New Methods in the Analysis of Electron Density and Electron Localizability – Applications to X–O–X Systems (X = C, Si)

Inaugural Dissertation
to obtain the academic degree
Doctor rerum naturalium (Dr. rer. nat.)
submitted to the Department of Biology, Chemistry and Pharmacy
of Freie Universität Berlin

by

Simon Grabowsky

from Berlin

December, 2009

from October, 2006 to December, 2009

supervised by Prof. Dr. Peter Luger

at the Institute of Chemistry and Biochemistry / Crystallography

1^{st} Reviewer: Prof. Dr. Peter Luger

2^{nd} Reviewer: Prof. Dr. Jens Beckmann

date of defence: February 12th, 2010

Contents

List of Tables

List of Figures

Introduction

Nearly one hundred years ago (1912), von Laue developed a mathematical model to describe constructive interference of X-rays scattered from atoms or molecules arranged in a crystal lattice. [1, 2] His predictions were verified in experiments performed by Friedrich and Knipping who obtained the first diffraction picture of a chemical compound by passing an X-ray beam through a crystal of copper sulfate. [3] Only one year later, the first crystal structures were solved by Ewald, Bragg, Sr. and Bragg, Jr. [4–7] But structure solution was only possible in exceptional cases because of the fundamental phase problem of crystallography. The first method to tackle this problem was introduced by Patterson in 1934. [8] Sayre, Karle and Hauptman developed equations in the 1950s to numerically solve the phase problem (direct methods, [9–11]) that gained general recognition in the 1960s and 1970s due to a rapid progress in computer technology. Since then, structure determination through X-ray diffraction on crystalline materials has become one of the most frequently used standard methods in analytical chemistry.

By 1915, Debye already pointed out that there is more information in the diffraction pattern than the atomic positions, namely the arrangement of the valence electrons. [12] This statement opened up the vision to fundamentally understand a chemical system's behaviour by means of its total electron density. But it took another 50 years until models were developed by Stewart and Hirshfeld to replace the spherical description of the electron density by an aspherical approach that allows to determine the arrangement of bonding and non-bonding valence distributions. [13–15] The multipole model of Hansen and Coppens finally established itself for broad application. [16] First electron-density studies showed that useful chemical information could indeed be obtained, but so far only on a qualitative level. [17–20]

When Bader introduced his Quantum Theory of Atoms in Molecules (QTAIM) in the 1980s, [21–25] the quantitative analysis of the electron density in terms of a full topological analysis with bond and atomic properties became accessible.

Accompanied by a rapid advance of technology (area detectors, computer hardware power and software quality) in the 1990s, electron-density determination and analysis from X-ray diffraction experiments have become an increasingly standardised and powerful method. The first experimental electron-density study employing synchrotron radiation was published by Luger et al. in 1998, [26] so that electron-density experiments on small and weakly diffracting samples like large organic compounds of biological interest were rendered possible. This intention is promoted by the build-up of databanks containing multipole parameters for atomic fragments of organic compounds [27–32] relying on the transferability concept of submolecular properties in the electron density [21, 23]. Now, a century after the first X-ray diffraction experiment, we are at a point where the electron-density determination and analysis from X-ray diffraction on single-crystals is not far from becoming a standard method. [33–35]

Electron-density distribution in a compound can also be derived from theoretical calculations. With modern computers, the calculation of the density for any moderately sized compound is carried out routinely. As the electron density can be calculated directly from the square of the absolute value of the wave function, it is accessible from any method that provides the wave function, e.g. often used ab-initio methods like Hartee-Fock and Møller-Plesset or very new methods like constrained wave-function fitting (CWF) [36–39]. CWF yields a wave function fitted to experimental data and therefore opens up access to properties which can otherwise not be deduced from experiments.

Hohenberg and Kohn proved in 1964 that the ground-state electron density uniquely determines all molecular electronic properties. [40] In the density-functional theory (DFT), the ground-state electronic energy is a functional of the ground-state electron density, and therefore the calculation of the wave function, which lacks direct physical significance, can be omitted. Kohn and Sham devised a practical method for finding the ground-state electron density, but it contains an unknown functional that must be approximated. [41] However, mainly hybrid methods that base on DFT methods, e.g. B3LYP including exchange and correlation terms, have established themselves and are widely used in computational chemistry.

Normally, theoretical calculations are carried out for an isolated molecule in the vacuum at 0 K. To get results comparable to the electron density derived from the X-ray diffraction experiment, calculations for molecules with periodic boundaries, i.e. within the crystal lattice, can be carried out. These calculations are much

more time-consuming, and the analysis of the electron density is more demanding, so that they cannot be applied routinely for molecular crystals. [42]

In the last years, a harsh debate on the fundamentals of chemical physics erupted in the literature. One side [43, 44] argues that the electron density is more fundamental than the wave function because the latter has no direct physical meaning and is not accessible to human imagination and senses, whereas the electron density is an observable in real space and can therefore be grasped intuitively. The other side [45–47] counters that the wave function is more fundamental because it is the mathematically underlying concept and "...it is only the wave function that gives an explanation for the chemical bond, whereas all attempts to explain the chemical bond in terms of the electron density have failed." [45] In the present doctoral thesis, methods from both fields are used to describe chemical bonding. Both electron density and wave function give valuable information on electronic properties. By neglecting the explanatory power of either of them, researchers deprive themselves of the potential to adequately treat a given chemical problem. A combination of the advantages of both fields provides a variety of new tools that are best suited for each individual chemical question, as the following two examples from both fields show.
The electron localization function (ELF) [48–50] and the recently introduced electron localizability indicator (ELI) from Kohout [51–53] are calculated directly from the wave function, but are real-space representations and topologically interpretable. ELF and ELI separate space into regions of electron-pair localisation, and thus give a chemical image of bonding and non-bonding effects in a quantifiable manner. Furthermore, an ELF or ELI analysis can be combined with an electron-density or molecular-orbital evaluation. Within this doctoral work, a way was found to deduce the ELI from the X-ray diffraction experiment as it is already possible for the ELF [54–56]. Moreover, the topological analysis of the experimental ELF and ELI are newly introduced in this doctoral thesis.
The source function from Gatti [57–59] is a new tool to analyse scalar fields like the electron density. Contributions of any atom in the molecule to the density of a given reference point, and thus intramolecular interactions along the molecules' scaffolds, can be detected, analysed, and visualised.

X–O–X systems, with X being silicon or carbon, more precisely siloxanes (Si–O–Si), silyl ethers (Si–O–C), open-chain ethers, and epoxides (C–O–C), were chosen as

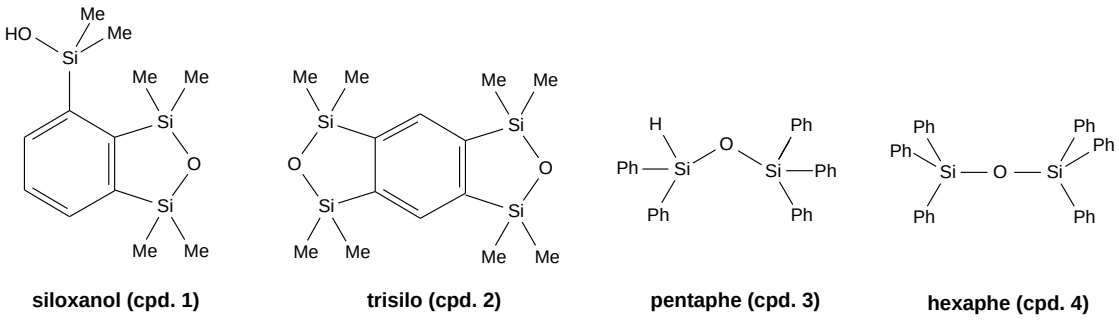

Figure 1: Molecular structures of scrutinised siloxane compounds with short names

the chemical topic of this doctoral thesis because these systems are among the most common and important chemical classes, while their bonding situation is still not sufficiently understood. Therefore, it appeared to be indispensable to use the newest methods in electron-density evaluation and alternative methods like ELF and ELI.

The Si–O–Si angle in open-chain siloxanes is very flexible and spans a wide range from 130 ° to about 180 °. Forced into ring systems, smaller Si–O–Si angles to about 80 ° are possible. The Si-O bonds are assumed to be of strong ionic character. The C–O–C angle in open-chain ethers covers a much smaller range from about 110 ° to 120 °, whereas the C–O–C angle in epoxides is fixed to 60 °. The C–O bonds are of predominantly covalent character. Thus, between the extreme angles of 60 ° and 180 ° - between strong ionic and covalent bonds - there is a very interesting development of bonding types and conditions that depend on the bond angle X–O–X, giving rise to very different chemical properties. This means that in a selective synthesis of compounds containing the Si–O–Si, Si–O–C or C–O–C linkage, respectively, chemical properties can be tuned with respect to the X–O–X angle.

The Si–O bond is the most common chemical bond in the earth's crust due to the high natural abundance of these elements and the high affinity of oxygen for silicon. Ubiquitous minerals, such as quartz, crystobalite, tridymit, feldspars or natural zeolites, but also man-made silica materials, such as unnatural zeolites or mesoporous silica (e.g. MCM-41, SBA-15), comprise a high content of siloxane linkages (Si–O–Si). Important industrial applications of zeolites and mesoporous silica involve, for instance, the use as heterogeneous catalyst supports and as selective molecular adsorbents. [60, 61] There is still a vivid controversy on the correct description of the Si-O bond character in silica materials, ranging from "very

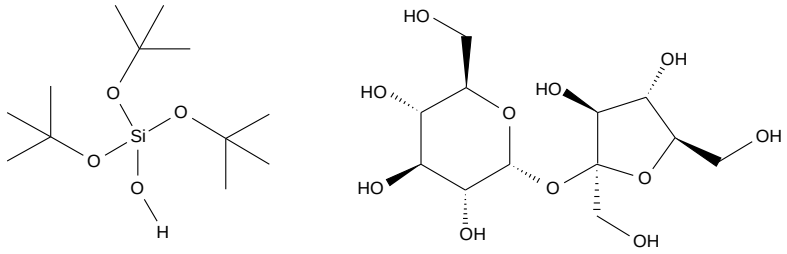

Figure 2: Molecular structures of scrutinised butoxysilanol and sucrose

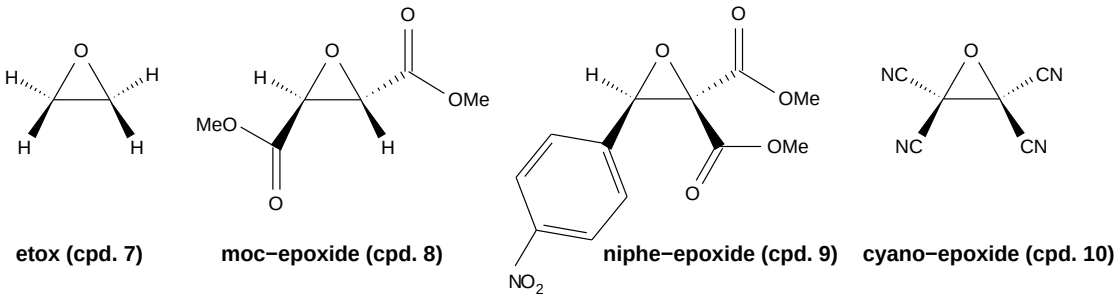

Figure 3: Molecular structures of scrutinised epoxide compounds with short names

ionic" [62–65] to a still "substantial covalent character" [62, 66–68] or a "mixture of covalent and strong ionic bonding" [62, 69]. Therefore, the Si-O bond is also referred to as "the elusive bond". [70]

Not only for minerals, but also for molecular or polymeric compounds containing the siloxane linkage (Si–O–Si), there is an ongoing discussion on the correct description of the chemical properties of the siloxane linkage. [56, 71, 72] A major point is the inherently low basicity of the siloxane linkage and its inability to form hydrogen bonds with polar molecules such as water. For example, linear and branched silicones, the most important class of organometallic polymers used in the chemical industry, also contain the siloxane linkage (Si–O–Si) in their backbones. Silicone polymers containing -Me_2Si-O-SiMe_2- units are highly hydrophobic and frequently find applications as water repellents. [73–75]

Figure 1 shows the structures of the molecular compounds **1** to **4** that were chosen as model compounds for the examination of the siloxane linkage by high-resolution X-ray diffraction experiments in this doctoral thesis. Siloxanol (cpd. **1**) and trisilo (cpd. **2**, [76, 77]) comprise strained siloxane linkages between 115 ° and 120 °. These Si–O–Si angles do not normally occur in siloxanes (see above) and

therefore give rise to unusual chemical behaviour. For example, the siloxane linkage in siloxanol (**1**) serves as an acceptor for a very exceptional intermolecular silanol-siloxane hydrogen bond, since it additionally contains a silanol group as a possible hydrogen-bond donor. This compound class is generally called siloxanols. Pentaphe (cpd. **3**, [78]) and hexaphe (cpd. **4**, [79, 80]) comprise unstrained siloxane linkages between 160 ° and 180 °, so that exceptionally strained and relaxed siloxane linkages can be compared.

The ether linkage (C–O–C) possesses a considerably higher basicity than the siloxane linkage, which is reflected in its pronounced hydrophilicity. Many ethers, such as tetrahydrofurane and crown ethers, are highly miscible with or soluble in water because of their ability to form hydrogen bonds of the type HO-H$\cdots$ O$(CX_3)_2$. [81, 82] Therefore, the inherent differences between the Si–O–Si and the C–O–C linkages, which cause the pronounced differences in basicity and the ability to form hydrogen bonds, are of interest. The Si–O–C linkage serves as an intermediate model between the two symmetrical linkages. The compounds chosen for X-ray diffraction experiments are shown in Figure 2. For the analysis of the Si–O–C linkage, butoxysilanol (cpd. **5**, [83]) was selected because therein one of three Si–O–C linkages (Si–O–C = 129 ° to 132 °) serves as a hydrogen-bond acceptor group while the others do not. For the ether linkage, sucrose (cpd. **6**, [84]) was chosen because it comprises one open ether linkage adjacent to two sterically demanding rings (compare pentaphe (**3**) and hexaphe (**4**)), one ether linkage incorporated into a six-membered ring, and one ether linkage incorporated into a five-membered ring (compare siloxanol (**1**) and trisilo (**2**)). In contrast to the siloxane linkage, the C–O–C angles for these three different cases are similar (C–O–C = 111 ° to 116 °). Moreover, there are several inter- and intramolecular hydrogen bonds in sucrose (**6**) with the C–O–C groups as acceptors.

Epoxides (oxiranes, ethylene oxides, oxacyclopropanes) containing a C–O–C linkage of about 60 ° are worth further research because of the unusually high bond strength and the broad synthetical and pharmaceutical applications. There are different concepts to describe this bonding situation, but it is still not sufficiently understood how bond character and bond shape can be correctly described (three bent σ bonds, i.e. banana bonds, or one stable six-electrons-three-center bond). [19, 85, 86] Epoxides are widely used reagents in organic synthesis because the strained bonding situation leads to a synthetically very useful balance between stability and reactivity. [87, 88] Their application is so broad and straightforward that they are a key element of the so called click-chemistry. [89, 90] There

is also a pharmaceutical relevance of epoxides as potential protease inhibitors against various diseases like cancer and HIV. [91–93] Moreover, numerous efforts are presently made to find an inhibitor against the SARS coronavirus, of which the ones involving an epoxide derivative are very promising. [94, 95] Two of the chosen epoxide derivatives of this doctoral thesis (moc-epoxide (cpd. **8**) and niphe-epoxide (cpd. **9**), see Figure 3) are model compounds for drug design in this field. The aim is to develop cysteinic [91, 96] and aspartic [97, 98] protease inhibitors consisting of an electrophilic building block, which can covalently block the nucleophilic amino acids of the enzyme's active sites (Cys in cysteine proteases or Asp in aspartate proteases). The electronic properties of the model compounds can give valuable insight into their mode of action regarding the recognition and inhibition process with the enzyme. [99, 100] Etox (cpd. **7**, [101, 102]) and cyano-epoxide (cpd. **10**, [19, 103]) are examined for comparison because they contain a very weak or a very strong electron-withdrawing substitution pattern, respectively.

Part I

Theoretical Foundations

Chapter 1

Determination of Electron Density

1.1 Experimental Determination of Electron Density

1.1.1 Setup of the Electron-Density Experiment

Single-crystal X-ray diffraction experiments suited to determine the electron density are much more demanding than conventional measurements for structure determination. This is due to the fact that the number of parameters to be refined increases from a maximum of nine per atom to a maximum of 41 in the aspherical case. Thus, the number of symmetry-independent reflections measured must be increased enormously. It follows that a complete set of data must be measured to high resolutions of at least $\frac{\sin(\theta_{max})}{\lambda}$=1.0 Å^{-1}. Moreover, the measurement has to be more exact than a standard experiment, as the effects to be modelled are much smaller. So high redundancy of data is necessary to guarantee a good merging procedure and error model. Low temperatures of at least 100 K also improve the electron-density model because thermal smearing of the density must be deconvolved from valence density. [104]

The most promising way to meet the requirements described above is the use of large area detectors and intensive primary X-radiation from synchrotron sources. Most of the data sets used in this doctoral thesis were measured at synchrotron facilities (DESY in Hamburg and APS in Chicago). The beamlines F1 and D3

of HASYLAB at DESY (Hamburger Synchrotron-Strahlungslabor des Deutschen Elektronen-Synchrotrons) in Hamburg, Germany, were employed, which are connected to the storage ring DORIS III. Tunable wavelengths in the high-energy region between 0.56 and 0.51 Å were used. The high primary intensity gives rise to strong reflection intensities and sharp profiles at high resolution and low absorption. Figures 1.1 (a) and (b) show the experimental setup of these beamlines, which are both equipped with a large marCCD 165 area detector. F1 consists of a large Huber kappa five-circle diffractometer and open-flow nitrogen gas-stream cooling. D3 consists of a large Huber Eulerian four-circle diffractometer with open-flow helium gas-stream cooling.

With increasing size of the area detector and decreasing wavelength at small crystal-detector distances, the mean free path of the diffracted beam through the phosphorescent layers of the detector (Tb doped $Gd_2O_2S_2$) varies significantly between centre and margin of the detector. Therefore, the reflection intensities at the detector margins are biased because of oblique incidence angles and must be corrected. For F1 and D3, an oblique incidence correction programme was developed by Johnas [105] and could successfully be employed for the HASYLAB data sets of this work.

The beamline 15-ID-B at APS (Advanced Photon Source) of the Argonne National Laboratories in Chicago, USA, is designated for electron-density experiments, too. It is equipped with a Bruker D8 diffractometer with fixed chi angle. A Bruker APEXII detector and an open-flow helium gas-stream cooling device are installed, see Figure 1.1 (c). The X-ray energy (0.41 Å) and the primary intensity of the beam at the APS are even higher than at DORIS III.

One of the data sets of this doctoral thesis (etox (**7**)) was measured by Buschmann with a conventional sealed Mo-K_α X-ray tube and a scintillation counter about 25 years ago on a Stoe four-circle diffractometer. Another data set (moc-epoxide (**8**)) was collected at the in-house Huber Eulerian four-circle diffractometer, which is equipped with a sealed Mo-K_α X-ray tube, a Bruker APEX CCD area detector, and a closed-cycle helium cryostat with a transparent kapton vacuum chamber [106,107], see Figure 1.1 (d). These data sets are less resolved than the synchrotron data sets. The data set of etox (**7**) is still sufficient for an experimental electron-density study, but the data set of moc-epoxide (**8**) had to be treated with additional theoretical information to get access to the electron-density distribution.

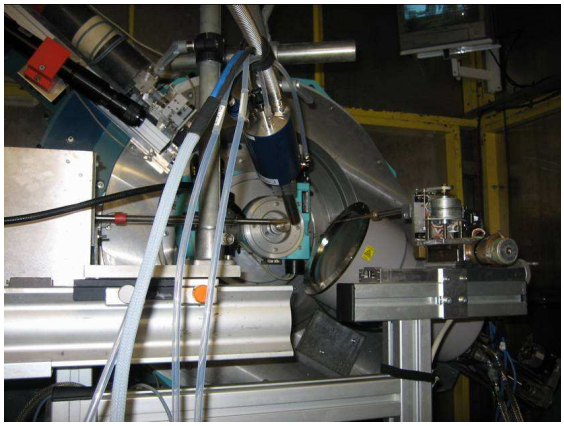

(a) Beamline F1 of HASYLAB

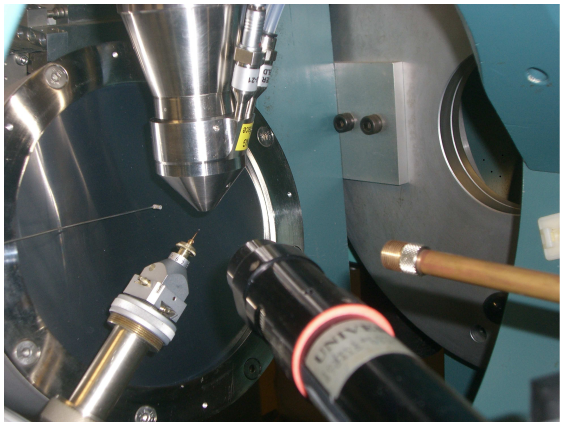

(b) Beamline D3 of HASYLAB

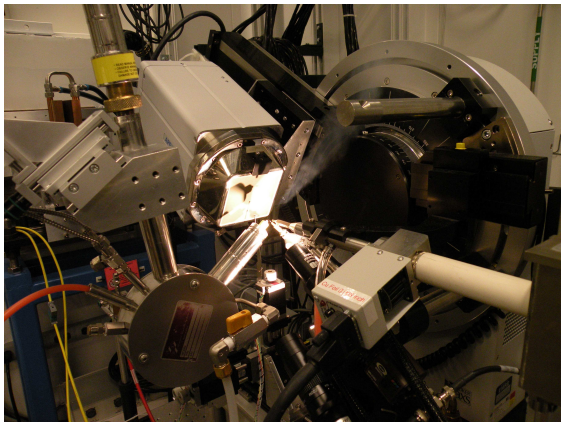

(c) Beamline 15-ID-B of APS

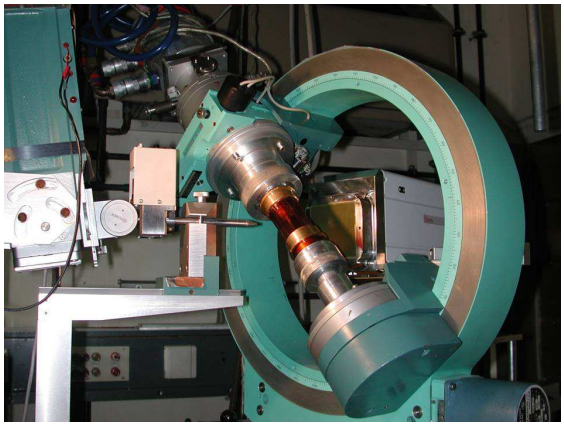

(d) In-house diffractometer with kapton cylinder

Figure 1.1: Experimental setups employed in this work

1.1.2 Conventional X-ray Structure Analysis

An X-ray beam is diffracted by the periodical arrangement of the molecules in a crystal as a three-dimensional lattice. The periodicity is defined by the regular recurrence of the unit cell with the lattice constants $a, b, c, \alpha, \beta, \gamma$. The fractional coordinates x, y, z determine the position vector of each atom in the unit cell with respect to the lattice constant vectors as basis of the internal coordinate system: $\vec{r} = x\vec{a} + y\vec{b} + z\vec{c}$. The reciprocal space of the crystal is spanned by the reciprocal lattice vector $\vec{h}$ according to Eq. 1.1 with $a^*, b^*, c^*, \alpha^*, \beta^*, \gamma^*$ being the reciprocal lattice constants and h, k, l being integer numbers.

$$\vec{h} = h\vec{a}^* + k\vec{b}^* + l\vec{c}^* \tag{1.1}$$

$\vec{h} \cdot |\vec{h}|^{-1}$ is the normal vector of a lattice plane according to the Hessian normal form. A reflection can be observed if a lattice plane is aligned towards the direction of the primary beam ($\vec{s}_0$) and towards the direction of the diffracted beam ($\vec{s}$) following the Ewald condition (Eq. 1.2).

$$\vec{h} = h\vec{a}^* + k\vec{b}^* + l\vec{c}^* = \frac{\vec{s} - \vec{s}_0}{\lambda} \tag{1.2}$$

The X-radiation interacts with the electrons of the atoms. Thus, the electron-density distribution is in principle accessible through the X-ray diffraction experiment. The probability to find the electron, i.e. the square of the absolute value of the wave function, is proportional to the electron density: $\varrho(\vec{r}) \sim |\Psi(\vec{r})|^2$. The structure factor $F(\vec{h})$ is the Fourier transform of the electron density $\varrho(\vec{r})$ according to Eq. 1.3.

$$F(\vec{h}) = \int_V \varrho(\vec{r}) \cdot e^{2\pi i \vec{h}\vec{r}} dV \tag{1.3}$$

In the conventional X-ray structure analysis, the atomic electron densities are approximated as being of spherical symmetry (Independent Atom Model, IAM). They are referred to as atomic scattering factors f_j and are tabulated for each atom type. Hence, the Fourier transformation (Eq. 1.3) simplifies to a sum of scattering factors with associated complex phases for each atom type j, yielding Eq. 1.4.

$$F(\vec{h}) = \sum_{j=1}^{N} f_j(|\vec{h}|) \cdot e^{2\pi i \vec{h}\vec{r}_j} \tag{1.4}$$

Since it is important to account for the thermal motion of the atoms in the crystal, an additional term is added to the structure factor that contains the isotropic

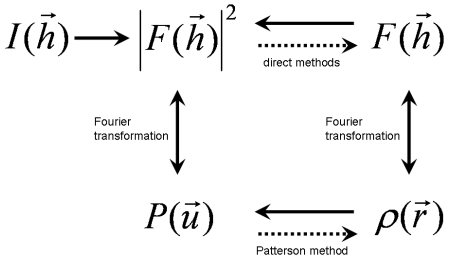

Figure 1.2: Hosemann diagram

Debye-Waller factor B_j, which is calculated from the mean isotropic oscillation amplitude of the thermal motion of the atom j (Eq. 1.5).

$$F(\vec{h}) = \sum_{j=1}^{N} f_j(|\vec{h}|) \cdot e^{2\pi i \vec{h}\vec{r}_j} \cdot e^{-B_j(\frac{sin^2\Theta}{\lambda^2})} \tag{1.5}$$

An anisotropic description of the thermal motion is more appropriate. But with the use of the anisotropic displacement parameters (adps) B_{ij}, six additional parameters per atom are introduced. The anisotropic decription of the thermal motion is routinely applied for non-hydrogen atoms, but there is also a way to describe the hydrogen-atom motion anisotropically by a rigid body approximation using the SHADE code. [108, 109]

The square of the absolute value of the structure factor can be calculated from the intensities $I(\vec{h})$ of the reflections if several corrections are applied (see Eq. 1.6). k scales to the total number of electrons using the F(000) value. LP are Lorentz and polarisation correction terms, whereas A corrects for the absorption of the X-ray beam upon travelling through the crystal.

$$I(\vec{h}) = k \cdot LP \cdot A \cdot |F(\vec{h})|^2 \tag{1.6}$$

But to calculate the Fourier transformations in equations 1.3, 1.4 or 1.5, respectively, which are necessary to solve the crystal structure, the complex-valued structure factor $F(\vec{h})$ itself is needed, the phase of which can generally not be determined from the square of the absolute value $|F(\vec{h})|^2$. This phase problem of crystallography prevents the electron density from being directly deducible from the experiment. The Hosemann diagram in Figure 1.2 shows the relations of the functions. The dotted arrows indicate the phase problem.

The Hosemann diagram includes the two methods that circumvent the phase problem mathematically: direct methods and the Patterson method. Direct methods

make use of statistical relationships between intensities and signs for centrosymmetric structures (Sayre's equation, [9]) or generally between intensities and phases (tangent formula from Karle and Hauptman, [10]), respectively, to get the structure factor from the square of the absolute value. Direct methods have established themselves for small-molecule crystallography. Within the Patterson method, [8] the Fourier transformation of $|F(\vec{h})|$ itself is calculated to get the Patterson function $P(\vec{u})$. $P(\vec{u})$ being the convolution square of $\varrho(\vec{r})$ can be interpreted to obtain the electron density. This method is still used for large protein structures or if heavy atoms are included.

After solving the phase problem, the structure model is still only a raw approximation. Therefore, in a subsequent difference Fourier synthesis the phases of the structure factors calculated from the present structure model (F_c) are assigned to the structure factors of all observed reflections: $F_o = |F_o| \cdot e^{i\varphi(F_c)}$. Hence, the structure model can be improved by the adjustment method of least squares. The best structure model is found if Eq. 1.7 gives a minimum value for Q.

$$Q = \sum_{\vec{h}} (|F_o(\vec{h})| - |F_c(\vec{h})|)^2 \tag{1.7}$$

One of a multitude of different figures of merit to test the structure model is the calculation of a residual index that quantifies the relative differences between the observed and the calculated structure factors according to Eq. 1.8.

$$R = \frac{\sum_{\vec{h}} ||F_o(\vec{h})| - |F_c(\vec{h})||}{\sum_{\vec{h}} |F_o(\vec{h})|} \tag{1.8}$$

More details on conventional X-ray structure analysis can be found in various textbooks. [110–112]

1.1.3 The Multipole Model

The Hansen-Coppens multipole formalism [16] replaces the spherically symmetric atomic scattering factors by aspherical terms. Thus, the structure factor $F(\vec{h})$ can be expressed as Eq. 1.9 shows.

$$F(\vec{h}) = \sum_{i=0}^{N_{atoms}} \sum_{j=0}^{N_{sym}} \Bigg[P_{i,core} f_{i,core}(\vec{h}) + P_{i,val} f_{i,val}(\vec{h}, \kappa) + \sum_{l=0}^{4} \Phi_{il}(\vec{h}, \kappa'_l) \sum_{m=-l}^{l} P_{ilm} Y^i_{lm}(\vec{h}_j/|\vec{h_j}|) \Bigg] e^{2\pi i \vec{h} \cdot \vec{r}_{ij}} \cdot T_i(\vec{h}) \tag{1.9}$$

The structure factor is generated by three contributions: the core electrons (first summand), the spherically symmetrical valence electrons (second summand) and the asphericaly distributed valence electrons (third summand). P are population parameters which are to be refined, f are core-only or valence-only scattering factors that are extracted from tabulated IAM scattering factors. κ and κ' are expansion-contraction parameters that can also be refined. Y_{lm} are spherical harmonics that account for the aspherical expansion. T_i stands for the description of the thermal motion of the ith atom, either isotropic or anisotropic. The function Φ_{il} is the Fourier-Bessel transform (Eq. 1.10) of the atomic radial function R_{il} (Eq. 1.11).

$$\Phi_{il}(\vec{h}, \kappa'_l) = 4\pi i^l \int_0^\infty R_{il}(\vec{r}, \kappa'_l) \cdot j_l \cdot 2\pi\vec{h}\vec{r}^3 dr \tag{1.10}$$

j_l is a Bessel function of the lth order.

$$R_{il}(\vec{r}, \kappa'_l) = \frac{\zeta_{il}^{n_{il}+3}}{(n_{il}+2)!}(\kappa'_l\vec{r})^{n_{il}} \cdot e^{-\kappa'_l\zeta_{il}\vec{r}} \tag{1.11}$$

The radial functions R_{il} are single-zeta Slater functions that differ for each atom type. The radial power coefficients n_{il} can be varied, but are normally fixed to default values per atom type. The ζ_{il} values are calculated for each atom type and tabulated. [113–116] The index l gives the order of the multipole expansion, the number of the involved multipoles per expansion step can be calculated according to $m = 2l + 1$. Thus, the order $l = 0$ stands for one monopole, $l = 1$ for three dipoles, $l = 2$ for five quadrupoles, $l = 3$ for seven octupoles and $l = 4$ for nine hexadecapoles. So the maximum number of refinable parameters per atom in the multipole formalism is 41.[1] To prevent high correlations between the parameters in the refinement, P_{00} and κ'_0 are never refined. κ'_l parameters (l>0) are not refined independently. Furthermore, the spherical harmonics are dependent on the symmetry of the local atomic site as Eq. 1.9 shows. Therefore, some population parameters are not refined because of symmetry considerations [117], so that in general, the maximum number of refineable parameters is not reached.

With all these considerations, it is possible to calculate the electron density of the whole system as the Fourier transform of the aspherical structure factor of Eq. 1.9. This final aspherical electron density of the system is given in Eq. 1.12 as a

[1] $x, y, z, u_{11}, u_{12}, u_{13}, u_{22}, u_{23}, u_{33}, P_{val}, P_{00}, P_{10}, P_{1\bar{1}}, P_{11}, P_{20}, P_{2\bar{1}}, P_{21}, P_{2\bar{2}}, P_{22}$,
$P_{30}, P_{3\bar{1}}, P_{31}, P_{3\bar{2}}, P_{32}, P_{3\bar{3}}, P_{33}, P_{40}, P_{4\bar{1}}, P_{41}, P_{4\bar{2}}, P_{42}, P_{4\bar{3}}, P_{43}, P_{4\bar{4}}, P_{44}, \kappa, \kappa'_0, \kappa'_1, \kappa'_2, \kappa'_3, \kappa'_4$

superposition of atomic densities $\varrho_i(\vec{r})$ called pseudoatoms: $\varrho(\vec{r}) = \sum_{i=1}^{N} \varrho_i(\vec{r})$.

$$\varrho(\vec{r}) = \sum_{i=1}^{N} \left[P_{i,core}\varrho_{i,core}(\vec{r}) + P_{i,val}\kappa^3 \varrho_{i,val}(\vec{r},\kappa) + \sum_{l=0}^{4} \kappa_l'^3 R_{il}(\vec{r},\kappa_l') \sum_{m=-l}^{l} P_{ilm} Y_{lm} \right] \tag{1.12}$$

It is common practice to evaluate the quality of the multipolar modelling by means of the deformation density and the residual density. The deformation density $\Delta\varrho(\vec{r})$ is the difference between the total multipolar density $\varrho_{mult}(\vec{r})$ and the total IAM density $\varrho_{IAM}(\vec{r})$ according to Eq. 1.13. As electron density and thermal motion are already deconvolved in both the multipolar and the IAM density, the deformation density is referred to as static deformation density. It visualises regions of increase or decrease of the electron density, respectively, upon expanding the model from the IAM towards the multipolar description.

$$\Delta\varrho(\vec{r}) = \varrho_{mult}(\vec{r}) - \varrho_{IAM}(\vec{r}) = \frac{1}{V} \sum_{\vec{h}} (F_{c,mult}(\vec{h}) - F_{c,IAM}(\vec{h})) \cdot e^{-2\pi i \vec{h}\vec{r}} \tag{1.13}$$

The residual density is the density accessible by the Fourier transformation of the difference of the observed structure factors $F_o(\vec{h})$ and the calculated multipolar structure factors $F_{c,mult}(\vec{h})$ as given in Eq. 1.14. The residual density is a dynamic difference density, as thermal motion and electron density are both included in $F_o(\vec{h})$, but already deconvolved in $F_{c,mult}(\vec{h})$. In the optimum case, the residual density should vanish as both total electron-density distribution and thermal motion should be described by the final model.

$$\delta_{res}\varrho(\vec{r}) = \frac{1}{V} \sum_{\vec{h}} (F_o(\vec{h}) - F_{c,mult}(\vec{h})) \cdot e^{-2\pi i \vec{h}\vec{r}} \tag{1.14}$$

1.2 Theoretical Determination of Electron Density

1.2.1 Methods

There are two major ways to determine the electron density by quantum-chemical calculations: wave function-based ab-initio or density-functional treatments of molecules. In the density-functional theory (DFT), the electron density is the fundamental property itself. In wave function-based ab-initio methods, the electron density can be calculated from the square of the absolute value of the wave

function, i.e. the probability density to find an electron according to Eq. 1.15. Therein, integration over the coordinates of all electrons except the one considered $(2, 3, \ldots, n)$ and summation over all possible spin states $m_{s1}, \ldots, m_{sn}$ gives the electron probability density (electron density, charge density) to find an electron at the position $\vec{r}$. For a many-electron molecular orbital (MO) wave function, ϱ is likewise found by multiplying the probability-density function ϕ of each MO by the number of electrons occupying it and summing the results.

$$\varrho(\vec{r}) = n \sum_{all\ m_s} \int \cdots \int |\psi(\vec{r}, \vec{r_2}, \ldots, \vec{r_n}, m_{s1}, \ldots, m_{sn})|^2 d\vec{r_2} \cdots d\vec{r_n} = \sum_j n_j |\phi_j|^2 \tag{1.15}$$

Wavefunction-Based Ab-Initio Methods

Wavefunction-based ab-initio methods [118] try to solve the time-independent three-dimensional Schrödinger equation $\hat{H}\Psi = E\Psi$ (detailed in Eq. 1.16) by different approximations. The Hamiltonian $\hat{H}$ for an n-electron case is given in square brackets. m_i is the mass of electron i, V is the potential energy.

$$\left[-\sum_{i=1}^{n} \frac{\hbar^2}{2m_i} \nabla_i^2 + V(\vec{r_1}, \ldots, \vec{r_n}) \right] \Psi(\vec{r_1}, \ldots, \vec{r_n}) = E\Psi(\vec{r_1}, \ldots, \vec{r_n}) \tag{1.16}$$

The Schrödinger equation $\hat{H}\Psi = E\Psi$ can be transposed to get an equation for the ground-state energy of the system as an integral over the elements of space $d\tau$ (Eq. 1.17).

$$\int \Psi^\star \hat{H} \Psi d\tau = E \tag{1.17}$$

As the correct wave function for a many-electron system can never be found analytically, the correct ground-state energy E of the system can never be calculated. According to the variation theorem, any trial variation function ϕ that can be chosen to calculate the ground-state energy of the system will yield an energy value that is higher than, or in the optimum case equal to, the correct energy, but never lower. Thus, the quality of test functions can be evaluated in a way that the function that yields the lowest energy is the best approximation for the system. The variation theorem is given in Eq. 1.18.

$$\int \phi^\star \hat{H} \phi d\tau \geq E \tag{1.18}$$

The challenge is to find an appropriate trial variational function that on the one hand gives reliable results, but on the other hand is not too time-consuming in

computational calculations. The Hartree-Fock (HF) method to find such a trial variational function has established itself for broad application. Within this approach, the instantaneous interactions between one electron and all the other electrons are averaged out. Electrons 2,3,...,n are being smeared out to form a static distribution of electric charge through which the first electron moves. This effective potential affecting the considered electron is referred to as self-consistent field (SCF). The Schrödinger equation reduces to a differential equation (Eq. 1.19) for finding the atomic Hartee-Fock spin-orbital u_i. The Fock operator $\hat{F}$ is the effective Hartree-Fock Hamiltonian to give the orbital energy ε_i of spin-orbital i.

$$\hat{F}u_i = \varepsilon_i u_i \tag{1.19}$$

The trial wave function ϕ of a whole system results from the superposition of all i atomic spin-orbitals (Eq. 1.20). Constructing a wave function for a molecule from the i atomic Hartree-Fock spin-orbitals is called the linear combination of atomic orbitals to molecular orbitals (LCAO-MO). According to Eq. 1.20, optimal coefficients c_i for the system have to be calculated iteratively (Roothaan-Hartree-Fock formalism).

$$\phi = \sum_i c_i u_i \tag{1.20}$$

The energies calculated by the Hartree-Fock SCF method are typically in error by about 0.5 % for light atoms. It is an improvement to introduce the instantaneous electron correlations into the wave functions, which is done in so-called configuration-interaction (CI) methods. But these methods are so time-consuming that they cannot be employed in this doctoral thesis.

A different approach to approximately solve the Schrödinger equation is the so-called perturbation theory. Therein, the difference between a correct system with the Hamiltonian $\hat{H}$, for which the Schrödinger equation cannot be solved, and an unperturbed system with the Hamiltonian $\hat{H}^0$, for which the Schrödinger equation can be solved, is referred to as the perturbation $\hat{H}'$. This perturbation is applied gradually to the known eigenvalues and eigenfunctions to relate them to the unknown eigenvalues and eigenfunctions. Eq. 1.21 shows how the Lagrangian multiplier λ, which lies between zero and one, is mixed to the unperturbed system to yield the correct system.

$$\hat{H} = \hat{H}^0 + \lambda\hat{H}' \tag{1.21}$$

The Møller-Plesset (MP) perturbation theory is often used in quantum chemical

calculation, but it is not employed within this doctoral thesis. However, the same ansatz is used in the theory of the constrained wave-function fitting (CWF) and will therefore be discussed in further detail in Chapter 1.3.

Density-Functional Theory

In density-functional theory (DFT) (for the original literature, see ref. [40,41]; for reviews on the DFT, see [119–121]), the ground-state electron density is used in place of the wave function as the basic descriptor of an electronic system. The total ground-state molecular energy, the wave function and all other molecular electronic descriptors are uniquely determined by the ground-state electron density. The total ground-state molecular energy $E[\varrho]$ is given by Eq. 1.22 as a functional of the electron density. The functional $F[\varrho]$ is the sum of the kinetic energy functional and the electron-electron repulsion functional. $v(\vec{r})$ is the external potential of the nuclei.

$$E[\varrho] = F[\varrho] + \int v(\vec{r})\varrho(\vec{r})d\vec{r} \tag{1.22}$$

Unfortunately, Eq. 1.22 does not provide a practical way to calculate the energy and the density because the functional $F[\varrho]$ is unknown. Thus, approximations have to be introduced. The Hohenberg-Kohn variational theorem states that $E[\varrho]$ is a minimum when ϱ is the correct ground-state density. For every suitable trial density $\varrho_{tr}(\vec{r})$, the inequality $E \leq E[\varrho_{tr}]$ holds. Therefore, similar to the variation method to solve the Schrödinger equation (see above), it can be judged which density is best suited as it has to yield the smallest energy. The Kohn-Sham method is a practical way of finding an appropriate ϱ_{tr} and deriving E_{tr} from it. It considers a ficticious reference system of n non-interacting electrons, so that each one experiences the same external potential energy $v_{ref}(\vec{r}_i)$. With this approximation that is simimlar to the SCF method descibed above, a pseudo-Schrödinger equation Eq. 1.23 can be introduced that includes the one-electron Kohn-Sham Hamiltonian $\hat{h}_i^{KS} = -\frac{1}{2}\nabla_i^2 + v_{ref}(\vec{r}_i)$, the Kohn-Sham one-electron orbitals θ_i^{KS} and the corresponding orbital energies ϵ_i^{KS}.

$$\hat{h}_i^{KS}\theta_i^{KS} = \epsilon_i^{KS}\theta_i^{KS} \tag{1.23}$$

The wanted electron density can be obtained by summing up the squares of the absolute values of the Kohn-Sham orbitals: $\varrho_{tr} = \sum_{i=1}^{n} |\theta_i^{KS}|^2$. But even after obtaining the electron density, the energy can still not be calculated due to the unknown functional of Eq. 1.22, more precisely the unknown exchange-correlation energy

functional (E_{xc}) which is included in $F[\varrho]$, amongst other contributions. Several methods were introduced to approximate this problem, for example the local-density approximation (LDA) or the local-spin-density approximation (LSDA) based on the uniform-electron-gas model. The most popular and successful modern methods are hybrid methods that use E_{xc} corrections from wave function-based methods like Hartree-Fock, and therefore do not depend on the uniform-electron-gas model, but take the variation of the electron density with position into consideration. There are numerous hybrid methods in the literature [118] from which the B3LYP method (Becke, Lee, Yang and Parr) [122, 123] is the most commonly used and is also applied in this doctoral thesis. The exchange-correlation energy in question is a sum of several contributions from different methods according to Eq. 1.24.

$$E_{xc}^{B3LYP} = 0.08E_x^{LSDA} + 0.20E_x^{HF} + 0.72E_x^{B88} + 0.19E_c^{VWN} + 0.81E_c^{LYP} \quad (1.24)$$

The ab-initio SCF MO method is usually reliable for ground-state, closed-shell molecules, but especially the MP2 perturbation theory and DFT with hybrid functionals usually perform substantially better than HF methods. [118] Moreover, DFT with hybrid functionals is less time-consuming than MP2 perturbation theory.

1.2.2 Basis Sets

Molecular quantum-mechanical calculations start with the choice of a set of basis functions χ_r, which are used to express the MOs ϕ_i as $\phi_i = \sum_r c_{ri}\chi_r$. A commonly used set of basis functions is the set of Slater-type orbitals (STO) according to Eq. 1.25.

$$\frac{(2\zeta/a_0)^{n+0.5}}{[(2n)!]^{0.5}} r^{n-1} e^{-\zeta r/a_0} Y_l^m(\theta,\phi) \quad (1.25)$$

n, l and m are the quantum numbers, a_0 is the Bohr radius, r the distance from the nucleus, $Y_l^m(\theta,\phi)$ are the spherical harmonics and ζ are tabulated parameters. The form of Eq. 1.25 is similar to the single-zeta radial functions of Eq. 1.11 used in the multipolar modelling. The ζ values used in the multipolar modelling can also be used here. [113, 114]

Gaussian-type functions (GTF) that speed up molecular integral evaluation are used more often. GTF are generally defined as Eq. 1.26 shows.

$$g_{ijk} = \left(\frac{2\alpha}{\pi}\right)^{3/4} \left[\frac{(8\alpha)^{i+j+k} i!j!k!}{(2i)!(2j)!(2k)!}\right]^{0.5} x_b^i y_b^j z_b^k e^{-\alpha r_b^2} \quad (1.26)$$

i,j and k are positive integers, α is a positive orbital exponent and x_b, y_b and z_b are Cartesian coordinates with the origin at nucleus b. Each basis function χ_r is a normalised linear combination of a few Gaussians according to Eq. 1.27

$$\chi_r = \sum_u d_{ur} g_u \tag{1.27}$$

The g_u's are called primitive Gaussians. They are centred on the same atom and have the same i, j, k but different α values. The contraction coefficients d_{ur} are constant and are held fixed during the calculation. χ_r is called a contracted Gaussian-type function (CGTF).
Classification and nomenclature of different CGTF-based basis sets describe the number of primitive Gaussians for each atom type in the molecule. For example, the Pople basis set 6-311++G(d,p) is composed as follows: One CGTF as a linear combination of six primitive Gaussians describes the inner shells (6). The valence shell is built from a CGTF as linear combination from three primitive Gaussians, a medium expanded primitive Gaussian and an expanded primitive Gaussian (311). Two diffuse functions are used to describe charges and interactions (++). All used functions are Gaussian-type functions (G). For hydrogen atoms, a polarisation function is used that is similar to p orbitals (p). For non-hydrogen atoms, a polarisation function is used that is similar to d orbitals (d). Current state of the art are the correlation consistent (cc) CGTF-based basis sets by Dunning. Their nomenclature is cc-pVXZ. For example, the cc-pVTZ basis set stands for correlation consistent polarised valence triple-zeta basis set. Pople and Dunning basis sets are used in this doctoral thesis.

1.2.3 Isolated Molecules vs. Periodic Boundaries

The predefinition made in standard computational-chemistry procedures [118,124, 125] is that of an isolated molecule, i.e. the molecule is considered to be in vacuum at 0 K without any intermolecular interactions and thermal motion. This makes it possible to determine exclusively properties inherent to the molecule and its geometry. The geometry can be input from an X-ray structure determination. Alternatively, it can be optimised according to the energetical ground state in the vacuum. Furthermore, a relaxed potential-energy surface (PES) scan can be carried out. Therein, one geometrical parameter can be varied gradually, and all the other geometrical parameters are optimised at each step. This way, the development of the potential energy along one coordinate can be observed.

Besides the electron density and the ELF/ELI (for further details see Chapter 3), a number of other interesting properties can be calculated by isolated-molecule calculations. The total molecular energy is routinely given, but also interaction energies E_{int} can be obtained, for example of a hydrogen-bonded adduct. In this case, the interaction energy is the best possible approximation to the hydrogen-bond energy E_{HB} because the hydrogen bond should be the most important interaction in these adducts. To get E_{HB}, the total molecular energies of the hydrogen bonded adduct and of both isolated molecules are calculated and substracted from each other. As a basis set superposition error (BSSE) occurs in this procedure, a correction term has to be calculated seperately by the counterpoise procedure. [126]
A frequency analysis yields the harmonic and anharmonic vibration frequencies of the molecule. If negative frequencies are observed, the molecule is not in its relaxed energetical ground state, but in a transition state, i.e. a saddle point on the energy hypersurface. Moreover, the IR red shift of the donor-H stretching vibrations upon hydrogen-bond formation can be calculated by substracting the frequencies of the vibrations before and after complexation. A term for the zero-point vibration can be calculated to correct the total molecular energy. But this term has to be scaled due to an inconsistency of the absolute values of a frequency analysis with special basis sets. The value for scaling is 0.9877 for Pople basis sets [127] and 0.9800 for Dunning basis sets [128].
In a natural bond orbital (NBO) analysis, [129–131] negative hyperconjugation of the type $n(A) \rightarrow \sigma^{\star}(D-H)$ (A=acceptor, D=donor, H=hydrogen) has been invoked as the main contribution to hydrogen-bond energies. They can be quantitatively assessed by NBO analyses in the form of hydrogen-bond delocalisation energies ΔE_{deloc}.

The neglection of intermolecular interactions is not appropriate if the theoretical results are to be compared with experimental results from the crystal. Especially for biologically active molecules, where intermolecular bonding plays a key role in the mode of action, the electron density from isolated-molecule calculations is not sufficient to predict properties in biological environments. [99,132] Therefore, mimicking the crystal environment, which is indeed a much better approximation to the biological environment, [132] by periodic boundaries is necessary. In periodic-boundary calculations, the molecular geometry as well as the symmetry information of the crystal are input. Upon geometry optimisation, the atomic coordinates and the lattice constants are optimised at a fixed space group. [133] Hartree-Fock

and DFT calculations can be carried out for periodic systems. [42, 134] The wave function in periodic cases is a plane wave which is propagated to infinity. The basis sets are nearly exclusively based on Pople molecular basis sets but separately defined for each different atom type in the crystal.
However, periodic-boundary calculations are much more demanding and time-consuming than isolated-molecule calculations. Therefore, periodic calculations at the experimental geometry were performed for all cpds. **1** to **10**, but geometry optimisations could only be carried out for cpds. **7** to **10**. Moreover, the direct analysis of the density yielded by periodic calculations is limited to the classical QTAIM. Otherwise, calculation of theoretical structure factors (see Chapter 1.2.4) and multipolar modelling must be performed.

1.2.4 Theoretical Structure Factors

The calculation of structure factors from a given structure model ($F_c(\vec{h})$) according to Eq. 1.4 is routinely done to improve the structure model in the least-square method (Eq. 1.7) or to calculate the R-value (Eq. 1.8). It is therefore also simple to obtain structure factors from theoretical calculations under pseudo-periodic conditions (from isolated-molecule calculations) or under fully periodic conditions (from periodic-boundary calculations). Lattice constant vector $\vec{r}$ and reciprocal lattice vector $\vec{h}$ are given arbitrarily (pseudo-periodic way) or are known (fully periodic way). Normally, thermal motion is not considered, so that the structure factors are static. [135]
To calculate structure factors in a pseudo-periodic way has the advantage that any molecule for which the crystal structure is not known or simple model compounds can be made accessible to a multipole modelling and subsequent analyses. For example, the Invariom formalism relies on the multipole modelling of the static theoretical structure factors of simple model compounds from pseudo-periodic calculations. [31, 32] This way, experimental geometry and multipole electron density of non-sufficient data sets can be improved if kappa values and multipole populations from multipole modelling on model compounds are transferred.
But if the crystal structure is known, it is more appropriate to improve the geometry and density of a non-sufficient data set by the multipole modelling of theoretical structure factors from a fully periodic calculation on the whole molecule because it is accounted for crystal effects in this way. Moreover, fully periodic structure factors yield best possible comparative topological results with respect

to the experiment. All structure factors calculated in this doctoral thesis are fully periodic static structure factors.

1.3 Constrained Wave-Function Fitting

The constrained wave-function fitting (CWF) approach [36–39] is a combination of theoretical and experimental methods. A wave function based on methods and basis sets as described above is fitted to experimental structure factors. The resulting wave function is referred to as experimental wave function. The electron density can be calculated from this experimental wave function according to Eq. 1.15. But also other functions, like experimental ELF or experimental ELI that can otherwise not be determined from the experiment due to fundamental reasons, become accessible this way.

The Lagrange function $L(\mathbf{c}, \boldsymbol{\epsilon}, \lambda)$ of Eq. 1.28 ($\mathbf{c}$ = molecular-orbital coefficients, $\boldsymbol{\epsilon}, \lambda$ = Lagrange multipliers) is minimized with respect to the energy $E(\mathbf{c}, \boldsymbol{\epsilon})$, and a term which depends on the difference of the observed and calculated structure factors controlled by the agreement statistic function $\chi^2(\mathbf{c})$ given in Eq. 1.29. A value of a Lagrange multiplier λ can be chosen to constrain the agreement statistic to reasonable values. A good value of λ is found if the weighted R-value $\mathrm{R}_W(\mathrm{F})$ is similar to the one obtained from a multipolar modelling of the same experimental structure factors. Δ is the desired error in the χ^2 term. N_r and N_p are the numbers of reflections and fitted parameters, respectively.

$$L(\mathbf{c}, \boldsymbol{\epsilon}, \lambda) = E(\mathbf{c}, \boldsymbol{\epsilon}) - \lambda[\chi^2(\mathbf{c}) - \Delta] \tag{1.28}$$

$$\chi^2 = \frac{1}{N_r - N_p} \sum_{\vec{h}}^{N_r} \frac{[F_c(\vec{h}) - F_o(\vec{h})]^2}{\sigma^2(\vec{h})} \tag{1.29}$$

If the minimum energy with respect to the experimental structure factors has been calculated, the wave function must be determined. This is done by an SCF calculation according to the Hartree-Fock (Eq. 1.19) or Kohn-Sham theory (Eq. 1.23).

Chapter 2

Methods to Analyse Electron Density

2.1 The Quantum Theory of Atoms in Molecules

2.1.1 Bond-Topological Properties

According to the Quantum Theory of Atoms in Molecules (QTAIM) by Bader, [23] the chemical structure of a molecule is determined by the topology of the electron density. A topological analysis is the search for the extrema of the electron density scalar field $\varrho(\vec{r})$. An extremum is referred to as critical point (cp). It occurs if the gradient-vector field of $\varrho(\vec{r})$ vanishes as Eq. 2.1 shows.

$$\nabla\varrho(\vec{r}_{cp}) = \begin{pmatrix} \frac{\partial\varrho}{\partial x} \\ \frac{\partial\varrho}{\partial y} \\ \frac{\partial\varrho}{\partial z} \end{pmatrix} = 0 \tag{2.1}$$

Extrema can be found at nuclear positions, at bonds, in rings and in cages. A mathematical classification of these different critical points is carried out by the interpretation of the diagonalised Hessian $D(\vec{r})$ of electron density as Eq. 2.2 shows.

$$D(\vec{r}) = \begin{pmatrix} \frac{\partial^2\varrho}{\partial x^2} & 0 & 0 \\ 0 & \frac{\partial^2\varrho}{\partial y^2} & 0 \\ 0 & 0 & \frac{\partial^2\varrho}{\partial z^2} \end{pmatrix} = \begin{pmatrix} \lambda_1 & 0 & 0 \\ 0 & \lambda_2 & 0 \\ 0 & 0 & \lambda_3 \end{pmatrix} \tag{2.2}$$

The diagonal elements of the Hessian are labelled with λ_i. A set of curvature parameters (ω, σ) that classify the critical points according to Table 2.1 can be deduced from λ_i. The rank ω is the number of non-zero diagonal elements that

Table 2.1: Classification of critical points according to their curvature parameters

type of critical point	λ_1	λ_2	λ_3	(ω, σ)
nuclear attractor (na)	-	-	-	(3,-3)
bond critical point (bcp)	-	-	+	(3,-1)
ring critical point (rcp)	-	+	+	(3,+1)
cage critical point (ccp)	+	+	+	(3,+3)

are three in any case. σ is the sum of the signs of λ_i. A nuclear attractor (na) is a local maximum in all three dimensions. A bond critical point (bcp) is a saddle point, a maximum in two dimensions but a minimum of the bond path, the path of maximum density between two nuclei constituting a chemical bond. A ring critical point (rcp) is a saddle point, too, a maximum in the direction perpendicular to the ring plane and a minimum in the two directions of the ring plane. A cage critical point is a local minimum in the density.

The Laplacian results from the application of the Laplace operator to the electron-density scalar field according to Eq. 2.3. Additionally, it is the trace of the diagonalised Hessian.

$$\nabla^2 \varrho(\vec{r}) = \frac{\partial^2 \varrho(\vec{r})}{\partial x^2} + \frac{\partial^2 \varrho(\vec{r})}{\partial y^2} + \frac{\partial^2 \varrho(\vec{r})}{\partial z^2} = \lambda_1 + \lambda_2 + \lambda_3 \tag{2.3}$$

A region of negative Laplacian values indicates a charge concentration. Isolated charge concentrations around an atom represent bonding or non-bonding effects and are referred to as valence shell charge concentrations (VSCCs). [136] Accordingly, valence shell charge depletions (VSCDs) are defined for isolated regions of positive Laplacian values. [136]

The ellipticity ϵ is another bond-topological parameter. It quantifies the deviation from a cylindrically symmetrical electron-density distribution of the bond axis at the bcp and is defined as the ratio of the two negative curvatures λ_1 and λ_2 of the Laplacian (Eq. 2.4).

$$\epsilon = \frac{\lambda_1}{\lambda_2} - 1 \tag{2.4}$$

For an ideally cylindrically symmetrical bond like the single bond in ethane or the triple bond in ethine, ϵ equals zero; for a 1.5-fold bond in benzene, ϵ equals 0.23 and for a double bond in ethane, ϵ equals 0.45. [137]

2.1.2 Atomic Properties

A molecule can be uniquely partitioned into its atoms with the help of the gradient-vector field of the electron density. All gradients end in one nuclear attractor and never cross so-called zero-flux surfaces (ZFSs), which Eq. 2.5 expresses. $\vec{n}$ is the normal vector of the ZFS.

$$\nabla\varrho(\vec{r}) \cdot \vec{n} = 0 \tag{2.5}$$

The ZFSs are the boundary surfaces between the atoms and therefore constitute a special atomic shape, which is referred to as the atomic basin Ω. An atom is thus defined as the entity of a nuclear attractor and a corresponding atomic basin. Atomic properties can be determined by an integration of a wanted property over all volume elements $d\tau$ of the basin Ω. The atomic volume is given in Eq. 2.6 and the atomic charge as difference of atomic number and atomic electron population is given in Eq. 2.7.

$$V(\Omega) = \int_{\Omega} d\tau \tag{2.6}$$

$$Q(\Omega) = Z - N(\Omega) = Z - \int_{\Omega} \varrho(\vec{r}) d\tau \tag{2.7}$$

It is common practice to cut the atomic properties at the isovalue 0.001 a.u. = $0.0067\,\mathrm{e\AA^{-3}}$ of the electron density to assure a reasonable comparison between experimental and theoretical data as theoretical basins from isolated-molecule calculations extend towards infinity.

2.2 The Source Function

Bader and Gatti showed that the electron density at any point $\vec{r}$ (called reference point) within a molecule consists of contributions from a source operating at all other points $\vec{r}\,'$. [57–59] Such a decomposition enables one to view the properties of the density from a new perspective and establishes a new tool to provide chemical information.

The electron density at the reference point $\vec{r}$ within an atomic basin Ω is given in Eq. 2.8 by the sum of two contributions: (i) the basin average of the electric potential at $\vec{r}$ exerted by the Laplacian of the density at any other point $\vec{r}\,'$ within the same atomic basin (first summand of Eq. 2.8) and (ii) the electric field at $\vec{r}$ owing to the gradient of the electron density at the zero-flux surface point $\vec{r}_S$

(second summand of Eq. 2.8).

$$\varrho(\vec{r}) = -\frac{1}{4\pi}\left[\int_{\Omega}\frac{\nabla^2\varrho(\vec{r}\,')}{|\vec{r}-\vec{r}\,'|}d\vec{r}\,' + \oint_{S_\Omega}\frac{\nabla\varrho(\vec{r}_S)}{|\vec{r}-\vec{r}_S|}dS(\vec{r}_S)\right] \tag{2.8}$$

The integrand of the first summand is called the local source $G(\vec{r},\vec{r}\,')$ of the atomic basin Ω (Eq. 2.9). There are as many local sources as there are atoms in the molecule, as a local source is defined for one atomic basin bounded by its zero-flux surface.

$$G(\vec{r},\vec{r}\,') = \frac{\nabla^2\varrho(\vec{r}\,')}{|\vec{r}-\vec{r}\,'|} \tag{2.9}$$

Eq. 2.8 holds for the atomic basin Ω as an open system. That means that the density at the reference point $\vec{r}$ is influenced by all atomic basins in the molecule. These contributions are expressed in the second summand, because the density at the zero-flux surface point $\vec{r}_S$ exerting an electric field at $\vec{r}$ is itself influenced by the neighbouring atomic basins according to the same equation. Therefore, one can expand the description from an open system with boundaries to a closed system with boundaries at infinity. All the contributions to the density at the reference point $\vec{r}$ can now be described as the sum over all local sources $G_i(\vec{r},\vec{r}\,')$ (Eq. 2.10).

$$\varrho(\vec{r}) = -\frac{1}{4\pi}\sum_{i}^{N_\Omega}\int_{\Omega}G_i(\vec{r},\vec{r}\,')d\vec{r}\,' = \sum_{i}^{N_\Omega}S_i(\vec{r},\Omega) \tag{2.10}$$

The function $S_i(\vec{r},\Omega)$ is called the source function. Eq. 2.10 states that the density at the reference point $\vec{r}$ is given by the contributions of source functions from each atom in the total system. The source function is thus a measure of the relative importance of an atom's contribution to the density at any chosen reference point. $S(\vec{r},\Omega)$ is often also called the integrated source function of the atom Ω because it is the integration of the local source $G(\vec{r},\vec{r}\,')$ of atom Ω over all points $\vec{r}\,'$ within the basin. $S(\vec{r},\Omega)$ is therefore only dependent on the reference point and the choice of the basin Ω. A single value of the same unit as the density ($e\text{Å}^{-3}$) can be given for each atomic basin by using the integrated source function.

Special points like bond- or ring-critical points are normally used as reference points to describe the contributions of atoms or functional groups to the specified bond or ring. But it is an open question if substituent effects or the bond character of the examined bond can be characterised by the source function. [138] For an ionic bond, the contributions to the bcp of the examined bond are generally more widely spread out over the whole molecule than for a covalent bond. [139–141] For

a weak interaction like a hydrogen bond, the contributions of the hydrogen atom to the bcp of the interaction can even be negative. [58]

2.3 The Electrostatic Potential

The electrostatic potential $V(\vec{r})$ (ESP) is one of the most important properties in the study of molecular reactivity and the analysis of molecular bonding and packing in crystals. For example, a biological recognition process can be explained by the principle of electrostatic complementarity. [142, 143]
The ESP is defined as the potential energy that is needed to move a positively charged test particle from infinity to the point $\vec{r}$ devided by the particle's charge. A negative ESP corresponds to an attraction of the test charge, a positive ESP corresponds to a repulsion. As Eq. 2.11 shows, the ESP is dependent on position $\vec{R}_i$ and atomic number Z_i of the cores in the vicinity of $\vec{r}$ and the electron density of all points $\vec{r}\,'$ of the system.

$$V(\vec{r}) = V_{nuc}(\vec{r}) + V_{elec}(\vec{r}) = \sum_{i=1}^{N} \frac{Z_i}{|\vec{R}_i - \vec{r}|} - \int \frac{\varrho(\vec{r}\,')}{|\vec{r}\,' - \vec{r}|} d\vec{r}\,' \tag{2.11}$$

The core contributions $V_{nuc}(\vec{r})$ can simply be computed, the electronic contributions $V_{elec}(\vec{r})$ have to be appoximated by the multipolar formalism to make the ESP accessible to the experimental electron density or the electron density from theoretical structure factors. [144, 145] The ESP originating from a pseudoatom is expanded in the same way as the density itself: $V_{elec}(\vec{r}) = V_{core}(\vec{r}) + V_{val}(\vec{r}) + \Delta V(\vec{r})$ (spherical core, spherical valence and aspherical deformation contributions), see Eq. 1.12. The three contributions to the ESP are given in Eq. 2.12, Eq. 2.13 and Eq. 2.14. For the meaning of the terms and symbols that are defined by the Hansen-Coppens multipolar formalism, see the corresponding Chapter 1.1.3.

$$V_{core}(\vec{r}) = \frac{Z}{|\vec{r} - \vec{R}|} - \int_0^\infty \frac{\varrho_{core}(\vec{r}\,')}{|\vec{r} - \vec{R} - \vec{r}\,'|} d\vec{r}\,' \tag{2.12}$$

$$V_{val}(\vec{r}) = - \int_0^\infty \frac{P_{val} \kappa\,'^3 \varrho_{val}(\kappa\,', \vec{r}\,')}{|\vec{r} - \vec{R} - \vec{r}\,'|} \tag{2.13}$$

$$\Delta V(\vec{r}) = -4\pi \sum_{lm} \frac{\kappa\,' P_{lm}}{2l+1} \left[\frac{1}{\kappa\,'^{l+1} |\vec{r} - \vec{R}|^{l+1}} \int_0^{\kappa\,'|\vec{r} - \vec{R}|} t^{l+1} R_l(t) dt + \right.$$
$$\left. \kappa\,'^{l} |\vec{r} - \vec{R}|^{l} \int_{\kappa\,'|\vec{r} - \vec{R}|}^\infty \frac{R_l(t)}{t^{l-1}} dt \right] d_{lm}(\Omega) \tag{2.14}$$

This description of the $V_{elec}(\vec{r})$ term of the ESP is used within the van der Waals surface of the molecule, where the electron density is high. Outside the van der Waals surface of the molecule, the contributions are small, as the density is typically smaller than 0.001 a.u. in this region. Therefore, a further approximation can be made in which only the distance from the centre of the molecule is important. These small contributions are calculated according to the Amsterdam Density Functional (ADF) method. [146]

2.4 Interaction Energies

In Chapter 1.2.3, it was described how interaction energies of two molecules or molecular fragments can be derived from isolated-molecule calculations. It is also possible to approximately calculate the interaction energy of two molecules, molecular fragments or atoms from the electron density. The total interaction energy E_{int} may be expressed (Eq. 2.15) as the sum of electrostatic, exchange-repulsion, dispersion and induction terms. [147]

$$E_{int} = E_{es} + E_{ex-rep} + E_{disp} + E_{ind} \tag{2.15}$$

The electrostatic term is usually the major contribution to the interaction energy. The exchange-repulsion terms arise from the anti-symmetrisation requirements of the Pauli principle, the dispersion terms from the induced charge distribution on different fragments. The induction terms originate from the interaction of the unperturbed electron density of one fragment with the induced charge distribution of another, and vice versa. The induction effects of the crystal lattice should normally already be included in the determined pseudoatom parameters and will not be further accounted for.

The exchange-repulsion and dispersion terms are calculated according to the method by Williams and Cox for light atoms (H, C, N, O) [148] and by Spackman for heavier atoms (Al-Cl) [149]. The main contribution, i.e. the electrostatic energy, is calculated according to the exact potential/multipole moment hybrid method (EPMM) after Volkov. [150] Therein, the calculation switches at critical distances from the calculation of the exact potential (EP) to a pseudoatom approximation using atomic multipolar moments (aMM) and finally to a pseudoatom approximation using molecular multipolar moments (mMM). The expression for the exact potential (Eq. 2.16) is similar to Eq. 2.11 of the electrostatic potential. In the case of the ESP, a molecule interacts with a test charge; in the case of

the EP, the two pseudoatom charge distributions $\varrho_a(\vec{r}_a)$ and $\varrho_b(\vec{r}_b)$ interact with each other. The EP is calculated by numerical integration over both pseudoatoms. Multipolar approximations aMM and mMM are used when the critical distances are reached that are given by the user.

$$E_{es}(EP) = \int_a \int_b \frac{\varrho_a(\vec{r}_a)\varrho_b(\vec{r}_b)}{|\vec{r}_a - \vec{r}_b|} d\vec{r}_a d\vec{r}_b \tag{2.16}$$

The electrostatic crystal binding energy of a molecule, i.e. the lattice energy, is calculated using the same methodology as for the interaction energies. All intermolecular interactions are calculated directly within the spherical approximation of a cell shell and summed up. The size of the cell shell can be varied until the lattice energy value converges. This depends on the size of the unit cell.

2.5 The Delocalization Index

The quantity $\delta(A, B)$ introduced by Bader [151] is called delocalization index and represents a measure of the number of electron pairs delocalised between the atoms A and B. Although it is defined for any two atoms A and B in the system that do not have to be in close vicinity, [152] it can be used as a tool to decide on the bond character of a bond between the atoms A and B. [153] For homopolar covalent bonds, $\delta(A, B)$ is identical to the formal bond order or very close to it. Polar bonds have a $\delta(A, B)$ smaller than the predicted bond order, because ionic contributions mix into the bond character. Ionic bonds have very small $\delta(A, B)$ values, but not zero, because some residual electron sharing persists due to small covalent contamination of a purely closed-shell form. Thus, the degree of ionic contributions to a covalent bond or covalent contributions to an ionic bond, respectively, can be quantified by $\delta(A, B)$.

2.6 Molecular Surfaces

2.6.1 Electron-Density Isosurfaces

The outer contour of an atom is usually defined as a surface constructed from the van der Waals radius of the atom. If other atoms approach they come into touch with this surface. So it is consequential to define a van der Waals envelope of a molecule as an electron-density (ED) isosurface in a distance to the atomic

cores that is in the magnitude of the atomic van der Waals radii. Bader defined the ED isosurface of 0.001 a.u.=0.0067 eÅ^{-3} as being this molecular van der Waals envelope. [22] It has become common practice to evaluate properties like the ESP on the 0.001 a.u. molecular surface to correlate them with reactivity or biological activity. [154, 155]
The 0.001 a.u.-molecular surfaces are meaningful if non-covalent interactions are to be considered. To get an idea of the individual impact of the atoms in the molecule to properties that guide the building of a covalent bond, a molecular surface that is closer to the covalence radii is used. The 0.5 eÅ^{-3}-ED isosurface is in a distance to the atom cores of light atoms that is in the magnitude of the covalence radii. [100, 156]
The zero Laplacian isosurface is another reactive surface of a molecule. It is defined by $\nabla^2\varrho = 0$. Valence-shell charge depletions (VSCDs) can be found as holes in the isosurface. They represent electrophilic centres of the molecule. [157]

2.6.2 Hirshfeld Surfaces

Hirshfeld surfaces were introduced by Spackman as a new definition of a molecule in a crystal. [158] They are based on Hirshfeld's stockholder partitioning concept. [159] A molecular weight function $w(\vec{r})$ is introduced according to Eq. 2.17 that describes the contribution of the molecular density to the total crystal density at point $\vec{r}$. $\varrho_A(\vec{r})$ is a spherically-averaged atomic electron density centred on nucleus A. The promolecule and procrystal densities are sums over the atoms belonging to the molecule and to the crystal, respectively.

$$w(\vec{r}) = \frac{\sum_{A_{mol}} \varrho_A(\vec{r})}{\sum_{A_{cryst}} \varrho_A(\vec{r})} = \frac{\varrho_{promolecule}(\vec{r})}{\varrho_{procrystal}(\vec{r})} \tag{2.17}$$

A molecule is defined as region of $w(\vec{r}) \geq 0.5$, i.e. the region in which the contribution of the molecule to the total crystal density exceeds all the contributions from all neighbouring molecules. The Hirshfeld surface is the isosurface of $w(\vec{r}) = 0.5$. The Hirshfeld partitioning is not space filling as there are regions in the crystal that are not made up by the density of one molecule by more than 50 %.
Figure 2.1 exemplifies the Hirshfeld partitioning on a one-dimensional atomic chain. The atomic electron densities of three atoms and the total electron density of this system (pink curve) are given. The positions of the nuclei correspond to the maxima of the ED. The region of atom 2 as defined by the Hirshfeld partitioning is bounded by the intersections of the ED curves of atom 2 (blue curve) with the

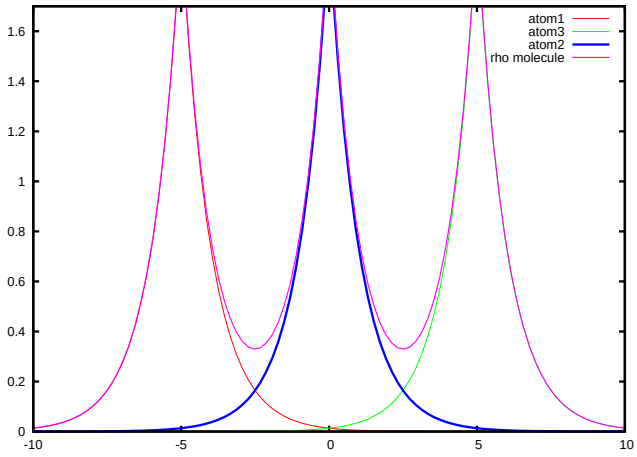

Figure 2.1: Illustration of the Hirshfeld partitioning for a one-dimensional chain of atoms; x-axis: distance in Å, y-axis: ED in $e\text{Å}^{-3}$

ones of its neighbours (red and green curves). Within these intersections, atom 2 contributes more than 50 % to the total density of the system.

Chapter 3

Alternatives to Electron Density: ELF and ELI

3.1 The Electron Localization Function (ELF)

The family of the ELF and ELI functions is an alternative method to analyse chemical bonding beneath ED or wave-function-based methods. The wave-function-based methods that use molecular orbitals (MO) or natural bond orbitals (NBO) to describe chemical bonding have the disadvantage that MO and NBO are not physically observable and that bonds cannot be described as localised and real-space phenomena. ED and ELF/ELI methods describe bonds in a localised way and are real-space representations. But ELF and ELI are generally not physically observable in contrast to ED.

Figure 3.1 schematically shows the behaviour of the ED, ELF and ELI functions in the case of a two-electron-two-centre single bond. The atomic nuclei are located at the positions +10 and -10 on the abscissa, the bond-critical point in the ED or bond attractor in the ELF/ELI is located at the position 0. In terms of ED, the function has a minimum at the position 0 and huge maxima at the positions of the nuclei. It is a disadvantage of the ED that the smallest effects are the most interesting ones. In the ELF/ELI description, there is a maximum at the position of the bond that is even more pronounced for the ELI than for the ELF, which is an advantage of the ELI over the ELF. For a real bond that can be polarised, the positions of the bcp in terms of the ED and the maxima in terms of ELF/ELI do not necessarily coincide.

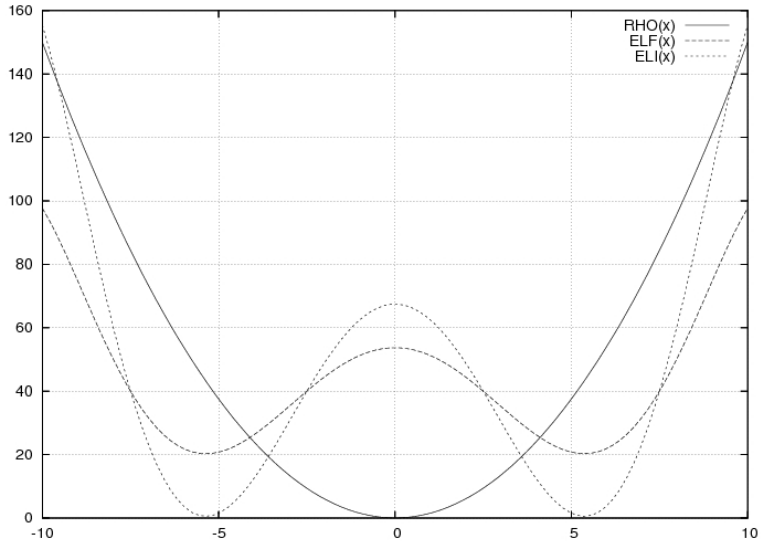

Figure 3.1: Idealised curves of the ED (solid), ELF (dashed) and ELI (dotted) for a homopolar 2e-2c single bond

Nuclei at +10/-10 on the abscissa, bcp/attractors at 0 on the abscissa, arbitrary scale

The ELF tests if there is an electron pair in the neighbourhood of another, i.e. it calculates the electron-pair probability for the mutual perturbation of two electron pairs within the radius R. Figure 3.2 exemplifies this gedanken experiment. An electron pair is situated at the point $\vec{r} = (x, y, z)$. A sphere with radius R is spanned for which $\vec{r}$ is the centre. The probability to find another electron pair inside this sphere is calculated. The electron-pair probability for this event is identical to the probability to find an electron inside a sphere with radius R in which there already is another electron with the same spin. Thus, the calculation is reduced to the calculation of the so-called same-spin probability $W(\vec{r}, R)$. The same-spin probability is based on the Pauli principle and thus $W(\vec{r}, R)$ decreases if the radius R decreases. In summary, one can state: Where electron pairs mutually perturb each other, $W(\vec{r}, R)$ is large; where electron pairs do not meet, $W(\vec{r}, R)$ is small.

The ELF is defined by $W(\vec{r}, R)$, but a Lorentzian-type scaling is applied yielding Eq. 3.1 with c as a constant for scaling. Due to this scaling, ELF values always lie between 0 and 1. Where electron pairs are localised, i.e. where $W(\vec{r}, R)$ is small, ELF is close to 1; in regions between electron pairs where mutual perturbation is

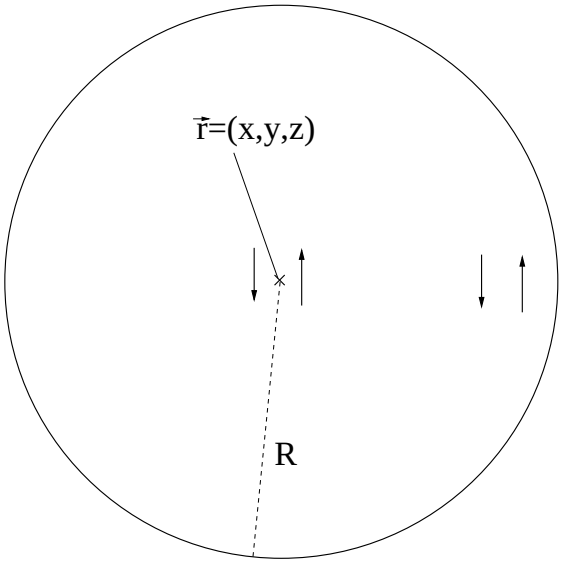

Figure 3.2: Gedanken experiment to derive the ELF

Probability to find an electron pair inside a sphere with the radius R in which another electron pair is located at $\vec{r}$

large, i.e. where $W(\vec{r}, R)$ is large, ELF is close to 0.

$$ELF = \frac{1}{1 + (c \cdot W(\vec{r}, R))^2} \tag{3.1}$$

In the original definition from Becke and Edgecombe, [48] $W(\vec{r}, R)$ is given as the spherically averaged conditional same-spin probability density from the quadratic term of a Taylor expansion (Eq. 3.2).

$$W(\vec{r}, R) = \frac{1}{3}\left[\sum_{i}^{\sigma} |\nabla \Psi_i(\vec{r})| - \frac{1}{4}\frac{|\nabla \varrho_\sigma(\vec{r})|^2}{\varrho_\sigma(\vec{r})}\right] \cdot R^2 = \frac{1}{3}\left[D(\vec{r})\right] \cdot R^2 \tag{3.2}$$

$\varrho_\sigma(\vec{r})$ is the σ-spin density which is not accessible via experiment but must also be calculated from the wave function: $\varrho_\sigma(\vec{r}) = \sum_i^\sigma |\Psi_i|^2$. The term $D(\vec{r})$ is directly proportional to $W(\vec{r}, R)$ and is used to define the ELF, see Eq. 3.3.

$$ELF = \frac{1}{1 + [\frac{D(\vec{r})}{D_h(\vec{r})}]^2} \tag{3.3}$$

The reciprocal of $D_h(\vec{r})$ is the scaling constant c of Eq. 3.1. It is proportional to the spherically averaged conditional same-spin probability density of the imagined homogeneous electron gas of the same substance, see Eq. 3.4. This scaling to a

reference system makes the ELF a relative property without dimension. Therefore, ELF values from different substances cannot be compared with each other.

$$D_h(\vec{r}) = \frac{3}{5}(6\pi^2)^{\frac{3}{5}} \cdot \varrho_\sigma^{5/3}(\vec{r}) \tag{3.4}$$

If ELF = 0.5, the effect of the Pauli repulsion at $\vec{r}$ is the same as in the homogeneous electron gas of the same compound. But no other analogy with physical properties of the homogenous electron gas is possible. If ELF >0.5, the electron pair at $\vec{r}$ is more localised than in the homogeneous electron gas. ELF values smaller than 0.5 occasionally occur, too, but their interpretation is difficult.

As Eq. 3.2 shows, the ELF can only be calculated from the wave function, i.e. from wave function-based ab-initio methods. Savin et al. introduced a variant of the ELF that can be deduced from density-functional theory. [160] They used kinetic-energy densities that are defined within the framework of the DFT. The Pauli kinetic-energy density $t_P(\vec{r})$ is the kinetic energy of the electrons that is due to the redistribution of the electrons caused by the Pauli principle. The Pauli kinetic-energy density $t_h(\vec{r})$ refers to the homogeneous electron gas of the same substance. With these properties, the formal kernel of the ELF can be mimicked to give the ELF_{Savin} according to Eq. 3.5. This formula indeed produces identical ELF values compared to the original definition.

$$ELF_{Savin} = \frac{1}{1 + [\frac{t_P(\vec{r})}{t_h(\vec{r})}]^2} \tag{3.5}$$

Kinetic-energy densities are not accessible by experiment either. So Tsirelson and Stash developed a set of approximations to calculate the kinetic-energy densities from experimental densities. [54] A method that provides more accurate results is the constrained wave-function-fitting approach described in Chapter 1.3 which can be used to derive the ELF from an experimental wave function. [55] The topology of the ELF derived this way is very similar to the one from theoretical calculations and gives reliable quantitative results. [56, 161]

3.2 The Electron Localizability Indicator (ELI)

The ELI is based on the same gedanken experiment as described for the ELF (see Figure 3.2) as the idea is closely related to the ELF. However, the physical definition is different. In contrast to the ELF, which is based on abitrary scaling to

an external reference system, and therefore lacks the quality of being a measure for Pauli repulsion or electron-pair localisation, the ELI is not scaled so that the absolute values are interpretable as a direct measure of electron localisation and Pauli repulsion. Therefore, absolute ELI values are comparable between different substances. The ELF is a function of the electron-pair density, whereas the ELI is a functional of the electron-pair density. Thus, the ELI provides in principle more information in its topology than the ELF, which is revealed only for correlated wave functions (CI methods). At the HF or B3LYP level, this advantage of the ELI is cancelled owing to the SCF approximation, and only the advantage of directly interpretable absolute values remains. At the levels of theory used in this doctoral thesis, the ELI is directly proportional to the ELF and the topology is identical.

Kohout introduced the ELI in 2004. [51–53] It is based on ω-restricted space partitioning: The space is divided into i mutually exclusive space-filling regions Ω_i that must fulfil the condition that a probe quantity integrated over each region Ω_i always yields the same value ω. Furthermore, the regions Ω_i must be compact, i.e. the volume that is needed to fulfil the condition of the ω-restriction must be enclosed by the smallest possible surface area to ensure the locality of the examined effects. The choice of the value ω and the initial region fixes the complete partitioning. Then, the analysis of how the regions Ω_i enclosing the same amount ω of the probe quantity are arranged over space gives a certain spatial density of Ω_i caused by the distribution of the probe quantity in the molecule.

The ω-restriction operative in the definition of the ELI ($=\Upsilon$) is that each region Ω_i encloses the same fraction ω of an electron pair, i.e. the probability to find an electron pair inside Ω_i is the same for all regions. The ELI value is proportional to the charge found in the respective region, i.e. it is proportional to the charge that is needed to form an electron pair. To demonstrate this, a same-spin electron pair ($\sigma\sigma$) is chosen that couples to a triplet state (t). (Compare the gedanken experiment described above to yield the ELF from the same-spin probability: A same-spin electron-electron interaction is sufficient to describe the interaction of two electron pairs.) The fixed fraction ω of this same-spin electron pair is denoted as $D^{\sigma\sigma}$. The ELI yielded from this ansatz is denoted as ELI-D(t)=$\Upsilon_D^{\sigma(t)}$. [162, 163] The property ELI-D(t) is used throughout this doctoral thesis.

The calculation of the σ-spin charge Q_i^σ in each region Ω_i centred around the position $\vec{r}_i$ yields the values of $\Upsilon_D^{\sigma(t)}(\vec{r}_i)$. Q_i^σ is given by the same-spin density

$\varrho_\sigma(\vec{r}_i)$ (see Eq. 3.2) multiplied by the volume V_i of the region Ω_i: $Q_i^\sigma = \varrho_\sigma(\vec{r}_i) \cdot V_i$. In turn, the volume can be approximately calculated from the same-spin electron pair fraction $D^{\sigma\sigma}$ and the so-called Fermi whole curvature $g_\sigma(\vec{r}_i)$ according to Eq. 3.6.

$$V_i = \left[12 \frac{D^{\sigma\sigma}}{g_\sigma(\vec{r}_i)}\right]^{3/8} \tag{3.6}$$

Then, the σ-spin charge Q_i^σ can be written as given in Eq. 3.7.

$$Q_i^\sigma = \varrho_\sigma(\vec{r}_i) \cdot V_i = (D^{\sigma\sigma})^{3/8} \left[12 \frac{\varrho_\sigma^{8/3}(\vec{r}_i)}{g_\sigma(\vec{r}_i)}\right]^{3/8} \tag{3.7}$$

The charge distribution is dependent on the fixed same-spin pair population $D^{\sigma\sigma}$ which is a constant over all regions of the ω-restricted partitioning. ELI-D(t) is the $D^{\sigma\sigma}$-independent part of the expression for Q_i^σ (Eq. 3.7) so that $Q_i^\sigma = (D^{\sigma\sigma})^{3/8} \cdot \Upsilon_D^{\sigma(t)}$. Hence, ELI-D(t) is defined as Eq. 3.8 shows.

$$\Upsilon_D^{\sigma(t)}(\vec{r}_i) = \varrho_\sigma(\vec{r}_i) \cdot \left[\frac{12}{g_\sigma(\vec{r}_i)}\right]^{3/8} \tag{3.8}$$

As long as the Fermi-hole curvature $g_\sigma(\vec{r}_i)$ is not approximated according to an SCF ansatz, it is a sum over all occupied σ-spin orbitals and thus electron-correlation effects can be accounted for. But for SCF calculations like HF and B3LYP, $g_\sigma(\vec{r}_i)$ reduces to the term given in Eq. 3.9.

$$g_\sigma(\vec{r}) = \varrho_\sigma \sum_i^\sigma |\nabla \Psi_i(\vec{r})|^2 - \frac{1}{4}(\nabla \varrho_\sigma(\vec{r}))^2 \tag{3.9}$$

At these levels, the ELI formula for the same-spin electron pairs resembles the kernel of the ELF formula (compare Eq. 3.2), but without any reference to the homogeneous electron gas.

There is no approximation to the ELI so far to make it deducible from experimental electron density. Moreover, the formula of the ELI was hitherto also not accessible to the constrained wave function fitting (CWF). In cooperation with Prof. Jayatilaka, the ELI formula was implemented into the programme TONTO (see Chapter 11.1.2) to make it accessible to the CWF approach to be used within this doctoral thesis. Thus, the ELI is now accessible from the experiment for the first time.

3.3 Analysis of ELF and ELI

The ELF and the ELI are scalar fields that can be topologically analysed. The mathematical method to partition the space into ELF/ELI basins bounded by zero-flux surfaces is identical to the partitioning of the ED within the QTAIM methodology as described in chapter 2.1. But the difference is the number and position of the attractors. Within the ELF/ELI topology, there is an attractor with a corresponding basin for each atomic shell, each bond, each multi-centre interaction and each non-bonding effect like lone pairs. Therefore, the volume demand and the electron population of bonds and lone pairs can be determined. The volume can be calculated by an integration over the basin according to Eq. 2.6, and the population can be calculated by an integration of the ED within the ELF/ELI basin similar to Eq. 2.7. Even a combination of the ELF/ELI bond basins and the ED atomic basins is possible as a way to find out which absolute or relative amount of the population or volume of a bond belongs to either Bader atoms of the bond. These calculations are performed by an intersection of the ELF/ELI and ED basins and an integration of the split basins generated this way. The descriptors from this analysis are called Jansen indices. [164]

The nomenclature of the ELF/ELI basins is governed by the differentiation between core and valence electrons. There is a core basin for each atomic shell according to the main quantum number. The descriptor for a core basin of atom A would be C(A). The populations and volumes of the core basins should not change from the free atom to the atom in the molecule and are therefore applicable to test the accuracy of the calculations. It must be noted that the integrated electron populations differ slightly from the integers expected from the aufbau principle due to atomic orbital overlap in the basins. [165, 166]

The valence electrons can be attributed to either bonding or non-bonding effects. A valence basin of a two-centre bond between atoms A and B is denoted as V_2(A,B), the index marks the synaptic order of the bond. A two-centre bond is called a disynaptic bond, as the bond basin shares two common zero-flux surfaces with the outer core basins of the atoms A and B. With the help of the synaptic-order concept, [167, 168] different types of multi-centre bonding can be discerned by counting with how many adjacent atoms the bond basin shares common zero-flux surfaces. Lone pairs are monosynaptic, as they share only one common zero-flux surface with the corresponding atom. Therefore, a lone pair of atom A is denoted V_1(A). Due to the fact that there is no core basin for hydrogen atoms, as there

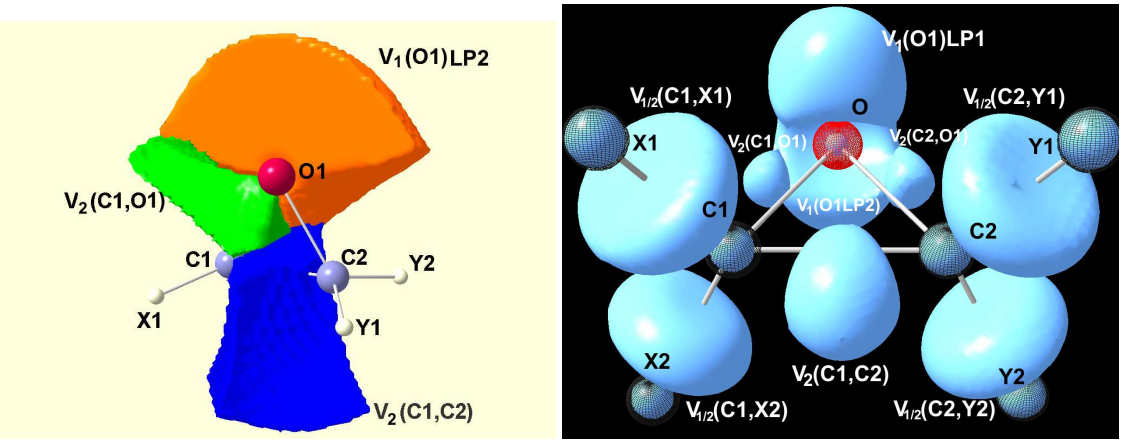

(a) Basin representation: outer contour of basins cut at ϱ=0.001 eÅ^{-3}, disynaptic valence basin of the C–C bond (V_2(C,C)) in blue, disynaptic valence basin of one C–O bond (V_2(C,O)) in green, monosynaptic valence basin (V_1(O)) of the backmost oxygen lone pair (LP2) in orange, other basins not shown because the partitioning is space filling

(b) Localization-domain representation: isosurface plot of the ELI-D, localisation domains representing bond basins (V_2(A,B)) are irreducible, localisation domain of oxygen lone pairs is reducible (it encloses space belonging to the two lone-pair basins V_1(O)LP1 and V_1(O)LP2)

Figure 3.3: Two different representations of the topology of the ELF/ELI of a substituted epoxide molecule

is only one valence electron, bonds to hydrogen atoms are monosynaptic, too. They are referred to as protonated monosynaptic valence basins and denoted as V_1(A,H).

Saddle points in the ELF/ELI topology are commonly not interpreted and discussed. One reason is that there are many more saddle points than in the ED topology and their distribution can become very confusing. Moreover, the comparison of absolute values is not suitable in the ELF topology, it becomes reasonable only when the ELI is considered. Consequently, there are very few examples of a full topological analysis of the ELI including saddle points until now. [169] Krokidis et al. applied the catastrophe theory to the ELF and stated that a change of number and position of saddle points and attractors in the topology is an indicator for a chemical process. [170]

A graphical representation of the ELF or ELI of a molecule normally cannot consist of the display of basins because they are space filling and conceal the rest of the molecule. An example only displaying a few basins of the given molecule is shown in Figure 3.3 (a). A widely used alternative to the basin representation is the use of

isosurfaces of the ELF or ELI function. At a certain isovalue, the isosurface builds separated domains enclosing the attractors. These domains are called localisation domains. An example is given in Figure 3.3 (b). Localization domains are irreducible if they enclose only one attractor and therefore represent one basin. If they enclose more than one attractor, they are called reducible localisation domains and can be split into irreducible ones by increasing the isovalue. An isosurface representation of localisation domains gives an impression where the vast amount of electron-pair localisation takes place. For the epoxide molecule in the given examples, the total C–O bond basin (V_2(C,O), coloured green) completely encloses the internuclear axis, whereas the localisation-domain representation shows that the electrons are mainly localised outside the internuclear bond axis, indicating a bent bond. Characteristic localisation-domain shapes for different bond types can be distinguished, [50] for example the cap-like shape of the reducible localisation domain of the oxygen lone pairs as shown in Figure 3.3 (b). Normally, the nomenclature of the corresponding basin is also used for irreducible localisation domains or attractors, respectively.

Chapter 4

Bonding Theories of X–O–X Linkages (X = C, Si)

4.1 Siloxanes Si–O–Si

The two most important questions concerning the siloxane linkage (Si–O–Si) are about the bond character of the Si–O bonds and about the basicity of the oxygen atom. It is generally accepted that the Si–O bond is predominantly ionic, but the question is discussed to which extent covalent contributions mix into the bond character and how these contributions depend on the variation of the Si–O–Si bond angle. The material properties of compounds incorporating siloxane linkages are generally governed by the weak basicity and the inability to form hydrogen bonds as acceptor group. But the question remains if the basicity can be increased significantly by decreasing the Si–O–Si bond angle to values usually adopted by ethers, so that compounds with rather different material properties can be synthesised. Hence, it is examined in this doctoral thesis if and how the reactivity of siloxanes can be tuned by variation of the Si–O–Si bond angle.

It is known that the range of Si–O–Si angles spanned by open-chain siloxane compounds is unusually large (from 130 ° to about 180 °). To examine the geometries of molecular siloxanes in general, the Cambridge Structural Database (CSD, [171]) was searched. The first search (Figures 4.1 (a) and 4.1 (b)) gave all compounds containing the fragment Si–O–Si. There are 1191 entried including 4943 Si–O–Si fragments, i.e. the majority of the 1191 molecules found comprises several siloxane fragments. Figure 4.1 (a) shows that indeed the vast majority of all compounds contains Si–O–Si angles between 130 ° and 180 ° with a maximum at 150 °. There

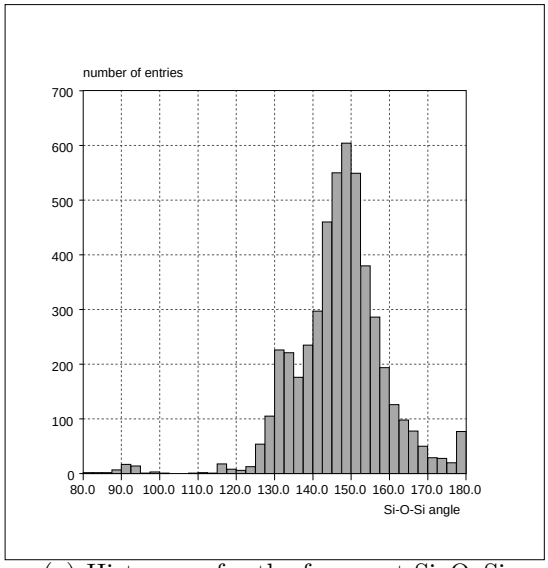

(a) Histogram for the fragment Si–O–Si

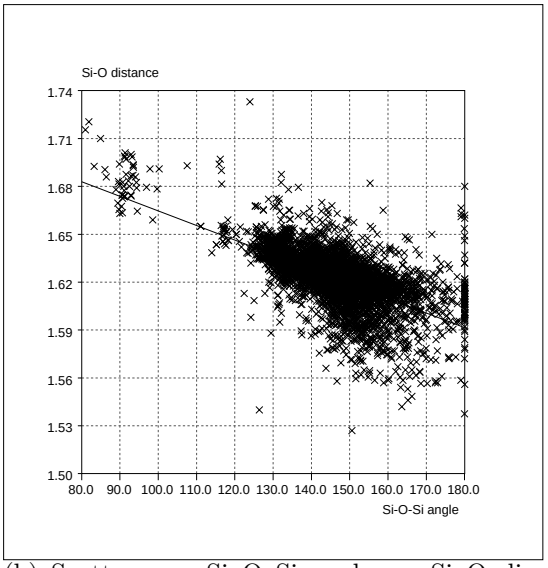

(b) Scattergram Si–O–Si angle vs. Si–O distance for the fragment Si–O–Si

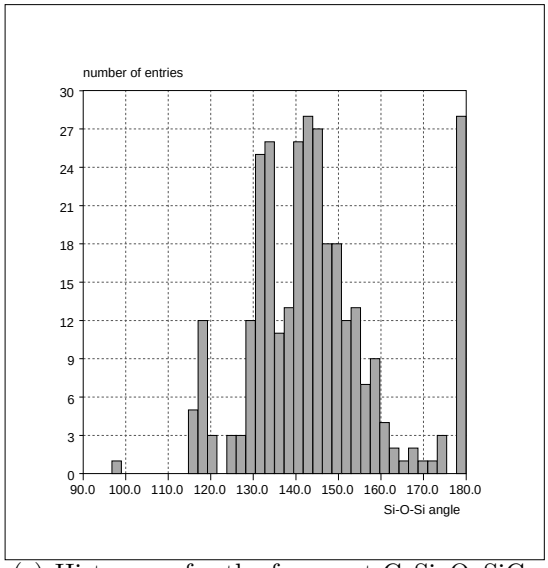

(c) Histogram for the fragment $C_3Si–O–SiC_3$

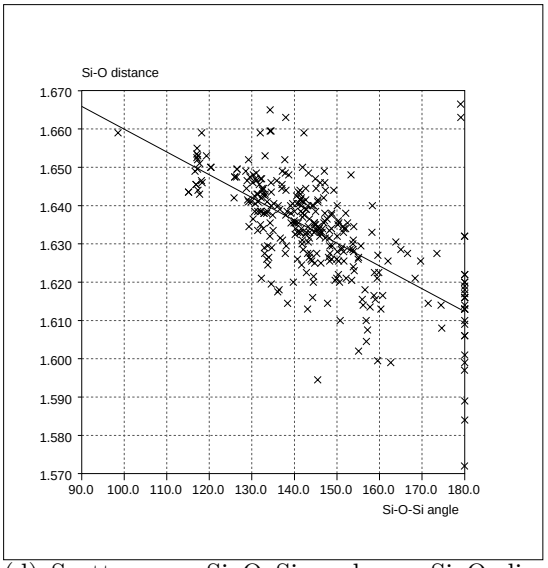

(d) Scattergram Si–O–Si angle vs. Si–O distance for the fragment $C_3Si–O–SiC_3$

Figure 4.1: Histograms and scattergrams for Si–O–Si and $C_3Si–O–SiC_3$ fragments in the CSD

are only very few examples (39 of 1191 compounds) that have Si–O–Si angles between 115 ° and 125 ° as siloxanol (**1**) and trisilo (**2**) have. (The structure of cpd. **1** is not yet included in the CSD because this compound was synthesised by Dipl.-Chem. Maxie F. Hesse for the first time for this study (see Chapter 5.1.1). For the structure determination of cpd. **2**, see Ref. [76, 77].) All these 39 compounds have in common that the siloxane linkage is forced to adopt this small angle by being incorporated into a five- or six-membered ring structure. Furthermore, there are 30 siloxane compounds in the CSD with Si–O–Si angles between 85 ° and 100 ° in which the siloxane linkage is incorporated into a three- or four-membered ring structures. As it was not possible to get single-crystals of one of these compounds for experimental electron-density determination, model calculations on three-membered Si–O–Si rings were performed.

Only three of 1191 compounds in the CSD contain a siloxane linkage that is an acceptor for hydrogen bonding. These three exceptional cases exhibit strained Si–O–Si linkages incorporated into five- or six-membered rings, respectively: 116.2 ° [172], 133.0 ° [173] and 134.4 ° [174]. Cpd. **1** with Si–O–Si = 116.4 ° is the fourth example. These four compounds have in common that they belong to the compound class of siloxanols, which means they possess a silanol group (Si–O–H) in addition to the siloxane group (Si–O–Si). The silanol group acts as the hydrogen-bond donor and the siloxane group as the hydrogen-bond acceptor. This is an exceptional case because there are 79 siloxanols in the CSD, of which only the three cases mentioned above exhibit a silanol-siloxane hydrogen bond. In the other 76 compounds, the silanol group acts as both hydrogen-bond donor and acceptor, because the basicity of the silanol oxygen atom is generally much higher than the basicity of the siloxane oxygen atom. Only if the siloxane linkage is strained, it can compete with the silanol group as hydrogen-bond acceptor. The increase of basicity of the siloxane oxygen atom upon decrease of the Si–O–Si angle is examined in further detail in Chapter 6.

Figure 4.1 (b) shows the correlation between the Si–O bond distance (average value over both Si–O bonds in the siloxane linkage Si–O–Si) and the Si–O–Si angle. The trend is obvious: The bond lengths increase if the bond angles decrease. Both ring and open-chain structures fulfil this relationship. The electronic details of this relation are also studied in Chapter 6.

Shklover et al. searched the CSD for compounds containing a C_3Si-O-SiC_3 fragment in 1991. [175] This search was repeated here (246 entries including 314 fragments) and the results are shown in Figures 4.1 (c) and 4.1 (d) as a subset of the entries

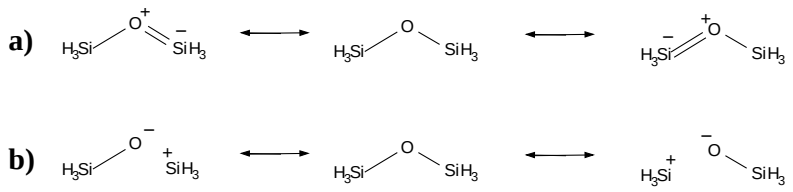

Figure 4.2: Lewis-formula representations discussed for the siloxane linkage in $H_3SiOSiH_3$

a) Obsolete back-bonding model, b) Ionic bond model

found for the fragment Si–O–Si (see above). Again, there are only a few strained siloxanes (one three-membered ring, [176] 23 five- or six-membered rings) and the distribution of angles has its maximum at about 145 °. But here it is obvious that there are only a few entries between 160 ° and 180 ° yet a lot of entries at exactly 180 °. A chemically symmetrical substitution pattern does not necessarily cause linearity with an inversion centre at the oxygen position. Shklover et al. stated that the accumulation of linear Si–O–Si fragments can be related to disorder of the oxygen atom that in fact occupies two equivalent positions above and below the linear Si–O–Si axis. They proposed a correction method based on the mean-square displacement amplitudes. [175] Therefore, the position of the oxygen atom in hexaphe (**4**) deserves closer attention. Figure 4.1 (d) again shows the linear regression between Si–O distance and Si–O–Si angle.

A historic explanation for the large Si–O–Si angles and the low basicity still found in some textbooks involves the obsolete back-bonding models in Figure 4.2 a) of the type p(O)→ d(Si) or more recently of the type n(O)→ σ*(Si–X). However, both back-bonding models have now been discarded in favour of the ionic bond model in Figure 4.2 b), which attributes the large Si–O–Si angles to the electronegativity difference of the elements. [71] But given that the ionic bond model is operative, the low basicity is counterintuitive to the high electron-density accumulation and the negative charge situated at the oxygen atom, the two properties that are usually associated with a good acceptor for hydrogen bonding. [177] This aspect deserves closer attention.

Previously, several relationships between the Si–O bond length, the Si–O–Si angle, Si and O Mulliken charges and the degree of Si–O bond ionicity have already been proposed. [63, 71, 72, 178] It has even been suggested that the Si–O–Si angles can be used as a direct measure of the Si–O bond character because an increase of the angle leads to greater charges at the silicon and oxygen atoms, which increases the

Si–O bond ionicity. [62] These relationships will be further analysed with newest methods in ED and ELF/ELI analyses in this doctoral thesis.

4.2 Epoxides C–O–C

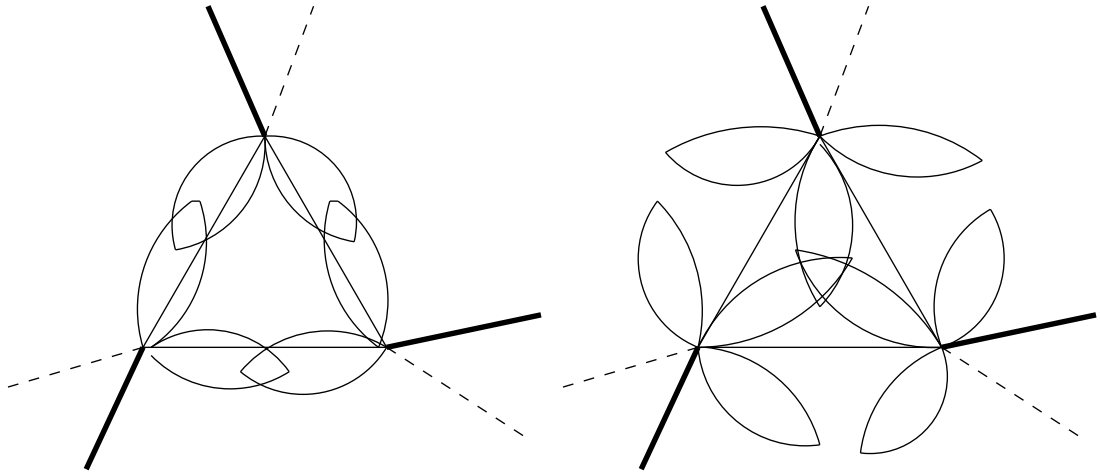

(a) Förster-Coulson-Moffitt model (b) Walsh model

Figure 4.3: Molecular-orbital models for cyclopropane

Interpretation in terms of valence-bond theory suggests that both models resemble atomic sp^2-type hybridisation states with additional p-orbitals perpendicular to the ring plane. This allows π-interactions with suitable substituents.

It is another goal of this doctoral thesis to find a way to adequately describe the strained bond character of the epoxide three-membered ring by ED and ELF/ELI methods, and how this special bonding situation influences the reactivity of the epoxides. This is especially important as moc-epoxide (**8**) and niphe-epoxide (**9**) serve as model compounds in drug design, and the mode of action regarding the recognition and inhibition process with the enzyme is not sufficiently understood. The geometric arrangement of the bonds owing to mechanical forces within a ball-and-stick model suggests that the bonds must bend outwards to master the high strain (so-called banana bonds, [179]). Similar considerations apply for molecular-orbital (MO) and valence-bond (VB) theories, respectively: A non-bent bond scenario is not possible because overlap of ordinary atomic hybrid orbitals can only produce 90 ° (pure p character) and not 60 ° as would be necessary for a non-bent bond description. Therefore, ordinary hybridisation states, e.g. sp^3 or sp^2, are

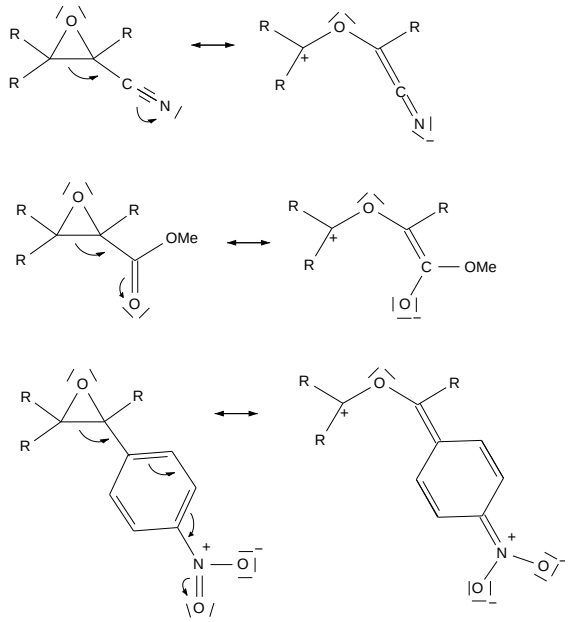

Figure 4.4: Resonance formulae for the epoxide ring substituted with a cyano, methyl ester or nitro-phenyl substituent

modified with increased or decreased s-orbital character in order to accommodate a particular molecular geometry. Corresponding MO models [1] were developed for cyclopropane, but can also be considered for epoxide. [85, 86, 180]

The Förster-Coulson-Moffitt model [181–183] makes use of hybrid orbitals with a relation between s- and p-character similar to sp^2 hybridisation. This leads to an orbital overlapping outside the direct bond axis forming three σ-type bonds, which is depicted in Figure 4.3 (a). An alternative model is the Walsh model, [184, 185] in which a stable central three-centre bond is formed from inward-directed sp^2 atomic orbitals. Additionally, two weak peripheral three-center bonds are formed from the tangential in-plane p-π orbitals of the CH_2 fragments. The complete Walsh scenario is shown in Figure 4.3 (b). The Walsh model does not correspond to the ground state of cyclopropane/epoxide so that the bent bond description of the Förster-Coulson-Moffitt model is the commonly considered one. [180]

The Förster-Coulson-Moffitt model suggests that most electron density is accumulated outside the direct bond axis, and there is no accumulation in the centre of

[1] The discussed models are referred to as MO models in the literature, but they are commonly interpreted in terms of a VB description involving atomic hybridisation states to explain chemical reactivity.

the ring. In contrast, the Walsh model suggests that most electron density is accumulated in the centre of the ring, but there should also be delocalised electrons outside the ring. Experimentally, bent bonds according to the Förster-Coulson-Moffitt model could be detected by several ED analyses of cyclopropane. [186–189] For epoxide, so far published ED results are ambiguous: Difference density maps show maxima within and outside the ring, but not in the centre. [190–192] It is therefore the aim of this doctoral thesis to clarify the description of the epoxide ring.

The involvement of sp^2-type orbitals in the epoxide ring instead of sp^3 like in a normal single bond suggests that the bonds are not saturated and can interact with π-electron systems. Evidence by various methods (UV spectroscopy, heat of combustion, MO calculations) has been found for such conjugation of the epoxide ring. [85, 193, 194] The epoxide ring preferably exhibits conjugation with electron-donating groups because the epoxide ring itself can act as the electron-withdrawing group. [194] However, cpds. **8** to **10** are substituted with electron-withdrawing groups because this is a preferable situation for the underlying drug design purposes, so that the epoxide ring must act as the electron-donating group. The resonance formulae that show this potential conjugation are given in Figure 4.4.

It is an open question to which extent this electron-withdrawing character of the substituents is reflected in the electronic properties of the epoxide ring. According to Figure 4.4, the C–C bond should widen and the ED value at the bcp of this bond should decrease if the C–C bond vanishes in the resonance formulae. Moreover, the ED value of the bcp of the bond to the substituent should increase as partial double-bond character is suggested by Figure 4.4.

Part II

The Siloxane Linkage Si–O–Si

Chapter 5

Experimental and Computational Details

5.1 Experimental Details

5.1.1 Synthesis, Crystallisation and Measurement

Compounds **1** to **4** (see Figure 1) were synthesised or purchased from Dipl.-Chem. Maxie F. Hesse and Prof. Dr. Jens Beckmann, Freie Universität Berlin. 5-Dimethylhydroxysilyl-1,3-dihydro-1,1,3,3-tetramethyl-2,1,3-benzoxadisilole (siloxanol (**1**)) was prepared by the catalytic oxidation of 1,2,3-tris(dimethylsilyl)benzene using Pearlman's catalyst ($C/Pd(OH)_2$), initially giving rise to the formation of the intermediate 1,2,3-tris(hydroxydimethylsilyl)benzene, which spontaneously underwent self-condensation (for details see [56] and [195]). 3,7-Dihydro-1,1,3,3,5,5,7,7-octamethyl-1,5-dihydro-benzo[1,2-c:4,5-c']bis[1,2,3]oxadisilole (trisilo, (**2**)) was synthesised by the silylation of hexabromobenzene with dimethylchlorosilane and magnesium in tetrahydrofurane. [196] Pentaphenyldisiloxane (pentaphe (**3**)) was obtained by the reaction of triphenylsilanole with diphenylchlorosilane and triethylamine. [78] Hexaphenyldisiloxane (hexaphe (**4**)) was purchased from the company TCI Europe as a crystalline powder. It can generally be synthesised through the reaction of sodium triphenylsilanolate with triphenylchlorosilane. [197]

Crystals from cpds. **1** to **4** were obtained by dissolving the crude materials in a solvent or in a mixture of solvents after stirring and moderately heating. Then, the solvents were slowly evaporated. For siloxanol (**1**), the solvent was pure hexane; for

trisilo (**2**), it was a mixture of diethylether and methanol; for pentaphe (**3**), it was pure ethanol; for hexaphe (**4**), it was dichloromethane and hexane. In each case, colourless crystals of good quality in any required size could be obtained. Relatively large crystals were selected, which had a maximum dimension of 0.6 mm and a minimum dimension of 0.3 mm (see Table 5.1) to guarantee sufficient diffracting power for the high-resolution X-ray diffraction experiment. The crystals were mounted on cactus needles with Paratone N oil or high vacuum grease as glue.

The data set of siloxanol (**1**) was measured at synchrotron beamline F1 of HASYLAB in Hamburg at a wavelength of 0.5600(2) Å. As it turned out, the compound undergoes several phase transitions between room temperature and 100 K so that every tested crystal burst upon cooling. After many attempts, a high-resolution data set could finally be obtained at 240 K. For the special case of a very rigid cyclic structure like siloxanol (**1**) exhibits, thermal motions were small enough for an accurate electron-density determination. [198] A resolution of 1.04 Å^{-1} and an overall completeness of data of 96.3 % within the monoclinic space group $P2_1/n$ was achieved. A total of 208742 reflections was measured. Due to the high temperature, only 5899 out of 14536 unique reflections were observed according to the criterium $F^2 \geq 2\sigma(F^2)$. However, this amount of reflections still yielded an excellent ratio of reflections over parameters in the multipole refinement. For more details on the measurement and the crystallographic data, see Table 5.1.

The data sets of cpds. **2** to **4** were measured at beamline D3 of HASYLAB at a wavelength of 0.5166(2) Å. The crystals could be quick-freezed by inserting them into a helium open-flow gas-stream, and the temperature was maintained at 8 K during the measurement. Resolutions of 1.11 Å^{-1} were reached, yielding an overall completeness of 100.0 % for trisilo (**2**) (monoclinic space group $P2_1/c$), 89.2 % for pentaphe (**3**) (triclinic space group $P\bar{1}$) and 88.6 % for hexaphe (**4**) ($P\bar{1}$). Between 150000 and 270000 reflections were measured, and between 62 and 75 % of the unique reflections were also observed according to the criterium $F^2 \geq 2\sigma(F^2)$ and used in the refinements (see Table 5.1). Very high ratios of reflections over parameters were achieved with these observed data.

Integration of data was carried out with the programme XDS (revision August 2006 for cpd. **1** and revision Dec 2007 for cpds. **2** to **4**). [199–201] Subsequently, oblique incidence correction was performed. [105] Scaling and merging of data were carried out using the programme SORTAV. [202–204] The structures were solved with direct methods using the programme SHELXS. [205] All four compounds crystallise without solvent molecules. The asymmetric units of siloxanol (**1**) and

Table 5.1: Crystallographic and refinements details of cpds. **1** to **4**

Spherical refinement, multipole refinement and constrained wave-function fitting (CWF)

	siloxanol (**1**)	trisilo (**2**)	pentaphe (**3**)	hexaphe (**4**)
chemical formula	$C_{12}H_{22}O_2Si_3$	$C_{14}H_{26}O_2Si_4$	$C_{30}H_{26}OSi_2$	$C_{36}H_{30}OSi_2$
M ($g{\cdot}mol^{-1}$)	282.57	338.71	458.69	534.78
space group, Z	$P2_1/n$, 4	$P2_1/c$, 2	$P\bar{1}$, 2	$P\bar{1}$, 1
a (Å)	8.922(2)	10.489(2)	9.110(2)	8.493(2)
b (Å)	16.700(3)	8.941(2)	10.543(2)	9.477(2)
c (Å)	11.151(2)	11.421(2)	13.597(3)	10.933(2)
α (°)	90.00	90.00	94.30(3)	96.17(3)
β (°)	103.59(3)	115.95(3)	106.90(3)	111.74(3)
γ (°)	90.00	90.00	92.96(3)	113.15(3)
V ($Å^3$)	1615.0(6)	963.1(4)	1242.3(5)	717.8(4)
ϱ_x ($g{\cdot}\ cm^{-3}$)	1.162	1.168	1.226	1.237
F(000)	608	364	484	282
μ (mm^{-1})	0.15	0.13	0.07	0.07
crystal size (mm^3)	$0.4x0.4x0.3$	$0.5x0.3x0.3$	$0.6x0.4x0.3$	$0.6x0.5x0.4$
beamline	F1	D3	D3	D3
T (K)	240	8	8	8
λ (Å)	0.5600(2)	0.5166(2)	0.5166(2)	0.5166(2)
min./ max. 2θ (°)	3.6/ 71.0	3.1/ 70.0	2.3/ 70.0	3.1/70.0
$\frac{sin\theta_{max}}{\lambda}$ ($Å^{-1}$)	1.04	1.11	1.11	1.11
no. of coll. refl.	208742	161141	273011	156723
no. of unique refl.	14536	11033	25392	14557
cond. for obs. refl.	$F^2 \geq 2\sigma(F^2)$	$F^2 \geq 2\sigma(F^2)$	$F^2 \geq 2\sigma(F^2)$	$F^2 \geq 2\sigma(F^2)$
no. of obs. refl.	5899	8622	15819	9974
redundancy	14.4	10.5	10.8	10.8
completeness (%)	96.3	100.0	89.2	88.6
R_{int} (%)	2.88	3.50	6.31	5.11
spherical ref.:				
R(F) (%)	4.20	2.23	3.67	3.56
wR(F^2) (%)	14.95	7.26	12.32	12.32
GooF	0.90	1.05	1.01	1.11
multipole ref.:				
refinement on	F^2	F^2	F^2	F^2
ratio refl./par.	19.66	50.72	38.49	42.99
R(F)/ R(F^2) (%)	2.85/ 3.07	1.38/ 2.02	1.90/ 2.87	2.05/ 3.04
wR(F)/ wR(F^2) (%)	2.63/ 5.19	1.87/ 3.70	2.50/ 5.00	2.88/ 5.77
GooF	1.01	0.69	0.56	0.80
min./ max./ mean				
$\delta_{res}\varrho(\vec{r})$ ($eÅ^{-3}$)	-0.21/ 0.20/ 0.02	-0.25/ 0.19/ 0.03	-0.32/ 0.30/ 0.03	-0.22/ 0.46/ 0.03
CWF:		–	–	–
R(F)/ wR(F) (%)	7.65/4.27	–	–	–
χ^2/λ	0.93/ 0.60	–	–	–
GooF	0.97	–	–	–

pentaphe (**3**) consist of one molecule, whereas for trisilo (**2**) and hexaphe (**4**) the asymmetric units consist of half a molecule. For trisilo (**2**), there is an inversion centre in the middle of the phenyl ring and for hexaphe (**4**), there is an inversion centre at the atomic position of the oxygen atom O1 that is therefore in a special crystallographic position.

5.1.2 Refinement and Analysis of Data

Conventional spherical refinement was carried out by the programme SHELXL [205] to establish the starting positional and displacement parameters for the aspherical refinement steps. Anisotropic displacement parameters (adps) were refined for the non-hydrogen atoms. For the hydrogen atoms, adps were calculated by a rigid body approximation using the SHADE approach. [108, 109] This was not possible for siloxanol (**1**) owing to greater atomic motion in the methyl groups at 240 K. Isotropic displacement parameters were used instead. Table 5.1 lists important figures of merit for the spherical refinement. Figure 5.1 shows the final structures after multipole modelling (ORTEP representation [206]) with the atomic-numbering scheme that is used in the following discussions. It is visible in Figure 5.1 that the adps of oxygen atom O1 in hexaphe (**4**) are as small as the other non-hydrogen adps in the structure and as small as the adps of the O1 atoms in trisilo (**2**) and pentaphe (**3**). The values of the adps of O1 are: $u_{11} = 0.0116, u_{12} = 0.0091, u_{13} = 0.0050, u_{22} = 0.0049, u_{23} = 0.0045, u_{33} = 0.0013$. These results confirm that the Si–O–Si fragment in hexaphe (**4**) is strictly linear and that no deviation from linearity by disorder is indicated (compare discussion on this topic in Chapter 4.1).

For aspherical refinement, the multipole formalism was used as implemented in the programme XDLSM of the XD2006 suite of programmes [207]. The usage of chemical site symmetries and constraints is identical in cpds. **1** to **4** as far as that was possible. Local mirror (m) symmetry was imposed on all non-hydrogen atoms in the rings of siloxanol (**1**) and trisilo (**2**) including Si1, Si2 and O1. Methyl groups were refined with local threefold (3) symmetry and hydrogen atoms with local sixfold (6) symmetry as approximation to linear groups. Si3 in siloxanol (**1**) was refined without local symmetry (1), but m symmetry was imposed on the silanol oxygen atom O3. In pentaphe (**3**) and hexaphe (**4**), mm2 symmetry was introduced for all C atoms in the phenyl rings. In pentaphe (**3**), m symmetry was imposed on siloxane oxygen atom O1, but Si1 and Si2 were refined without

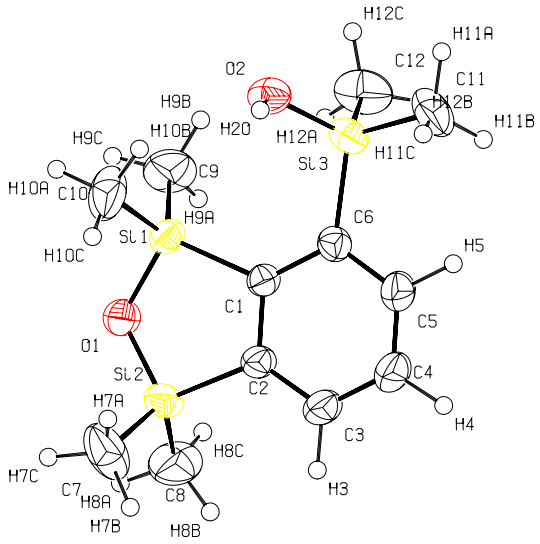

(a) Siloxanol (**1**) at 240 K with isotropic H atoms of arbitrary radii

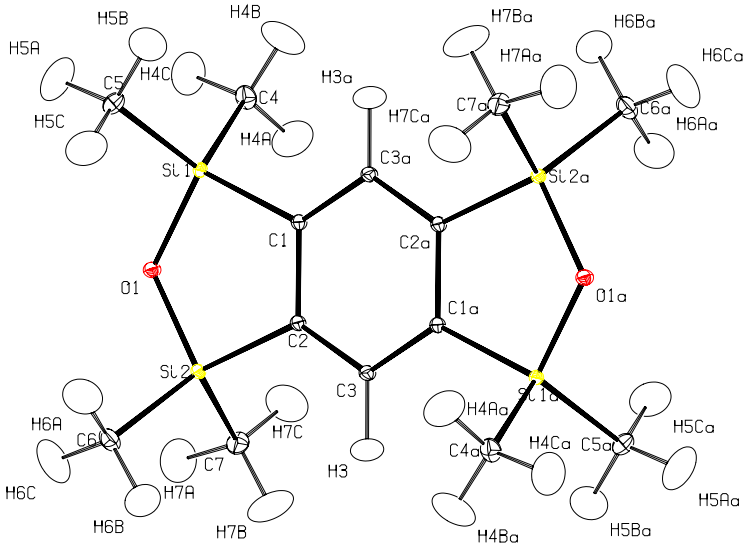

(b) Trisilo (**2**) at 8 K with anisotropic H atoms

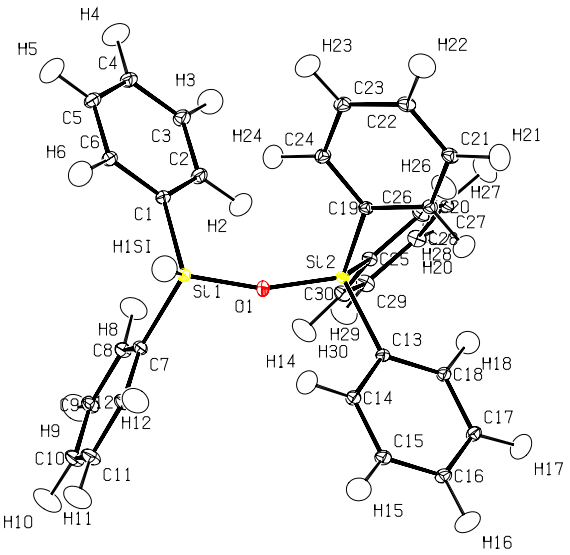

(c) Pentaphe (**3**) at 8 K with anisotropic H atoms

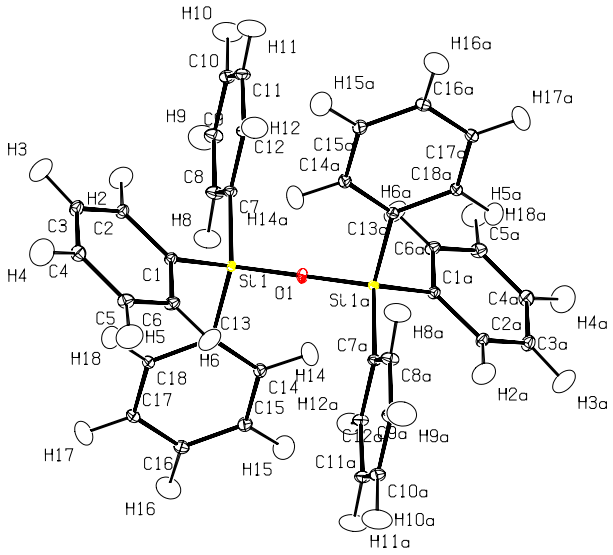

(d) Hexaphe (**4**) at 8 K with anisotropic H atoms

Figure 5.1: ORTEP representations of cpds. **1** to **4**

Thermal ellipsoids at 50 % probability, atomic-numbering scheme as used in the discussion

symmetry, as was Si1 in hexaphe (**4**). Due to the special position of O1 in hexaphe (**4**), local $\overline{3}$ symmetry (threefold axis and inversion centre) was used. In siloxanol (**1**) and trisilo (**2**), Si2 was chemically constrained to Si1. Furthermore, the methyl groups were constrained to each other as well as some C and H atoms in the phenyl rings. In pentaphe (**3**) and hexaphe (**4**), most of the C and H atoms in the phenyl rings were chemically constrained to each other. For more details on the usage of local site symmetries and chemical constraints, see Tables A.1 and A.2 of the Appendix.

All non-hydrogen atoms were treated up to the hexadecapole level of expansion, whereas monopoles, bond-directed dipoles and bond-directed quadrupoles were introduced for hydrogen atoms. The expansion-contraction parameter κ was refined independently for all non-constrained non-hydrogen atoms (see Tables A.1 and A.2). κ' values of C and O atoms were left at their default values κ'=1.0. For Si atoms, κ' values were calculated from theoretical structure factors from periodic-boundary calculations modelled with XD2006 (see below). For all four compounds, similar κ'(Si) values were obtained, which were averaged and rounded to give overall κ'(Si)=0.85 used in the refinement steps. For hydrogen atoms, optimised values κ=1.13 and κ'=1.29 [208] were used, except for H1Si of pentaphe (**3**) because it is bonded to a more electropositive atom (Si) instead of a more electronegative atom (C). κ=1.05 and κ'=1.05 were obtained in the same way as for κ'(Si).

All distances of bonds involving hydrogen atoms were fixed to mean neutron diffraction values from the literature. [209] H–C–H bond angles in methyl groups were fixed to the tetrahedral angle. An electroneutrality constraint concerning the monopole populations was applied for the asymmetric unit. Figures of merit for the multipole refinement on F^2 are collected in Table 5.1. As expected, there is a significant improvement of the R values compared to the spherical refinement.

The minimum and maximum residual densities are in a typical range, especially when atoms heavier than oxygen are involved. This is due to the inflexibility of the single-zeta radial functions in the multipole formalism (see Chapter 1.1.3), which causes the residual density to increase with the weight of the atom. Therefore, more diffuse values of the radial power coefficient n_{il} and a different ζ(Si) value than given by default in the scattering table were chosen (ζ(Si)=3.0628, n_0=2, n_1=2, n_2=4, n_3=6, n_4=8). These values have established themselves for the third period of the periodic table [210, 211] and have already sucessfully been tested for silicon before [212]. It is known that the use of these values improves the description

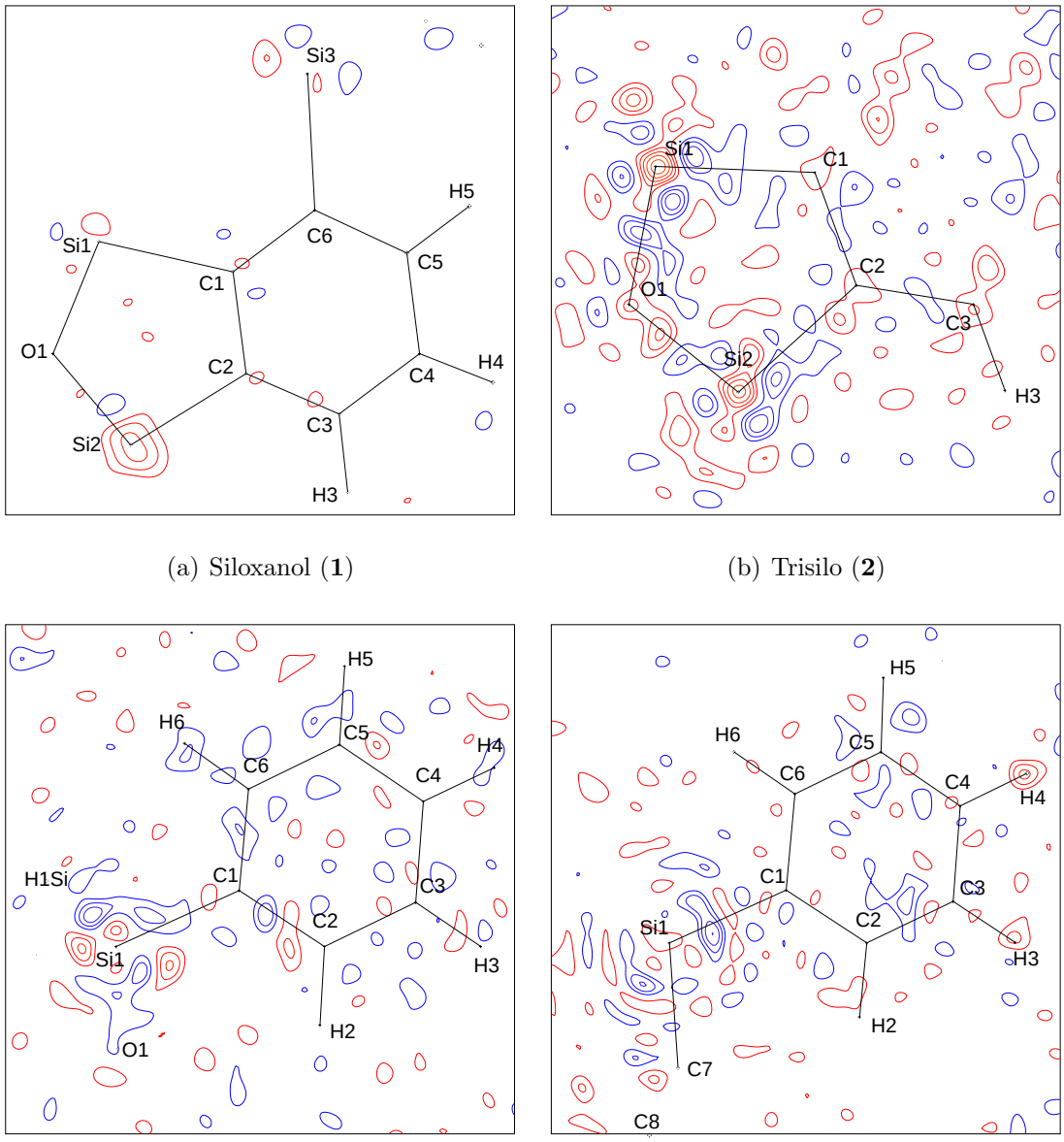

(a) Siloxanol (**1**)

(b) Trisilo (**2**)

(c) Pentaphe (**3**)

(d) Hexaphe (**4**)

Figure 5.2: Residual-density maps in selected planes of cpds. **1** to **4**
Contour interval = 0.05 eÅ^{-3}; red=negative, blue=positive

of the ED in the middle of bonds, which are most important for an ED analysis, but corrupts the description of the ED at the atomic positions, where the relative errors remain negligible due to the high absolute value at these positions. [213]
The residual-density distributions of cpds. **1** to **4** with isocontour intervals of $0.05\,e\text{Å}^{-3}$ are visualised in Figure 5.2. The most striking effects are located at the Si positions or in close vicinity to them, but they do not exceed $0.25\,e\text{Å}^{-3}$. Although optimised n_l and ζ values were used, not all Si–O and Si–C bonds are featureless, but effected with no more than $0.15\,e\text{Å}^{-3}$ of residual density. This constitutes approximately 10 % of the absolute value of the ED at the bcp. All regions of the molecules further away from a Si atom are flat and featureless because the visual impression of many features in the residual density is caused by the choice of the small iso-contour interval. Overall, the analysis of the residual density distribution confirms a successful modelling of the ED in the framework of the multipole formalism.
The final ED distributions were topologically analysed with the programme XDPROP of the XD2006 suite of programmes. The calculation of the Source function, the electrostatic potential, interaction energies as well as molecular surfaces were performed with XDPROP, too. Deformation density, residual density and Laplacian maps were generated with the programme XDGRAPH of the XD2006 suite. For one-dimensional plots, the programme GNUPLOT [214] was used. Graphical Source function representations were obtained with the programme DIAMOND. [215] Molecular surfaces were plotted with the programme MOLISO [216] and properties like the electrostatic potential were mapped on these iso-surfaces. Geometries and molecular graphs were visualised with the programme SCHAKAL99 [217].

Constrained wave-function fitting (CWF, [36–39]) at the HF/cc-pVDZ level of theory was performed for siloxanol (**1**) with the programme TONTO [218] using experimental geometry and experimental structure factors. The λ value was iteratively increased from 0.00 to 0.60 in steps of 0.05. Between λ=0.55 and 0.60, the figures of merit (summarised in Table 5.1) did not improve, so that the constrained wavefunction at λ=0.60 was used for the calculation of ED and ELF. It was decided to derive the experimental ELF for siloxanol (**1**) as described in Ref. [55] and not the experimental ELI-D to have pictures and values from an established method, which can be compared with the experimental ELI-D applied for the first time for epoxide cpds. **7** to **10** in Chapter 12.3.
Grids of ED and ELF were written by TONTO in cube format (stepsize=0.1 a.u.)

and analysed with the programme DGRID-4.4 [219]. A topological analysis of the experimental ELF according to Bader's method [220] was performed to define basins for core and valence electron pairs. The ED was integrated within the ELF basins to get electron populations. The topological analysis of the experimental ELF was introduced only recently by Hübschle and Grabowsky (see Chapter "Additional Studies"). [56, 161]

5.2 Details of Theoretical Calculations

5.2.1 Calculations on Compounds 1 to 4

Isolated-molecule calculations on the B3LYP/cc-pVTZ level of theory were performed for cpds. **1** to **4** at experimental and optimised geometries, as well as for hydrogen-bonded complexes of cpds. **1**, **2** and the model compound $H_2Si(OSiH_2)_2O$ (see Chapter 7.1.3) with silanol and water at optimised geometries with the programme GAUSSIAN03, revision E.01 [221]. Only for siloxanol (**1**), the HF/cc-pVDZ level of theory was additionally used at experimental geometry to compare with CHF/cc-pVDZ from CWF. Hydrogen-bond energies E_{HB} and IR red shifts $\Delta\tilde{\nu}(OH)$ of the hydrogen-bonded complexes were extracted directly from the GAUSSIAN output. A formatted checkpoint (fchk) file and a wavefunction (wfn) file were written from GAUSSIAN03, which served as input for other programs.
The topological analysis of the ED was carried out with the programme AIM2000 [222] from the wfn output to obtain bond-topological and atomic parameters as well as the delocalization indices. From the fchk files, the ELI-D, ED, and Laplacian of the ED were calculated on a grid of 0.07 a.u. stepsize with the programme DGRID-4.4. [219] The same programme was employed to topologically analyse the ELI-D grids. Graphical localisation domain and Laplacian isosurface representations were generated with MOLISO [216].

Furthermore, the experimental geometries of cpds. **1** to **4** were taken as input for periodic-boundary calculations with the programme CRYSTAL06 [223]. The method B3LYP and the following basis sets were used individually for each atom type: 88-31G(d,p) for Si [224], 6-31G(d) for O and C [225], and 3-1G(p) for H [225]. From the periodic wavefunction, static theoretical structure factors were calculated with the programme PROPERTIES06 belonging to the CRYSTAL06 suite. The list of experimentally obtained hkl indices was chosen to be calculated, but including

Table 5.2: Details of refinements on theoretical structure factors

Periodic-boundary calculations at experimental geometry

	siloxanol (**1**)	trisilo (**2**)	pentaphe (**3**)	hexaphe (**4**)
space group, Z	$P2_1/n$, 4	$P2_1/c$, 2	$P\bar{1}$/ 2	$P\bar{1}$/ 1
F(000)	608	364	484	282
no. of calc. refl.	5907	8634	15824	9984
refinement on	F	F	F	F
ratio refl./par.	47.26	107.93	119.39	107.47
R(F)/ R(F^2) (%)	0.31/0.52	0.40/0.63	0.44/0.73	0.43/0.78
min./ max./ mean $\delta_{res}\varrho(\vec{r})$ (e$Å^{-3}$)	-0.06/0.08/0.01	-0.16/0.14/0.01	-0.08/0.19/0.01	-0.07/0.11/0.01

a few reflections of very low resolution that were not observed in the experiment yet might contain important information.

The theoretical structure factors were modelled with XD2006. In a first step, multipoles and κ values were refined up to the hexadecapole level without constraints and local site symmetries to get optimised κ' values for Si atoms at fixed experimental geometry. κ'(Si)=0.85 was found and used in the experimental refinements (see above). After the experimental multipole modelling was fully converged and yielded the final experimental geometry, the periodic-boundary calculations were repeated with the slightly changed experimental geometry. The new theoretical structure factors were modelled using the same density model as in the experiments, i.e. constraints, site symmetries and κ values (as long as not refined, see Tables A.1 and A.2) were imposed as detailed in Chapter 5.1.2. The results of the aspherical modelling of the theoretical structure factors are summarised in Table 5.2. Even for theoretical structure factors, the description of polar bonds and heavier atoms like Si is subject to inaccuracies within XD2006, so that small but significant residual densities occur. From the final density model resulting from theoretical structure factors, the same properties were calculated with XDPROP as for the experimental ED distribution (see Chapter 5.1.2).

5.2.2 Calculations on Model Compounds of the Type $H_3SiOSiH_3$

Free disiloxane $H_3SiOSiH_3$ - the smallest compound containing the siloxane linkage Si–O–Si - as well as disiloxane$\cdots$silanol [$(H_3Si)_2O\cdots HOSiH_3$] and disiloxane$\cdots$water [$(H_3Si)_2O\cdots HOH$] hydrogen-bonded complexes were chosen as model compounds (see Figure 5.3). Relaxed PES scans with fixed Si–O–Si angles ϕ were

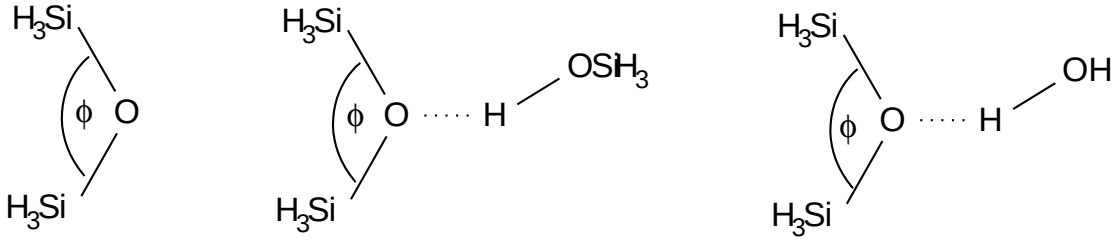

Figure 5.3: Scrutinised model compounds of the type $H_3SiOSiH_3$
Free disiloxane ($H_3SiOSiH_3$), disiloxane$\cdots$silanol hydrogen-bonded complex ($(H_3Si)_2O\cdots HOSiH_3$), and disiloxane$\cdots$water hydrogen-bonded complex ($(H_3Si)_2O\cdots HOH$)

performed between ϕ=50 ° and 180 ° in 5 ° intervals with GAUSSIAN03 at B3LYP/cc-pVTZ level of theory. In addition to the relaxed PES scans, full geometry optimisations of $H_3SiOSiH_3$, $(H_3Si)_2O\cdots HOSiH_3$, $(H_3Si)_2O\cdots HOH$, H_3SiOH and H_2O were performed at the same level of theory.

It is one of the major goals of this study to find out why hydrogen bonding is not possible for large Si–O–Si angles. It can be assumed that a chemical catastrophe [226] on the PES might take place between a chemical system of $H_3SiOSiH_3$ - as defined by catastrophe theory - with rather small Si–O–Si angles in which hydrogen bonding is possible (around ϕ=120 °) and a chemical system of $H_3SiOSiH_3$ with large Si–O–Si angles in which hydrogen bonding is not possible (close to ϕ=180 °). To develop concepts how such a chemical catastrophe in $H_3SiOSiH_3$ can be found and described within the framework of the topological ED and ELI-D analyses [170, 227], possibilities were sought to intentionally provoke another chemical catastrophe in $H_3SiOSiH_3$, so that a known chemical catastrophe could be compared with the assumed chemical catastrophe at larger Si–O–Si angles. Hence, it was chosen to start the PES scan with very small Si–O–Si angles (ϕ=50 °), yielding $H_3SiOSiH_3$ systems that are definitely only hypothetical, i.e. that are not stable in reality, and increase ϕ to values that yield stable systems. It will be analysed how the change between these two systems (hypothetical and stable) manifests in ED and ELI-D and shows the chemical catastrophe. This knowledge will then be transferred to investigate how the change from hydrogen-bonding to hydrogen-repelling systems at larger Si–O–Si angles takes place. Moreover, relaxed geometry optimisations (B3LYP/cc-pVTZ) were performed on disilaepoxide $H_2SiOSiH_2$ (three-membered ring) as a stable system with a small Si–O–Si angle, and on disilaepoxide$\cdots$silanol/water complexes.

For very large and very small Si–O–Si angles ϕ in the hydrogen-bonded adducts, convergence could not be reached easily. To solve this problem, the calculations were started with small basis sets, for which the time expenditure of the calculations is small, so that the number of optimisation cycles could be increased. Moreover, successfully optimised geometries from the next smaller or larger angle were used as input geometries. This strategy yielded optimised geometries only for some of the initially non-converged cases. For $(H_3Si)_2O\cdots HOSiH_3$, there are no optimised geometries between ϕ=50 and 80 ° nor between ϕ=170 and 180 °; for $(H_3Si)_2O\cdots HOH$, there are no optimised geometries between ϕ=50 and 85 ° nor between ϕ=170 and 180 °.

From the GAUSSIAN logfiles, a number of parameters could be determined directly: the bending potential (molecular energy relative to the minimum of the PES scan), the hydrogen-bond energies (E_{HB}) after BSSE correction, the delocalization energies (ΔE_{deloc}) after NBO analysis and the IR red shifts ($\Delta\tilde{\nu}(OH)$). Topological analyses of ED and ELI-D were performed as described above for theoretical calculations on cpds. **1** to **4**. The developments of the extracted properties against ϕ were plotted with the programme ORIGIN. [228]

Chapter 6

Results for Model Compounds of the Type $H_3SiOSiH_3$

6.1 Geometrical and Energetical Results

6.1.1 Bending-Potential and Hydrogen-Bond Energy

It was shown in Chapter 4.1 that most siloxanes contain large Si-O-Si angles ϕ between 130 ° and 180 °. This is an unusually wide region of angles, which can be explained by the bending potentials plotted in Figure 6.1. In the curve for free disiloxane $H_3SiOSiH_3$, the region between 130 ° and 180 ° is flat, so that variation of the bond angle ϕ is associated only with a small change of energy. The barrier to linearisation from the minimum-angle position (ϕ=151.4° obtained by relaxed optimisation of free disiloxane) is only 0.5 kJ mol^{-1}, so that the large number of linear Si–O–Si fragments in symmetrically substituted compounds (see Fig. 4.1) is easy to explain. In the crystal structure of free disiloxane at 108 K, [229] the Si–O–Si angle is ϕ=142.2(3) °.

The curve for free disiloxane also suggests that the siloxane linkage is strained for angles smaller than about 130 ° as the curve ascends rapidly towards smaller angles. To bend the Si–O–Si linkage to values around 115 ° as they occur in siloxanol (**1**) and trisilo (**2**), an energy loss of about 20 kJ mol^{-1} with respect to the minimum angle has to be compensated. This cannot be done by the energy gain associated with the formation of hydrogen bonds at small angles that are about 10 kJ mol^{-1} for silanol as donor and 3 kJ mol^{-1} for water as donor (see Figure 6.2 and discussion below). Consequently, the siloxane linkage has to be incorporated into a ring

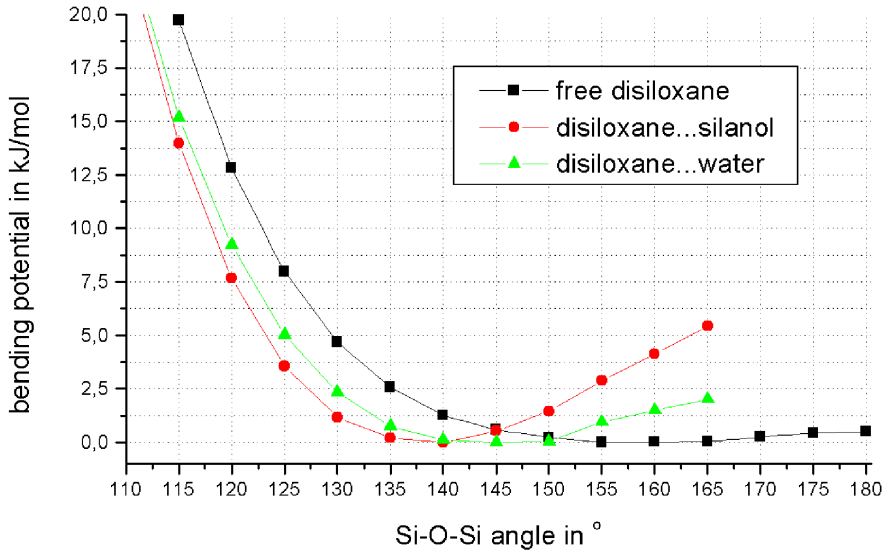

Figure 6.1: Bending-potential energies for free disiloxane and hydrogen-bonded complexes

system to force it into a strained situation. To bend the siloxane linkage to a value of ϕ=100 °, which only occurs in three-membered Si–O–Si rings (see Fig. 4.1 and Ref. [176]), about 61 kJ mol^{-1} are required; to bend the siloxane linkage to the hypothetical value of ϕ=60 °, which corresponds to the C–O–C angle in epoxides, 605 kJ mol^{-1} must already be provided (see also Table A.17 of the Appendix).

The situation changes when a hydrogen bond with the disiloxane oxygen atom as acceptor is formed. Figure 6.1 also shows the bending-potential curves for the disiloxane$\cdots$silanol [$(H_3Si)_2O\cdots HOSiH_3$] and disiloxane$\cdots$water [$(H_3Si)_2O\cdots$ HOH] complexes. The minima of the curves in the case of the complexes shift towards smaller angles. For disiloxane$\cdots$silanol, the minimum angle as obtained from relaxed optimisation is 137.8 °; for disiloxane$\cdots$water, it is 140.1 °. Moreover, it becomes energetically unfavourable to increase the Si–O–Si angle. 5.4 instead of 0.5 kJ mol^{-1} must be provided to increase the Si–O–Si angle in disiloxane$\cdots$silanol from the minimum position to ϕ=165 °; for disiloxane$\cdots$water, the corresponding value is 2.0 kJ mol^{-1}.

As already mentioned in Chapter 5.2.2, there are no optimised structures of disiloxane$\cdots$silanol and disiloxane$\cdots$water in the regions ϕ=50 ° to 80 ° and 170 ° to 180 °. This means that hydrogen bonding is generally not feasible in these regions. At first glance, this seems to be a contradiction to the results shown in

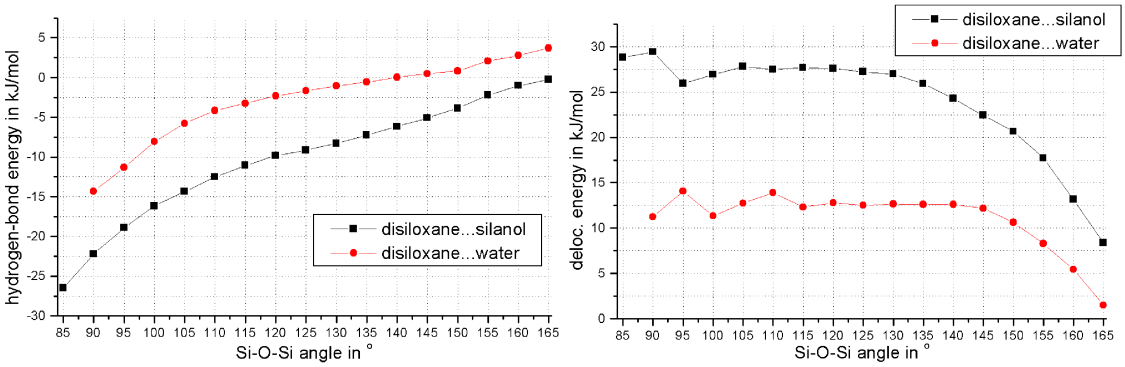

(a) Hydrogen-bond energies (b) Delocalization energies

Figure 6.2: Hydrogen-bond energies and delocalization energies from NBO analyses of hydrogen-bonded complexes

Figure 6.2 (a). Therein, the hydrogen-bond energies (E_{HB}) of the disiloxane$\cdots$silanol/water complexes are plotted. E_{HB} steadily decreases with a decreasing Si–O–Si angle, so that the strongest hydrogen bonds are found for the smallest angles (for disiloxane$\cdots$ silanol: E_{HB}=-26.5 kJ mol^{-1} at ϕ=85 °; for disiloxane$\cdots$water: E_{HB}=-14.3 kJ mol^{-1} at ϕ=90 °). Below these angles with the strongest hydrogens bonds, no optimised structures exist, and hydrogen bonding is generally not feasible. This contradiction can only be explained with a sudden change of the electronic situation between 80 ° and 85 °, so that the oxygen atom of the siloxane linkages completely loses its acceptor quality. This sudden change between 80 ° and 85 °, which will be analysed in detail in Chapters 6.2.2 and 6.3, can be identified as the chemical catastrophe that was sought between a hypothetical and a stable system of free disiloxane $H_3SiOSiH_3$.

In the curves of the delocalization energy ΔE_{deloc} in Figure 6.2 (b), the highest energy value stands for the strongest bond. For values between about 85 ° and 115 °, the curves show outliers and sudden steps because no unambiguous minimum in the energy hypersurface can be found upon optimisation with a frozen Si–O–Si angle. This ambiguousness for small angles will also be shown for many other properties in the following chapters. One consequence is that convergence was not reached at ϕ=85 ° for disiloxane$\cdots$water, although a high hydrogen-bond energy would most probably be associated with this minimum. But it will be shown later that the chemical catastrophe indeed takes place between ϕ=80 ° and 85 ° in free disiloxane. So the reason for the fact that no optimised structure was found for disiloxane$\cdots$water at ϕ=85 ° is only the ambiguousness of the energy hypersurface

at small Si–O–Si angles.
The fact that hydrogen bonding is generally not possible for very large Si–O–Si angles (ϕ= 170 ° to 180 °) can also be understood from Figure 6.2: The hydrogen-bond energies and the delocalization energies drop to zero between 165 ° and 170 °. For disiloxane$\cdots$water, E_{HB} is already slightly positive above 140 ° (see also Table A.18). It will be shown in Chapter 6.2.2 and 6.3 that the second chemical catastrophe in free disiloxane can be found between 165 ° and 170 °. This means that there is also a sudden change of the electronic situation that goes along with the loss of acceptor properties of the siloxane oxygen atom, which manifests in a similar way as for the first chemical catastrophe that was intentionally provoked.

One of the major questions that were brought up concerning the character of the siloxane linkage can already be answered from Figure 6.2: The basicity of the siloxane linkage can be improved strongly by decreasing the Si–O–Si angle, i.e. the siloxane linkage becomes a better hydrogen-bond acceptor at smaller Si–O–Si angles. Near the tetrahedral angle (110 °) that is usually adopted by ethers, the hydrogen-bond energy is -12.5 kJ mol^{-1} for disiloxane$\cdots$silanol and -4.2 kJ mol^{-1} for disiloxane$\cdots$water. At a Si–O–Si angle of 140 ° in the case of disiloxane$\cdots$silanol, the hydrogen bond is already half as strong (E_{HB} = -6.2 kJ mol^{-1}).
However, in almost all siloxanols the silanol sites themselves are better acceptors for hydrogen bonding than the siloxane linkage. For the model complex silanol$\cdots$silanol ($H_3SiOH\cdots O(H)SiH_3$), E_{HB} is -14.5 kJ mol^{-1}. Also, the comparison of different acceptors in model complexes of the type A$\cdots$HOSiH$_3$ - for example A = water, ether, and methanol - reveals that these hydrogen bonds are stronger (E_{HB}=-15 to -21 kJ/mol, [230]) than those in disiloxane$\cdots$silanol [$(H_3Si)_2O\cdots$ HOSiH$_3$] or disiloxane$\cdots$water [$(H_3Si)_2O\cdots$HOH], even if small Si–O–Si angles are considered. Nonetheless, for strained siloxane linkages with ϕ smaller than about 135 °, the hydrogen-bond energy is large enough to be chemically significant and compete with the silanol group as acceptor, as the existence of three hydrogen-bond complexes in the CSD (see Chapter 4.1) and one complex in this doctoral thesis proves.
Figure 6.2 also shows that the silanol group is a much better hydrogen-bond donor than water. In the whole range where hydrogen bonding is generally feasible (85 °$\leq \phi \leq$ 165 °), the hydrogen bond with silanol as donor is approximately twice as strong. This holds for E_{HB} and ΔE_{deloc}.

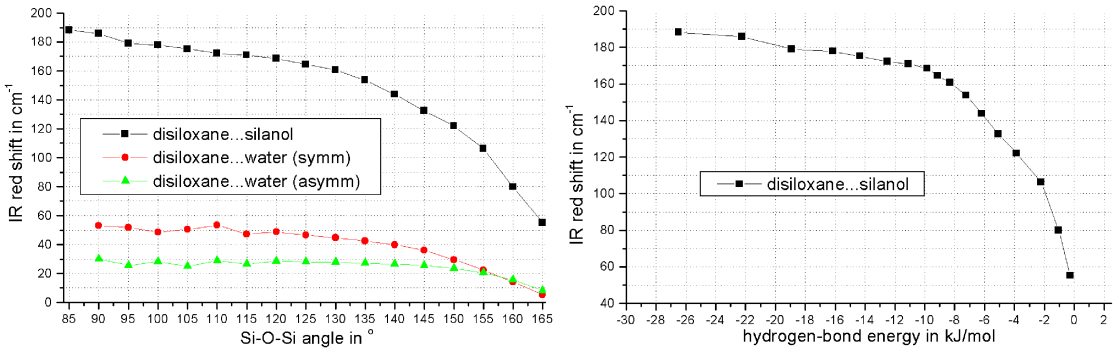

(a) IR red shift vs. ϕ (b) IR red shift vs. E_{HB}

Figure 6.3: IR red shift of hydrogen-bonded complexes vs. Si–O–Si angle ϕ and hydrogen-bond energy E_{HB}, respectively

It is known that the IR red shift of the OH-stretching vibration of the hydroxy group ($\Delta\tilde{\nu}(OH)$) in silanol is indicative of hydrogen bonding. [231] $\Delta\tilde{\nu}(OH)$ ranges from 55 to 188 cm^{-1} for disiloxane$\cdots$silanol as depicted in Figure 6.3 (a). The IR red shift decreases continuously from ϕ=85 ° to 165 °, showing that the hydrogen bond becomes weaker. The IR red shift can therefore be referred to as a measure of the hydrogen-bond strength. Thus, it was plotted against the hydrogen-bond energy to evaluate if it follows the same trend. In studies that involve different silanol$\cdots$acceptor complexes, it was found that $\Delta\tilde{\nu}(OH)$ correlates linearly with E_{HB}. [230] Figure 6.3 (b) shows that in this case where different Si–O–Si angles are examined for the same complex (disiloxane$\cdots$silanol), the correlation is not linear. The IR red shift increases more rapidly when E_{HB} is small (corresponding to large Si–O–Si angles) and the hydrogen-bond energy increases more rapidly than the IR red shift at small Si–O–Si angles. The range of $\Delta\tilde{\nu}(OH)$ covered here (about 130 cm^{-1}) is comparable to the range covered by different silanol$\cdots$acceptor complexes (about 140 cm^{-1}, [230]).

The IR red shift of the symmetric and asymmetric OH-stretching vibrations in the water molecule are also plotted in Figure 6.3 (a). They cover a much smaller range and the absolute values are also much smaller than for silanol, being consistent with a weaker hydrogen bond. There is no trend visible in the region of the ambiguous hypersurface between 90 ° and 130 °, but the IR red shift significantly drops off when the Si–O–Si angle approaches 165 °. This behaviour matches the observed behaviour for the delocalization energies.

Properties that describe the hydrogen bonds in disiloxane$\cdots$silanol/ water can in general be classified into three categories:

- properties that are a measure of the hydrogen-bond strength, i.e. that are indicative of hydrogen bonding, because they unambiguously correlate with the hydrogen-bond energy;
- properties that show no meaningful trend in the region of the ambiguous energy hypersurface approximately between 85 and 130 °, but significantly drop off or rise for large Si–O–Si angles; they are in general indicative of hydrogen bonding;
- properties that are not affected by hydrogen-bond formation; as they do not change over the whole range of Si–O–Si angles, they are not indicative of hydrogen bonding.

Any property discussed below will be interpreted according to this classification because it is an important hint on the nature of the hydrogen bonds even if a property is not affected upon hydrogen-bond formation.

6.1.2 Geometries of Siloxane Linkage and Hydrogen Bonds

For free disiloxane, the energetically most favourable conformation at each frozen Si-O-Si angle ϕ is the one that retains C2v-symmetry, with the exception of ϕ=180 ° where the highest symmetry is D3h-symmetry. This means that free disiloxane is in its eclipsed conformation as Figure 6.4 (a) depicts for ϕ=140 °. As a consequence, all properties for the Si atoms and Si–O bonds, respectively, are identical and therefore only given once or as the sum over both properties (compare Tables A.7 to A.32 of the Appendix).
Figure 6.5 shows the Si–Si and the Si–O distances against the Si–O–Si angle. At small angles, the Si–Si distance is smaller (2.139 to 2.238 Å between 50 ° and 75 °) than the Si–O distance (2.648 to 1.855 Å between 50 ° and 75 °). This suggests that a Si–Si bond is initially present that is broken with an increasing Si–O–Si angle, but a Si–O bond forms only when a Si–O–Si angle of about 70 ° to 75 ° is reached (see Chapters 6.2 and 6.3). Interestingly, the Si–Si bond becomes even shorter from 50 ° to 60 ° to form an equilateral Si–O–Si triangle and then increases steadily from 60 ° to 180 °. The Si–O bond distance is strictly monotonically decreasing over the whole range of Si–O–Si angles. In the linear case, the Si–O

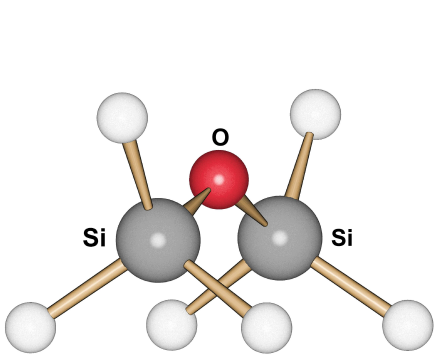

(a) Free disiloxane in its eclipsed conformation at ϕ=140 °

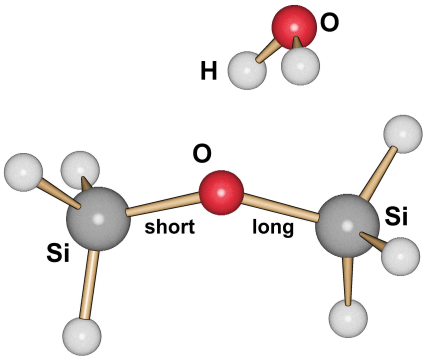

(b) Disiloxane···water at ϕ=140 °

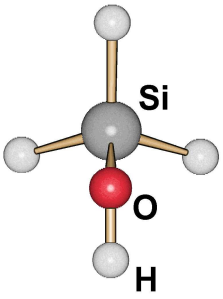

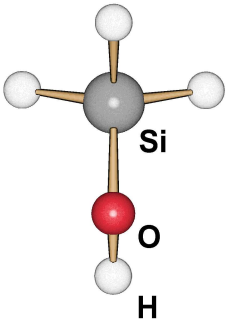

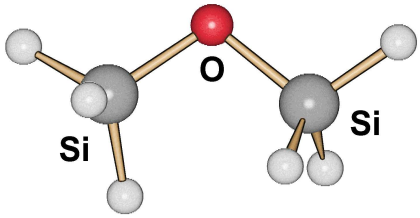

(c) Disiloxane···silanol in its staggered conformation at ϕ=105 °

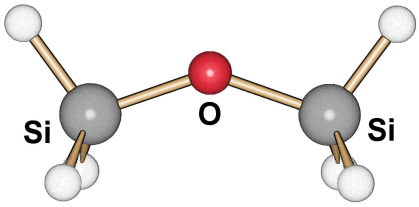

(d) Disiloxane···silanol in its eclipsed conformation at ϕ=140 °

Figure 6.4: Representative geometries of model compounds

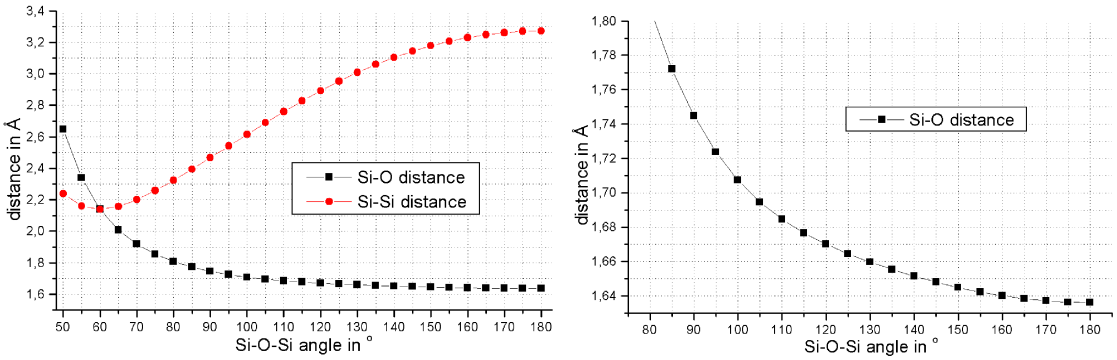

(a) Si–O and Si–Si bond distances over the complete range of Si–O–Si angles

(b) Detail of (a): Si–O bond distances between ϕ=85 ° and 180 °

Figure 6.5: Si–O and Si–Si bond distances in free disiloxane

distance is as short as 1.635 Å. The shortening of the Si–O bond with increasing Si–O–Si angle is due to larger Coulomb interactions (see Bader charge separation in Chapter 6.2) and shows that the ionic character of the bond increases in agreement with the ionic bond model (see Figure 4.2). From the fully relaxed geometry optimisation, the Si–O distance is 1.645 Å, and from the crystal structure [229], it is 1.632(5)/ 1.630(5) Å.

Figure 6.4 shows the geometries of representative model complexes disiloxane$\cdots$silanol and disiloxane$\cdots$water. Between 110 ° and 165 °, disiloxane$\cdots$silanol retains Cs-symmetry in its optimised geometries, i.e. that again the eclipsed conformation is present (Figure 6.4 (d)), so that properties for the $Si_{siloxane}$ atoms and the Si–$O_{siloxane}$ bonds, respectively, are identical. Between 85 ° and 105 °, the symmetry is reduced because a staggered conformation is present (Figure 6.4 (c)), and the properties are formally not to be considered identical. But as they are practically nearly identical because the hydrogen bond is still in the same plane as before, the average over the properties of both $Si_{siloxane}$ atoms or Si–$O_{siloxane}$ bonds is given.

For disiloxane$\cdots$water, the situation is different. The water molecule is shifted towards one of the silyl groups (Figure 6.4 (b)), so that the corresponding Si–O bond elongates. Therefore, properties of $Si_{siloxane}$ atoms and Si–$O_{siloxane}$ bonds in the short and in the long bond are given separately.

Figure 6.6 (a) shows that the Si–O bonds in free disiloxane, disiloxane$\cdots$silanol and disiloxane$\cdots$water follow the same trend, i.e. they shorten when the Si–O–Si

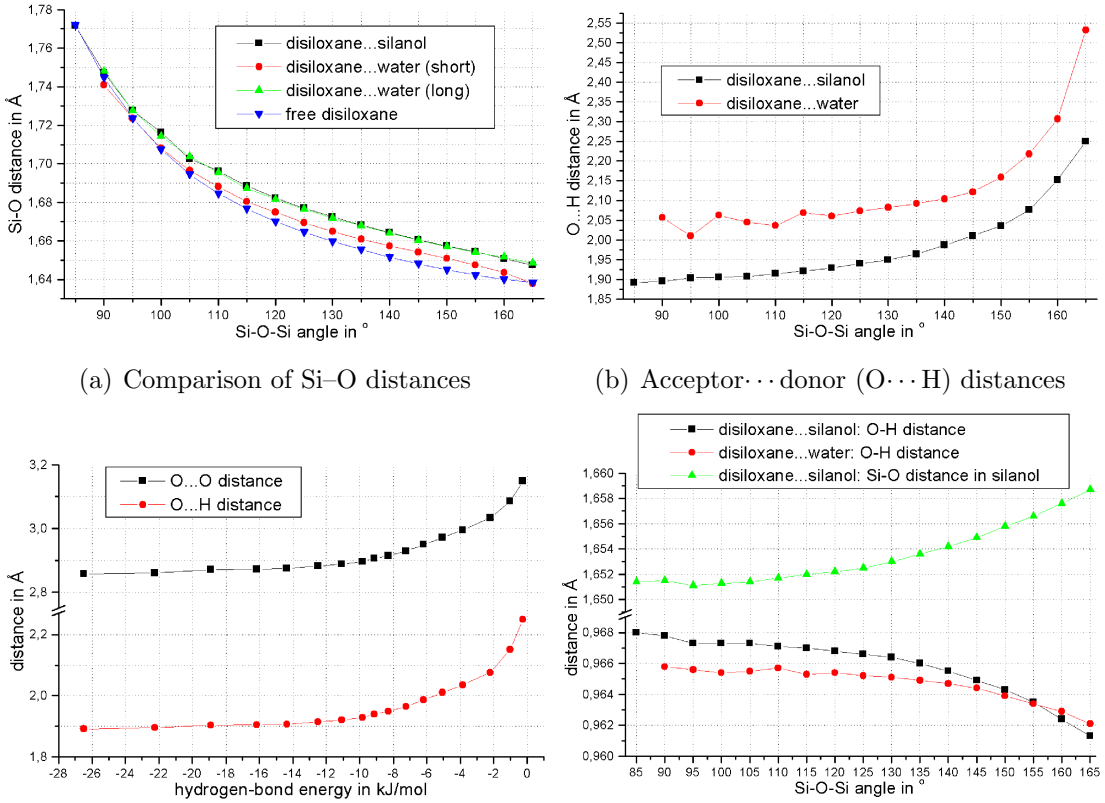

(a) Comparison of Si–O distances

(b) Acceptor···donor (O···H) distances

(c) Acceptor···donor (O···H and O···O) distances vs. E_{HB} in disiloxane···silanol

(d) O–H and Si–O distances in donor molecules silanol/water

Figure 6.6: Bond distances in hydrogen-bonded complexes

angle increases. Moreover, the effect of the formation of the hydrogen bond can be observed: The Si–O bond at any frozen Si–O–Si angle is shortest in free disiloxane, and the Si–O bonds in the hydrogen-bonded complexes elongate. The Si–O bond in disiloxane···water that is further away from the water molecule elongates only a little (referred to as the *short* one) whereas the *long* Si–O bond in disiloxane···water and the Si–O bonds in disiloxane···silanol are affected to the same extent upon hydrogen-bond formation. They elongate by an average of about 0.015 Å.

It has been shown in studies involving different acceptor···silanol complexes [230] that the A···$H_{silanol}$, A···O, O-$H_{silanol}$ and Si–$O_{silanol}$ distances are indicative of hydrogen bonding, and the A···H–O angle is not. This finding is confirmed here: The O···H–O angle in disiloxane···silanol [$(H_3Si)_2O$···$HOSiH_3$] and disiloxane···

water [$(H_3Si)_2O\cdots HOH$] does not correlate with the hydrogen-bond strength, whereas all the mentioned distances in both complexes do as Figure 6.6 shows. If the properties of two different complexes are compared, the Si–O–Si angles are used as common x-coordinate; if two different properties of one complex are compared, the correlation to the hydrogen-bond energy is shown. The relation between E_{HB} and Si–O–Si angles was given in Figure 6.2.

The acceptor$\cdots$donor O$\cdots$H and O$\cdots$O distances in disiloxane$\cdots$silanol [$(H_3Si)_2O\cdots HOSiH_3$] and disiloxane$\cdots$water [$(H_3Si)_2O\cdots HOH$] increase when the hydrogen bond becomes weaker with an increasing Si–O–Si angle (Figures 6.6 (b) and (c)). While in disiloxane$\cdots$silanol both distances are a direct measure of the bond strength (Figure 6.6 (c)), there are uncertainties at small angles in disiloxane$\cdots$water (referred to as category 2 in Chapter 6.1.1). This again demonstrates that the energy hypersurface for small angles in the case of water as donor is much more ambiguous, and the properties much more unstable, than for silanol as donor. That O$\cdots$H and O$\cdots$O distances in disiloxane$\cdots$silanol are much smaller than in disiloxane$\cdots$water, although the silanol molecule is sterically more demanding than the water molecule, also circumstantiates the better donor quality of the silanol group.

The O–H distance in the water molecule decreases when the hydrogen bond becomes weaker with increasing Si–O–Si angle (Figures 6.6 (d)), but this property also belongs to category 2. The O–H distance in the silanol molecule decreases, too, whereas the Si–O distance increases when the hydrogen bond becomes weaker with increasing Si–O–Si angle (Figures 6.6 (d)). The Si–O distance in the silanol molecule is in the range from 1.651 to 1.659 Å, whereas in the siloxane molecule of the disiloxane$\cdots$silanol complex it is in the range from 1.772 to 1.647 Å. This shows that the effect of changing the Si–O–Si angle is much greater than the effect of forming a hydrogen bond, but both are nonetheless detectable. In the cases of the fully relaxed geometries of free disiloxane and free silanol, the Si–$O_{siloxane}$ distance is 1.645 Å, whereas the Si–$O_{silanol}$ distance is 1.660 Å.

6.2 Results of the Topological Analysis of the ED

6.2.1 Bond-Topological Properties of Free Disiloxane

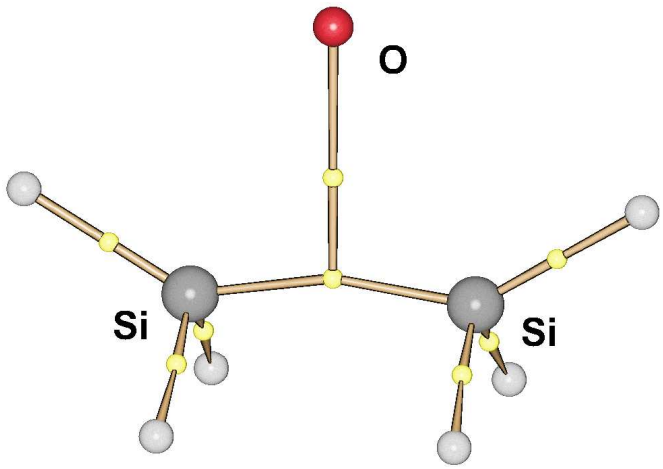

(a) ϕ=55 °, T-type shape of molecular graph

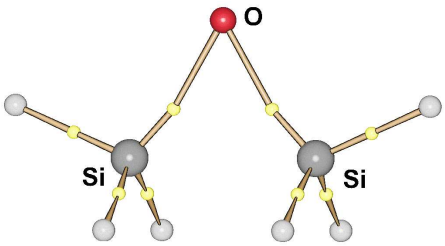

(b) ϕ=70 °, open form of molecular graph, strained Si–O bonds

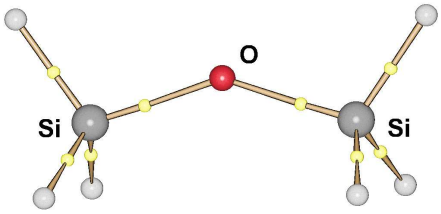

(c) ϕ=145 °, open form of molecular graph, relaxed Si–O bonds

Figure 6.7: Representative molecular graphs of free disiloxane

The molecular graphs of free disiloxane at three representative angles are shown in Figure 6.7. In the hypothetical case of very small Si–O–Si angles (between 50 ° and 60 °), there is a bond-critical point (bcp) between the Si atoms indicating the existence of a Si–Si bond, see Figure 6.7 (a). There are no bcps between Si and O, but one critical point between the bcp of the Si–Si bond and the O atom, giving the molecular graph a T-type shape. This fact shows that there is indeed an interaction between the oxygen atom and the Si–Si bond, but no

Si–O bonds exist. This kind of T-shaped molecular graphs is known for unstable complexes. [232, 233] The O–bcp$_{Si-Si}$ interaction is in the range of very strong hydrogen bonds [234] as the value of the ED and the Laplacian of the ED at the bcp show: for ϕ=50 °, ϱ(O–bcp$_{Si-Si}$)=0.21 eÅ^{-3} and $\nabla^2\varrho$(O–bcp$_{Si-Si}$)=1.1 eÅ^{-5}; for ϕ=55 °, ϱ(O–bcp$_{Si-Si}$)=0.38 eÅ^{-3} and $\nabla^2\varrho$(O–bcp$_{Si-Si}$)=1.0 eÅ^{-5}; for ϕ=60 °, ϱ(O–bcp$_{Si-Si}$)=0.50 eÅ^{-3} and $\nabla^2\varrho$(O–bcp$_{Si-Si}$)=0.1 eÅ^{-5}. The interaction becomes stronger with increasing Si–O–Si angle, but then vanishes by splitting into two bcps for the two Si–O bonds that appear at 65 °.

In Figure 6.5 (a), an initial decrease of the Si–Si bond distance was shown, which might be associated with a stengthening of the bond before it vanishes between ϕ=60 ° and 65 °. But the bond-topological properties show that the bond has the highest ED value at ϕ=50 ° where it is longest (d=2.238 Å, ϱ(Si–Si)=0.60 eÅ^{-3}, $\nabla^2\varrho$(Si–Si)=-3.7 eÅ^{-5}), that it decreases at ϕ=55 ° where the distance decreases, too (d=2.161 Å, ϱ(Si–Si)=0.59 eÅ^{-3}, $\nabla^2\varrho$(Si–Si)=-3.5 eÅ^{-5}), and that it has the lowest value at ϕ=60 ° where the bond is shortest (d=2.139 Å, ϱ(Si–Si)=0.56 eÅ^{-3}, $\nabla^2\varrho$(Si–Si)=-2.8 eÅ^{-5}). For nearly every other known case, the ED at the bcp increases if the bond distance decreases, which is like piling up the ED by shortening the bond. In this case, the ED at the bcp is the more plausible indicator for the bond strength as the delocalization index δ(Si–Si) also decreases from 50 ° towards 65 °(δ(Si–Si)=0.454, 0.328, 0.221, 0.125). The Si–Si bond becomes weaker with increasing Si–O–Si angle before it vanishes between 60 ° and 65 °and only shortens because the geometry of an equilateral triangle has to be fulfilled at 60 °. Beyond 60 °, it quickly lengthens (Figure 6.5 (a)). The small negative value of the Laplacian of the ED at the Si–Si bcp demonstrates that there are significant covalent contributions in the Si–Si bonding interaction.

Figure 6.7 (a) also shows that the Si–Si bond path is bent inwards towards the oxygen atom so that the Si–Si bcp is not located on the direct internuclear Si–Si axis. At the smallest Si–O–Si angle ϕ=50 °, the bond path is longer than the bond distance by only 0.019 Å, at ϕ=55 °, it is longer by 0.028 Å and at ϕ=60 °, the bond path is longer by 0.042 Å. This is an indicator for the fact that the direct Si–Si bond distance shortens by geometrical necessities from ϕ=50 ° to ϕ=60 °. It becomes more strained towards 60 °.

In the PES scan of free disiloxane, the open form of the molecular graph directly replaces the T-type shape between 60 ° and 65 °. The open form is characterised by the existence of two Si–O bonds and no Si–Si bond. Figure 6.7 (b) shows the open form in which the Si–O bonds are highly strained, so that the bond path is

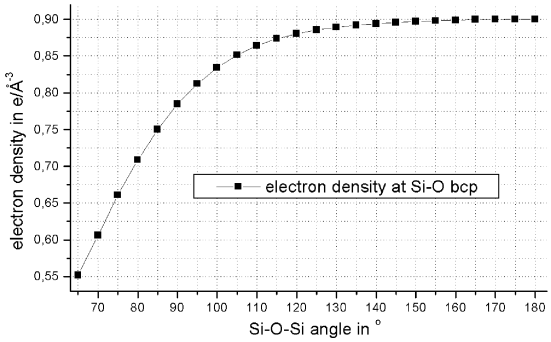

(a) Electron density at Si–O bcps over the complete range of Si–O–Si angles

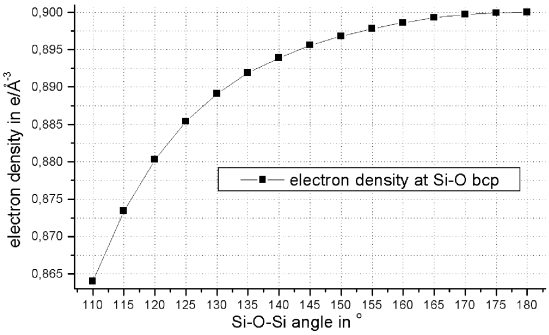

(b) Detail of (a): Electron density at Si–O bcps between ϕ=110 and 180 °

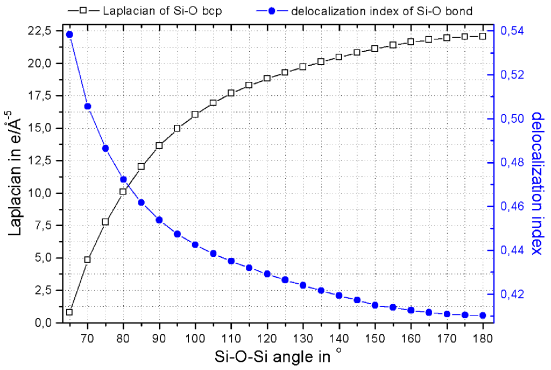

(c) Laplacian of the ED at the Si–O bcps and delocalization index of the Si–O bonds over the complete range of Si–O–Si angles

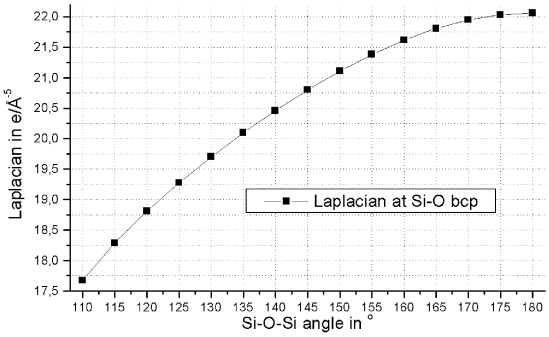

(d) Detail of (c): Laplacian of the ED at the Si–O bcps between ϕ=110 and 180 °

Figure 6.8: Electron density and Laplacian of the ED at the Si–O bcps of free disiloxane as well as delocalization index of the Si–O bonds

bent inwards (between 65 ° and 80 °). Figure 6.7 (c) shows the open form in which the Si–O bonds are not strained (between 85 ° and 180 °). For ϕ=65 °, the bond path is longer by 0.070 Å than the direct internuclear axis, for 80 ° it is 0.010 Å and for 85 ° it is only 0.002 Å. Beyond ϕ=85 °, the difference is smaller than 0.001 Å. Interestingly, the range from ϕ=50 ° to 80 ° is the range in which hydrogen bonding is generally not possible and the range from 85 ° upwards is the range where it is possible. So the sudden change in the bending of the bonds might be a sign for a chemical catastrophe taking place between ϕ=80 ° and 85 ° showing the transition from a hypothetical chemical system to a stable chemical system. However, there is no sudden change in the bond path lengths between ϕ=165 ° and 170 ° indicating a chemical catastrophe between a hydrogen-bonding and a hydrogen-repelling system.

Figure 6.8 shows the development of the bond-topological properties and the delocalization index for the Si–O bonds. The density and the Laplacian at the Si–O bcp increase from ϱ(Si–O)=0.55 eÅ^{-3} and $\nabla^2\varrho$(Si–O)=0.8 eÅ^{-5} at 65 ° to ϱ(Si–O)=0.90 eÅ^{-3} and $\nabla^2\varrho$(Si–O)=22.1 eÅ^{-5} at 180 °. The curves become flat at about 110 ° upwards, but Figures 6.8 (b) and 6.8 (d) make clear that it increases smoothly also for large Si–O–Si angles. The Laplacian being positive on the whole range shows that the Si–O bond is of ionic character in agreement with the ionic bond model. A high degree of ionicity can be found for large Si–O–Si angles that most existing siloxane compounds exhibit. The ionicity is increased upon widening the Si–O–Si angle so that the most ionic situation can be found at ϕ=180 °. However, the fact that the Laplacian adopts smaller values when the Si–O–Si angle decreases until it is close to zero at ϕ=65 ° also suggests that covalent contributions mix into the bond character and become significant at very small Si–O–Si angles. The value of the Laplacian at the bcp mainly helps to learn about the bond character, while the value of the ED at the bcp makes a statement on the bond strength. Thus, it can be concluded that the Si–O bond becomes steadily more ionic and stronger when the Si–O–Si angle increases.
The angular dependence of the delocalization index δ(Si,O) for the Si–O bond is given in Figure 6.8 (c). It supports the findings on the bond character: As δ(Si,O) is significantly smaller than the formal Si–O bond order of 1.0 over the whole range of angles, a predominantly ionic bond character can be found that increases with increasing Si–O–Si angle because δ(Si,O) decreases. At small Si–O–Si angles, δ(Si,O) is higher than 0.5, showing that also covalent bond contributions exist and at large Si–O–Si angles, δ(Si,O) is close to 0.4, showing that the ionicity has its maximum at the linear situation. This means that a relaxed siloxane linkage is highly ionic, but that a strained siloxane linkage exhibits significant covalent contributions.

6.2.2 Valence-Shell Charge Concentrations in Free Disiloxane and in Hydrogen-Bonded Complexes

In order to learn about the hydrogen-bonding acceptor qualities, i.e. the basicity, of the siloxane linkage, it is important to study the location and shape of the oxygen lone pairs. These lone pairs interact with the acidic hydrogen atom of the donor group via negative hyperconjugation (n(O)→ σ*(O–H)) to form the hydrogen

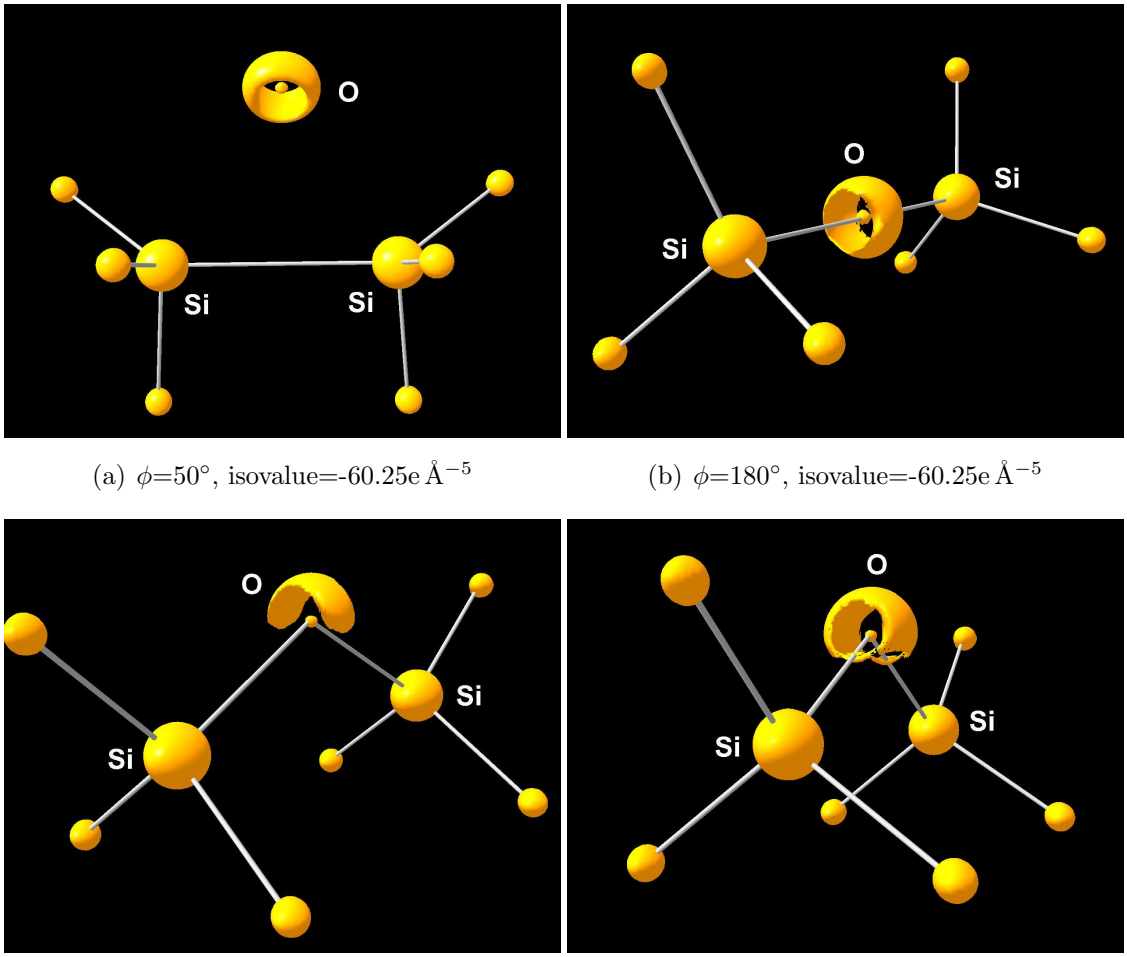

(a) ϕ=50°, isovalue=-60.25e Å^{-5}

(b) ϕ=180°, isovalue=-60.25e Å^{-5}

(c) ϕ=120°, isovalue=-72.30e Å^{-5}

(d) ϕ=120°, isovalue=-60.25e Å^{-5}

Figure 6.9: Laplacian isosurface representations of free disiloxane at representative Si–O–Si angles

Different shapes of the valence-shell charge concentrations (VSCCs) around the oxygen atoms within different chemical systems of $H_3SiOSiH_3$

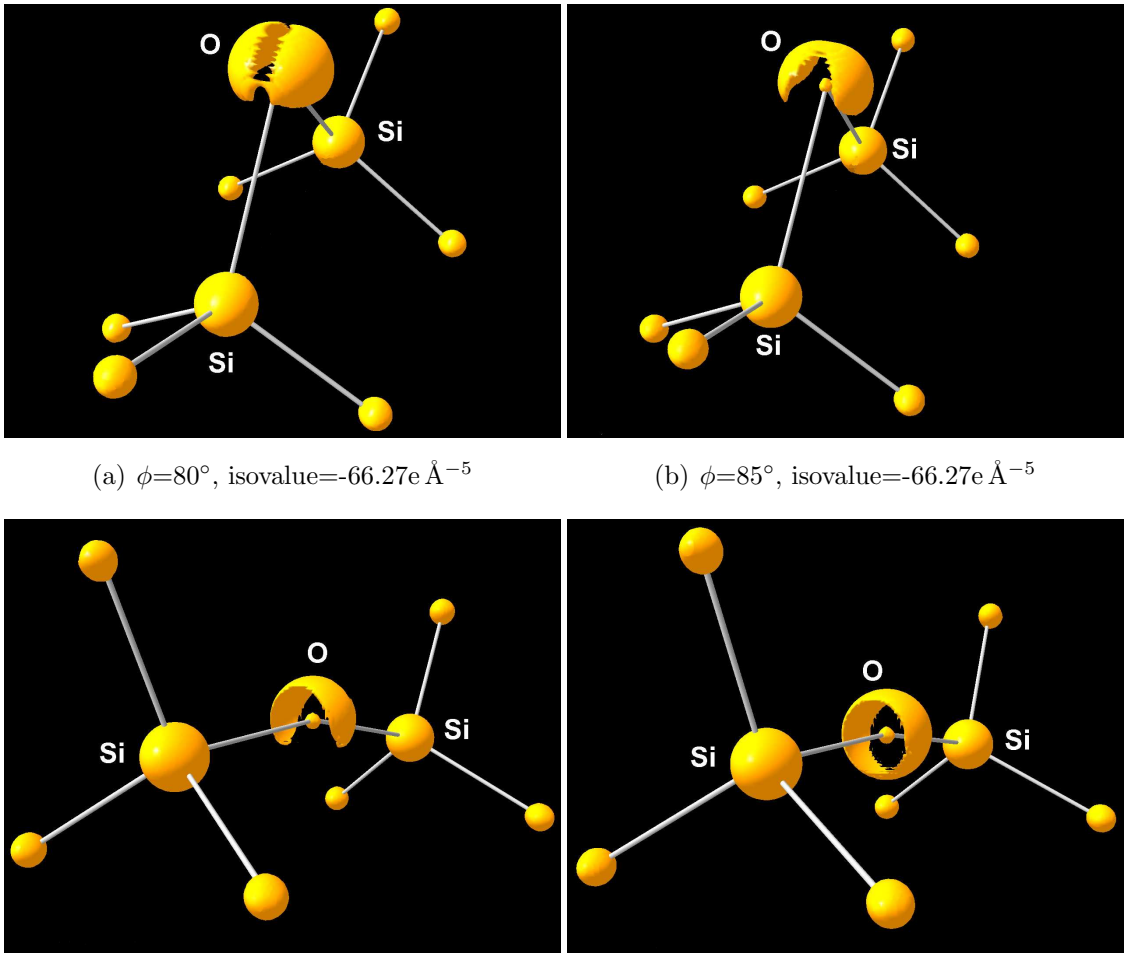

(a) ϕ=80°, isovalue=-66.27e Å^{-5} (b) ϕ=85°, isovalue=-66.27e Å^{-5}

(c) ϕ=165°, isovalue=-62.66e Å^{-5} (d) ϕ=170°, isovalue=-62.66e Å^{-5}

Figure 6.10: Laplacian isosurface representations of free disiloxane at representative Si–O–Si angles

Different shapes of the valence-shell charge concentrations (VSCCs) around the oxygen atoms show chemical catastrophes between different chemical systems of $H_3SiOSiH_3$

bond. In order to enable this n(O)→ σ^*(O–H) interaction, the lone pairs have to be properly concentrated, localised and adjusted towards the hydrogen atom. A qualitative way to examine the lone pairs is to represent them via valence-shell charge concentrations (VSCCs) visible in the Laplacian distribution. Figures 6.9 and 6.10 show three-dimensional Laplacian isosurfaces of free disiloxane at certain isovalues that show the orientation and shape of the lone pairs.

As discussed above, there are three different regions in free disiloxane: between 50 ° and 80 °, hydrogen bonding is not possible; between 85 ° and 165 °, hydrogen bonding is possible; and between 170 ° and 180 °, hydrogen bonding is again not possible. Figures 6.9 (a), (b) and (c) show the extreme example from each region. At ϕ=50 °, the oxygen atom is isolated; there are no Si–O bonds and the lone-pair electrons are delocalised around the equator of the atom in the form of a ring. There is no special concentration of the lone pairs that could selectively be attacked by an electrophilic proton. Hydrogen bonding is not feasible for such a situation. At ϕ=180 °, the situation is similar. Here, the oxygen atom is most strongly bonded to the silicon atoms, but again, the lone-pair electrons are distributed ringlike around the oxygen atom without giving an attacking proton a special position of electron concentration for the attack. The ring is oriented with respect to the cylindrical symmetry of the bond, i.e. it is turned by 90 ° to the situation at ϕ=50 °. At ϕ=120 °, where hydrogen bonding is observed not only within the PES scans but also in crystal structures of model compounds (compare siloxanol (**1**) and trisilo (**2**)), the lone-pair electrons are concentrated above the oxygen atom in the form of a cap. Even if the isovalue is decreased, the lower side of the oxygen atom is never enclosed (see Figure 6.9 (d)) and the cap-like shape is preserved. At lower isovalues, VSCCs for the Si–O bonds appear.

Figure 6.9 illustrates that the shape of the lone pairs coincides with the observation of possible hydrogen bonding. But it is still an open question what happens between ϕ=80 ° and 85 ° to cause a sudden change in the oxygen's basicity even though the hydrogen-bond energy has its maximum value at ϕ=85 °. In the same context, the change between ϕ=165 ° and 170 ° might be understood. It will be shown in the following that a catastrophe in the topology of the ED takes place between the Si–O–Si angles in question that involves the chemical process of re-orientation of the lone-pair electrons. These catastrophes represent the transition from one chemical system of free disiloxane $H_3SiOSiH_3$ - as defined by catastrophe theory applied to chemistry [226] - to another one with a different chemical behaviour. In these terms, it can also be understood why not only the hydrogen-

bonding ability but also different electronical properties undergo sudden changes between the Si–O–Si angles in question (compare for example the bending of the bond paths).

Figures 6.10 (a) and (b) compare the situation before and after the chemical catastrophe, i.e. the situations at ϕ=80 ° and 85 °. At ϕ=80 °, the shape of the VSCC is still more similar to the ring at ϕ=50 ° because the surface is closed at the sides near to the equator of the oxygen atom but it is open at the upper side. At ϕ=85 °, there is a totally different shape of the VSCC that is already very similar to the cap at ϕ=120 °. This cap-like shape does not change as long as hydrogen-bonding is possible and can therefore also be found at ϕ=165 ° (Figure 6.10 (c)). Then, there is the next sudden change of the shape of the VSCC towards ϕ=170 ° (Figure 6.10 (d)) yielding the ringlike shape of the VSCC that can be found at all angles up to the linear geometry (Figure 6.9 (b)).

In Figure 6.11, the Laplacian isosurfaces of the complexes disiloxane$\cdots$silanol and disiloxane$\cdots$water are depicted at ϕ=120 °. The shapes of the oxygens' VSCCs do not change upon hydrogen-bond formation. It is clearly visible that the hydrogen atom points towards the middle or the top of the cap-like VSCC, forming a symmetrical complex. It can be assumed that none of the two lone pairs is favoured, but the interaction takes place with the central region of negative Laplacian distribution, i.e. electron concentration. This is true also in the case of disiloxane$\cdots$water, where the water molecule is shifted towards one side of the disiloxane molecule (towards the long Si–O bond) but the hydrogen atom nevertheless points towards the middle or the top of the cap-like VSCC of the siloxane's oxygen atom. If there was a hole in the VSCC just at this very point where the hydrogen atoms point to as it is the case between ϕ=50 ° and 80 °, the hydrogen bond could not be formed. Moreover, the shape of the VSCCs at the silanol's and water's oxygen atoms, which are very good hydrogen-bond acceptors themselves, shows that a cap is the preferred shape.

The application of the theory of chemical catastrophes [226] to the VSCCs explains adequately the chemical behaviour of the siloxane linkage concerning hydrogen bonding and basicity. By means of the analysis of the ELI-D (see Chapter 6.3), the qualitative results will be supported. Additionally, they will be substantiated by quantitative results, for which the ELI-D is a much better tool than the Laplacian of the ED.

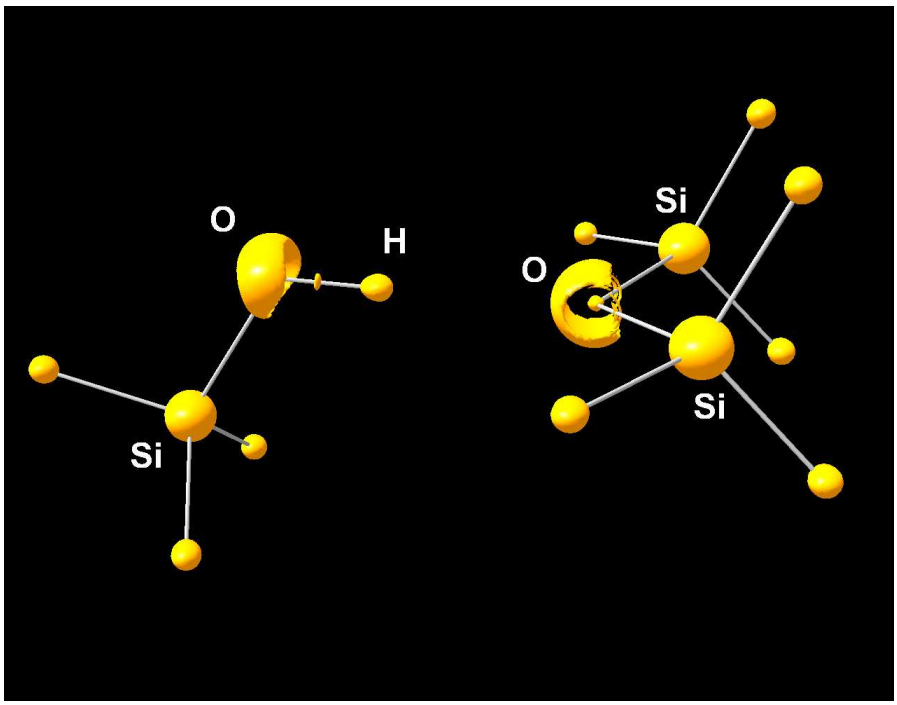

(a) ϕ=120°, isovalue=-61.45e Å^{-5}

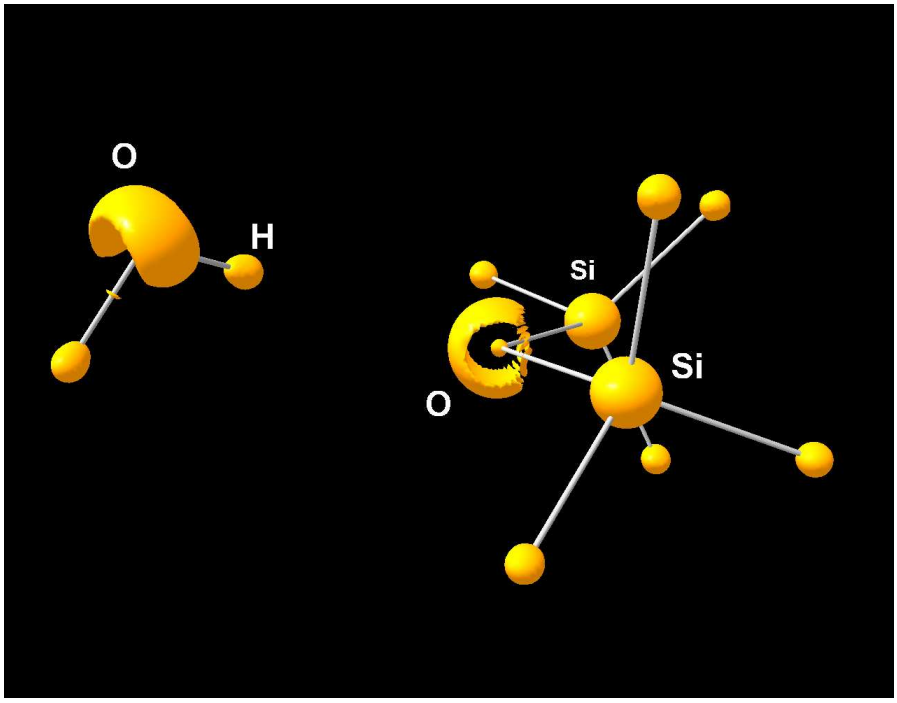

(b) ϕ=120°, isovalue=-60.85e Å^{-5}

Figure 6.11: Laplacian isosurface representations of hydrogen-bonded complexes at representative Si–O–Si angles

6.2.3 Bond-Topological Properties of Hydrogen-Bonded Complexes

Figure 6.12 shows the curves of the electron density and the Laplacian at the Si–$O_{siloxane}$ bcp as well as the delocalization index of Si–$O_{siloxane}$ for the hydrogen-bonded complexes compared to free disiloxane. In the complexes, the trend is the same as for free disiloxane, i.e. the Si–O bonds become more ionic and stronger when the Si–O–Si angle increases towards linearity. As already seen for the Si–O distances (Figure 6.6 (a)), the Si–$O_{siloxane}$ bonds in disiloxane$\cdots$silanol and the long Si–$O_{siloxane}$ bond in disiloxane$\cdots$water are most affected upon hydrogen-bond formation. As an average value, their Si–$O_{siloxane}$ bond properties are lowered by $0.03\,e\text{Å}^{-3}$, $1.0\,e\text{Å}^{-5}$ and 0.15 compared to free disiloxane, which is caused by the formation of the hydrogen bond. The variation of the Si–$O_{siloxane}$ bond properties of the short bond in the complex disiloxane$\cdots$water is only half the amount.

It has been shown in many publications ([230, 235, 236]) that the value of the electron density and the Laplacian at the O$\cdots$H bcp are a measure of the hydrogen-bond strength. Figure 6.13 shows that the O$\cdots$H hydrogen bond in disiloxane$\cdots$silanol is stronger than in disiloxane$\cdots$water, since the value of the ED at the bcp as well as the Laplacian is higher for disiloxane$\cdots$silanol over the whole range of angles. In the region from ϕ=85 ° to about 135 °, the curves are flat, and especially for disiloxane$\cdots$water, the curves belong to category 2, i.e. the trend for small angles is ambiguous.

However, the variation for small angles is not large so that a classification of the hydrogen bonds can nevertheless be made: For disiloxane$\cdots$silanol, ϱ(O$\cdots$H) varies from $0.18\,e\text{Å}^{-3}$ (ϕ=85 °) to $0.16\,e\text{Å}^{-3}$ (ϕ=135 °) and $\nabla^2\varrho$(O$\cdots$H) varies from $2.0\,e\text{Å}^{-5}$ (ϕ=85 °) to $1.8\,e\text{Å}^{-5}$ (ϕ=135 °). These values are typical for strong hydrogen bonds compared to other sets of hydrogen bonds [230, 234] or within the criteria of Koch and Popelier [237]. The hydrogen bond in disiloxane$\cdots$water is still of considerable strength owing to these criteria as the values vary between ϱ(O$\cdots$H)=0.14 to $0.12\,e\text{Å}^{-3}$ and $\nabla^2\varrho$(O$\cdots$H)=1.8 to $1.6\,e\text{Å}^{-5}$ from ϕ=90 to 135 °. Beyond about ϕ=135 °, the curves drop off significantly to show how the hydrogen bond becomes weaker at larger Si–O–Si angles. The delocalization index δ(O,H) for the O$\cdots$H hydrogen bonds does not show any correlation to the hydrogen-bond stength, and thus a curve for this property is not shown.

The bond-topological properties of bonds in the donor group that are further apart from the hydrogen atom are affected upon hydrogen-bond formation, too, and their

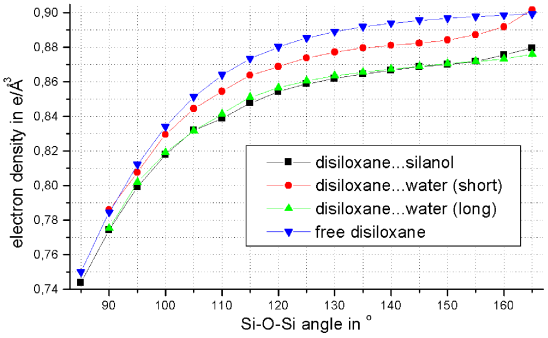

(a) Electron density at Si–O bcps

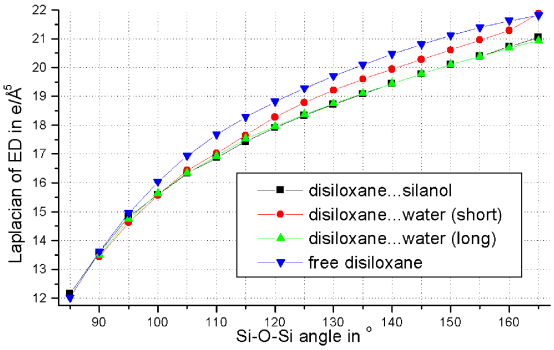

(b) Laplacian of the ED at Si–O bcps

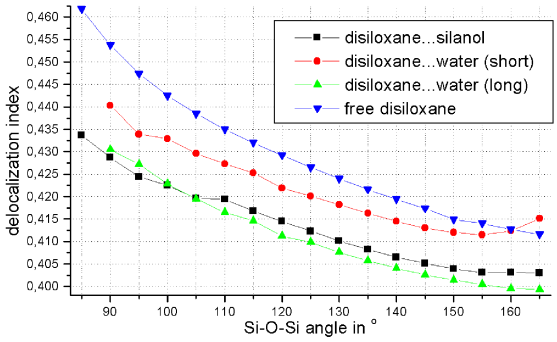

(c) Delocalization index of the Si–O bonds

Figure 6.12: Electron density and Laplacian of the ED at the Si–O bcps as well as delocalization index of the Si–O bonds; comparison between free disiloxane and hydrogen-bonded complexes

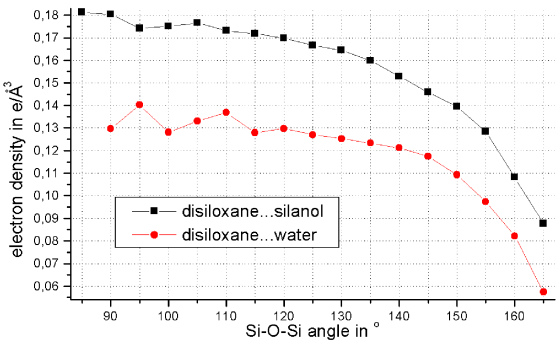

(a) Electron density at O···H bcps

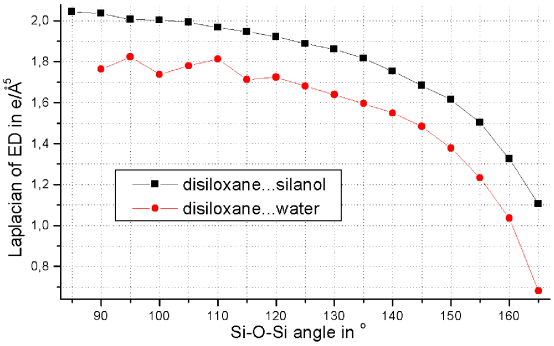

(b) Laplacian of the ED at O···H bcps

Figure 6.13: Electron density and Laplacian of the ED at the bcps of the acceptor···donor (O···H) bonds in hydrogen-bonded complexes

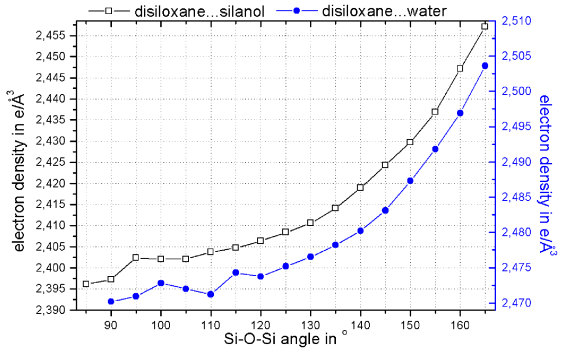

(a) Electron density at the O–H bcps in silanol/water

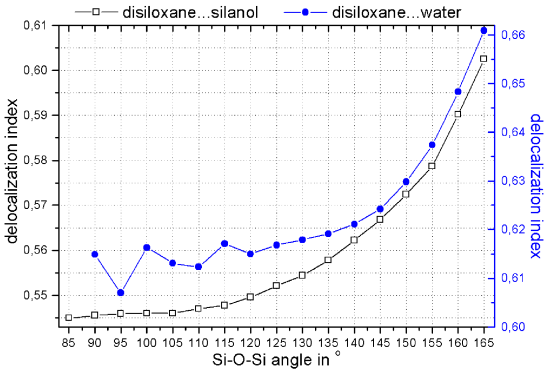

(b) Delocalization index of the O–H bonds in silanol/water

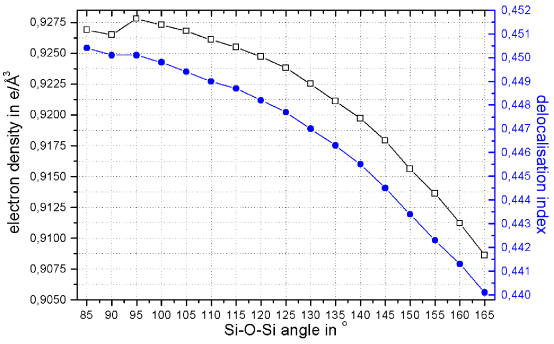

(c) Electron density and delocalization index of the Si–O bond in silanol

Figure 6.14: Electron density at the bcps and delocalization index of the O–H and Si–O bonds in silanol/water of hydrogen-bonded complexes

changes can additionally be examined to study the hydrogen-bond strength. This applies to the O–H bonds in silanol and water as well as to the Si–O bond in silanol. Figure 6.14 shows that ϱ(O–H) in silanol and water, δ(O,H) for the O–H bond in silanol and water as well as ϱ(Si–O) and δ(Si,O) in silanol correlate with the hydrogen-bond strength that decreases with increasing Si–O–Si angles, while the Laplacian in each case is not indicative (curves not shown). The stronger the hydrogen bond is, the lower is the value of the ED at the bcp of the O–H bond in the donor group (Figure 6.14 (a)). This means that the O–H bond becomes weaker if the hydrogen bond becomes stronger, which is consistent with the chemical picture of acidity of the proton that is being detached from its donor atom upon hydrogen-bond formation. This effect is more pronounced for disiloxane$\cdots$silanol (left y-axis) than for disiloxane$\cdots$water (right y-axis), as the hydrogen bond in disiloxane$\cdots$silanol is stronger over the whole range of angles. For the strongest hydrogen bond in disiloxane$\cdots$silanol, ϱ(O–H) is only 2.396 eÅ^{-3}, whereas for the weakest hydrogen bond, ϱ(O–H) is already 2.457 eÅ^{-3}, which is closest to the value of ϱ(O–H)=2.483 eÅ^{-3} obtained from the free silanol molecule after relaxed geometry optimisation. For disiloxane$\cdots$water, the strongest hydrogen bond possesses the value ϱ(O–H)=2.470 eÅ^{-3}, whereas the weakest has ϱ(O–H)=2.504 eÅ^{-3} (ϱ(O–H)=2.515 eÅ^{-3} for free water after relaxed geometry optimisation).
The delocalization index for the O–H bond in silanol and water (Figure 6.14 (b) supports this finding by a corresponding curve progression. Figure 6.14 (c) shows that the effect of the hydrogen-bond formation is still clearly observeable in the Si–O bond in silanol. The curve progressions of the electron density at the Si–$O_{silanol}$ bcp and the delocalization index $\delta(Si,O)$ in silanol both suggest that the Si–O bond becomes stronger upon hydrogen-bond formation because ϱ(Si–O) increases from 0.909 to 0.927 eÅ^{-3} and $\delta(Si,O)$ from 0.440 to 0.450 from the weakest (ϕ=165 °) to the strongest (ϕ=85 °) hydrogen bond. The corresponding values in free silanol after relaxed geometry optimisation are ϱ(Si–O)=0.906 eÅ^{-3} and $\delta(Si,O)$=0.436.

6.2.4 Atomic Properties of Free Disiloxane and Hydrogen-Bonded Complexes

An increase of the ionicity of the Si–O bond with an increasing Si–O–Si angle must be accompanied by an increase of the atomic charge separation. Figure 6.15 shows that the charge separation in the case of free disiloxane indeed increases with

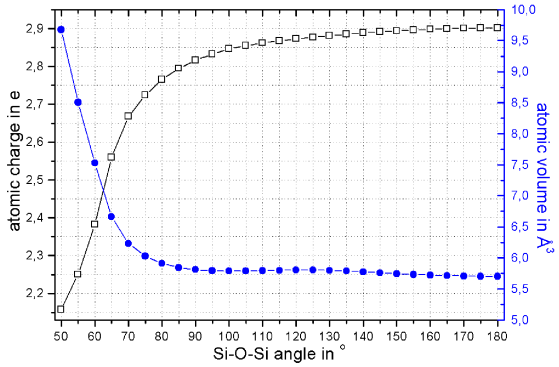

(a) Atomic charge Q_{001} and volume V_{001} of the Si atoms over the complete range of Si–O–Si angles

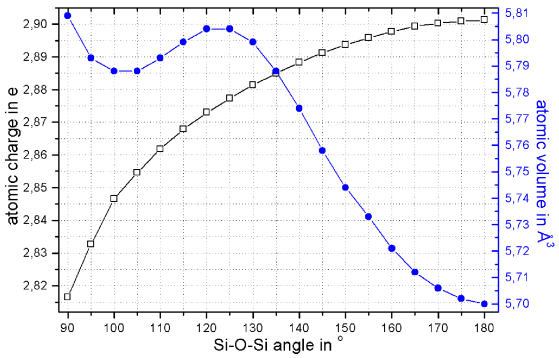

(b) Detail of (a): Atomic charge Q_{001} and volume V_{001} of the Si atoms between ϕ=90 ° and 180 °

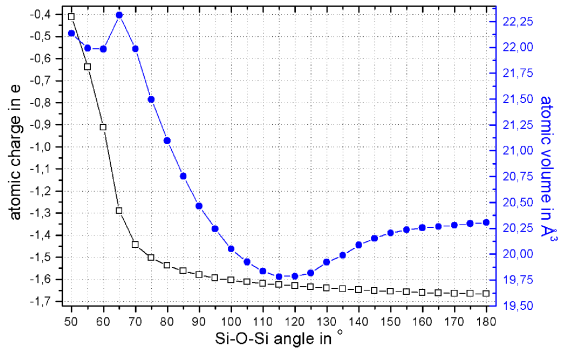

(c) Atomic charge Q_{001} and volume V_{001} of the O atoms over the complete range of Si–O–Si angles

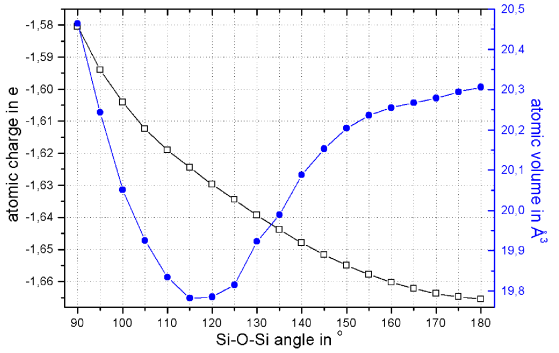

(d) Detail of (a): Atomic charge Q_{001} and volume V_{001} of the O atoms between ϕ=90 ° and 180 °

Figure 6.15: Atomic properties of free disiloxane

increasing Si–O–Si angle: The silicon atoms become more positive and the oxygen atom more negative. At ϕ=50 °, the silicon atoms are charged by Q_{001}(Si)=2.16 e, but the charge increases quickly to Q_{001}(Si)=2.80 e at ϕ=85 °. At ϕ=180 °, the curve has its maximum value of Q_{001}(Si)=2.90 e. For free disiloxane after relaxed geometry optimisation, the charge is Q_{001}(Si)=2.89 e. The curve shape for the oxygen atom's charge is very similar. At ϕ=50 °, the oxygen atom is charged by only Q_{001}(O)=-0.41 e, but the negative charge increases quickly to Q_{001}(O)=-1.56 e at ϕ=85 °. At ϕ=180 °, the curve has its minimum value of Q_{001}(O)=-1.67 e. For free disiloxane after relaxed geometry optimisation, the charge is Q_{001}(O)=-1.66 e. The increase of the charge separation explains the shortening of the Si–O bonds with increasing Si–O–Si angles due to stronger Coulomb interactions, which in

turn explains the increase of the density at the Si–O bcps (see above).

Figure 6.15 also shows the progression of the atomic volumes against the Si–O–Si angle. It is obvious that there is no correlation between atomic charge and atomic volume. For the silicon atom, the volume decreases while the positive charge increases as it is intuitively expected (from $V_{001}(Si)$=9.7 Å^3 at ϕ=50 ° to $V_{001}(Si)$=5.7 Å^3 at ϕ=180 °), but between ϕ=100 ° and 125 °, it surprisingly increases even though the charge still increases smoothly in this region, too. This phenomenon can only be explained together with the curve progression of the oxygen atom. For the oxygen atom, the values run against intuition, as the oxygen atom loses volume from ϕ=50 ° ($V_{001}(O)$=22.1 Å^3) to ϕ=180 ° ($V_{001}(O)$=20.3 Å^3) although it becomes significantly more negatively charged. From ϕ=70 ° to 115 °, there is a dramatic volume loss; beyond ϕ=115 °, the volume increases again towards 180 °.

One possible explanation is the change of the geometry of free disiloxane from a situation at very small angles where the oxygen atom is isolated or only weakly bound to the Si atoms, i.e. where the space opposite to the Si–Si fragment is large (see Figures 6.7 (a) and (b)), to a situation at larger Si–O–Si angles where the oxygen atom is more strongly bound by the two adjacent Si atoms, and therefore restricted in the volume to fill out (Figure 6.7 (c)). It was shown by many properties that the geometry changes are severe for small Si–O–Si angles in the range from ϕ=50 ° to 115 ° (compare Figures 6.5 and 6.8), but that these changes are moderate for the range from ϕ=115 ° to 180 °. Therefore, the geometry changes from ϕ=50 ° to 115 ° can be made responsible for the volume loss. In turn, in the range where the geometry changes do not dominate, the increase of negative charge causes a volume growth. The point of inflexion in the curve of the silicon atoms' volumes agrees with the minimum of the curve of the oxygen volumes, so that it can be assumed that the change of the oxygen atom's volume and shape influences the silicon atoms. In general, this means that the progression of the atomic charges is driven by the change of the bond character from significant covalent contribution to more and more solely ionic character, but the progression of the volumes is overruled in some regions by the geometrical conditions upon Si–O–Si angle variation.

The atomic properties $Q_{001}(Si)$, $Q_{001}(O)$ and $V_{001}(Si)$ in the disiloxane group in disiloxane$\cdots$silanol and disiloxane$\cdots$water are not indicative of hydrogen bonding. No significant charge transfer from the acceptor towards the donor group or vice

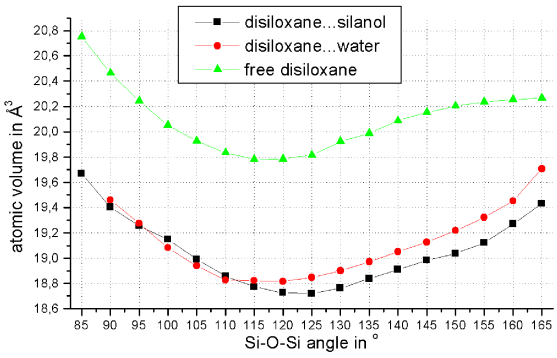

(a) Comparison of atomic volumes V_{001} of the O atom in siloxane

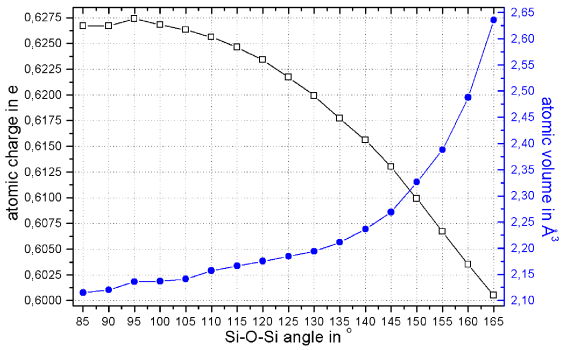

(b) Atomic charge Q_{001} and volume V_{001} of the donor H atom in silanol

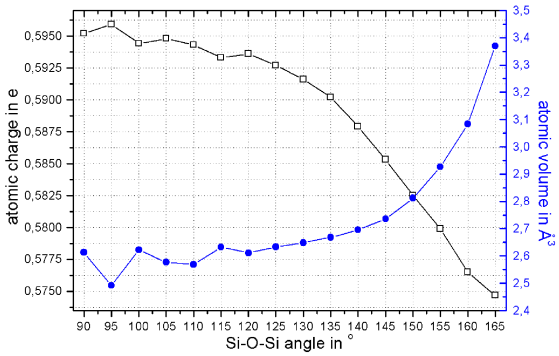

(c) Atomic charge Q_{001} and volume V_{001} of the donor H atom in water

Figure 6.16: Atomic properties of hydrogen-bonded complexes

versa can be found. In contrast, the atomic volume $V_{001}(O)$ of the oxygen acceptor atom is significantly affected upon hydrogen-bond formation, Figure 6.16 (a): The curves for disiloxane$\cdots$silanol and disiloxane$\cdots$water are shifted by a constant difference of about 1 Å^3 towards smaller volumes at each Si–O–Si angle. This also means that $V_{001}(O)$ cannot be referred to as a measure of the hydrogen-bond strength upon variation of the Si–O–Si angle because the shift is constant. There is also no significant difference in the oxygen's atomic volumes between disiloxane$\cdots$silanol and disiloxane$\cdots$water, so that the different hydrogen-bond strengths between the two complexes also cannot be detected in this property.

In contrast to the oxygen atom, the atomic volume of the hydrogen atom of the donor group is a measure of the hydrogen-bond strength. In both complexes, the volume decreases when the hydrogen bond becomes stronger towards smaller

Si–O–Si angles (Figures 6.16 (b) and (c)). In disiloxane$\cdots$silanol, $V_{001}(H)$ varies from 2.12 Å^3 for the strongest hydrogen bond at ϕ=85 ° to 2.64 Å^3 in the weakest hydrogen bond at ϕ=165 °; in disiloxane$\cdots$water, $V_{001}(H)$ varies from 2.61 Å^3 for the strongest hydrogen bond at ϕ=90 ° to 3.37 Å^3 in the weakest hydrogen bond at ϕ=165 °. In free silanol from relaxed geometry optimisation, $V_{001}(H)$ equals 3.19 Å^3, and in free water from the same procedure, $V_{001}(H)$ equals 3.42 Å^3. This means that the hydrogen atom's volume also decreases upon hydrogen-bond formation by a maximum of ΔV_{001}=1 Å^3. The volume loss of both partners of the hydrogen bond, acceptor oxygen and donor hydrogen, can be understood as a mutual penetration of these atoms as included in the hydrogen-bond criteria of Koch and Popelier. [237]

When the hydrogen bond becomes stronger with decreasing Si–O–Si angles, the decrease of the atomic volumes is accompanied by an increase of the atomic charges, as Figures 6.16 (b) and (c) show. This charge increase also correlates with the hydrogen-bond strength even though it is as small as 0.02 e from ϕ=165 ° to 85 ° for both complexes. Free silanol exhibits a charge of $Q_{001}(H)$=0.60 e and free water $Q_{001}(H)$=0.57 e. As the value for the weakest hydrogen bond for each is still larger, a general charge increase of the donor hydrogen atom upon hydrogen-bond formation can be detected.

In contrast to the bond-topological properties, atomic properties in the donor groups further away from the hydrogen bond are unaffected for disiloxane$\cdots$silanol. For disiloxane$\cdots$water, there is at least the trend that the oxygen atom in water becomes more negatively charged when the Si–O–Si angle becomes smaller and the hydrogen bond becomes stronger (see Table A.23).

6.3 Results of the Topological Analysis of the ELI-D

6.3.1 Topology of the ELI-D of Free Disiloxane

The ELI-D distribution was calculated for all model compounds of the PES scans and topologically analysed. As there is one attractor with its corresponding basin for each bond and each lone pair, the bonding situation in terms of the ELI-D can be compared to the one in terms of the QTAIM of the ED where there is one attractor for each atom and one saddle point (critical point) for each bond (see

Figure 6.7). For free disiloxane, the ELI-D localisation-domain representations in Figures 6.17 and 6.18 depict the bonding situations in terms of ELI-D. Each irreducible localisation domain (i.e. there is only one attractor under the surface) stands for one ELI-D basin. All bonds (disynaptic valence basins V_2) are represented by irreducible localisation domains. The oxygen lone pairs (monosynaptic valence basins V_1) are represented by reducible localisation domains (i.e. there is more than one attractor under the surface, so that the isosurface encloses space belonging to different basins). The labelling of the attractors (V_1(O)) shows how many attractors belong to the reducible domain and where they are approximately located under the surface. Isovalues around ELI-D=1.5 are chosen that are suited to depict the regions of maximum electron localisation. These regions give the best possible impression of the bonding situations.

Identical to the QTAIM of the ED of free disiloxane, there is no Si–O bond at very small Si–O–Si angles but a Si–Si bond instead. In contrast to the QTAIM, this bonding situation prevails from ϕ=50 ° to 70 °, and the Si–O bonds do not form until ϕ=85 °. At ϕ=75 ° and 80 °, there are neither Si–O bonds nor a Si–Si bond. Between ϕ=85 ° and 180 °, there are two Si–O bonds and no Si–Si bond.

In terms of the ELI-D or the ELF, a chemical catastrophe is defined by the change of the number of attractors and thus bonding features indicating the transition from one chemical system to another. [170, 227] This again involves the chemical process of reorientation of electrons as observed for the Laplacian of the ED (see above). One chemical system is found between ϕ=85 ° and 165 ° in which two Si–O bonds and two oxygen lone pairs exist, each indicated by an attractor in the ELI-D. This bonding situation corresponds to the classical Lewis picture for the disiloxane molecule. In this chemical system, hydrogen bonding is generally possible. Figures 6.17 (c) and (d) as well as 6.18 (a) and (b) show the localisation domains in this chemical system for ϕ=95 °, 120 °, 150 ° and 165 °. Two irreducible domains for V_2(Si,O) are found, and one reducible domain for the two oxygen lone pairs V_1(O). The lone pairs are situated above the oxygen atom in the form of a cap as already found for the Laplacian of the ED (compare Figure 6.9 (c) and (d) as well as Figure 6.10 (b) and (c)). That means that the lone pair electrons are localised above the oxygen atom in a way to allow and guide an attack of an electrophilic proton during hydrogen-bond formation.

Between ϕ=165 ° and 170 °, another attractor for the oxygen lone-pair electrons appears that is situated below the oxygen atom (see Figure 6.18 (c)). This chemical catastrophe leads to a different chemical system (ϕ=170 ° to 180 °) with two Si–O

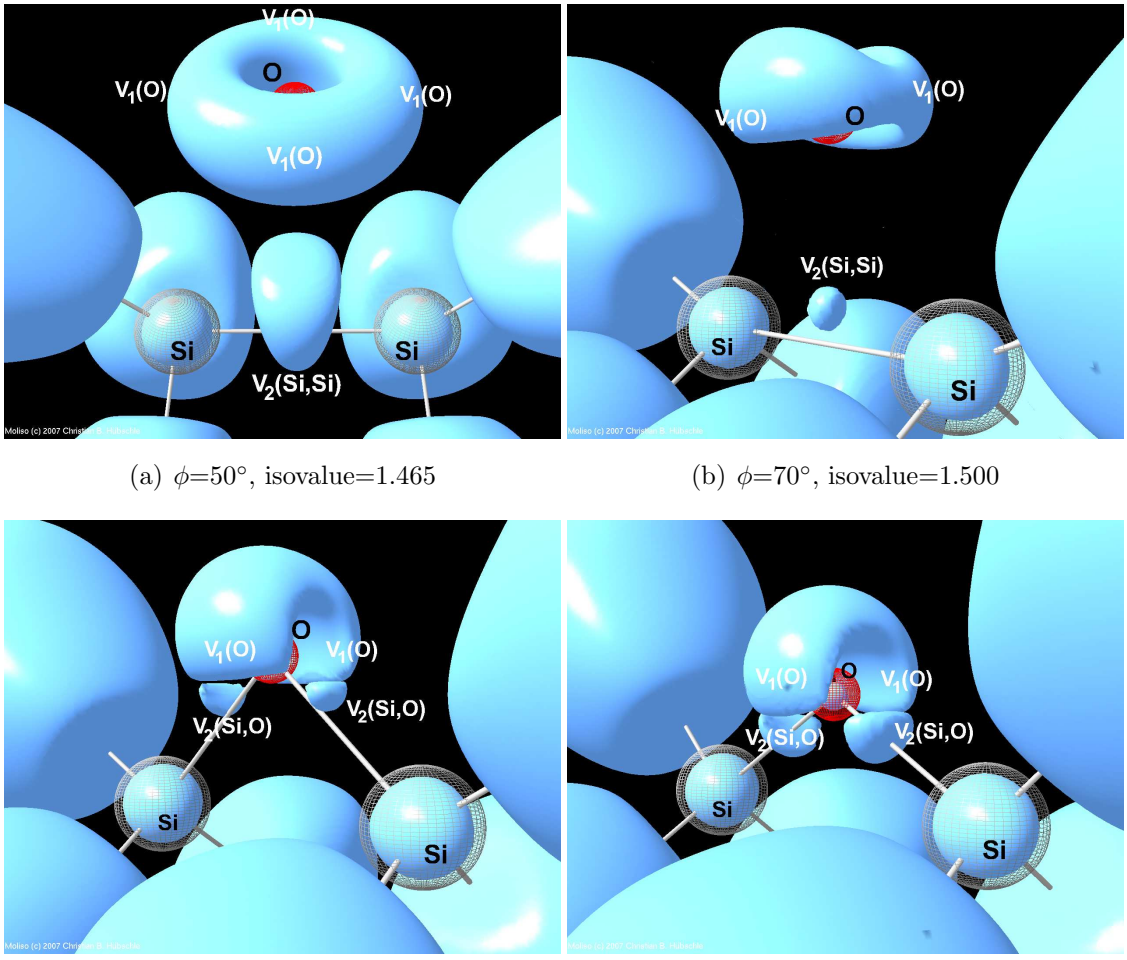

(a) ϕ=50°, isovalue=1.465

(b) ϕ=70°, isovalue=1.500

(c) ϕ=95°, isovalue=1.467

(d) ϕ=120°, isovalue=1.470

Figure 6.17: ELI-D localisation-domain representations of free disiloxane at representative angles

Different shapes of the localisation domains and different numbers of basins define the different chemical systems of $H_3SiOSiH_3$, chemical catastrophe between ϕ=80° and 85° is graphically more obvious by looking at the differences between ϕ=70° and 95° inbetween which massive electronic reorientation takes place, locations of attractors under the surfaces are marked

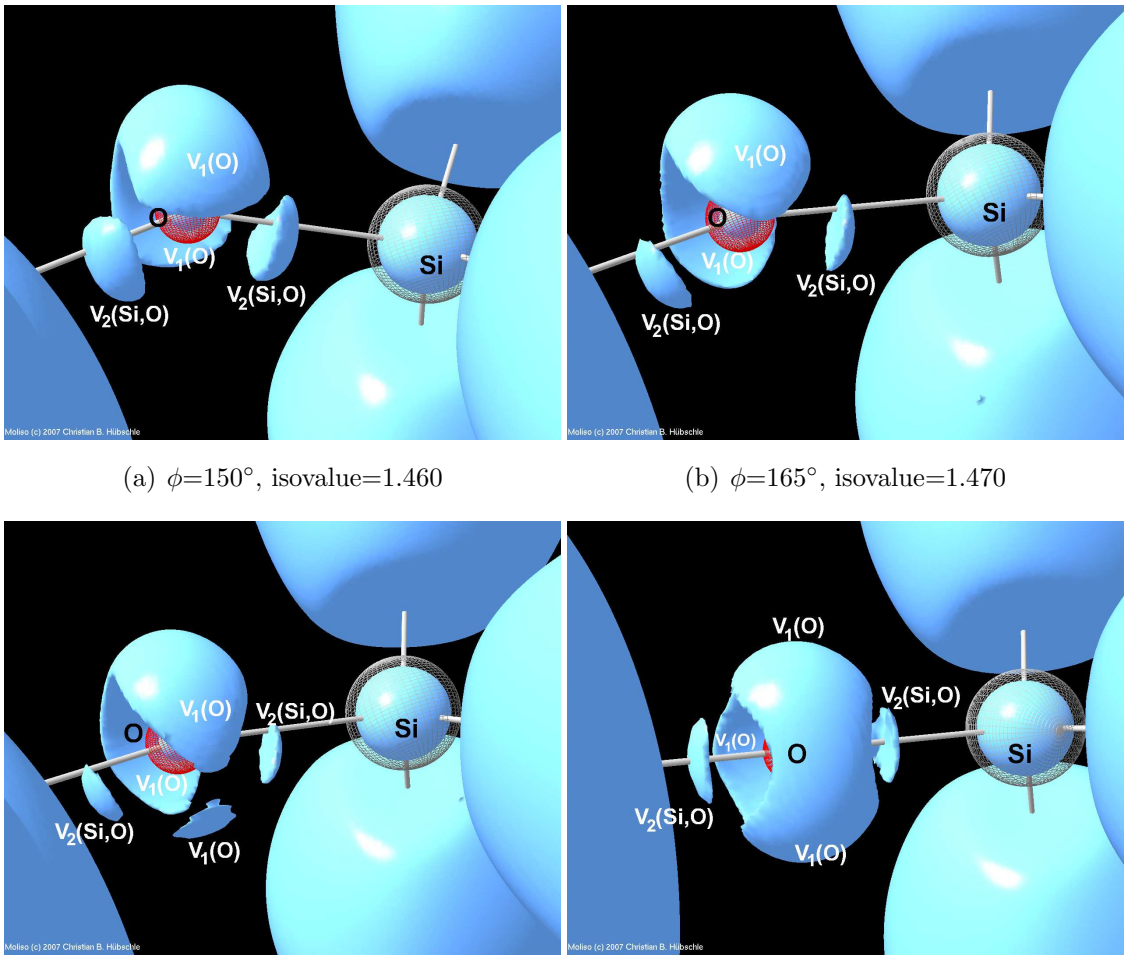

(a) ϕ=150°, isovalue=1.460

(b) ϕ=165°, isovalue=1.470

(c) ϕ=170°, isovalue=1.470

(d) ϕ=180°, isovalue=1.465

Figure 6.18: ELI-D localisation-domain representations of free disiloxane at representative angles

Different shapes of the localisation domains and different numbers of basins define the different chemical systems of $H_3SiOSiH_3$, chemical catastrophe between ϕ=165° and 170° is obvious, locations of attractors under the surfaces are marked

bonds but three lone-pair basins. The expansion of the space of the lone pairs towards the lower side of the oxygen atom provides a straightforward explanation for the fact that hydrogen bonding is not feasible in this region anymore. For the Laplacian of the ED, it was discussed (compare Figures 6.9 (b) and 6.10 (d)) that there is no pronounced concentration of the lone-pair electrons anymore that could selectively be attacked by a proton. Here, localisation of electrons is made visible, but the same argumentation holds: There is no longer a pronounced localisation of the lone-pair electrons to guide an electrophilic attack. This can best be seen by the formation of a torus or ring around the oxygen atom at ϕ=180 °. Three attractors can unambiguously be found also in the case of the torus at ϕ=180 °, because the three-fold symmetry caused by the substitution pattern (three hydrogen atoms in eclipsed conformation) is reflected in the toroidal shape.

For ϕ=50 °, it is not staightforward to locate the attractors as there is only a weak gradient of the ELI-D values indicating delocalisation of the electrons within this ringlike isosurface. Four attractors are present that are plotted in Figure 6.17 (a). For ϕ=55 ° to 80 °, two attractors V_1(O) are found. The shape of the localisation domain at ϕ=70 ° in Figure 6.17 (b) with two swellings depicts this finding. Similar to the Laplacian isosurfaces (compare Figures 6.9 (a) and 6.10 (a)), this ringlike shape of the localisation domains explains why hydrogen bonding is not possible in this region.

The region from ϕ=50 ° to 80 ° cannot be referred to as one chemical system as there are a few changes in the number of attractors (firstly: from four attractors V_1(O) at ϕ=50 ° to two attractors V_1(O) at ϕ=55 °; secondly: from one attractor for the Si–Si bond at ϕ=70 ° as depicted in Figures 6.17 (a) and (b) to no bond attractors at all). However, in this region (ϕ=50 ° to 80 °) the same explanation for the fact that hydrogen bonding is generally not possible holds (ringlike shape of localisation domains), and this region can clearly be distinguished from the next chemical system (ϕ=85 ° to 165 °) by the chemical catastrophe of the appearance of the attractors of the Si–O bonds between ϕ=80 ° and 85 °. Therefore, the region from ϕ=50 ° to 80 ° will nonetheless be referred to as a single chemical system hereafter.

It is not common practice to draw a molecular graph from the locations of the ELI-D attractors as it is done within the QTAIM analysis of the electron density. However, it is interesting to compare the locations of the ELI-D attractors of the Si–O bonds with the locations of the bcps. A strained Si–O bond for small

Si–O–Si angles is characterised by a bond path that is bent inwards in the molecular graph, i.e. the bcps are shifted inwards (Figure 6.7 (b). In contrast, the Si–O bond attractors in the ELI-D are shifted outwards, so that the maximum localisation of bond electrons is located outwards the internuclear axis (Figure 6.17 (c). This means that bond strain for small angles is detectable in both ED and ELI-D, but it manifests itself in two different ways. At ϕ=120 °, the bcps as well as the ELI-D attractors of the Si–O bond are located on the internuclear axis (Figure 6.17 (d). Surprisingly, the attractors do not coincide with the internuclear axis when the Si–O–Si angle increases like the bcps do but they are shifted inwards. Figures 6.18 (a), (b) and (c) illustrate this phenomenon and show how the attractors shift away from the axis although the linkage becomes more and more linear. It can be found in the literature that this shift is an indicator for ionicity of a bond. [50] The more the position of an attractor differs from the straight internuclear connectivity line, the more ionic is the bond. At ϕ=180 °, the attractors are forced to the internuclear axis by the D3h-symmetry of the linear configuration. Figure 6.19 (a) illustrates this progression of the distance of the Si–O bond attractor to the internuclear axis against the Si–O–Si angle. At ϕ=85 °, the attractor is away from the axis perpendicular to it by 0.238 Åand then approaches as the bond strain diminishes. Between ϕ=115 ° and 120 °, the attractor hits the direct internuclear axis. Beyond this point the attractor again shifts away, this time inwards, indicating an increasing ionic character of the Si–O bond. At ϕ=175 °, the attractor is again away from the axis by 0.192 Å.

The distance of the bond attractors from the electronegative atom is an additional indicator for ionicity. [50] The closer the attractor is to the more electronegative atom, the more ionic is the bond. This can qualitatively be seen in Figure 6.18 or quantitatively in 6.19 (a). At the most covalent Si–O bond (ϕ=85 °), the Si–O bond attractor is away from the oxygen atom by 0.634 Å; at the most ionic Si–O bond (ϕ=180 °), the attractor is away from the oxygen atom by 0.620 Å. In between these values, the distance decreases steadily. The situation is different in the ED where the bcp is located closer to the more electropositive atom because it is the minimum of the electron density along the bond path.

Figure 6.19 (b) shows the distance of the oxygen lone-pair attractors V_1(O) to each other. For ϕ=50 °, the positions could not be located reliably, but for ϕ=170 ° to 180 °, the distances fit well into the graph, as the three attractors are distributed at same distances around the oxygen atom. The curve shows that the lone pair

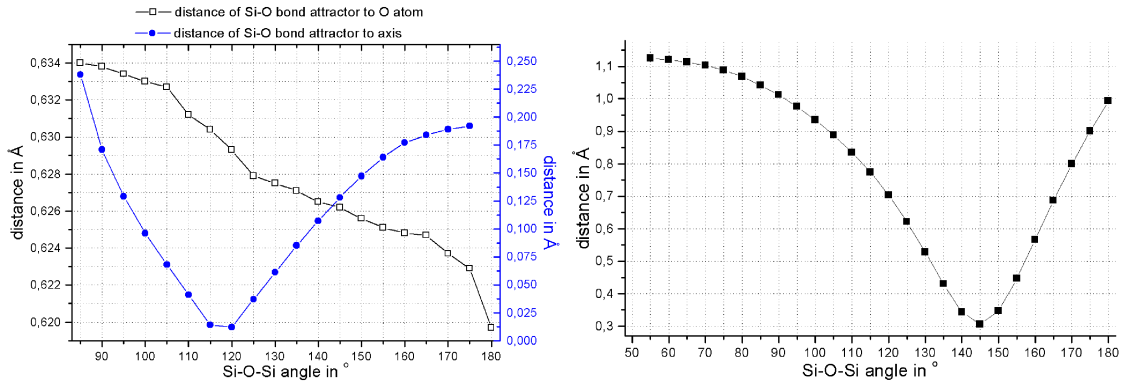

(a) Distance of the Si–O bond attractors to the O atom and the bond axis

(b) Distance between two oxygen lone-pair attractors

Figure 6.19: Distances to or between ELI-D attractors in free disiloxane

attractors are separated from each other initially by 1.125 Åand then approach each other to a minimum distance of 0.306 Å at ϕ=145 °. Towards ϕ=180 °, the attractors depart to again 0.993 Å. The curve exhibits its minimum around the Si–O–Si angle determined by full geometry optimisation of free disiloxane, which also coincides with the minimum of the bending potential energy curve (Figure 6.1). A minimum distance of the attractors towards each other seems to be energetically favoured, it does not coincide with the maximum of the hydrogen-bond energy, which would be another intuitively expected possibility.

The ELI has the advantage over the ELF that absolute function values can be compared and discussed. In Figure 6.20, the ELI-D values for oxygen lone-pair attractors and Si–O bond attractors of free disiloxane are plotted. There is no comparable study in the literature where the progression of ELI-D values at attractors or saddle points is discussed with respect to inherent molecular properties. So it is not clear whether the ELI-D values that stand for the quantification of electron-pair localisation are indicative of molecular properties like hydrogen-bonding ability in this case. However, the curve for the oxygen lone pairs has its maximum at the smallest and its minimum at the largest Si–O–Si angle, varying from ELI-D=1.498 to 1.797. In the earlier discussion, it was concluded that a pronounced electron localisation is crucial for the formation of a hydrogen bond. The curve supports this argumentation because the localisation of lone-pair electrons by means of the ELI-D values at the lone-pair attractors increases with increasing hydrogen-bond strength of the complexes from large to small Si–O–Si angles. However, the high-

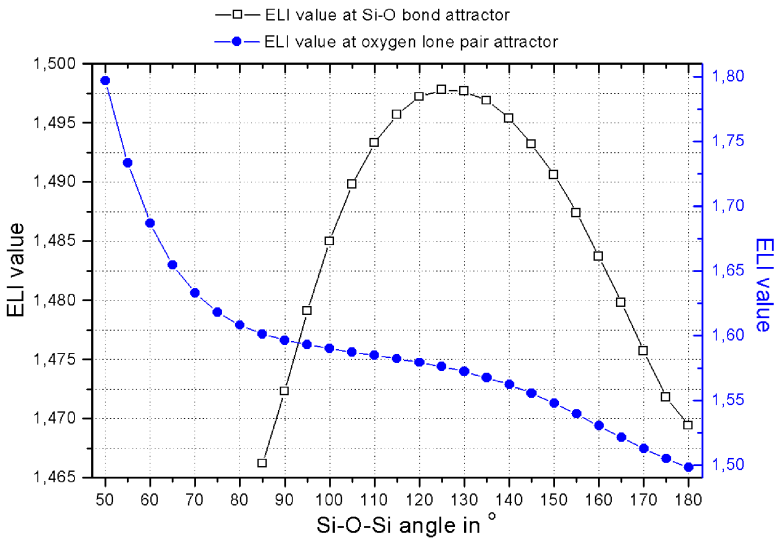

Figure 6.20: ELI-D values of the Si–O bond attractors and the oxygen lone-pair attractors of free disiloxane

est localisation can be found at the smallest angles where hydrogen bonding is not feasible anymore. The topological catastrophes cannot be detected in the ELI-D values.

The ELI-D values for the Si–O bond attractors that can also be found in Figure 6.20 are smaller than for the lone pairs, they range from ELI-D=1.466 to 1.498. The maximum value belongs to ϕ=125 °, so that the curve shape is totally different to that of the oxygen lone-pair attractors. The maximum approximately correlates with the minimum of the attractor distance to the bond axis, see Figure 6.19 (a). This means that the localisation of the electron pair constituting the Si–O bond is highest when the attractor is located nearest to the internuclear axis. The electron-pair localisation is smallest when the attractor position is farthest from the internuclear axis, regardless of whether the attractor is shifted inwards or outwards.

6.3.2 Electron Populations of ELI-D Basins in Free Disiloxane

The integration of the ED inside the volumes allocated to ELI-D basins yields core, bond and lone-pair populations. Figure 6.21 shows the dependency of the valence-basin populations and volumes on the Si–O–Si angle. The red curves show

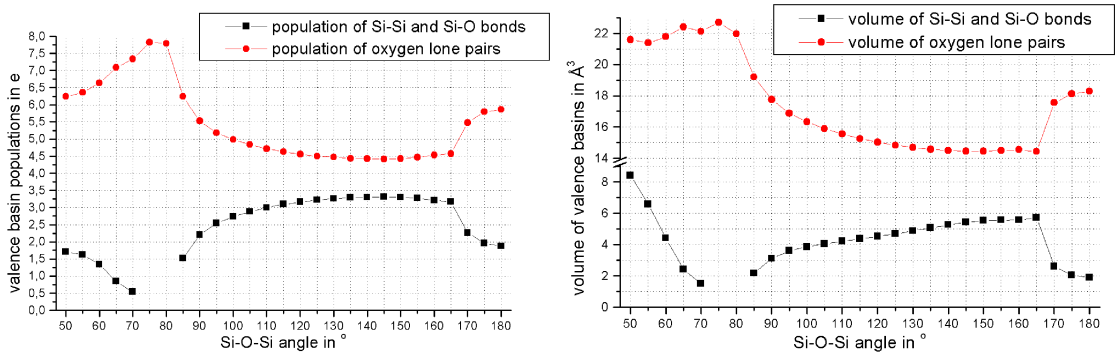

(a) N_{001} of Si–Si bond (ϕ=50 ° to 70 °), sum of N_{001} of both Si–O bonds (ϕ=85 ° to 180 °) and sum of N_{001} of both oxygen lone pairs (ϕ=50 ° to 180 °)

(b) V_{001} of Si–Si bond (ϕ=50 ° to 70 °), sum of V_{001} of both Si–O bonds (ϕ=85 ° to 180 °) and sum of V_{001} of both oxygen lone pairs (ϕ=50 ° to 180 °)

Figure 6.21: Electron populations N_{001} and volumes V_{001} of ELI-D basins for Si–Si and Si–O bonds as well as oxygen lone pairs in free disiloxane

the sum of all lone-pair electrons at the oxygen atom or the sum of all lone-pair basins' volumes, respectively. The black curves show the population/volume of the Si–Si bonds as long as they exist (ϕ=50 ° to 70 °) and the sum of the populations/volumes of the Si–O bonds beginning at ϕ=85 °. As the populations of the atomic core and hydrogen basins are generally constant upon different substitution or other chemical changes, the sum of electrons in all valence basins (V_1(O), V_2(Si,Si)/V_2(Si,O)) must be constant, too. This is shown in Figure 6.21 (a) in terms of the highly symmetric curve shapes between lone-pair and bond basins. The total constant number of electrons in valence basins is about N_{001}=7.75 e. If bond basins lose electron population, the lone-pair basins gain the same number, and vice versa. One has to consider that in the framework of the ELI-D or ELF, an electron pair does not necessarily have to consist of 2 e. This is only given for strong homonuclear covalent bonds like a C–C single bond. In the systems scrutinised here, the population of the electron pair - or paired electrons - constituting the Si–Si bond ranges from 0.54 to 1.71 e. One Si–O bond is made up of 0.76 to 1.66 e, whereas one oxygen lone pair consists of 2.21 to 3.91 e.

Figure 6.21 very impressively confirms the finding made by Laplacian and ELI-D isosurface analyses - namely the existence of three different chemical systems separated by chemical catastrophes between ϕ=80 ° and 85 ° and between ϕ=165 ° and 170 ° involving electron reorientations - by quantitative results. Cusps in the curves (both populations and volumes) occur only between ϕ=80 ° and 85 ° as

well as between ϕ=165 ° and 170 °. In the first $H_3SiOSiH_3$ chemical system between ϕ=50 ° and 85 °, the lone-pair populations ($\Sigma N_{001}(V_1(O))$) increase from 6.24 to 7.79 e, whereas the Si-Si bond population ($N(V_2(Si,Si))$) decreases from 1.71 to 0.54 e at ϕ=70 ° before the Si–Si bond disappears and the total amount of valence basin population is carried by the oxygen lone pairs. Between ϕ=80 ° and 85 °, the first chemical catastrophe occurs: The lone pairs immediately lose about 1.5 e, which the newly formed Si–O bonds ($\Sigma N_{001}(V_2(Si,O))$) obtain. In the second $H_3SiOSiH_3$ chemical system between ϕ=85 ° and 165 °, the lone pairs continue losing electron population from 6.24 e at ϕ=85 ° to 4.41 e at ϕ=145 ° where a minimum is located, and then gain electrons until $\Sigma N_{001}(V_1(O))$=4.57 e is reached at ϕ=165 °. On the other hand, the Si–O bonds' populations increase from $\Sigma N_{001}(V_2(Si,O))$=1.51 e at ϕ=85 ° to 3.31 e at ϕ=145 ° where a maximum is located and then lose electrons until $\Sigma N_{001}(V_2(Si,O))$=3.17 e is reached at ϕ=165 °. The location of the minimum/ maximum of these curves coincide with the location of the minimum/maximum of the lone pair attractor distance (Figure 6.19 (b)) and the bending potential energy curve (Figure 6.1), see above. Between ϕ=165 ° and 170 °, the second chemical catastrophe occurs: The lone pairs immediately gain about 1.0 e, which the Si–O bonds lose as the third $V_1(O)$ attractor forms. In the third $H_3SiOSiH_3$ chemical system between ϕ=170 ° and 180 °, the lone pair populations still increase and the Si–O bond populations decrease. At the linear geometry, the lone pairs are populated with as much as $\Sigma N_{001}(V_1(O))$=5.86 e, whereas the two Si–O bonds are populated with 1.87 e altogether.

It is counterintuitive that the only system in which hydrogen-bonding is possible (ϕ=85 ° to 165 °) is the one with the smallest electron populations of the oxygen lone pairs. The reason for this fact was already given above (see Figures 6.17 and 6.18): The spatial distribution of the lone-pair electrons, delocalised in the form of rings or localised in the form of a cap above the oxygen atom, is crucial and not their total number. Figure 6.21 (b) confirms that the sum of the lone-pair basin volumes is smallest in the region where hydrogen-bonding is possible.

The curves in Figure 6.21 (b) are not symmetrical, but a correlation between basin population and volume is more obvious than for the QTAIM analysis of the ED (Figures 6.15). The chemical catastrophes, and therefore also the three different chemical systems, are nicely visible in the progression of the volumes, too. In the first $H_3SiOSiH_3$ chemical system, the lone pair volumes are approximately constant around $\Sigma V_{001}(V_1(O))$=22 Å^3 as the oxygen atom is more or less isolated from the Si–Si fragment. The volume of the Si–Si bond decreases

drastically (from 8.41 to 1.51 Å^3) before the bond vanishes. Within the first chemical catastrophe, the lone pairs lose 2.77 Å^3 and the newly formed Si–O bonds possess $\Sigma V_{001}(V_2(Si,O))$=2.17 Å^3. In the second $H_3SiOSiH_3$ chemical system, the lone pairs steadily lose volume from $\Sigma V_{001}(V_1(O))$=19.20 Å^3 at ϕ=85 ° to $\Sigma V_{001}(V_1(O))$=14.42 Å^3 at ϕ=165 °. The Si–O bonds gain volume up to ΣV_{001} $(V_2(Si,O))$=5.72 Å^3 at ϕ=165 °. As the lone pairs gain electron populations within the second chemical catastrophe between ϕ=165 ° and 170 °, their volumes increase by 3.13 Å^3 and the Si–O bonds' volumes decrease by 3.13 Å^3, too. In the third $H_3SiOSiH_3$ chemical system between ϕ=170 and 180 °, the lone pair volumes still increase and the Si–O bond volumes decrease. At the linear geometry, the lone pair volumes are $\Sigma V_{001}(V_1(O))$=18.29 Å^3, whereas the two Si–O bonds volumes are $\Sigma V_{001}(V_2(Si,O))$=1.89 Å^3.

6.3.3 ELI-D Properties of Hydrogen-Bonded Complexes

In free disiloxane in the range from ϕ=85 ° to 165 ° where hydrogen bonding is possible, the unperturbed oxygen atom exhibits two lone pairs according to the Lewis model, which can be identified by two attractors in the ELI-D (see above). But as found in Figure 6.11, the complex is symmetric and the hydrogen atom therefore seems to interact with both lone pairs. Thus, it is important that the VSCC is closed in form of a cap even at rather high isovalues. A similar finding can be made within the framework of the ELI-D. Figures 6.22 (a) and (c) show that the hydrogen atom in both disiloxane$\cdots$silanol and disiloxane$\cdots$water points somehow towards the centre of the cap-like localisation domain. This again explains why a ringlike arrangement of the localisation domains with a hole at the very position where the hydrogen atom points to prevents hydrogen bonding. But it is still an open question if the hydrogen-bonded complex is indeed perfectly symmetrical and no lone pair is favoured in the interaction or if the interaction with the hydrogen atom is guided by one of them although the hydrogen atom points towards the centre of the VSCC or ELI-D localisation domain, respectively.

In contrast to the Laplacian distribution, the ELI-D provides an opportunity to determine the number of lone pairs according to the number of attractors in this region and to mark unambiguously which region of space belongs to which lone-pair basin. For disiloxane$\cdots$silanol, there are two lone pairs from ϕ=85 ° to 125 °. In Figure 6.22 (b) for ϕ=100 °, the cap-like reducible localisation domain is separated into the regions of the two lone pairs using a colour code. Having a close look, the

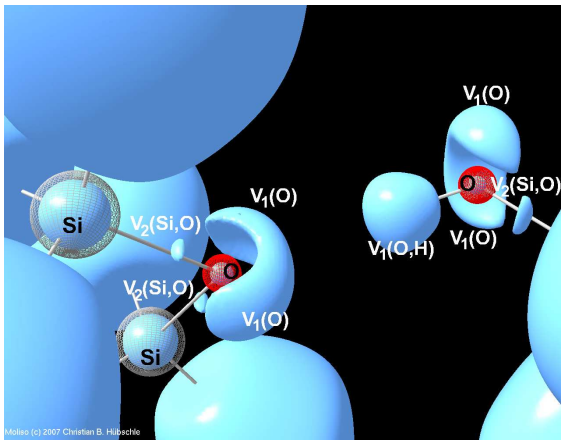

(a) disiloxane···silanol, ϕ=100°, isovalue=1.500

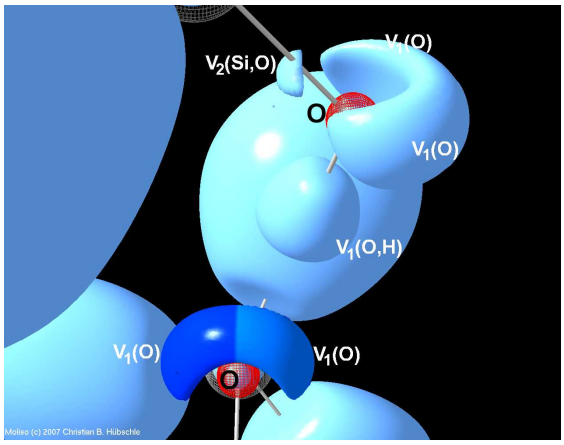

(b) Detail of situation in (a): disiloxane···silanol, ϕ=100°, isovalue=1.515, different acceptor-oxygen lone-pair basins are differently coloured

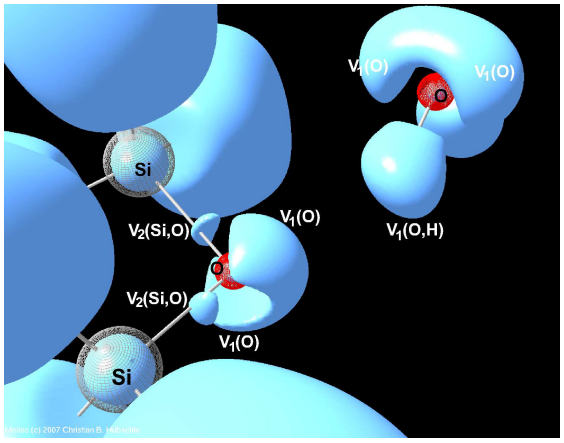

(c) disiloxane···water, ϕ=100°, isovalue=1.478

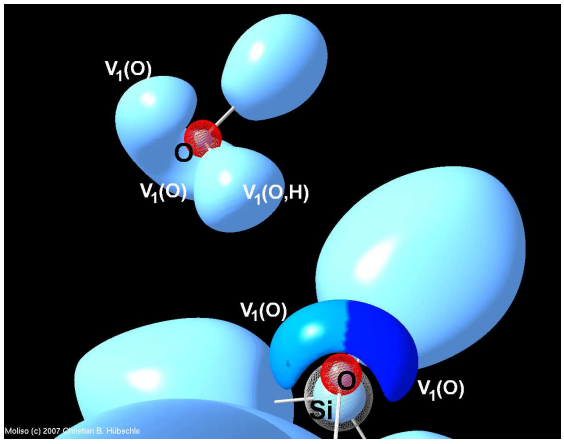

(d) Detail of situation in (c): disiloxane···water, ϕ=100°, isovalue=1.510, different acceptor-oxygen lone-pair basins are differently coloured

Figure 6.22: ELI-D localisation-domain representations of hydrogen-bonded complexes at representative angles

hydrogen atom may point rather to the region of the right lone pair over which the hydroxy group is located. This lone pair is also more affected by the interaction as its volume is reduced by 2.1 Å^3 (ϕ=85 °) in contrast to the other lone pair. The difference decreases until it is only 0.1 Å^3 at ϕ=125 °(see Appendix).
Between ϕ=125 ° and 130 °, the two lone pairs merge into one, i.e. only one attractor for all approximately 4.5 lone-pair electrons exists between ϕ=130 ° and 165 °. The hydrogen-bonded complex in this region is truely symmetrical and therefore causes the lone pairs to merge into one large lone pair. The same phenomenon can be observed for disiloxane$\cdots$water except for the fact that the initially two lone pairs merge into one already between ϕ=115 ° and 120 °. Figure 6.22 (d) shows the situation before the merger. Afterwards, the water molecule is still located closer to one of the Si–O bonds (compare Figures 6.4 and 6.6 (a)), but the hydrogen atom points exactly to the middle of the cap-like localisation domain.
The hydrogen bond is stronger at smaller Si–O–Si angles. This means that a situation where the interaction of the donor hydrogen atom with the acceptor oxygen atom is guided by only one lone pair is more efficient. In this case, it is also possible for the oxygen atom to form two or more hydrogen bonds with different acceptor groups. For example, trisilo (**2**) is able to form two C–H$\cdots$O$_{siloxane}$ hydrogen bonds although the C–H fragment is a very weak hydrogen-bond donor, which will be discussed in further detail below (compare Table 7.2).
The water and the silanol oxygen atoms that are good hydrogen bond acceptors show the same cap-like shaped ELI-D localisation domains in Figure 6.22, just like the siloxane oxygen atom does in the chemical system between ϕ=85 ° and 165 °. The two lone pairs of the water and silanol oxygen atoms do not merge because they do not participate in a hydrogen bond as acceptor. The sum of the electron populations of both lone pairs of the silanol oxygen atom is constant at 4.54 e, the value of the water oxygen atom is constant at 4.52 e.

Finally, it will be examined which parameters in the framework of the ELI-D are indicative of hydrogen bonding and which ones correlate with the hydrogen-bond energy to be a measure of the hydrogen-bond strength. The properties ΣN$_{001}$(V$_1$(O)), ΣN$_{001}$(V$_2$(Si,O)) and ΣV$_{001}$(V$_2$(Si,O)) in the disiloxane group in disiloxane$\cdots$silanol and disiloxane$\cdots$water are not indicative of hydrogen bonding. No charge transfer from the acceptor towards the donor group or vice versa can be found, the populations remain unaffected (similar to the atomic charges within the QTAIM of the ED). In contrast, the oxygen lone-pair volume ΣV$_{001}$(V$_1$(O)) is

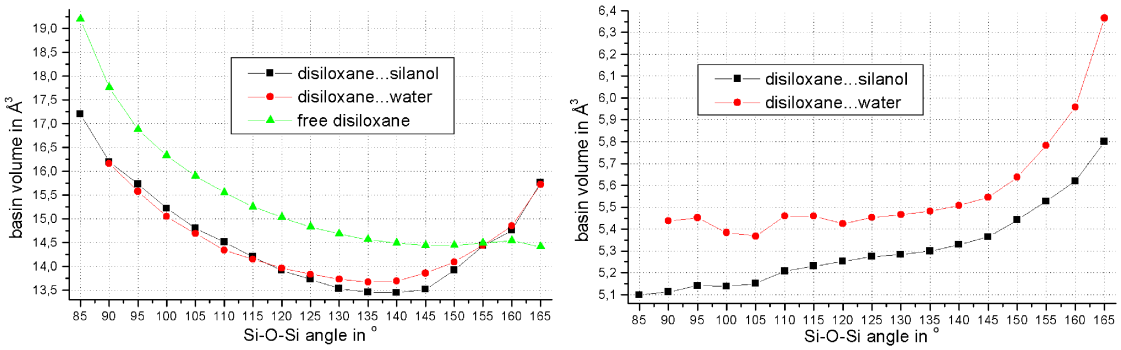

(a) Comparison of V_{001} of acceptor-oxygen lone-pair basins, sum of volumes where two lone pairs exist

(b) V_{001} for donor H atoms in silanol/ water of hydrogen-bonded complexes

Figure 6.23: ELI-D basin volumes V_{001} of acceptor-oxygen lone pairs in siloxane and H atoms in silanol/water for hydrogen-bonded complexes

significantly affected upon hydrogen-bond formation, Figure 6.23 (a): The curves for disiloxane$\cdots$silanol and disiloxane$\cdots$water are shifted towards smaller volumes at each Si–O–Si angle compared to free disiloxane. There is no difference between the two curves for the complexes, so that this property does not show which hydrogen bond is stronger. However, the following trend can be observed: The volume loss of the lone pairs of the complexes compared to free disiloxane increases with the strength of the hydrogen bond, i.e. the smaller the Si–O–Si angle is. At ϕ=85 °, the difference is about 2 Å^3; at ϕ=120 °, it is about 1 Å^3 and at ϕ=155 °, the difference has vanished.

Figure 6.23 (b) shows the progression of the volume of the protonated monosynaptic valence basin V_1(O,H). The volume $V_{001}(V_1(O,H))$ of free silanol from a full geometry optimisation is 6.84 Å^3; the volume $V_{001}(V_1(O,H))$ of free water from a full geometry optimisation is 6.64 Å^3. As these values are larger than any of those in the complexes, a decrease of the hydrogen atom's volume indicates the formation of the hydrogen bond. Therefore, the curves of $V_{001}(V_1(O,H))$ clearly show that the hydrogen bond in disiloxane$\cdots$silanol is stronger than the hydrogen bond in disiloxane$\cdots$water at each Si–O–Si angle because the volume loss of the hydrogen atom is on average higher by 0.4 Å^3 in disiloxane$\cdots$silanol. Moreover, $V_{001}(V_1(O,H))$ correlates with the hydrogen-bond strength. The stronger the hydrogen bond becomes with decreasing Si–O–Si angle, the smaller the hydrogen atom's volume becomes. Not only the volume of the hydrogen atom in a hydrogen bond changes but also the shape of the corresponding localisation domain,

see Figure 6.23 (d). In this respresentation, both hydrogen atoms of water are depicted. The one in the hydrogen bond is significantly flattened, indicating the interaction with the oxygen atom.
These results are very similar to the results found in the analysis of the atomic properties from the QTAIM analysis of the ED (compare Figure 6.16). There, a reduction of the atomic volumes of the oxygen and the hydrogen atom involved in the hydrogen bond were found, here, a reduction of the volumes of the oxygen lone pairs and the protonated monosynaptic valence basin of the hydroxy group were found. Both findings indicate a mutual penetration of the involved atoms. In contrast to the QTAIM analysis of the ED, where a correlation of the atomic charge of the hydrogen atom with the hydrogen-bond strength could be found, the population of the protonated monosynaptic valence basin of the hydroxy group is not affected upon hydrogen-bond formation. No other examined ELI-D property in the silanol and water group is indicative of hydrogen bonding.

6.4 Results for Disilaepoxide $H_2SiOSiH_2$

In the preceding chapters, the hypothetical chemical system of free disiloxane $H_3SiOSiH_3$ was defined in the angle region ϕ=50 ° to 80 °. Massive chemical reorientations take place between 80 ° and 85 °. Silaepoxide $H_2SiOSiH_2$ was chosen to be compared with free disiloxane $H_3SiOSiH_3$ because disilaepoxide is a stable system (there are a few crystal structures including a disilaepoxide fragment in the CSD, for example [176]) with a Si–O–Si angle close to 80 °. The Si–O–Si angle is exactly 80.54 ° as obtained from a full geometry optimisation, see Table 6.1. In contrast to disiloxane at ϕ=80 °, there are convergent hydrogen-bonded complexes with silanol and water as donor molecules for disilaepoxide. The Si–O–Si angles do not change upon hydrogen-bond formation but remain close to ϕ=80 °, see Table 6.1.
The molecular structures of free disilaepoxide and the hydrogen-bonded complexes are given in form of the molecular graphs as obtained from a QTAIM analysis in Figure 6.24. The disilaepoxide$\cdots$silanol complex is symmetrical so that the properties for Si–O bonds and Si atoms listed in Table 6.1 are identical; in disilaepoxide$\cdots$water, the properties are different because the water molecule is shifted towards one of the silylene groups. The Si–O bond that is nearer to the water molecule is the shorter one in contrast to disiloxane$\cdots$water, where it is the longer one (compare Figure 6.4 (b)). The Si–Si bond in free disilaepoxide

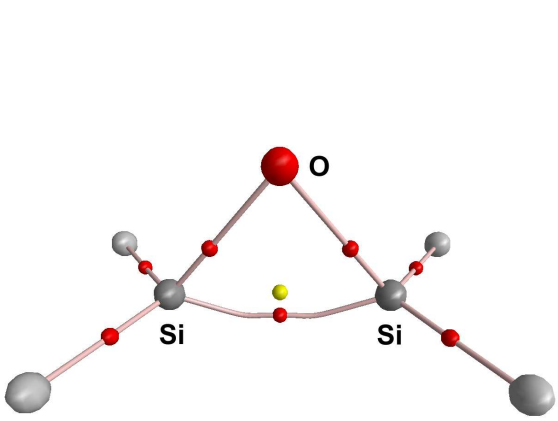

(a) Molecular graph of free disilaepoxide

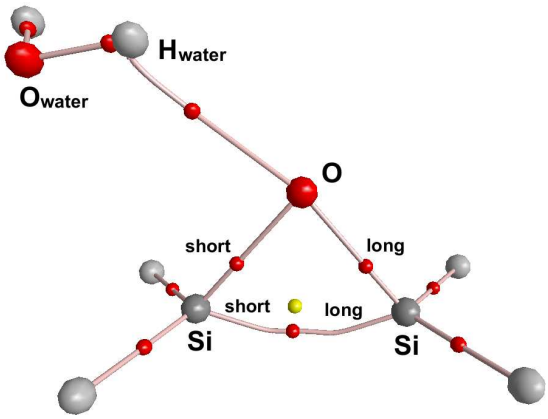

(b) Molecular graph of disilaepoxide$\cdots$water

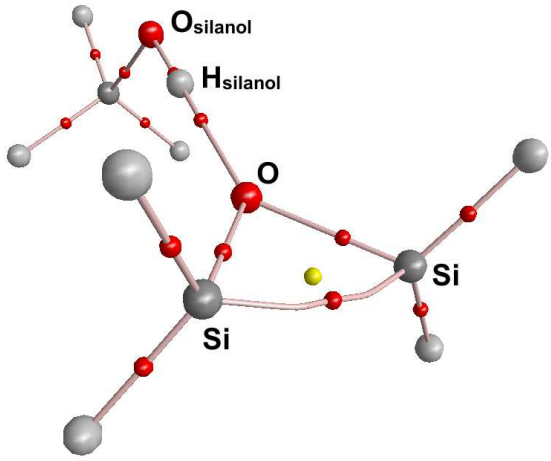

(c) Molecular graph of disilaepoxide$\cdots$silanol

Figure 6.24: Molecular graphs of free disilaepoxide and hydrogen-bonded complexes of disilaepoxide

(d=2.209 Å) is shorter than the Si–Si distance in free disiloxane at ϕ=80 ° (d = 2.324 Å) where there is no Si–Si bond. But the Si–O bonds in free disilaepoxide are shorter by 0.1 Å, too (d=1.709 Å compared to d=1.808 Å). Like for disiloxane, the Si–O bonds elongate upon hydrogen-bond formation in disilaepoxide, which also holds for the Si–Si bond.

Figure 6.24 shows that the bond path of the Si–Si bond is curved but the Si–O bonds are straight. A bond-path analysis, values are given in Table 6.1, shows that the Si–Si bond path is by 0.1 Å longer than the bond distance. The bcp of the Si–Si bond is shifted by about 0.2 Å towards the silicon atom which is closer to the water molecule in disilaepoxide$\cdots$water. The rcp is very close to the Si–Si bcp. Therefore, the values of the ED at these cps are similar (ϱ(Si-Si)=0.60 e Å^{-3} and ϱ(rcp)=0.58 e Å^{-3}). But the Laplacian values are different: $\nabla^2\varrho$(Si-Si) is small but negative (Table 6.1) showing that the Si–Si bond consists of a shared interaction with mainly covalent contributions. The delocalization index is also significantly larger than 0.5. But for example in the case of a solely covalent C–C bond, the delocalization index would be closer to 1.0 and the Laplacian would be more negative. The delocalization index δ(Si,Si) decreases upon hydrogen-bond formation.

In contrast to the Si–Si bond, the Si–O bonds are strongly ionic as found for disiloxane. But the bonds in free disilaepoxide are stronger and more ionic than for free disiloxane at ϕ=80 ° (ϱ(Si-O)=0.83 e Å^{-3} and $\nabla^2\varrho$(Si-O)=16.8 e Å^{-5} for disilaepoxide compared with ϱ(Si-O)=0.71 e Å^{-3} and $\nabla^2\varrho$(Si-O)=10.1 e Å^{-5} for disiloxane). The Si–O bond character of disilaepoxide is rather comparable to the one of disiloxane at ϕ=100 °(d=1.707 Å, ϱ(Si-O)=0.83 e Å^{-3} and $\nabla^2\varrho$(Si-O)=16.0 e Å^{-5}). The charge separation in terms of atomic Bader charges is on the other hand not comparable with free disiloxane at a special Si–O–Si angle because the oxygen atom is charged by -1.64 e corresponding to free disiloxane at ϕ=130 °, but the silicon atoms are charged less positively (Q_{001}(Si)=2.15) than for any Si–O–Si angle in free disiloxane.

As expected, the hydrogen bond in disilaepoxide$\cdots$silanol is much stronger than in disilaepoxide$\cdots$water, as every value in Table 6.2 confirms. In terms of the hydrogen-bond energy, the hydrogen bond is twice as strong in disilaepoxide$\cdots$silanol (E_{HB}=-18.92 kJ mol^{-1} compared to E_{HB}=-8.76 kJ mol^{-1}). These values are similar to the ones of disiloxane in hydrogen-bonded complexes approximately at a Si–O–Si angle of ϕ=100 °, compare Figure 6.2. For hypothetical disiloxane complexes at ϕ=80 °, the negative values of the hydrogen-bond energies would be much

Table 6.1: Selected geometrical, ED and ELI-D properties of free disilaepoxide and hydrogen-bonded complexes

property	free disilaepoxide	disilaepoxide$\cdots$silanol	disilaepoxide$\cdots$water
geometry:			
d(Si-Si) in Å	2.209	2.214	2.221
d(Si-O) in Å	1.709	1.719	long: 1.725
			short: 1.708
a(Si-O-Si) in °	80.54	80.20	80.63
a(O-Si-Si) in °	49.73	49.90	long: 49.63
			short: 50.01
ED topology			
bond path Si-Si in Å	2.297	2.304	long + short:
			1.246+1.064=2.310
bond path Si-O in Å	1.709	1.719	long: 1.725
			short: 1.708
ϱ(Si-Si) in e Å^{-3}	0.60	0.61	0.60
$\nabla^2\varrho$(Si-Si) in e Å^{-5}	-2.8	-3.0	-2.9
ϱ(Si-O) in e Å^{-3}	0.83	0.81	long: 0.80
			short: 0.84
$\nabla^2\varrho$(Si-O) in e Å^{-5}	16.8	16.1	long: 15.8
			short: 16.8
ϱ(rcp) in e Å^{-3}	0.58	0.58	0.58
$\nabla^2\varrho$(rcp) in e Å^{-5}	0.0	0.2	0.1
δ(Si,Si)	0.722	0.653	0.644
δ(Si,O)	0.610	0.568	long: 0.602
			short: 0.545
Q_{001}(Si) in e	2.15	2.19	long: 2.05
			short: 2.32
V_{001}(Si) in Å^3	13.0	12.5	long: 14.0
			short: 11.0
Q_{001}(O) in e	-1.64	-1.61	-1.62
V_{001}(O) in Å^3	20.9	19.8	19.8
ELI-D topology			
$ELI_{att}(V_2(Si,Si))$	2.397	2.449	2.427
$N_{001}(V_2(Si,Si))$ in e	2.00	1.99	1.99
$V_{001}(V_2(Si,Si))$ in Å^3	16.40	16.07	16.20
$ELI_{att}(V_2(Si,O))$	1.481	1.503	long: 1.495
			short: 1.495
$N_{001}(V_2(Si,O))$ in e	1.42	1.41	long: 1.40
			short: 1.49
$V_{001}(V_2(Si,O))$ in Å^3	2.24	2.26	long: 2.18
			short: 2.21
$ELI_{att}(V_1(O))$	1.605	1.605	1.602
$N_{001}(V_1(O))$ in e	4.79	4.80	4.75
$V_{001}(V_1(O))$ in Å^3	16.23	15.21	15.35

Table 6.2: Selected properties of the disilaepoxide$\cdots$silanol/water hydrogen bonds *Angles a in °, distances d in Å, ED ϱ(bcp) in e Å^{-3}, Laplacian of ED $\nabla^2\varrho$(bcp) in e Å^{-5}, hydrogen-bond energy E_{HB} in kJ mol^{-1}, IR red shift $\Delta\tilde{\nu}(OH)$ in cm^{-1} (sym/asym)*

a(Si–O–Si)	d(H$\cdots$O)	d(O$\cdots$O)	a(O-H$\cdots$O)	ϱ(H$\cdots$O)	$\nabla^2\varrho$(H$\cdots$O)	E_{HB}	$\Delta\tilde{\nu}(OH)$
disilaepoxide$\cdots$silanol:							
80.20	1.836	2.807	179.67	0.21	2.2	-18.92	257.1
disilaepoxide$\cdots$water:							
80.63	2.058	2.747	126.56	0.14	2.1	-8.76	68.2/33.2

higher from an extrapolation of the curves in Figure 6.2 (about E_{HB}= -30 kJ mol^{-1} for disiloxane$\cdots$silanol and -20 kJ mol^{-1} disiloxane$\cdots$water). The fact that disilaepoxide is a stable compound makes its properties rather comparable with a stable disiloxane analogon at a larger Si–O–Si angle than with an unstable disiloxane analogon at the same Si–O–Si angle (compare discussion of Si–O-bond properties above).

Figure 6.25 shows the ELI-D localisation-domain and Laplacian iso-surface representations of free disilaepoxide and the disilaepoxide$\cdots$silanol complex. The VSCCs as well as the localisation domains of the oxygen lone pairs exhibit the typical cap-like shapes as found before for disiloxane in hydrogen-bonding systems. VSCCs and ELI-D basins V_2(Si,O) for the two Si–O bonds were found. Additionally, a very large Si–Si bond basin V_2(Si,Si) exists. Its volume ($V_{001}(V_2(Si,Si))$= 16.40 Å^3) is twice as large as the volume of one of the oxygen lone-pair basins, see Table 6.1. It is populated with exactly 2.00 e, and the ELI-D localisation value of 2.397 is significantly larger than for the Si–O-bond attractors and the oxygen lone pairs found before.

The ELI-D values at the Si–O bond and oxygen lone-pair attractors (see Table 6.1) for free disilaepoxide fit into the curves for free disiloxane (Figure 6.20) again at about ϕ=100 °. The sum of the Si–O-bonds' populations ($\Sigma N_{001}(V_2(Si,O))$=2.84 e) fits into the curve of the Si–O-bonds' populations of free disiloxane (Figure 6.21) at about ϕ=102 °, whereas the sum of the basins' volumes ($\Sigma V_{001}(V_2(Si,O))$=4.48 Å^3) is larger than for ϕ=102 ° in free disiloxane.

Two basins for the oxygen lone-pair electrons were found for free disilaepoxide. For disilaepoxide$\cdots$silanol and disilaepoxide$\cdots$water, the two lone pairs merge into one upon hydrogen-bond formation. This merger takes place at larger Si–O–Si angles in the case of disiloxane, which also shows that the disilaepoxide systems

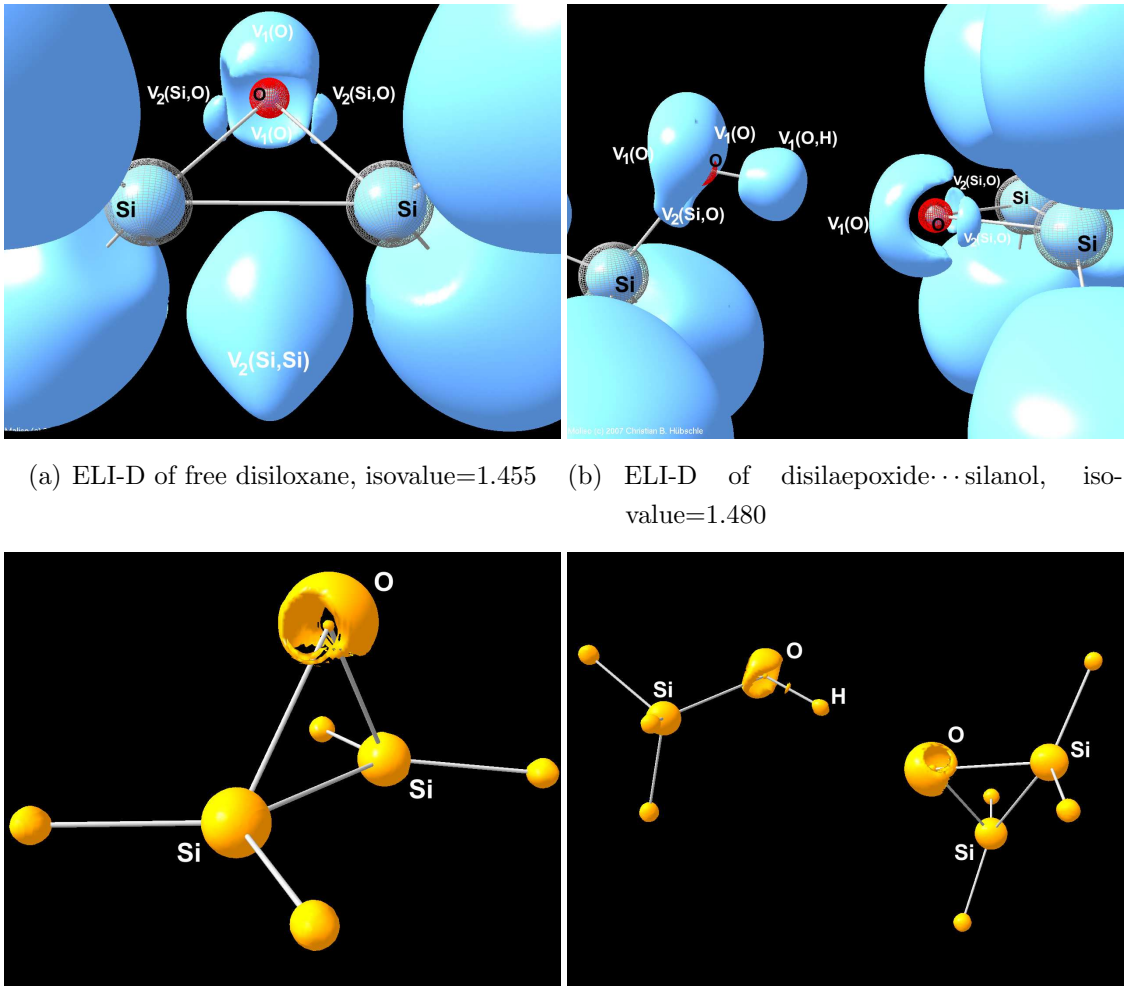

(a) ELI-D of free disiloxane, isovalue=1.455

(b) ELI-D of disilaepoxide···silanol, isovalue=1.480

(c) Laplacian of the ED of free disiloxane, isovalue=-58.08 $e Å^{-5}$

(d) Laplacian of the ED of disilaepoxide···silanol, isovalue=-58.08 $e Å^{-5}$

Figure 6.25: ELI-D localisation-domain and Laplacian isosurface representations of free disilaepoxide and disilaepoxide···silanol

are rather comparable with disiloxane systems at larger angles. Figures 6.25 (b) and (d) show how the hydrogen atom of the silanol group points towards the centre of the cap-like VSCC or localisation domain to form the hydrogen bond. The sum of populations and volumes of the oxygen lone-pair basins in free disilaepoxide ($\Sigma N_{001}(V_1(O))$=4.79 e and $\Sigma V_{001}(V_1(O))$=16.23 Å) correspond to the values of free disiloxane at about ϕ=105 °.

Chapter 7

Results of the Analyses of Compounds 1 to 4

7.1 Geometrical and Energetical Results

7.1.1 Experimental and Optimised Geometries

The crystal structures of cpds. **1** to **4** including the atomic-numbering scheme can be found in Figure 5.1. The most important geometric parameters are listed in Table 7.1, the complete lists of bond distances, angles and torsion angles are given in the Appendix, Tables A.33 to A.44. Siloxanol (**1**) and trisilo (**2**) exhibit strained Si–O–Si linkages with small Si–O–Si angles (ϕ=116.37(7)° for siloxanol (**1**) and ϕ=117.81(3)° for trisilo (**2**)) that are incorporated into a five-membered ring to force them into the strained situation. In contrast, pentaphe (**3**) and hexaphe (**4**) exhibit relaxed Si–O–Si linkages with large Si–O–Si angles (ϕ=162.03(2)° for pentaphe (**3**) and ϕ=180.00° for hexaphe (**4**)) that are caused by bulky phenyl groups as substituents. As expected from the considerations in Chapter 6.1.2, the Si–O bonds are longer in siloxanol (**1**) and trisilo (**2**) with small Si–O–Si angles (d(Si1–O1)=1.679(1) Å and d(Si2–O1)=1.657(1) Å for siloxanol (**1**); d(Si1–O1)= d(Si2–O1)= 1.657(1) Å for trisilo (**2**)) and become shorter in pentaphe (**3**) and hexaphe (**4**) when the ionic bond character increases with increasing Si–O–Si angle (d(Si1–O1)=1.619(1) Å and d(Si2–O1)=1.626(1) Å for pentaphe (**3**); d(Si1–O1)= 1.621(1) for hexaphe (**4**)).

Values of the full geometry optimisations of cpds. **1** to **4** are given in the second column in Table 7.1. For siloxanol (**1**) and trisilo (**2**), the Si–O–Si angles do not

Table 7.1: Selected bond distances and angles of cpds. **1** to **4**

First column: experiment, second column: isolated-molecule optimisations, bond distances A–B in Å, bond angles A–B–C in °, standard uncertainties from the experiment or standard deviations from averaging in brackets at the last digit

Siloxanol (**1**)								
Si1–O1	1.679(1)	1.677	Si2–C2	1.870(1)	1.890	Si3–O2	1.650(1)	1.675
Si2–O1	1.657(1)	1.663	C1–C2	1.412(1)	1.417	Si–C_{methyl}	1.849(1)	1.880(1)
Si1–C1	1.895(1)	1.919	Si3–C6	1.882(1)	1.894	O–H	0.967	0.959
Si1–O1–Si2	116.37(7)	118.07	O1–Si2–C2	98.63(5)	98.32	Si2–C2–C1	114.40(5)	114.20
O1–Si1–C1	99.28(4)	98.77	Si1–C1–C2	109.97(5)	110.43	O2–Si3–C6	108.65(3)	110.44
Trisilo (**2**)								
Si1–O1	1.657(1)	1.672	Si2–C2	1.880(1)	1.894	Si–C_{methyl}	1.857(1)	1.878(1)
Si2–O1	1.657(1)	1.672	C1–C2	1.419(1)	1.414			
Si1–C1	1.881(1)	1.894	C2–C3	1.401(1)	1.396			
Si1–O1–Si2	117.81(3)	117.64	O1–Si2–C2	99.01(3)	98.72	Si2–C2–C1	111.98(3)	112.46
O1–Si1–C1	98.79(3)	98.71	Si1–C1–C2	112.37(3)	112.46			
Pentaphe (**3**)								
Si1–O1	1.619(1)	1.648	Si1–C7	1.861(1)	1.881	Si2–C19	1.863(1)	1.885
Si2–O1	1.626(1)	1.652	Si1–H1Si	1.484	1.488	Si2–C25	1.864(1)	1.884
Si1–C1	1.863(1)	1.878	Si2–C13	1.862(1)	1.888			
Si1–O1–Si2	162.03(2)	153.90	O1–Si1–C1/C7	109.49(3)	108.96(1)	O1–Si2–C13/19/25	109.34(2)	108.40(1)
O1–Si1–H1Si	108.07	109.74	H1Si–Si1–C1	109.67	109.87			
Hexaphe (**4**)								
Si1–O1	1.621(1)	1.644	Si1–C1/7/13	1.864(1)	1.886(1)			
Si1–O1–Si1a	180.00	180.00	O1–Si1–C1/C7/13	108.97(3)	108.60(1)			

change much due to the restriction of the five-membered ring and the Si–O distances only increase slightly. As the Si–O–Si angles of siloxanol (**1**) and trisilo (**2**) conform to each other by geometry optimisation (ϕ=118.07 ° for siloxanol (**1**) and ϕ=117.64 ° for trisilo (**2**)), the Si–O distances (varying from d=1.663 to 1.677 Å) are very similar, too. These values fit very well into the curve of Si–O distances against Si–O–Si angles obtained from the PES scans shown in Figure 6.5 (b) although the silicon atoms are differently substituted. From this curve, values of about d(Si–O)=1.67 Å are expected for ϕ=120 °.

For pentaphe (**3**), the Si–O–Si angle is reduced by about 10 ° upon full geometry optimisation from ϕ=162.03 to 153.90 °. It comes close to the value ϕ=151.4 ° found for the model compound $H_3SiOSiH_3$ at full geometry optimisation, which additionally is the minimum of the bending potential energy curve of $H_3SiOSiH_3$. This shows that this angle is energetically more favourable also in the case of large bulky substitutents for isolated-molecule calculations. In the crystal, the bulky phenyl groups cause the molecule to pack in a way that causes the Si–O–Si angle to enlarge. In contrast, the Si–O–Si angle in hexaphe (**4**) does not decrease, but it retains the linear geometry as energetically most favourable in the case of a symmtrical substitution pattern. From the curve in Figure 6.5 (b), values of around d(Si–O)=1.645 to 1.635 Å can be expected in the range from ϕ=150 ° to 180 °. The Si–O distances found for pentaphe (**3**) and hexaphe (**4**) are larger than for the experimental case and close to these expected values from the PES scans of $H_3SiOSiH_3$: d(Si1–O1)=1.648 Å and d(Si2–O1)=1.652 Å for pentaphe (**3**); d(Si1–O1)=1.644 Å for hexaphe (**4**).

The Si–O distance in the silanol group of siloxanol (**1**) (d(Si3–O2)=1.650 Å in experiment and 1.675 Å in theory) is very similar to the ones in siloxane at small Si–O–Si angles around ϕ=120 °. In their relaxed states after full geometry optimisation, free silanol H_3SiOH exhibits a longer Si–O bond (d(Si–O)=1.660 Å) compared to free disiloxane $H_3SiOSiH_3$ (d(Si–O)=1.645 Å).

Si–C bonds are about 0.2 Å longer than Si–O bonds. Comparing different Si–C bonds, Si–C distances in the five-membered rings are largest (averaged to 1.882 Å in experiment and 1.899 Å in theory), Si–C_{phenyl} distances are smaller (averaged to 1.863 Å in experiment and 1.884 Å in theory) and Si–C_{methyl} distances are smallest (averaged to 1.853 Å in experiment and 1.879 Å in theory). The theoretical Si–C distances are larger in any of the discussed cases. The Si–H bond in pentaphe (**3**), in which the hydrogen atom is rather hydridic because silicon is more electropositive than hydrogen, is significantly longer than any C–H bond. It was fixed to

a value of d(Si–H)=1.484 Å from averaged neutron-diffraction studies [209]. The optimised geometry exhibits the value d(Si–H)=1.488 Å, which is very close to the experimental one. The O–H bond in silanol was fixed to 0.967 Å from [209] (theoretical value d(O–H)=0.959Å), which is the other extreme where hydrogen is much more electropositive. All C–H distances that were also fixed to averaged neutron diffraction values in the multipole refinement are very reliably resembled by the optimised geometry, too (compare Tables A.33, A.36, A.39 and A.42). The values are d(C–H)=1.083/ 1.083 Å (experiment/theory) for phenyl groups and d(C–H)=1.059/ 1.092 Å (experiment/theory) for methyl groups.

7.1.2 Intermolecular Interactions in the Crystals

It was discussed in Chapter 4.1 that there are only three compounds in the CSD that exhibit a classical hydrogen bond with the siloxane oxygen atom as acceptor. They belong to the compound class of siloxanols and they have in common that they contain exceptionally small Si–O–Si angles. Siloxanol (**1**) is the fourth example of a siloxane compound in which the siloxane group acts as hydrogen-bond acceptor. These facts prove the considerations made according to the analysis of the PES scans: The hydrogen-bond strength of hydrogen bonds with the siloxane oxygen atom as acceptor is large enough for small Si–O–Si angles (here ϕ=116.37(7) °) to compete with the silanol group as acceptor. The silanol$\cdots$siloxane hydrogen bond O2–H2O$\cdots$O1 is visualised in Figure 7.1 (a) showing the crystal packing scheme of siloxanol (**1**). Besides O2–H2O$\cdots$O1, there are two weak C–H$\cdots$O2 hydrogen bonds with the silanol oxygen atom as acceptor that are not visualised in Figure 7.1 (a). However, details of all hydrogen bonds are listed in Table 7.2.
With respect to the H2O$\cdots$O1 and O2$\cdots$O1 distances as well as the O2–H2O$\cdots$O1 angle, the O2–H2O$\cdots$O1 hydrogen bond can be classified as a classical medium-strength hydrogen bond according to the geometric criteria of Jeffrey and Steiner. [238–240] The experimental bond-topological properties of the H2O$\cdots$O1 bcp are ϱ(H2O$\cdots$O1)=0.16(3) eÅ^{-3} and $\nabla^2\varrho$(H2O$\cdots$O1)=2.7(1) eÅ^{-5}. Within the criteria of Koch and Popelier [237], and compared to other hydrogen bonds [234], the O2–H2O$\cdots$O1 hydrogen bond can be classified as strong from its bond-topological properties. The experimental interaction energy E_{int}=-9.55 kJ mol^{-1} between the two molecules in the crystal that are connected by the hydrogen bond via the symmetry operation 1/2+x, 1/2-y, 1/2+z shall serve as an approximation of the hydrogen-bond energy. From theoretical periodic-boundary calculations,

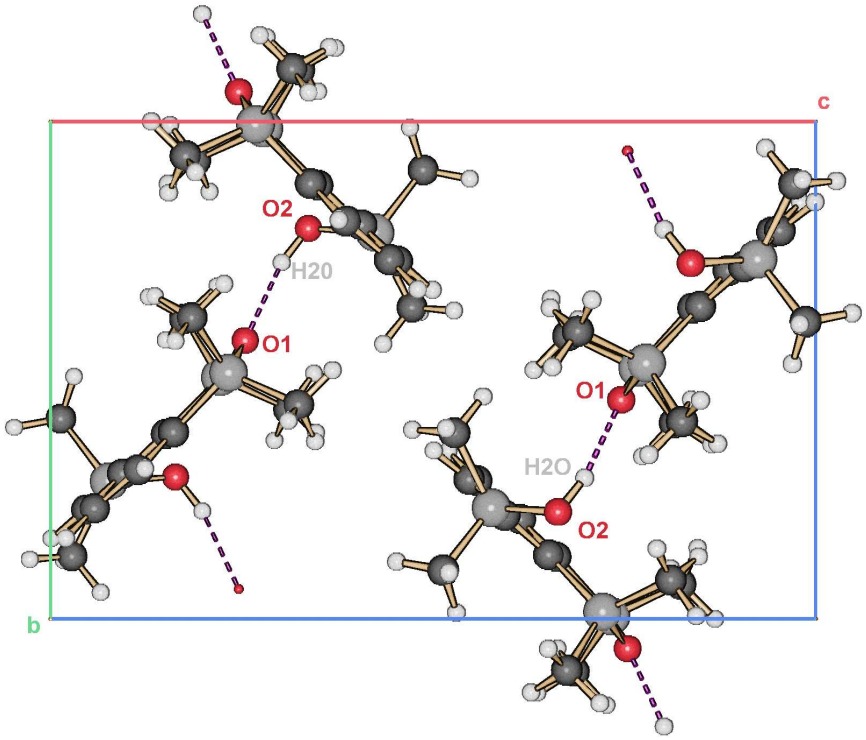

(a) Siloxanol (**1**)

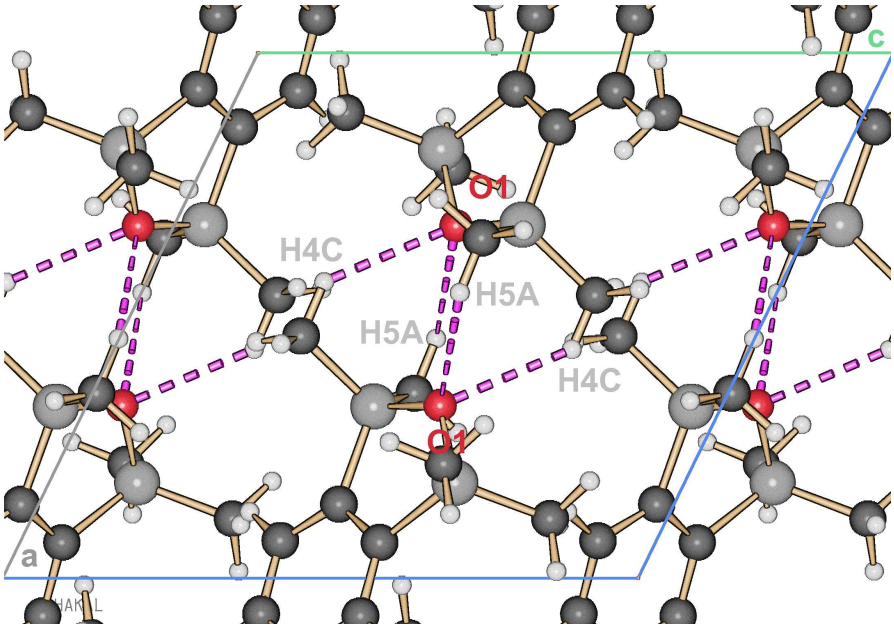

(b) Trisilo (**2**)

Figure 7.1: Crystal packing and hydrogen-bonding network

Table 7.2: Selected properties of the hydrogen bonds of cpds. **1** to **4**
First row: experiment, second row: periodic-boundary calculations at experimental geometries, hydrogen$\cdots$acceptor (H$\cdots$A) distance in Å, donor$\cdots$acceptor (D$\cdots$A) distance in Å, donor–hydrogen$\cdots$acceptor (D–H$\cdots$A) angle in °, electron density ϱ at H$\cdots$A bcp in e$Å^{-3}$, Laplacian $\nabla^2\varrho$ at H$\cdots$A bcp in e$Å^{-5}$, interaction energy in kJ mol^{-1}, symmetry operation to generate acceptor molecule

labels	H$\cdots$A	D$\cdots$A	D–H$\cdots$A	ϱ_{bcp}	$\nabla^2\varrho_{bcp}$	E_{int}	sym
Siloxanol (**1**):							
O2–H2O$\cdots$O1	1.918	2.869	167.28	0.16(3)	2.7(1)	-9.55	1/2+x, 1/2-y, 1/2+z
				0.22	1.5	-27.80	
C10–H10B$\cdots$O2	2.436	3.264	134.25	0.08(1)	1.0(1)	–	intra
				0.08	1.0	–	
C3–H3$\cdots$O2	2.517	3.589	170.53	0.07(1)	0.2(1)	-10.24	-1+x, y, z
				0.07	0.6	-5.84	
Trisilo (**2**):							
C4–H4C$\cdots$O1	2.582	3.428	136.40	0.06(1)	0.7(1)	-4.38	1-x, 1-y, 2-z
				0.06	0.7	-2.24	
C5–H5A$\cdots$O1	2.751	3.557	132.83	0.04(1)	0.5(1)	-4.38	1-x, 1-y, 2-z
				0.04	0.5	-2.24	
Pentaphe (**3**): no hydrogen bond							
Hexaphe (**4**): no hydrogen bond							

the interaction energy is three times larger (E_{int}=-27.80 kJ mol^{-1}), but also the hydrogen bond-topological properties are significantly changed, so that they indicate a stronger hydrogen bond: ϱ(H2O$\cdots$O1)=0.22 e$Å^{-3}$ and $\nabla^2\varrho$(H2O$\cdots$ O1)= 1.5 e$Å^{-5}$.

From the PES scan of disiloxane$\cdots$silanol [$(H_3Si)_2O\cdots HOSiH_3$], a hydrogen-bond energy of about E_HB=-10.5 kJ mol^{-1} was found at ϕ=115 ° (Figure 6.2). This value better compares with the experimental E_{int}. Moreover, ϱ(H$\cdots$O)=0.17 e$Å^{-3}$ and $\nabla^2\varrho$(H$\cdots$O)=1.9 e$Å^{-5}$ were predicted by the PES scan for ϕ=115 ° (Figure 6.13). Although there is no classical hydrogen-bond donor group in trisilo (**2**), there are nevertheless two hydrogen bonds in the crystal structure as Figure 7.1 (b) shows. The siloxane oxygen atom is the acceptor of two weak C–H$\cdots$O1 hydrogen bonds: C4–H4C$\cdots$O1 and C5–H5A$\cdots$O1. This impressively demonstrates that the basicity of the siloxane linkage at small Si–O–Si angles (here ϕ=117.81(3)) is even large enough to be acceptor for hydrogen bonds with protons that are only slightly acidic. C–H$\cdots$O hydrogen bonds are commonly found in molecular crystals with strong acceptor groups and play a key role in many biological interactions. [241,242]

In both experiment and theory, a bond critical point for the H$\cdots$O1 interactions can be found. The small values of the density and the Laplacian at the H$\cdots$O1 bcps are typical for these weak hydrogen bonds (here ϱ(H$\cdots$O1)=0.04 to 0.06 eÅ^{-3} and $\nabla^2\varrho$(H$\cdots$O1)=0.5 to 0.7 eÅ^{-5}, compare [99, 243]). Accordingly, the interaction energies per hydrogen bond between the two fragments in the crystal that are connected via the hydrogen bonds are small (-4.38/-2.24 kJ mol^{-1} (exp/theo)). In Chapter 6.3, it was shown that the interaction of one hydrogen donor atom with the siloxane oxygen atom is rather symmetrical, i.e. the hydrogen atom points to the centre of a VSCC or localisation domain of both oxygen lone pairs, causing the two lone pairs to merge into one for larger Si–O–Si angles. Figure 7.1 (b) shows that the two lone pairs of the siloxane group can also interact independently from each other with two different hydrogen atoms.

There are no hydrogen bonds in the crystal structures of pentaphe (**3**) and hexaphe (**4**) as there are neither hydrogen bond donors nor acceptors present. This does not necessarily mean that the crystal packing is less efficient and the lattice energy is smaller. This point is addressed in detail in the following discussion.

The electrostatic potential (ESP) of siloxanol (**1**) (Figure 7.2 (a)) is less strongly polarised than the ESP of pentaphe (**3**) in Figure 7.2 (c). For siloxanol (**1**), only the hydrogen atom H2O involved in the hydrogen bond is strongly positively polarised, showing the electrostatic contributions to the hydrogen bond O2–H2O$\cdots$O1. On the other hand, the ESP of pentaphe (**3**) exhibits a strong gradient between the positively and the negatively polarised sides of the molecule. The crystal packing of pentaphe (**3**) is therefore guided by the differences in the ESP in a way that a stacking of the negative phenyl groups alternating with the positive phenyl groups is most effective according to the principle of electrostatic complementarity. [143] Figure 7.2 (b) shows by means of the electron density mapped on the Hirshfeld surface of siloxanol (**1**) that strong covalent interactions within the hydrogen bond O2–H2O$\cdots$O1 are dominant and guide the crystal packing of siloxanol (**1**). On the other hand, there are no significant covalent intermolecular interactions in pentaphe (**3**), as the Hirshfeld surface in Figure 7.2 (d) shows.

The lattice energies of siloxanol (**1**) and pentaphe (**3**) are very similar even though the type of intermolecular interactions is very different. Table 7.3 confirms that electrostatic interactions are much more important for pentaphe (**3**) than for siloxanol (**1**) as 87.1/85.1 % (exp/theo) of the lattice energy of pentaphe (**3**) comes from electrostatic interactions but only 68.4/67.7 % in the case of siloxanol (**1**). The

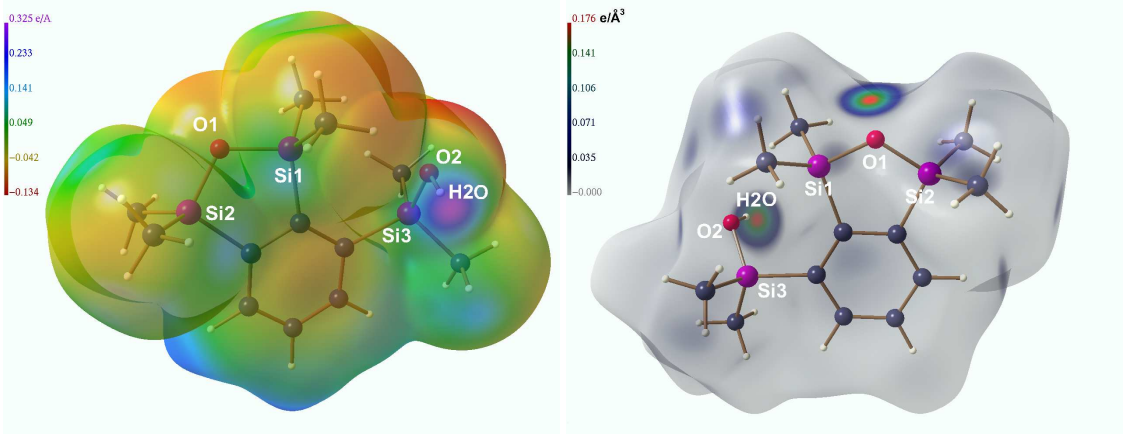

(a) ESP ($eÅ^{-1}$) of siloxanol (**1**) mapped on an ED isosurface of $0.0067\,eÅ^{-3}$

(b) ED ($eÅ^{-3}$) of siloxanol (**1**) mapped on a Hirshfeld surface

(c) ESP ($eÅ^{-1}$) of pentaphe (**3**) mapped on an ED isosurface of $0.0067\,eÅ^{-3}$

(d) ED ($eÅ^{-3}$) of pentaphe (**3**) mapped on a Hirshfeld surface

Figure 7.2: Experimental electrostatic potentials (ESPs) mapped on ED molecular surfaces and experimental ED mapped on Hirshfeld surfaces

Table 7.3: Lattice energies of cpds. **1** to **4** in kJ mol^{-1}
First row: experiment, second row: periodic-boundary calculations at experimental geometries, contributions of exchange+repulsion+dispersion terms (erd, absolute) and of the electrostatic term (es, absolute and relative) to the total lattice energy

cpd.	total	erd	es	es (%)
siloxanol (**1**)	-105.35	-33.30	-72.05	68.4
	-103.25	-33.30	-69.95	67.7
trisilo (**2**)	-41.30	-27.40	-13.90	33.7
	-62.55	-27.40	-35.15	56.2
pentaphe (**3**)	-103.88	-13.35	-90.53	87.1
	-89.31	-13.35	-75.96	85.1
hexaphe (**4**)	-82.02	7.15	-89.17	108.7
	-87.52	7.16	-94.68	108.2

percentage contribution of the ESP to the lattice energy is even more dominant for hexaphe (**4**) as only the electrostatic contributions are attractive but the exchange-repulsion and dispersion terms are overall repulsive. The negative lattice energy of hexaphe (**4**) is nevertheless by about 30-40 kJ mol^{-1} higher than for trisilo (**2**), where both covalent and electrostatic contributions to the lattice energy are small. The sum of exchange-repulsion and dispersion terms is constant between experiment and theory. Its negative value is highest for siloxanol (**1**) and decreases towards hexaphe (**4**). On the contrary, the electrostatic contributions show large variations between experiment and theory. However, it is clear that they are much larger for pentaphe (**3**) and hexaphe (**4**) without hydrogen bonds and are caused by stacking of phenyl groups that are polarised complementary to each other.

7.1.3 Interactions with Selected Donor Molecules

To get a better impression of the acceptor qualities of siloxanol (**1**) and trisilo (**2**) compared to disiloxane and compared to the other siloxanols involved in hydrogen bonds found in the CSD, isolated-molecule calculations on silanol and water complexes were performed. Figures 7.3 (a) to (d) show the structures of the hydrogen-bonded complexes of siloxanol (**1**) and trisilo (**2**) with silanol and water

after full geometry optimisation. Figure 7.3 (e) shows the fully optimised complex $H_2Si(OSiH_2)_2O\cdots$silanol of a model compound that is structurally closely related to the siloxanols $HOMe_2SiN(SiMe_2O)_2$-$SiMe_2$ [173] and $HOMe_2SiCH(SiMe_2O)_2$-$SiMe_2$ [174], which were found in the CSD and are also involved in hydrogen bonding (see Chapter 4.1). The siloxane linkages in these compounds are incorporated into a six-membered ring so that the Si–O–Si angle (ϕ=131.39 °) is larger than in the five-membered rings of siloxanol (**1**) and trisilo (**2**) (ϕ=117.39 and 117.92 °).

Considering the properties summarised in Table 7.4, it can be shown that the hydrogen bonds of siloxanol (**1**) and trisilo (**2**) to silanol are much stronger than the $H_2Si(OSiH_2)_2O\cdots$silanol hydrogen bond. The hydrogen-bond energies E_{HB}= -20.75 and -18.77 kJ mol^{-1} of the siloxanol$\cdots$silanol HB complex (**1s**) and the trisilo$\cdots$silanol HB complex (**2s**) are nearly twice as large as E_{HB}=-10.50 kJ mol^{-1} for the $H_2Si(OSiH_2)_2O\cdots$silanol HB complex. Any other property in Table 7.4 characterising the hydrogen bonds (geometrical parameters, bond-topological properties and the IR red shift) supports this finding. This can be explained by the fact that the Si–O–Si angles in siloxanol (**1**) and trisilo (**2**) are by about 14 ° smaller than in $H_2Si(OSiH_2)_2O$, which is consistent with the results of the PES scans.

The hydrogen bond in the siloxanol$\cdots$silanol HB complex (**1s**) is by 2 kJ mol^{-1} stronger than the one in the trisilo$\cdots$silanol HB complex (**2s**), which indicates that siloxanol (**1**) is a slightly better hydrogen-bond acceptor and the oxygen atom is more basic than in trisilo (**2**). This finding is again confirmed by all the other properties in Table 7.4. A comparison of the siloxanol$\cdots$water HB complex (**1w**) and trisilo$\cdots$water HB complex (**2w**) also shows that siloxanol (**1**) forms the stronger hydrogen bond.

If the siloxanol$\cdots$silanol HB complex (**1s**) is compared with the siloxanol$\cdots$water HB complex (**1w**) and the trisilo$\cdots$silanol HB complex (**2s**) with the trisilo$\cdots$water HB complex (**2w**), respectively, it can be found that the water molecule is a poor hydrogen-bond donor compared to silanol. The hydrogen bonds to silanol are about twice as strong as the hydrogen bonds to water, which can be seen from the hydrogen-bond energies. ϱ(H$\cdots$O)=0.23/0.22 eÅ^{-3} and $\nabla^2\varrho_{bcp}$=2.2/2.2 eÅ^{-5} of siloxanol$\cdots$silanol (**1s**) / trisilo$\cdots$silanol (**2w**) indicate a strong hydrogen bond [234, 237]. The values are close to the ones for O2–H2O$\cdots$O1 in the crystal structure of siloxanol (**1**) from theoretical calculations in periodic boundaries (ϱ(H$\cdots$O) = 0.22 eÅ^{-3} and $\nabla^2\varrho_{bcp}$ = 1.5 eÅ^{-5}).

Siloxanol (**1**) and trisilo (**2**) are better hydrogen-bond acceptors than the model

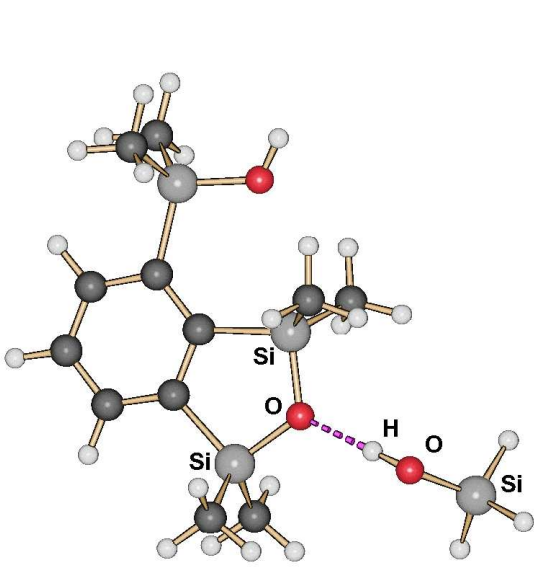

(a) Siloxanol···silanol HB complex (**1s**)

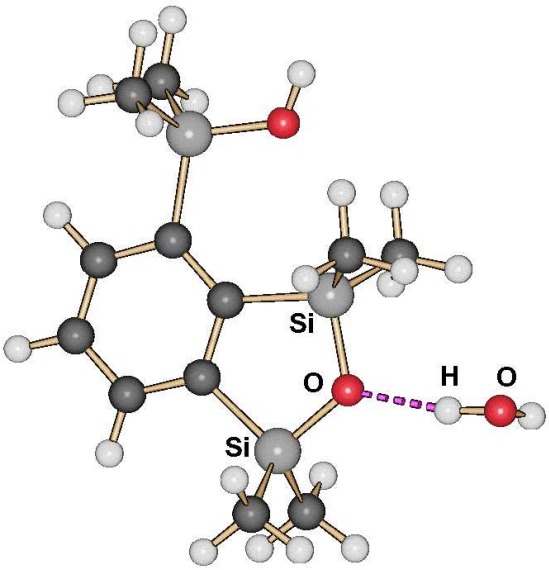

(b) Siloxanol···water HB complex (**1w**)

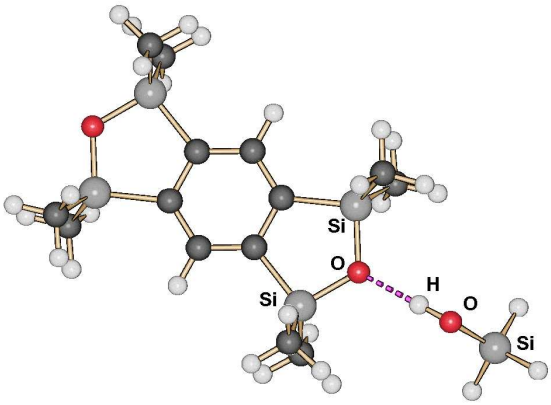

(c) Trisilo···silanol HB complex (**2s**)

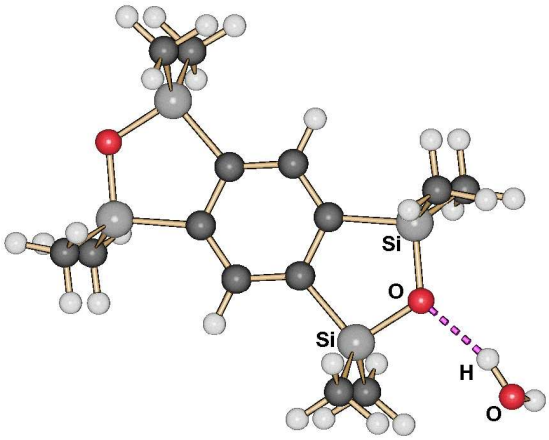

(d) Trisilo···water HB complex (**2w**)

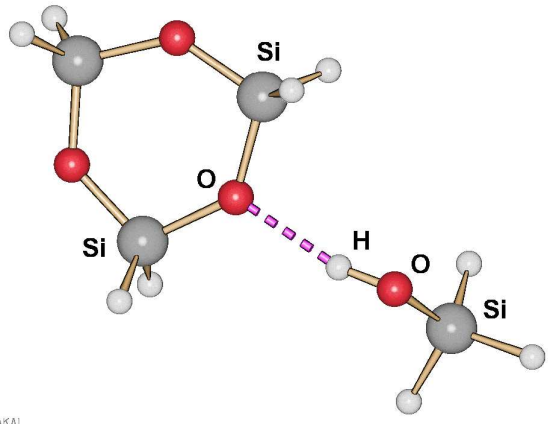

(e) $H_2Si(OSiH_2)_2O$···silanol HB complex

Figure 7.3: Geometries from isolated-molecule optimisations of scrutinised hydrogen-bonded (HB) complexes of cpds. **1** and **2** as well as of the model compound $H_2Si(OSiH_2)_2O$ with silanol (s) and water (w)

Table 7.4: Selected properties of hydrogen-bonded (HB) complexes of cpds. **1**, **2**, model compound $H_2Si(OSiH_2)_2O$ and model compound disiloxane ($H_3SiOSiH_3$) with silanol and water from isolated-molecule optimisations
Angles a in °, distances d in Å, ED ϱ(bcp) in e Å^{-3}, Laplacian of ED $\nabla^2\varrho$(bcp) in e Å^{-5}, hydrogen-bond energy E_{HB} in kJ mol^{-1}, IR red shift $\Delta\tilde{\nu}(OH)$ in cm^{-1}

a(Si–O–Si)	d(H...O)	d(O...O)	a(O-H...O)	ϱ(H···O)	$\nabla^2\varrho$(H···O)	E_{HB}	$\Delta\tilde{\nu}(OH)$
siloxanol···silanol HB complex (**1s**):							
117.92	1.824	2.797	177.51	0.23	2.2	-20.75	308.6
siloxanol···water HB complex (**1w**):							(symm/asymm)
118.16	1.922	2.882	169.74	0.17	1.9	-11.22	130.2/36.0
trisilo···silanol HB complex (**2s**):							
117.39	1.830	2.803	177.84	0.22	2.2	-18.77	292.2
trisilo···water HB complex (**2w**):							(symm/asymm)
117.58	1.947	2.890	163.50	0.18	2.0	-9.71	115.1/35.5
$H_2Si(OSiH_2)_2O$···silanol HB complex:							
131.39	1.979	2.925	166.15	0.16	1.8	-10.50	141.2
disiloxane···silanol HB complex:							
130.00	1.949	2.914	176.14	0.16	1.9	-8.30	160.7
disiloxane···silanol HB complex:							
120.00	1.929	2.896	178.43	0.17	1.9	-9.84	168.4
disiloxane···water HB complex:							(symm/asymm)
120.00	2.061	2.920	147.30	0.13	1.7	-2.31	48.8/28.5

compound disiloxane. This becomes clear by a comparison of the E_{HB} values of siloxanol/trisilo$\cdots$silanol (**1s**/**2s**) (E_{HB}=-20.75 and -18.77 kJ mol^{-1}) with disiloxane$\cdots$silanol at ϕ=120 ° (E_{HB} = -9.84 kJ mol^{-1}) as well as by a comparison between siloxanol/trisilo$\cdots$water (**1w**/**2w**) (E_{HB}=-11.22 and -9.71 kJ mol^{-1}) with disiloxane$\cdots$water at ϕ=120 ° (E_{HB} = -2.31 kJ mol^{-1}). It is not clear if $H_2Si(OSiH_2)_2O$ in the HB complex $H_2Si(OSiH_2)_2O\cdots$silanol is a better acceptor than disiloxane in the complex disiloxane$\cdots$silanol at ϕ=130 °. On the one hand, the hydrogen-bond energy of $H_2Si(OSiH_2)_2O\cdots$silanol is higher (E_{HB}= -10.50 kJ mol^{-1} compared to E_{HB}=-8.30 kJ mol^{-1}), but on the other hand, mainly the distances listed in Table 7.4 imply that disiloxane is the better acceptor.

7.2 Results of the Topological Analysis of the ED

7.2.1 Deformation Density and Laplacian

The one-dimensional plots of the Laplacian of the ED along different bond types shown in Figure 7.4 reveal the different bond characters. Figures 7.4 (a) and (c) compare a typical ionic bond (Si–O in siloxanol (**1**)) with a typical covalent bond (C–C in siloxanol (**1**)). The covalent bond exhibits two VSCCs (minima) at the carbon atoms forming the typically saddle-shaped bond region with the maximum at the position of the bcp. The maximum is still significantly negative, indicating that the VSCCs overlap to form a shared interaction. In the Si–O bond, the bcp is shifted towards the electropositive atom and is significantly positive. The whole bond region is shifted towards positive values. There is no maximum, but a plateau in the middle of the bond instead because there is no VSCC at the silicon atom, only a deep one at the oxygen atom. The Si–C bond (Figure 7.4 (b)) and the Si–H bonds (Figure 7.4 (d)) are in-between ionic and covalent character. There is not a plateau but a point of inflexion. The Laplacian values at the bcps are positive because the position of the bcp is shifted towards silicon, but the bonding region, i.e. the middle of the bond, is already at negative Laplacian values. The shape of the hydrogen bonds (Figures 7.4 (e) and (f)) in terms of the Laplacian is different. The oxygen lone pair (deep VSCC, minimum in the Laplacian) is directed towards the hydrogen atom. The bcps are located at a minimum of the Laplacian that is close to zero but still positive.

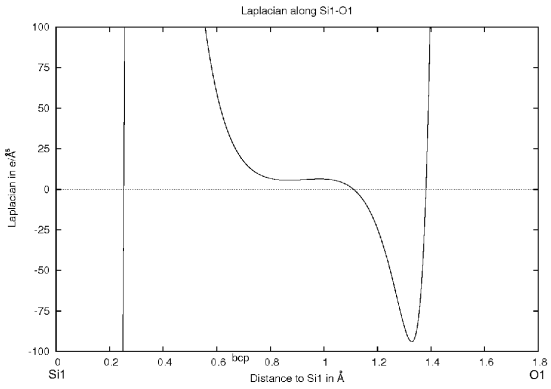

(a) Si1-O1 in siloxanol (**1**)

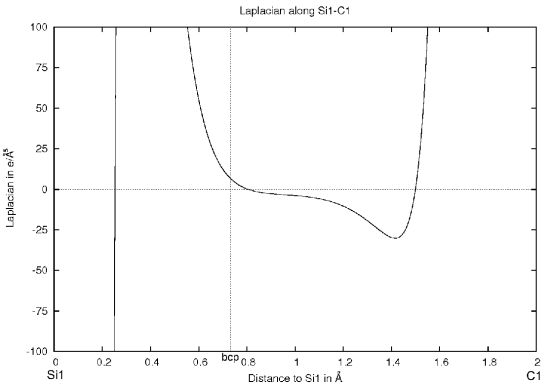

(b) Si1-C1 in siloxanol (**1**)

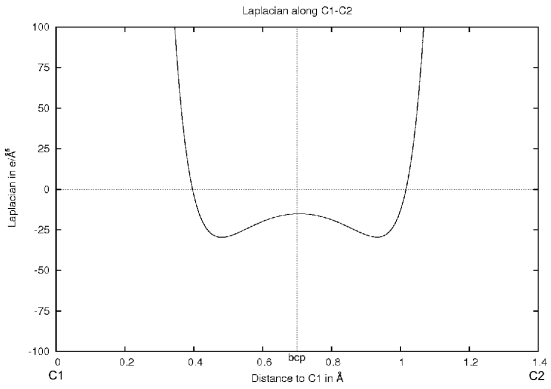

(c) C1-C2 in siloxanol (**1**)

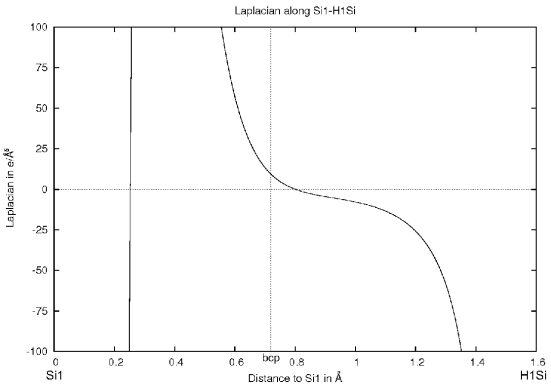

(d) Si1-H1Si in pentaphe (**3**)

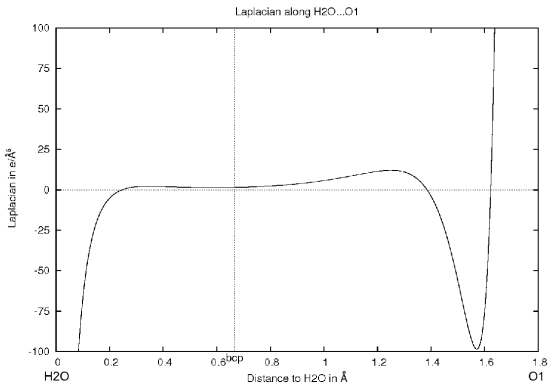

(e) hydrogen bond H2O$\cdots$O1 in siloxanol (**1**)

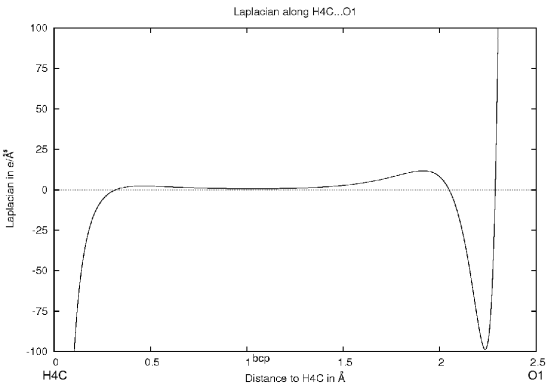

(f) hydrogen bond H4C$\cdots$O1 in trisilo (**2**)

Figure 7.4: One-dimensional Laplacian of the ED along various bonds of different types *Periodic-boundary calculations at experimental geometries, positions of bcps are plotted as vertical lines*

Figure 7.5 shows the experimental static deformation density and Laplacian distributions in the bicyclic fragment and in the plane of the hydrogen bond of siloxanol (**1**). Figure 7.5 (a) exemplifies the difference between homopolar covalent bonds (C–C), heteropolar covalent bonds (Si–C), and ionic bonds (Si–O) in terms of deformation density. The maximum of the deformation density is observed in the middle of C-C bonds. For Si-C bonds, there are two kinds of maxima: The smaller ones are situated at the silicon atoms and the larger ones are located at carbon atoms. For the Si-O bonds there are only maxima situated at the oxygen atoms.

The effects found in the one-dimensional Laplacian graphs can also be found in the contour plots (Figure 7.5 (c) and (d)). There is one VSCC at each carbon atom of the C-C bond forming the typically saddle-shaped region of a homopolar covalent bond (compare Figure 7.4 (c)). There is one VSCC at the carbon atom but none at the silicon atom for the Si-C bond (compare Figure 7.4 (b)); however, there is a pronounced deformation of the Laplacian toward the silicon atom. Finally, there is one large VSCC at the oxygen atom that is not deformed toward the silicon atom for the Si-O bond, so that silicon and oxygen atoms nearly retain the spherical form of ions (compare Figure 7.4 (a)). As can be seen from Figures 7.5 (b) and (d), the deformation of the oxygen lone pair toward the hydrogen atom is consistent with the formation of the hydrogen bond O2–H2O$\cdots$O1.

The static deformation-density distribution of trisilo (**2**) is shown in Figure 7.6 (a) from experimental and in Figure 7.6 (b) from theoretical refinements. Both maps indicate successful multipolar modelling because every expected feature (compare discussion above for the deformation-density maps of siloxanol (**1**)) is developed and the maps are quite similar. However, some differences between experimental and theoretical deformation-density maps shall be discussed here. In theory, bonds seem to be more ionic because silicon and oxygen atoms are more isolated. In the experiment, there is at least one isocontour line connecting Si and C or O atoms, respectively. This indicates the presence of some covalent contributions also to the ionic Si–O bond, which cannot be seen in the theoretical case. The deformation-density maxima at the oxygen atom in the Si–O bond are much more pronounced in experiment than in theory. This trend can be seen in the bond-topological properties, too, where the density at the Si–O bcp is higher for experimental than for theoretical refinements for all four compounds (compare Table 7.5). In contrast, the oxygen lone pairs are much more pronounced in the theoretical map. The reason for the discussed differences are different values of κ in experiment and theory, compare Table A.1.

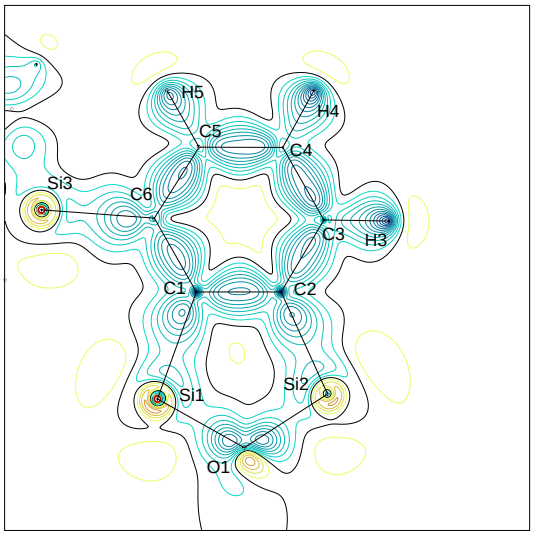

(a) Deformation-density map of bicyclic fragment of siloxanol (**1**)

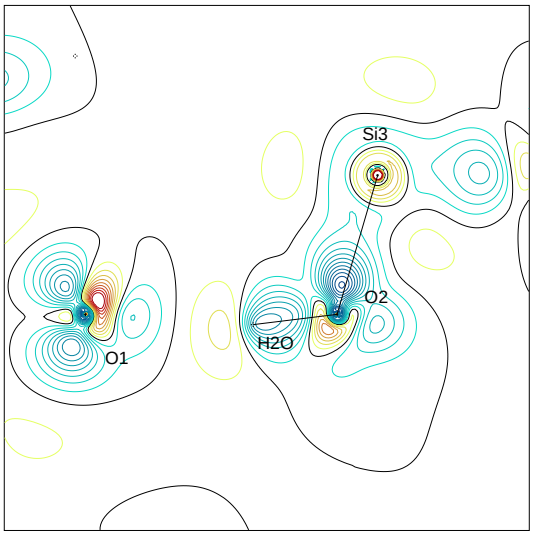

(b) Deformation-density map of hydrogen bond in siloxanol (**1**)

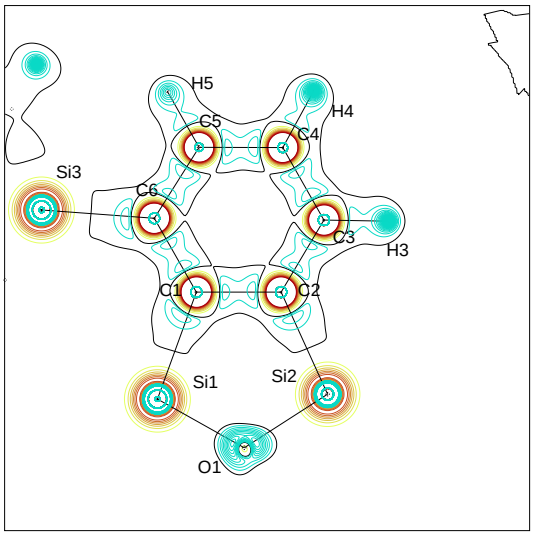

(c) Laplacian-distribution map of bicyclic fragment of siloxanol (**1**)

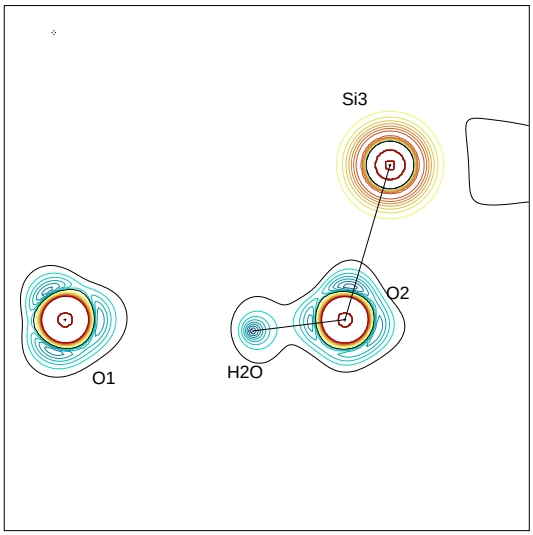

(d) Laplacian-distribution map of hydrogen bond in siloxanol (**1**)

Figure 7.5: Experimental static deformation-density and Laplacian-distribution maps *Deformation-density maps: contour interval = 0.1 e Å^{-3}, blue = positive, red = negative, black = zero; Laplacian-distribution maps: contour interval = 25 e Å^{-5}, blue = negative, red = positive, black = zero*

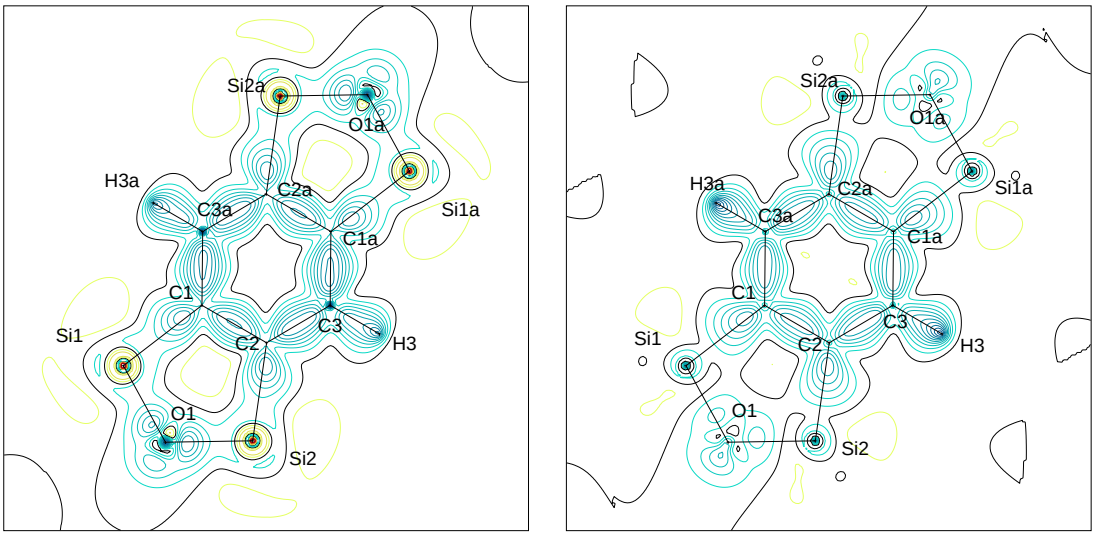

(a) Experimental deformation-density map (b) Theoretical deformation-density map

Figure 7.6: Comparison between experimental and theoretical (periodic-boundary calculation at experimental geometry) static deformation-density maps for the molecular plane of trisilo (**2**)
Contour interval = 0.1 e Å^{-3}, blue = positive, red = negative, black = zero

The three-dimensional deformation densities of trisilo (**2**) and hexaphe (**4**) as derived from theoretical refinements are depicted in Figure 7.7. They are compared to the three-dimensional Laplacian distributions. For trisilo (**2**), i.e. for ϕ=117.81(3)°, both deformation density and Laplacian show the expected cap-like shape of the oxygen lone pair electrons, which can be found for the Laplacian as well as for the ELI-D in the PES scans of disiloxane ($H_3SiOSiH_3$). This underlines the good hydrogen-bond acceptor qualities of trisilo (**2**) and confirms a connection between the cap-like lone pair shape and the basicity of the oxygen atom. The same holds for siloxanol (**1**) (not shown here), for which the three-dimensional deformation density and Laplacian distribution close to the siloxane oxygen atom is nearly identical to trisilo (**2**). If one compares the VSCCs in Figure 7.7 (b) closely with the ones for ϕ=120° in $H_3SiOSiH_3$ (Figures 6.9 (c) and (d)), it is obvious that the VSCC for the Si–O bonds are much more pronounced here. In the PES scans, VSCCs for the Si–O bonds are small and only appear if the isovalue is reduced. Here, VSCCs for the Si–O bonds are large and merge with the VSCCs of the lone pairs at lower isovalues.

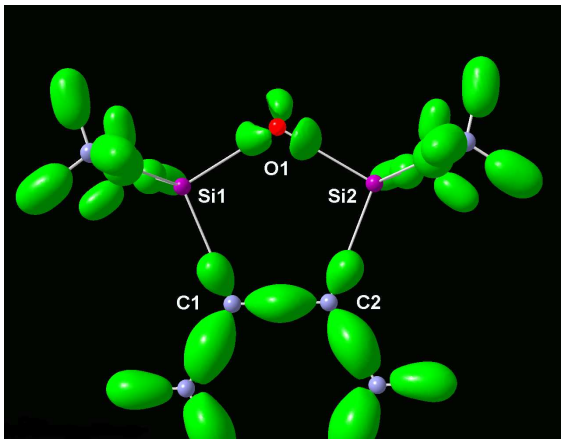

(a) Deformation density of trisilo (**2**), ϕ=117.81 °

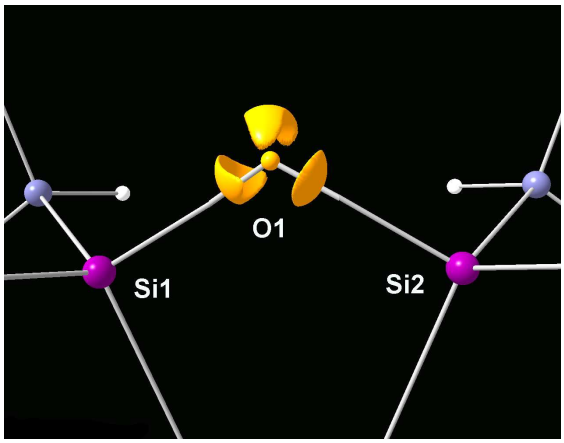

(b) Laplacian of trisilo (**2**) only around O1, ϕ=117.81 °

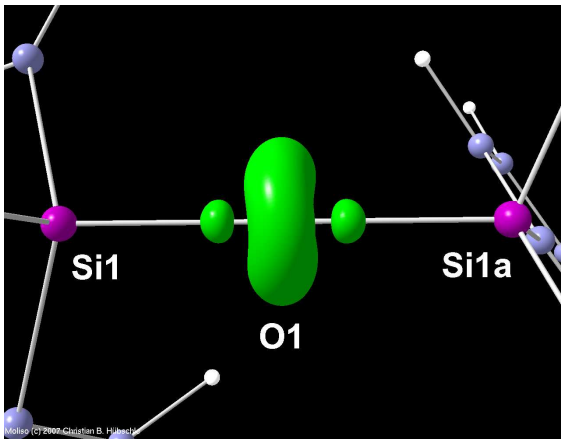

(c) Deformation density of hexaphe (**4**) only around O1, ϕ=180.00 °

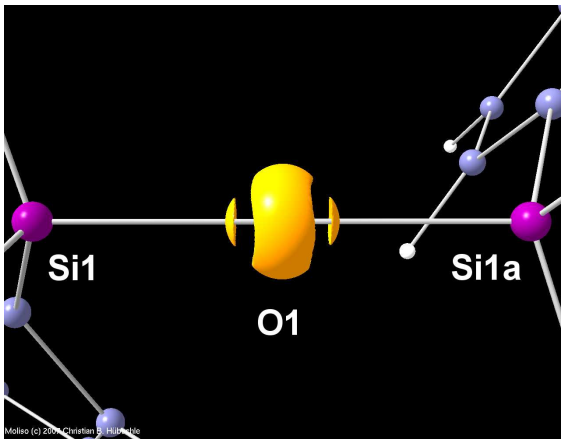

(d) Laplacian of hexaphe (**4**) only around O1, ϕ=180.00 °

Figure 7.7: Three-dimensional isosurface representations of the static deformation density and the Laplacian of trisilo (**2**) and hexaphe (**4**)

Periodic-boundary calculations at experimental geometries, isovalue for deformation density = 0.25 eÅ^{-3}, isovalue for Laplacian = -83.00 eÅ^{-5}

For ϕ=180 °, a ringlike shape of the VSCCs is expected from the PES scans (Figures 6.9 (b) and 6.18 (d)). For hexaphe (**4**), both deformation density (Figure 7.7 (c)) and Laplacian (Figure 7.7 (d)) show that the lone-pair electrons are indeed distributed as expected. However, deformation-density and Laplacian maxima for the Si–O bonds can still be clearly identified in Figure 7.7. The results for siloxanol (**1**) are similar to the ones of trisilo (**2**) and are therefore not shown; the results for pentaphe (**3**) are ambiguous because the Si–O–Si angle of ϕ=162.03 ° is very near the point of the chemical catastrophe and are thus also not shown.

7.2.2 Gradient-Vector Field and Bond-Path Analysis

Representations of the experimental gradient-vector fields of cpds. **1** to **4** in planes including the siloxane linkage are shown in Figure 7.8. Zero-flux surfaces enclosing atomic basins are plotted together with bond paths, bond- and ring-critical points, which are the main features of the QTAIM. An atom is bounded by zero-flux surfaces so that a visual impression of the atomic shape can be obtained. Carbon and silicon atoms have a triangular shape in this plane and are smaller than the hydrogen atoms that are not involved in hydrogen bonds.

Significant differences in the shapes of the oxygen atoms are visible in the siloxane linkages at small Si–O–Si angles (siloxanol (**1**) and trisilo (**2**)) compared to large Si–O–Si angles (pentaphe (**3**) and hexaphe (**4**)): The oxygen atom has lot of space towards the upper side for small angles, but for large angles, the oxygen atom is nearly totally enclosed by the silicon atoms. Hydrogen-bonding is only feasible if there is the possibility of forming a common zero-flux surface between the donor hydrogen atomic basin and the acceptor oxygen atomic basin. It is obvious that this is only feasible for small Si–O–Si angles. For trisilo (**2**), it was possible to force the bond paths of the weak hydrogen bonds C4–H4C$\cdots$O1 and C5–H5A$\cdots$O1 into the plane (H4C and H5A of the molecule generated by symmetry are far outside this plane).

In Chapter 6.2.1 it was shown for the PES scan of $H_3SiOSiH_3$ that the Si–O bonds are not strained, i.e. the difference between bond path and bond distance was smaller than 0.001 Å between ϕ=85 and 180 °. It can be seen in Figure 7.8 that the Si–O bonds in cpds. **1** to **4** are also not significantly bent. But additionally, a bond-path analysis was performed. The maximum difference between bond-path length and bond distance in all four cpds. is 0.004 Å and the mean difference is 0.001 Å. The maximum displacement of the bcp from the direct internuclear axis

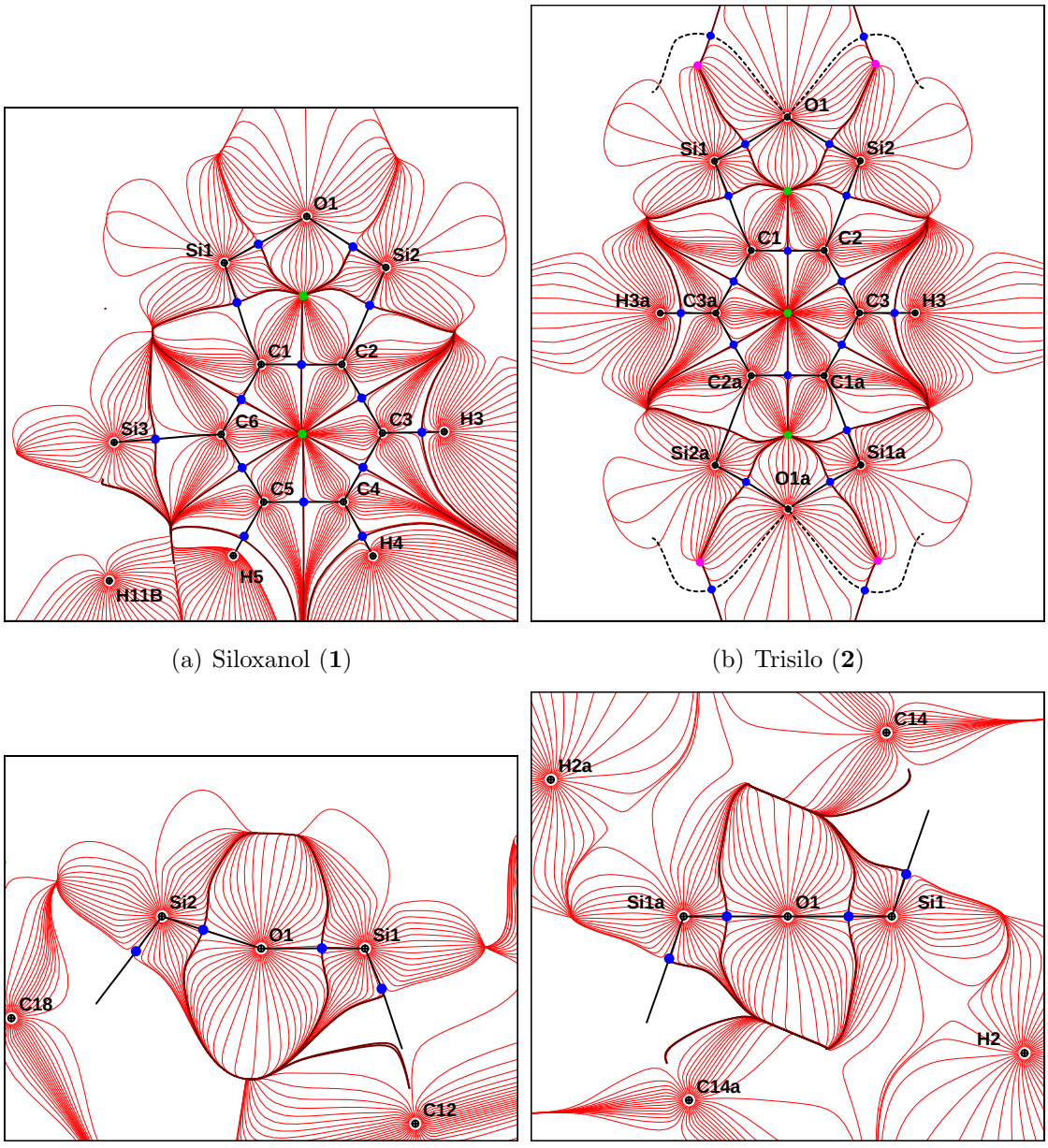

(a) Siloxanol (**1**)

(b) Trisilo (**2**)

(c) Pentaphe (**3**)

(d) Hexaphe (**4**)

Figure 7.8: Experimental gradient-vector fields and molecular graphs of molecular planes including the siloxane linkage Si–O–Si of cpds. **1** to **4**

is 0.03 Å. These values are small so that the bonds might be considered as being straight. However, the differences are a bit larger than 0.001 Å as found for the PES scans. In contrast, it could be shown in Figure 6.19 that the Si–O bond attractor in the ELI-D is significantly shifted away from the internuclear axis for the PES scans of $H_3SiOSiH_3$. The displacement of the ELI-D attractor between 85 ° and 180 ° ranges from 0.238 to 0.192 Å. All results concerning gradient-vector fields and bond-path analysis are nearly identical for experimental and theoretical structure factors.

7.2.3 Bond-Topological Properties

Table 7.5 summarises bond- and ring-topological properties of cpds. **1** to **4**. Each first line gives experimental results, lines two to four give theoretical results (periodic-boundary calculations at experimental geometry, isolated-molecule calculations at experimental geometry and at optimised geometry). Properties of bonds to or within phenyl or methyl groups are averaged as well as properties of the phenyl ring-critical points (rcp), complete lists can be found in Tables A.45 to A.51.
The properties agree between the experiment and the different theoretical methods in a way that general chemical conclusions can be drawn. The bcp is located closer to the more electropositive atom as expected, but relative to the bond distance, it is located closer to the Si atom in the Si–C bonds than in the Si–O bonds although the electronegativity difference is larger in the latter one. From the PES scans of $H_3SiOSiH_3$ it can be expected that the Si–O bonds in pentaphe (**3**) and hexaphe (**4**) are more ionic and stronger than in siloxanol (**1**) and trisilo (**2**). It cannot be confirmed that the Si–O bonds in pentaphe (**3**) and hexaphe (**4**) are stronger because the values of the ED at the Si–O bcps scatter between ϱ(Si–O)=0.81 and 0.95 eÅ^{-3}. But the positive Laplacian of the ED at the Si–O bcp is larger by 3 to 5 eÅ^{-5} for pentaphe (**3**) and hexaphe (**4**) compared to siloxanol (**1**) and trisilo (**2**), so that it can be confirmed that the Si–O bonds are more ionic for larger Si–O–Si angles. The bond ellipticity is close to zero for Si–O bonds, indicating a cylinder-symmetrical shape. If there was partial back-bonding character as the obsolete bond model depicted in Figure 4.2 suggests, the ellipticity should be around 0.2.

Table 7.5: Bond-topological properties of cpds. **1** to **4**
First line: experiment, second line: periodic-boundary calculation at experimental geometry, third line: isolated-molecule calculation at experimental geometry, fourth line: isolated-molecule calculation at optimised geometry, ED ϱ(bcp) in e$Å^{-3}$, Laplacian $\nabla^2\varrho$(bcp) in e$Å^{-5}$, ellipticity ε and delocalization index δ(A,B) without units

bond	ϱ(bcp)	$\nabla^2\varrho$(bcp)	ε	δ(A,B)	bond	ϱ(bcp)	$\nabla^2\varrho$(bcp)	ε	δ(A,B)
siloxanol (**1**):					trisilo (**2**):				
Si1–O1	0.86(1)	16.7(1)	0.04		Si1–O1	0.94(1)	16.0(1)	0.00	
	0.76	20.0	0.03			0.82	20.6	0.03	
	0.86	18.4	0.03	0.368		0.90	20.1	0.03	0.378
	0.87	18.5	0.03	0.378		0.88	18.9	0.03	0.381
Si2–O1	0.90(1)	18.3(1)	0.04		Si2–O1	0.95(1)	16.4(1)	0.03	
	0.79	21.5	0.03			0.82	20.7	0.03	
	0.91	20.1	0.03	0.380		0.90	20.1	0.03	0.377
	0.89	19.6	0.03	0.384		0.87	18.9	0.03	0.381
Si3–O2	0.97(1)	19.6(1)	0.13		Si1–Cph	0.77(1)	2.8(1)	0.04	
	0.87	21.0	0.01			0.75	7.6	0.04	
	0.93	20.9	0.07	0.382		0.82	4.9	0.07	0.415
	0.87	18.8	0.07	0.382		0.81	4.3	0.07	0.424
Si1–C1	0.78(1)	2.3(1)	0.03		Si1–Cmethyl	0.81(1)	4.5(1)	0.03	
	0.74	6.7	0.11			0.78	8.2	0.07	
	0.81	4.2	0.07	0.428		0.85	4.8	0.03	0.456
	0.78	3.4	0.07	0.430		0.83	4.1	0.03	0.456
Si2–C2	0.82(1)	2.9(1)	0.03		C1–C2	2.05(1)	-17.7(1)	0.18	
	0.77	7.6	0.09			1.98	-14.9	0.16	
	0.83	5.2	0.07	0.414		2.04	-21.8	0.11	1.403
	0.81	4.4	0.07	0.422		2.06	-22.3	0.11	1.400
Si3–C6	0.74(1)	4.4(1)	0.06		C1–C3a	2.19(3)	-19.4(1)	0.05	
	0.72	8.1	0.10			2.05	-15.9	0.19	
	0.82	4.7	0.08	0.427		2.12	-24.2	0.16	1.395
	0.81	4.1	0.08	0.438		2.14	-24.8	0.16	1.397
Si-Cmethyl	0.82(1)	7.4(1)	0.06		C2–C3	2.15(2)	-17.8(1)	0.12	
	0.79	8.6	0.07			2.04	-15.8	0.19	
	0.86	5.3	0.03	0.452		2.12	-24.3	0.16	1.398
	0.83	4.5	0.03	0.465		2.14	-24.8	0.16	1.395
Cph–Cph	2.14(4)	-19.7(1)	0.20		silox	0.17	3.4		
	2.04	-16.5	0.16		ring	0.21	3.4		
	2.12	-24.2	0.16	1.390		0.20	3.1		
	2.13	-24.3	0.16	1.404		0.19	3.0		
O2–H2O	1.82(13)	-31.7(6)	0.05		phenyl	0.22	3.1		
	2.42	-48.7	0.00		ring	0.21	3.0		
	2.44	-60.8	0.00	0.669		0.17	3.5		
	2.49	-63.4	0.00	0.652		0.17	3.6		
silox	0.19	2.7							
ring	0.17	3.3							
	0.20	3.1							
	0.19	3.0							
phenyl	0.17	3.3							
ring	0.22	3.0							
	0.17	3.5							
	0.17	3.6							

pentaphe (**3**):					hexaphe (**4**):				
Si1–O1	0.92(1)	20.9(1)	0.02		Si1–O1	0.92(1)	22.4(1)	0.03	
	0.84	24.3	0.03			0.85	25.2	0.01	
	0.94	23.4	0.00	0.389		0.93	23.6	0.01	0.372
	0.89	20.5	0.01	0.392		0.89	21.4	0.01	0.373
Si2–O1	0.87(1)	23.3(1)	0.01		Si1–Cph	0.79(1)	5.3(1)	0.07	
	0.81	24.7	0.01			0.74	10.1	0.03	
	0.93	22.4	0.00	0.376		0.84	5.0	0.07	0.435
	0.88	20.4	0.01	0.377		0.82	4.2	0.07	0.446
Si–Cph	0.74(1)	7.0(1)	0.05		Cph–Cph	2.15(1)	-19.0(1)	0.16	
	0.74	8.8	0.06			2.05	-16.3	0.20	
	0.85	5.2	0.07	0.438		2.15	-24.9	0.18	1.399
	0.82	4.4	0.06	0.447		2.16	-25.4	0.18	1.410
Cph–Cph	2.16(1)	-19.5(1)	0.17		phenyl	0.21	3.2		
	2.06	-17.3	0.20		C1	0.20	3.0		
	2.15	-24.9	0.18	1.400		0.16	3.6		
	2.16	-25.4	0.18	1.413		0.17	3.6		
Si1–H1Si	0.73(2)	5.7(1)	0.05						
	0.72	9.5	0.03						
	0.82	4.5	0.03	0.460					
	0.82	4.4	0.03	0.465					
phenyl	0.20	3.1							
	0.20	3.0							
	0.16	3.6							
	0.17	3.6							

The values of the ED at the Si–C bcp are not higher than for ionic Si–O bonds (ϱ(Si–C)=0.72 to 0.85 eÅ^{-3} compared to ϱ(Si–O)=0.82 to 0.97 eÅ^{-3}), but the value of the Laplacian is significantly smaller ($\nabla^2\varrho$(Si–C)=2.3 to 8.8 eÅ^{-5} compared to $\nabla^2\varrho$(Si–O)=16.0 to 25.2 eÅ^{-5}) yet still positive. That means that Si–O bonds have highly ionic character but Si–C bonds have mainly ionic character with strong covalent contributions. In cpds. **1** to **4** there are only aromatic C–C bonds which exhibit a much larger value of the ED at the bcp and a large negative Laplacian value (ϱ(C–C)=1.98 to 2.19 eÅ^{-3} and $\nabla^2\varrho$(C–C)=-14.9 to -25.4 eÅ^{-5}). This classification of the bonds agrees with the classification according to the deformation density maps of Figure 7.5.

The values of the delocalization index for Si–O bonds are smallest, but the ones for the Si–C bonds are only a bit larger. As these values are more than 0.5 away from the formal bond order of 1, both bond types have to be referred to as having mainly ionic bond character. For C–C bonds in the phenyl rings, the values of the delocalization index are close to the formal bond order of 1.5, indicating predominant covalent bond character.

It is interesting to compare the bond-topological properties of the short O–H bond with a protonic hydrogen atom (0.967 Å) with the ones of the long Si–H bond with

a hydridic hydrogen atom (1.484 Å). The bond O2–H2O possesses a large amount of ED at the bcp (up to 2.49 eÅ^{-3}) and a large negative Laplacian value (up to -63.4 eÅ^{-5}); the bond Si1–H1Si has a small amount of ED at the bcp (a minimum of 0.72 eÅ^{-3}) and a small positive Laplacian value (a minimum of 4.4 eÅ^{-5}). C–H bonds range in between these values (averaged values: ϱ(C–H)=1.70 eÅ^{-3} and $\nabla^2\varrho$(C–C)=-20.0 eÅ^{-5} , see Appendix).

The five-membered rings incorporating the siloxane linkage and the phenyl rings exhibit very similar properties at the rcp. The values range from ϱ(rcp)=0.17 to 0.22 eÅ^{-3} and $\nabla^2\varrho$(C–C)=2.7 to 3.6 eÅ^{-5}. These values are typical for five- or six-membered rings. If the ring size decreases accompanied by a decrease of the distance of the rcp to the atoms, the density increases (compare properties for three-membered rings within this doctoral thesis).

It seems to be a general trend that the values from experimental and from theoretical structure factors - both contain crystal effects and multipole modelling - vary most strongly. The values from isolated-molecule calculations are closer to the experimental values than the values from periodic-boundary calculations are. It is striking that the ED at the bcp is lowest for periodic-boundary calculations and the Laplacian most positive. A reason might be that more elaborated basis sets could be used in the case of isolated-molecule calculations. The values from isolated-molecule calculations are very close to each other even though different geometries were the basis for the calculations (experimental vs. optimised geometry). These results imply on the one hand that it is more important which basis sets are used than if experimental or optimised geometries are considered or crystal effects are present or not. On the other hand, this discussion shows that the experimental results are very reliable.

7.2.4 Atomic Properties

Table 7.6 summarises the atomic properties of cpds. **1** to **4**. Like for the bond-topological properties, the experimental (first line) and three different theoretical results are shown. Atomic properties for carbon atoms in methyl groups, in phenyl groups not bonded to Si and in phenyl groups bonded to Si are averaged. Complete lists can be found in Tables A.52 to A.55.

As expected for a highly ionic bond, the silicon atoms in the Si–O bonds are highly positive whereas the oxygen atoms are highly negative. The charges are in the range found from the PES scans of $H_3SiOSiH_3$. But the expected increase of

the charge separation upon increasing the Si–O–Si angle can be found here only for experiment and periodic-boundary calculations, but not for isolated-molecule calculations. This shows for Si and O atoms that the charges coming from a crystal environment (experiment and periodic-boundary calculations, both incorporating crystal effects) are similar as expected and vary from the values coming from isolated-molecule calculations. This trend cannot be found for C and H atoms as it also could not be found for bond-topological properties, see above. The charges of the silicon atoms within the crystal environments (no differences between Si atoms in siloxane or silanol groups) vary between Q=2.43 to 2.98 e, whereas the charges from isolated-molecule calculations are larger and in a much smaller range (Q=2.95 to 3.02 e). In contrast, the atomic volumes V_{001} slightly decrease from periodic-boundary to isolated-molecule calculations.

For the oxygen atoms in the siloxane group, the same trend on the volumes V_{001} can be found: They increase from periodic-boundary (ranging from V_{001}=13.7 to 16.8 Å^3) to isolated-molecule (V_{001}=18.1 to 19.5 Å^3) calculations. For the charges, the range of values is Q=-1.23 (at the smallest Si–O–Si angle) to -1.92 e (at the largest Si–O–Si angle), but there is no systematic trend. Within the isolated-molecule results, a differentiation between the oxygen atoms in the siloxane linkage and the silanol group can be made: O2 in siloxanol (**1**) is charged less negatively, but its volume is largest.

The differences between the protonic hydrogen atom H2O in siloxanol (**1**) and the hydridic hydrogen atom H1Si in hexaphe (**4**) are obvious. H2O is positively charged by 0.59 to 0.70 e and its volume is small (1.7 to 3.4 Å^3); H1Si is negatively charged by -0.56 to -0.76 e and its volume is slightly larger than an average carbon atom (12.9 to 14.2 Å^3). The average values for a hydrogen atom bonded to a carbon atom are about Q=0.00 e and V_{001}=6.5 Å^3 (see Tables A.52 to A.55).

For the carbon atoms, there are also no discrepancies between the different compounds but only between different carbon types, i.e. neighbouring spheres, as expected from Bader's proposition of transferability [23]. The carbon atoms bonded to a silicon atom, regardless of if they are incorporated into methyl groups or phenyl groups, are negatively charged by -0.42 to -0.83 e. The charges of the C_{ph} atoms are on average close to neutrality, which makes them clearly distinguishable from the silicon-bonded atoms. The volumes are a bit larger than for the carbon atoms in the phenyl groups not bonded to a Si atom.

Table 7.6: Atomic properties of cpds. **1** to **4**

First line: experiment, second line: periodic-boundary calculation at experimental geometry, third line: isolated-molecule calculation at experimental geometry, fourth line: isolated-molecule calculation at optimised geometry, charge Q_{001} cut at ϱ=0.001 e$\AA^{-3}$ is equal to charge of total basin Q_{tot}, Q in e, volumes V_{001} and V_{tot} in $\AA^3$

atom	Q	V_{001}	V_{tot}	atom	Q	V_{001}	V_{tot}	atom	Q	V_{001}	V_{tot}
siloxanol (**1**):											
Si1	2.49	5.7	5.8	O1	-1.23	14.1	15.6	Cph(–Si)	-0.42	12.0	12.5
	2.82	4.5	4.7		-1.57	13.7	16.8		-0.61	12.1	13.2
	2.97	4.3			-1.64	19.0			-0.69	13.9	
	2.95	4.6			-1.63	19.3			-0.69	14.1	
Si2	2.50	5.8	5.8	O2	-1.61	19.7	21.5	C_{ph}	0.29	10.6	12.0
	2.82	4.6	4.6		-1.48	17.4	19.9		-0.15	12.5	14.4
	2.99	4.2			-1.39	19.5			0.01	12.2	
	2.97	4.5			-1.39	19.7			0.01	12.1	
Si3	2.46	5.9	6.0	H2O	0.70	1.7	1.7	C_{Me}	-1.33	17.3	18.8
	2.78	4.8	5.1		0.59	1.8	1.9		-0.64	12.0	13.5
	2.99	4.2			0.59	3.4			-0.67	13.6	
	2.97	4.5			0.59	3.3			-0.73	14.4	
trisilo (**2**):											
Si1	2.43	5.5	5.7	C1	-0.39	11.1	13.2	C3	-0.23	11.4	12.8
	2.75	4.7	4.8		-0.69	12.7	14.3		-0.03	11.1	12.4
	2.98	4.3			-0.69	13.9			0.00	12.3	
	2.96	4.6			-0.68	14.1			0.01	12.2	
Si2	2.43	5.8	6.2	C2	-0.39	11.3	12.8	C_{Me}	-0.83	13.2	14.5
	2.74	5.2	5.5		-0.69	12.8	14.1		-0.60	12.0	13.2
	2.98	4.3			-0.70	14.1			-0.67	14.0	
	2.96	4.5			-0.68	14.1			-0.71	14.6	
O1	-1.56	14.9	17.5								
	-1.73	15.5	18.0								
	-1.64	19.2									
	-1.64	19.5									
pentaphe (**3**):											
Si1	2.52	6.3	6.3	O1	-1.59	15.8	18.3	C_{ph}	-0.10	12.3	12.8
	2.82	4.9	5.1		-1.72	15.7	18.0		-0.03	12.0	12.6
	2.98	4.5			-1.71	18.4			0.00	12.3	
	2.96	4.8			-1.69	18.7			-0.01	12.3	
Si2	2.79	5.0	5.2	C(–Si)	-0.44	11.6	12.3	H1Si	-0.56	12.9	15.9
	2.88	4.6	4.7		-0.61	12.3	12.9		-0.76	14.2	17.2
	3.02	4.1			-0.74	13.7			-0.68	14.0	
	2.98	4.4			-0.76	14.1			-0.67	14.2	
hexaphe (**4**):											
Si1	2.71	4.7	4.9	C(–Si)	-0.51	11.5	12.8	C_{ph}	-0.12	12.1	12.8
	2.98	4.0	4.1		-0.73	12.8	13.5		-0.01	11.8	12.5
	3.02	4.1			-0.74	13.5			-0.05	12.3	
	2.98	4.4			-0.73	13.7			-0.05	12.2	
O1	-1.47	14.8	18.0								
	-1.92	16.8	18.3								
	-1.72	18.1									
	-1.71	18.1									

7.2.5 Source Function

The local source function along a bond path helps to reveal the bond character. It is correlated to the Laplacian of the same bond path. [59] Therefore, the same six bonds as in Figure 7.4 are displayed in Figure 7.9. VSCCs at oxygen atoms that are minima in the Laplacian can be found in the local source function as maxima. Their values are always positive, i.e. they contribute to the density at the bcp of the bond which was chosen as reference point. The remaining positive contributions come from the core electrons of the atoms, for Si atoms the outer core shell is visible as a large maximum. In the case of a covalent bond, see Figure 7.9 (c), the region around the bcp acts as a source for the density. The bond can be described as a localised phenomenon.

Regarding bonds for which ionic contributions dominate in terms of the local source function, the region around the bcp acts as a sink. Hence, Si–O, Si–C, Si–H and hydrogen bonds can be referred to as mainly ionic. But there are significant differences between them. Si–O as a strongly ionic bond (Figure 7.9 (a)) exhibits a deep minimum around the bcp and the asymmetry of the graph is pronounced. For Si–C (Figure 7.9 (b)), the region around the bcp acts only moderately as a sink, suggesting that significant covalent contributions are present, too. The Si–H bond (Figure 7.9 (d)) rather resembles the ionic case of Si–O. For the hydrogen bonds (Figure 7.10 (e) and (f)), the oxygen lone pairs which dominate the interaction are clearly visible. The strong hydrogen bond H2O$\cdots$O1 in siloxanol (**1**) has clearly ionic character because there is a pronounced minimum at the bcp. For the weak hydrogen bond H4C$\cdots$O1 in trisilo (**2**), the interaction is hardly detectable in the local source function (consider the different scales at the y-axes).

The four bond types Si–O, Si–C, C–C and Si–H shall also be compared using the integrated source function, Figure 7.10. Percentage source contributions of the atoms to the reference points are represented by the atoms' radii, blue indicating positive contribution (source), red indicating negative contribution (sink). The contributions of the substituents are given as the sum over all atoms of the corresponding substituent. The absolute numbers of the contributions can be found in Tables A.56 to A.59. In the experiment, the contributions from the directly bonded atoms are larger than in theory, i.e. in theory, the influence of the substituents is more pronounced. However, the agreement between experiment and theory is high enough so that chemical differences will only be discussed for the

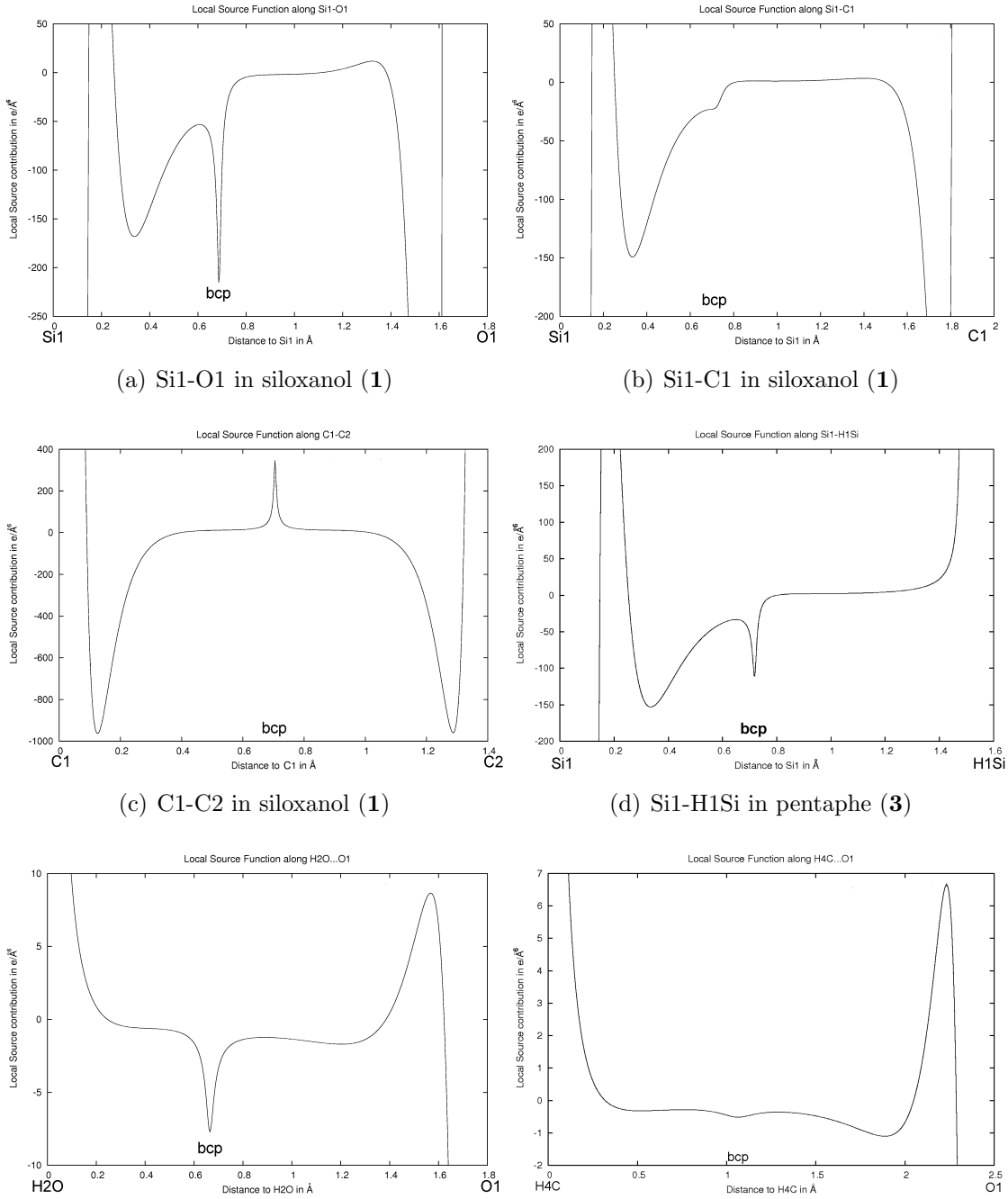

(a) Si1-O1 in siloxanol (**1**)

(b) Si1-C1 in siloxanol (**1**)

(c) C1-C2 in siloxanol (**1**)

(d) Si1-H1Si in pentaphe (**3**)

(e) hydrogen bond H2O$\cdots$O1 in siloxanol (**1**)

(f) hydrogen bond H4C$\cdots$O1 in trisilo (**2**)

Figure 7.9: Local source function along various bonds of different types
Periodic-boundary calculations at experimental geometries, positions of bcps are plotted as vertical lines

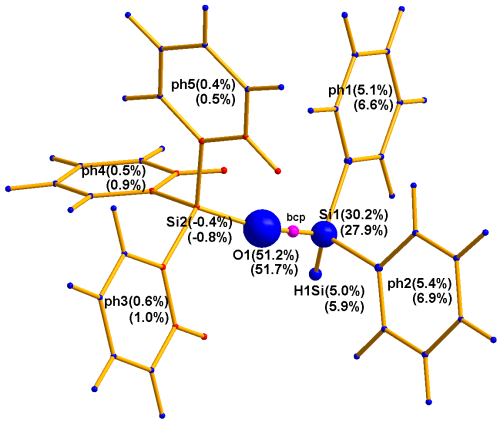

(a) Relative source contributions to Si1–O1 bcp in pentaphe (**3**)

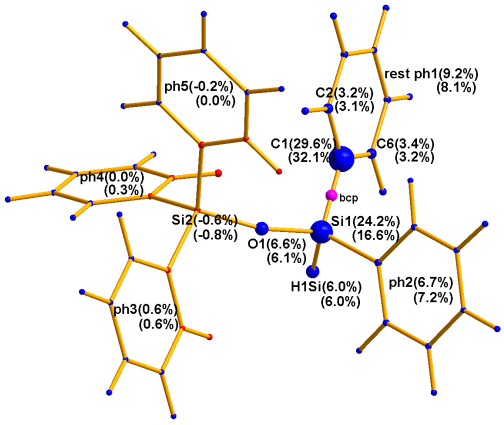

(b) Relative source contributions to Si1–C1 bcp in pentaphe (**3**)

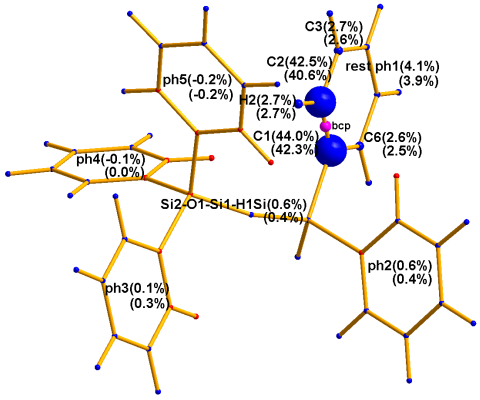

(c) Relative source contributions to C1–C2 bcp in pentaphe (**3**)

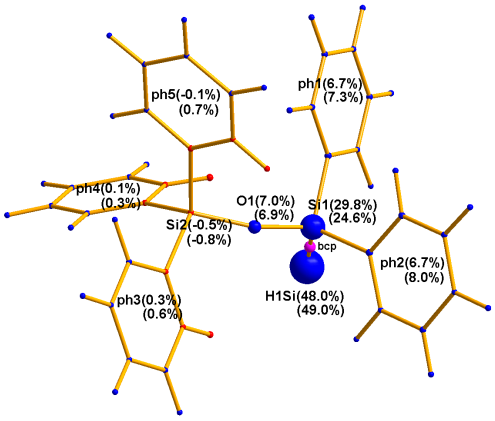

(d) Relative source contributions to Si1–H1Si bcp in pentaphe (**3**)

Figure 7.10: Integrated source function for various bonds in pentaphe (**3**)
First value = experiment, second value = periodic-boundary calculations at experimental geometry, relative source contributions of the atoms to the plotted bcps are represented by the atom's radii, blue = positive, red = negative

experimental values.

The sum of the contributions of the directly bonded atoms is 81.4 % for Si–O, 53.8 % for Si–C, 86.5 % for C–C, and 77.8 % for Si–H. These parameters of the integrated source function are not indicative of the bond character in contrast to the local source function. It is also not indicative of the amount of electron density concentrated around the reference point as Si1–O1 and Si1–C1 have nearly the same value of the ED at the bcp (compare Table 7.5). In fact, the integrated source function only indicates whether there are many donating next neighbours or not. For example, the oxygen atom, carbon atoms within the phenyl group and the hydridic hydrogen atom contribute significantly to an adjacent bond, whereas the silicon atom rather acts as a sink for a neighbouring bond. Therefore, the Si–O bond must cumulate more density from the directly bonded atoms than for example the Si–C bond. Thus, the integrated source function is rather a tool to examine substituent effects than to examine the bond character or strength of different bonds.

The oxygen atom contributes about 7 % to the density of an adjacent bond regardless of the type of this reference bond. The hydridic hydrogen atom H1Si contributes 5-6 % to an adjacent bond regardless of its type, whereas the protic atom H2 donates less than 3 %. Carbon atoms within the phenyl groups contribute about 3 % to an adjacent bond regardless of its type if at least one bond partner is located within the ring, whereas a carbon atom of the phenyl groups contributes only about 1 % to an adjacent bond if both bond partners are outside the ring. However, applying orbital decomposition to the source function, [138] it was shown that delocalisation within an aromatic system cannot be detected by means of the source function because the bcp as reference point is located at a node of the wave function. The total contribution of phenyl groups to adjacent bonds is quite constant at 5-7 % regardless of which type of bond is the reference. If the reference bond is more than one bond away, the contribution of a phenyl group is close to zero.

There is indeed a significant difference in the integrated source function between strong interactions (bonds) and weak interactions (hydrogen bonds). The source contributions of atoms to the bcps of the hydrogen bond H2O$\cdots$O1 in siloxanol (**1**) and both hydrogen bonds in trisilo (**2**) are plotted in Figure 7.11. The sum of the directly bonded atoms is negative for both hydrogen bonds, -26.2 % for H2O$\cdots$O1 and close to -100 % for the hydrogen bonds in trisilo (**2**). Major positive contributions come from the donor oxygen or carbon atoms and the rest of the molecule.

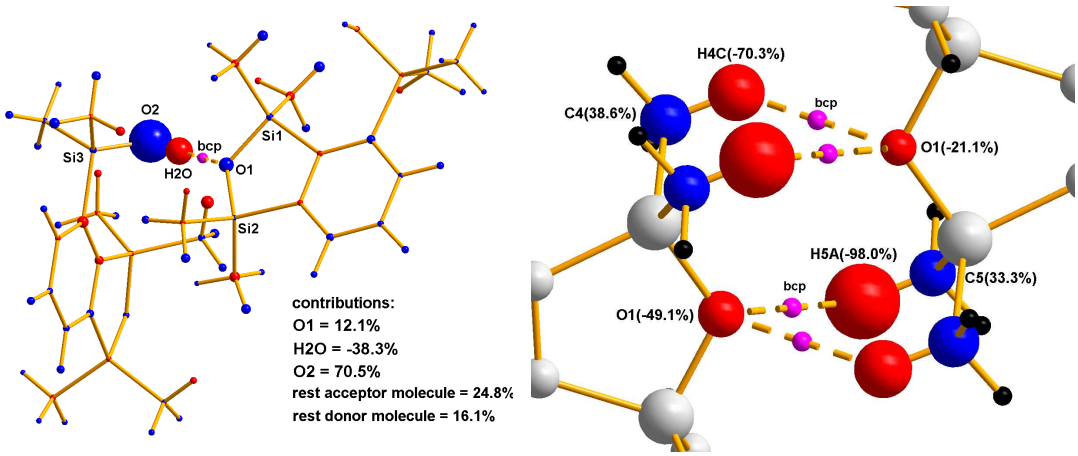

(a) Relative source contributions to hydrogen bond H2O···O1 in siloxanol (**1**)

(b) Relative source contributions to hydrogen bonds in trisilo (**2**), only acceptor and donor groups shown

Figure 7.11: Experimental integrated source function for hydrogen bonds in siloxanol and (**1**) trisilo (**2**)
Relative source contributions of the atoms to the plotted bcps are represented by the atoms' radii, blue = positive, red = negative

This behaviour is typical for hydrogen bonds. From the sign and the amount of the contributions of the atoms involved in the hydrogen bond, a classification can be carried out according to the criteria of Gatti, Gilli and Gilli. [58] In H2O···O1, the donor H atom is negative, the acceptor O atom is only slightly positive and the donor H atom is about twice as positive as the absolute value of the hydrogen atom. These kinds of hydrogen bonds are referred to as polarized assisted hydrogen bonds (PAHB). In H4C···O1 and H5A···O1, donor and acceptor are both negative, which is true for very weak hydrogen bonds that are not covered by the abovementioned criteria.
In Table 7.7, a comparison between the same bond (Si1–O1) in different compounds is carried out. Again, it is obvious that in the theoretical case the influence of the substituents (sum2) is higher than in the experimental case by 4-7 %. This is due to the fact that the contribution of the atom Si1 is in theory smaller to the same degree, whereas the contribution of O1 is constant. A difference of the Si–O bond character in the different compounds with different Si–O–Si angles cannot be detected. However, the substituent effects are most interesting. A methyl group directly bonded to Si1 contributes 5 to 8 % to the adjacent bond. If the methyl group is bonded to Si2, it still contributes 1 to 2 %. A phenyl or aryl group donates

Table 7.7: Absolute (realtive) source contributions to the Si1–O1 bcps in cpds. **1** to **4** *Absolute source contributions in eÅ^{-3}, first column: experiment, second column: periodic-boundary calculations at experimental geometries, sum1 refers to the directly bonded atoms, sum2 refers to the rest of the molecule, Me$_2$(C9/C10) refers to the sum of all atoms of both methyl groups including atoms C9 and C10, correspondingly for Me$_2$(C7/C8) and Me$_2$(C4/C5), ph1(C1) refers to the sum of all atoms of the phenyl group including C1 acoording to Figures 7.10 (a) to (d), reference values are taken from Table 7.5*

group/atom	exp	theo	group/atom	exp	theo
siloxanol (**1**):			trisilo (**2**):		
Si1	0.288(33.5)	0.209(27.5)	Si1	0.276(29.4)	0.183(22.3)
O1	0.409(47.6)	0.375(49.3)	O1	0.411(43.7)	0.374(45.6)
sum1	0.697(81.1)	0.584(76.8)	sum1	0.687(73.1)	0.557(67.9)
Si2	0.006(0.7)	0.006(0.7)	Si2	-0.005(-0.5)	-0.011(-1.3)
Me$_2$(C9/C10)	0.094(10.9)	0.116(15.2)	Me$_2$(C4/C5)	0.090(9.6)	0.111(13.5)
Me$_2$(C7/C8)	0.016(1.9)	0.022(2.9)	Me$_2$(C6/C7)	0.020(2.1)	0.025(3.1)
aryl	0.054(6.2)	0.064(8.4)	aryl	0.043(4.6)	0.058(7.1)
silanol+Me2	0.005(0.6)	0.001(0.1)	rest	0.001(0.1)	0.003(0.3)
sum2	0.175(20.3)	0.209(27.3)	sum2	0.149(15.9)	0.186(22.7)
reference	0.86	0.76	reference	0.94	0.82
pentaphe (**3**):			hexaphe (**4**):		
Si1	0.278(30.2)	0.234(27.9)	Si1	0.308(33.5)	0.219(25.8)
O1	0.471(51.2)	0.434(51.7)	O1	0.441(48.0)	0.417(49.1)
sum1	0.749(81.4)	0.668(79.6)	sum1	0.749(81.5)	0.636(74.9)
Si2	-0.003(-0.4)	-0.006(-0.8)	Si1a	0.011(1.2)	0.006(0.7)
H1Si	0.046(5.0)	0.050(5.9)	ph1(C1)	0.049(5.3)	0.054(6.4)
ph1(C1)	0.048(5.1)	0.055(6.6)	ph2(C7)	0.049(5.3)	0.057(6.8)
ph2(C7)	0.049(5.4)	0.058(6.9)	ph3(C13)	0.050(5.4)	0.058(6.8)
ph3(C13)	0.007(0.6)	0.008(1.0)	ph4(C1a)	0.006(0.6)	0.007(0.8)
ph4(C19)	0.004(0.5)	0.007(0.9)	ph5(C7a)	0.007(0.7)	0.009(1.1)
ph5(C25)	0.003(0.4)	0.003(0.5)	ph6(13a)	0.008(0.9)	0.009(1.1)
sum2	0.154(16.6)	0.175(21.0)	sum2	0.180(19.4)	0.200(23.7)
reference	0.92	0.84	reference	0.92	0.85

the same amount of electron density to the reference point as the metyhl groups, namely 5-8 % if it is directly bonded to Si1 but only 0.5-1.0 % if it is bonded to Si2, respectively.

7.3 Results of the Topological Analyses of ELF and ELI-D

7.3.1 Experimental ELF of Siloxanol (1)

The experimental ELF qualitatively resembles the expected localisation-domain shapes from theoretical calculations as depicted in Figure 7.12 for siloxanol (**1**). A colour code was used to visually separate different basins from each other. This is especially helpful to see if a localisation domain is reducible or irreducible, meaning for example if there are two lone pairs or only one lone pair at an oxygen atom (compare Figure 6.22). For the experimental ELF of siloxanol (**1**), there is only one oxygen lone pair that is populated with 4.50 e (see Table 7.8). A merger of the two lone pairs of oxygen was found in the PES scans (Chapter 6.3.3) only upon hydrogen-bond formation if the hydrogen bond becomes totally symmetric. Figure 7.1 confirms that donor hydrogen H2O in siloxanol (**1**) points towards the centre of acceptor oxygen O1. As crystal effects are incorporated into the experimental ELF via the experimental structure factors and the experimental geometry, it is thus not surprising that this merger can be found.
However, to examine this point in more detail, isolated-molecule calculations on a single molecule of siloxanol (**1**) at the experimental geometry and a corresponding hydrogen-bonded dimer on HF/cc-pVDZ and B3LYP/cc-pVTZ levels of theory were performed. In both cases and for both levels of theory, the lone pairs have merged. This means that it is only the geometry and not the hydrogen-bonding interaction that causes the putative two lone pairs to merge. After a geometry optimisation of a single molecule of siloxanol (**1**), there is still only one lone pair. On the other hand, the silanol oxygen atom, which is acceptor of two weak C–H$\cdots$O hydrogen bonds in the crystal structure, possesses two lone pairs in all the mentioned cases. It is also not a feature of the ELF compared to the ELI-D, as the next chapter will show. Therefore, it must be concluded that the existence of only one basin for the 4.5 lone-pair electrons is an inherent property of the siloxane linkage in this molecule and not caused by intermolecular interactions. In the

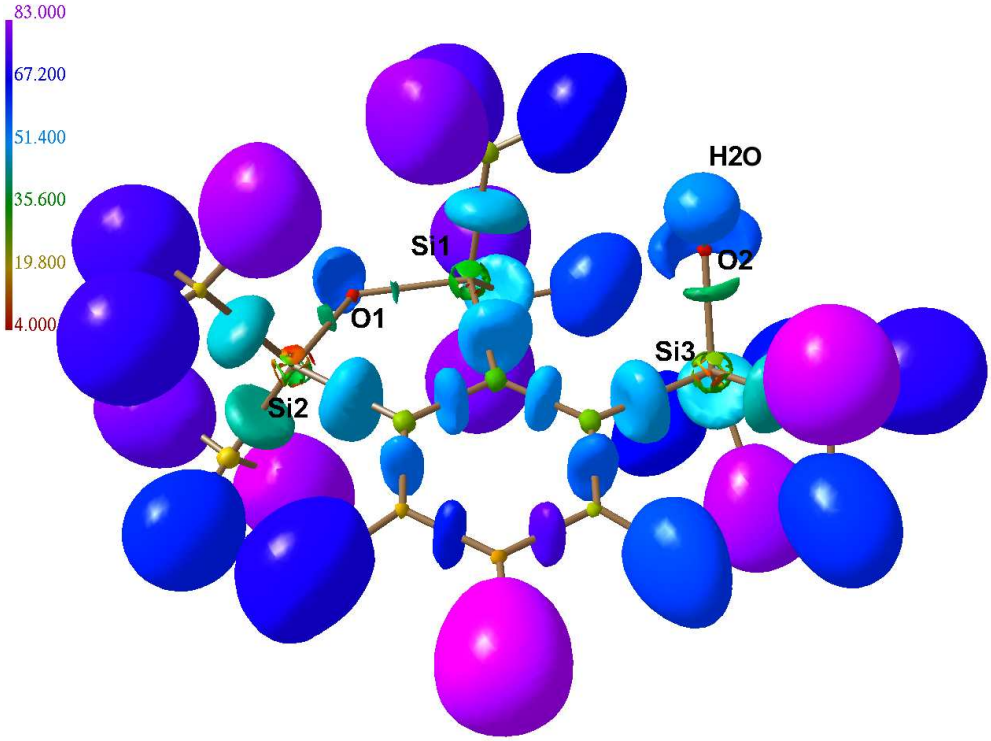

Figure 7.12: Experimental ELF localisation domains of siloxanol (**1**)
Isovalue = 0.86, colour code representing the volumes of the basins on a linear scale beginning with the smallest basin (no. 1 in the scale) ending with the largest basin (no. 83 in the scale)

Table 7.8: Electron populations of ELF basins in the siloxane and silanol groups of siloxanol (**1**)
N_{001} in e cut at ϱ=0.001 a.u., CHF refers to experimental ELF from CWF, HF and B3LYP refer to isolated-molecule calculations for a single molecule at experimental geometry

basin	CHF/cc-pVDZ	HF/cc-pVDZ	B3LYP/cc-pVTZ
$V_1(O1)_{silox}$	4.50	4.20	4.32
sum of both $V_2(Si,O1)_{silox}$	3.30	3.60	3.45
sum of both $V_1(O2)_{silanol}$	4.23	4.33	4.47
$V_2(Si3,O2)_{silanol}$	1.81	1.73	1.69

case of the $H_3SiOSiH_3$ model compounds, the hydrogen bond is the reason for the merger of the two oxygen lone pairs. Here, the merger might be the reason for the exceptionally strong hydrogen bond found in the crystal structure.
Table 7.8 only lists the populations of the ELF basins for the calculations on the single molecule to compare the experimental to the theoretical ELF. The deviation of the experimental from the theoretical results is not larger than the deviation between the two different theoretical calculations. The oxygen lone pairs of the siloxane linkage are more highly populated in the experiment than in theory, the siloxane Si–O bonds are less populated. In the silanol group, the opposite is true. The values for the siloxane group fit very well into the curves of the oxygen lone-pair and Si–O-bond populations obtained from the PES scans at a corresponding Si–O–Si angle (Figure 6.21).

7.3.2 Theoretical ELI-D of Compounds 1 to 4

The theoretical ELI-D of cpds. **1** to **4** at B3LYP/cc-pVTZ level of theory was calculated for optimised geometries. The resulting localisation-domain representations for details of the molecules containing the siloxane linkage are shown in Figure 7.13. The numbering of the basins which the domains represent is given as used in Table 7.9.
Siloxanol (**1**) and trisilo (**2**) comprising small Si–O–Si angles close to ϕ=120 ° show the typical cap-like shape of the localisation domain of the oxygen lone-pair electrons. This shape was expected for this value of ϕ from the PES scans (Chapter

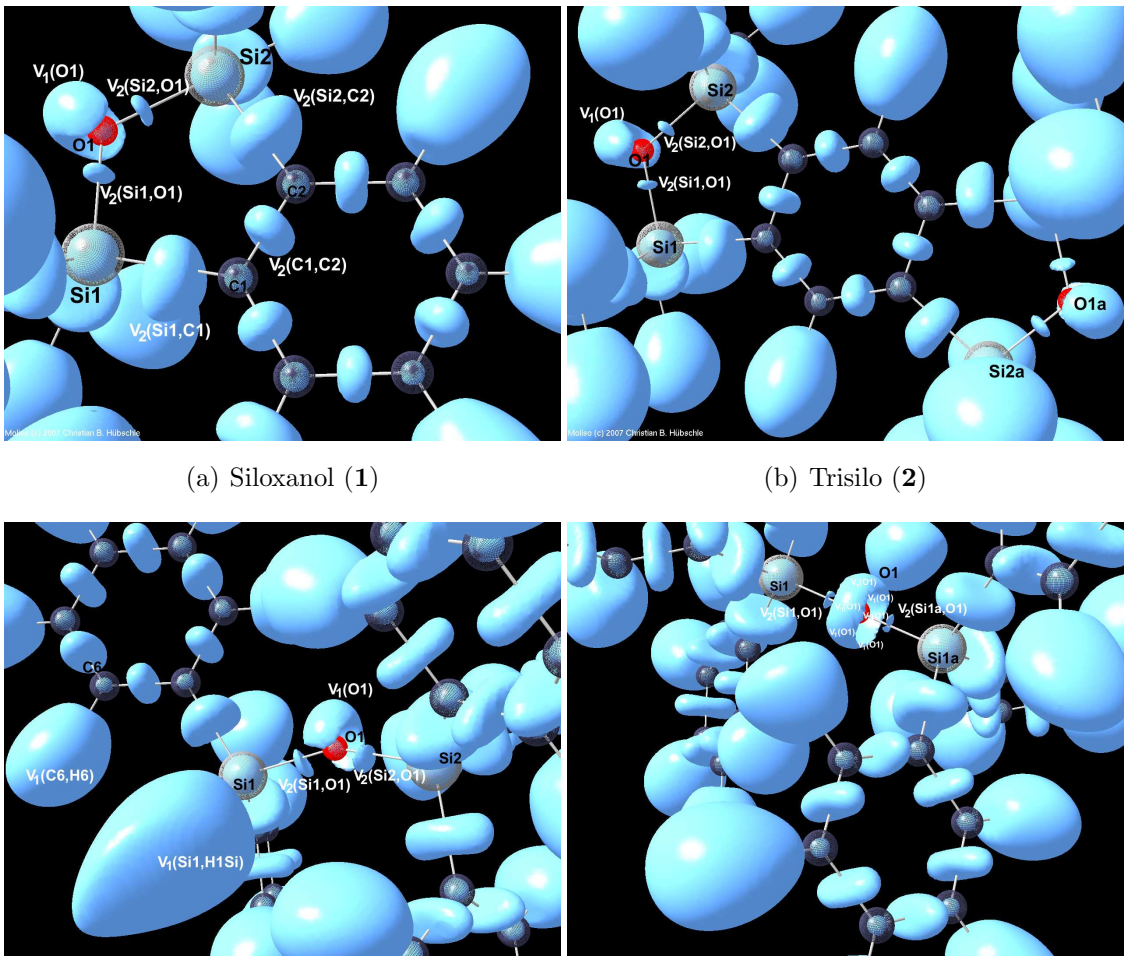

(a) Siloxanol (**1**) (b) Trisilo (**2**)

(c) Pentaphe (**3**) (d) Hexaphe (**4**)

Figure 7.13: Theoretical ELI-D localisation-domain representations of cpds. **1** to **4** *Isolated-molecule calculations at optimised geometries, isovalue = 1.50*

6.3.1) and corresponds to the shape of the VSCCs and the deformation density around oxygen (compare Figure 7.7). As discussed in the preceding chapter, there is only one basin for the lone-pair electrons of the siloxane oxygen atom even though the ELI-D originates from an isolated-molecule geometry optimisation. This suggests that the merger of the two putative lone pairs is an inherent property of the siloxane linkage in these compounds, since they are good hydrogen-bond acceptors.

For siloxanol (**1**), a comparison of the different bond types Si–O, Si–C and aromatic C–C will be carried out as already done for various ED properties in this chapter. Figure 7.13 (a) shows the different shapes of the localisation domains of these

bonds. Table 7.9 confirms that the order of the volumes of the bond basins agrees with the impression one gets from the localisation domains: The Si-C bonds are largest (V_{001}=8.34 Å^3), the aromatic C–C bonds are a bit smaller (V_{001}=7.12 Å^3) and the Si–O bonds are by far the smallest bonds (V_{001}=2.35/2.44 Å^3). The population of the aromatic C–C bond is N_{001}=2.56 e, which is less than 3.0 e, which would be expected from a bond order of 1.5. In turn, the Si–C bond possesses more electrons (N_{001}=2.33 e) than a formal bond order of 1.0 would suggest. It is known for the ionic Si–O bond from the PES scans (Chapter 6.3.2) that the electron number of the electron pair constituting the bond is significantly smaller than 2.0, as would be expected from a formal bond order of 1.0 (here: N_{001}=1.67/1.72 e). The values for Si–O found here for siloxanol (**1**) and trisilo (**2**) at about ϕ=120 ° (ΣN_{001}=3.39/3.38 e) are a bit larger than the value expected from the curve of the PES scan of $H_3SiOSiH_3$ at ϕ=120 ° (Figure 6.21, ΣN_{001}=3.16 e).

Upon geometry optimisation, the Si–O–Si angle in pentaphe (**3**) decreases from ϕ=162.03 ° to 153.90 °. Therefore, the siloxane linkage of pentaphe (**3**) should belong to the same chemical system as the one in siloxanol (**1**) and trisilo (**2**) because the chemical catastrophe in the model compound $H_3SiOSiH_3$ occurs between ϕ=165 ° and 170 °. This is confirmed in Figure 7.13 (c). The lone-pair electrons of the oxygen atom exhibit the same cap-like shape as in siloxanol (**1**) and trisilo (**2**). There is no isosurface enclosing the lower side of the oxygen atom even at very low isovalues. There is also only one attractor for the lone-pair electrons just like for siloxanol (**1**) and trisilo (**2**), in contrast to free disiloxane. So the siloxane linkage in pentaphe (**3**) should generally be enabled to act as hydrogen-bond acceptor, but the hydrogen-bond energy would be too low to be competitive compared to any other potential acceptor group.

The difference between a rather protic (H6) and a hydridic (H1Si) hydrogen atom can be seen in Figure 7.13 (c) and Table 7.9. The volume is larger for H1Si than for H6, which agrees with the visual impression of the shapes of the corresponding localisation domains in Figure 7.13 (c). The ELI-D value at the attractor of V_1(Si1,H1Si) is much higher than for V_1(C6,H6), but surprisingly, the population of the hydridic H1Si atom (N_{001}=1.98 e) is lower than for the protic H6 atom (N_{001}=2.13 e). This finding cannot be understood intuitively but one has to be aware that V_1(Si/C,H) are protonated bond basins and not atomic basins. C–H bonds are highly covalent whereas Si–H bonds are rather ionic. In the comparison of the ionic Si–O bond with more covalent Si–C or highly covalent C–C bonds, it was also demonstrated that ionic bonds have a smaller population.

Table 7.9: Electron populations, volumes and attractor values of ELI-D valence basins of the siloxane group in cpds. **1** to **4**, the silanol group and selected reference bonds of other types in siloxanol (**1**) and pentaphe (**3**)
Isolated-molecule calculations at optimised geometries, electron population of the ELI-D basin (N_{001}) in e, volume of the ELI-D basin (V_{001}) in $Å^3$, ELI value at the attractor of the ELI-D basin (ELI_{att}) without dimension

basin		siloxanol (**1**)	trisilo (**2**)	pentaphe (**3**)	hexaphe (**4**)
V_2(Si1,O1)	ELI_{att}	1.528	1.529	1.520	1.504
	N_{001}	1.67	1.69	1.64	1.02
	V_{001}	2.35	2.41	2.71	1.11
V_2(Si2/1a,O1)	ELI_{att}	1.528	1.529	1.521	1.504
	N_{001}	1.72	1.69	1.64	1.02
	V_{001}	2.44	2.41	2.46	1.11
sum V_2(Si,O1)	N_{001}	3.39	3.38	3.28	2.04
V_1(O1)	ELI_{att}	1.615	1.619	1.574	1.522
	N_{001}	4.37	4.38	4.49	6x0.96=5.76
	V_{001}	15.24	15.44	15.81	6x2.70=16.20
siloxanol (**1**)		V_2(Si3,O2)	V_1(O2)	V_1(O2)	sum V_1(O2)
silanol group	ELI_{att}	1.567	1.658	1.660	
	N_{001}	1.61	2.23	2.30	4.53
	V_{001}	2.28	6.03	7.91	13.94
siloxanol (**1**)		V_2(Si1,C1)			
Si1–C1	ELI_{att}	2.097			
	N_{001}	2.33			
	V_{001}	8.34			
siloxanol (**1**)		V_2(C1,C2)			
C1–C2	ELI_{att}	1.817			
	N_{001}	2.56			
	V_{001}	7.12			
pentaphe (**3**)		V_1(C6,H6)			
C6–H6	ELI_{att}	6.196			
	N_{001}	2.13			
	V_{001}	11.48			
pentaphe (**3**)		V_1(Si1,H1Si)			
Si1–H1Si	ELI_{att}	11.17			
	N_{001}	1.98			
	V_{001}	15.98			

In hexaphe (**4**) (Figure 7.13 (d)) with ϕ=180 °, a ringlike shape of the localisation domain around the oxygen atom is expected and indeed found (compare Chapter 6.3.1 and Figure 7.7). This compound belongs to a chemical system in which hydrogen bonding is generally not feasible. Six attractors and thus six basins for the lone-pair electrons can be found because perfect cylindrical symmetry is perturbed by six phenyl groups that are arranged in a staggered conformation. In free disiloxane $H_3SiOSiH_3$, where the six hydrogen atoms are arranged in an eclipsed conformation, consequently only three attractors were found. Localization domains for the bond basins of Si–O are clearly visible in Figure 7.13 (d) although the linkage is the most ionic. The population of one of the Si–O bonds (N_{001}=1.11 e) is higher than for free disiloxane at the linear geometry (N_{001}=0.94 e).
In general, the trends observed for free disiloxane upon variation of the Si–O–Si angle (compare Figures 6.20 and 6.21) can also be observed within a comparison between cpds. **1** to **4**. The Si–O–Si angle increases from cpd. **1** to **4**, and thus, the ELI values at the oxygen lone pairs and the Si–O bonds decrease. The populations and the volumes of the Si–O bonds in siloxanol (**1**), trisilo (**2**) and pentaphe (**3**) are rather constant but then suddenly drop off towards the linear case in hexaphe (**4**). For the populations and volumes of the oxygen lone pairs, a constant increase of the values can be found, but again with a large increase towards the linear case. For the oxygen atom of the silanol group in siloxanol (**1**), there are two lone pairs. The sum of their populations is larger than for the siloxane group, but the volume is smaller. Population and volume of the Si3–O2 bond in silanol are smaller than in the siloxane group. The ELI-D values at the attractors are larger for both oxygen lone pairs and the Si–O bond.

Part III

From Silyl Ethers (Si–O–C) to Ethers (C–O–C)

Chapter 8

Experimental and Computational Details

8.1 Experimental Details

Tris(*tert*-butoxy)silanol (butoxysilanol (**5**)) was synthesised by Prof. Dr. Jens Beckmann. The reaction of silicon tetrachloride with potassium *tert*-butoxylate initially provided tris(*tert*-butoxy)chlorosilane $(t\mathrm{BuO})_3\mathrm{SiCl}$. Hydrolysis with a large excess of water in the presence of a small amount of pyridine produced the corresponding silanol $(t\mathrm{BuO})_3\mathrm{SiOH}$ (cpd. **5**). [83] Crystals were grown from pure hexane, but crystal quality was poor: The crystals were rather soft and sensitive to mechanical stress so that they were destroyed by cutting. Moreover, they dissolved in each tested glue at room temperature, even in shellac or honey, so that a simple test measurement at room temperature was impossible. Therefore, a test measurement was performed at 200 K in a dry-air stream where the crystals showed to be stable. The measurement was performed by Dr. Malte Hesse at a Stoe IPDS-2 diffractometer equipped with an image plate in the Inorganic Chemistry Department of the Freie Universität Berlin. The crystal structure exhibits strong disorder at the *tert*-butoxy groups as Figure 8.1 illustrates. Further details of this measurement can be found in Table 8.1 in the column "disordered cpd. **5**".

Figure 8.1 shows the strong silanol$\cdots$silyl ether hydrogen bond (the second molecule is generated by a twofold axis, monoclinic space group C2/c) that is of great interest for a comparison with the discussed basicity properties of siloxanes. Thus, great effort seemed to be justified to obtain the desired electronic properties of the Si–O–C linkage and its intermolecular interactions. But severe disorder was also

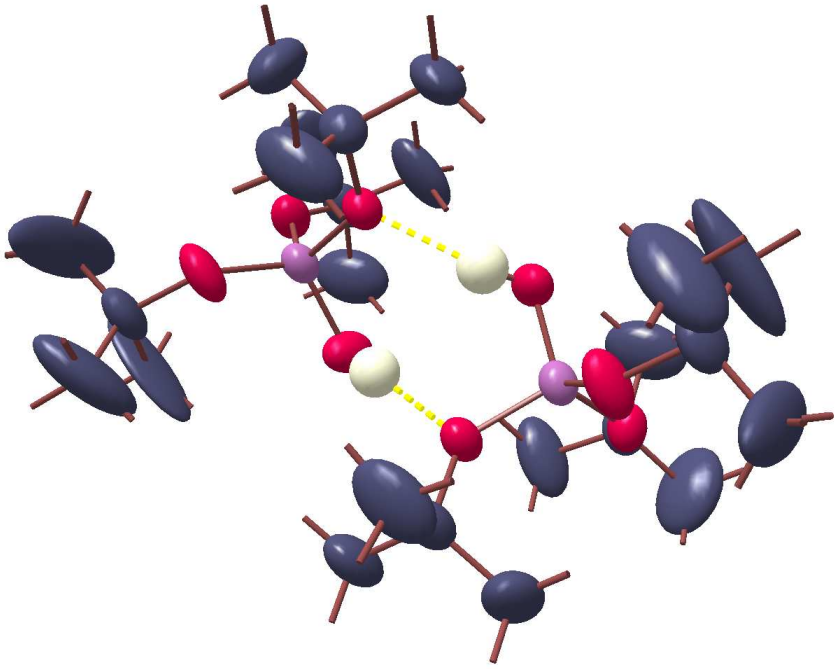

Figure 8.1: Disordered symmetry-related pair of cpd. **5** in the monoclinic modification

found at 173 K by Beckmann et al. [83], so that reliable electron-density determination was out of reach at a standard experimental setup. Therefore, butoxysilanol (**5**) was measured again at the synchrotron beamline 15-ID-B of APS in Chicago at 15 K in a helium cold-gas stream at a wavelength of 0.41328 Å.

Unfortunately, all crystals had to be cut because of the small diameter of the very sharp and intense primary synchrotron beam. Therefore, no single crystal could be found and measured since all crystals were severly damaged by the mechanical stress. Finally, a crystal was found that was internally broken into no more than two parts, so that the diffraction pattern looked like the one of a twinned crystal. However, the integration software of the BRUKER APEX II suite [244] allowed the use of big integration boxes, enclosing the whole intensity for one twinned reflection. Therefore, the data set was good enough to be considered for further investigation (211897 collected reflections, 30497 observed, max. resolution = 1.11 $Å^{-1}$, completeness = 91.6 %, R_{int} = 6.36 %, see Table 8.1). Data reduction was carried out with the programmes SADABS [244] and XPREP [244]. It turned out that another disorder-free modification (triclinic, $P\bar{1}$) is present at 15 K. But the structure could only be solved (programmes SHELXS and SHELXL [205])

Table 8.1: Crystallographic and refinement details of cpds. **5** and **6**
Spherical refinement of experimental structure factors, multipole refinement of theoretical structure factors

	disordered cpd. **5**	butoxysilanol cpd. **5**	sucrose [84] cpd. **6**
chemical formula	$C_{12}H_{28}O_4Si$	$C_{12}H_{28}O_4Si$	$C_{12}H_{22}O_{11}$
M ($g{\cdot}mol^{-1}$)	264.43	264.43	342.30
space group, Z	C2/c, 8	$P\bar{1}$, 4	$P2_1$, 2
a (Å)	16.866(3)	9.311(1)	7.736(3)
b (Å)	9.596(2)	9.608(1)	8.702(4)
c (Å)	21.232(4)	21.063(2)	10.846(5)
α (°)	90.00	76.86(1)	90.00
β (°)	101.86(3)	79.85(1)	102.97(2)
γ (°)	90.00	61.20(1)	90.00
V ($Å^3$)	3362.9(1)	1603.0(3)	711.5(6)
ϱ_x ($g{\cdot}\ cm^{-3}$)	1.045	1.096	1.598
F(000)	1168	584	364
μ (mm^{-1})	0.14	0.08	0.14
crystal size (mm^3)	$0.65x0.60x0.20$	$0.30x0.20x0.02$	$0.40x0.35x0.30$
beamline	IPDS-2, AC	15-ID-B, APS	in-house
T (K)	200	15	20
λ (Å)	0.71073	0.41328	0.71073
max. 2θ (°)	58.5	54.8	109.6
$\frac{sin\theta_{max}}{\lambda}$ ($Å^{-1}$)	0.69	1.11	1.15
no. of coll. refl.	17829	211897	86373
no. of unique refl.	4488	33907	8732
cond. for obs. refl.	$F \geq 4\sigma(F)$	$F \geq 4\sigma(F)$	$F^2 \geq 2\sigma(F^2)$
no. of obs. refl.	2935	30497	8481
redundancy	4.0	6.2	10.0
completeness (%)	99.0	91.6	93.2
R_{int} (%)	10.93	6.36	1.37
spherical refinement of experimental structure factors			
R(F) (%)	7.50	15.84	2.67
wR(F^2) (%)	23.51	39.44	6.94
GooF	1.06	1.16	1.07
multipole refinement of theoretical structure factors			
refinement on	–	F	F
ratio refl./par.	–	160.70	16.54
R(F)/ R(F^2) (%)	–	0.78/ 1.02	0.46/ 0.72
min./ max./ mean $\delta_{res}\varrho(\vec{r})$ ($eÅ^{-3}$)	–	-0.25/ 0.36/ 0.02	-0.13/ 0.10/ 0.01

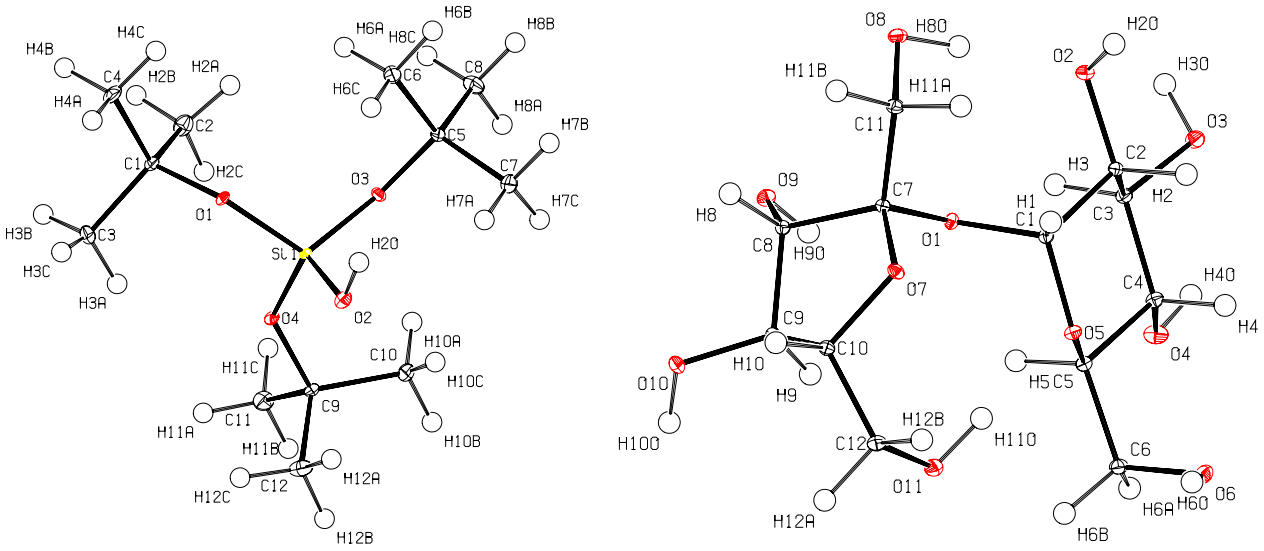

(a) Butoxysilanol (**5**) at 15 K in its triclinic modification with isotropic H atoms of arbitrary radii

(b) Sucrose (**6**) at 20 K with isotropic H atoms of arbitrary radii

Figure 8.2: ORTEP representations of cpds. **5** and **6**

Thermal ellipsoids at 50 % probability, atomic-numbering scheme as used in the discussion

encountering many problems. Mainly, numerous residual-density peaks that are distributed throughout the asymmetric unit prevent the R-value from dropping below 15 %. Hydrogen atoms with isotropic displacement parameters were added according to the riding model in SHELXL, but the X–H distances were fixed to average neutron-diffraction values [209]. Experimental ED determination was again not possible, but a disorder-free molecular structure with reasonable adps was obtained that could serve as the input geometry for theoretical calculations under periodic-boundary conditions.

There are two molecules of butoxysilanol (**5**) in the asymmetric unit connected by only one strong silanol$\cdots$silyl ether hydrogen bond because the twofold symmetry is cancelled in the new modification. A detailed discussion of the hydrogen bonds can be found in Chapter 10.1.2. Figure 8.2 (a) shows the final structure of one molecule of the asymmetric unit (asu) with adps at 15 K and the atomic-numbering scheme. Corresponding non-hydrogen atoms in the other molecule of the asu have the same label, but extended by the capital letter A.

Since the Si–O–C linkages in butoxysilanol (**5**) are in the vicinity of three other oxygen atoms [(O_3)Si–O–C], sucrose (**6**) was chosen for comparison because for the

ether linkages of sucrose (**6**), the situation is similar [(O)C–O–C and (O_2)C–O–C]. However, one has to be aware of the different chemical environments when comparing the linkages in butoxysilanol (**5**) and sucrose (**6**) with PES scans of methoxysilane and dimethylether on the one hand (see below) and with the siloxane linkage Si–O–Si in cpds. **1** to **4** and the epoxide three-membered C–O–C ring in cpds. **7** to **10** on the other hand.

A crystal of commercially available sugar was selected and measured by Dr. Stefan Mebs and M. Sc. Da'san Jaradat at the in-house diffractometer. Measurement, ED determination and ED analysis were performed as the master thesis of Da'san Jaradat. This study can be found in Ref. [84]. Only a few details are listed in Table 8.1. The experimental ED will not be considered again in this doctoral thesis, but the geometry after multipole modelling was taken to perform periodic theoretical calculations corresponding to butoxysilanol (**5**). The atomic-numbering scheme for sucrose (**6**) used here can be found in Figure 8.2 (b).

8.2 Details of Theoretical Calculations

8.2.1 Calculations on Compounds 5 and 6

Although an experimental ED determination is not possible for butoxysilanol (**5**), the analysis of the theoretical ED, obtained by periodic-boundary calculations at experimental geometry, nevertheless grants access to all electronic properties including all measured inter- and intramolecular interactions. Also for sucrose (**6**), properties were only derived from a modelling of theoretical structure factors from a periodic-boundary calculation at the experimental geometry in this work. It is not intended to investigate sucrose (**6**) in other respects because it was already done before. [84] Periodic-boundary calculations were performed as disclosed in Chapter 5.2.1 for siloxane compounds.

In the multipole modelling with XD2006, [207] chemical site symmetries and constraints as similar as possible to cpds. **1** to **4** were chosen. Therefore, many constraints were used in butoxysilanol (**5**) (all methyl groups were constrained to each other), all oxygen atoms were refined with local mirror symmetry, but without constraints, and all carbon atoms were refined with local three-fold symmetry. Only the silicon atoms were refined without symmetry. For details, see Table A.60 of the Appendix. This rather inflexible model with a high ratio of reflections over parameters yields unusually high residual densities regarding theoretical structure

factors, see Table 8.1. If more parameters are refined, e.g. no constraints and site symmetries, the residual densities slightly decrease. But as deformation densities, ED values at the bcps and other parameters are physically most reasonable for the inflexible model that is similar to the ones for siloxane compounds **1** to **4**, this model was chosen despite residual densities. Moreover, polar bonds and heavier atoms like Si are not modelled accurately within XD2006, which also contributes to residual densities. Another reason might be that the experimental geometry frozen at 15 K is far from the minimum geometry on the energy hypersurface, so that the theoretical calculation is more erroneous. However, the results from this modelling are the best results on a periodic structure one can get from butoxysilanol (**5**) if one considers the enormous experimental problems encountered for this compound (see above).

In sucrose (**6**), fewer constraints and site symmetries were imposed because there are few similar atoms and few planar fragments. Only H6B was constrained to H6A, as well as H11B to H11A and H12B to H12A. Oxygen atoms O1, O4 and O7 (the ones without strong hydrogen bonds) as well as carbon atoms C2, C3, C4, C6, C8, C9, C11 and C12 were refined with local mirror symmetry; all other non-hydrogen atoms were refined without symmetry.

For both butoxysilanol (**5**) and sucrose (**6**), all non-hydrogen atoms were treated up to the hexadecapole level of expansion, whereas monopoles, bond-directed dipoles and bond-directed quadrupoles were introduced for hydrogen atoms. The expansion-contraction parameter κ was refined independently for all chemically non-similar non-hydrogen atoms. κ' values were left at their default values κ'=1.0, but for silicon atoms, the optimised value κ'=0.85 and for hydrogen atoms, optimised values κ=1.13 and κ'=1.29 [208] were used. More details on the refinements can be found in Tables 8.1, A.60 and A.61.

Additionally, geometry optimisations of the isolated molecules were performed with GAUSSIAN03 [221] to obtain and analyse the ELI-D on a grid of 0.07 a.u. with the programme DGRID-4.4 [219].

8.2.2 Calculations on Model Compounds of the Type H_3SiOCH_3 and H_3COCH_3

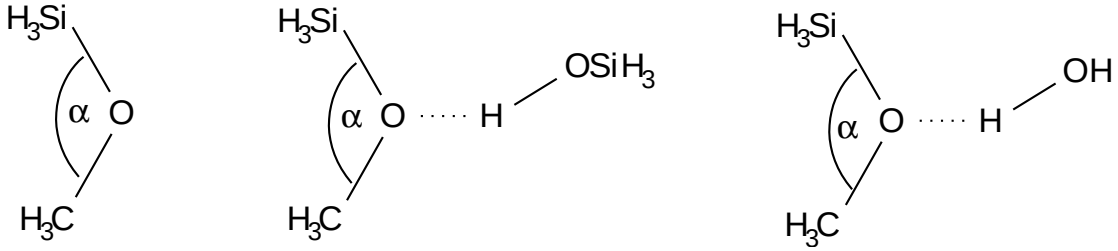

(a) Free methoxysilane H_3SiOCH_3, methoxysilane$\cdots$silanol hydrogen-bonded complex $(H_3Si)(H_3C)O\cdots HOSiH_3$ and methoxysilane$\cdots$water hydrogen-bonded complex $(H_3Si)(H_3C)O\cdots HOH$

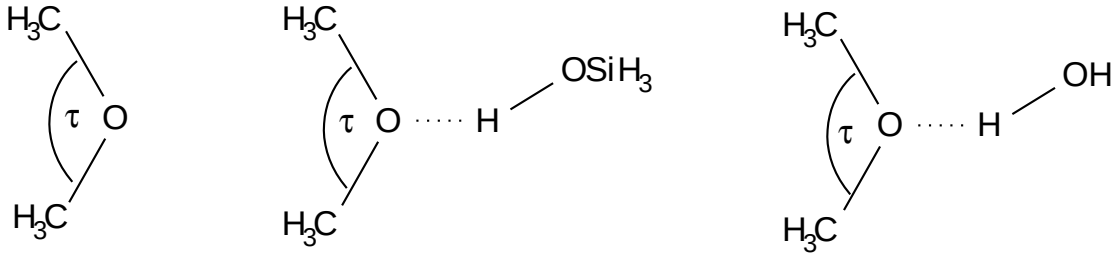

(b) Free dimethylether H_3COCH_3, dimethylether$\cdots$silanol hydrogen-bonded complex $(H_3C)_2O\cdots HOSiH_3$ and dimethylether$\cdots$water hydrogen-bonded complex $(H_3C)_2O\cdots HOH$

Figure 8.3: Scrutinised model compounds of the types H_3SiOCH_3 and H_3COCH_3

PES scans of methoxysilane H_3SiOCH_3 and dimethylether H_3COCH_3 as free compounds and as corresponding hydrogen-bonded complexes with silanol and water were performed and analysed according to the procedure outlined in Chapter 5.2.2 for disiloxane $H_3SiOSiH_3$. Reasonably optimised structures at frozen X–O–X angles could not be obtained below α/τ=65 °. However, it is not the purpose of these scans to discuss the hypothetical chemical systems of these compounds at small X–O–X angles as it was done for $H_3SiOSiH_3$ because the general question of how to find a chemical catastrophe in ED and ELI-D has already been answered. In fact, the two major chemical questions that were discussed for the siloxane linkage, namely of how the X–O bond character and the oxygen basicity change upon variation of the X–O–X angle, are to be examined in detail here for the Si–O–C and C–O–C linkages. Moreover, it has also been sufficiently investigated for $H_3SiOSiH_3$ which properties within molecular geometry, ED and ELI-D are indicative for hydrogen bonding and a change of the bond character. Therefore,

only the parameters that are most indicative will be employed in the following. It was again not easy to reach convergence for all hydrogen-bonded complexes. But after the same procedure as detailed in Chapter 5.2.2 for $H_3SiOSiH_3$ hydrogen-bonded complexes, optimised structures could finally be obtained for all X–O–X angles except α/τ=180 ° and except α=65 ° to 75 ° for methoxysilane$\cdots$water, the complex with the weakest acceptor and the weakest donor. The fact that hydrogen bonding is generally feasible over the whole range of scrutinised angles in the systems H_3SiOCH_3 and H_3COCH_3 is the first general difference to $H_3SiOSiH_3$ and will be discussed in the following chapters.

Chapter 9

Results for the Model Compounds H_3SiOCH_3 and H_3COCH_3

9.1 Geometrical and Energetical Results

9.1.1 Bending-Potential and Hydrogen-Bond Energies

The bending-potential energy curves of methoxysilane (H_3SiOCH_3) and dimethylether (H_3COCH_3) (Figure 9.1) generally differ from each other and from the ones of disiloxane ($H_3SiOSiH_3$) given in Figure 6.1. The curve of free disiloxane is added in Figures 9.1 (a) and (b) for comparison. The barrier to linearisation from the minimum angle is $0.5\,\mathrm{kJ\,mol^{-1}}$ for free disiloxane, see Chapter 6.1.1. For free methoxysilane, this barrier ($26.5\,\mathrm{kJ\,mol^{-1}}$) is significantly larger and increases upon hydrogen-bond formation. For dimethylether, the shown potential well is the opposite to the flat curve of disiloxane. It is virtually no different if the C–O–C angle is increased or decreased from the minimum position, both scenarios are energetically unfavourable. In contrast, increasing the Si–O–Si angle in disiloxane does not need activation energy, but decreasing the angle leads to high bond strain. Si–O–C and C–O–C linkages are also significantly strained at angles smaller than about 100 °, but the curve of disiloxane already ascends at higher angles.

The energy minimum was found to be located at ϕ=151.4° for free disiloxane. For free methoxysilane, it is shifted to α=123.91 ° as obtained by a relaxed geometry optimisation (α=120.13(16) ° in the crystal structure at 110 K, [245]). For

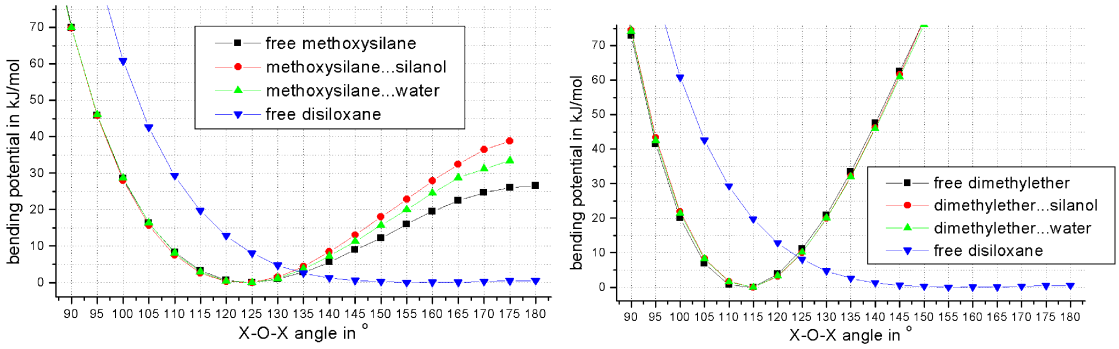

(a) Methoxysilane (b) Dimethylether

Figure 9.1: Bending-potential energies for free methoxysilane, free dimethylether and corresponding hydrogen-bonded complexes, comparison with free disiloxane

free dimethylether, the minimum is again at a smaller X–O–X angle: τ=112.66 ° from relaxed geometry optimisation and τ=111.0(1) ° in the crystal structure at 110 K [246]. In contrast to disiloxane where the minimum angle shifts to smaller values upon hydrogen-bond formation, it remains the same for hydrogen-bonded complexes of methoxysilane and dimethylether. This means that the impact of the X–O–X angle on the hydrogen bond or vice versa is much more pronounced in disiloxane. This can also be seen by the differences in the bending-potential energies before and after complex formation at any given X–O–X angle: For disiloxane, there are large differences at any angle (see Figure 6.1); for methoxysilane, there are small differences for angles larger than the minimum position, i.e. linearisation of the system becomes energetically more difficult after hydrogen-bond formation, but differences have vanished at smaller angles; for dimethylether, there are no energy differences at all between free and hydrogen-bonded compounds regarding bending of the C–O–C linkage.

The curves of the hydrogen-bond energies in Figure 9.2 clearly support the finding that the X–O–X angle has the largest impact on the hydrogen bonds in disiloxane: The curves for disiloxane in both complexes, with silanol and with water, cover the largest range of energies and include the energetical extreme values (-0.26 to -26.49 kJ mol^{-1} for the silanol complex and 3.70 to -14.30 kJ mol^{-1} for the water complex) while hydrogen bonding is feasible in a smaller range of X–O–X angles than for methoxysilane and dimethylether. In general, the curves follow a similar trend that is most pronounced for disiloxane: Hydrogen bonds become stronger

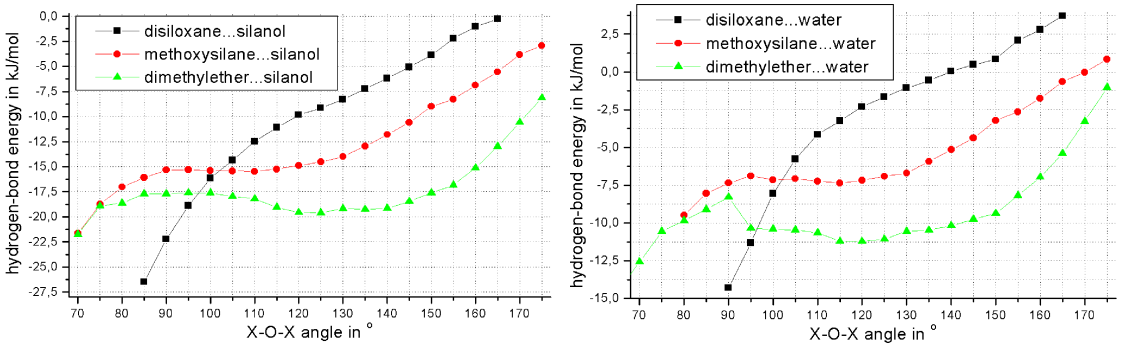

(a) Hydrogen bonds to silanol (b) Hydrogen bonds to water

Figure 9.2: Comparison of hydrogen-bond energies of hydrogen-bonded complexes

with decreasing X–O–X angle, i.e. the basicity of the oxygen atom can be significantly improved by decreasing the X–O–X angle.

A search in the CSD reveals that there are actially 119325 compounds incorporating the C–O–C linkage, of which 35.4% exhibit classical hydrogen bonds (H$\cdots$acceptor distance within sum of van der Waals radii). The maximum number of these hydrogen-bonded complexes lies at 115 ° according to the fact that hydrogen bonding does not affect the energetical minimum (see above). There are 7151 Si–O–C fragments of which 18.7% exhibit hydrogen bonds with a maximum at τ=125 °. It was discussed in Chapter 4.1 that there are only four out of 4944 Si–O–Si fragments which exhibit hydrogen bonds as acceptor.

The curves in Figure 9.2 reflect this finding for X–O–X angles larger than 105 °: Hydrogen bonds with disiloxane as acceptor are weakest, the ones with dimethylether as acceptor are strongest - the difference between disiloxane and dimethylether is on average larger than 10 kJ mol^{-1} - and the ones with methoxysilane as acceptor are in-between. Most compounds containing the X–O–X linkage occur in the range of angles between 105 ° and 180 ° where the curves are rather parallel to each other. For angles smaller than 105 °, the hydrogen-bond energies no longer drop or even begin to rise for methoxysilane and dimethylether, but quickly decrease for disiloxane. Hydrogen-bond energies for X–O–X angles smaller than 100 ° are more negative for disiloxane, indicating that the siloxane linkage is a better acceptor than the ether linkage at these angles.

For angles smaller than ϕ=85 ° and larger than 165 °, hydrogen bonding is no longer possible in disiloxane due to chemical catastrophes involving massive reorientation of electrons, see detailed discussions in Chapter 6. For methoxysilane

and dimethylether, these catastrophes do not occur, since hydrogen bonding is generally possible between α/τ=65 ° and 175 °. Only for α/τ=180 °, hydrogen bonding is generally not possible. There are also no entries of linear X–O–X fragments incorporated in hydrogen bonds in the CSD. The symmetrical arrangement of the electrons caused by the linear geometry leads to maximum delocalisation and prevents hydrogen bonding, see discussion in Chapter 6. These arrangements of the electrons at 180 ° are not a chemical property of the given substance but only due to geometrical necessities. Thus, there will be no discussion on the chemical catastrophe between the angulated and the linear geometry in the following. Instead, the differences of the electronical properties in disiloxane, methoxysilane and dimethylether close to the point of the catastrophe in disiloxane between a hydrogen-bonding and a hydrogen-repelling chemical system (between ϕ=165 ° and 170 °) will be examined.

9.1.2 Geometries and Molecular Graphs

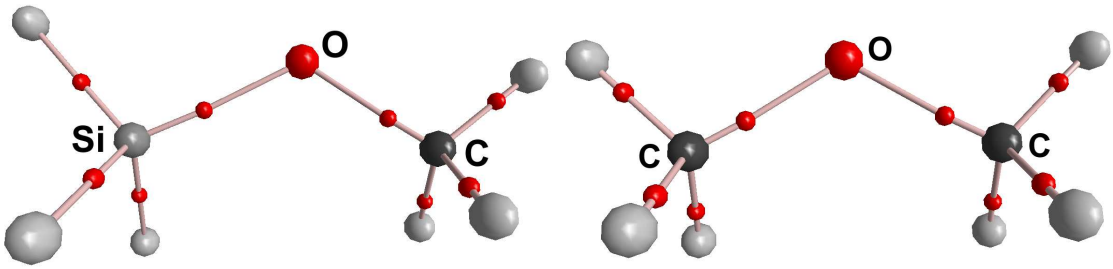

(a) Free methoxysilane at α=120 ° (b) Free dimethylether at τ=120 °

Figure 9.3: Representative molecular graphs of free methoxysilane and free dimethylether

In this chapter, the geometries of the Si–O–C and the C–O–C linkages will be discussed, combined with the molecular graphs displayed in Figures 9.3 to 9.5 in anticipation of the results of the topological analysis of the ED. The free compounds (Figure 9.3) exhibit eclipsed conformation. Only for α/τ=65 ° and 70 °, a small deviation from perfect eclipsed conformation occurs. Thus, the properties for free dimethylether are given as an average over both bonds/ carbon atoms at very small angles (compare Tables A.64 to A.72 in the Appendix). The C–O bonds are not bent over the complete range of angles, but the Si–O bonds are slightly bent at small angles. The deviations of the lengths of the bond paths from the

bond distances are in a range as found for the Si–O bonds in free disiloxane at small angles (0.001 to 0.010 Å), but without a sudden change towards non-strained bonds (compare discussion in Chapter 6.2.1).

Figures 9.4 (a) and (c) show the geometry by means of the molecular graphs for the methoxysilane$\cdots$silanol/water hydrogen-bonded complexes at α=95°. Corresponding representations for dimethylether$\cdots$silanol/ water at τ=95° can be found in Figures 9.5 (a) and (c). The situation at α/τ=95° is representative of the range from 65° to 165°, the overall geometry does not change therein. Eclipsed conformation prevails and the Si–O bond is only slightly strained at small angles. While the complex is perfectly symmetric for dimethylether$\cdots$silanol/water, the donor molecule is shifted towards the methyl group in methoxysilane$\cdots$silanol/ water complexes. The axis of the H$\cdots$O interaction lies in projection of the Si–O bond axis, i.e. there are nearly 180° between these two axes. This fact will be explained with the location of the VSCCs and the ELI-D localisation domains in Chapter 9.3.1.

Within the systems dimethylether$\cdots$silanol/water, the situation does not change upon increasing the C–O–C angle from τ=165° to 170°; the hydrogen-bonding interaction is the same, see Figures 9.5 (b) and (d). This is a fundamentally different behaviour than in disiloxane$\cdots$silanol/ water hydrogen-bonded complexes where a chemical catastrophe occurs between ϕ=165° and 170° so that hydrogen bonding becomes impossible (Chapter 6). This fundamental difference will be explained in Chapter 9.3. It is related to the fact that the ether linkage is a much better hydrogen-bond acceptor than the siloxane linkage at large X–O–X angles (difference of the hydrogen-bond energies (ΔE_{HB}) with silanol as donor at ϕ/τ=165° is 12.71 kJ mol^{-1}, compare Figure 9.2).

On the one hand, the silyl ether linkage is still a better hydrogen-bond acceptor at large Si–O–C angles compared to the siloxane linkage (ΔE_{HB} with silanol as donor at ϕ/α=165° is 5.28 kJ mol^{-1}) so that there are converged methoxysilane$\cdots$silanol/ water complexes at α=170° and 175°. But on the other hand, the O–H$\cdots$O hydrogen bond at α=170° is already not strong enough to stabilise the complex, so that an additional C_{methyl}–H$\cdots O_{silanol}$ interaction is necessary, see Figures 9.4 (b) and (d). The molecular graph with two interactions exists for α=170° and 175°. This is an intermediate behaviour between disiloxane, where no hydrogen bonds are possible at these X–O–X angles, and dimethylether, where there is no difference between these and smaller X–O–X angles. It will be discussed in Chapter 9.3 whether this behaviour is accompanied by a chemical catastrophe in free

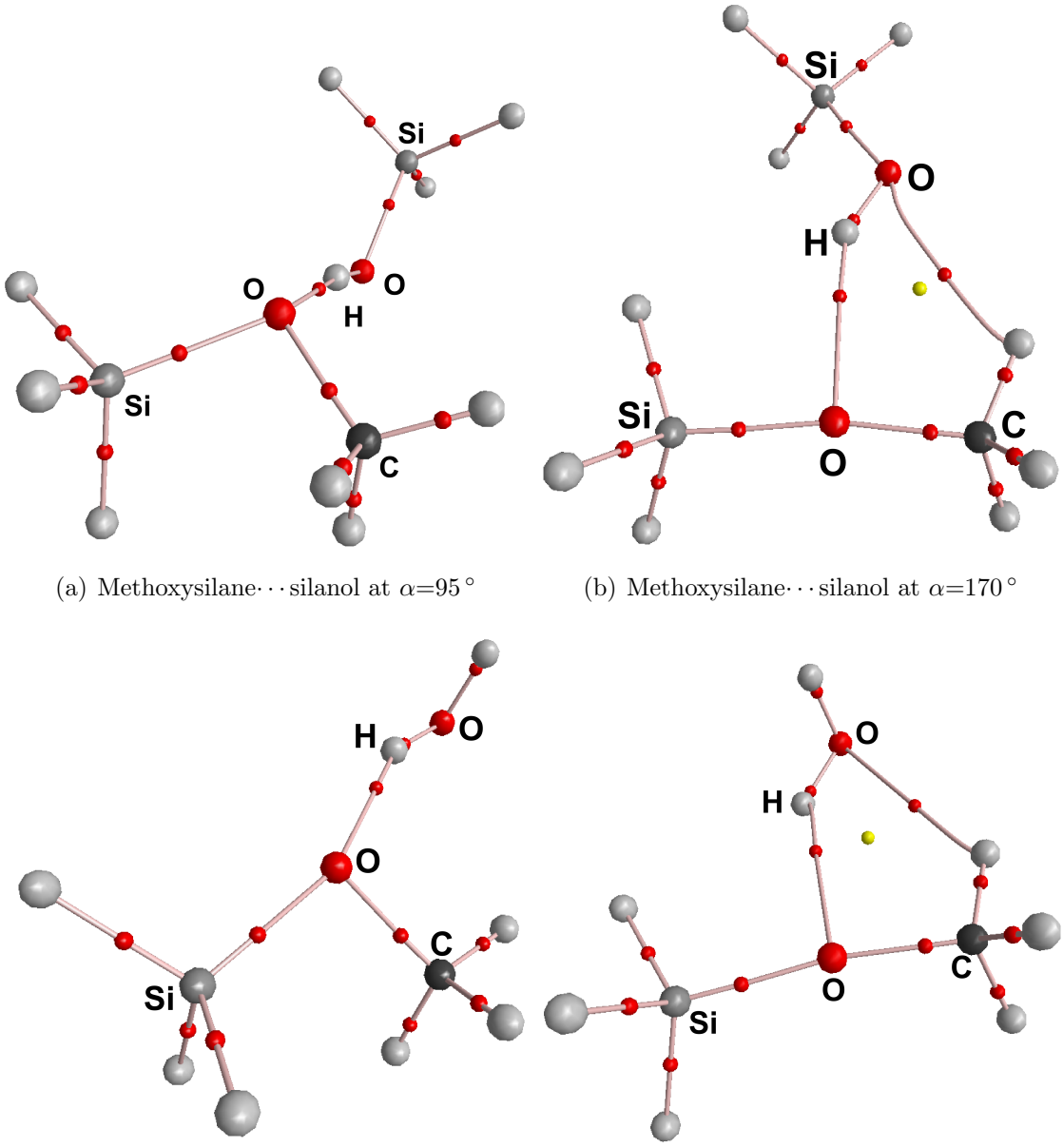

(a) Methoxysilane···silanol at α=95 °

(b) Methoxysilane···silanol at α=170 °

(c) Methoxysilane···water at α=95 °

(d) Methoxysilane···water at α=170 °

Figure 9.4: Representative molecular graphs of methoxysilane hydrogen-bonded complexes

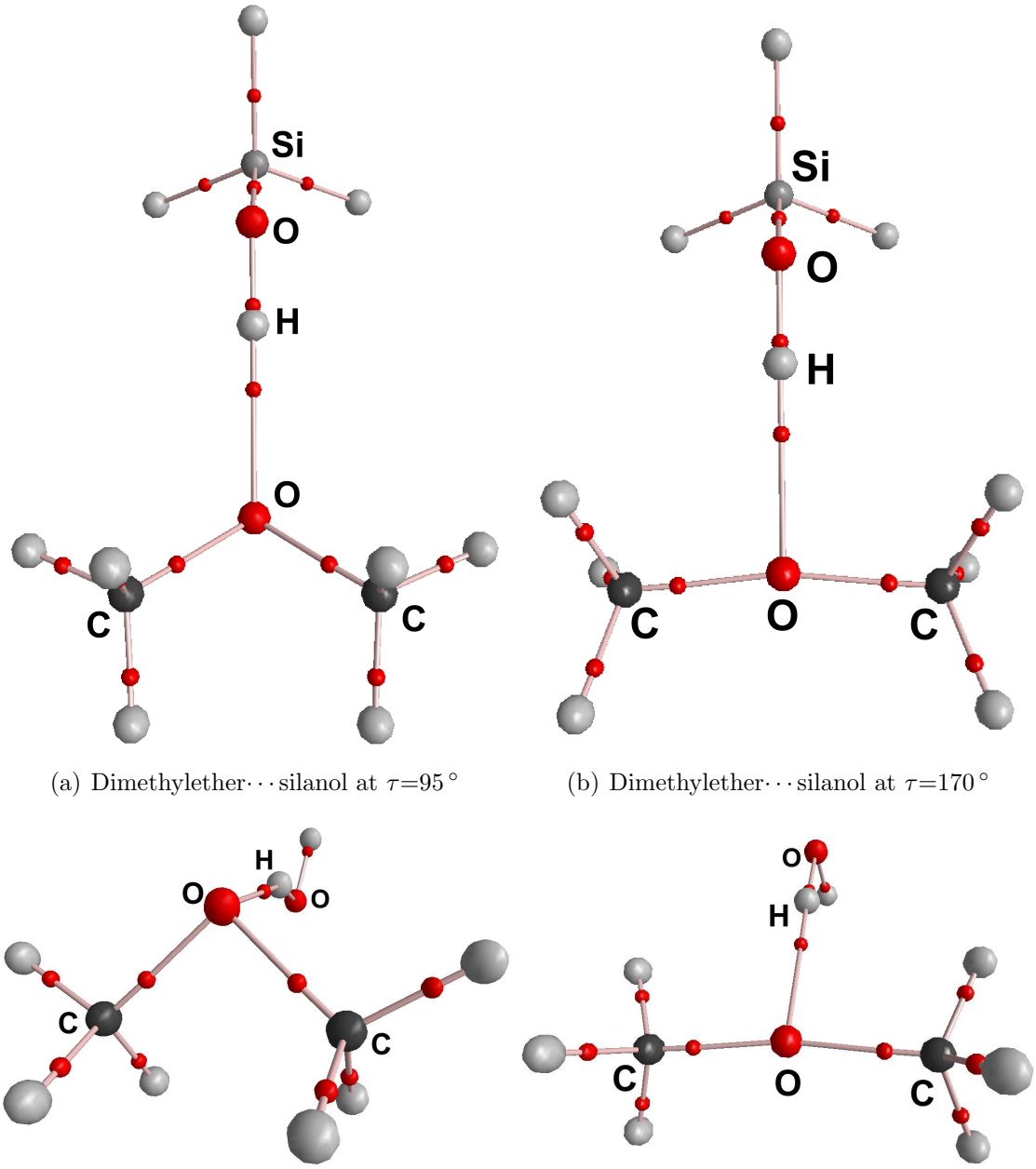

(a) Dimethylether···silanol at τ=95 °

(b) Dimethylether···silanol at τ=170 °

(c) Dimethylether···water at τ=95 °

(d) Dimethylether···water at τ=170 °

Figure 9.5: Representative molecular graphs of dimethylether hydrogen-bonded complexes

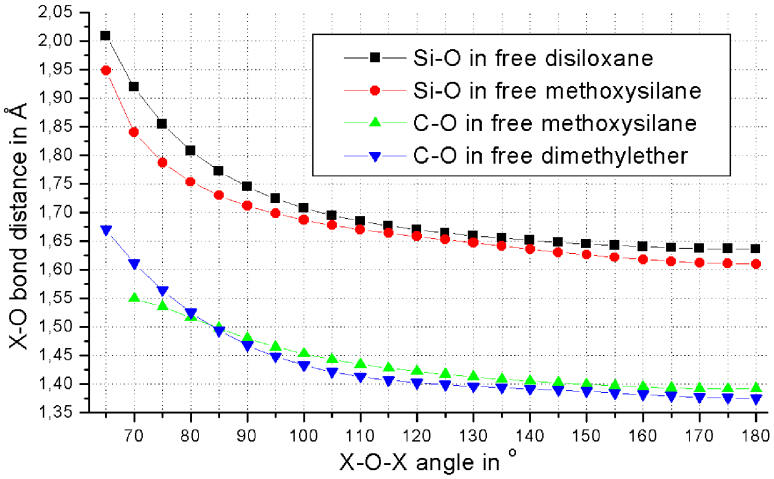

Figure 9.6: Si–O and C–O bond distances in free model compounds

methoxysilane like in disiloxane or not like in dimethylether.

The Si–O bonds in the model compounds are significantly longer (ranging from 2.008 to 1.610 Å) than the C–O bonds (ranging from 1.670 to 1.365 Å), see Figure 9.6. From the fully relaxed geometry optimisation of free methoxysilane, the Si–O distance is 1.654 Å and the C–O distance is 1.418 Å. From the crystal structure of methoxysilane, [245] d(Si–O)=1.651(2) Å and d(C–O)=1.424(3) Å. For free dimethylether the C–O distance is 1.410 Å after relaxed geometry optimisation and 1.413(1)/ 1.415(1) Å from the crystal structure [246]. The Si–O bonds in free methoxysilane are slightly shorter over the full range of angles than the Si–O bonds in free disiloxane, whereas the C–O bonds in free methoxysilane are slightly longer for most C–O–C angles than the C–O bonds in free dimethylether. All bonds shorten when the X–O–X angle is increased, but this effect is strongest for small X–O–X angles.

9.2 Results of the Topological Analysis of the ED

9.2.1 Bond-Topological Properties

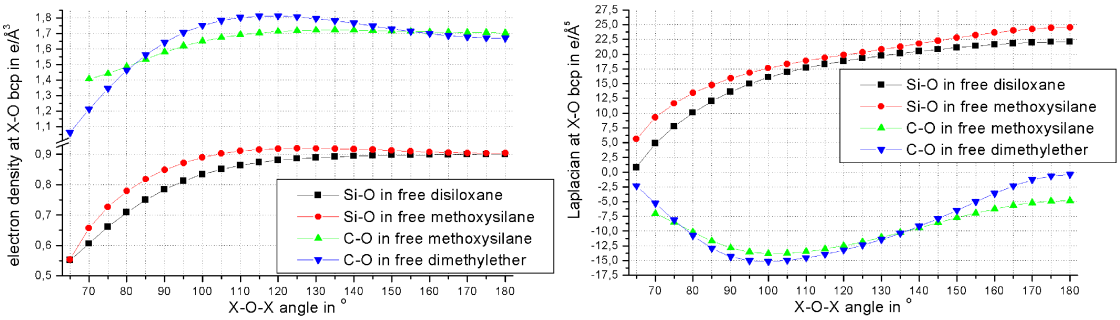

(a) Electron density (b) Laplacian

Figure 9.7: Electron density and Laplacian at X–O bcps in free model compounds

It was stated before that the value of the electron density at the bcp is predominantly indicative of the bond strength while the Laplacian indicates the bond character. Thus, it occurred that the Si–O bonds in free disiloxane become stronger and more ionic upon increasing the Si–O–Si angle. This means that not only the basicity of the oxygen atom but also the bond character can be tuned by angle variation. The curves for free disiloxane are again plotted in Figure 9.7, where they are compared to corresponding curves for free methoxysilane and free dimethylether. The behaviour of the Si–O bond in free methoxysilane is similar to the behaviour in free disiloxane: The bond is weaker at small angles than at larger angles (ranging from $\varrho(bcp)$=0.55 to 0.92 eÅ^{-3}) and the constant increase of the Laplacian (ranging from $\nabla^2\varrho(bcp)$=5.6 to 24.5 eÅ^{-5}) shows that it also becomes more and more ionic towards large angles. The Si–O bond is even stronger and more ionic at any given angle in free methoxysilane than in free disiloxane according to the decrease of the bond distance. A small difference in the behaviour of the curves can nevertheless be found for the electron density. Whereas the curve for free disiloxane constantly ascends, it runs through a small maximum at α=125 ° for free methoxysilane ($\varrho(bcp)$=0.92 eÅ^{-3} compared to 0.90 eÅ^{-3} at α=180 °). This means that the Si–O bond in free methoxysilane is strongest at the minimum-angle position but most ionic at the linear geometry.

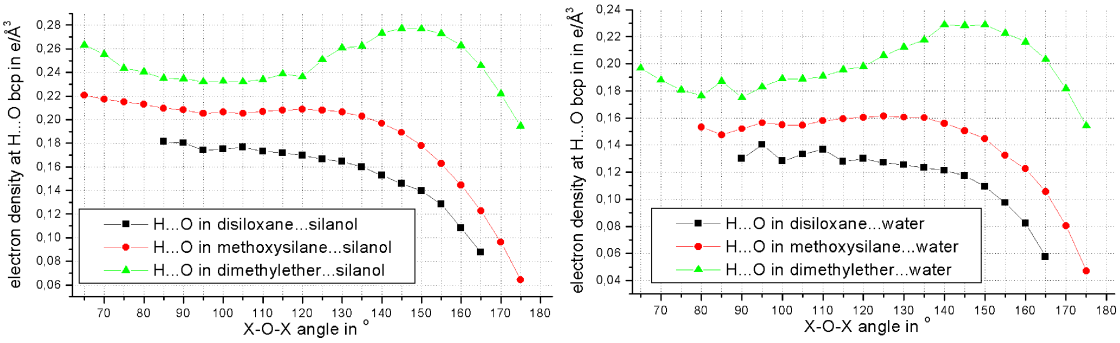

(a) Hydrogen bonds to silanol

(b) Hydrogen bonds to water

Figure 9.8: Electron density at H···O bcps in hydrogen-bonded complexes

However, a similar effect is found for the C–O bonds, but much more pronounced. For free methoxysilane, there is again only a small maximum in the curve of the electron density, shifted to α=135 °. But for the Laplacian, there is a pronounced minimum in the curve at α=100 °. This means that the C–O bond in methoxysilane is strongest and most covalent at medium angles, but ionic contributions mix into the bond character for very large and very small Si–O–C angles. The C–O bond is a bit stronger and a bit more ionic at very large angles compared to very small angles.

In free dimethylether, the effect is stronger. On the one hand, the C–O bonds are clearly stronger and more covalent at medium angles close to the minimum-angle position than in methoxysilane because the curves run through pronounced extrema. On the other hand, the Laplacian is less negative at very large and very small angles compared to free methoxysilane, indicating that ionic contributions become more important for the C–O bonds in free dimethylether.

The value of the electron density at the H···O bcp in the hydrogen-bonded model complexes was chosen as one example for a property that is indicative of hydrogen-bond formation. The curves for the silanol complexes and the water complexes are given in Figure 9.8. The curves for methoxysilane and dimethylether do not correlate with the curves for the hydrogen-bond energy (Figure 9.2) in a simple manner. The first striking difference is that the value of the electron density for disiloxane hydrogen-bonded complexes is lowest at any given X–O–X angle, indicating that hydrogen bonds of disiloxane as acceptor are weakest, whereas hydrogen bonds of dimethylether as acceptor are strongest in any case. For disiloxane

and methoxysilane, the trend is confirmed that the basicity of the oxygen atom, and thus, the ability to form hydrogen bonds as acceptor, can be improved by decreasing the X–O–X angle. However, for dimethylether this trend is nearly reversed since a maximum of the electron density is located at τ=150 ° for both dimethylether$\cdots$silanol and dimethylether$\cdots$water. However, the lowest values of the electron density can be found at very large angles according to weak hydrogen bonding and towards very small angles, the electron density rises according to a strengthening of the hydrogen bonds.

9.2.2 Atomic Properties

An increasing charge separation of silicon/carbon atoms and the oxygen atom indicates increasing ionic character of the Si/C–O bonds. This can be found for all compounds as shown in Figures 9.9 (a) and (b). The silicon or carbon atom, respectively, becomes more positively charged while the oxygen atom becomes more negatively charged with increasing X–O–X angle. There are no extrema in the curves at medium angles, so that the atomic charges indicate a constant increase of ionicity. According to the electronegativity differences, the oxygen atom is charged most strongly in free disiloxane (-1.3 to -1.7 e), less strongly in free methoxysilane (-0.9 to -1.5 e) and least strongly in free dimethylether (-0.6 to -1.3 e). The carbon atoms are charged by 0.7 e or less, but the silicon atoms are charged by 2.5 e or more. However, the carbon atom in free methoxysilane is less positively charged than the corresponding atoms in free dimethylether, whereas the silicon atom is more positively charged than the ones in free disiloxane. The differences for C and Si atoms are largest for small X–O–X angles but nearly vanish for large angles.

The order of the atomic volumes (Figures 9.9 (c) and (d)) for the three different model compounds is reversed compared to the charges. The most positively charged atoms possess the smallest volume and the most negatively charged atoms possess the largest. But within a system, this correlation cannot be found. The charges ascend or descend monotonously whereas the volumes run through extrema at medium angles. The shapes of the curves for the different model compounds are very similar; the extrema are located at the same positions, only the height of the maxima differs. These facts confirm that the occurrence of the extrema has to be explained with geometrical changes upon variation of the X–O–X angle and cannot be attributed to inherent chemical differences. The same explanantion by

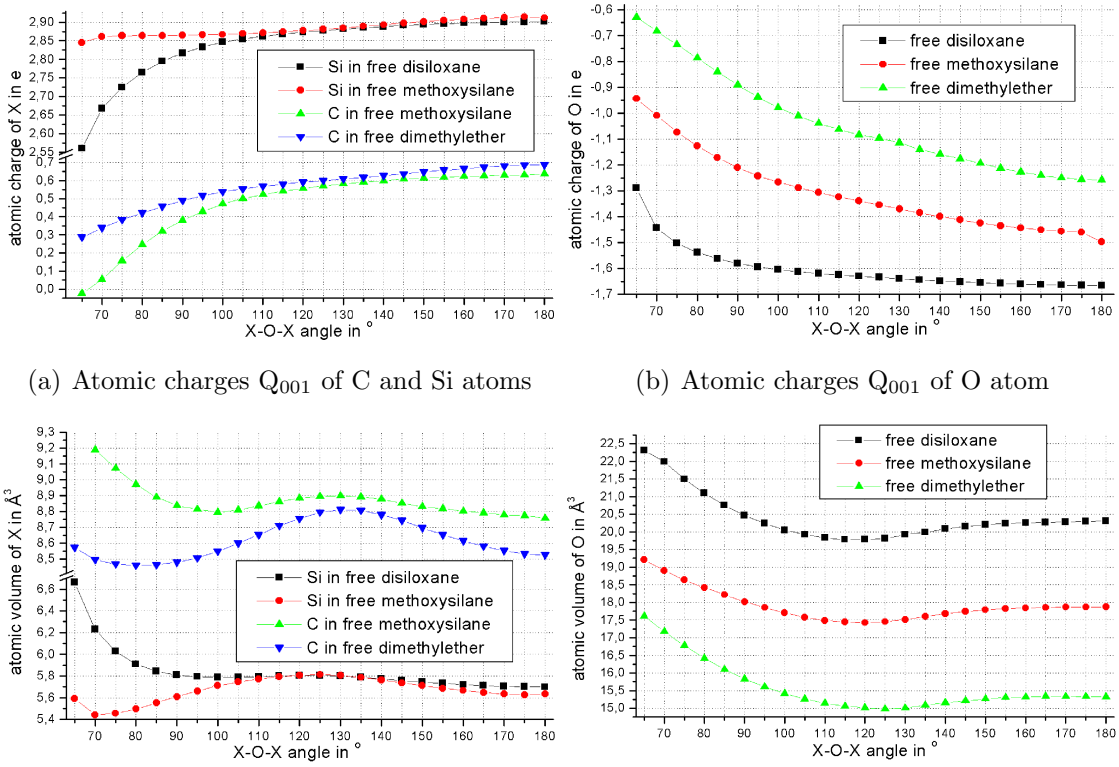

(a) Atomic charges Q_{001} of C and Si atoms

(b) Atomic charges Q_{001} of O atom

(c) Atomic volumes V_{001} of C and Si atoms

(d) Atomic volumes V_{001} of O atom

Figure 9.9: Atomic charges and volumes in free model compounds

means of geometry that holds for the disiloxane system (compare Chapter 6.2.4) therefore also holds for methoxysilane and dimethylether.

9.3 Results of the Topological Analysis of the ELI-D

9.3.1 Localisation Domains vs. VSCCs

In contrast to free disiloxane, there is no change in the number of attractors within the topological ELI-D analysis for both free methoxysilane and free dimethylether upon variation of the X–O–X angle. Over the full range of X–O–X angles (α/τ=65 ° to 175 °), there is no Si–C or C–C bond but two X–O bonds and two oxygen lone pairs, in each case indicated by the existence of corresponding ELI-D attractors and basins. Hence, no chemical catastrophe occurs upon variation of the X–O–X angle. This means that the same chemical system is existent within the full range of angles and accordingly, no sudden change in a chemical property like hydrogen-bonding ability must be present. This explains why hydrogen bonding is feasible from α/τ=65 ° to 175 °. A third lone-pair attractor and a ringlike shape of the ELI-D localisation domain and the VSCCs around the oxygen atoms only appear for the linear geometry in free methoxysilane and free dimethylether, consequently hydrogen bonding is no longer possible at α/τ=180 °. Free disiloxane behaves fundamentally differently because it exhibits several different chemical systems in the same range of angles divided by topological catastrophes and indicated by different chemical behaviour like hydrogen-bonding ability.

To exemplify these findings and go into more detail concerning the ELI-D results, localisation-domain representations of free methoxysilane and free dimethylether at representative angles are shown in Figures 9.10 (a),(c) and 9.11 (a),(c) in comparison to the corresponding VSCC representations in Figures 9.10 (b),(d) and 9.11 (b),(d). A cap-like shape of the ELI-D localisation domains and the VSCCs of the oxygen lone pairs has been anticipated with the general ability of a system to form hydrogen bonds as acceptor, see detailed discussion in Chapter 6 and Figures 6.17 and 6.18. This shape can be seen for all examples in Figures 9.10 and 9.11 at respresentative X–O–X angles of α/τ=95 ° and 170 °.

For free dimethylether, the situation is simple over the full range of angles (Figure 9.11). Symmetric and rather strong hydrogen-bonded complexes are possible because the shape of the oxygen lone pairs does not change in principle. They only differ in details: While the two different lone-pair basins might be recognisable by means of two swellings of the reducible localisation domain at τ=95 °, the reducible localisation domain at τ=170 ° is narrower and more homogeneous. But

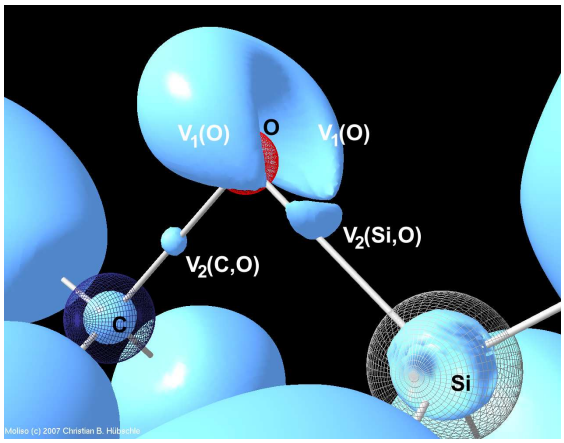

(a) ELI-D localisation domains at α=95°, isovalue=1.467

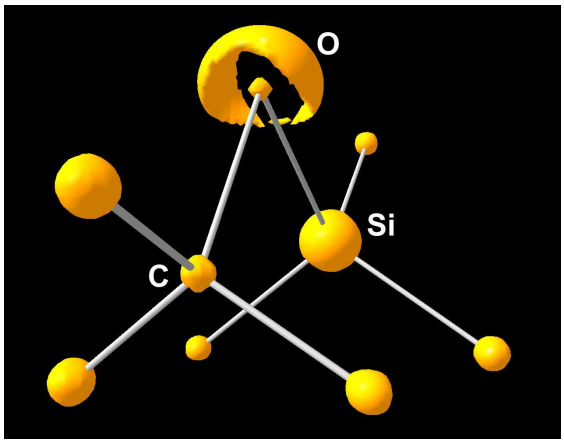

(b) VSCCs at α=95°, isovalue=-68.68 e Å^{-5}

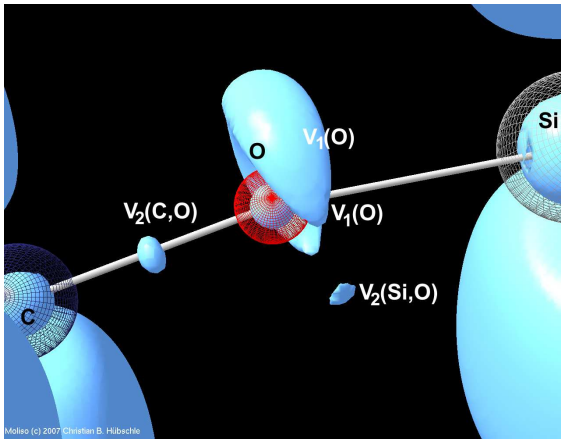

(c) ELI-D localisation domains at α=170°, isovalue=1.509

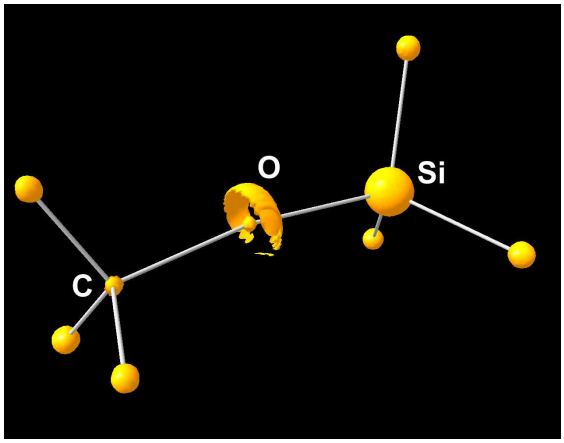

(d) VSCCs at α=170°, isovalue=-72.30 e Å^{-5}

Figure 9.10: ELI-D localisation-domain and Laplacian isosurface representations of free methoxysilane at representative angles

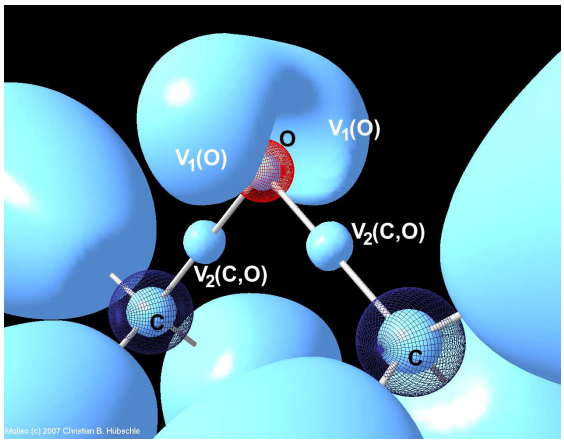

(a) ELI-D localisation domains at τ=95°, isovalue=1.467

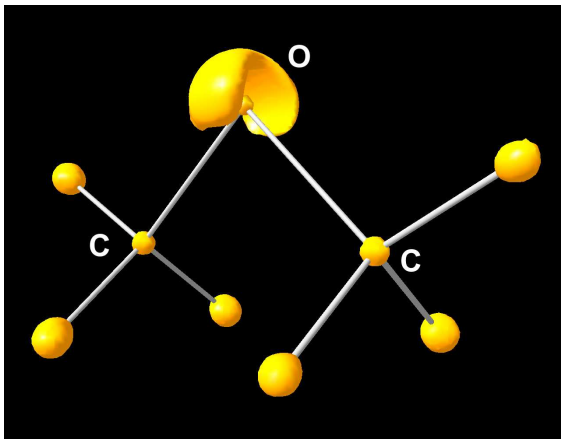

(b) VSCCs at α=95°, isovalue=-66.03 e Å^{-5}

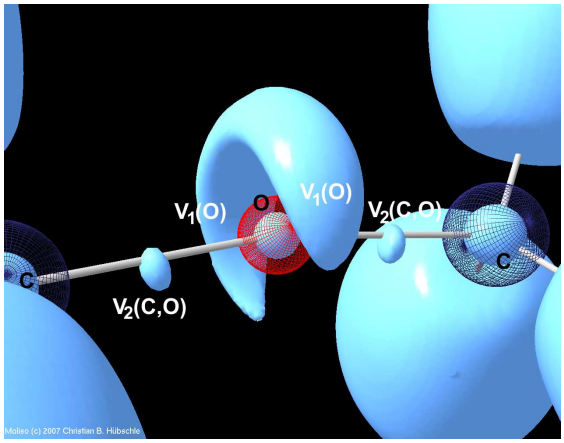

(c) ELI-D localisation domains at τ=170°, isovalue=1.470

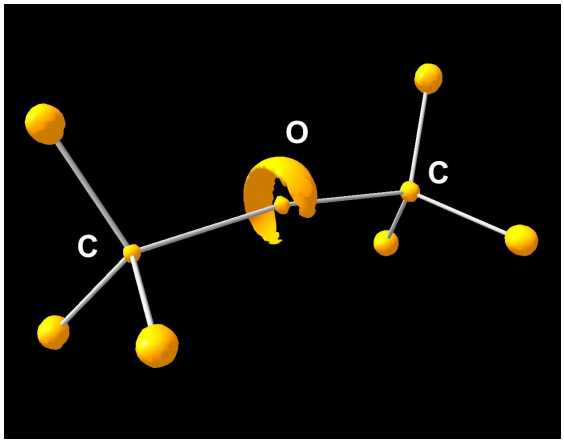

(d) VSCCs at α=170°, isovalue=-62.66 e Å^{-5}

Figure 9.11: ELI-D localisation-domain and Laplacian isosurface representations of free dimethylether at representative angles

the most important point is that electrons do not localise underneath the oxygen atom. This does not even occur at higher isovalues and not at τ=175 °. The isovalue chosen is the same as for disiloxane in Figure 6.18, where an extension of the space of the lone pairs towards the lower side of the oxygen atom is clearly visible. Corresponding explanations are true for the Laplacian isosurface representations showing the oxygen VSCCs in Figures 9.11 (b),(d).

For free methoxysilane, the situation is a bit more complex due to the unsymmetrical linkage. The cap of ELI-D localisation or VSCCs, respectively, is situated on top of the oxygen atom but oblique (Figures 9.10 (a) and (b)). The open side points towards the Si–O bond basin V_2(Si,O) so that the closed side is situated in projection of the Si–O bond axis. If a protic hydrogen atom approaches the oxygen atom in an electrophilic attack, it is guided towards the centre of the cap yielding a geometry of the hydrogen as found in Figures 9.4. There, a geometry was described in which the axis of the H$\cdots$O interaction lies in projection of the Si–O bond axis. A similar shape of lone-pair localisation domain and VSCC can be found for the oxygen atom in a silanol group which is included in an unsymmetrical Si–O–H linkage, too, compare for example Figures 6.11 and 6.22.

When the Si–O–C angle increases, the cap must consequently straighten up (Figures 9.10 (c) and (d)). It is still not symmetrical but shifted towards the silicon atom. In the course of this straightening, the Si–O bond attractor strongly shifts away from the Si–O bond axis as if it is bonded to the lone-pair domains. Actually, the localisation domains or the VSCCs, respectively, merge at larger isovalues so that the phenomenological appearance of this situation is similar to the one of disiloxane at large Si–O–Si angles, compare Figure 6.10 (d) and 6.18 (c). Thus, it can be understood why hydrogen bonding is at least difficult for α=170 ° and 175 ° so that an additional interaction must stabilise the complexes, see Figures 9.4 (b) and (d).

However, it must be noted that there is not an additional valence attractor in the ELI-D that appears between α=165 ° and 170 °, but an existing bond attractor continuously shifts away from its initial position at the bond axis to the same degree the cap of the lone pairs straightens up. This is not the scenario of a topological catastrophe and thus a fundamental difference compared to the situation for free disiloxane. Moreover, the attractor V_2(Si,O) remains a bond attractor although it is situated closer to the oxygen atom and the lone pairs than to the bond axis and the silicon atom. This is reflected in the fact that the basin belonging to the attractor still shares a common boundary (zero-flux surface) with the outer

core basin of the silicon atom, i.e. the basin remains di-synaptic.

The ELI-D localisation domains of the C–O and Si–O bond basins (V_2(C,O) and V_2(Si,O)) have a different shape. The C–O bond domains are smaller and more spherical than the Si–O bond domains (see Figure 9.10 (a)). Actually, the C–O bond basins really have the smaller volume and are less populated than the Si–O bonds, see next chapter.
The Si–O bond attractor is slightly shifted outwards with respect to the Si–O bond axis at α=95 °, indicating bond strain. The effect is larger for smaller Si–O–C angles. At large angles, the Si–O bond attractor significantly shifts inwards as depicted and discussed for α=170 ° indicating a strong ionic bond character. These shifts are generally the same for the Si–O bond attractors of free disiloxane (compare Chapter 6.3.1 and Figure 6.19) but the inwards shift is stronger for free methoxysilane according to the fact that the Si–O bond in methoxysilane is more ionic than in disiloxane (see discussion on the Laplacian in Chapter 9.2.1).
In contrast, the positions of the C–O bond attractors are nearly invariant upon variation of the X–O–X angle (see Figures 9.10 (a),(c) and 9.11 (a),(c)). There is a small shift inwards for dimethylether at τ=170 °(Figure 9.11 (c)) indicating some degree of ionic contributions to the mainly covalent bond (compare again discussion on the Laplacian in Chapter 9.2.1). In general, no bond strain and only a small degree of ionicity is indicated by the position of the C–O bond attractor.

9.3.2 Populations and Volumes of ELI-D Basins

Within the discussion of the chemical catastrophes in disiloxane, the curves of the populations of Si–O bonds and oxygen lone pairs (Figure 6.21) very clearly confirmed the conclusions drawn from the qualitative pictures of the localisation domains and VSCCs. Between ϕ=80 ° and 85 ° as well as ϕ=165 ° and 170 °, sudden changes in the populations could be found, indicating the transition from one chemical system to another by means of electron reorganisation. In Figure 9.12 for free methoxysilane and free dimethylether, there is neither a sudden change in the population between α/τ=165 ° and 170 ° nor between any other two angles in the region of large X–O–X angles. This again confirms that there is no chemical catastrophe and all X–O–X angles except α/τ=180 ° belong to the same chemical system in which hydrogen bonding is possible.
However, there is a sudden change between α/τ=70 ° and 75 ° similar to the ones

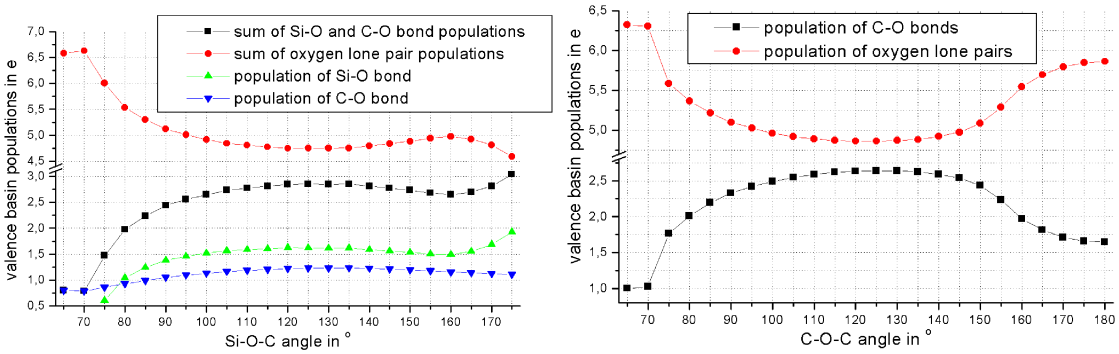

(a) Free methoxysilane, sum as well as individual populations of Si–O and C–O bonds, sum of oxygen lone-pair populations

(b) Free dimethylether, sum of C–O bond populations, sum of oxygen lone-pair populations

Figure 9.12: Electron populations N_{001} of ELI-D basins for Si–O bonds, C–O bonds as well as for oxygen lone pairs in free methoxysilane and in free dimethylether

found for free disiloxane. This change cannot belong to a topological catastrophe because the number of attractors does not change in the same region. Nevertheless, a transition from a hypothetical to a real form of H_3SiOCH_3 and H_3COCH_3 might be indicated as the ELI-D populations have been proven to be a very sensitive parameter to detect chemical variations.

In general, the curves for the sum of the populations of the bond basins and lone-pair basins - which must be totally symmetric to each other - are similar for all three model compounds. At very small angles, the oxygen lone pairs possess almost all valence electrons of the systems. With increasing strength of the X–O bonds, they gain electrons and the oxygen lone pairs lose population. A maximum of the bond populations is located at medium angles. Towards very large X–O–X angles, the oxygen lone pairs in turn gain electrons, which the bonds lose. This takes place continuously in free methoxysilane and free dimethylether, but suddenly in free disiloxane. In methoxysilane, there is a special situation regarding the V_2(Si,O) basin. It gains electrons as it mimics a third oxygen lone pair. Hence, the sum of the X–O bond populations increases again between α=165 ° and 175 °.

In Figure 9.12 (a), the individual populations of Si–O and C–O bonds are compared. It turns out that the Si–O bond is generally more highly populated than the C–O bond by an average of about 0.4 e. Thus, the electron population of a bond in terms of an ELI-D analysis is not indicative of the bond character. An ionic bond can possess more electrons than a covalent bond of the same strength, as this example shows. A corresponding conclusion can be drawn for the ELI-D

bond volumes. The volumes of the Si–O bonds are larger than the volumes of the C–O bonds, which was already implied by the shapes of the associated localisation domains. The difference is about 1 to 2 $Å^3$, see Tables A.70 to A.72.

Chapter 10

Results of the Analyses of Compounds 5 and 6

10.1 Geometrical and Energetical Results

10.1.1 Experimental Geometries

The molecular structures of butoxysilanol (**5**) and sucrose (**6**), including the used atomic-numbering schemes, can be found in Figure 8.2. Bond distances and angles of six different Si–O–C linkages in the asymmetric unit (asu) of butoxysilanol (**5**) are given in Table 10.1. The asu of butoxysilanol (**5**) consists of two independent molecules, one being the acceptor of the silanol$\cdots$silyl ether hydrogen bond O2A–H2OA$\cdots$O1, the other one being the donor. Additionally, distances and angles of three different C–O–C linkages in sucrose (**6**) (consisting of one molecule in the asu) are listed. Complete lists can be found in Tables A.73 to A.75 and in Ref. [84].

The Si–O–C angles in butoxysilanol (**5**) range from α=129.59(4)° to 131.82(5)°. They are by about 6° to 7° larger than the minimum angle in methoxysilane H_3SiOCH_3, which was found to be 123.91°. Accordingly, the Si–O bond distances are shorter; they range from 1.611(1) to 1.643(1) Å (1.654 Å at the minimum-angle position in methoxysilane). However, the C–O bonds in butoxysilanol (**5**) are significantly longer than in methoxysilane, ranging from 1.439(1) to 1.448(1) Å (1.418 Å at the minimum-angle position in methoxysilane).

The C–O–C angles in sucrose (**6**) are smaller than the Si–O–C angles in butoxysilanol (**5**) by about 15° to 20°. They range from τ=111.64(1)° to 115.57(1)° and

Table 10.1: Selected bond distances (Å) and angles (°) in butoxysilanol (**5**) and sucrose (**6**) from high-resolution X-ray diffraction experiments

bond/angle	butoxysilanol (**5**)	bond/angle	sucrose (**6**)
Si1–O1	1.638(1)		
Si1–O3	1.615(1)		
Si1–O4	1.618(1)		
Si1A–O1A	1.620(1)		
Si1A–O3A	1.643(1)		
Si1A–O4A	1.611(1)		
C1–O1	1.446(1)	C1–O1	1.430(1)
C5–O3	1.439(1)	C7–O1	1.439(1)
C9–O4	1.443(1)	C1–O5	1.419(1)
C1A–O1A	1.440(1)	C5–O5	1.448(1)
C5A–O3A	1.448(1)	C7–O7	1.415(1)
C9A–O4A	1.443(1)	C10–O7	1.454(1)
Si1–O1–C1	130.03(5)	C1–O1–C7	113.73(1)
Si1–O3–C5	131.41(5)	C1–O5–C5	115.57(1)
Si1–O4–C9	131.82(5)	C7–O7–C10	111.64(1)
Si1A–O1A–C1A	130.30(5)		
Si1A–O3A–C5A	129.59(4)		
Si1A–O4A–C9A	130.16(5)		

thus scatter closely around the minimum-angle position of 112.66 ° in dimethylether. But again, the C–O distances are significantly longer (ranging from 1.415(1) to 1.454(1) Å) than the ones in dimethylether at the minimum-angle position (1.410 Å). In contrast, the Si–O bond behaves as expected from the PES scans, which was also found for the siloxane linkage in Chapter 7.

10.1.2 Intermolecular Interactions in the Crystals

The hydrogen-bonding pattern of butoxysilanol (**5**) is fundamentally different to the one of sucrose (**6**), compare Figure 10.1 and Table 10.2. In butoxysilanol (**5**), there is only one medium-strength hydrogen bond (O2A–H2OA$\cdots$O1) and a few weak C–H$\cdots$O interactions. O2A–H2OA$\cdots$O1 connects the two independent molecules of the asu while the C–H$\cdots$O interactions are mainly intramolecular;

only one interaction connects the asu with symmetry-related molecules. In sucrose (**6**), there are many intra- and intermolecular strong O–H···O hydrogen bonds and also a few C–H···O interactions. Consequently, sucrose (**6**) has a high lattice energy (-270.82 kJ mol^{-1}, see Table 10.3) whereas butoxysilanol (**5**) has a low lattice energy (-15.61 and -12.07 kJ mol^{-1} for donor and acceptor molecule in the asu).

Every hydroxy donor group in sucrose (**6**) exhibits one or even two hydrogen bonds. In contrast, the silanol group Si1–O2–H2O does not act as a hydrogen-bond donor at all. The linkage C1–O1–C7 in sucrose (**6**) is not involved in a hydrogen bond as acceptor, but C1–O5–C5 forms a strong O–H···O hydrogen bond and C7–O7–C10 forms a weaker O–H···O hydrogen bond. In butoxysilanol (**5**), Si1–O3–C5 is not involved in hydrogen bonding as acceptor, whereas Si1–O1–C1 forms the only O–H···O hydrogen bond and Si1–O4–C9 forms two weak C–H···O interactions as acceptor.

For siloxane, the occurrence of C–H···O interactions with the siloxane linkage as acceptor was discussed as a noteworthy peculiarity, see Chapter 7.1.2. The two C–H···O interactions in trisilo (**2**) are even a bit stronger than the ones in butoxysilanol (**5**) regarding the interaction energies and the density at the H···O bcps (compare Tables 7.2 and 10.2). Within the same criteria, the C–H···O interactions in sucrose (**6**) must be referred to as being twice as strong as the ones in butoxysilanol (**5**) and trisilo (**2**) due to the fact that the ether oxygen atom is more basic.

The silanol···siloxane hydrogen bond in siloxanol (**1**) is clearly stronger than the silanol···silyl ether hydrogen bond. From methoxysilane···silanol, E_{HB}=-13.99 kJ mol^{-1} and ϱ(H···O)=0.21 eÅ^{-3} were expected at α=130 °. Thus, the PES scans predict a considerably stronger hydrogen bond than those found in the scrutinised triclinic modification of butoxysilanol (**5**).

The silanol···siloxane hydrogen bond in siloxanol (**1**) is rather comparable to the hydroxy···ether hydrogen bonds in sucrose (**6**). For the latter ones, E_{HB}=-11.21/ -19.56 kJ mol^{-1} and ϱ(H···O)=0.20/0.24 eÅ^{-3} were predicted from the PES scans of dimethylether···water/silanol at α=115 °. These values are in accordance with the ones of the hydroxy···ether hydrogen bonds as given in Table 10.2 with the exception of O4–H4O···O6/O7, which have a much longer H···O distance.

As already mentioned above, the negative lattice energy of sucrose (**6**) is nearly 20 times larger than the ones for butoxysilanol (**5**), given separately for the donor and

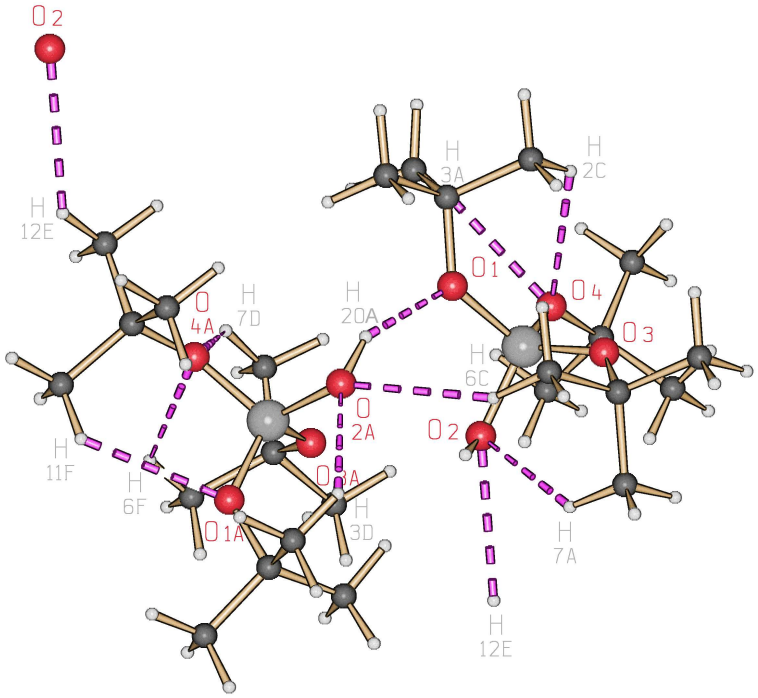

(a) Two molecules of butoxysilanol (**5**) in the asu connected mainly via the silanol···silyl ether hydrogen bond O2A–H2OA···O1

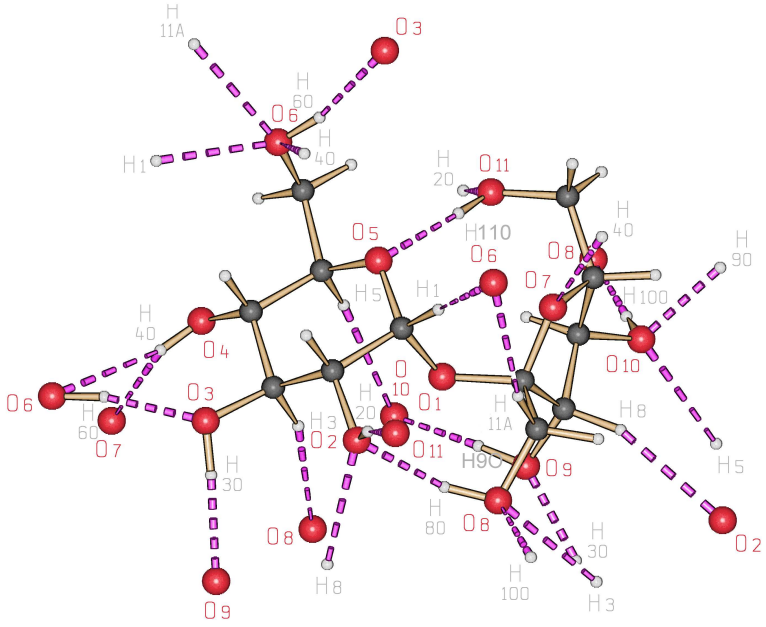

(b) One molecule of sucrose (**6**) in the asu exhibiting many intra- and intermolecular hydrogen bonds

Figure 10.1: Representation of the hydrogen-bonding networks of the asymmetric units (asus) of butoxysilanol (**5**) and sucrose (**6**)
All symmetry-related hydrogen-bonding partners are plotted and labelled

Table 10.2: Selected properties of the hydrogen bonds of cpds. **5** and **6**
Hydrogen$\cdots$acceptor (H$\cdots$A) distance in Å, donor$\cdots$acceptor (D$\cdots$A) distance in Å, donor-hydrogen$\cdots$acceptor (D–H$\cdots$A) angle in °, electron density ϱ at H$\cdots$A bcp in eÅ^{-3}, Laplacian $\nabla^2\varrho$ at H$\cdots$A bcp in eÅ^{-5}, interaction energies E_{int} in kJ mol^{-1}, symmetry operation to generate second molecule

labels	H$\cdots$A	D$\cdots$A	D–H$\cdots$A	ϱ_{bcp}	$\nabla^2\varrho_{bcp}$	E_{int}	sym
Butoxysilanol (**5**):							
O2A–H2OA$\cdots$O1	1.888	2.779	151.99	0.15	0.4	-3.17	intra asu
C7–H7A$\cdots$O2	2.485	3.241	127.60	0.04	1.0	–	intramolecular
C12A–H12E$\cdots$O2	2.696	3.417	125.18	0.03	0.5	-0.59	-1+x, 1+y, z
C2–H2C$\cdots$O4	2.671	3.339	120.79	0.03	0.5	–	intramolecular
C3–H3A$\cdots$O4	2.437	3.225	130.36	0.04	0.8	–	intramolecular
C11A–H11F$\cdots$O1A	2.627	3.315	122.24	0.03	0.5	–	intramolecular
C6–H6C$\cdots$O2A	2.612	3.576	151.15	0.05	0.3	-1.06	intra asu
C3A–H3D$\cdots$O2A	2.569	3.273	123.44	0.03	0.6	–	intramolecular
C6A–H6F$\cdots$O4A	2.540	3.250	123.78	0.04	0.6	–	intramolecular
C7A–H7D$\cdots$O4A	2.523	3.257	125.82	0.04	0.7	–	intramolecular
Sucrose (**6**):							
O8–H8O$\cdots$O2	1.836	2.776	161.36	0.25	1.4	–	intramolecular
O11–H11O$\cdots$O5	1.886	2.833	164.49	0.20	1.6	–	intramolecular
O6–H6O$\cdots$O3	1.873	2.811	167.01	0.23	1.1	-15.10	-x, 1/2+y, -z
O4–H4O$\cdots$O6	2.499	3.357	157.29	0.07	0.6	-4.60	-x, -1/2+y, -z
O4–H4O$\cdots$O7	2.323	2.815	113.70	0.07	1.5	-11.56	x, -1+y, z
O10–H10O$\cdots$O8	1.744	2.706	168.14	0.30	1.4	-17.08	-1+x, y, z
O3–H3O$\cdots$O9	1.881	2.835	173.51	0.19	1.4	-17.97	-x, -1/2+y, 1-z
O9–H9O$\cdots$O10	1.884	2.831	165.68	0.22	1.2	-13.74	1-x, -1/2+y, 1-z
O2–H2O$\cdots$O11	1.874	2.835	169.59	0.21	1.2	-11.39	-1+x, y, z
C8–H8$\cdots$O2	2.399	3.437	156.41	0.08	0.8	-7.57	-x, 1/2+y, 1-z
C1–H1$\cdots$O6	2.239	3.326	167.85	0.11	1.0	-7.22	-x, 1/2+y, -z
C11–H11A$\cdots$O6	2.418	3.450	156.58	0.08	0.8	-5.25	-x, 1/2+y, -z
C3–H3$\cdots$O8	2.445	3.503	161.54	0.07	0.7	-6.62	-x, -1/2+y, 1-z
C5–H5$\cdots$O10	2.603	3.678	164.63	0.05	0.6	-3.12	1-x, -1/2+y, 1-z

Table 10.3: Lattice energies of butoxysilanol (**5**) and sucrose (**6**) in kJ mol^{-1}
Contributions of exchange+repulsion+dispersion terms (erd, absolute) and of the electrostatic term (es, absolute and relative) to the total lattice energy

cpd.	total	erd	es	es(%)
butoxysilanol (**5**) donor	-15.61	-9.49	-6.12	39.2
butoxysilanol (**5**) acceptor	-12.07	-1.32	-10.75	89.1
sucrose (**6**)	-270.82	87.44	-358.26	132.3

the acceptor molecule in the asu in Table 10.3. For both molecules of butoxysilanol (**5**), the exchange-repulsion-dispersion (erd) term as well as the electrostatic term contribute to the lattice energy. In the donor molecule, the erd term dominates whereas in the acceptor molecule, the ESP term contributes with about 90 %. In sucrose (**6**), the erd term is positive, which means that the whole crystal lattice is held together by the huge amount of electrostatic interactions between the molecules. The lattice energies of siloxane cpds. **1** to **4** (compare Table 7.3) range from about -50 to -100 kJ mol^{-1}, which shows that the value of sucrose (**6**) is exceptionally large and implies very effective crystal packing with strong intermolecular contacts. This in turn guides diverse biological modes of actions of sucrose in the body since it is consumed in its crystalline form.

The electrostatic potentials as well as the Hirshfeld surfaces in Figure 10.2, which are best suited to depict the intermolecular interaction pattern, show that there is only one significant interaction in butoxysilanol (**5**), namely O2A–H2OA$\cdots$O1. Towards symmetry-related molecules, i.e. outwards directed, there are neither notable electrostatic polarisation nor covalent interactions because the butoxy groups shield the centres of the molecules, which are directed towards each other to build a dimer. The ESP exhibits values of -0.02 to 0.05 eÅ^{-1} (green to light blue) towards molecules outside the asu for both the donor and the acceptor molecule. This is quite sufficient to form a crystal packing but explains the exceptionally low lattice energies, see above. The Hirshfeld surfaces show that there also is not any interaction with covalent contributions in the crystal packing but very nicely depicts strength and direction of the O2A–H2OA$\cdots$O1 hydrogen bond. In the representations of the ESP of the donor molecule (Figure 10.2 (a)), it can be seen clearly that the hydrogen atom H2O is strongly positively polarised and points

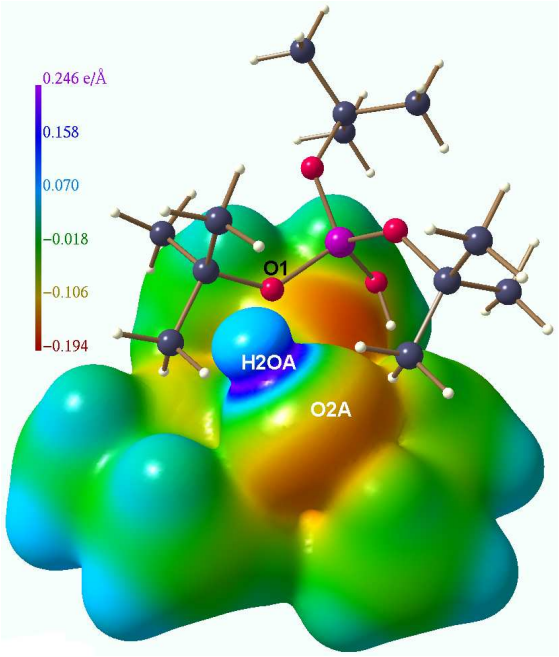

(a) ESP ($e\text{Å}^{-1}$) of the donor molecule mapped on a corresponding ED isosurface of $0.0067\,e\text{Å}^{-3}$, acceptor molecule given as molecular scaffold

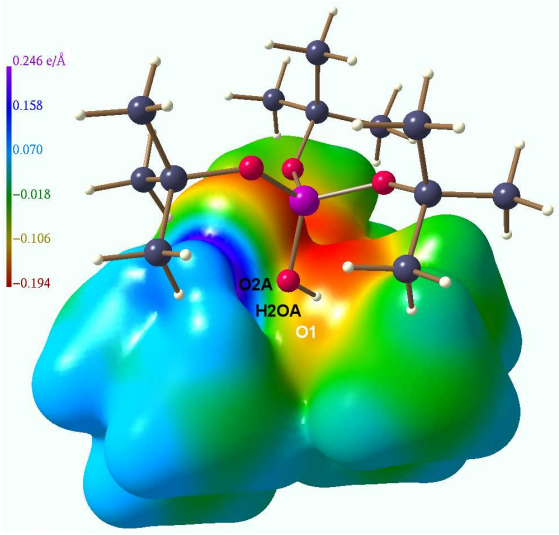

(b) ESP ($e\text{Å}^{-1}$) of the acceptor molecule mapped on a corresponding ED isosurface of $0.0067\,e\text{Å}^{-3}$, donor molecule given as molecular scaffold

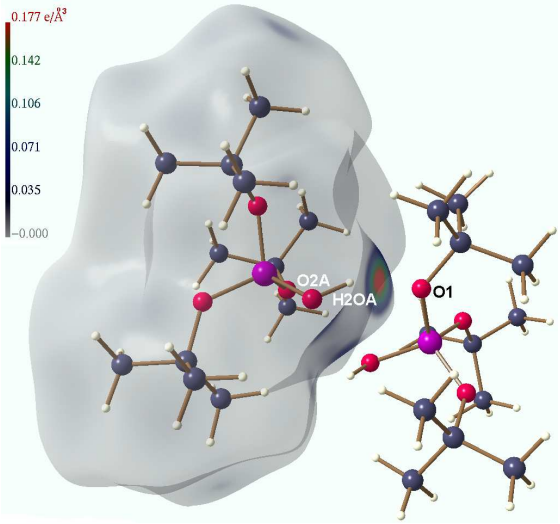

(c) Total ED ($e\text{Å}^{-3}$) mapped on a Hirshfeld surface of the donor molecule, acceptor molecule given as molecular scaffold

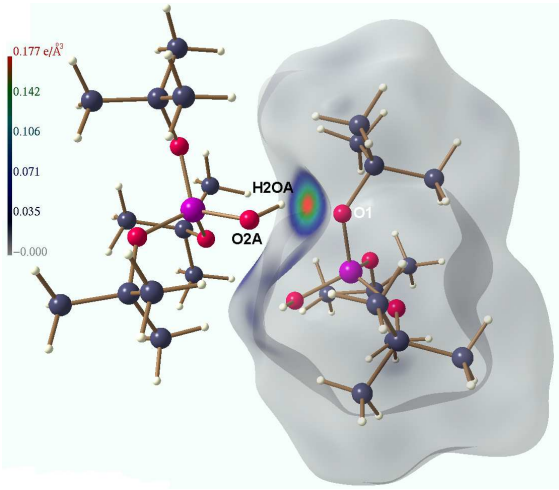

(d) Total ED ($e\text{Å}^{-3}$) mapped on a Hirshfeld surface of the acceptor molecule, donor molecule given as molecular scaffold

Figure 10.2: Representations of the electrostatic potential (ESP) and the Hirshfeld surface of butoxysilanol (**5**)

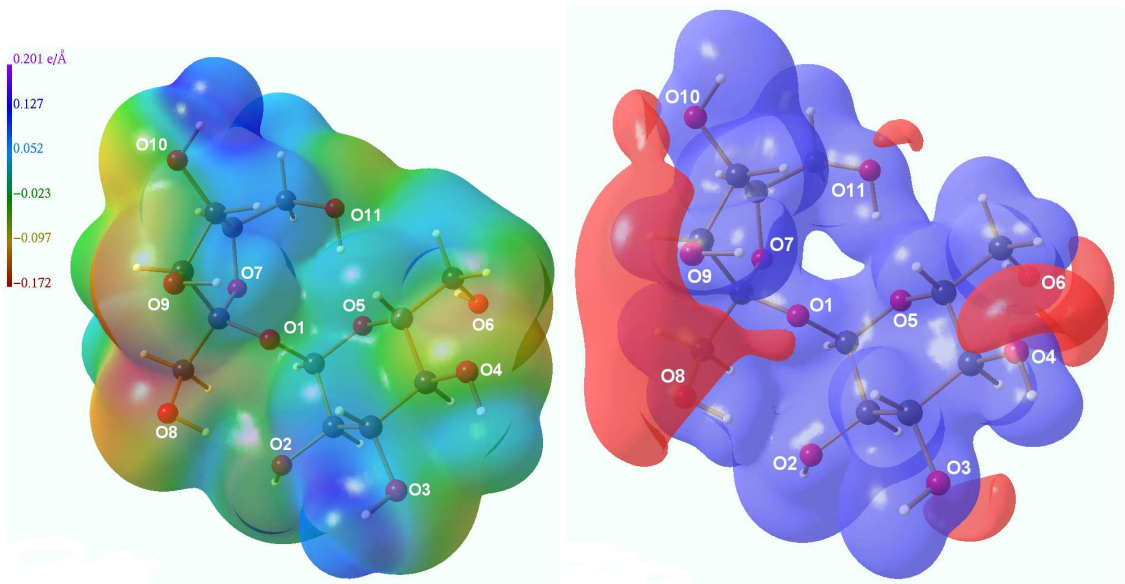

(a) ESP ($e\text{Å}^{-1}$) mapped on an ED isosurface of 0.0067 $e\text{Å}^{-3}$

(b) Blue = isosurface of the ESP at 0.1 $e\text{Å}^{-1}$; red = isosurface of the ESP at -0.1 $e\text{Å}^{-1}$

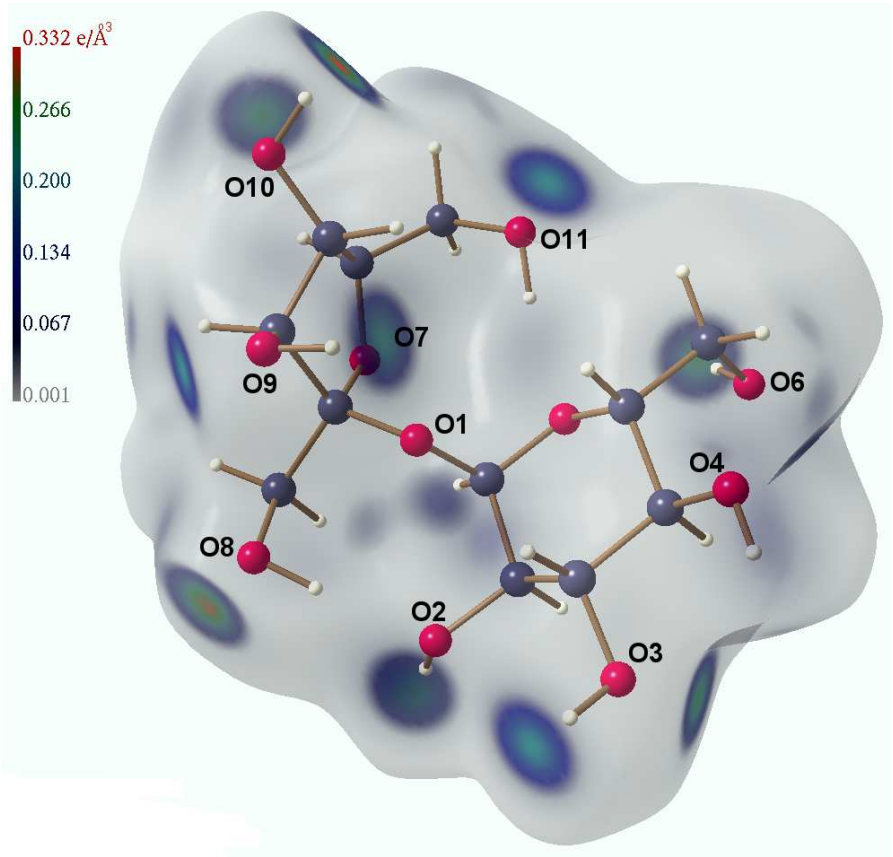

(c) Total ED ($e\text{Å}^{-3}$) mapped on a Hirshfeld surface

Figure 10.3: Representations of the electrostatic potential (ESP) and the Hirshfeld surface of sucrose (**6**)

towards O1. In turn, the pocket in the molecular shape incorporating the acceptor atom O1 (Figure 10.2 (b)) is strongly negatively polarised and thus fits to the donor group like a key to a keyhole.
In sucrose (**6**), regions of intermolecular contacts can be easily identified with their electrostatic contributions on the 0.001 a.u.-ED molecular surface (Figure 10.3 (a)) as well as with their covalent contributions on the Hirshfeld molecular surface (Figure 10.3 (c)). Electrostatic contributions to the hydrogen bonds are strong, as individual regions around oxygen atoms are negatively polarised up to -0.17 $e\text{Å}^{-1}$ and regions around hydrogen atoms are positively polarised up to 0.20 $e\text{Å}^{-1}$. It is noteworthy that the region around pentose (O8, O9, O10) is more negative than corresponding regions around hexose so that a continuous area of negative potential forms at the pentose site, see Figure 10.3 (b). This effect might guide the crystal packing and explain the exceptionally high value of electrostatic contributions to the lattice energy (see above). On the Hirshfeld surface, all O–H$\cdots$O hydrogen bonds can be individually identified with their strength and direction.

10.2 Results of the Topological Analysis of the ED

10.2.1 Deformation Density and Laplacian

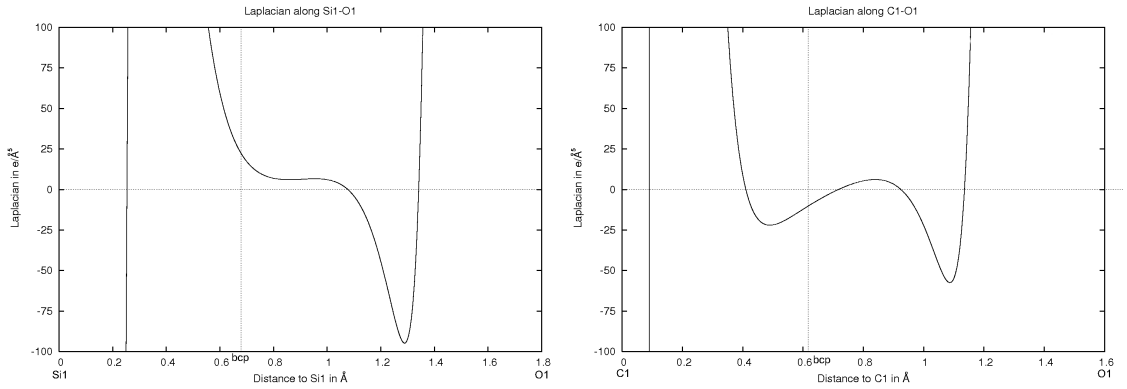

(a) Si1–O1 (b) C1–O1

Figure 10.4: One-dimensional plots of the Laplacian of the ED along Si1–O1 and C1–O1 bonds in butoxysilanol (**5**)
Positions of bcps and atomic cores are plotted

The one-dimensional plots of the Laplacian of the ED along the Si1–O1 and the C1–O1 bond paths of butoxysilanol (**5**) (Figure 10.4) show the characteristics of these two bond types. Si–O as a highly ionic bond shows a deep VSCC in the valence shell of the oxygen atom, a plateau in the bonding region that is completely located at positive Laplacian values and thus a highly positive Laplacian value at the bcp (compare discussion for Figure 7.4). C–O as a polar covalent bond shows a VSCC at the oxygen atom and a VSCC at the carbon atom which merge together and thus form a maximum in the bonding region. In contrast to a homopolar covalent bond (compare 7.4 (c)), the maximum is located at positive Laplacian values, but the value at the bcp is nevertheless unambiguously negative. The typically saddle-shaped form of a covalent bond is retained.
Figure 10.5 shows the static deformation-density and Laplacian-distribution maps of a plane in butoxysilanol (**5**) containig the linkage Si1–O1–C1 and the hydrogen bond O2A–H2OA$\cdots$O1. The differences between a Si–O and a C–O bond can be seen in these maps. There is a common maximum of the deformation density between C1 and O1 and there are two VSCCs along the bond in the Laplacian map.

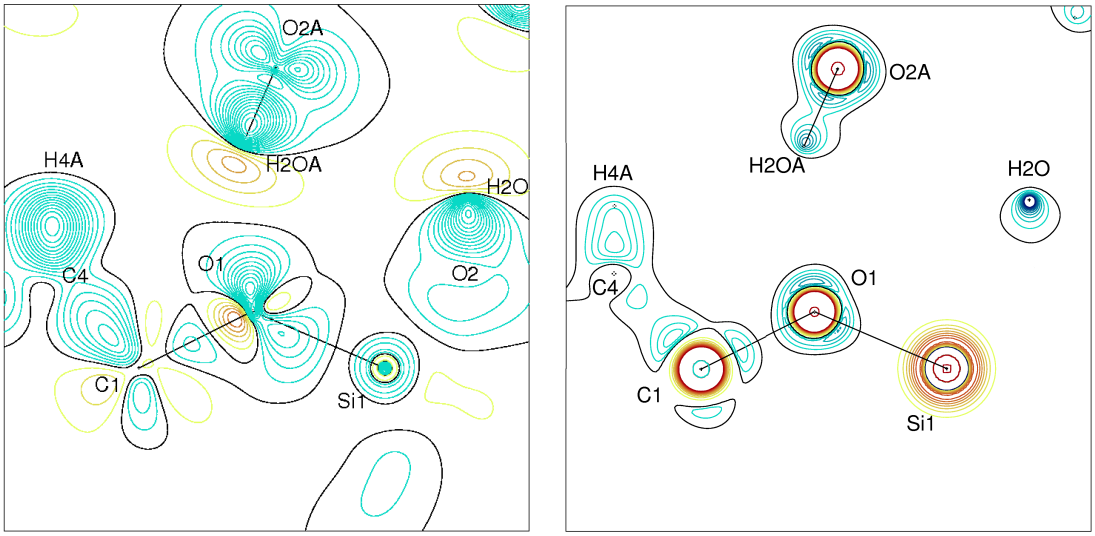

(a) Deformation density in the plane of the Si1–O1–C1 linkage, contour intervals: 0.07 for positive deformation density and 0.1 for negative deformation density

(b) Laplacian in the plane of the Si1-O1–C1 linkage, contour intervals: 25 for positive Laplacian, 25 for negative Laplacian around oxygen atoms, 8 for negative Laplacian around carbon atoms

Figure 10.5: Static deformation-density and Laplacian-distribution maps of butoxysilanol (**5**)
Deformation density in e Å^{-3}, blue = positive, red = negative, black = zero; Laplacian in e Å^{-5}, blue = negative, red = positive, black = zero

For Si1–O1, one VSCC of the oxygen atom is oriented towards the silicon atom, which remains isolated. The Si–O bond seems to be a bit strained because the maxima of deformation density and Laplacian are located below the internuclear axis. There is one lone-pair lobe of O1 in this plane which is oriented towards hydrogen atom H2OA to form the intra-asu hydrogen bond.
The difference between homonuclear covalent C–C bonds and polar C–O bonds is visualised in figure 10.6 for sucrose (**6**). The two bonded C atoms as well as the bonded C and O atom share a common maximum in the deformation density, but in contrast to the C–C bond, the maximum is isolated for the C–O bond and separated from the O atom by a region of negative deformation density. In the Laplacian map, C–C and C–O bonds show the typically saddle-shaped bonding region, but in contrast to C–C, there is a zero crossing in the middle of the C–O bond. In the plane of the C1–O5–C5 linkage, there is one lobe of the lone pairs of the oxygen atom like in the plane Si1–O1–C1 in Figure 10.5. For sucrose (**6**), the

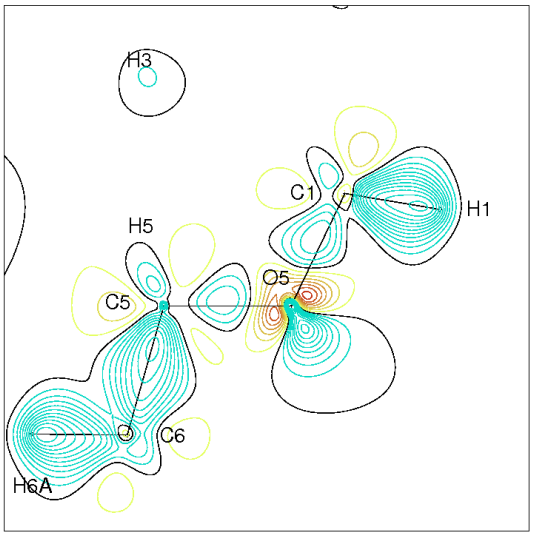

(a) Deformation density in the plane of the C1– O5–C5 linkage, contour intervals: 0.07 for positive deformation density and 0.1 for negative deformation density

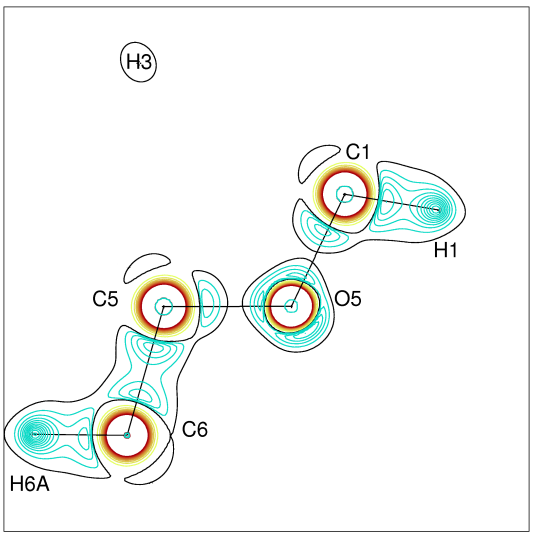

(b) Laplacian in the plane of the C1–O5–C5 linkage, contour intervals: 25 for positive Laplacian, 25 for negative Laplacian around oxygen atoms, 8 for negative Laplacian around carbon atoms

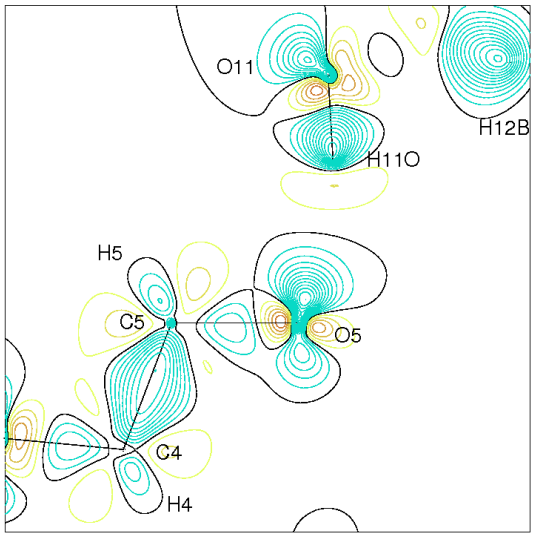

(c) Deformation density in the plane of C5– O5···H11O, contour intervals: 0.07 for positive deformation density and 0.1 for negative deformation density

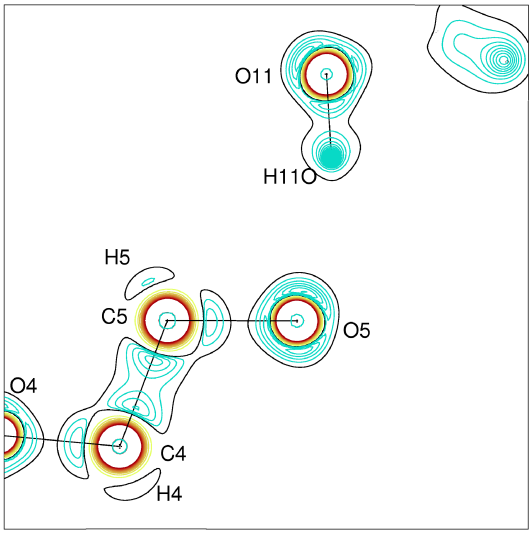

(d) Laplacian in the plane of C5–O5···H11O, contour intervals: 25 for positive Laplacian, 25 for negative Laplacian around oxygen atoms, 8 for negative Laplacian around carbon atoms

Figure 10.6: Static deformation-density and Laplacian-distribution maps of sucrose (**6**)

Deformation density in e Å^{-3}, blue = positive, red = negative, black = zero; Laplacian in e Å^{-5}, blue = negative, red = positive, black = zero

hydrogen bond is not in the same plane. Figures 10.6 (c) and (d) show the plane of the hydrogen bond O11–H11O$\cdots$O5 and how the lone pairs of the oxygen atom are directed towards the hydrogen atom. In this plane, another lobe of the lone pairs is additionally visible.

The three-dimensional deformation-density and Laplacian distributions of butoxysilanol (**5**) and sucrose (**6**) are represented in Figure 10.7. The expected cap-like shapes of the deformation density and the VSCCs around the acceptor-oxygen atoms can be determined. All four pictures show how the donor hydrogen atom of the O2A–H2OA$\cdots$O1 hydrogen bond in butoxysilanol (**5**) and of the O11–H11O$\cdots$O5 hydrogen bond in sucrose (**6**) points towards the centre of the cap of the acceptor oxygen lone pairs.

The deformation density of butoxysilanol ((**5**) Figure 10.7 (a)) around O1 looks symmetric, whereas the asymmetry that was found in ELI-D localisation domains and VSCCs of methoxysilane (Figure 9.10) is again found in Figure 10.7 (b). In the PES scans, the centre of the cap was located in projection of the Si–C bond axis which dictates the geometry of a hydrogen bond optimised for the isolated case. In the crystal structure, the hydrogen bond cannot follow the same geometry due to steric reasons, so that the axis O2A–H2OA is not located in the projection of Si1–O1. This leads to a deformation of the VSCCs of the acceptor oxygen atom compared to the PES scans that bends the cap backwards to allow the hydrogen atom to point towards the centre of the cap again. This finding confirms the conclusion that hydrogen bonding is only possible if the precondition of pronounced electron concentration and localisation in hydrogen-bonding direction is fulfilled. Only if the electrons are able to reorganise in a way to fulfill the given geometrical requirements can a hydrogen bond form.

The one-dimensional Laplacian graphs and the contour plots have shown that along a Si–O bond, there must be one VSCC visible in the Laplacian near the oxygen atom but none near the silicon atom. This is demonstrated in the three-dimensional Laplacian isosurface representations of Figures 10.7 (b) and 9.10 for methoxysilane as well as in Figures 7.7 and 6.9 (d). But it was also shown that the VSCCs along the Si–O bond are no longer visible if the isovalue is increased, compare Figure 6.9 (c) with 6.9 (d).

It is difficult to see the cap-like arrangement of the oxygen lone pairs together with the VSCCs near the C and O atoms along C–C and C–O bonds in the same isosurface representation because they appear at completely different isovalues.

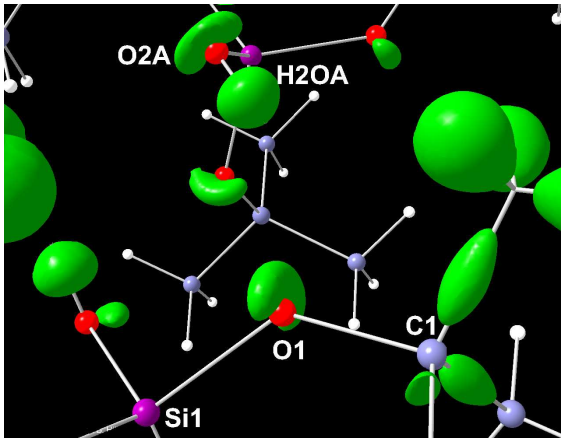

(a) Deformation density of butoxysilanol (**5**), Si1–O1–C1 linkage and O2A–H2OA···O1 hydrogen bond, isovalue = 0.30

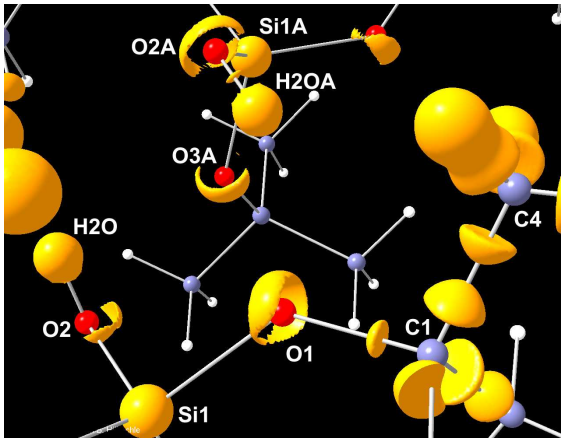

(b) Laplacian of butoxysilanol (**5**), Si1–O1–C1 linkage and O2A–H2OA···O1 hydrogen bond, isovalue = -95.0 around oxygen atoms and -15.0 around carbon atoms

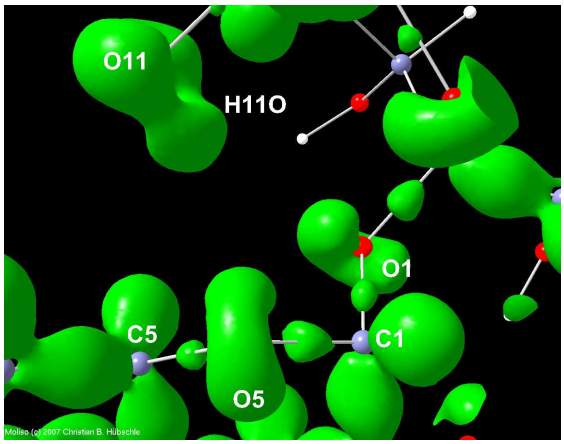

(c) Deformation density of sucrose (**6**), C1–O5–C5 linkage and O11–H11O···O5 hydrogen bond, isovalue = 0.15

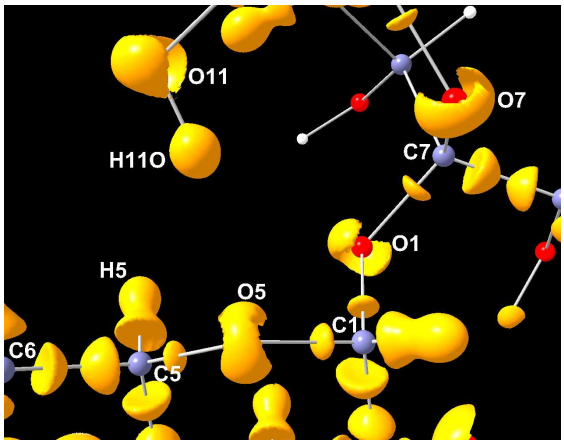

(d) Laplacian of sucrose (**6**), C1–O5–C5 linkage and O11–H11O···O5 hydrogen bond, isovalue = -85.0 around oxygen atoms and -15.0 around carbon atoms

Figure 10.7: Three-dimensional isosurface representations of the static deformation density and the Laplacian of butoxysilanol (**5**) and sucrose (**6**)
Deformation density in eÅ^{-3}, Laplacian in eÅ^{-5}

Therefore, a representation with two different isovalues around different atom types was chosen in Figures 10.7 (b) and (d) (compare different contour intervals in Figures 10.5 and 10.6). Consequently, the saddle-shaped bonding regions of C–C bonds can be seen for C1–C4 (Figure 10.7 (b)) and C5–C6 (Figure 10.7 (d)). In addition, VSCCs at the carbon atoms for the Si–O bonds (C1–O1 in butoxysilanol (**5**), C1–O5 and C5–O5 in sucrose (**6**)) are visible. Corresponding VSCCs at the oxygen atoms are still invisible due to the higher negative isovalue around oxygen.

10.2.2 Bond-Path Analyses and Gradient-Vector Fields

The gradient-vector field in the plane of the Si1–O1–C1 linkage and O2A–H2OA$\cdots$O1 hydrogen bond in butoxysilanol (**5**) is shown in Figure 10.8 (a). Silicon and carbon atoms enclose the oxygen atom at the lower side, but towards hydogen atom H2OA, there is a lot of free space for the oxygen atom to form a common zero-flux surface with the hydrogen atom. This situation was found for siloxane cpds. **1** and **2** at small Si–O–Si angles, but not for cpds. **3** and **4** at large Si–O–Si atoms. In this respect, silicon resembles carbon as Figure 10.8 (b) for the ether linkage in sucrose (**6**) depicts, where O5 also has lots of space on the upper side. In another plane (Figure 10.8 (c)), this space is used to form the hydrogen bond O11–H11O$\cdots$O5.

The hydrogen atoms involved in the hydrogen bonds (H2OA and H11O) are compressed by the two oxygen atoms, their volumes decrease compared to other hydrogen atoms. The hydrogen atom H2O of the silanol group Si1–O2–H2O, which is not involved in hydrogen bonding although it is a classical hydrogen-bond donor, is also represented in the given plane of butoxysilanol (**5**) in Figure 10.8 (a). The oxygen atom O2A is the only possible acceptor atom in the vicinity of H2O. These two atoms indeed share a common zero-flux surface. But this is only a necessary and not a sufficient condition for the existence of a hydrogen bond. There is neither a bond path nor a bcp, so that these two atoms do not interact with each other although they share a common zero-flux surface.

The bond paths in Figure 10.8 suggest that there is no strain in the systems unlike the deformation-density and Laplacian maps do (see above). A detailed bond-path analysis shows that the differences between bond path and bond distance are smaller than 0.005 Å for all analysed cases. These differences are very small but larger than 0.001 Å, which was found to be the border between strained and non-strained Si–O bonds in the PES scans of disiloxane, see chapter 6.2.1. Therefore,

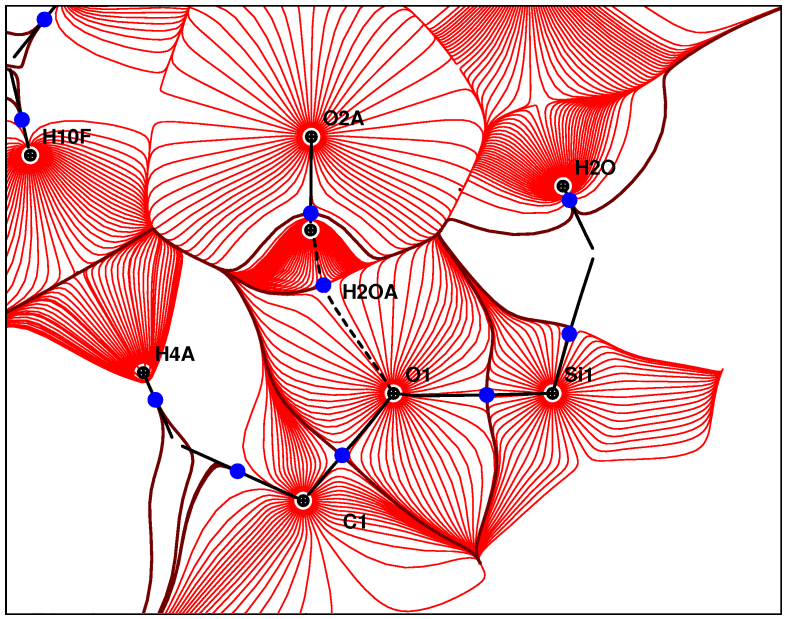

(a) Plane of Si1–O1–C1 linkage and O2A–H2OA···O1 hydrogen bond in butoxysilanol (**5**), oxygen O2 connecting Si1 and H2O is not in the chosen plane

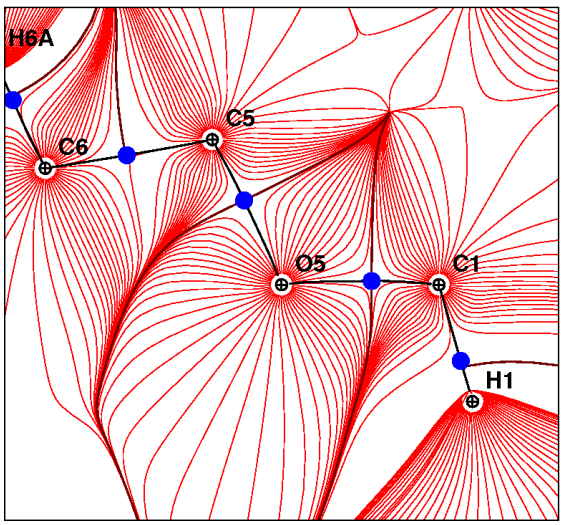

(b) Plane of C1–O5–C5 linkage in sucrose (**6**)

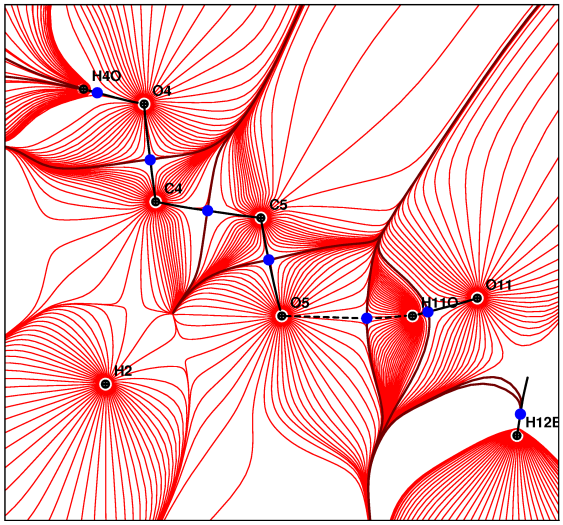

(c) Plane of O11–H11O···O5 hydrogen bond in sucrose (**6**)

Figure 10.8: Gradient-vector fields and molecular graphs in molecular planes of butoxysilanol (**5**) and sucrose (**6**)

a more detailed discussion on the differences of Si–O and C–O bonds follows.
The differences in the case of C–O bonds of the Si–O–C linkage are 0.0001 to 0.0002 Å, which means that the bonds are straight and not bent. Si–O bond paths in the Si–O–C linkage are 0.001 to 0.003 Å longer than the internuclear vector. These small differences were also found for the Si–O bonds in the siloxane linkage Si–O–Si and will be found for C–O bonds in epoxides (compare Table 12.5). In sucrose (**6**), the same differences of 0.001 to 0.003 Å were found for the C–O bonds. The ether linkages incorporated in the ring systems therefore seem to be slightly bent, whereas the C–O bonds in butoxysilanol (**5**) are straight.

10.2.3 Bond-Topological Properties

The differences in the Laplacian distribution between Si–O and C–O bonds as found qualitatively in the one-dimensional plots along the bond path (see Figure 10.4) are given quantitatively in Table 10.4. The Laplacian at the bcps of Si–O bonds varies between $\nabla^2\varrho$=21.7 and 25.6 eÅ^{-5}, indicating highly ionic character, whereas the Laplacian at the bcps of C–O bonds ranges from $\nabla^2\varrho$=-9.0 to -13.6 eÅ^{-5}, indicating predominantly covalent character. The value of the ED at the bcps is twice as high for C–O bonds (ϱ=1.64 to 1.89 eÅ^{-3}) compared to Si–O bonds (ϱ=0.85 to 0.92 eÅ^{-3}).
From the PES scans of methoxysilane, ϱ(Si–O)=0.92 eÅ^{-3} and $\nabla^2\varrho$(Si–O)= 20.8 eÅ^{-5} were predicted for α=130 °. The Si–O bonds in butoxysilanol (**5**) are slightly weaker and more ionic. For the C–O bonds in methoxysilane at α=130 °, ϱ(C–O)=1.72 eÅ^{-3} and $\nabla^2\varrho$(C–O)=-11.1 eÅ^{-5} were found, but for dimethylether at τ=115 °, ϱ(C–O)=1.81 eÅ^{-3} and $\nabla^2\varrho$(C–O)=-13.9 eÅ^{-5}. This means that the C–O bonds in butoxysilanol (**5**) and sucrose (**6**) are slightly weaker and less covalent compared to the model compounds at corresponding C–O–C angles. However, the PES scans predict a difference of 0.11 eÅ^{-3} and 2.8 eÅ^{-5}, i.e. the C–O bonds in the ether linkage are stronger and more covalent than the ones in the silyl ether linkage. In fact, the mean value of the ED at the C–O bond bcps in sucrose (**6**) is by 0.12 eÅ^{-3} higher than the one in butoxysilanol (**5**), the difference of the mean values of the Laplacian is 1.7 eÅ^{-5}. At least the ED difference is larger than a corresponding reproducibility margin as found in Ref. [247]. Therefore, it can be concluded according to the PES scans (see Chapter 9.2.1) that the C–O bond in the ether linkage is stronger than in the silyl ether linkage.
All Si–O bonds except Si1–O2/Si1A–O2A in the silanol groups are in the same

Table 10.4: Bond-topological properties of butoxysilanol (**5**) and sucrose (**6**) in X–O–X linkages

ED ϱ(bcp) in e$Å^{-3}$, Laplacian $\nabla^2\varrho$(bcp) in e$Å^{-5}$, distances of the bcp to the first (d1) and second (d2) atom of the bond in Å, ellipticity ε without unit, complete lists are given in Tables A.76 and A.77

bond	ϱ	$\nabla^2\varrho$	d1	d2	ε
butoxysilanol (**5**):					
Si1–O1	0.85	22.5	0.678	0.961	0.03
Si1–O2	0.90	25.6	0.669	0.946	0.08
Si1–O3	0.91	23.7	0.674	0.942	0.02
Si1–O4	0.88	24.4	0.672	0.946	0.04
C1–O1	1.65	-10.3	0.617	0.830	0.01
C5–O3	1.66	-10.8	0.604	0.836	0.01
C9–O4	1.65	-10.6	0.606	0.837	0.00
Si1A–O1A	0.87	24.5	0.672	0.948	0.02
Si1A–O2A	0.92	24.8	0.670	0.949	0.03
Si1A–O3A	0.85	21.7	0.680	0.963	0.02
Si1A–O4A	0.91	24.7	0.671	0.941	0.02
C1A–O1A	1.66	-10.9	0.604	0.837	0.01
C5A–O3A	1.64	-10.2	0.613	0.835	0.00
C9A–O4A	1.65	-10.4	0.607	0.835	0.01
C–C	1.71(1)	-12.3(2)	0.775(1)	0.749(1)	0.06(1)
sucrose (**6**):					
C1–O1	1.78	-12.1	0.817	0.613	0.03
C7–O1	1.75	-11.3	0.820	0.620	0.04
C1–O5	1.84	-13.4	0.812	0.609	0.03
C5–O5	1.68	-10.4	0.832	0.617	0.04
C7–O7	1.89	-13.6	0.803	0.611	0.03
C10–O7	1.65	-9.0	0.830	0.626	0.05

chemical environment and thus the spread of values is small. The values for the silanol group also do not deviate from the other Si–O bonds, a behaviour which was also found in siloxanol (**1**) when comparing the silanol group with the siloxane linkage. The same holds true for all C–O bonds in butoxysilanol (**5**): The spread is small because the chemical environment is identical, i.e. transferability is given. In contrast, three different types of C–O bonds can be identified within sucrose (**6**). The values (ED and negative Laplacian at the bcps) for C1–O5 and C7–O7 are highest. Both carbon atoms are bonded to another oxygen atom and they are incorporated into the ring systems. The values for the bonds in the linkage C1–O1–C7 are on average lower by 0.1 eÅ^{-3} and 2 eÅ^{-5}. The carbon atoms are also bonded to another oxygen atom, but the linkage is more flexible as it is not incorporated into a ring. The values for C5–O5 and C10–O7 are again lower by 0.1 eÅ^{-3} and 2 eÅ^{-5}. C5 and C10 are not bonded to an oxygen atom but to two carbon atoms and one hydrogen atom. These differences are indicative of the chemical environments of the C–O bonds, see discussion on transferability and reproducibility margins in Ref. [247].

The averaged values of the ED, the negative Laplacian and the ellipticity at the C–C bcps are only marginally higher than the values for the C–O bonds in butoxysilanol (**5**), showing that both are strong covalent bonds. The polar nature of the C–O bonds, which was discussed by means of the shape of the Laplacian and the deformation density, see Figures 10.4 and 10.6, is only reflected here in terms of the distances of the bcp to the atoms (d1 and d2). The bcp shifts towards the carbon atoms in C–O but is in the middle of the C–C bond. Relative to the bond length, the bcp is nearer to the silicon atoms in Si–O bonds (40-41 %) than to the carbon atoms in C–O bonds (43-44 %) according to the electronegativity difference between silicon and carbon. (Compare discussion on Si–C versus Si–O bonds in Chapter 7.2.3).

10.2.4 Atomic Properties

It was demonstrated for the bond-topological properties that differences in the chemical environments of the bonds can be detected. The same holds true for atomic properties (Table 10.5) so that averaged values (atomic charge Q and atomic volumes V_{001}/V_{tot}) for chemically equal atoms defined by their environments are used in the following discussion.

In butoxysilanol (**5**), the silicon atoms are charged by Q=3.09 e with a volume

Table 10.5: Atomic properties of butoxysilanol (**5**) and sucrose (**6**)
Charge Q_{001} cut at ϱ=0.001 a.u. is equal to charge of total basin Q_{tot}, Q in e, volumes V_{001} and V_{tot} in Å^3, complete lists are given in Tables A.78 and A.79

atom	Q	V_{001}	V_{tot}	atom	Q	V_{001}	V_{tot}
butoxysilanol (**5**):							
Si1	3.07	3.5	3.5	Si1A	3.11	3.2	3.2
O1	-1.36	13.6	14.9	O1A	-1.40	15.1	16.1
O2	-1.62	17.7	18.5	O2A	-1.67	18.2	19.5
O3	-1.38	14.6	15.5	O3A	-1.34	13.5	14.5
O4	-1.42	14.9	15.8	O4A	-1.39	14.4	15.6
C1	0.38	5.6	5.6	C1A	0.41	5.3	5.3
C5	0.39	5.6	5.6	C5A	0.38	5.7	6.1
C9	0.39	5.6	5.6	C9A	0.39	5.6	5.6
H2O	0.73	2.5	2.6	H2OA	0.81	0.7	0.7
sucrose (**6**):							
O1	-0.87	12.0	12.0	C5	0.33	6.7	6.7
O5	-0.89	11.9	12.0	C7	0.71	4.8	4.8
O7	-0.88	12.1	12.6	C10	0.33	6.6	6.7
O11	-0.99	15.3	16.1	H11O	0.58	1.9	1.9
C1	0.71	5.6	5.6				

of V=3.4/3.4 Å^3. From the PES scan of methoxysilane at α=130 °, Q=2.88 e and V_{001}=5.8 Å^3 were predicted. In cpds. **1** to **4**, charges were smaller and volumes larger, too, see Table 7.6. The oxygen atoms in the silyl ether linkages possess the values Q=-1.38 e and V=14.4/15.4 Å^3. In the siloxane linkages (Table 7.6), the oxygen atoms are more negative and their volumes larger. Thus, the charge separation within the Si–O bonds is about the same. The oxygen atoms O2/O2A in the silanol group are on average 0.27 e and 3.6/3.6 Å^3 more negative and larger than the ones in the silyl ether linkages. The hydrogen atom H2OA, which is involved in a hydrogen bond, is more positive and significantly smaller than H2O, which is not involved in a hydrogen bond. All carbon atoms in the Si–O–C linkage are chemically equal with the values Q=0.39 e and V_{001}=5.6/5.6 Å^3.

In sucrose (**6**), there are two types of carbon atoms in the C–O–C linkages. C5 and C10, which are bonded only to carbon and hydrogen beneath the oxygen atom of

the ether linkage, exhibit Q=0.33 e and V_{001}=6.7/6.7 Å^3. These values are similar to the values of the carbon atoms in butoxysilanol (**5**), which are themselves only bonded to other carbon atoms beneath the O atom of the silyl ether linkage. C1 and C7 are bonded to another oxygen atom and thus their charges are larger by 0.38 e and their volumes smaller. The oxygen atoms in the C–O–C linkages are equal and show the values Q=-0.88 e and V_{001}=12.0/12.2 Å^3. So there are C–O bonds with a charge separation of 1.21 e (C5–O5 and C10–O7) and other ones with a charge separation of 1.59 e (C1–O1, C7–O1, C1–O5, C7–O7). The latter ones have significantly higher values of the electron density and the negative Laplacian at the bcps than the first ones, see above. The charge separation within the C–O bonds of butoxysilanol (**5**) is higher (1.77 e). This is in line with the findings of the PES scans in Chapter 9.2.2. Therein, the charge separation of the C–O bond was higher for methoxysilane than for dimethylether.

Finally, the silanol group in butoxysilanol (**5**) (O2, H2O or O2A, H2OA, respectively) shall be compared with a hydroxy group in sucrose (**6**) (O11, H11O). H11O is involved in a hydrogen bond like H2OA, but it is even less charged than H2O, which is not involved in a hydrogen bond. However, H2O and H2OA are both bonded to oxygen atoms that are clearly more negatively charged (-1.62 and -1.67 e) than O11 (-0.99 e). This in turn is due to the electronegativity differences of silicon (silanol group) compared to carbon (hydroxy group). These values reflect the fact that a hydrogen atom in a silanol group is generally more protic than a hydrogen atom in a hydroxy group and thus a better hydrogen-bond donor. This is another reason for the fact that the silanol$\cdots$siloxane/silyl ether hydrogen bonds discussed in Chapter 10.1.2 are comparable in their strengths to hydroxy$\cdots$ether hydrogen bonds.

10.2.5 Source Function

The local source function along a bond path was shown in Chapter 7.2.5 to be indicative of the bond character of this bond. There, the Si–O bond was already discussed. Here, it is compared to the C–O bond in butoxysilanol (**5**), Figure 10.9. The ionicity of the Si–O bond is mainly implied by three facts. Firstly, there is a minimum around the bcp, which means that the region around the bcp acts as a deep sink for the ED at the bcp. Secondly, the bond region is asymmetric, which means that the values to the left and to the right of the minimum around the bcp are clearly different. Thirdly, these values left and right of the minimum, i.e.

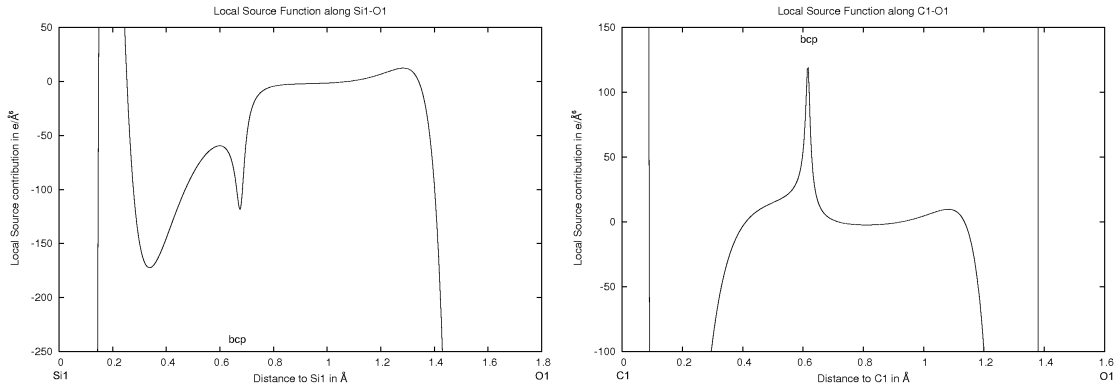

(a) Si1–O1 (b) C1–O1

Figure 10.9: Local source function along Si–O and C–O bonds in butoxysilanol (**5**)

the whole bond region, are clearly negative (-75 e$Å^{-6}$ to -10 e$Å^{-6}$). For a covalent bond, the opposite of these three points is true: There is a maximum of the local source around the bcp in C–O and the values to the left and to the right of the maximum are about the same and close to zero or positive (-5 to 10e $Å^{-6}$).

The integrated source-function contributions of atoms or functional groups, respectively, in butoxysilanol (**5**) and sucrose (**6**) to selected Si–O, C–O and hydrogen bonds are listed in Tables 10.6 and 10.7, complete lists are given in tables A.80 to A.82. It was stated in Chapter 7.2.5 that the integrated source function is not indicative of bond character or bond strength, but of the bond's environment. This can be exemplified by a comparison of the Si–O bonds in butoxysilanol (**5**) and siloxane cpds. **1** to **4**. The Si1–O1 bond in the latter ones was made up by 67.9 to 79.6 % (periodic-boundary calculations) by the directly bonded atoms Si and O and by only 21.0 to 27.3 % by the rest of the molecules. In butoxysilanol (**5**), source contributions of directly bonded Si and O atoms are smaller (57.8 % in Si1–O1 and 68.5 % in Si1–O3) and the influence of the environment is larger (33.4 and 30.8 %). The reason is that the carbon atom in Si–O–C is a source for the Si–O bond, whereas the silicon atom in Si–O–Si is a sink. *Tert*-butyl groups including the carbon atom of the Si–O–C linkage contribute 7-9 % as nearest neighbours and 3-4 % if they are bonded over another oxygen atom as next nearest neighbours. So they are better donors in terms of source contribution in the first as well as the second neighbouring sphere than phenyl or methyl groups, see Table 7.7 for siloxane compounds. Moreover, the Si–O bonds in butoxysilanol (**5**) are surrounded by

Table 10.6: Absolute (relative) source-function contributions to selected bonds in butoxysilanol (**5**)

Absolute source-function contributions in eÅ^{-3}, sum1 refers to the directly bonded atoms, sum2 refers to the rest of the molecule, tert-butyl(C1) refers to the sum of all atoms of the tert*-butyl group including atom C1, reference values are taken from Table 10.4*

group/atom	Si1–O1	group/atom	C1–O1	group/atom	Si1–O3
Si1	0.140(16.5)	C1	0.566(34.3)	Si1	0.190(20.9)
O1	0.351(41.3)	O1	0.770(46.7)	O3	0.433(47.6)
sum1	0.491(57.8)	sum1	1.336(81.0)	sum1	0.623(68.5)
O3	0.043(5.1)	O3	0.002(0.1)	O1	0.041(4.5)
O4	0.045(5.3)	O4	-0.001(-0.1)	O4	0.045(4.9)
		Si1	0.000(0.0)		
silanol	0.068(8.0)	silanol	0.012(0.7)	silanol	0.068(7.5)
tert-butyl(C1)	0.074(8.7)	rest tert-butyl	0.288(17.5)	tert-butyl(C1)	0.037(4.1)
tert-butyl(C5)	0.027(3.2)	tert-butyl(C5)	0.014(0.8)	tert-butyl(C5)	0.062(6.8)
tert-butyl(C9)	0.026(3.1)	tert-butyl(C9)	0.015(0.9)	tert-butyl(C9)	0.027(3.0)
sum2	0.283(33.4)	sum2	0.330(19.9)	sum2	0.280(30.8)
ref	0.85	ref	1.65	ref	0.91
group/atom	C5–O3	group/atom	H2OA$\cdots$O1		
C5	0.568(34.2)	O1	0.014(9.3)		
O3	0.762(45.9)	H2OA	-0.092(-61.3)		
sum1	1.330(80.1)	O2A	0.139(92.7)		
O1	0.003(0.2)	rest			
O4	0.006(0.4)	donor			
Si1	-0.001(-0.1)	molecule	0.052(34.7)		
silanol	0.010(0.6)				
tert-butyl(C1)	0.020(1.2)	rest			
rest tert-butyl	0.274(16.5)	acceptor			
tert-butyl(C9)	0.011(0.7)	molecule	0.090(60.0)		
sum2	0.323(19.5)				
ref	1.66	ref	0.15		

three adjacent oxygen atoms, which generally are strong donors within the source function. Here, they contribute about 5 % each to the Si–O bond, the silanol group as a whole even about 8 %.

For Si1–O1 in butoxysilanol (**5**), the directly bonded atoms and the rest of the molecule contribute 91.2 % altogether, but for Si1–O3, the contributions add up to 99.3 %. This means that a significant amount of electron density at the Si1–O1 bcp comes from the crystal environment, whereas nearly no crystal effect is detected for Si1–O3. This is consistent with the fact that oxygen O1 is the acceptor of the only classical hydrogen bond of medium strength in butoxysilanol (**5**), whereas oxygen O3 is not involved in any intermolecular contact. This again shows that the source contributions for Si–O bonds are highly sensitive to changes in the chemical environment.

The situation changes for C–O bonds. Within butoxysilanol (**5**), sucrose (**6**) and epoxide compounds **7** to **10** (see Chapter 12.2.5), the directly bonded C and O atoms always contribute about 80 % to the C–O bcp and the rest of the molecule about 20 %. Substituent and crystal effects are not detectable in the value of sum1 because a direct contribution of quite precisely 80 % seems to be characteristic of C–O bonds. It is not a characteristic of distinctively covalent or strong bonds because C–C bonds, for example, behave differently (compare discussion in Chapter 12.2.5). However, substituent effects can still be seen in the way how the 20 % that are left for all substituents are divided among them. For example, the influence of *tert*-butyl groups as next next nearest neighbours is still significantly positive, whereas it is zero or even slightly negative for phenyl groups (see Figure 7.10). Hexose and pentose in sucrose (**6**) behave quite similarly although the number of ring and of oxygen atoms is different.

The source contributions to the hydrogen bonds O2A–H2OA$\cdots$O1 in butoxysilanol (**5**) and O11–H11O$\cdots$O5 in sucrose (**6**) are also given in Tables 10.6 and 10.7. The latter one can be referred to as a polarized assisted hydrogen bond (PAHB) according to the criteria of Gatti, Gilli and Gilli. [58] It is therefore in the same class as the silanol$\cdots$siloxane hydrogen bond (see Figure 7.11 and associated explanations), which is in agreement with the findings discussed in Chapter 10.1.2. The hydrogen bond O2A–H2OA$\cdots$O1 in butoxysilanol (**5**) was already found to be weaker than the comparable ones in siloxanol (**1**) and sucrose (**6**), which is also reflected in the source function. The contributions of the donor hydrogen atom H2OA are significantly more negative than those of H11O in sucrose (**6**) or H2O in siloxanol (**1**), but the positive contributions of the donor oxygen atom O2A

Table 10.7: Absolute (relative) source-function contributions to selected bonds in sucrose (**6**)

Absolute source contributions in eÅ^{-3}, sum1 refers to the directly bonded atoms, sum2 refers to the rest of the molecule, reference values are taken from Table 10.4

group/atom	C1–O1	group/atom	C7–O1	group/atom	C1–O5	group/atom	C5–O5
C1	0.623(35.0)	C7	0.606(34.7)	C1	0.648(35.2)	C5	0.586(34.9)
O1	0.809(45.5)	O1	0.812(46.4)	O5	0.837(45.5)	O5	0.743(44.2)
sum1	1.432(80.5)	sum1	1.418(81.1)	sum1	1.485(80.7)	sum1	1.329(79.1)
C7	0.010(0.6)	C1	0.012(0.7)	C5	0.005(0.3)	C1	0.017(1.0)
				O1	0.074(4.0)	O1	0.006(0.4)
rest hexose	0.259(14.6)	rest pentose	0.274(15.7)	rest hexose	0.216(11.7)	rest hexose	0.285(17.0)
rest pentose	0.066(3.4)	rest hexose	0.064(3.7)	pentose	0.035(1.9)	pentose	0.021(1.3)
sum2	0.335(18.6)	sum2	0.350(20.1)	sum2	0.330(17.9)	sum2	0.329(19.7)
ref	1.78	ref	1.75	ref	1.84	ref	1.68
group/atom	C7–O7	group/atom	C10–O7	group/atom	O5$\cdots$H110		
C7	0.654(34.6)	C10	0.590(35.7)	O5	0.014(7.0)		
O7	0.864(45.7)	O7	0.729(44.2)	H11O	-0.057(-28.3)		
sum1	1.518(80.3)	sum1	1.319(79.9)	sum1	-0.043(-21.3)		
C10	0.016(0.8)	C7	0.014(0.9)	O11	0.105(52.4)		
O1	0.072(3.8)	O1	0.013(0.8)	O1	0.001(0.7)		
rest pentose	0.221(11.7)	rest pentose	0.270(16.3)	rest hexose	0.080(40.0)		
hexose	0.034(1.8)	hexose	0.017(1.0)	rest pentose	0.042(20.8)		
sum2	0.343(18.1)	sum2	0.314(19.0)	sum2	0.228(113.9)		
ref	1.89	ref	1.65	ref	0.20		

are less than twice as high as the absolute value of H2OA. This kind of hydrogen bonds is referred to as isolated hydrogen bonds (IHB) within Ref. [58].
The pentose fragment is the donor of the hydrogen bond O11–H11O$\cdots$O5, the hexose fragment the acceptor. Hexose contributes 40 % to the ED of the H11O$\cdots$O5 bcp, but pentose only 20 %. A similar finding can be made regarding O2A–H2OA$\cdots$O1 in butoxysilanol (**5**): The acceptor molecule contributes about twice as much as the donor molecule (60 and 35 %).

10.3 Results of the Topological Analysis of the ELI-D

The ELI-D of butoxysilanol (**5**) and sucrose (**6**) was calculated for the optimised geometries of the isolated molecule. Resulting localisation-domain representations are given in Figure 10.10. The phenomenological behaviour of oxygen lone pairs, Si–O and C–O bonds is the same as the PES scans of free methoxysilane and free dimethylether have shown. In butoxysilanol (**5**), the cap-like localisation domain of the lone pairs is opened at the side which points towards the Si–O bond domain. The asymmetry of the cap seems to be slightly reduced compared to free methoxysilane. The localisation domains of the C–O bonds are quite spherical, but the ones of the Si–O bonds are more elongated. As the PES scans have also shown, the volumes and the electron populations of the C–O bond basins are significantly smaller than corresponding values of the Si–O bond basins as listed in Table 10.8. The shapes of lone-pair localisation domains and C–O bonds in sucrose (**6**) are as expected, too.

It was described in Chapter 7.3 that it seems to be an inherent property of the siloxane linkage in cpds. **1** to **3** that the two attractors of the oxygen lone pairs merge. This finding is also true for the silyl ether linkage in butoxysilanol (**5**): There is only one lone-pair attractor with a corresponding basin for the lone-pair electrons of atoms O1, O2 and O3. But for O2 in the silanol group, there are two lone pairs as found for any other silanol group examined in this doctoral thesis, compare for example oxygen atom O2 in siloxanol (**1**) in Chapter 7.3.1. Moreover, oxygen atoms O1, O5 and O7 in the ether linkage also comprise two lone pairs. Perhaps it might be necessary for systems that are rather weak hydrogen-bond acceptors like siloxane and silyl ether linkages to localise the accepting electrons to a

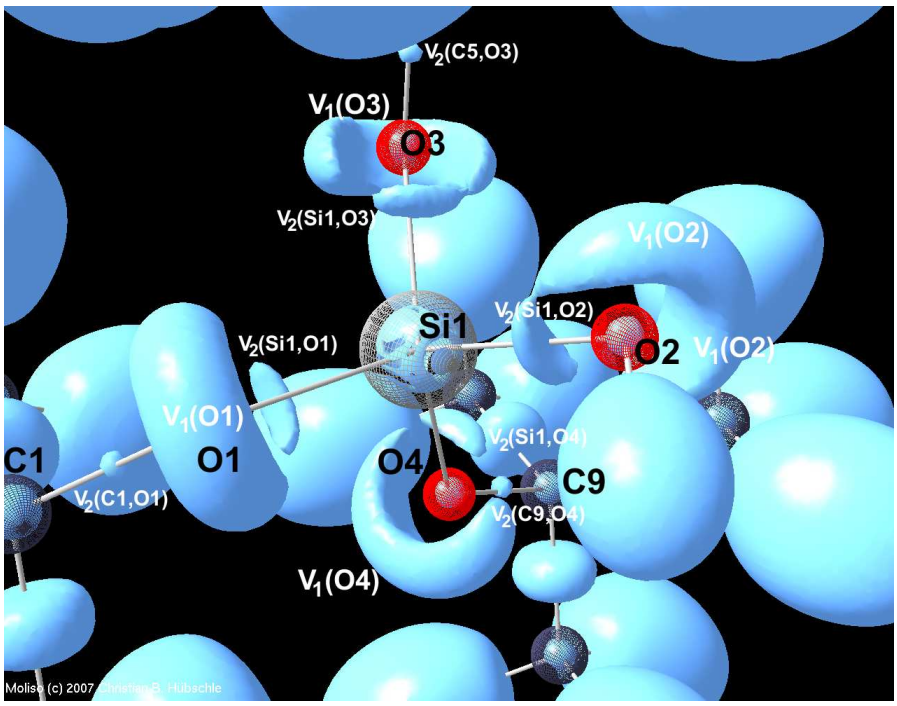

(a) Butoxysilanol (**5**), isovalue = 1.54

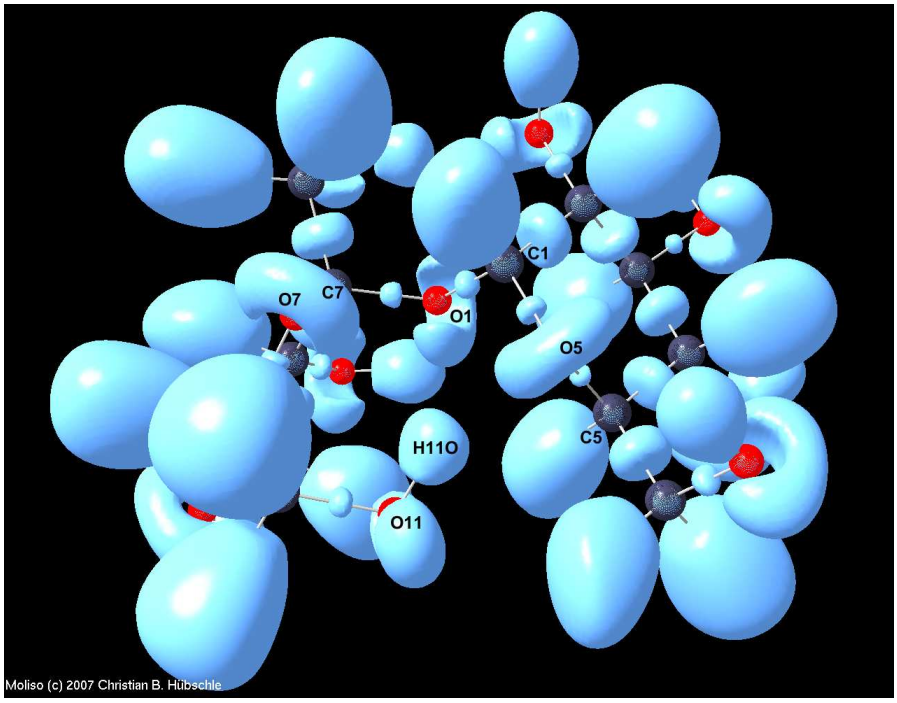

(b) Sucrose (**6**), isovalue = 1.50

Figure 10.10: ELI-D localisation-domain representations of butoxysilanol (**5**) and sucrose (**6**)

Isolated-molecule calculations at optimised geometries

Table 10.8: Attractor values, electron populations and volumes of ELI-D valence basins of the Si–O–C and C–O–C linkages in butoxysilanol (**5**) and sucrose (**6**)
Isolated-molecule calculations at optimised geometries, ELI value at the attractor of the ELI-D basin (ELI_{att}) without unit, electron population of the ELI-D basin (N_{001}) in e, volume of the ELI-D basin (V_{001}) in $Å^3$, ELI-D values at the attractors are averaged over both lone pairs $V_1(O)$ if two basins exist, populations and volumes are summed up in this case

basin	ELI_{att}	N_{001}	V_{001}	basin	ELI_{att}	N_{001}	V_{001}
butoxysilanol (**5**):				sucrose (**6**):			
V_2(Si1,O1)	1.563	1.77	2.74	V_2(C1,O1)	1.588	1.35	1.13
V_2(Si1,O2)	1.574	1.74	2.55	V_2(C7,O1)	1.576	1.31	1.12
V_2(Si1,O3)	1.563	1.78	2.70	V_2(C1,O5)	1.600	1.37	1.16
V_2(Si1,O4)	1.564	1.75	2.65	V_2(C5,O5)	1.587	1.28	1.07
V_2(C1,O1)	1.567	1.22	0.99	V_2(C7,O7)	1.591	1.36	1.11
V_2(C5,O3)	1.565	1.21	0.99	V_2(C10,O7)	1.582	1.25	1.00
V_2(C9,O4)	1.566	1.22	0.99	sum/av V_1(O1)	1.718	4.95	10.79
V_1(O1)	1.655	4.69	13.00	sum/av V_1(O5)	1.737	4.90	11.43
sum/av V_1(O2)	1.660	4.43	14.08	sum/av V_1(O7)	1.729	4.94	12.29
V_1(O3)	1.658	4.69	12.75				
V_1(O4)	1.656	4.72	12.64				

maximum degree, which is reflected in the merger of the attractors in order to be able to form hydrogen bonds of a considerable strength. Systems that are strong hydrogen-bond acceptors like ether or silanol groups still exhibit two lone pairs. So this behaviour might be related to the inherent basicity of the oxygen atom. This interpretation is consistent with the fact that the hydrogen atom H11O of the intramolecular hydrogen bond O11–H11O$\cdots$O5 in sucrose (**6**) (Figure 10.10 (b)) does no longer point to the centre of the reducible localisation domain of oxygen atom O5 like in the experimental geometry (Figures 10.7 (c) and (d)) but to the side of it, clearly favouring one of the lone pairs. Nonetheless, a significant flattening of the localisation domain of H11O indicates that the interaction is still of considerable strength.

The ELI-D values of the bond and lone-pair attractors (Table 10.8) are in a range as found for the siloxane linkage at comparable X–O–X angles (between 1.5 and 1.8, see Figure 6.20). The averaged values for the two oxygen lone-pair attractors

at the ether oxygen atoms are still by 0.1 larger than the values of the merged attractors in the silyl ether linkages.
The electron populations and volumes of the Si–O or C–O bonds that are in the same chemical environment are very close to each other as already found for bond-topological and atomic properties above. This means that the concept of transferability in the framework of the ED analysis can be transferred to the ELI-D analysis. Consequently, atoms in different chemical environments can be distinguished from one another. For example, the population of both lone pairs in the silanol group is lower than for oxygen atoms in the silyl ether linkages, but the volume of the lone pairs is larger. In sucrose (**6**), the three pairs of C–O bonds as distinguished by their ED and Laplacian values at the bcp can also be found here. C1–O5 and C7–O7, which have the highest value of the ED at the bcp, are also populated with the highest absolute number of electrons. C1–O1 and C7–O1 follow with medium values. C5–O5 and C10–O7 with the lowest ED values also have the lowest populations of their ELI-D basins. This means that the fact that C5–O5 and C10–O7 are not neighboured by another oxygen atom in contrast to the other linkages lowers the ED values at the bcps as well as the absolute electron population.

Part IV

The Strained C–O–C Linkage in Epoxides

Chapter 11

Experimental and Computational Details

11.1 Experimental Details

11.1.1 Synthesis, Crystallisation and Measurement

Oxacyclopropane (etox (**7**), see Figure 3), which is a colourless gas at room temperature (m.p.=161 K and b.p.=284 K), was purchased by Dr. Jürgen Buschmann and Prof. Dr. Peter Luger in the 1980s . They crystallised it in situ on a Stoe four-circle diffractometer by a method described in Ref. [248] and determined the crystal structure with Cu-K_α radiation and a scintillation counter at 150 K [102]. They repeated the experiment in 1986 on another Stoe four-circle diffractometer with Mo-K_α radiation and a scintillation counter at 100 K to get a high-resolution data set, which was not further examined at that time. This data set was used in this doctoral thesis. 4382 reflections were collected to a maximum resolution of 1.0 $Å^{-1}$ with an overall completeness of 100 % within the monoclinic space group $P2_1/n$. The data were integrated and reduced with the in-house programme REDUC. 1314 of 2081 unique reflections were observed within the criterium $F \geq 4\sigma(F)$. The structure was solved with the programme SHELXS [205]. There is one molecule in the asymmetric unit. Details are summarised in Table 11.1.

Compounds **8** to **10** (see Figure 3) were synthesised by Dipl.-Chem. Thomas Pfeuffer from the work group of Prof. Dr. Tanja Schirmeister, Julius-Maximilians-Universität Würzburg. For the preparation of (2S,3S)-Dimethyl-oxacyclopropane-2,3-dicarboxylate (moc-epoxide (**8**)), (R,R)-dimethyl-tartrate was put into a

Table 11.1: Crystallographic and refinements details of cpds. **7** to **10**

Spherical refinement, multipole refinement and constrained wave-function fitting (CWF)

	etox (**7**)	moc-epoxide (**8**)	niphe-epoxide (**9**)	cyano-epoxide (**10**)
chemical formula	C_2H_4O	$C_6H_8O_5$	$C_{12}H_{11}NO_7$	C_6N_4O
M ($g{\cdot}mol^{-1}$)	44.05	160.12	281.22	144.09
space group, Z	$P2_1/n$, 4	C2, 8	$P\bar{1}$, 2	$P2_1/c$, 4
a (Å)	4.633(5)	21.304(4)	7.7460(3)	9.586(2)
b (Å)	8.400(1)	4.046(1)	8.0800(2)	6.082(1)
c (Å)	6.577(3)	17.685(4)	11.8350(5)	11.994(2)
α (°)	90.00	90.00	86.198(1)	90.00
β (°)	100.37(6)	107.05(3)	74.105(1)	110.79(3)
γ (°)	90.00	90.00	60.673(1)	90.00
V ($Å^3$)	251.8(3)	1457.3(6)	619.07(4)	653.7(2)
ϱ_x ($g{\cdot}\ cm^{-3}$)	1.162	1.460	1.509	1.464
F(000)	96	672	292	288
μ (mm^{-1})	0.09	0.13	0.08	0.07
crystal size (mm^3)	$0.30x0.30x0.30$	$0.50x0.50x0.25$	$0.60x0.40x0.15$	$0.50x0.40x0.20$
beamline	in-house	in-house	F1	F1
T (K)	100	25	100	100
λ (Å)	0.71073	0.71073	0.5600(2)	0.5600(2)
min./ max. 2θ (°)	8.0/ 90.0	4.0/ 90.6	2.8/ 83.6	3.6/105.3
$\frac{sin\theta_{max}}{\lambda}$ ($Å^{-1}$)	1.00	1.00	1.19	1.42
no. of coll. refl.	4382	41152	126224	186756
no. of unique refl.	2081	6618	14724	15522
cond. for obs. refl.	$F \geq 4\sigma(F)$	$F^2 \geq 3\sigma(F^2)$	$F^2 \geq 3\sigma(F^2)$	$F^2 \geq 3\sigma(F^2)$
no. of obs. refl.	1314	4723	8523	9689
redundancy	2.1	6.2	8.6	19.3
completeness (%)	100.0	99.0	84.2	99.0
R_{int} (%)	2.86	5.31	7.62	5.31
spherical ref.:				
R(F) (%)	4.11	5.70	4.45	3.45
$wR(F^2)$ (%)	12.18	15.95	13.94	11.73
GooF	1.05	1.15	0.97	0.91
multipole ref.:				
refinement on	F	F^2	F^2	F^2
ratio refl./par.	16.22	23.85	16.55	53.24
R(F)/ $R(F^2)$ (%)	2.61/3.15	3.41/ 5.55	3.09/4.60	1.87/ 4.26
wR(F)/ $wR(F^2)$ (%)	2.21/ 4.42	3.59/ 7.00	4.22/ 8.34	2.87/ 5.61
GooF	1.31	1.25	0.95	0.55
min./ max./ mean				
$\delta_{res}\varrho(\vec{r})$ ($eÅ^{-3}$)	-0.13/ 0.11/ 0.03	-0.25/ 0.25/ 0.05	-0.31/ 0.19/ 0.04	-0.27/ 0.14/ 0.05
CWF:				
R(F)/ wR(F) (%)	5.57/ 2.50	3.50/ 3.68	3.22/ 3.01	1.80/ 2.70
χ^2/λ	1.30/ 0.36	0.82/ 0.60	0.96/ 0.60	0.74/ 0.60
GooF	1.14	0.91	0.98	0.84

solution of hydrobromic acid (HBr) in pure acetic acid. The product was isolated and again treated with HBr/acetic acid in methanol under reflux. Finally, potassium carbonate in acetone was added to achieve the ring closure. [249] Dimethyl-3-(4-nitrophenyl)oxacyclopropane-2,2-dicarboxylate (niphe-epoxide (**9**)) was synthesised by the Knoevenagel condensation of malonate with p-nitro benzaldehyde, followed by treatment with hypochlorite for the epoxidation. [99] Tetracyanooxacyclopropane (cyano-epoxide (**10**)) was obtained from tetracyano-ethylene upon reaction with hydrogen peroxide (35 %) in acetonitrile. [250]

Crystals of cpds. **8** to **10** were obtained by using the evaporation method (see Chapter 5.1.1). Suited solvents were a mixture of etyhl acetate and acetone for moc-epoxide (**8**), a mixture of dichloromethane and methanol for niphe-epoxide (**9**) and a mixture of 1,2-dichloroethane and acetone for cyano-epoxide (**10**), respectively. All crystals were colourless. Moc-epoxide (**8**) produces needle-shaped crystals that were soft and flexible. Although they were very sensitive to mechanical stress, they had to be cut in order to get crystals of suitable size. Therefore, severe problems with crystal quality occurred. Moreover, once removed from their mother liquor, the crystals decompose slowly, but quick insertion into a gas stream of liquid helium or nitrogen also destroys the crystals. So a data set could only be obtained at the in-house diffractometer after slowly cooling down and protecting the crystal by a vacuum chamber. Still, bad crystal quality and limited resolution lowered the quality of the data set. The data set could only be used with the inclusion of theoretical information (see below). Crystals of niphe-epoxide (**9**) tend to suffer from twinning problems. But once a non-twinned crystal was found, crystal quality was sufficient for a high-resoluted data set at the synchrotron. Cyano-epoxide (**10**) delivered crystals of very good quality in any required size. Crystals of all compounds were mounted on cactus needles with high-vacuum grease.

Moc-epoxide (**8**) was measured at the in-house Huber diffractometer with an APEX CCD detector (for details see Chapter 1.1.1). The temperature could be maintained at 25 K during the measurement. At a resolution of 1.00 $Å^{-1}$, the data set was complete within the face-centred monoclinic space group C2 (41152 measured reflections, 6618 unique). Within the criterium $F^2 \geq 3\sigma(F^2)$, there are 4723 observed reflections. For more details, see Table 11.1. Integration of data was carried out with the programme SAINT [251]. For scaling and merging of data, SORTAV [202–204] was used. The structure was solved using direct methods as implemented in SHELXS. [205] Moc-epoxide (**8**) crystallises with two individual molecules in the asymmetric unit and without solvent molecules. There are

two chiral carbon atoms in the molecule (C1 and C2 of the epoxide ring). Both molecules of the asymmetric unit belong to the same enantiomer and as C2 is a chiral space group, it follows that moc-epoxide (**8**) crystallises enantiomerically pure. Thomas Pfeuffer determined the rotational direction of polarised light sent through a solution of moc-epoxide (**8**). From this experiment, S-configuration was assigned to both C atoms.

The data sets of niphe-epoxide (**9**) and cyano-epoxide (**10**) were measured at beamline F1 of HASYLAB/DESY at a wavelength of 0.5600(2) Å with a marCCD area detector (for details see Chapter 1.1.1). A constant temperature of 100 K was reached by an open-flow nitrogen gas stream. The resolutions of the data sets are higher than for the in-house data sets, the resolution for cyano-epoxide (**10**) is even 1.42 $Å^{-1}$. The data set of niphe-epoxide (**9**) is not complete (84.2 %) due to the triclinic space group $P\bar{1}$, but the data set of cyano-epoxide (**10**) is 99 % complete to the maximum resolution. Between 120000 and 190000 reflections were measured, of which 8000 to 10000 unique reflections are observed within the criterium $F^2 \geq 3\sigma(F^2)$ (see Table 11.1 for details). Integration of data was carried out with the programme XDS ([199–201], revision August 2006 for niphe-epoxide (**9**) and revision June 2008 for cyano-epoxide (**10**)) and oblique incidence correction [105] was performed subsequently. For scaling and merging of data, SORTAV was used and the structures were solved with SHELXS (direct methods). Both asymmetric units consist of one molecule, no solvent molecules are embedded in the crystal packing. Niphe-epoxide (**9**) crystallises as racemic mixture of the S- and R-configuration.

11.1.2 Refinement and Analysis of Data

Conventional spherical refinement was carried out by the programme SHELXL [205] to establish the starting positional and displacement parameters for the aspherical refinement steps. Anisotropic displacement parameters (adps) were refined for the non-hydrogen atoms. For the hydrogen atoms, adps were calculated by a rigid-body approximation using the SHADE approach. [108, 109] The rigid-body approximation requires at least five non-hydrogen atoms for the estimation of the hydrogen adps. Therefore, a more simple approach (riding-model approximation) had to be used for etox (**7**). Table 11.1 lists some figures of merit for the spherical refinement. The final structures (after multipole modelling) are shown in Figure 11.1, including the atomic-numbering scheme that is used throughout this doctoral

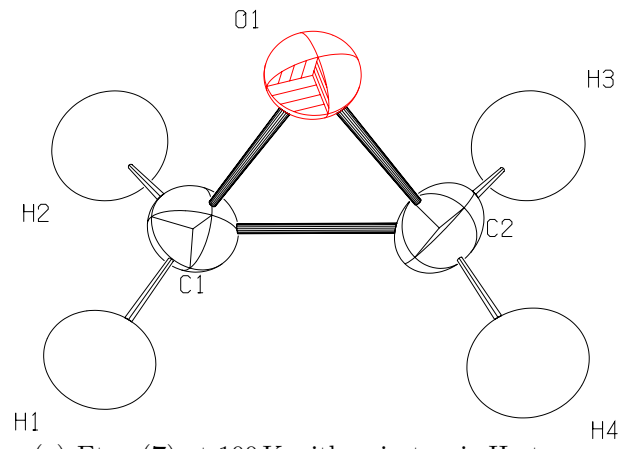

(a) Etox (**7**) at 100 K with anisotropic H atoms

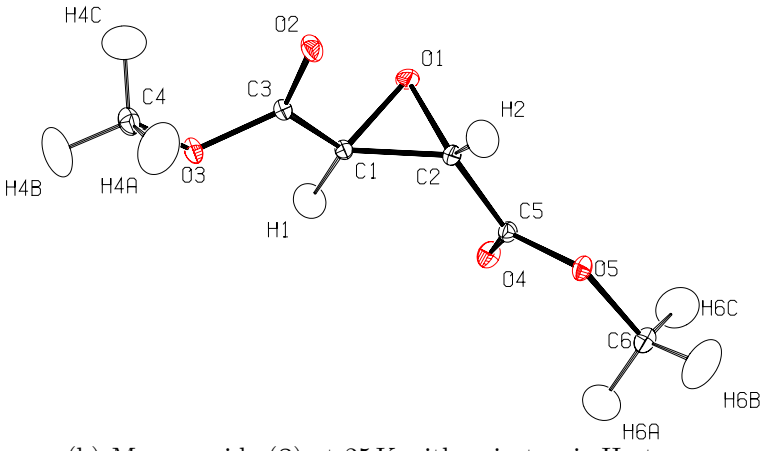

(b) Moc-epoxide (**8**) at 25 K with anisotropic H atoms

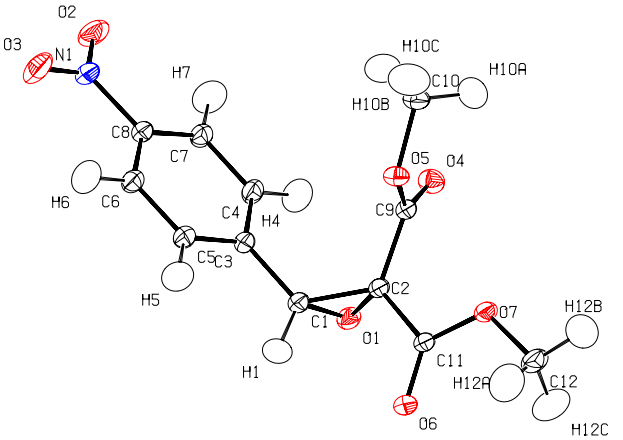

(c) Niphe-epoxide (**9**) at 100 K with anisotropic H atoms

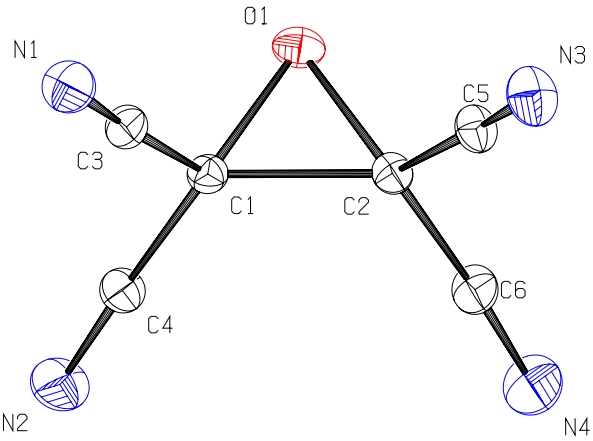

(d) Cyano-epoxide (**10**) at 100 K

Figure 11.1: ORTEP representations of cpds. **7** to **10**

Thermal ellipsoids at 50 % probability, atomic-numbering scheme given

thesis. The numbering of the second molecule in the asymmetric unit of moc-epoxide (**8**) corresponds to the first one. The capital letter A is added to each label to relate the atom to the second molecule. The ED properties of the two molecules are very similar, so that averaged values are used in the discussion.

The programme XDLSM of the XD2006 suite, [207] which uses the Hansen-Coppens multipole formalism for aspherical modelling, was employed. Local mm2 symmetry was imposed on the epoxide oxygen atom O1. In etox (**7**) and cyano-epoxide (**10**), local m symmetry was used for the epoxide carbon atoms C1 and C2, whereas no symmetry was applied for C1 and C2 in moc-epoxide (**8**) and niphe-epoxide (**9**). M symmetry was also imposed on all nitrogen, oxygen and carbon atoms in

ester, phenyl and nitro groups, except for C3 and C8 in niphe-epoxide (**9**), for which mm2 symmetry was used. Methyl groups were refined with local threefold (3) symmetry. Carbon and nitrogen atoms in the cyano groups of cyano-epoxide (**10**) as well as hydrogen atoms were refined with local sixfold (6) symmetry to approximate the linearity of these groups. A detailed summary of the used local site symmetries can be found in Tables A.83 and A.84. Due to the fact that the ratio of reflections over parameters is excellent for these small molecules, no chemical constraints were used.

All non-hydrogen atoms were treated up to the hexadecapole level of expansion, whereas monopoles, bond-directed dipoles and bond-directed quadrupoles were introduced for hydrogen atoms. The expansion-contraction parameter κ was refined independently for all chemically non-similar non-hydrogen atoms, values can be found in Tables A.83 and A.84. κ' values were left at their default values κ'=1.0, but for hydrogen atoms, optimised values κ=1.13 and κ'=1.29 [208] were used. All distances of bonds involving hydrogen atoms were fixed to mean neutron-diffraction values from the literature. [209] H–C–H bond angles in methyl groups were fixed to the tetrahedral angle. An electroneutrality constraint concerning the monopole populations was applied for the asymmetric unit. Figures of merit for the multipole refinement on F^2 are collected in Table 11.1. The structure factors of etox (**7**) from the measurement from 1986 were only available as F values, therefore refinement was not carried out on F^2 but on F.

The described procedure for the multipole modelling of the experimental structure factors could not be applied for moc-epoxide (**8**). Multipole populations and κ values could only be refined to physically unreasonable results. This is due to the problems with crystal quality described above. However, a method related to the invariom transfer [31, 32] was successfully applied to model the electron density from this otherwise insufficient data set. A periodic-boundary calculation using the experimental geometry of both molecules in the asymmetric unit after spherical refinement was performed and fully periodic theoretical structure factors for the whole asymmetric unit were determined. Subsequent multipole modelling was carried out against these periodic theoretical structure factors to determine theoretical multipole populations and κ parameters. These multipole populations and κ parameters were transferred and fixed during a subsequent experimental refinement of the geometry and the adps against the experimental structure factors. As the geometry and the electron density were very stable after this treatment, it was even possible to introduce anisotropic hydrogen adps as detailed above.

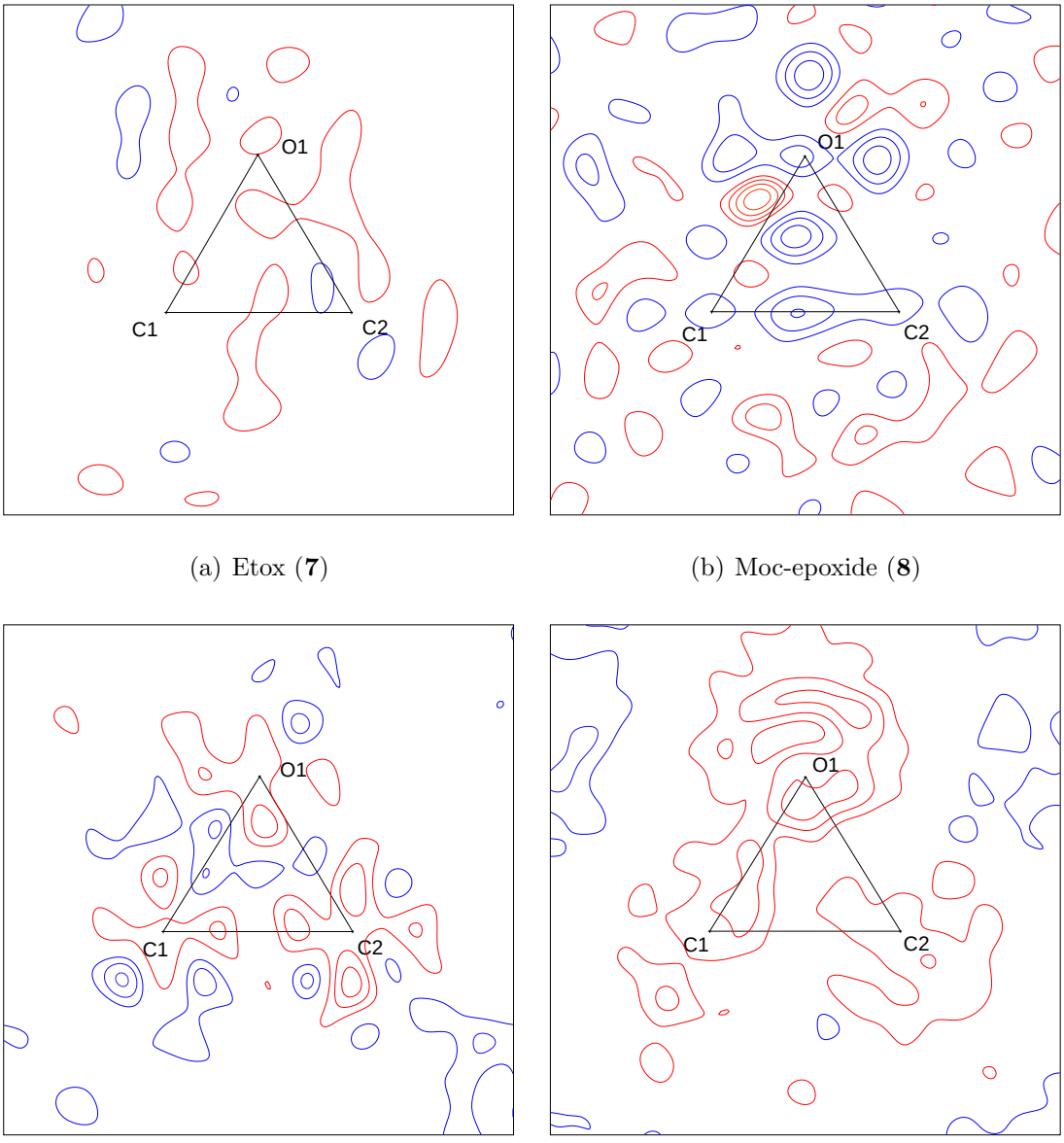

(a) Etox (**7**)

(b) Moc-epoxide (**8**)

(c) Niphe-epoxide (**9**)

(d) Cyano-epoxide (**10**)

Figure 11.2: Residual-density maps of the epoxide rings of cpds. **7** to **10**
Contour interval = 0.05 e$\AA^{-3}$, red = negative, blue = positive

Minimum and maximum residual densities (compare Table 11.1) are acceptable. Figure 11.2 shows the residual density in the plane of the epoxide rings with contour intervals of 0.05 eÅ^{-3}. For etox (**7**), the modelling is nearly perfect, the map is flat and featureless. There are more features for cyano-epoxide (**10**), but they are small and distributed unsystematically. The only peculiarity in both cases is that there is predominantly or exclusively negative residual density in the epoxide ring. In moc-epoxide (**8**) and niphe-epoxide (**9**), features concentrate in the region of the epoxide ring. For niphe-epoxide (**9**), the effects are still small, there is no more than 0.10 e of residual density in the region of the bonds, which is less than 7 % of the densities at the bcps of the C–O and C–C bonds. For moc-epoxide (**8**), the effects are larger: There are up to 0.20 e of residual density near bond- or ring-critical points. This is due to the fact that theoretical multipole populations were used and fixed before the refinement of the geometry. Otherwise, the electron density could not have been determined at all. Therefore, the residual densities must be accepted. However, the results of the topological analysis (deformation density, bond topological and atomic properties) could be determined very reliably, which can be shown by comparing with the other compounds (see Chapter 12.2).

As already mentioned in Chapter 3.2, the code of the ELI-D was implemented into the programme TONTO in cooperation with Prof. Jayatilaka. Equations 3.8 and 3.9 defining the ELI-D for triplet pairs and the corresponding Fermi-hole curvature were converted into programme code. Everything that must be determined to calculate the ELI-D according to the implemented equations 3.8 and 3.9 are the σ-spin orbitals $\Psi_i(\vec{r})$ and the same-spin density $\varrho_\sigma(\vec{r}_i)$. It was decided to use $\Psi_i(\vec{r})$ and $\varrho_\alpha(\vec{r}_i)$ for electrons with α-spin that are available in TONTO in form of their orbital gradients from the process of constraining the wave function. Finally, a routine was included to write the experimental ELI-D function values calculated in TONTO into a grid file. The programme TONTO containing the described modifications can be downloaded free of charge, including the source code, from http://tonto-chem.sourceforge.net.

Epoxide cpds. **7** to **10** were chosen as first test cases for the experimental ELI-D. Constrained wave-function fitting (CWF) on experimental geometry and experimental structure factors was performed at HF/cc-pVDZ level of theory. For cpds. **8** to **10**, the same iterative procedure could be used as described in Chapter 5.1.2 with a final λ-value of 0.60. But for etox (**7**), convergence was not reached easily,

so that steps of 0.02 were used to end up with a λ-value of 0.36. Figures of merit for CWF of cpds. **7** to **10** are listed in Table 11.1.
Grids of the ED and the new experimental ELI-D were written in cube format with a stepsize of 0.1 a.u. A topological analysis of the experimental ELI-D was performed with the programme DGRID-4.4 as well as an integration of the ED within the ELI-D basins. Hence, shape, number, and electron population of basins can be compared with the experimental ELF and the theoretical ELI-D. The function values at the attractors within the experimental ELI-D are accessible, too, which can be analysed with respect to the theoretical ELI-D values. These function values are the advantage of the ELI-D over the ELF as discussed in Chapter 3.
Unfortunately, a full topological analysis of the experimental ELI-D is not yet possible because on the one hand, DGRID-4.4 is not able to determine (3,-1) and (3,+1) saddle points in the ELI-D from a cube file and on the other hand, TONTO does not write another grid-file format that DGRID-4.4 can read. This problem must be tackled in the future to establish the analysis of critical points within the ELI-D in analogy to the ED analysis, which is not present in the literature so far. As a first approach, a full topological analysis of the theoretical ELI-D of cpds. **7** to **10** was performed in this doctoral thesis.

11.2 Details of Theoretical Calculations on Compounds 7 to 10

Isolated-molecule calculations were performed for cpds. **7** to **10** with the programme GAUSSIAN03 [221] at experimental geometries after multipole refinement and at optimised geometries. To compare with the results from the experimental ED determination, the B3LYP/cc-pVTZ level of theory was used; to compare with the experimental ELI-D, HF/cc-pVDZ was employed. Topological analysis of the ED was performed with AIM2000 [222]; for determination and topological analysis of the ELI-D, DGRID-4.4 [219] was employed. Moreover, geometry optimisations of hydrogen-bonded complexes of cpds. **7** to **10** with silanol and water as donors were carried out at the B3LYP/cc-pVTZ level of theory to get access to hydrogen-bond energies.

The experimental geometries of cpds. **7** to **10** were used as input for periodic-boundary calculations with the programme CRYSTAL06 [223] (levels of theory:

Table 11.2: Details of refinements on theoretical structure factors

Periodic-boundary calculations at eperimental and optimised geometries

	etox (**7**)	moc-epoxide (**8**)	niphe-epoxide (**9**)	cyano-epoxide (**10**)
exp. geometry:				
space group, Z	$P2_1/n$, 4	C2, 8	$P\bar{1}$, 2	$P2_1/c$, 4
a (Å)	4.633	21.304	7.7460	9.586
b (Å)	8.400	4.046	8.0800	6.082
c (Å)	6.577	17.685	11.8350	11.994
α (°)	90.00	90.00	86.198	90.00
β (°)	100.37	107.05	74.105	110.79
γ (°)	90.00	90.00	60.673	90.00
V (Å^3)	251.8	1457.3	619.1	653.7
F(000)	96	672	292	288
no. of calc. refl.	2082	4738	8048	9672
refinement on	F	F	F	F
ratio refl./par.	38.56	12.21	32.98	116.53
R(F)/ R(F^2) (%)	0.73/0.95	0.40/0.65	0.59/0.96	0.73/1.25
min./ max./ mean				
$\delta_{res}\varrho(\vec{r})$ (eÅ^{-3})	-0.09/0.11/0.01	-0.09/0.06/0.01	-0.14/0.13/0.02	-0.26/0.22/0.03
opt. geometry:				
space group, Z	$P2_1/n$, 4	C2, 8	$P\bar{1}$, 2	$P2_1/c$, 4
a (Å)	4.819	21.506	7.910	10.128
b (Å)	8.408	4.160	8.179	6.971
c (Å)	6.825	18.273	11.961	11.862
α (°)	90.00	90.00	88.585	90.00
β (°)	91.298	107.173	73.186	100.825
γ (°)	90.00	90.00	65.962	90.00
V (Å^3)	276.5	1562.0	667.0	822.6
F(000)	96	672	292	288
no. of calc. refl.	2082	4738	8048	9672
refinement on	F	F	F	F
ratio refl./par.	38.56	12.21	32.98	116.53
R(F)/ R(F^2) (%)	0.48/0.83	0.46/0.69	0.65/0.98	0.87/1.35
min./ max./ mean				
$\delta_{res}\varrho(\vec{r})$ (eÅ^{-3})	-0.08/0.08/0.01	-0.08/0.05/0.01	-0.12/0.12/0.01	-0.23/0.19/0.02

6-31G(d) for O, N and C [225], 3-1G(p) for H [225]). Not only calculations at fixed experimental geometry were performed, but also geometry optimisations within the crystal environment. The space group was fixed, but lattice constants as well as bond distances and angles were optimised. These optimisations took a few weeks for etox (**7**) and cyano-epoxide (**10**), but a few months for moc-epoxide (**8**) and niphe-epoxide (**9**) at the available computer capacities. Therefore, these calculations could only be performed for epoxide cpds. **7** to **10**, which are rather small molecules, and not for cpds. **1** to **6**, which are larger.

The final optimised crystal geometries are summarised in Table 11.2 and compared to the experimental values, the molecular geometries will be discussed in Chapter 12.1.1. The cell lengths do not change dramatically upon optimisation, the largest difference is 0.89 Å in cyano-epoxide (**10**). For moc-epoxide (**8**) and niphe-epoxide (**9**), the cell angles also only change by a maximum of 5.3 °, but for etox (**7**) and cyano-epoxide (**10**), the monoclinic angle is reduced by about 10 °. These changes in the cell constants are mainly reflected in differences within the hydrogen-bonding network, see Chapter 12.1.2. In all four cases, the cell volume increases significantly. For etox (**7**), moc-epoxide (**8**), and niphe-epoxide (**9**), the changes range from 6 to 9 %, but for cyano-epoxide(**10**) , the difference is 20.5 %.

From the periodic wave function for both experimental and optimised geometries, static theoretical structure factors were calculated with the programme PROPERTIES06. The same list of hkl indices as measured was chosen to be calculated, but including a few non-observed reflections of very low resolution. Within a modelling of the theoretical structure factors with XD2006, the same density models were used as for experimental structure factors, see preceding Chapter and Table A.83. Details of the refinements are also given in Table 11.2.

The experimental geometries used as input for theoretical calcuations under periodic-boundary conditions were taken after multipole refinement of the experimental structure factors for cpds. **7**, **9** and **10**. But as discussed above, multipole refinement of experimental structure factors did not work for moc-epoxide (**8**) due to severe problems with crystal quality. Therefore, the experimental geometry was taken after spherical refinement. Table 11.2 shows that the R-values and the residual densities after aspherical modelling of the theoretical structure factors at fixed spherical geometry are very low and thus indicate successfull determination of theoretical multipole parameters. Multipole populations and κ values obtained this way were transferred to refine the experimental geometry against the experimental structure factors at fixed theoretical multipoles, see above. In the following

discussion, experimental geometry and experimental properties of moc-epoxide (**8**) are given after this last refinement step. It must be noted that theoretical results referred to in the following as values from modelling of theoretical structure factors at experimental geometry of moc-epoxide (**8**) belong to the spherical structure.
R-values and residual densities are small as expected for modelling of theoretical structure factors. Without an exception, the residual densities decrease for optimised geometries. This fact argues for the assumption discussed regarding the unusually high residual densities in butoxysilanol (**5**) that residual densities are higher when the geometry is not in an energetically ideal state. This point was true for butoxysilanol (**5**), which was quick-frozen. For cyano-epoxide (**10**), residual densities are significantly higher than for the other epoxide compounds. This might also be an effect of the geometry because the differences between experimental and optimised geometry indicated in terms of the cell volumes are most severe for cyano-epoxide, see above.

Chapter 12

Results of the Analyses of Compounds 7 to 10

12.1 Geometrical and Energetical Results

12.1.1 Experimental and Optimised Geometries

Figure 4.4 in Chapter 4.2 depicts resonance formulae of the epoxide ring interacting with the electron-withdrawing groups that occur in cpds. **8** to **10**, compare molecular structures as given in Figure 11.1. It is assumed in organic chemistry that the cyano substituent is the most powerful electron-withdrawing group (EWG) of the three in cpds. **8** to **10**. But the methyl ester and nitro-phenyl group are also known as good EWGs. There are four cyano groups in cyano-epoxide (**10**), three EWGs (two methyl ester and one nitro-phenyl group) in niphe-epoxide (**9**) and only two methyl ester groups in moc-epoxide (**8**). Therefore, the influence on the properties of the epoxide ring should steadily increase from cpd. **8** towards cpd. **10**. Etox (**7**) serves as reference without EWGs.

If the open forms of the resonance formulae in Figure 4.4 really have some impact on the situation of the epoxide ring, the C–C bonds should lengthen and the C–O–C angles should widen upon substitution with EWGs compared to etox (**7**). The more EWGs are present, the more significant the effect should be. This can be seen unambiguously in Table 12.1, which summarises bond lengths and angles for cpds. **7** to **10** (complete lists in Tables A.89 to A.100). In all three methods (experiment, geometry optimisations within periodic boundary and of the isolated molecule), the bond C1–C2 is shortest for etox (**7**) (1.46-1.47 Å) and

Table 12.1: Selected bond distances (Å) and angles ° in cpds. **7** to **10**
First row: experiment, second row: periodic-boundary optimisation, third row: isolated-molecule optimisation

bond, angle	etox (**7**)	moc-epoxide (**8**)	niphe-epoxide (**9**)	cyano-epoxide (**10**)
epoxide ring				
C1–O1	1.434(1)	1.424(2)	1.435(1)	1.426(1)
	1.449	1.431	1.436	1.433
	1.428	1.416	1.426	1.423
C2–O1	1.441(1)	1.427(2)	1.420(1)	1.422(1)
	1.454	1.434	1.428	1.429
	1.428	1.416	1.420	1.424
C1–C2	1.457(1)	1.472(2)	1.488(1)	1.499(1)
	1.468	1.477	1.497	1.519
	1.464	1.479	1.486	1.517
C1–O1–C2	60.91(4)	62.15(8)	62.80(3)	63.54(3)
	60.78	62.06	63.05	64.13
	61.68	62.99	62.95	64.38
O1–C1–C2	59.79(3)	59.03(8)	58.10(3)	58.10(3)
	59.78	59.05	58.22	57.79
	59.15	58.50	58.34	57.81
O1–C2–C1	59.30(3)	58.82(7)	59.09(3)	58.36(3)
	59.44	58.88	58.73	58.08
	59.18	58.51	58.71	57.81
bonds	C1–H1	C1–H1	C1-H1	C1–C3
to	1.099	1.099	1.099	1.450(1)
substituents	1.088	1.085	1.089	1.454
	1.085	1.083	1.085	1.448
	C1–H2	C1–C3	C1–C3	C1–C4
	1.099	1.507(2)	1.487(1)	1.449(1)
	1.089	1.505	1.491	1.453
	1.085	1.504	1.487	1.448
	C2–H3	C2–H2	C2–C9	C2–C5
	1.098	1.099	1.514(1)	1.451(1)
	1.087	1.086	1.518	1.455
	1.085	1.083	1.513	1.448
	C2–H4	C2–C5	C2–C11	C2–C6
	1.099	1.507(2)	1.516(1)	1.450(1)
	1.088	1.506	1.521	1.454
	1.085	1.504	1.521	1.448

lengthens towards cyano-epoxide (**10**) (1.50-1.52 Å). The angle C1–O1–C2 widens significantly from etox (**7**) (60.7-60.9 °) to cyano-epoxide (**10**) (63.5-64.4 °). The impact on the C–O bonds and the O–C–C angles is not that clear, but there is a trend: The C–O bonds are longest in etox (**7**) and shorten upon substitution with EWGs. They are shorter than the C–C bonds in the epoxide ring for every compound and method. The mean difference is 0.02 Å in etox (**7**) and increases towards cyano-epoxide (**10**) (0.09 Å). The O–C–C angles are largest for etox (**7**) and narrow upon substitution with EWGs. They are smaller than the C–O–C angles for any compound and method so that the smallest mean difference again exists for etox (**7**) (1.7 °) and the largest for cyano-epoxide (**10**) (6.0 °).

Bond distances C1–O1 and C2–O1 are different within experiment and periodic-boundary optimisations, although cpds. **7**, **8** and **10** are symmetrically substituted. The reason is that the hydrogen-bonding networks within experiment and periodic-boundary calculations are not symmetric. Etox (**7**), for example, exhibits only three C–H$\cdots$O hydrogen bonds, see next chapter. Within isolated-molecule calculations, the distances C1–O1 and C2–O1 are equal for cpds. **7**, **8** and **10**. The same holds true for the angles O1–C1–C2 and O1–C2–C1. It is not clear from Table 12.1 whether the two methods incorporating crystal effects produce values that are closer together or the two theoretical methods. In general, the deviations between experiment and the two theoretical methods are not large. There is a trend that C–O bonds and O–C–C angles are smallest for isolated-molecule calculations and C–O–C angles are largest.

In the second part of Table 12.1, the bonds to the four substituents of the epoxide ring are listed. C–H distances range from 1.085 to 1.089 Å for the two geometry optimisations and were fixed to 1.099 Å from averaged neutron-diffraction values within the experimental geometry. The C–C bonds can clearly be distinguished with respect to the different EWGs. In the resonance formulae in Figure 4.4, the C–C bonds are assigned partial double-bond character and should therefore shorten according to the electron-withdrawing capability of the corresponding EWG. Consequently, the C–C bonds in cyano-epoxide (**10**) are shortest since the cyano groups are the most powerful EWGs. They range from 1.448 Å (optimisation on isolated molecule) to 1.455 Å (optimisation in periodic boundary) with the experimental values in-between. The bond C1–C3 to the nitro-phenyl group in niphe-epoxide (**9**) is second shortest (1.487 Å for isolated-molecule optimisation and experiment, 1.491 Å for periodic-boundary calculations), indicating that this group is the second most powerful EWG. The bonds to the methyl ester groups in

moc-epoxide (**8**) and niphe-epoxide (**9**) are longest, ranging from 1.504 to 1.521 Å.

12.1.2 Intermolecular Interactions in the Crystals

There are no classical hydrogen-bond donor groups like O–H or N–H in cpds. **7** to **10**. In cyano-epoxide (**10**), there are not even hydrogen atoms. Therefore, the discussion on intermolecular interactions is about C–H$\cdots$O hydrogen bonds and N$\cdots$C contacts. The individual contact patterns are depicted in Figures 12.1 and 12.2. The asymmetric units and symmetry-related donor or acceptor atoms, respectively, are shown for the experimental cases. The patterns change slightly for the optimised cases, see discussion below.

As already mentioned, etox (**7**) (Figure 12.1 (a)) exhibits three C–H$\cdots$O interactions so that the hydrogen-bonding pattern is unsymmetrical, which is reflected in differing C–O distances and O–C–C angles. In the optimised geometry, the hydrogen bond C1–H1$\cdots$O1 does not exist but C2–H3$\cdots$O1 exists instead, which is in turn not present in the experimental lattice, see Table 12.2. In moc-epoxide (**8**) and niphe-epoxide (**9**), numerous C–H$\cdots$O hydrogen bonds are present (Figure 12.2), but only ester and nitro oxygen atoms are acceptors and not the epoxide oxygen O1. Therefore, the question arises whether the basicity of the epoxide oxygen atom is not competitive to the ester or nitro groups, so that only etox (**7**) forms C–H$\cdots$O$_{epoxide}$ interactions in the absence of alternative acceptor atoms. This question will be tackled with theoretical calculations on model complexes of cpds. **7** and **10** with silanol and water in the next chapter. For cyano-epoxide (**10**) (Figure 12.1 (b)), there are many N$\cdots$C contacts with several bcps and rcps, but only the two that are shorter than 3.0 Å will be discussed in the follwing for comparison with the C–H$\cdots$O hydrogen bonds.

Table 12.2 lists properties of all discussed C–H$\cdots$O hydrogen bonds and N$\cdots$C contacts for etox (**7**) and cyano-epoxide (**10**), but only a selection of C–H$\cdots$O hydrogen bonds for moc-epoxide (**8**) and niphe-epoxide (**9**). A complete list can be found in the Appendix, Tables AA.101 to A.104. In moc-epoxide (**8**) and cyano-epoxide (**10**), the pattern is identical between experiment and geometry optimisation, only strength and direction vary. For niphe-epoxide (**9**), there is an additional hydrogen bond (C10–H10A$\cdots$O4) in the optimised crystal lattice. But for etox (**7**), the lattice changes almost completely upon optimisation. As already mentioned, C1–H1$\cdots$O1 only exists in the experiment and C2–H3$\cdots$O1 only in the optimised case. Moreover, the contact C2–H4$\cdots$O1 originates from another

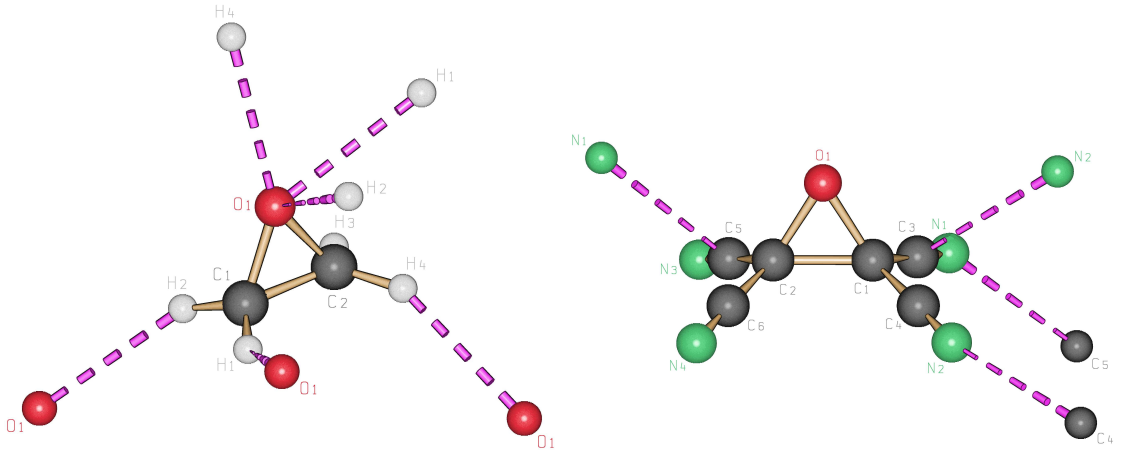

(a) Etox (**7**) exhibiting three C–H···O hydrogen bonds

(b) Cyano-epoxide (**10**) exhibiting numerous N···C contacts, of which only the ones shorter than 3.0 Å are plotted

Figure 12.1: Representation of the experimental interaction networks of etox (**7**) and cyano-epoxide (**10**)
All symmetry-related partners are plotted and labelled

symmetry operation.

In general, the strength of the C–H···O hydrogen bonds by means of interaction energies (E_{int}) and electron density at the bcp (ϱ_{bcp}) is typical for these kinds of interactions, see corresponding interactions in trisilo (**2**) and sucrose (cpd. **6**) (Tables 7.2 and 10.2). E_{int} are close to -10 kJ mol^{-1} or lower (absolute values), ϱ(bcp) varies between 0.03 and 0.09 eÅ^{-3}. But the C–H···O interactions in etox (**7**) with the epoxide oxygen atom as acceptor are slightly weaker, indicated by both E_{int} and ϱ_{bcp}, than in moc-epoxide (**8**) and nitro-epoxide with ester and nitro oxygen atoms as acceptors. The N···C contacts in cyano-epoxide (**10**) are exactly within the ranges given above, while the distances of these contacts are larger than H···O distances due to a larger sum of the van der Waals radii.

Optimisation of the crystal structures does not necessarily lead to closer and stronger intermolecular contacts. Changes of up to 0.2 Å in H···O or C···O distances, 10 ° in C–H···O angles, 4 kJ mol^{-1} in interaction energies and not more than 0.03 eÅ^{-3} in ϱ(bcp) and 0.3 eÅ^{-5} in $\nabla^2\varrho$(bcp) occur, but in both directions. The values of the ED and the Laplacian at the H···O bcps are closer between experiment and periodic-boundary calculations at experimental geometry than between the two theoretical methods, but this is not true for the interaction energies that spread more widely.

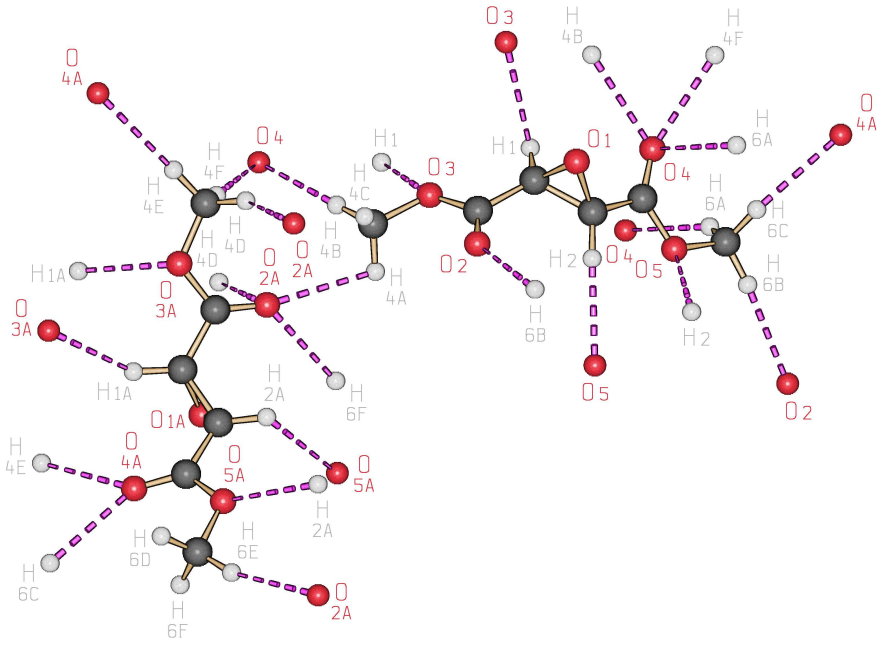

(a) Two molecules of moc-epoxide (**8**) in the asu

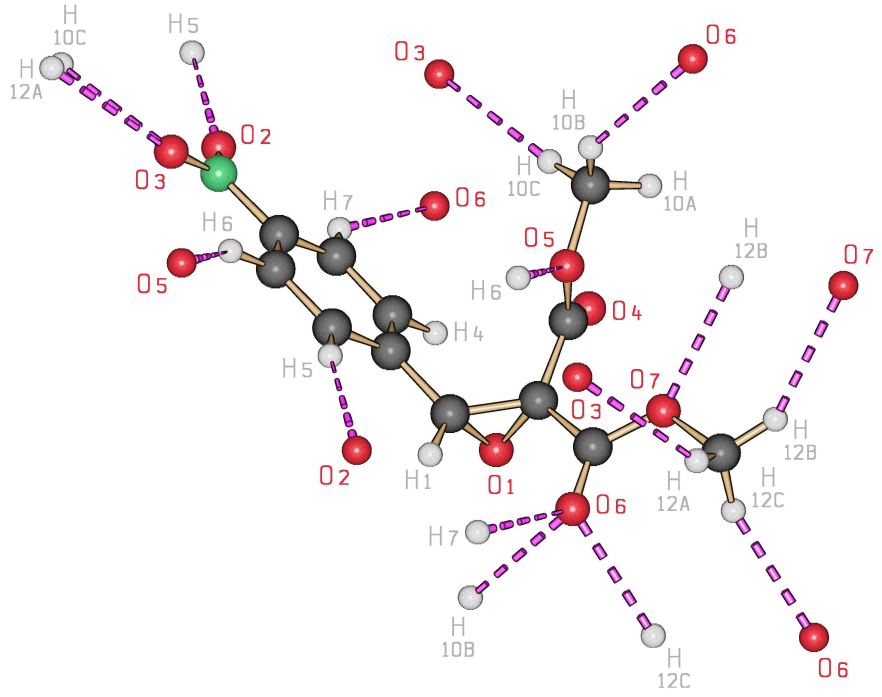

(b) One molecule of niphe-epoxide (**9**) in the asu

Figure 12.2: Representation of the experimental hydrogen-bonding networks of the asymmetric units (asus) of moc-epoxide (**8**) and niphe-epoxide (**9**)
All symmetry-related hydrogen-bonding partners are plotted and labelled

Table 12.2: Selected properties of intermolecular interactions of cpds. **7** to **10**
*Hydrogen$\cdots$acceptor (H$\cdots$A) or N$\cdots$C distance in Å, donor$\cdots$acceptor (D$\cdots$A) distance in Å, donor-hydrogen$\cdots$acceptor (D-H$\cdots$A) angle in °, electron density ϱ at H$\cdots$A or N$\cdots$C bcp in eÅ^{-3}, Laplacian $\nabla^2\varrho$ at H$\cdots$A or N$\cdots$C bcp in eÅ^{-5}, interaction energies E_{int} in kJ mol^{-1}, symmetry operation to generate second molecule; for moc-epoxide (**8**) and niphe-epoxide (**9**), only a few hydrogen bonds are given here, a complete list can be found in Tables A.101 to A.104*

labels	H$\cdots$A	D$\cdots$A	D-H$\cdots$A	ϱ_{bcp}	$\nabla^2\varrho_{bcp}$	E_{int}	sym
etox (**7**):							
C1–H1$\cdots$O1	2.584	3.579	150.20	0.03(1)	0.5(1)	-3.56	1/2+x, 3/2-y, 1/2+z
SP periodic				0.05	0.6	-1.45	
opt periodic	–	–	–	–	–	–	–
C1–H2$\cdots$O1	2.520	3.481	145.42	0.05(1)	0.7(1)	-4.29	1/2-x, 1/2+y, 1/2-z
SP periodic				0.06	0.7	-5.56	
opt periodic	2.453	3.470	154.89	0.07	0.7	-5.58	
C2–H3$\cdots$O1	–	–	–	–	–	–	–
SP periodic	–	–	–	–	–	–	–
opt periodic	2.502	3.377	136.73	0.06	0.8	-4.90	-x, -y, -z
C2–H4$\cdots$O1	2.519	3.503	148.39	0.03(1)	0.5(1)	-4.78	-1/2+x, 3/2-y, 1/2+z
SP periodic				0.05	0.6	-4.52	
opt periodic	2.596	3.529	143.40	0.05	0.5	-4.43	-1/2+x, -1/2-y, 1/2+z
moc-epoxide (**8**):							
C2–H2$\cdots$O5	2.352	3.391	157.28	0.07	1.0	-4.72	1-x, y, 1-z
SP periodic				0.07	1.0	-4.85	
opt periodic	2.351	3.410	164.32	0.08	0.9	-4.78	
C4–H4B$\cdots$O4	2.543	3.602	172.38	0.06	0.6	-9.89	1/2-x, 1/2+y, 1-z
SP periodic				0.06	0.6	-10.25	
opt periodic	2.380	3.465	175.01	0.08	0.9	-6.84	
C6–H6A$\cdots$O4	2.689	3.647	149.55	0.05	0.5	-11.51	x, 1+y, z
SP periodic				0.05	0.5	-12.64	
opt periodic	2.644	3.580	143.55	0.05	0.6	-10.04	
...							
niphe-epoxide (**9**):							
C5–H5$\cdots$O2	2.446	3.486	160.35	0.07	0.6	-5.62	x, -1+y, z
SP periodic				0.06	0.7	-8.58	
opt periodic	2.554	3.607	162.98	0.05	0.5	-5.50	
C6–H6$\cdots$O5	2.282	3.248	147.30	0.09	0.8	-11.70	1-x, 1-y, 1-z
SP periodic				0.09	1.0	-10.40	
opt periodic	2.422	3.367	145.08	0.06	0.8	-8.14	
C7–H7$\cdots$O6	2.264	3.150	137.65	0.09	1.2	-7.22	x, 1+y, z
SP periodic				0.08	1.1	-11.44	
opt periodic	2.318	3.197	137.23	0.08	1.0	-8.80	
C10–H10A$\cdots$O4	–	–	–	–	–	–	–
SP periodic	–	–	–	–	–	–	–
opt periodic	2.571	3.534	147.06	0.05	0.6	-6.49	2-x, 1-x, -z
...							
cyano-epoxide (**10**):							
N1$\cdots$C5	2.932			0.08	0.9	-7.77	x, 3/2-y, 1/2+z
SP periodic				0.07	0.9	-9.88	
opt periodic	3.107			0.06	0.8	-11.00	
N2$\cdots$C4	2.993			0.07	0.8	-8.72	-x, -1/2+y, 1/2-z
SP periodic				0.06	0.8	-11.27	
opt periodic	3.272			0.05	0.8	-9.34	

Electrostatic and covalent contributions of the hydrogen bonds and N···C contacts are visualised by the experimental ESP on ED molecular surfaces and the experimental ED on Hirshfeld surfaces for etox (**7**) and cyano-epoxide (**10**) in Figure 12.3. In the ESP representation of etox (**7**) on an ED isosurface of 0.0067 $e Å^{-3}$ (Figure 12.3 (a)), the contacts of H1 and H4 are clearly visible as pronounced positive regions (about 0.38 $e Å^{-1}$). Around oxygen atom O1, there is a continuous distribution of negative ESP with a magnitude of about -0.10 $e Å^{-1}$. On the Hirshfeld surface, individual contacts are also visible at the oxygen atom. H1, H2 and H4 exhibit contacts with covalent contributions up to 0.07 $e Å^{-3}$ on the Hirshfeld surface (more than at the bcps, which are minima in the ED along the direction of the interaction), whereas H3 only shows a weak colouring, which exemplifies that there is no C2–H3···O1 interaction of reasonable strength in the experiment.

The experimental ESP of cyano-epoxide (**10**) was mapped on an ED isosurface of 0.5 $e Å^{-3}$ (Figure 12.3 (c)), which is much closer to the nuclei. Therefore, the scale of the ESP is shifted towards much more positive values. However, it is obvious that the nitrogen atoms are more negatively polarised than the oxygen atom. Around carbon atoms in the cyano groups and in the epoxide ring, regions of strong positive polarisation are located. Thus, N···C contacts guide the crystal packing of this compound. In the corresponding Hirshfeld representation (Figure 12.3 (d)), these contacts are visualised. Each nitrogen atom is involved in contacts (only a selection is given in Table 12.2). Instead of a localised charge accumulation, which is always found for classical hydrogen bonds, the Hirshfeld surface close to the carbon atoms is covered by large areas of ED being donated from the nitrogen atoms. The strength of these interactions is comparable to the C–H···O interactions in the other compounds, compare Table 12.2 and the scales in Figures 12.3 (b), 12.4 and 12.5.

The analysis of intermolecular interactions is even more important for moc-epoxide (**8**) and niphe-epoxide (**9**) because they are model compounds for drug design in pharmacological research. The goal is to find protease inhibitors against deseases like SARS or HIV. [91–100] The principle of electrostatic complementarity plays an important role in the recognition process of biologically active low molecular-weight ligands and corresponding target enzymes. [142,143] It is thus an important finding that the experimental ESPs of both moc-epoxide (**8**) and niphe-epoxide (**9**) are not distributed in a simple manner (positive at each hydrogen atom, negative at each

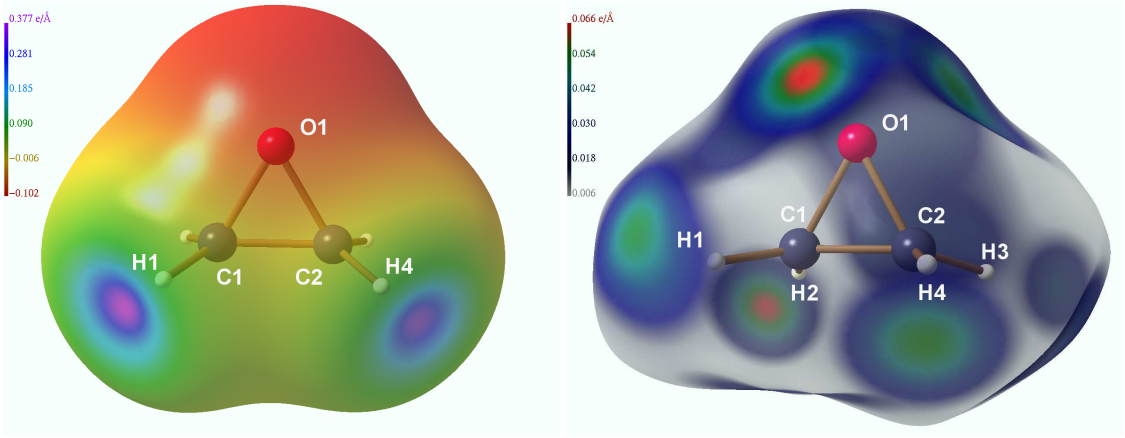

(a) ESP ($eÅ^{-1}$) of etox (**7**) mapped on an ED isosurface of $0.0067\,eÅ^{-3}$

(b) ED ($eÅ^{-3}$) of etox (**7**) mapped on a Hirshfeld surface

(c) ESP ($eÅ^{-1}$) of cyano-epoxide (**10**) mapped on an ED isosurface of $0.5\,eÅ^{-3}$

(d) ED ($eÅ^{-3}$) of cyano-epoxide (**10**) mapped on a Hirshfeld surface

Figure 12.3: Representations of the ESPs and the Hirshfeld surfaces of etox (**7**) and cyano-epoxide (**10**)

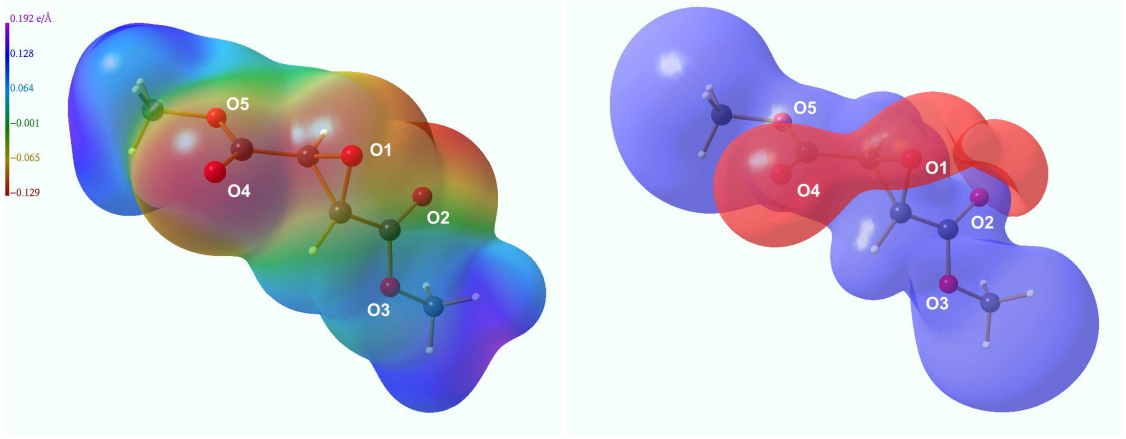

(a) ESP ($eÅ^{-1}$) mapped on an ED isosurface of $0.0067\,eÅ^{-3}$

(b) Blue = isosurface of the ESP at $0.1\,eÅ^{-1}$, red = isosurface of the ESP at $-0.1\,eÅ^{-1}$

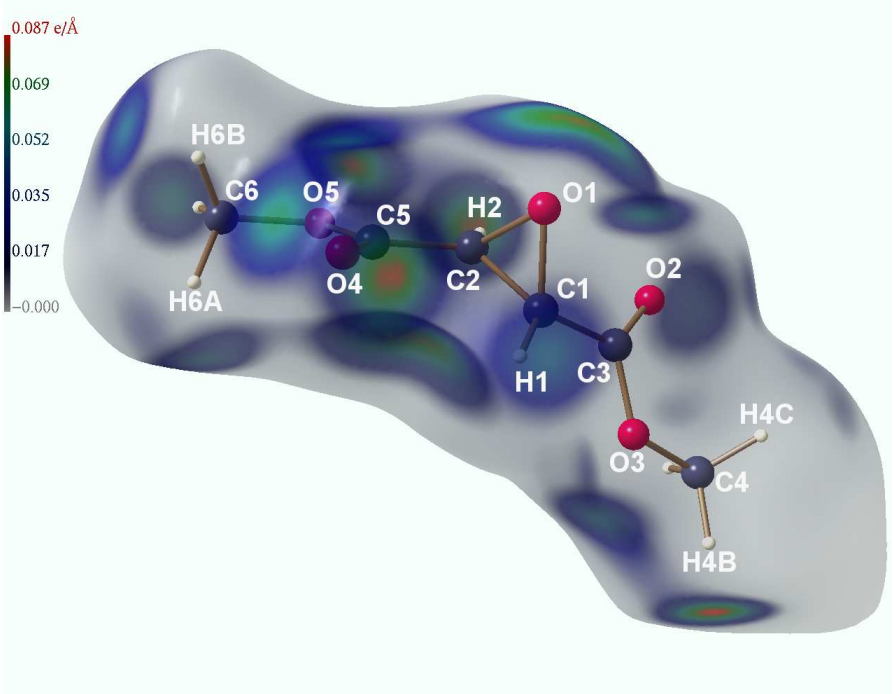

(c) ED ($eÅ^{-3}$) mapped on a Hirshfeld surface

Figure 12.4: Representations of the ESP and the Hirshfeld surface of moc-epoxide (**8**)

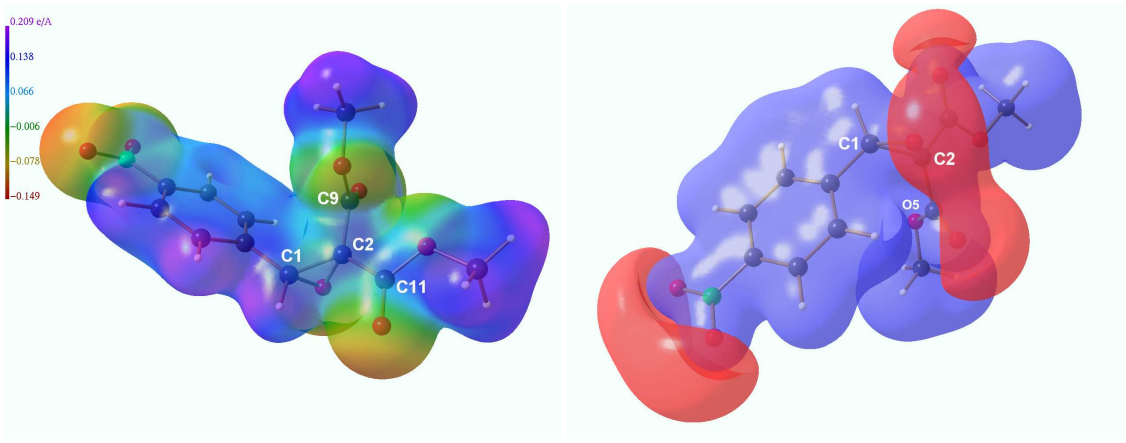

(a) ESP ($e\text{Å}^{-1}$) mapped on an ED isosurface of $0.0067\,e\text{Å}^{-3}$

(b) Blue = isosurface of the ESP at $0.1\,e\text{Å}^{-1}$, red = isosurface of the ESP at $-0.1\,e\text{Å}^{-1}$

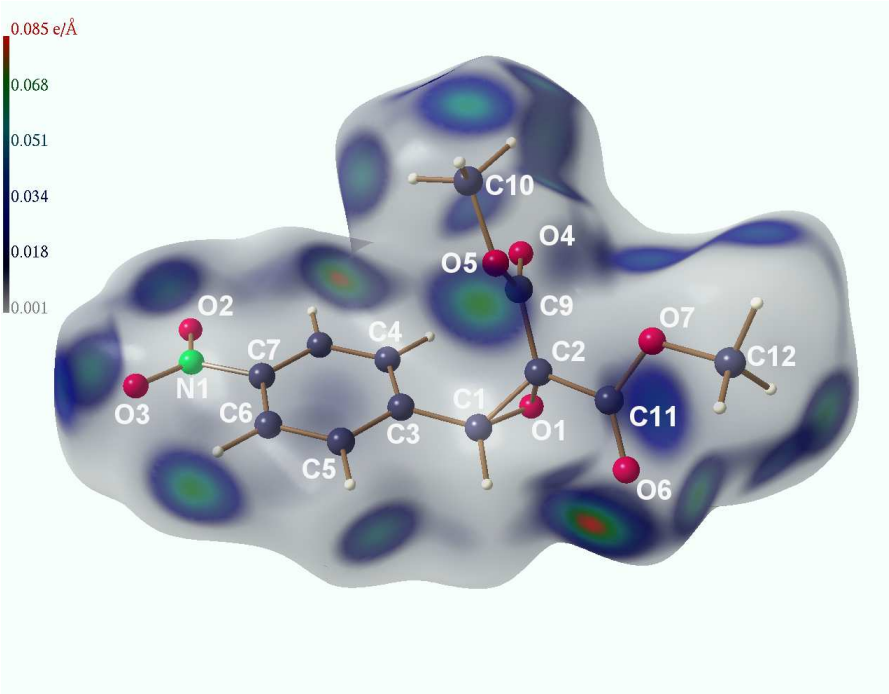

(c) ED ($e\text{Å}^{-3}$) mapped on a Hirshfeld surface

Figure 12.5: Representations of the ESP and the Hirshfeld surface of niphe-epoxide (**9**)

oxygen atom) but show a special pattern. There is a belt-region of distinctive negative potential spanning obliquely over the epoxide ring connecting the two ester groups. This can be seen in Figures 12.4 (a) and (b) for moc-epoxide (**8**). For niphe-epoxide (**9**), it is most obvious in the representation of two ESP isosurfaces in Figure 12.5 (b). The negative region around the nitro group is not part of the biologically active kernel of the molecule. It was only added synthetically to improve the crystallisation properties.

These belt-regions might play a substantial role in the biological mode of action of the compounds moc-epoxide (**8**) and niphe-epoxide (**9**) - or generally of compounds incorporating methyl ester groups bonded to an epoxide ring - because they represent the main nucleophilic sites of the molecules. Oxygen atoms which do not lie in this belt-region are polarised much more positively and are therefore far less nucleophilic. This underlines the special arrangement of the ESP in these biologically active model compounds. It can best be seen for oxygen atom O3 in moc-epoxide (**8**) (Figures 12.4 (a) and (b)), but also holds for O5 in niphe-epoxide (**9**) (Figure 12.5 (b)). In contrast, the oxygen atoms O1 in the epoxide rings are involved in the negative belt region.

The Hirshfeld representation of moc-epoxide (**8**) (Figure 12.4 (c)) additionally shows an accumulation of interactions in a region corresponding to the belt-region in the ESP with oxygen atoms O1, O2, O4, O5. Oxygen atom O3, which is polarised less negatively and therefore not included in the belt region, actually forms only one weak contact in contrast to the other oxygen atoms. This confirms that intermolecular interactions mainly take place in the belt-region, which can therefore be referred to as the active region. Epoxide oxygen atom O1 is involved in intermolecular interactions, as displayed on the Hirshfeld surface, as there is a large region of ED above O1. But no hydrogen bond to O1 could be localised by means of a bcp, see Tables 12.2 and A.101 to A.104.

In niphe-epoxide (**9**), the interactions are spread more widely on the Hirshfeld surface (12.5 (c)), which is related to the fact that there are additional nucleophilic sites at the nitro group, which is not biologically active regarding protease inhibition. Oxygen atom O1 in the epoxide ring is not an acceptor for an intermolecular interaction. The search for electrophilic and nucleophilic sites within niphe-epoxide (**9**) compared to aziridine and olefin analoga was the topic of another study that was carried out during the time of this doctoral research. The results were published in Ref. [99,100] and will be summarised in the Chapter "Additional Studies".

Table 12.3: Lattice energies of cpds. **7** to **10** in kJ mol^{-1}

First row: experiment, second row: periodic-boundary calculations at experimental geometries, third row: periodic-boundary calculations at optimised geometries, contributions of exchange+repulsion+dispersion terms (erd, absolute) and of the electrostatic term (es, absolute and relative) to the total lattice energy

cpd.	total	erd	es	es(%)
etox (**7**)	-51.24	-16.75	-34.49	67.3
	-50.41	-16.75	-33.66	66.8
	-46.53	-16.57	-29.95	64.4
moc-epoxide (**8**)	-114.83	-36.04	-78.80	68.6
molecule 1	-94.29	-38.31	-55.98	59.4
	-119.02	-36.00	-83.02	69.8
moc-epoxide (**8**)	-97.76	-38.28	-59.49	60.9
molecule 2	-90.48	-36.37	-54.11	59.8
	-96.82	-37.38	-59.44	61.4
niphe-epoxide (**9**)	-192.13	-89.32	-102.81	53.5
	-205.59	-92.45	-113.15	55.0
	-183.48	-88.29	-95.19	51.9
cyano-epoxide (**10**)	-101.17	-31.34	-69.83	69.0
	-128.86	-31.34	-97.51	75.7
	-102.72	-24.09	-78.64	76.6

Lattice energies of cpds. **7** to **10** are listed in Table 12.3. Etox (**7**) exhibits the weakest crystal lattice whereas niphe-epoxide (**9**) exhibits the strongest. In all compounds, electrostatic contributions dominate the crystal packing, but in niphe-epoxide (**9**) they are only slightly larger than 50 % because absolute values of the exchange-repulsion-dispersion term are much larger for niphe-epoxide (**9**) than for the other compounds. It is also evident from Table 12.3 that geometry optimisation within periodic boundaries does not yield the maximum of the negative lattice energy. There is no trend in Table 12.3 which method gives highest or lowest energies.

12.1.3 Interactions with Selected Donor Molecules

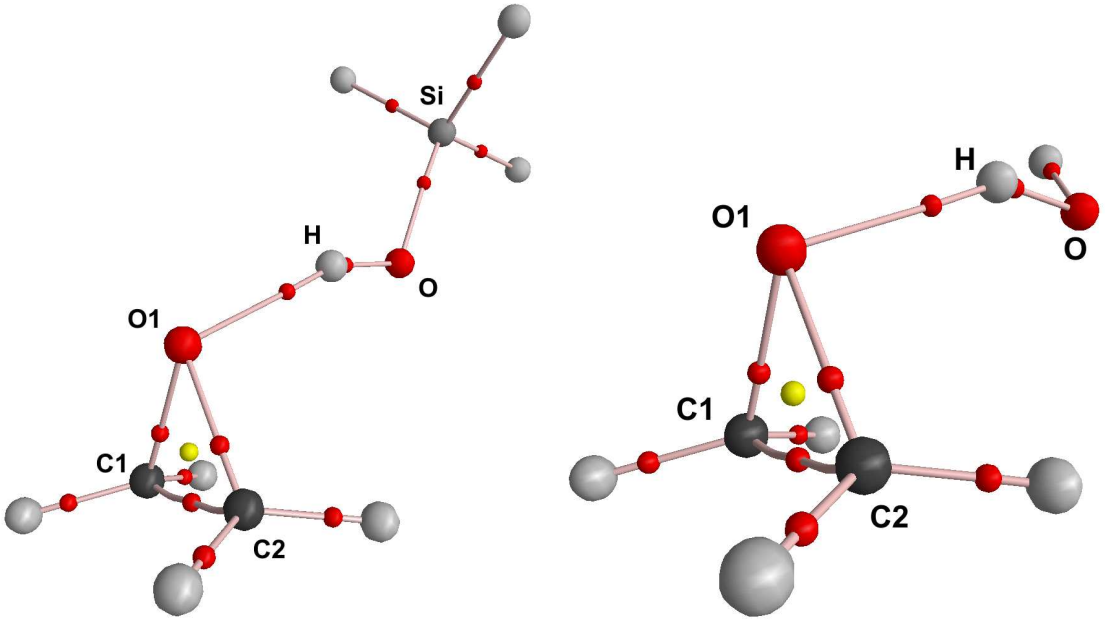

(a) Etox···silanol HB complex (**7s**) (b) Etox···water HB complex (**7w**)

Figure 12.6: Molecular graphs of hydrogen-bonded (HB) complexes of etox (**7**) with silanol (s) and water (w)
Obtained from isolated-molecule geometry optimisation

Geometry optimisations on hydrogen-bonded complexes of etox (**7**) - the epoxide without EWGs - and cyano-epoxide (**10**) - the epoxide affected most by the EWGs - were carried out with silanol and water as donor molecules. Complexes of etox (**7**) converged without problems, the resulting molecular graphs are shown in Figure 12.6. In contrast, it was very difficult to obtain converged structures of complexes of cyano-epoxide (**10**). Different start geometries were tested, but in every case the donor group moved away from the epoxide oxygen atom to interact with the cyano groups. Finally, converged structures were obtained in which no hydrogen bond with the epoxide oxygen atom but several contacts with the cyano groups existed. It can therefore be concluded that EWGs reduce the basicity of the epoxide oxygen atom in a way that hydrogen bonding with the epoxide oxygen as an acceptor is no longer preferred. This explains why no hydrogen bonds with oxygen atom O1 as the acceptor could be found in the crystal structures of cpds. **8** to **10**.
In the following, the results for hydrogen-bonded complexes of etox (**7**) will be discussed. In Table 12.4, selected properties of epoxide···silanol/water (**7s**/**7w**)

Table 12.4: Selected properties of etox···silanol/water hydrogen bonds (**7s**/**7w**) compared to disilaepoxide and dimethylether as acceptors
Angles a in °, distances d in Å, ED ϱ(bcp) in e Å^{-3}, Laplacian of ED $\nabla^2\varrho$(bcp) in e Å^{-5}, hydrogen-bond energy E_{HB} in kJ mol^{-1}, IR red shift $\Delta\tilde{\nu}(OH)$ in cm^{-1}

d(H···O)	d(O···O)	a(O-H···O)	ϱ(H···O)	$\nabla^2\varrho$(H···O)	E_{HB}	$\Delta\tilde{\nu}(OH)$
etox···silanol HB complex (**7s**):						
1.823	2.761	160.83	0.23	2.3	-18.37	300.2
etox···water HB complex (**7w**):						(symm/asymm)
1.940	2.839	153.05	0.18	2.1	-10.02	135.9/31.3
disilaepoxide···silanol:						
1.836	2.807	179.67	0.21	2.2	-18.92	257.1
disilaepoxide···water:						(symm/asymm)
2.058	2.747	126.56	0.14	2.1	-8.76	68.2/33.2
dimethylether···silanol at τ=65 °:						
1.788	2.740	163.34	0.26	2.3	-23.83	412.1
dimethylether···water at τ=65 °:						(symm/asymm)
1.917	2.835	156.13	0.20	2.1	-14.56	202.6/34.3
dimethylether···silanol at τ=110 °:						
1.814	2.787	179.88	0.23	2.2	-18.20	287.8
dimethylether···water at τ=110 °:						(symm/asymm)
1.907	2.877	178.00	0.19	2.0	-10.64	129.4/34.8

hydrogen bonds are compared with corresponding bonds in disilaepoxide (values from Chapter 6.4) and in dimethylether at the smallest angle (τ=65 °) and near the tetrahedral angle (τ=110 °) (see Chapter 9.1.1). Hydrogen bonds with epoxide as the acceptor are not generally stronger than those with disilaepoxide as the acceptor. Considering silanol as the donor, d(H...O), ϱ(H···O), $\nabla^2\varrho$(H···O), and E_{HB} are nearly identical. For water as the donor, epoxide is a slightly better acceptor. The fact that the C–O–C linkage is not a better hydrogen-bond acceptor than the Si–O–Si linkage at strained angles is not surprising because this was already discovered concernig the PES scans of disiloxane and dimethylether (Chapter 9.1.1, especially Figure 9.2).

Hydrogen bonds with disilaepoxide as the acceptor (about ϕ=80 °) are as strong as hydrogen bonds with disiloxane as the acceptor at larger angles (about ϕ=100 °), see Chapter 6.4. The same can be found here for epoxide (τ=60 °) as the acceptor compared with dimethylether. At τ=65 °, the hydrogen bonds of dimethylether are much stronger than the ones of epoxide. The differences in the hydrogen-bond energies are about 5 kJ mol^{-1}. On the other hand, the properties indicating the

hydrogen-bond strength are nearly identical for epoxide as acceptor compared with dimethylether at τ=110 °.
Thus, it can be concluded in general for Si–O–Si and for C–O–C linkages that the basicity of the oxygen atom is lowered significantly by ring formation from H_3XOXH_3 to H_2XOXH_2 at the same X–O–X angles. Moreover, substitution with electron-withdrawing groups also lowers the basicity significantly, so that the oxygen atom is no longer competitive to alternative acceptors.

12.2 Results of the Topological Analysis of the ED

12.2.1 Deformation Density and Laplacian

The description of the bond strain in the epoxide ring is the most important aspect of this chapter. Competing MO models were described in Chapter 4.2 that suggest different locations of ED concentration (exclusively outside the bond axes: Förster-Coulson-Moffitt model; major concentration in the middle of the ring and minor concentrations outside the bond axes: Walsh model). The first approach to answer this questions in terms of the ED is the consideration of deformation-density and Laplacian maps in the plane of the epoxide ring as shown in Figure 12.7. The maxima of the deformation density and the VSCCs in the Laplacian maps are located clearly outside the bond axes for both C–O and C–C bonds, and there are no maxima inside the ring. This favours the description of bent bonds (banana bonds) according to the Förster-Coulson-Moffitt model, which was also found for cyclopropane before [186–189].
However, the maps in the epoxide plane show noticeable but not general differences comparing the different compounds. In Figure 12.7, the most differing experimental maps are shown. The maps of the three symmetrically substituted compounds **7**, **8** and **10** are similar, they resemble the maps of moc-epoxide (**8**) given in Figures 12.7 (a) and (c). One lobe of the oxygen lone pairs is visible in both the deformation density and the Laplacian. There are less isocontour lines for the C–O bonds than for the C–C bond, for which the maximum in the deformation density is elongated between the two carbon atoms. The shape of the maps is not different between etox (**7**) without EWGs and cyano-epoxide (**10**) with the most powerful electron-withdrawing pattern, but the number of isocontour lines is lower

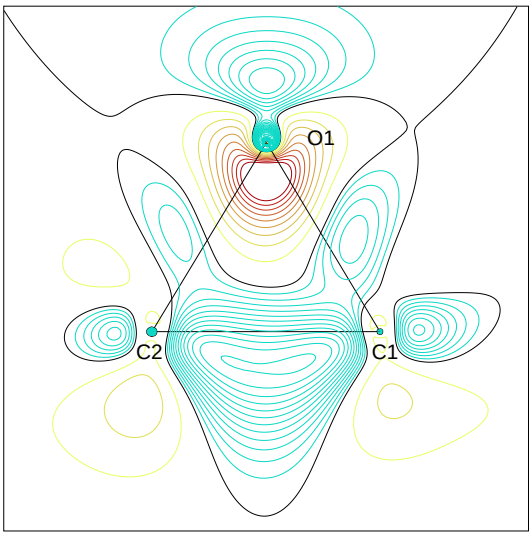

(a) Deformation density of moc-epoxide (**8**), contour interval = 0.025 e Å^{-3}

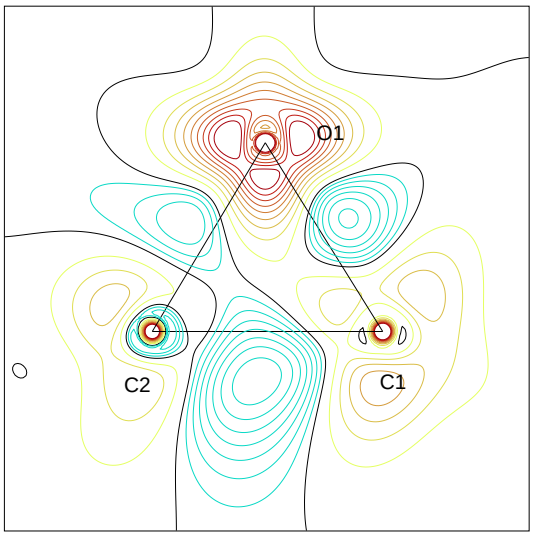

(b) Deformation density of niphe-epoxide (**9**), contour interval = 0.04 e Å^{-3}

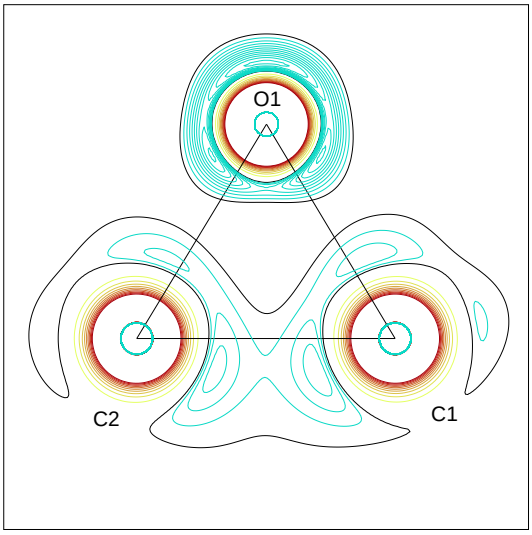

(c) Laplacian of moc-epoxide (**8**), contour interval = 7 e Å^{-5}

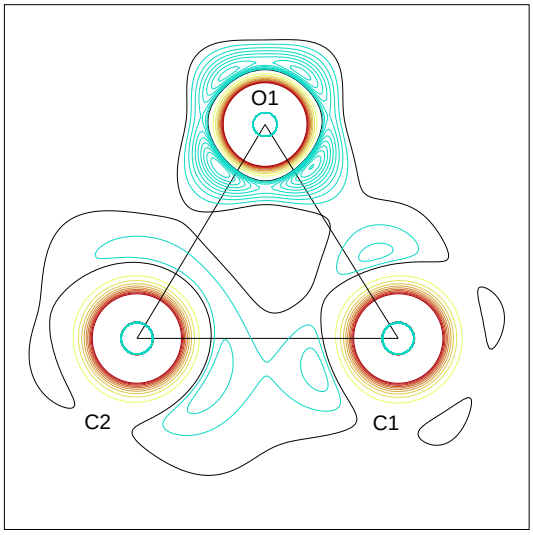

(d) Laplacian of niphe-epoxide (**9**), contour interval = 9 e Å^{-5}

Figure 12.7: Experimental static deformation-density and Laplacian-distribution maps in planes of the epoxide ring

Deformation-density maps: blue = positive, red = negative, black = zero; Laplacian-distribution maps: blue = negative, red = positive, black = zero

for the C–C bond in cyano-epoxide (**10**) yet higher for the C–O bonds.
For unsymmetrically substituted niphe-epoxide (**9**) (Figures 12.7 (b) and (d)), the maps reflect the asymmetry. The bond C2–O1 seems to be weaker and more ionic than C1–O1, C2 carries two EWGs whereas C1 carries only one EWG. Maxima in the deformation density are rather spherical compared to compounds **7**, **8** and **10**. There is no lobe of the oxygen lone pairs visible in the deformation density, but the region of negative deformation density is much more pronounced. In contrast, two lobes can be found in the Laplacian map. These phenomenological differences remain if corresponding maps from a modelling of theoretical structure factors are compared.

The three-dimensional representations of deformation density and Laplacian in the epoxide ring as shown in Figure 12.8 confirm that the maxima of the deformation density and the VSCCs are located outside the bond axes indicating bent-bond character. But a major difference can be found for the oxygen lone pairs. For etox (**7**) (Figures 12.8 (a) and (b)), the typical cap-like shape of deformation density and VSCCs resembles the shape found for disilaepoxide (Figure 6.25). It was discussed above that both epoxide and disilaepoxide are able to form hydrogen bonds of considerable strengths as acceptors.
It was also shown that the ability to form hydrogen bonds is reduced upon substitution with EWGs. In the crystal structure of niphe-epoxide (**9**), there is no hydrogen bond to epoxide oxygen O1. Therefore, the shape of the oxygen lone pairs in terms of deformation density and Laplacian (Figures 12.8 (c) and (d)) is fundamentally different from the typical cap-like shape in systems that form hydrogen bonds. There are two separate lobes of the two lone pairs in deformation density and Laplacian that do not merge even at much smaller isovalues. This means that there is no central concentration of electrons above the oxygen atom that was found to be crucial to forming hydrogen bonds. Even if there is not one symmetrical hydrogen-bonded complex but an asymmetrical one containing one or more hydrogen bonds, a cap-like shape was always found in this doctoral work (compare for example deformation density and Laplacian of trisilo (**2**) that exhibits two hydrogen bonds as the acceptor in the crystal structure, Figures 7.7 (a) and (b)).
However, the cases of an asymmetrical hydrogen-bonded complex were not considered in detail in this work. To completely rule out the possibility that systems like niphe-epoxide (**9**) could generally form hydrogen bonds would necessitate a

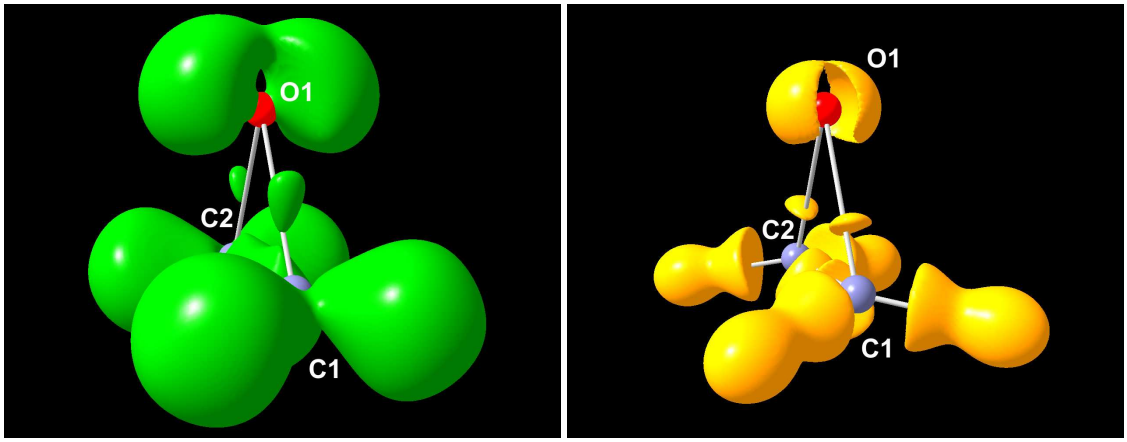

(a) Deformation density of etox (**7**), isovalue=0.085

(b) Laplacian of etox (**7**), isovalues = -73.0 around oxygen atoms and -13.0 around carbon atoms

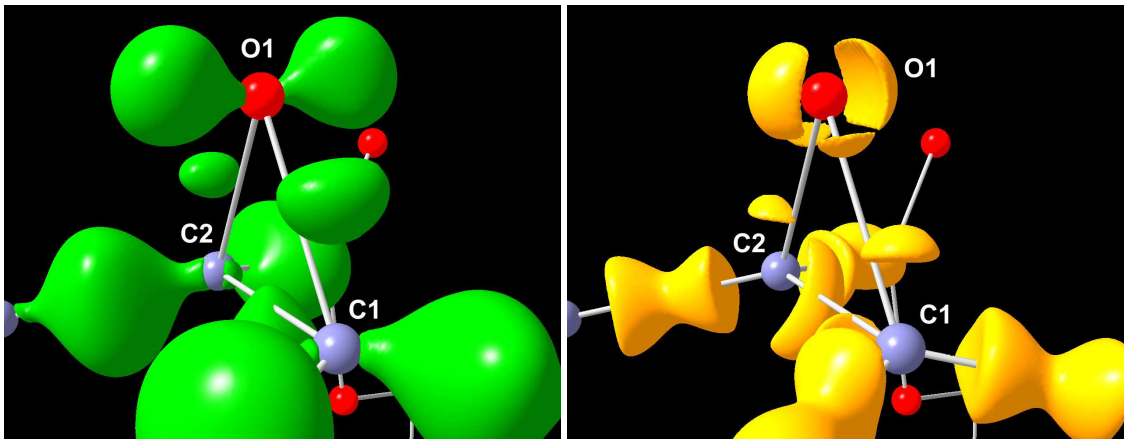

(c) Deformation density of niphe-epoxide (**9**), isovalue = 0.130

(d) Laplacian of niphe-epoxide (**9**), isovalues = -78.0 around oxygen atoms and -13.0 around carbon atoms

Figure 12.8: Three-dimensional isosurface representations of the static deformation density and the Laplacian of the epoxide ring in etox (**7**) and niphe-epoxide (**9**) *Periodic-boundary calculations at experimental geometry, deformation density in* $e\text{Å}^{-3}$*, Laplacian in* $e\text{Å}^{-5}$

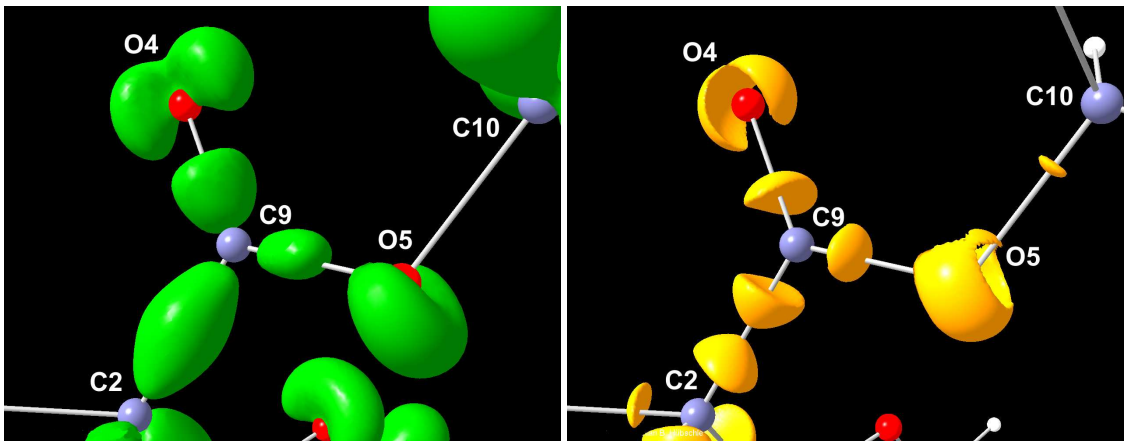

(a) Deformation density, isovalue = 0.250

(b) Laplacian, isovalues = -80.0 around oxygen atoms and -15.0 around carbon atoms

Figure 12.9: Three-dimensional isosurface representations of the static deformation density and the Laplacian of one of the ester groups in niphe-epoxide (**9**)
Periodic-boundary calculations at experimental geometry, deformation density in $e\text{Å}^{-3}$*, Laplacian in* $e\text{Å}^{-5}$

systematic study like PES scans on the aforementioned systems. Moreover, it might be possible that the lone pairs in niphe-epoxide (**9**) merge to form a symmetrical hydrogen-bonded complex if a donor of considerable strength is present despite the electron-withdrawing substitution pattern. However, the fact that no hydrogen bonds are formed in the studied case in combination with the shape of the lone pairs agrees with the considerations made for other systems.
Figure 12.9 shows the electronic situation in one of the ester groups of niphe-epoxide (**9**). Oxygen atom O5 is situated in an open C–O–C linkage of τ=116.67(5) °. The shape of deformation density and VSCCs is the same as for oxygen atoms in dimethylether (H_3C–O–CH_3) or sucrose ((O)C–O–C and (O_2)C–O–C). For O4 in the carbonyl group, the shapes of the lone pairs rather resemble the ones of O1 in etox (**7**) (Figures 12.8 (a) and (b)) than in the open C–O–C linkage. The individual lobes of the two lone pairs are more pronounced. However, O1 in etox (**7**) as well as O4 and O5 in niphe-epoxide (**9**) form C–H$\cdots$O hydrogen bonds in their crystal lattices.

12.2.2 Bond-Path Analyses and Gradient-Vector Fields

Bent-bond character was indicated by maxima in the deformation density located outside the bond axes, see above. Considering the total electron density, the situation is not that simple. For the C–C bond, the sum of d1 and d2 (distances from the atoms to the bcp) is larger than the bond distance, showing that the bond is bent in a way that the bcp is not located on the internuclear axis. But for the C–O bonds, the sum of d1 and d2 exactly yields the bond distance. This means that the bcp must be located directly on the internuclear axis.

However, a bond-path analysis reveals that the bond path of the C–O bonds is nevertheless longer than the C–O bond distance, the difference ranges from 0.001 Å to 0.014 Å within the different compounds and methods, see Table 12.5. In the preceding chapters, a difference of 0.001 Å and larger was referred to as being indicative of a slightly bent bond, a difference of 0.010 Å and larger was found to be indicative of a significantly bent bond. If the bcps of the C–O bonds are located directly on the internuclear axis but the bond path is nevertheless longer than the bond distance, a S- or W-type shape of the bond must be the reason. Figure 12.10 shows the S-type shapes of the C–O bond paths within the epoxide ring. From O1 to the bcp, the bond is curved outwards, whereas it is curved inwards from C1 to the bcp.

Figure 12.10 (a) shows the epoxide ring for the experimental case of etox (**7**) where the effect is most pronounced (diff = 0.014 and 0.012 Å, see Table 12.5), whereas Figure 12.10 (b) shows the epoxide ring for the theoretical case (optimised geometry from periodic-boundary calculation) of cyano-epoxide (**10**) (diff = 0.002 and 0.001 Å) where the effect is weakest but nonetheless existent. As Table 12.5 shows, the C–O bonds are generally more bent in the experiment than in theory, including isolated-molecule calculations. However, C–O bonds therefore cannot be referred to as banana bonds with respect to their bond paths that exhibit S-type shape. Valence density accumulates and concentrates outside the bond axes as shown by deformation density and Laplacian, see above, but the maxima of the total electron density are not shifted away perpendicular to the bond axes.

In contrast to the C–O bonds, the C–C bond in the epoxide ring is bent in the shape of a banana bond as the deformation density suggests. The bcp of the C–C bond is located outside the bond axis, Figure 12.10 exemplifies this fact. The differences between the length of the bond path and the bond distance range from 0.007 to 0.023 Å and are therefore on average larger than for the C–O bonds.

Table 12.5: Lengths of bond paths (bp), bond distances (dist) and differences (diff) between bp and diff in the epoxide rings of cpds. **7** to **10**
Exp = experimental, per SP/opt = periodic-boundary calculations at experimental/optimised geometry, isol SP/opt = isolated-molecule calculations at experimental/optimised geometry

bond	method	dist	bp	diff	dist	bp	diff
		etox (**7**)			moc-epoxide (**8**)		
C1–O1	exp	1.434	1.448	0.014	1.424	1.427	0.003
	per SP	1.434	1.437	0.003	1.424	1.426	0.002
	per opt	1.449	1.453	0.004	1.431	1.433	0.002
	isol SP	1.434	1.436	0.002	1.424	1.426	0.002
	isol opt	1.428	1.430	0.002	1.416	1.418	0.002
C2–O1	exp	1.441	1.453	0.012	1.427	1.431	0.004
	per SP	1.441	1.444	0.003	1.427	1.430	0.003
	per opt	1.454	1.457	0.003	1.434	1.437	0.003
	isol SP	1.441	1.443	0.002	1.427	1.429	0.002
	isol opt	1.428	1.429	0.001	1.416	1.418	0.002
C1–C2	exp	1.457	1.467	0.010	1.472	1.481	0.009
	cryst SP	1.457	1.471	0.014	1.472	1.480	0.008
	cryst opt	1.468	1.481	0.013	1.477	1.490	0.013
	isol SP	1.457	1.472	0.015	1.472	1.485	0.013
	isol opt	1.464	1.479	0.015	1.479	1.492	0.013
		niphe-epoxide (**9**)			cyano-epoxide (**10**)		
C1–O1	exp	1.435	1.446	0.011	1.426	1.427	0.001
	per SP	1.435	1.438	0.003	1.426	1.427	0.001
	per opt	1.436	1.438	0.002	1.433	1.435	0.002
	isol SP	1.435	1.437	0.002	1.426	1.427	0.001
	isol opt	1.426	1.427	0.001	1.423	1.426	0.003
C2–O1	exp	1.420	1.423	0.003	1.422	1.423	0.001
	per SP	1.420	1.424	0.004	1.422	1.423	0.001
	per opt	1.428	1.430	0.002	1.429	1.430	0.001
	isol SP	1.420	1.422	0.002	1.422	1.423	0.001
	isol opt	1.426	1.427	0.001	1.424	1.426	0.002
C1–C2	exp	1.488	1.511	0.023	1.499	1.507	0.008
	per SP	1.488	1.498	0.010	1.499	1.506	0.007
	per opt	1.497	1.507	0.010	1.519	1.527	0.008
	isol SP	1.488	1.502	0.014	1.499	1.512	0.013
	isol opt	1.486	1.500	0.014	1.517	1.531	0.014

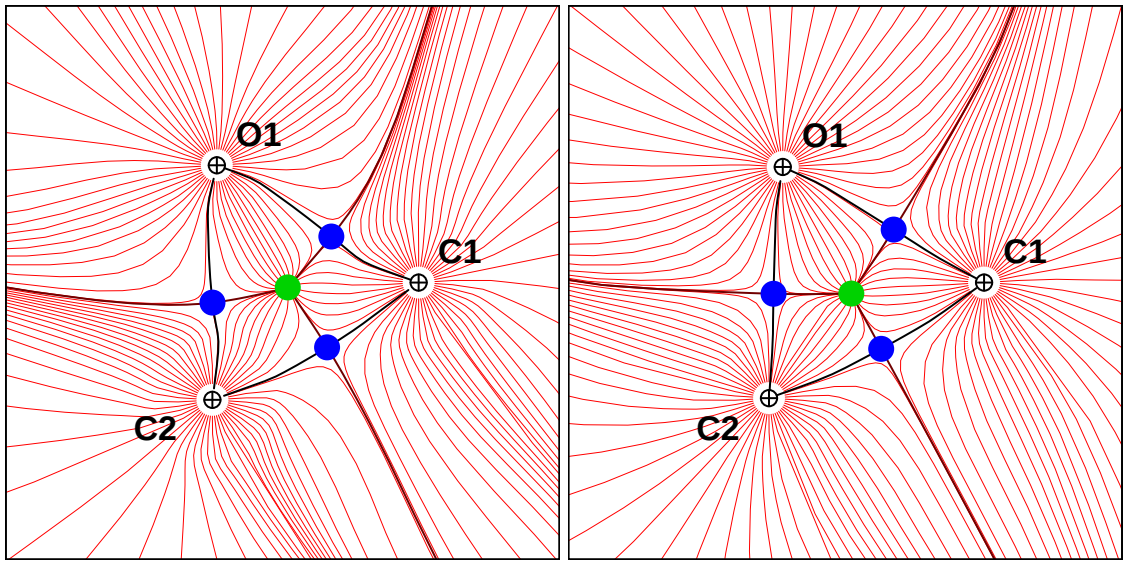

(a) Experimental case for etox (**7**)

(b) Periodic-boundary calculation at optimised geometry for cyano-epoxide (**10**)

Figure 12.10: Gradient-vector fields and molecular graphs in the plane of the epoxide ring of etox (**7**) and cyano-epoxide (**10**)

Moreover, the bending of the C–C bond is also significant within the theoretical methods, which is not the case for C–O bonds. In the case of the isolated molecule, the difference is larger than for periodic boundaries.

12.2.3 Bond-Topological Properties

Electron density and Laplacian at the bcps of C–O and C–C bonds in the epoxide rings as well as the bcps to the substituents are plotted in Figure 12.11. Comparisons between the four different compounds, but also between the five different methods employed can be drawn from these plots. Corresponding values are given in Tables A.105 to A.110. The most important chemical effect concerns the bond C1–C2. According to the lengthening of this bond from etox (**7**) to cyano-epoxide (**10**), which was explained by resonance formulae and increasing number and power of electron-withdrawing groups (EWGs), the values of the ED at the C1–C2 bcps as well as the negative Laplacian decrease, Figure 12.11 (a), right block. The effect is clearly visible, for example, in the isolated-molecule calculations at experimental geometry. The ED decreases from 1.81 $e Å^{-3}$ (etox,7) over 1.73 $e Å^{-3}$ (moc-epoxide,8) and 1.68 $e Å^{-3}$ (niphe-epoxide,9) to 1.65 $e Å^{-3}$ (cyano-epoxide,10).

Corresponding values for the Laplacian are -16.7 eÅ^{-5}, -14.6 eÅ^{-5}, -13.2 eÅ^{-5} and -12.4 eÅ^{-5}.

Besides this expected chemical effect for C1–C2, the most striking feature in Figure 12.11 (a) is that the differences between the methods are larger than the differences between the compounds. Whereas the agreement between the methods is in a typical range for the ED (smaller than 0.1 eÅ^{-3}, [247]), the differences are large in the Laplacian. The two values from periodic-boundary calculations are close to each other, which also holds true for the two values from isolated-molecule calculations, but the differences between these theoretical methods are on average larger than 5 eÅ^{-5}, which is more than typically found between different methods. [247] The negative Laplacian values from isolated-molecule calculations are significantly larger than the ones from modelling of theoretical structure factors. This is due to the so-called λ_3-effect discovered by Volkov et al. [252] In most cases, the experimental value is closer to the theoretical values considering periodic boundaries. But in some cases, see C1–O1,9 and C2–O1,7, the experiment exhibits severe outliers. In general, the value of the ED at the C–O bcps ranges from 1.61 eÅ^{-3} to 1.80 eÅ^{-3} in all methods. The Laplacian covers a range of 14.8 eÅ^{-5} from -1.8 eÅ^{-5} to -16.6 eÅ^{-5}.

The strained situation of the epoxide ring cannot be detected in the values of the ED and the Laplacian at the C–O and C–C bcps. The range of values covered by these bonds is the same as can be found for C–O bonds in open C–O–C linkages (compare butoxysilanol (**5**) and sucrose (**6**), Table 10.4) or non-strained C–C bonds as given for example in Figure 12.11 (b). The bond strain is reflected in the values of the ellipticity at the bcps. For non-strained C–O and C–C single bonds, the values are close to zero, compare again Table 10.4. For C–O and C–C bonds in epoxide, the values are significantly larger, indicating bent single bonds. They vary strongly between 0.21 and 0.73, see Tables A.105 to A.110.

Concerning Figure 12.11 (b) (bond-topological properties of bonds from C1 and C2 to the substituents), it must be noted that the order of the presented values is different than in Figure 12.11 (a). Here, all bonds to the four substituents within one compound are compared within one block and not the same bond within different compounds. The values of the ED at C–H bcps are higher than for C–C bonds and the Laplacian is generally more negative. There is an obvious trend in the values of the C–H bonds concerning a comparison of the different methods. The ED and the negative Laplacian are lowest in the experiment and continuously increase towards geometry optimisation of the isolated molecule. The range covers about

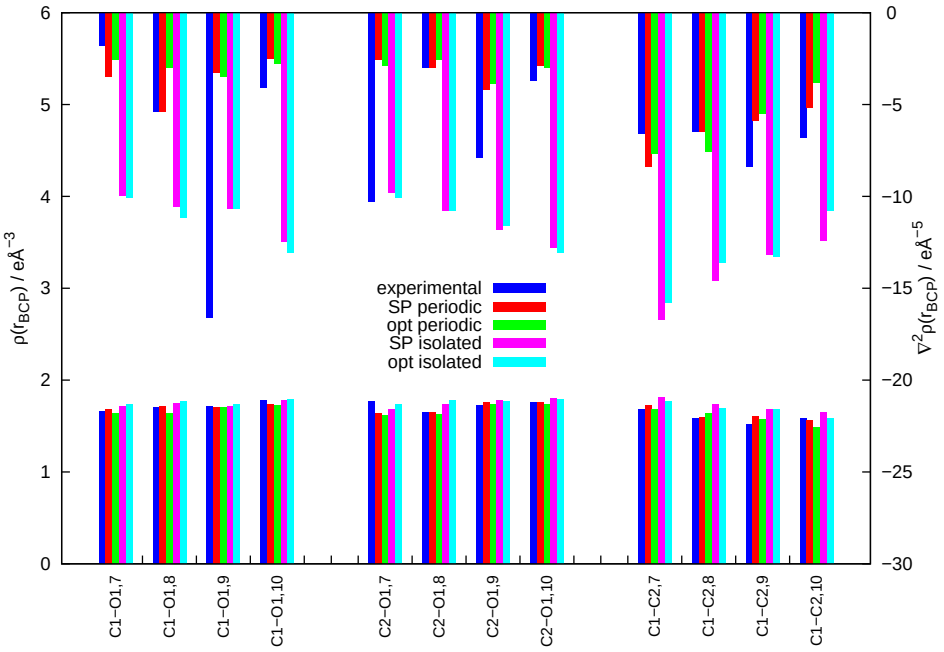

(a) Bonds within the epoxide rings

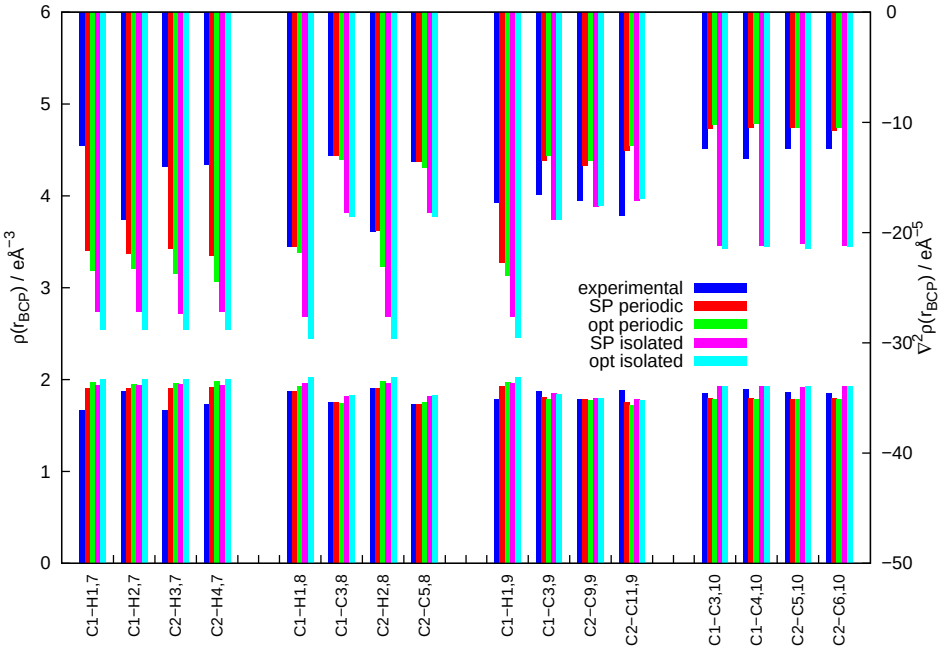

(b) Bonds to substituents

Figure 12.11: Bond-topological properties of cpds. **7** to **10**

Bars pointing from bottom to top refer to ED values ϱ(bcp) (left y-axis), bars from top to bottom refer to the Laplacian $\nabla^2\varrho$(bcp) (right y-axis), labelling 7 to 10 refers to cpds. **7** *to* **10**, *experimental, SP/ opt periodic = periodic-boundary calculations at experimental/ optimised geometry, SP/ opt isolated = isolated-molecule calculations at experimental/optimised geometry*

$0.3\,e\text{Å}^{-3}$ and $15\,e\text{Å}^{-5}$. The trend is the expected one as restrictions originating from the experiment, namely experimental geometry and periodic boundaries, are released one after the other in the ansatz of the theoretical calculations towards optimisation of the isolated molecule.

For C–C bonds, the same is found as for C–C and C–O bonds within the epoxide ring: ED and Laplacian values of the two theoretical methods including periodic boundaries are very similar, but strongly deviate from the values of the two isolated-molecule calculations, which themselves are very similar to each other (λ_3-effect). As expected, the experimental value is in general close to the values obtained from periodic-boundary calculations. But for niphe-epoxide (**9**), there are outliers again.

On the basis of a shortening of the C–C bonds to the EWGs due to partial double-bond character (compare resonance formulae in Figure 4.4), the ED at the C–C bcps should increase with the strength of the electron-withdrawing power of the EWG. For isolated-molecule calculations, this effect can indeed be observed. The average value for the four C–C bonds to methyl ester groups (C1–C3,8; C2–C5,8; C2–C9,9; C2–C11,9) for isolated-molecule calculations at experimental geometry is $1.81(2)\,e\text{Å}^{-3}$. It increases to $1.85\,e\text{Å}^{-3}$ for the nitro-phenyl group (C1–C3,9) and an average value of $1.93(1)\,e\text{Å}^{-3}$ for the four cyano groups in cyano-epoxide (**10**). The Laplacian behaves in the same way. Its negative value increases from -17.8(5) $e\text{Å}^{-5}$ to -18.8 $e\text{Å}^{-5}$ and -21.2(1) $e\text{Å}^{-5}$. However, the description of the cyano groups in experiment and periodic-boundary calculations is different, the trend is not visible or even reversed. In summary, electron-withdrawing power of the substituents in the row methyl ester, nitro-phenyl and cyano can be detected. But due to the fact that the differences between different methods are larger than between different compounds or substituents, this finding must be considered with care.

12.2.4 Atomic Properties

Atomic properties for the atoms in the epoxide ring and the directly bonded hydrogen and carbon atoms of the substituents are again shown by means of bar charts in Figure 12.12. Similar findings concerning chemical effects as made for the bond-topological properties can be made for the atomic properties, but the effects are more significant here and the trends clearer. The reason is that the variation of the values Q and V_{001} within the different methods is much smaller

than for the Laplacian. A continuous increase or decrease of the values from the experiment towards results from isolated-molecule optimisations as expected from a continuous release of restrictions in the ansatz of the calculations is generally observed in most of the atomic properties here, which was only true for C–H bonds in the preceding chapter.

Oxygen atoms in the epoxide rings are negatively charged by -0.53 to -0.89 e, their volumes V_{001} range from 14.1 to 16.7 Å^3. For carbon atoms, corresponding values are Q = 0.15 to 0.61 e and V_{001} = 6.0 to 10.7 Å^3. If only results from periodic-boundary calculations at experimental geometries are considered (see Tables A.111 to A.114) to compare with the results from butoxysilanol (**5**) and sucrose (**6**), Table 10.5, for which no other methods were employed, the following can be found: The charges of the oxygen atoms are smaller, but the volumes are larger than in Si–O–C and C–O–C in sucrose (**6**). This suggests that there is a lot of space for the oxygen atom's basin due to the small C–O–C angle, but the charge separation with the carbon atoms is less pronounced. This is confirmed by the atomic properties of the carbon atoms. The volumes are again larger than in Si–O–C and C–O–C linkages, but the charges are in the same range.

Carbon atoms C1 and C2 in cyano-epoxide (**10**) are significantly more positive than in the other compounds because they are bonded to the most powerful EWGs. The expected trend that is caused by the electron-withdrawing power of the substituents can best be seen for the volumes of the C2 atoms. The largest volumes (about 10 Å^3) can be found for etox (**7**) without EWGs. It decreases to about V_{001}=8 Å^3 in moc-epoxide (**8**), in which C2 is bonded to one methyl ester group, and again decreases to about V_{001}=7 Å^3 in niphe-epoxide (**9**), where C2 is bonded to two methyl ester groups. Finally, V_{001} is about 6 Å^3 in cyano-epoxide (**10**). This effect is larger than the differences between the different methods.

Charges and volumes of hydrogen atoms are quite similar in cpds. **7** to **9**. But carbon atoms can be assigned unambiguously to the different substituents they belong to by means of their atomic properties, which holds for all methods because the chemical effects are much larger here than the differences between the different computational methods. Carbon atoms in methyl ester groups have the highest positive charge Q (1.62(2) e averaged across C3,8; C5,8; C9,9 and C11,9, periodic-boundary calculations at experimental geometry) and the smallest volume (V_{001}= 5.1(4) Å^3), which is due to the fact that they are bonded to two oxygen atoms. In contrast, carbon atom C3 in the nitro-phenyl group in niphe-epoxide (C3,9) is nearly neutral (0.01 e) or even negative in experiment and possesses a much

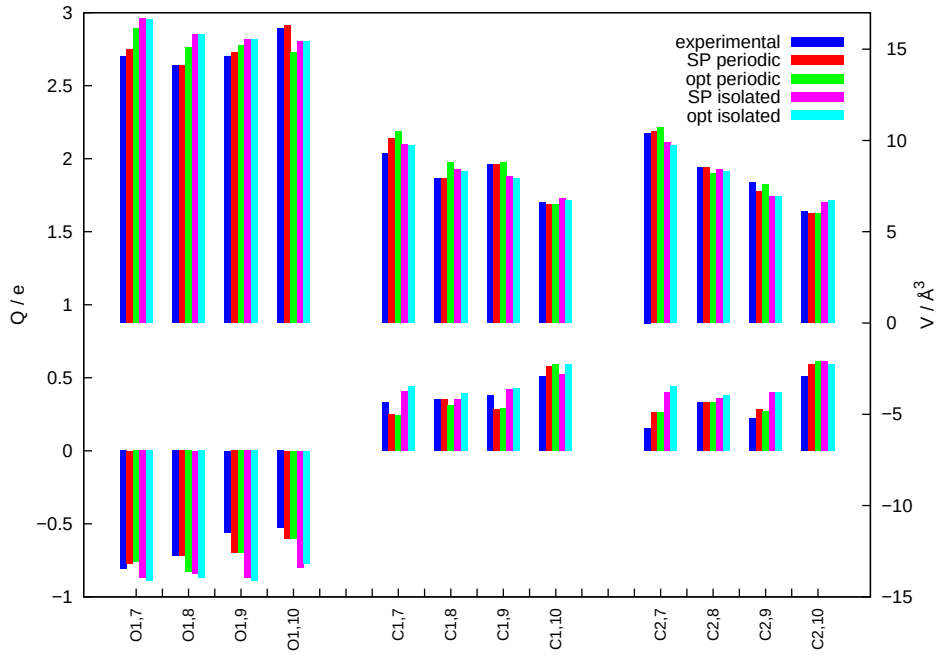

(a) Atoms in the epoxide rings

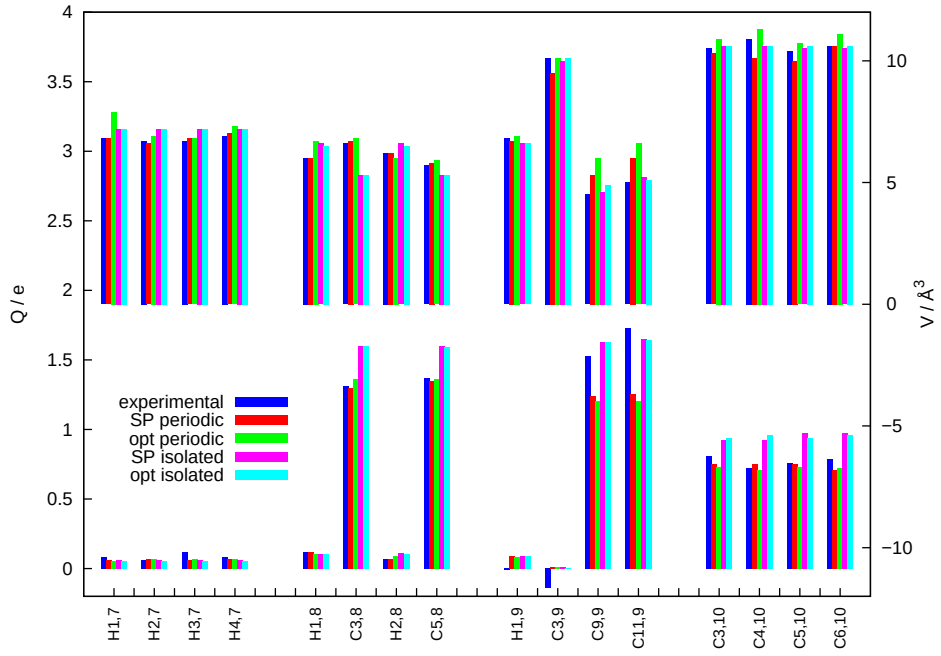

(b) Atoms in substituents that are directly bonded to the epoxide rings

Figure 12.12: Atomic properties of cpds. **7** to **10**

Bars in the lower half of each graphic refer to charges Q (left y-axis), bars in the upper half refer to volumes V_{001} (right y-axis), labelling 7 to 10 refers to cpds. **7** *to* **10**, *experimental, SP/ opt periodic = periodic-boundary calculations at experimental/ optimised geometry, SP/ opt isolated = isolated-molecule calculations at experimental/optimised geometry*

larger volume than the ester carbon atoms (10.0 Å^3). But the carbon atoms in the linear cyano groups in cyano-epoxide (**10**) have an even larger atomic volume (V_{001}= 10.6(1) Å^3 on average), although they are positively charged by nearly one electron (0.95(3) e). This is due to the fact that the number of adjacent atoms is smaller in the linear cyano group than in the other substituents. It was found recently that there is generally a linear relationship between the atomic volumes and the sum of the electronegativities of adjacent atoms. [253]

The total charge of the epoxide ring is significantly negative for etox (**7**) and significantly positive for cyano-epoxide (**10**) regardless of the method; moc-epoxide (**8**) and niphe-epoxide (**9**) range in-between . This again confirms the order of the electron-withdrawing power of the substituents. The effect is most pronounced for the experiment and least pronounced for the isolated-molecule calculations, compare Tables A.111 to A.114. In the experiment, the epoxide ring is charged by -0.33 e for etox (**7**) (unsubstituted), by -0.04 e for moc-epoxide (**8**) (two EWGs), by 0.04 e for niphe-epoxide (**9**) (three EWGs) and by 0.49 e for cyano-epoxide (**10**) (four EWGs).

12.2.5 Source Function

Relative source contributions to C–C and C–O bonds in the epoxide rings are represented in Figures 12.13 and 12.14. Results are given for experiment and both periodic-boundary calculations (experimental and optimised geometries). Absolute and relative source contributions for each atom are listed in Tables A.115 to A.118.

It was discussed in Chapter 10.2.5 that it is characteristic for C–O bonds that quite precisely 80 % of the density at the bcps is raised by the directly bonded atoms. In this respect, the bent C–O bonds in the epoxide rings do not behave differently from non-strained C–O bonds in butoxysilanol (**5**) (Si–O–C linkage) or sucrose (**6**) (C–O–C linkage). In the epoxide, the sum of contributions of directly bonded C and O atoms varies from 78.0 to 80.8 % (see Figure 12.13), which additionally means that the agreement between experiment and theory is high. The C–C bonds are more influenced by the substituents and therefore also more influenced by variation of the substituents than the C–O bonds (Figure 12.14). In etox (**7**), about 75 % of the density at the C1–C2 bcp originates from the directly bonded atoms. This contribution decreases upon substitution with methyl ester and nitro-phenyl groups. The sum of C1 and C2 contributions is about 69 % in

both moc-epoxide (**8**) and niphe-epoxide (**9**). In cyano-epoxide (**10**), the value significantly decreases again (about 65 %). This means that substituent effects cannot be detected by means of the source function in C–O bonds but in C–C bonds and again much better in Si–O bonds (see discussion in Chapter 10.2.5).

However, it is counterintuitive that the sum of the contributions of the directly bonded atoms (sum1) in the bond C1–C2 decreases if the number and the power of the EWGs is increased. The contribution of oxygen atom O1 in the epoxide ring increases by about 2 % from etox (**7**) towards cyano-epoxide (**10**), but this is not enough to explain the difference of about 10 % in sum1. So it must be stated as a paradox that in this example, the electron-donating power of substituents by means of the integrated source function increases (about 3.3 % for a hydrogen atom, 4.7 % for a methyl ester group, 5.3 % for the nitro-phenyl group and 5.1 % for a cyano group) if the electron-withdrawing power found thus far also increases. Since the electron-withdrawing capability of the substituents was confirmed by many different parameters in the preceding chapters, this paradox can only be explained with by fact that resonance effects are not reflected in the integrated source function. This was also found by Farrugia and Macchi recently. [138] They stated that "...when the reference point is close to the nodal plane of an orbital, this orbital makes a low to negligible contribution to the SF [source function], which has clear implications for the interpretation of π-interactions. This leads us to recommend caution in associating some chemical concepts with features of the SF..." As the epoxide ring is unsaturated and contains sp^2-like hybrid orbitals (MO model in chapter 4.2), the resonance formulae in Figure 4.4 can be explained with π-interactions. Therefore, resonance effects of substituents cannot be characterised by means of the integrated source function.

Considering the C–O bonds as reference points again (Figure 12.13), the difference between a carbon atom in the epoxide neighbouring the C–O bond and an oxygen atom neighbouring the C–C bond becomes clear. Oxygen is the better donor in terms of source contributions, its contributions are about twice as high. The contributions of the carbon atom decrease from about 8 % in etox (**7**) to 5,5 % in cyano-epoxide (**10**). The reason is that hydrogen atoms generally only provide 3.5 to 4.0 % if they are the nearest neighbours and 1.5 to 2.0 % if they are the next-nearest neighbours. Hence, carbon atom C2 in etox (**7**) must provide the difference. Each substituent (methyl ester, nitro-phenyl or cyano group, respectively) contributes about 5 to 6 % as the nearest neighbour and half of the amount as the next-nearest neighbour. So atom C2 in cyano-epoxide (**10**) must provide

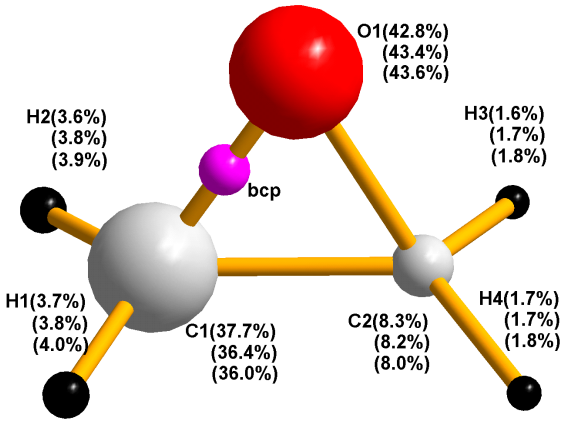

(a) Etox (**7**)

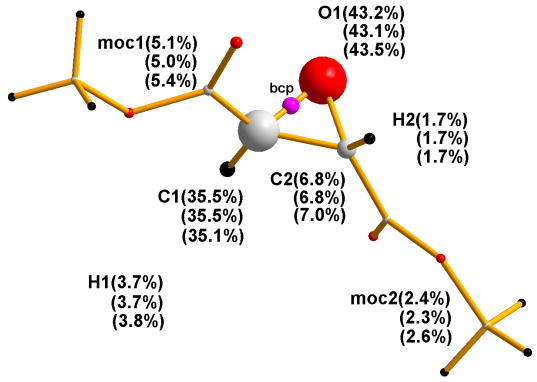

(b) Moc-epoxide (**8**)

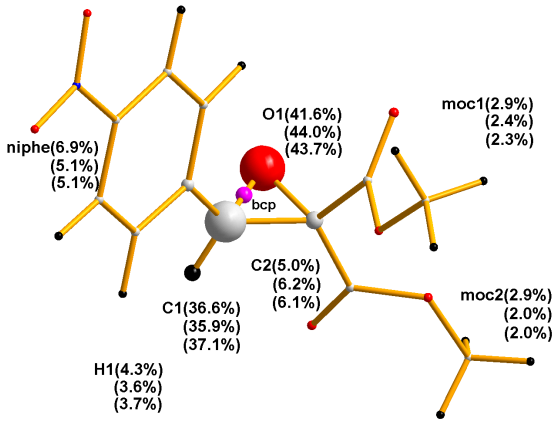

(c) Niphe-epoxide (**9**), C1–O1 bond

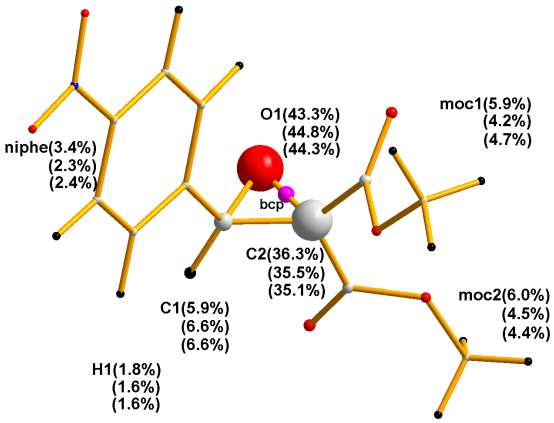

(d) Niphe-epoxide (**9**), C2–O1 bond

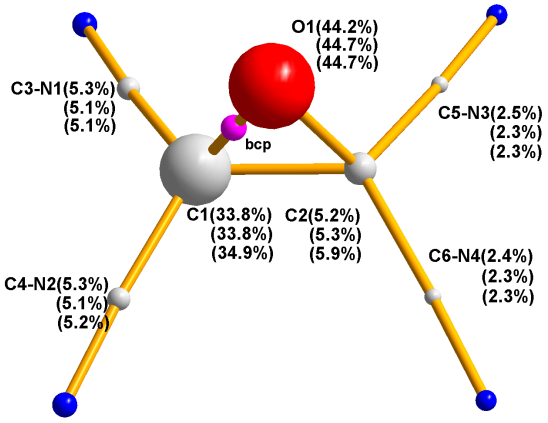

(e) Cyano-epoxide (**10**)

Figure 12.13: Relative atomic contributions to C–O bonds in the epoxide rings from the integrated source function of cpds. **7** to **10**

First value = experiment, second/third value = periodic-boundary calculations at experimental/optimised geometry, relative source contributions of the atoms to the plotted bcps are represented by the atom's radii, colour code only indicates atom type

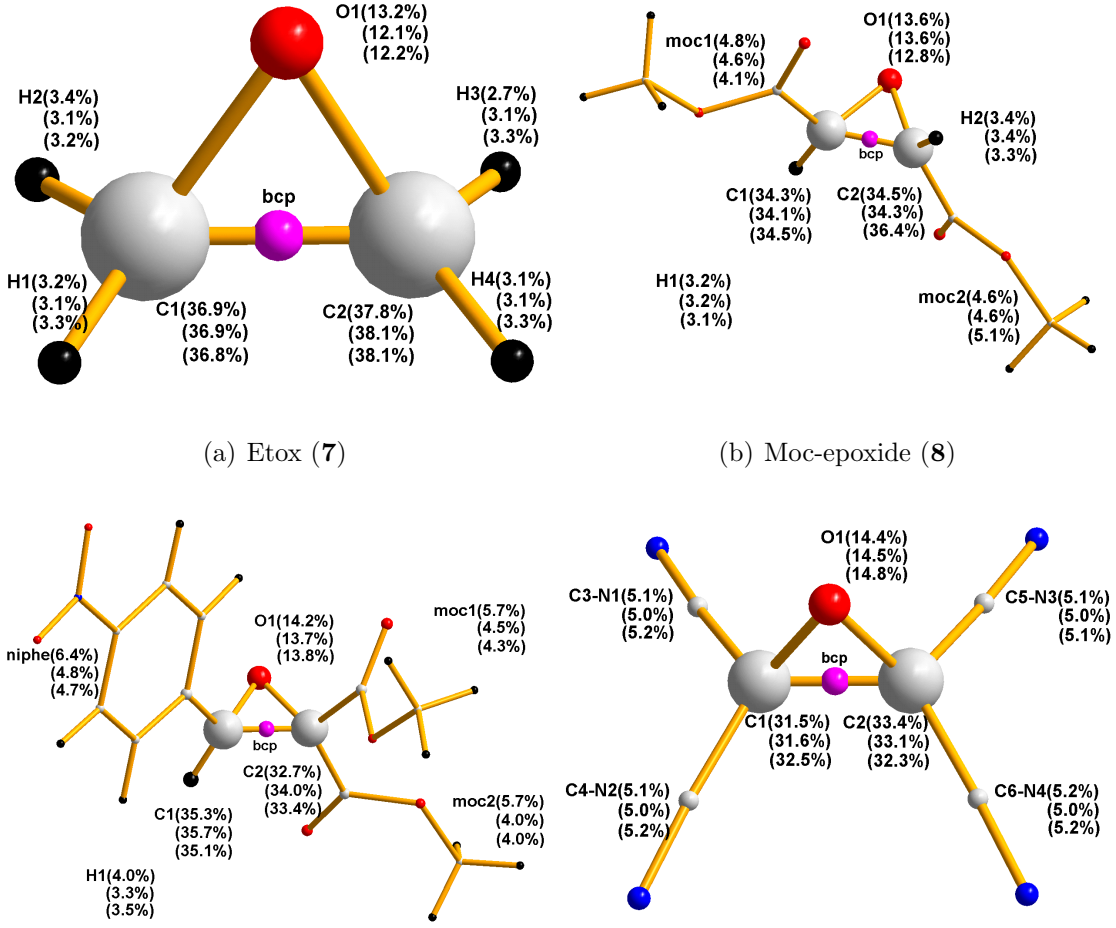

(a) Etox (**7**)

(b) Moc-epoxide (**8**)

(c) Niphe-epoxide (**9**)

(d) Cyano-epoxide (**10**)

Figure 12.14: Relative atomic contributions to C–C bonds in the epoxide rings from the integrated source function of cpds. **7** to **10**

First value = experiment, second/third value = periodic-boundary calculations at experimental/optimised geometry, relative source contributions of the atoms to the plotted bcps are represented by the atom's radii, colour code only indicates atom type

the least electron density because cyano-epoxide (**10**) is the only compound with four substituents.

In summary, the contributions of atoms as next nearest neighbours are in the order of the electronegativity (O > C > H > Si), see also Chapter 7.2.5. Consequently, the contributions of the directly bonded atoms change according to the electronegativities of the adjacent atoms. This can also be found for the carbon atom C2 in Figure 12.14 (consider values from periodic-boundary calculations at optimised geometry). C2 contributes 38.1 % to the C1–C2 bcp in etox (**7**) with two adjacent hydrogen atoms. The contribution decreases to 36.4 % in moc-epoxide (**8**) with one adjacent hydrogen atom and one more electronegative sp^2 carbon atom. It again decreases to 33.4 % in niphe-epoxide (**9**) with two adjacent sp^2 carbon atoms. In cyano-epoxide (**10**), the contribution is only 32.3 % because C2 is adjacent to two sp carbon atoms that are more electronegative than sp^2 carbon atoms.

12.3 Results of the Topological Analysis of the ELI-D

12.3.1 General ELI-D Topology Compared to General ED Topology of the Epoxide Ring

The analysis of the ED of the epoxide rings showed (Chapter 12.2) that on the one hand, valence density is accumulated clearly outside the C–O and C–C bond axes (maxima of deformation density), but on the other hand, the total ED exhibits maxima directly between the nuclei for C–O bonds or slightly shifted outwards for C–C bonds (locations of bcps). The analysis of the ELI-D yields unambiguous results for all different representations: attractor positions, basin shapes and positions of localisation domains, as exemplified in Figure 12.15.

The ELI-D topology of the epoxide ring is generally the same for all methods (experiment and theory) as well as for all compounds (**7** to **10**). The positions of the non-nuclear attractors A for C–O and C–C bonds, i.e. absolute maxima in the ELI-D, are significantly shifted away from the internuclear axes (Figure 12.15 (a)) but are still in the ring plane (Figure 12.15 (b)). This means that bent-bond character by means of electron-pair localisation is reflected in a banana-bond shape also for C–O bonds in contrast to the ED, where a S-type bond shape

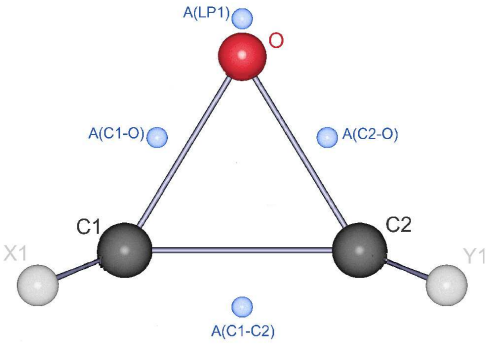

(a) Positions of non-nulcear attractors relative to the molecular scaffold

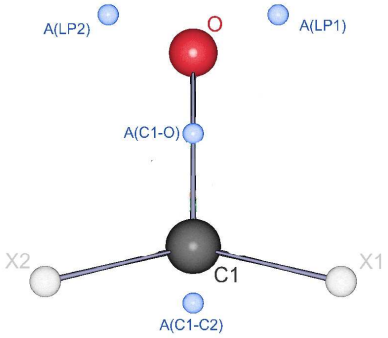

(b) Positions of non-nulcear attractors relative to the molecular scaffold rotated by 90 ° with respect to (a)

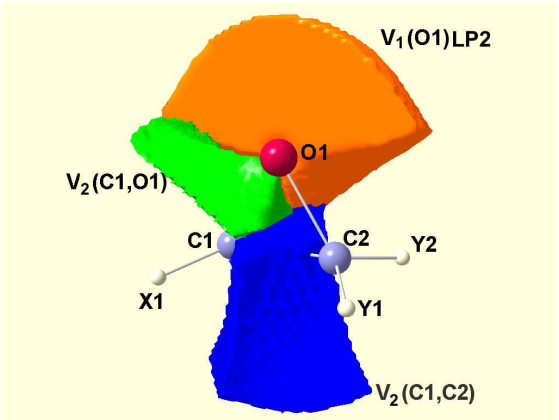

(c) Basin representation, outer contour of basins cut at ϱ=0.001 eÅ^{-3}, V_2(C,C) in blue, V_2(C,O) in green, V_1(O1) of the backmost oxygen lone pair LP2 in orange, other basins not shown

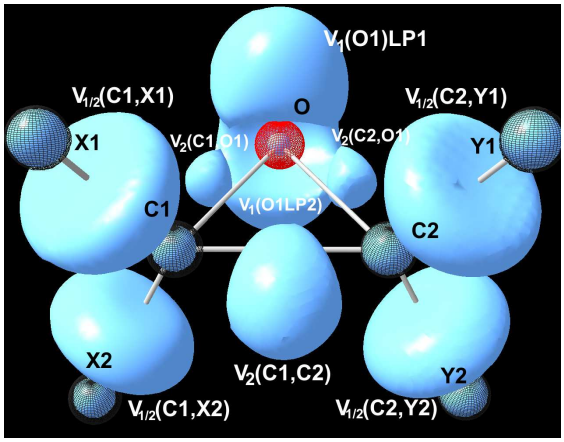

(d) Localization-domain representation of all bonds within the epoxide ring and to the substituents (irreducible), reducible localization domain of oxygen lone-pair basins V_1(O1)LP1 and V_1(O1)LP2

Figure 12.15: Different representations of the general ELI-D topology in the epoxide rings

General topology is identical for the experiment and theory, label A stands for non-nuclear attractors, LP for lone pairs, atoms of substituents bonded to C1 are labelled X1 and X2, atoms of substituents bonded to C2 are labelled Y1 and Y2, basins to substituents are either monosynaptic (V_1) if X/Y are hydrogen atoms or disynaptic (V_2) if X/Y are carbon atoms

prevails.[1] For all epoxide cpds. **7** to **10**, two attractors for the oxygen lone pairs exist (Figure 12.15 (b)). There is no merger of the attractors, which in contrast was found in some situations for siloxane and silyl ether linkages. But as it was in turn also not found for ether linkages; the presence of silicon seems to be crucial for this behaviour.

The basin representation in Figure 12.15 (c) shows the total shapes of three selected valence basins cut at ϱ=0.001 eÅ^{-3}. Due to the geometry of the three-membered ring, major regions of the basins are located outside the epoxide ring. For a non-strained single bond, the bond axis and the attractor are located in the middle of the basin, which is rather symmetrical the bond axis. The non-standard geometry in the epoxide ring causes an unusual pattern of saddle points located within common zero-flux surfaces of touching basins, see Chapter 12.3.3. Here, the bond basins of the two C–O bonds and the C–C bond touch each other in the middle of the ring, thus forming a ring-critical point, see Figure 12.17 and discussion in Chapter 12.3.3. The C–O and C–C bonds share common zero-flux surfaces with two core regions of the C or O atoms, respectively; they are disynaptic. The plotted lone-pair basin V_1(O1)LP2 is monosynaptic as it only comes into touch with the core basin of oxygen O1, represented by a red sphere.

The localisation-domain representation in Figure 12.15 (d) confirms that the major localisation effects of the C–O and C–C bonds take place outside the bond axes. The cap-like shape of the reducible localisation domain of the two lone pairs LP1 and LP2 at the oxygen atom is expected from the ELI-D analyses in preceding chapters. There is no general difference in this shape in the experiment and theory between etox (**7**) and the other epoxide compounds **8** to **10** carrying electron-withdrawing groups (EWGs). Localisation domains of bond basins to the substituents X1 and X2 at C1 as well as Y1 and Y2 at C2 are depicted. They are disynaptic if X/Y are carbon atoms and monosynaptic if X/Y are hydrogen atoms.

[1] Banana-bond shape is assumed by the location of the ELI-D attractors. However, a bond path connecting the atomic attractors by running through the bond attractor is not yet defined within the framework of the ELI.

12.3.2 Experimental Compared to Theoretical ELI-D

Figure 12.16 shows the shape of the localisation domains of the experimental ELI-D for cpds. **7** to **10**. It was already stated in the preceding chapter that there is no general difference to the topology originating from theoretical calculations. A comparison with the experimental ELF in Figure 7.12 also shows that the topology is correct. For example, the typical shape of the elongated domains of C–C bonds in an aryl group can be found in both the already established experimental ELF in Figure 7.12 and the new experimental ELI-D. However, the shape of the C–O bond domains in etox (**7**) (Figure 12.16 (a)), which can be discerned from the lone-pair domain only by the colour code, is different. They are smaller and shifted to the oxygen atom. This is not the case in theory or for the other three compounds, respectively.

The C–O bonds in etox (**7**) carry only 0.67 e on average (Table 12.6). C–O bonds in the other compounds are populated with about 1.0 to 1.2 e, which is only half of the population expected for a formal single bond. The population of C–O bonds in dimethylether at τ=65 ° was also found to be 1.0 e, but quickly increases with increasing C–O–C angle. So the small population is a clear indicator of the high bond strain of C–O bonds in epoxide. In disilaepoxide, with a Si–O–Si angle of about 80 °, the Si–O bond population is 1.42 e. The populations of C–C bonds in epoxide, also listed in Table 12.6, are much closer to the expected value than C–O bonds, see discussion in the next chapter. The C–C bond population in etox (**7**) originating from the experiment is close to theorical values, but the lone-pair populations are higher to compensate the loss in the C–O bonds.

Overall, the agreement in electron populations between the experiment and theory is very good, the differences are not higher than between the different theoretical methods. This also holds true for the ELI-D values at the attractors, the very property for which the implementation of the ELI-D formula into TONTO was carried out. These values cannot be deduced from an analysis of the ELF. As Table 12.6 shows that the experimental values are reasonable, it will be attempted in future projects to find a way to perform a full topological analysis of the experimental ELI-D. Within the scope of the present doctoral thesis, it will be shown for the theoretical ELI-D of cpds. **7** to **10** in the next chapter which conclusions can be drawn from such an analysis.

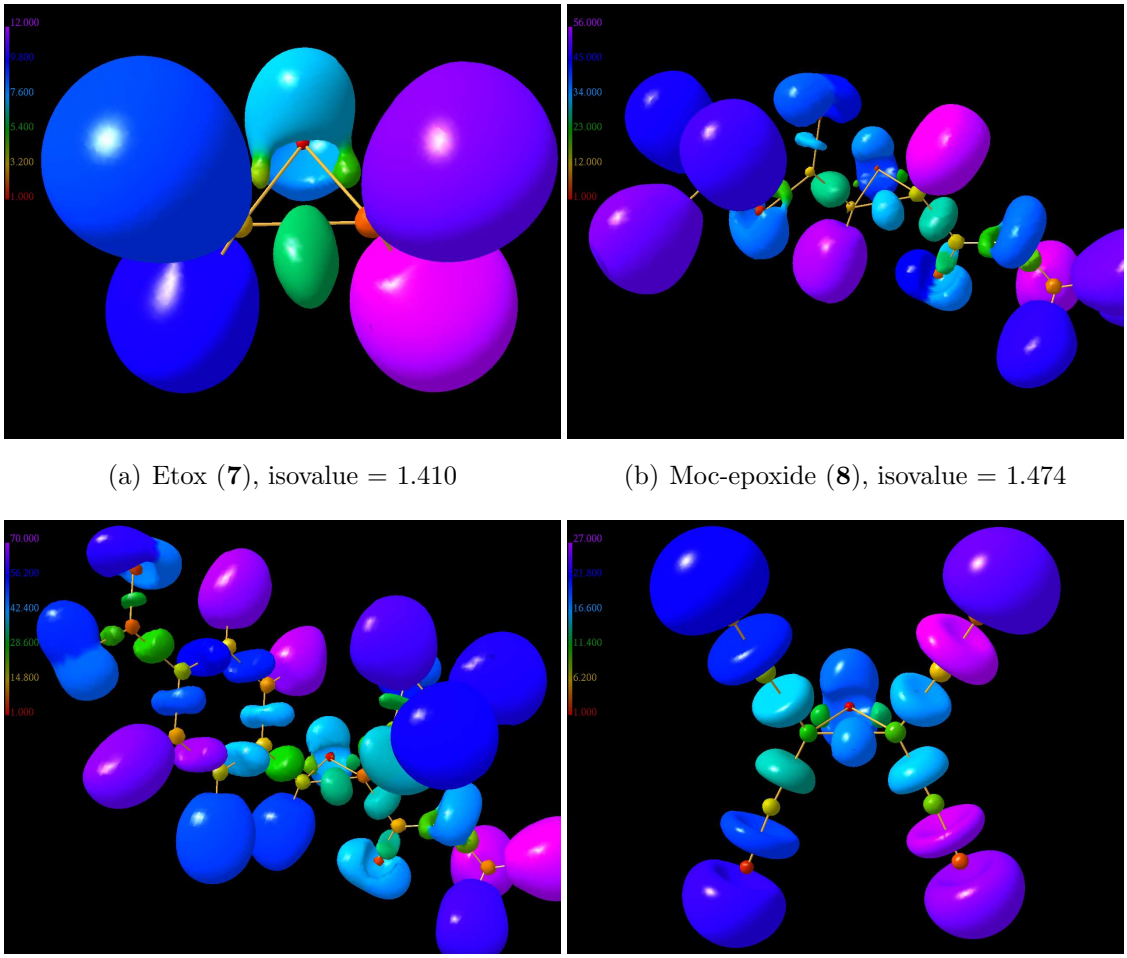

(a) Etox (**7**), isovalue = 1.410

(b) Moc-epoxide (**8**), isovalue = 1.474

(c) Niphe-epoxide (**9**), isovalue = 1.450

(d) Cyano-epoxide (**10**), isovalue = 1.450

Figure 12.16: Experimental ELI-D localisation-domain representations of cpds. **7** to **10**

Colour code representing the volumes of the basins on a linear scale beginning with the smallest basin

Table 12.6: Comparison of experimental and theoretical ELI-D populations N_{001} and values at the attractors ELI_{att} for valence basins in the epoxide rings of cpds. **7** to **10** *Experiment (exp) as well as isolated-molecule calculations at experimental (SP) and optimised geometry (opt), averages over both C–O bonds and both oxygen lone pairs (LPs) are given*

basin	method	cpd. **7**	cpd. **8**	cpd. **9**	cpd. **10**
V_2(C1/2,O1)	N_{001} exp	0.673	1.041	1.117	1.126
average	N_{001p} SP	1.022	1.058	1.085	1.127
over	N_{001} opt	1.098	1.124	1.143	1.200
both	ELI_{att} exp	1.474	1.529	1.547	1.560
bonds	ELI_{att} SP	1.463	1.514	1.532	1.533
	ELI_{att} opt	1.482	1.531	1.543	1.550
V_2(C1,C2)	N_{001} exp	1.863	1.877	1.893	1.848
	N_{001} SP	1.903	1.878	1.899	1.857
	N_{001} opt	1.876	1.853	1.902	1.879
	ELI_{att} exp	1.923	1.942	1.898	1.929
	ELI_{att} SP	1.895	1.898	1.912	1.913
	ELI_{att} opt	1.886	1.892	1.924	1.936
V_1(O1)LP1/2	N_{001} exp	2.941	2.686	2.695	2.614
average	N_{001} SP	2.661	2.635	2.629	2.600
over	N_{001} opt	2.600	2.584	2.574	2.543
both	ELI_{att} exp	1.729	1.779	1.813	1.563
LPs	ELI_{att} SP	1.736	1.798	1.801	1.809
	ELI_{att} opt	1.730	1.789	1.793	1.797

12.3.3 Full Topological Analysis of the Theoretical ELI-D

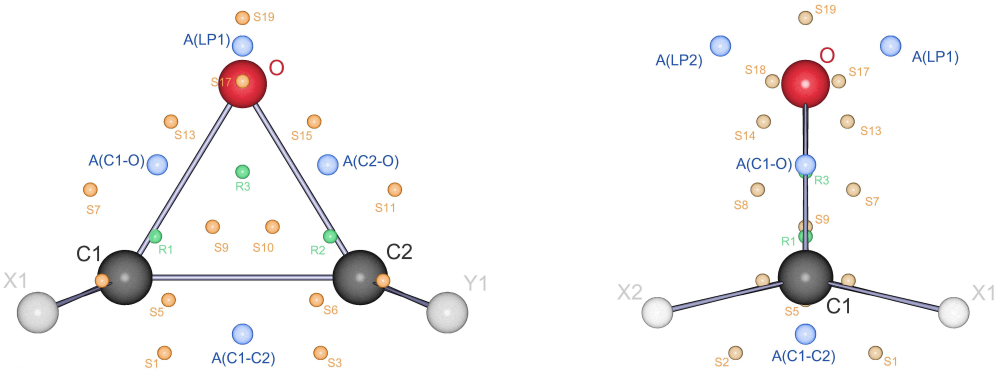

(a) (b) Rotated by 90 ° with respect to (a)

Figure 12.17: Positions of (3,-3) non-nuclear attractors A, (3,-1) saddle points S and (3,+1) ring-critical points R in the general theoretical ELI-D topology relative to the molecular scaffold

No example of the chemical interpretation of a full topological analysis of the ELI-D was found in the literature. Therefore, this is attempted here for the first time. The positions and ELI-D values at attractors, saddle points and ring-critical points are discussed together with basin populations, volumes and Jansen indices. The Jansen indices [164] show how much of the electron population of an ELI-D valence bond basin belongs to the Bader electron-density basin of each of the atoms of the bonds. It is calculated by an intersection of the ELI-D with the electron-density basins and a subsequent integration of the electron density in the intersected ELI-D basins. As already explained in Chapter 11.1.2, the determination of saddle points, ring-critical points and Jansen indices is not yet possible for the experimental ELI-D. Thus, the results were obtained from isolated-molecule calculations at experimental and optimised geometries.

Figure 12.17 shows the positions and the labelling of all critical points in the general topology of the ELI-D in contrast to Figure 12.15 (a) and (b) where only non-nuclear attractors A were plotted that can also be found in the experimental topology. Here, (3,-1) saddle points are denoted S and (3,+1) ring-critical points are labelled R. For a normal disynaptic single bond, saddle points in the ELI-D topology are expected between the valence basin of the bond and the core basins of the two atoms constituting this bond. For the C1–C2 bond, these saddle points are marked as S5 and S6 in Figure 12.17. Due to the unusual location of the

C1–C2 bond attractor, there are also saddle points (S1, S2, S3 and S4 in Figure 12.17) between the valence basins of the substituents X1, X2, Y1 and Y2 and the C1–C2 bond basin. These saddle points can be found regardless of X1, X2, Y1 or Y2 being a hydrogen atom or a carbon atom.

Quite surprisingly, no saddle points can be found between the core basins and the bond basins of the C–O bonds in the epoxide rings although they are disynaptic as shown in Figure 12.15 (c). This can be found regardless of the substitution pattern or method used. Therefore, this special feature in the topology can be attributed to the high ring strain and the unusual location of the C–O bond attractors. Moreover, it is characteristic of the C–O bonds in the epoxide ring because the C1–C2 bond exhibits the expected saddle points. Furthermore, any other C–O, C–C, C–N or N–O bond in cpds. **7** to **10** exhibits the expected saddle points, too. Another characteristic of this strained scenario is that the unusual location of the C–O bond attractors and therefore the unusual shape of the basins allow the formation of saddle points with the oxygen lone pairs LP1 and LP2 and the valence basins of the substituents X1, X2, Y1 or Y2. The saddle points between the basins of the C1–O1 bond and the C1–X1/X2 bonds are given as S7 and S8 in Figure 12.17; the saddle points between C2–O1 and C2–Y1/Y2 are S11 and S12. The saddle points between the attractors of the C–O bonds and the oxygen lone pairs are labelled as S13 to S16. The basins of the C1–C2 bond and the C–O bonds touch each other in the middle of the epoxide ring, which shows well in Figure 12.15 (c), yielding the saddle points S9 and S10 in the plane of the ring. The ELI-D topology described leads to several ring-critical points, of which the three ones in the ring plane are also plotted in Figure 12.17 (R1 to R3).

Table 12.7 lists all ELI-D values of the critical points depicted in Figure 12.17. In contrast to the topology of the electron density, the differences of the values at attractors (A, (3,-3)) compared to saddle points (S, (3,-1)) and ring-critical points (R, (3,+1))) are not large, only the saddle points between core basins and non-nuclear attractors (S5, S6, S17 and S18) are significantly smaller than the others. But as in the electron-density analysis, differences of the values between different compounds are interpretable in the ELI-D, which is not the case for the ELF. It is obvious that etox (**7**) has the lowest ELI-D values at all attractors and at most saddle and ring-critical points compared to the other compounds. This means that the electron-pair localisation at these special points that characterise the cores, bonds or lone pairs is lowest in the compound without electron-

Table 12.7: ELI-D values of the attractors, saddle points and ring-critical points for cpds. **7** to **10**

Isolated-molecule calculations at experimental (SP) and optimised geometry (opt), for labelling see Figure 12.17

crit. point	method	cpd. **7**	cpd. **8**	cpd. **9**	cpd. **10**	crit. point	method	cpd. **7**	cpd. **8**	cpd. **9**	cpd. **10**
(3,-3) nuclear attractors:						S8	SP	1.107	1.150	1.090	1.147
O1	SP	12.879	13.296	13.356	13.280		opt.	1.106	1.146	1.138	1.142
	opt.	12.824	13.243	13.307	13.226	S9	SP	1.100	1.142	1.067	1.138
C1	SP	16.817	17.243	17.435	17.167		opt.	1.097	1.140	1.135	1.134
	opt.	16.731	17.159	17.344	17.131	S10	SP	1.100	1.143	1.088	1.138
C2	SP	16.825	17.242	17.225	17.167		opt.	1.097	1.140	1.140	1.134
	opt.	16.731	17.159	17.143	17.131	S11	SP	1.107	1.158	1.096	1.147
(3,-3) non-nuclear attractors:							opt.	1.106	1.146	1.151	1.142
A(C1–O1)	SP	1.466	1.513	1.531	1.535	S12	SP	1.106	1.156	1.143	1.147
	opt.	1.482	1.531	1.549	1.550		opt.	1.106	1.148	1.153	1.142
A(C2–O1)	SP	1.460	1.515	1.533	1.531	S13	SP	1.371	1.417	1.435	1.410
	opt.	1.482	1.531	1.537	1.550		opt.	1.372	1.417	1.438	1.414
A(C1–C2)	SP	1.895	1.898	1.912	1.913	S14	SP	1.370	1.415	1.430	1.409
	opt.	1.886	1.892	1.924	1.936		opt.	1.372	1.415	1.434	1.414
A(LP1)	SP	1.736	1.799	1.795	1.809	S15	SP	1.369	1.408	1.418	1.409
	opt.	1.730	1.789	1.799	1.797		opt.	1.372	1.415	1.422	1.414
A(LP2)	SP	1.736	1.797	1.807	1.809	S16	SP	1.370	1.412	1.416	1.409
	opt.	1.730	1.789	1.787	1.797		opt.	1.372	1.417	1.415	1.414
(3,-1) saddle points:						S17	SP	0.762	0.789	0.714	0.789
S1	SP	1.220	1.254	1.247	1.234		opt.	0.761	0.788	0.790	0.787
	opt.	1.224	1.256	1.246	1.234	S18	SP	0.762	0.789	0.714	0.789
S2	SP	1.220	1.269	1.261	1.235		opt.	0.761	0.788	0.790	0.787
	opt.	1.224	1.267	1.268	1.234	S19	SP	1.571	1.597	1.608	1.608
S3	SP	1.223	1.264	1.266	1.236		opt.	1.555	1.632	1.622	1.631
	opt.	1.224	1.267	1.271	1.234	(3,+1) ring-critical points					
S4	SP	1.225	1.247	1.280	1.236	R1	SP	0.645	0.670	0.660	0.672
	opt.	1.224	1.256	1.269	1.234		opt.	0.608	0.665	0.652	0.659
S5	SP	0.659	0.679	0.669	0.681	R2	SP	0.648	0.668	0.659	0.672
	opt.	0.659	0.676	0.673	0.683		opt.	0.608	0.665	0.680	0.659
S6	SP	0.661	0.677	0.668	0.682	R3	SP	1.070	1.113	1.104	1.186
	opt.	0.659	0.676	0.691	0.683		opt.	1.174	1.211	1.113	1.100
S7	SP	1.106	1.149	1.070	1.147						
	opt.	1.106	1.148	1.134	1.142						

withdrawing substituents (EWGs). Consequently, cyano-epoxide (**10**) with four EWGs has the highest ELI-D values at the bond attractors (A(C1–O), A(C2–O) and A(C1–C2)) and saddle points to the C1–C2 bond (S5 and S6). Therefore, localisation of the remaining electrons is higher at the critical points in the ELI-D if electrons are withdrawn from this bond (see discussion on electron populations below or on critical points in the ED in Chapter 12.2.3). The localisation at the nuclear attractor of the oxygen atom is by about 4.0 lower than at the carbon attractors. This also shows that the ELI-D information on localisation are complementary to the electron-density concentrations in these regions. In summary, at the oxygen nuclear attractor and at attractors of bonds that are not subject to electron-withdrawing effects, electron density is more concentrated, but the electron localisation is lower.

Table 12.8 lists the populations and volumes of the bond basins in the epoxide ring, the oxygen lone pairs and the bond basins to the four substituents. The highly strained bond situation leads to extremely low populations in the C–O bonds with about 1.00 to 1.15 e and very low volumes with about 1.2 to 1.4 $Å^3$. The C1–C2 bond is populated with 1.85 to 1.90 e, which is also very low compared to non-strained C–C single bonds, see for example the bonds to the substituents in Table 12.8. This means that the sum of all three bond basins that correspond to three electron pairs is about 4 e. The two electron pairs of the oxygen lone pairs compensate for this and add up to more than 5 e, so that all valence electron pairs inside the epoxide ring carry about 9.3 e.

In the calculations at experimental geometry, it can be seen that most electrons are withdrawn from the C1–C2 bond in the case of cyano-epoxide (**10**) with four EWGs and fewest in the case of etox (**7**) without EWGs. However, the trend is more clear for the C–O bonds: The more electrons are withdrawn from the C1–C2 bond, the higher the population of the C–O bonds is. The C–O bond populations are highest for cyano-epoxide (**10**) with four EWGs, followed by niphe-epoxide (**9**) with three EWGs, moc-epoxide (**8**) with two EWGs and etox (**7**) without EWGs. This increase of the C–O bond populations seems to be due to losses in the lone-pair basins. The trend is clear for the sum of both oxygen lone-pair basins: The lowest lone-pair population can be found in cyano-epoxide (**10**) with four EWGs and increases continuously towards etox (**7**) without EWGs.

The populations of the bond basins C1/C2–C(cyano) are largest for all listed bonds with about 2.21 to 2.24 e. This fact confirms that the resonance formulae in Figure

Table 12.8: ELI-D populations (N_{001} in e) and volumes (V_{001} in Å^3) of valence basins in the epoxide region of cpds. **7** to **10**

*Isolated-molecule calculations at experimental (SP) and optimised geometry (opt), etox (**7**): X1=H, X2=H, Y1=H, Y2=H; moc-epoxide (**8**): X1=C, X2=H, Y1=H, Y2=C; niphe-epoxide (**9**): X1=C, X2=H, Y1=C, Y2=C; cyano-epoxide (**10**): X1=C, X2=C, Y1=C, Y2=C*

		etox(**7**)		moc-epoxide (**8**)		niphe-epoxide (**9**)		cyano-epoxide (**10**)	
basin	method	N_{001}	V_{001}	N_{001}	V_{001}	N_{001}	V_{001}	N_{001}	V_{001}
V_2(C1,O1)	SP	1.036	1.224	1.049	1.229	1.074	1.293	1.133	1.423
	opt.	1.098	1.207	1.124	1.240	1.157	1.259	1.200	1.343
V_2(C2,O1)	SP	1.007	1.205	1.066	1.378	1.095	1.375	1.120	1.405
	opt.	1.098	1.207	1.124	1.240	1.128	1.365	1.200	1.343
V_2(C1,C2)	SP	1.903	4.738	1.878	4.708	1.899	4.423	1.857	4.097
	opt.	1.876	4.779	1.853	4.881	1.902	4.606	1.879	4.352
sum of	SP	3.946		3.994		4.068		4.110	
all V_2	opt.	4.072		4.101		4.187		4.278	
V_1(O1)LP1	SP	2.682	7.228	2.643	6.949	2.602	6.434	2.616	6.749
	opt.	2.600	6.953	2.584	6.662	2.547	6.222	2.543	6.559
V_1(O1)LP2	SP	2.640	7.083	2.626	6.728	2.656	7.009	2.583	6.728
	opt.	2.600	6.953	2.584	6.662	2.600	6.959	2.543	6.559
sum of both	SP	5.322		5.269		5.258		5.199	
V_1(O1)	opt.	5.199		5.167		5.147		5.086	
sum of V_2	SP	9.268		9.262		9.325		9.309	
and V_1(O1)	opt.	9.271		9.269		9.334		9.364	
$V_{1/2}$(C1,X1)	SP	2.066	10.345	2.196	4.121	2.146	3.550	2.239	4.020
	opt.	2.069	10.251	2.203	4.089	2.132	3.508	2.213	3.948
$V_{1/2}$(C1,X2)	SP	2.065	10.405	2.098	9.764	2.091	9.493	2.233	3.994
	opt.	2.069	10.251	2.101	9.589	2.090	9.201	2.213	3.948
$V_{1/2}$(C2,Y1)	SP	2.075	10.329	2.097	9.773	2.189	3.639	2.243	3.990
	opt.	2.069	10.251	2.101	9.589	2.202	3.709	2.213	3.948
$V_{1/2}$(C2,Y2)	SP	2.059	10.418	2.200	4.110	2.197	4.277	2.232	4.001
	opt.	2.069	10.251	2.203	4.089	2.174	3.743	2.213	3.948

4.4, where this bond is a double bond, is quite significant and clearly carries the most significance out of all substituents. Corresponding populations for the methyl ester groups range from 2.17 in niphe-epoxide (**9**) to 2.20 e in moc-epoxide (**8**). In the case of the nitro-phenyl group, the C1–X1 bond population ranges from 2.13 to 2.15 e. Comparison with pure C–C single bonds (1.90 to 2.00 e) [161] and C–C double bonds (3.50 to 4.00 e) [161] confirms that the bonds C1/C2–C(substituent) are significantly more highly populated than single bonds, but have only partial double-bond character.

The Jansen indices of all bonds under discussion were calculated and listed in Table 12.9. They are a measure of how much of the populations of the bonds to the substituents belong to the carbon atoms in the epoxide ring. And thus, an overall estimate of the electron population of the ring and the withdrawing effects of the substituents can be made.
Only 0.94 to 0.96 e (about 43 % of 2.21 to 2.24 e) of the C1/C2-C(cyano) bond populations belong to the carbon atoms C1 and C2 in the epoxide ring. The methyl ester groups are the reason for the fact that 1.00 to 1.06 e (about 45 % of 2.17 to 2.20 e) of the C1/C2–C bonds belong to the carbon atoms in the epoxide ring, the nitro-phenyl group 1.09 to 1.10 e. This reflects the electron-withdrawing power of the cyano and methyl ester groups because less than 50 % of the electrons remain in the epoxide system. However, the electron population belonging to the carbon atoms of the epoxide ring, in the case of the nitro-phenyl group, is greater than 50 % and in the same range as for a hydrogen atom.
The total electron population of the epoxide rings can be calculated by a sum of the populations of all valence basins and the Jansen indices to the ring carbon atoms C1 and C2. As expected, this sum is smallest for cyano-epoxide (**10**) with four most powerful EWGs (13.12 to 13.16 e). It is not highest for etox (**7**), as the sum of the Jansen indices to the epoxide system in terms of absolute electron numbers is smaller than for moc-epoxide (**8**) and niphe-epoxide (**9**). But the average relative Jansen indices for the four compounds show that the hydrogen atoms in etox (**7**) donate to the epoxide carbon atoms C1 and C2 (50.7 to 51.4 %) and the cyano groups withdraw (43.0 to 43.4 %).
Jansen indices for C–O bonds show that about 75 % of the electrons and 65 % of the volumes of the ELI-D bond basins belong to the oxygen atom as expected from the electronegativity differences. For the bond C1–C2, the fractions are equal, at least for optimised geometries. Only niphe-epoxide (**9**), as the only unsymmetrically

Table 12.9: Jansen indices in the epoxide rings of cpds. **7** to **10**

Isolated-molecule calculations at experimental (SP) and optimised geometry (opt), cpd. **7***: X1=H, X2=H, Y1=H, Y2=H; cpd.* **8***: X1=C, X2=H, Y1=H, Y2=C; cpd.* **9***: X1=C, X2=H, Y1=C, Y2=C; cpd.* **10***: X1=C, X2=C, Y1=C, Y2=C; absolute (relative) populations N_{001} in e (%) and absolute (relative) volumes V_{001} in $Å^3$ (%) belonging to the basin fragments*

			etox (**7**)		moc-epoxide (**8**)		niphe-epoxide (**9**)		cyano-epoxide (**10**)	
basin	method		N_{001}	V_{001}	N_{001}	V_{001}	N_{001}	V_{001}	N_{001}	V_{001}
V_2(C1,O1)	SP	C1	0.264 (25.5)	0.425 (34.7)	0.272 (25.9)	0.441 (35.9)	0.269 (25.1)	0.468 (36.2)	0.357 (31.5)	0.630 (44.3)
		O	0.771 (74.5)	0.799 (65.3)	0.778 (74.1)	0.788 (64.1)	0.804 (74.9)	0.825 (63.8)	0.776 (68.5)	0.793 (55.8)
	opt.	C1	0.240 (21.9)	0.362 (29.9)	0.256 (22.8)	0.393 (31.7)	0.245 (21.2)	0.388 (30.8)	0.326 (27.2)	0.518 (38.6)
		O	0.858 (78.2)	0.845 (70.0)	0.868 (77.2)	0.846 (68.3)	0.912 (78.8)	0.871 (69.2)	0.873 (72.8)	0.825 (61.4)
V_2(C2,O1)	SP	C2	0.261 (25.9)	0.425 (35.3)	0.301 (28.2)	0.550 (39.9)	0.315 (28.7)	0.598 (43.5)	0.354 (31.6)	0.626 (44.5)
		O	0.746 (74.1)	0.780 (64.7)	0.765 (71.8)	0.828 (60.1)	0.780 (71.3)	0.776 (56.4)	0.767 (68.4)	0.780 (55.5)
	opt.	C2	0.240 (21.9)	0.362 (29.9)	0.256 (22.8)	0.393 (31.7)	0.286 (25.4)	0.582 (42.6)	0.326 (27.2)	0.518 (38.6)
		O	0.858 (78.2)	0.845 (70.0)	0.868 (77.2)	0.846 (68.3)	0.842 (74.6)	0.780 (57.2)	0.873 (72.8)	0.825 (61.4)
V_2(C1,C2)	SP	C1	0.922 (48.5)	2.269 (47.9)	0.942 (50.2)	2.434 (51.7)	0.847 (44.6)	1.963 (44.4)	0.913 (49.2)	1.997 (48.7)
		C2	0.958 (50.3)	2.442 (51.6)	0.908 (48.3)	2.207 (46.9)	1.024 (53.9)	2.386 (53.9)	0.918 (49.5)	2.068 (50.5)
	opt.	C1	0.925 (49.3)	2.372 (49.6)	0.907 (48.9)	2.382 (48.8)	0.832 (43.8)	1.970 (42.8)	0.922 (49.1)	2.154 (49.5)
		C2	0.925 (49.3)	2.372 (49.6)	0.907 (48.9)	2.382 (48.8)	1.035 (54.4)	2.536 (55.1)	0.922 (49.1)	2.154 (49.5)
$V_{1/2}$(C1,X1)	SP	C1	1.058 (51.2)	3.033 (29.3)	1.010 (46.0)	1.749 (42.4)	1.100 (51.2)	1.926 (54.2)	0.964 (43.1)	1.806 (44.9)
		X1	1.007 (48.8)	7.303 (70.6)	1.184 (53.9)	2.362 (57.3)	1.046 (48.8)	1.621 (45.7)	1.275 (56.9)	2.210 (55.00)
	opt.	C1	1.049 (50.7)	2.956 (28.8)	1.007 (45.7)	1.727 (42.2)	1.093 (51.3)	1.884 (53.7)	0.939 (42.4)	1.734 (43.9)
		X1	1.018 (49.2)	7.282 (71.0)	1.193 (54.2)	2.352 (57.5)	1.038 (48.7)	1.619 (46.2)	1.274 (57.6)	2.211 (50.0)
$V_{1/2}$(C1,X2)	SP	C1	1.058 (51.2)	3.074 (29.5)	1.178 (56.1)	3.266 (33.5)	1.156 (55.3)	3.033 (32.0)	0.958 (42.9)	1.777 (44.5)
		X2	1.007 (48.8)	7.319 (70.3)	0.919 (43.8)	6.462 (66.2)	0.934 (44.7)	6.448 (67.9)	1.276 (57.1)	2.217 (55.5)
	opt.	C1	1.049 (50.7)	2.956 (28.8)	1.147 (54.6)	3.059 (31.9)	1.140 (54.6)	2.893 (31.4)	0.939 (42.4)	1.734 (43.9)
		X2	1.018 (49.2)	7.282 (71.0)	0.952 (45.3)	6.493 (67.7)	0.948 (45.4)	6.288 (68.3)	1.274 (57.6)	2.211 (50.0)
$V_{1/2}$(C2,Y1)	SP	C2	1.064 (51.3)	3.001 (29.1)	1.169 (55.7)	3.261 (33.4)	1.053 (48.1)	1.703 (46.8)	0.970 (43.2)	1.782 (44.7)
		Y1	1.010 (48.7)	7.311 (70.8)	0.927 (44.2)	6.474(66.3)	1.134 (51.8)	1.926 (52.9)	1.273 (56.8)	2.207 (55.3)
	opt.	C2	1.049 (50.7)	2.956 (28.8)	1.147 (54.6)	3.059 (31.9)	1.064 (48.3)	1.763 (47.5)	0.939 (42.4)	1.734 (43.9)
		Y1	1.018 (49.2)	7.282 (71.0)	0.952 (45.3)	6.493 (67.7)	1.135 (51.6)	1.934 (52.2)	1.274 (57.6)	2.211 (50.0)
$V_{1/2}$(C2,Y2)	SP	C2	1.066 (51.8)	3.148 (30.2)	1.000 (45.4)	1.718 (41.8)	1.051 (47.8)	1.997 (46.7)	0.958 (42.9)	1.794 (44.8)
		Y2	0.992 (48.2)	7.258 (69.7)	1.199 (54.5)	2.385 (58.0)	1.143 (52.1)	2.264 (52.9)	1.274 (57.1)	2.207 (55.2)
	opt.	C2	1.049 (50.7)	2.956 (28.8)	1.007 (45.7)	1.727 (42.2)	1.029 (47.3)	1.674 (44.7)	0.939 (42.4)	1.734 (43.9)
		Y2	1.018 (49.2)	7.282 (71.0)	1.193 (54.2)	2.352 (57.5)	1.141 (52.5)	2.047 (54.7)	1.274 (57.6)	2.211 (50.0)
sum of J of C1 and C2	SP		4.245(51.4)		4.356(50.8)		4.358(50.6)		3.849(43.0)	
(av. relative)	opt.		4.196(50.7)		4.308(50.2)		4.327(50.4)		3.756(43.4)	
$\sum$N of epoxide ring plus	SP		13.513		13.619		13.684		13.158	
J of C1 and C2	opt.		13.467		13.577		13.661		13.119	

substituted epoxide in this study, is an exception. Therein, carbon atoms C1 and C2 are different. C2 is in the vicinity of two methyl ester groups and is therefore more electronegative. This fact is reflected in the Jansen partitioning of the ELI-D bond basins within the epoxide ring: 54 to 55 % of the population and volume of the C1–C2 bond basin belong to carbon atom C2. The fraction of C2 on the C2–O1 bond's population and volume is significantly larger than for C1 in the C1–O1 bond. The asymmetry can also be seen in the oxygen lone-pair populations: LP1, which is directed to the front of the molecule, has a smaller volume and a lower population. The reason is steric hindrance by the nitro-phenyl group that is also directed to the front of the molecule.

Conclusion and Outlook

The combined experimental-theoretical approach chosen in this doctoral thesis to determine and analyse the electron-density distribution (ED) and the electron localizability indicator (ELI) of X–O–X linkages (siloxanes, silyl ethers, open-chain ethers and epoxides) granted detailed insight into the electronic properties of bonds and atoms of the scrutinised linkages. Potential-energy surface (PES) scans of model compounds (disiloxane, methoxysilane and dimethylether) predicted chemical behaviours of the linkages that were verified by means of high-resolution X-ray diffraction experiments on single crystals of cpds. **1** to **10**.

It was shown that variation of the X–O–X angle influences electronic properties of the bonds and atoms in the linkages in a systematical way. Not only the Si–O and C–O bond characters can be fine-tuned by the choice of the bond angle, but also properties connected to reactivity like the basicity of the oxygen atom of the linkages. This opens up interesting applications for synthetical chemists, who can rationally design compounds with certain desired properties by adjusting the X–O–X angle in the synthesis to a value predicted by the PES scans carried out in this doctoral thesis. There are medium-strength hydrogen bonds and even weak C–H$\cdots$O interactions in the crystal structures of cpds. **1** and **2**, which is an exceptional case and due to the small Si–O–Si angles in these compounds. Thus, industrially used silicone polymers, which contain siloxane linkages in their backbones, could be gradually modified from water-repelling (large and medium Si–O–Si angles) to water-binding (small Si–O–Si angles) materials depending on the desired field of application.

A variety of procedures was applied to analyse substituent effects on the epoxide ring, which is especially important for the underlying drug-design purposes with epoxides as electrophilic building blocks. On the one hand, electron-withdrawing groups lower the hydrogen-bond acceptor capability of the epoxide oxygen atoms, but on the other hand, methyl ester groups in combination with the epoxide ring form a uniform region of negative electrostatic potential, in which the main

intermolecular interactions take place. This may contribute to rational drug design because intermolecular recognition plays a key role in biological processes. The expected order of the electron-withdrawing power of different substituents could be determined from geometrical, bond-topological and atomic ED properties as well as ELI populations. Thus, tools to analyse the power of different substituent effects were successfully tested and can be used for a rational design of molecules in various synthetic fields. Moreover, the actual impact of certain resonance formulae to the overall description of the electronic state of a molecule can be estimated by these methods. According to very recent findings, the source function is not applicable to detect resonance effects, but the sensitivity of different bond types to the chemical environment (Si–O is more sensitive than C–C and again C–O) can be characterised. The source contributions of atoms as next nearest neighbours increases with the atom type's electronegativity.

Bond strain in the epoxide rings manifests itself in bent bonds characterised in different ways. Valence electrons concentrate and electron pairs localise outside the C–O and C–C bond axes to form so-called banana bonds in accordance with the Förster-Coulson-Moffitt molecular-orbital model. But the maximum of the total electron density coincides with the C–O bond axes and bent bonds are expressed in an S-type shape of the bond path.

Chemical catastrophes were identified in the topologies of the ED and the ELI. The points of these topological catastrophes mark transitions from one chemical system into another, which exhibit different chemical behaviour. These catastrophes were found qualitatively in the Laplacian of the ED and the ELI in form of changes of typical shapes of the lone pairs at the oxygen atom within the different chemical systems. The ELI provides additional descriptors to unambiguously find the point of a chemical transition: The number of attractors and saddle points in the ELI topology changes accompanied by the appearance of cusps in the curves of electron populations and volumes of corresponding ELI basins upon variation of the X–O–X angle. It can be suggested that these changes also occur along reaction coordinates, so that the concept can be transferred to the study of reaction mechanisms and transition states in future projects.

It was found that the chemical interpretation of the full topology of the theoretical ELI is a valuable tool to describe the electronic characteristics of a functional group complementary to the ED. Substituent effects were detected in the ELI, and bent bonds were described by the location of bond attractors (see above), but also

by the absence of saddle points to the core basins that normally occur in non-strained bonds. The concept of submolecular transferability of ED properties of atoms or bonds in the same chemical environment was found also to be valid for ELI properties like electron populations of valence basins. The new experimental ELI that was introduced in this doctoral thesis was analysed in a first case study and proven to yield the correct topology compared to theory and the experimental ELF. As the chemical interpretations of the theoretical ELI provides valuable information, it is highly desirable to delve deeper into the interpretation of the experimental ELI in future projects in order to establish the method for broader chemical application.

Summary

A study of the X–O–X linkage with X being carbon or silicon was performed in this doctoral thesis, i.e. siloxanes (Si–O–Si), silyl ethers (Si–O–C), open-chain ethers and epoxides (C–O–C) were examined. For this purpose, high-resolution X-ray diffraction experiments on single crystals were carried out at low temperatures employing mainly synchrotron radiation (HASYLAB, Hamburg, and APS, Chicago). Additionally, ab-initio calculations were performed on model compounds and on the scrutinised molecules. From these experiments and calculations, electron-density (ED) distribution and electron localizability indicator (ELI) were determined and topologically analysed. New tools like the source function were employed to interpret the obtained topologies.
In this doctoral thesis, determination of the experimental ELI was rendered possible for the first time by making the ELI formula accessible to a constrained wave function. Features of this new experimental ELI were studied, and the first chemical interpretation of a full topological analysis of the theoretical ELI was carried out additionally.

Disiloxane $H_3SiOSiH_3$, methoxysilane H_3SiOCH_3, and dimethylether H_3COCH_3 as well as corresponding hydrogen-bonded complexes with silanol and water as donors served as model compounds. Potential-energy surface (PES) scans were performed by variation of the X–O–X angle from 50 ° to 180 °, from which resulted that ionic Si–O bonds become even more ionic and stronger with increasing angle, but significant covalent contributions mix into the bond character at small angles. Covalent C–O bonds are strongest and most covalent near the energetical minimum angle.
X–O–X linkages become more basic with decreasing angles and thus hydrogen bonds become stronger. This is most pronounced for the siloxane linkage, which is not a competitive hydrogen-bonding acceptor at large and medium X–O–X angles, but at small ones. Hydrogen bonding is generally feasible in siloxanes for Si–O–Si

angles between 85 ° and 165 °, but not at larger or smaller angles, respectively. This is confirmed by the finding of topological catastrophes in the ED and ELI of disiloxane, which are not found in methoxysilane and dimethylether.

Predictions from the PES scans were verified experimentally. Measured siloxane cpds. **1** and **2** comprise strained Si–O–Si linkages around 115 ° incorporated into five-membered rings. They indeed exhibit exceptional hydrogen bonds, even weak C–H$\cdots$O interactions. Siloxane cpds. **3** and **4** comprise relaxed Si–O–Si linkages (162 ° and 180 °) and no hydrogen bonds. Typical shapes of oxygen lone pairs dependent on the Si–O–Si angle as predicted by the PES scans were confirmed experimentally.
Results for cpd. **5** containing silyl-ether linkages were derived from a periodic-boundary calculation. Results of ether linkages in sucrose (cpd.**6**) were compared. The concept of submolecular transferability was found to be valid also for ELI results.
Unsubstituted epoxide (cpd. **7**) and epoxides substituted with electron-withdrawing groups (cpds. **8** to **10**) contain bent C–O and C–C bonds, which manifests itself differently in ED and ELI. Electron-withdrawing effects of the substituents were detected in the electronic properties. In terms of the source function, Si–O bonds are sensitive to the chemical environment while C–O bonds are not. The new experimental ELI proved to yield the correct topology qualitatively and quantitatively, thus making it suitable for future chemical application.

Zusammenfassung

Siloxane (Si–O–Si), Silylether (Si–O–C), offene Ether und Epoxide (C–O–C) wurden als systematische Reihe von X–O–X-Verknüpfungen in der vorliegenden Doktorarbeit untersucht. Dafür wurden sowohl hochauflösende Röntgenbeugungsexperimente an Einkristallen bei niedrigen Temperaturen durchgeführt - hauptsächlich unter Verwendung von Synchrotronstrahlung (HASYLAB in Hamburg und APS in Chicago) - als auch quantenchemische Rechnungen an den untersuchten Molekülen sowie an entsprechenden Modellverbindungen. Aus Experiment und Theorie wurden die Elektronendichteverteilung (ED) und der Elektronenlokalisierbarkeitsindikator (ELI) bestimmt sowie topologisch analysiert, wobei auch neue Hilfsmittel wie die ,,Source Function" zur Anwendung kamen.
Die Bestimmung des ELI aus dem Experiment über eine sogenannte experimentelle Wellenfunktion wurde in dieser Doktorarbeit erstmals ermöglicht und die Eigenschaften dieses neuen experimentellen ELI untersucht. Darüber hinaus wurde zum ersten Mal eine chemische Interpretation der vollständigen Topologie des theoretischen ELI vorgenommen.

Als Modellverbindungen dienten Disiloxan $H_3SiOSiH_3$, Methoxysilan H_3SiOCH_3 und Dimethylether H_3COCH_3 sowie entsprechende Wasserstoffbrückenkomplexe mit Silanol und Wasser als Donoren. An diesen wurden Scans der Potentialenergiefläche (PES) unter Variation des X–O–X-Winkels von 50 ° bis 180 ° durchgeführt. Es zeigte sich, dass die ionische Si–O-Bindung mit größer werdendem Winkel noch ionischer sowie stärker wird, was auch bedeutet, dass sie bei kleinem Winkel deutlich kovalente Anteile besitzt. Die kovalente C–O-Bindung ist am stärksten und am kovalentesten nahe des energetischen Minimumwinkels.
Die X–O–X-Verknüpfungen werden umso basischer, je kleiner der Winkel wird, und desto stärker werden folglich die Wasserstoffbrücken. Dies wurde für die Siloxan-Verknüpfung am deutlichsten, die bei großem und mittlerem Winkel ein schlechter Akzeptor, bei kleinem Winkel aber ein guter ist. Wasserstoffbrücken

sind in Siloxanen prinzipiell bei einem Si–O–Si-Winkel zwischen 85 ° und 165 ° möglich, nicht aber bei höherem bzw. niedrigerem Winkel. Bestätigt wurde dies durch das Auftreten topologischer Katastrophen in der ED und dem ELI bei Disiloxan, die bei Methoxysilan und Dimethylether nicht gefunden wurden.

Die Voraussagen durch die PES-Scans wurden experimentell verifiziert. Die gemessenen Siloxanverbindungen **1** und **2** beinhalten gespannte Si–O–Si-Einheiten von ca. 115 ° in fünfgliedrigen Ringen. Sie bilden tatsächlich Wasserstoffbrücken als Akzeptoren aus, sogar schwache C–H$\cdots$O-Wechselwirkungen. Verb. **3** und **4**, die entspannte Si–O–Si-Einheiten von 162 ° und 180 ° aufweisen, besitzen keine Wasserstoffbrücken im Kristallverbund. Es wurden in den PES-Scans typische Formen der freien Elektronenpaare am Sauerstoff in Abhängigkeit vom Winkel gefunden, die experimentell bestätigt werden konnten.
Die Ergebnisse für Verb. **5**, die Silylether-Einheiten trägt, stammen aus periodischen Rechnungen wie auch Vergleichsdaten für Ethergruppen in Saccharose (Verb. **6**). Es wurde gefunden, dass das Konzept submolekularer Transferierbarkeit auch für ELI-Eigenschaften gilt.
Unsubstituiertes Epoxid (Verb. **7**) sowie mit elektronenziehenden Gruppen substituierte Epoxide (Verb. **8** bis **10**) weisen gebogene C–O- und C–C-Bindungen auf, die sich in ED und ELI unterschiedlich manifestieren. Die ,,Source Function" reagiert für Si–O-Bindungen sensibel auf Veränderungen in der chemischen Umgebung, nicht jedoch für C–O-Bindungen. Anhand der Epoxide konnte auch gezeigt werden, dass der neue experimentelle ELI qualitativ und quantitativ die korrekte Topologie ausbildet, was zukünftige Anwendungen in Aussicht stellt.

Additional Studies

1) Experimental ELF of Thymidine

In cooperation with Dr. Christian B. Hübschle, the experimental ELF of the nucleoside thymidine was determined by constrained wave function fitting from a high-resolution X-ray diffraction data set at 20 K. The shape of the localization domain of one of the C–C bonds in the thymine ring, which has double-bond character in most of the corresponding resonance formulae, was found to be different from the other C–C bonds in the compound. As a topological analysis of the experimental ELF had not been done before, it was carefully carried out for thymidine to analyse the different C–C bonds quantitatively.
Electron populations of ELF basins were obtained and showed that the C–C bond in question possesses 3.5 e compared to 1.9 to 2.0 e for all other C–C bonds. Hence, it was characterised as a double bond and thus suggests that the thymine ring should be considered as only a partially delocalised system. The results were published in Ref. [161] and already included in the doctoral thesis of Christian B. Hübschle. This study served as a first test case for the detailed topological analysis of the experimental localisation functions and was a motivation to make some effort to derive the ELI from experiment, too.

2) A Comparative ED Study of Three Protease Inhibitor Model Compounds

The epoxide ring is one possible electrophilic building block to inhibit cysteine or aspartate proteases. Others are aziridines [254] and acceptor-substituted olefins [255]. In cooperation with Prof. Dr. Tanja Schirmeister (Universität Würzburg), niphe-epoxide (cpd. **9** in this doctoral thesis) was compared to identically substituted aziridine and olefin compounds on the basis of high-resolution, low-temperature X-ray diffraction experiments on single crystals as well as isolated-molecule calculations.
Geometries and topological properties within the ED are quite similar, but intermolecular interactions examined by means of interaction energies and a Politzer isosurface analysis [154, 155] showed that the aziridine compound behaves quite differently from the epoxide and olefin compounds. Pronounced electrophilic sites were found for the aziridine compound in the ESP and zero-Laplacian isosurfaces, which predict regio- and stereoselectivity of a nucleophilic attack. Model reactions with sulfur, nitrogen and oxygen nucleophiles were carried out by Dipl.-Chem. Thomas Pfeuffer (Universität Würzburg). They confirmed that the aziridine compound is most reactive and that regio- as well as stereoselectivity were correctly predicted.
The results were published in Ref. [99] and [100]. This study received broad appreciation in that one of the illustrations in Ref. [99] served as cover title of the European Journal of Organic Chemistry (17/2007, 2nd June issue) and in that it was awarded a research highlight of the year 2008 at HASYLAB/DESY [256].

3) Transferability and Reproducibility of Bond-Topological and Atomic Properties in Tripeptides of the Type L-Alanyl-X-L-Alanine

In the previous years, the group of Prof. Dr. Peter Luger has entered into a systematic study of tripeptides of the type L-alanyl-X-L-alanine. So far, experimental ED determinations were published on X = L-alanyl [257], L-tyrosyl [258], glycyl [259], and L-prolyl [260]. Within this doctoral thesis, two additional high-resolution X-ray diffraction data sets could be obtained, namely of X = L-histidinyl and L-phenylalanyl, so that a reasonable amount of experimental data for a concluding statistical evaluation existed.

Overall transferability indices $\overline{\sigma}^{o}_{trans,exp}$ with respect to the standard deviations σ of an averaging procedure of chemically equal atoms and bonds were introduced. For the experimental bond-topological and atomic properties of the scrutinised row of tripeptides, the following values were obtained: $\overline{\sigma}^{o}_{trans,exp}(\varrho_{bcp})$=0.09(2) eÅ^{-3}, $\overline{\sigma}^{o}_{trans,exp}(\nabla^2\varrho_{bcp})$=2.8(4) eÅ^{-5}, $\overline{\sigma}^{o}_{trans,exp}(\mathrm{Q}_{001})$=0.11(4) e and $\overline{\sigma}^{o}_{trans,exp}(\mathrm{V}_{001})$= 0.7(2) Å^3. Not only overall, but also individual transferability indices for each chemically different atom and bond of the tripeptide main chain were calculated. They were compared to overall reproducibility indices as benchmarks for experimental errors: $\overline{\sigma}^{o}_{rep,exp}(\varrho_{bcp})$=0.07 eÅ^{-3}, $\overline{\sigma}^{o}_{rep,exp}(\nabla^2\varrho_{bcp})$=3.3 eÅ^{-5}, $\overline{\sigma}^{o}_{rep,exp}(\mathrm{Q}_{001})$= 0.12 e and $\overline{\sigma}^{o}_{rep,exp}(\mathrm{V}_{001})$=0.4 Å^3. From these comparisons, it resulted that transferability is given for all bonds and atoms in the rigid inner main chain. But for termini (ammonium, carboxylate and carbonyl groups) that are involved in intermolecular interactions, transferability is reduced.

In addition to experimental data, isolated-molecule calculations were performed on all 20 different tripeptides of the type L-alanyl-X-L-alanine and the calculation of transferability indices was repeated. Terminal groups do not exhibit reduced transferability anymore because no crystal effects were accounted for. Nevertheless, chemical differences in the averaged bond and atoms cause transferability indices unequal to zero. The results were published in Ref. [247].

Bibliography

[1] M. von Laue, W. Friedrich, P. Knipping, *Sitzungsber. d. Bayr. Akad. der Wiss.* **1912**, 303–322.

[2] M. von Laue, *Sitzungsber. d. Bayr. Akad. der Wiss.* **1912**, 363–373.

[3] W. Friedrich, P. Knipping, M. von Laue, *Ann. Phys.* **1913**, *346*, 971–988.

[4] P. P. Ewald, *Ann. Phys.* **1914**, *349*, 257–282.

[5] P. P. Ewald, *Ann. Phys.* **1914**, *349*, 1183–1196.

[6] W. H. Bragg, W. L. Bragg, *Proc. R. Soc. Lond.* **1913**, 428–438.

[7] W. H. Bragg, *Phil. Mag.* **1914**, *27*, 881.

[8] A. L. Patterson, *Phys. Rev.* **1934**, *46*, 372–376.

[9] D. Sayre, *Acta Cryst.* **1952**, *5*, 60–65.

[10] J. Karle, H. A. Hauptman, *Acta Cryst.* **1956**, *9*, 635–651.

[11] H. A. Hauptman, *Angew. Chem.* **1986**, *98*, 600–610.

[12] P. Debye, *Ann. Phys.* **1915**, *46*, 809–823.

[13] R. F. Stewart, *J. Chem. Phys.* **1969**, *51*, 4569–4577.

[14] R. F. Stewart, *J. Chem. Phys.* **1973**, *58*, 1668–1676.

[15] F. L. Hirshfeld, *Acta Cryst. B* **1971**, *27*, 769–781.

[16] N. K. Hansen, P. Coppens, *Acta Cryst. A* **1978**, *34*, 909–921.

[17] P. Coppens, *Science* **1967**, *158*, 1577–1579.

[18] P. Coppens, T. M. Sabine, R. G. Delaplane, J. A. Ibers, *Acta Cryst. B* **1969**, *25*, 2451–2458.

[19] D. A. Matthews, G. D. Stucky, *J. Am. Chem. Soc.* **1971**, *93*, 5954–5959.

[20] M. Iwata, *Acta Cryst. B* **1977**, *33*, 59–69.

[21] R. F. W. Bader, A. Larouche, C. Gatti, M. T. Carroll, P. J. MacDougall, K. B. Wiberg, *J. Chem. Phys.* **1987**, *87*, 1142–1152.

[22] R. F. W. Bader, M. T. Carroll, J. R. Cheeseman, C. Chang, *J. Am. Chem. Soc.* **1987**, *109*, 7968–7979.

[23] R. F. W. Bader, *Atoms in Molecules: A Quantum Theory*, 1st edition, No. 22 in The International Series of Monographs on Chemistry, Clarendon Press, Oxford, U.K., **1990**.

[24] R. F. W. Bader, *Chem. Rev.* **1991**, *91*, 893–928.

[25] R. F. W. Bader, P. L. A. Popelier, T. A. Keith, *Angew. Chem. Int. Ed.* **1994**, *33*, 620–631.

[26] T. Koritsánszky, R. Flaig, D. Zobel, H.-G. Krane, W. Morgenroth, P. Luger, *Science* **1998**, *279*, 356–358.

[27] V. Pichon-Pesme, C. Lecomte, H. Lachekar, *J. Phys. Chem.* **1995**, *99*, 6242–6250.

[28] C. Jelsch, V. Pichon-Pesme, C. Lecomte, A. Aubry, *Acta Cryst. D* **1998**, *54*, 1306–1318.

[29] P. M. Dominiak, A. Volkov, X. Li, M. Messerschmidt, P. Coppens, *J. Chem. Theory. Comput.* **2007**, *3*, 232–247.

[30] A. Volkov, M. Messerschmidt, P. Coppens, *Acta Cryst. D* **2007**, *63*, 160–170.

[31] B. Dittrich, T. Koritsánszky, P. Luger, *Angew. Chem. Int. Ed.* **2004**, *43*, 2718–2721.

[32] B. Dittrich, C. B. Hübschle, P. Luger, M. A. Spackman, *Acta Cryst. D* **2006**, *62*, 1325–1335.

[33] P. Coppens, *Angew. Chem. Int. Ed.* **2005**, *44*, 6810–6811.

[34] T. S. Koritsánszky, P. Coppens, *Chem. Rev.* **2001**, *101*, 1583–1628.

[35] P. Luger, *Org. Biomol. Chem.* **2007**, *5*, 2529–2540.

[36] D. Jayatilaka, D. J. Grimwood, *Acta Cryst. A* **2001**, *57*, 76–86.

[37] D. J. Grimwood, D. Jayatilaka, *Acta Cryst. A* **2001**, *57*, 87–100.

[38] I. Bytheway, D. J. Grimwood, D. Jayatilaka, *Acta Cryst. A* **2002**, *58*, 232–243.

[39] I. Bytheway, D. J. Grimwood, B. N. Figgis, G. S. Chandler, D. Jayatilaka, *Acta Cryst. A* **2002**, *58*, 244–251.

[40] P. Hohenberg, W. Kohn, *Phys. Rev.* **1964**, *136*, B864–B871.

[41] W. Kohn, L. J. Sham, *Phys. Rev.* **1965**, *140*, 1133–1138.

[42] V. R. Saunders, *Faraday Symp. Chem. Soc.* **1984**, *19*, 79–84.

[43] R. J. Gillespie, P. L. A. Popelier, *Angew. Chem.* **2003**, *115*, 3452–3455.

[44] R. F. W. Bader, *Chem. Eur. J.* **2006**, *12*, 7769–7772.

[45] G. Frenking, *Angew. Chem. Int. Ed.* **2003**, *42*, 143–147.

[46] G. Frenking, *Angew. Chem.* **2003**, *115*, 3456.

[47] G. Frenking, C. Esterhuysen, A. Kovacs, *Chem. Eur. J.* **2006**, *12*, 7773–7774.

[48] A. D. Becke, K. E. Edgecombe, *J. Chem. Phys.* **1990**, *92*, 5397–5403.

[49] B. Silvi, A. Savin, *Nature* **1992**, *371*, 683–686.

[50] A. Savin, R. Nesper, S. Wengert, T. F. Fässler, *Angew. Chem. Int. Ed.* **1997**, *36*, 1808–1832.

[51] M. Kohout, *Int. J. Quant. Chem.* **2004**, *97*, 651–658.

[52] M. Kohout, *Faraday Discuss.* **2007**, *135*, 43–54.

[53] M. Kohout, F. R. Wagner, Y. Grin, *Theor. Chem. Acc.* **2008**, *119*, 413–420.

[54] V. Tsirelson, A. Stash, *Chem. Phys. Lett.* **2002**, *351*, 142–148.

[55] D. Jayatilaka, D. J. Grimwood, *Acta Cryst. A* **2004**, *60*, 111–119.

[56] S. Grabowsky, M. F. Hesse, C. Paulmann, P. Luger, J. Beckmann, *Inorg. Chem.* **2009**, *48*, 4384–4393.

[57] R. F. W. Bader, C. Gatti, *Chem. Phys. Lett.* **1998**, *287*, 233–238.

[58] C. Gatti, F. Cargnoni, L. Bertini, *J. Comput. Chem.* **2003**, *24*, 422–436.

[59] C. Gatti, L. Bertini, *Acta Cryst. A* **2004**, *60*, 438–449.

[60] R. K. Iler, *The Chemistry of Silica*, Wiley-VCH, New York, **1976**.

[61] G. J. Beall, *SILICA. Reviews in Mineralogy*, American Mineralogist, **1994**, 606.

[62] G. V. Gibbs, K. M. Rosso, D. M. Teter, M. B. Boisen, M. S. T. Bukowinski, *J. Mol. Struct.* **1999**, *485-486*, 13–25.

[63] R. J. Gillespie, S. A. Johnson, *Inorg. Chem.* **1997**, *36*, 3031–3039.

[64] T. Kudo, S. Nagase, *J. Am. Chem. Soc.* **1985**, *107*, 2589–2595.

[65] M. S. Gordon, T. J. Packwood, M. T. Carroll, J. A. Boatz, *J. Phys. Chem.* **1991**, *95*, 4332–4337.

[66] P. Coppens, *X-Ray Charge Densities and Chemical Bonding*, 1. edition, No. 4 in IUCr Texts on Crystallography, Oxford University Press, Oxford, **1997**.

[67] V. G. Tsirelson, O. A. Evdokimova, E. L. Belokoneva, V. S. Urusov, *Phys. Chem. Miner.* **1990**, *17*, 275–292.

[68] B. J. Teppen, D. M. Miller, S. Q. Newton, L. Schäfer, *J. Phys. Chem.* **1994**, *98*, 12545–12557.

[69] N. Binggeli, N. Troullier, J. L. Martins, J. R. Chelikowsky, *Phys. Rev. B.* **1991**, *44*, 4771–4777.

[70] G. V. Gibbs, J. W. Downs, J. Boisen, *Rev. Mineral.* **1994**, *29*, 331–368.

[71] H. Oberhammer, J. E. Boggs, *J. Am. Chem. Soc.* **1980**, *102*, 7241–7244.

[72] J. B. Nicholas, R. E. Winans, R. J. Harrison, L. E. Iton, L. A. Curtiss, A. J. Hopfinger, *J. Phys. Chem.* **1992**, *96*, 7958–7965.

[73] W. Noll, *Chemistry and Technology of the Silicones*, Academic Press, New York, **1969**.

[74] S. J. Clarson, J. A. Semlyen, *Siloxane Polymers*, Prentice Hall, Englewood Cliffs, **1993**.

[75] I. Manners, *Angew. Chem. Int. Ed.* **1996**, *35*, 1603–1621.

[76] J. J. Daly, F. Sanz, *J. Chem. Soc., Dalton Trans.* **1973**, *1973*, 2474–2475.

[77] Y.-L. Chen, J.-Q. Sun, X. Wei, W.-Y. Wong, A. W. M. Lee, *J. Org. Chem.* **2004**, *69*, 7190–7197.

[78] W. Wojnowski, B. Becker, K. Peters, E.-M. Peters, H. G. von Schnering, *Z. Anorg. Allg. Chem.* **1988**, *563*, 53–58.

[79] C. Glidewell, D. C. Liles, *Acta Cryst. B* **1978**, *34*, 124–128.

[80] B. Morosin, L. A. Harrah, *Acta Cryst. B* **1981**, *37*, 579–586.

[81] M. Berthelot, F. Besseau, C. Laurence, *Eur. J. Org. Chem.* **1998**, *1998*, 925–931.

[82] D. G. Lee, R. Cameron, *Can. J. Chem.* **1972**, *50*, 445–448.

[83] J. Beckmann, D. Dakternieks, A. Duthie, M. L. Larchin, E. R. T. Tiekink, *Appl. Organometal. Chem.* **2003**, *17*, 52–62.

[84] D. M. M. Jaradat, S. Mebs, L. Chęcińska, P. Luger, *Carbohydr. Res.* **2007**, *177*, 149–151.

[85] R. E. Parker, N. S. Isaacs, *Chem. Rev.* **1959**, *59*, 737–799.

[86] D.-K. Pan, J.-N. Gao, H.-L. Lin, M.-B. Huang, W. H. E. Schwarz, *Int. J. Quant. Chem.* **1986**, *29*, 1147–1154.

[87] A. K. Yudin, *Aziridines and Epoxides in Organic Synthesis*, Wiley-VCH, Weinheim, **2006**.

[88] A. Padwa, S. S. Murphree, *ARKIVOC* **2006**, *3*, 6–33.

[89] H. C. Kolb, M. G. Finn, K. B. Sharpless, *Angew. Chem. Int. Ed.* **2001**, *40*, 2004–2021.

[90] V. V. Fokin, P. Wu, *Aziridines and Epoxides in Organic Synthesis*, VCH-Wiley, chap. Epoxides and Aziridines in Click Chemistry, **2006**, 443–477.

[91] J. C. Powers, J. L. Asgian, Ö. D. Ekici, K. E. James, *Chem. Rev.* **2002**, *102*, 4639–4750.

[92] S. Ro, S.-G. Baek, B. Lee, J. H. Ok, *J. Pept. Res.* **1999**, *54*, 242–248.

[93] F. Schulz, C. Gelhaus, B. Degel, R. Vicik, S. Heppner, A. Breuning, M. Leippe, J. Gut, P. J. Rosenthal, T. Schirmeister, *ChemMedChem* **2007**, *2*, 1214–1224.

[94] T.-W. Lee, M. M. Cherney, C. Huitema, J. Liu, K. E. James, J. C. Powers, L. D. Eltis, M. N. G. James, *J. Mol. Biol.* **2005**, *353*, 1137–1151.

[95] E. Martina, N. Stiefl, B. Degel, F. Schulz, A. Breuning, M. Schiller, R. Vicik, K. Baumann, J. Ziebuhr, T. Schirmeister, *Bioorg. Med. Chem. Lett.* **2005**, *15*, 5365–5369.

[96] H.-H. Otto, T. Schirmeister, *Chem. Rev.* **1997**, *97*, 133–171.

[97] B. M. Dunn, *Chem. Rev.* **2002**, *102*, 4431–4458.

[98] B. Degel, P. Staib, S. Rohrer, J. Scheiber, E. Martina, C. Büchold, K. Baumann, J. Morschhäuser, T. Schirmeister, *Chem. Med. Chem.* **2008**, *3*, 302–315.

[99] S. Grabowsky, T. Pfeuffer, L. Chęcińska, M. Weber, W. Morgenroth, P. Luger, T. Schirmeister, *Eur. J. Org. Chem.* **2007**, *17*, 2759–2768.

[100] S. Grabowsky, T. Pfeuffer, W. Morgenroth, C. Paulmann, T. Schirmeister, P. Luger, *Org. Biomol. Chem.* **2008**, *6*, 2295–2307.

[101] P. Luger, C. Zaki, J. Buschmann, R. Rudert, *Z. Kristallogr.* **1986**, *174*, 138.

[102] P. Luger, C. Zaki, J. Buschmann, R. Rudert, *Angew. Chem. Int. Ed.* **1986**, *25*, 276–277.

[103] D. A. Matthews, J. Swanson, M. H. Mueller, G. D. Stucky, *J. Am. Chem. Soc.* **1971**, *93*, 5945–5953.

[104] A. E. Goeta, J. A. K. Howard, *Chem. Soc. Rev.* **2004**, *33*, 490–500.

[105] S. K. J. Johnas, W. Morgenroth, E. Weckert, *HASYLAB Annual Report* **2006**, 325–328.

[106] M. Messerschmidt, P. Luger, *Acta Cryst. A* **2002**, *58*, C262.

[107] M. Messerschmidt, M. Meyer, P. Luger, *J. Appl. Crystallogr.* **2003**, *36*, 1452–1454.

[108] A. Ø. Madsen, H. O. Sørensen, C. Flensburg, R. F. Stewart, S. Larsen, *Acta Cryst. A* **2004**, *60*, 550–561.

[109] A. Ø. Madsen, *J. Appl. Crystallogr.* **2006**, *39*, 757–758.

[110] P. Luger, *Modern X-Ray Analysis on Single Crystals*, de Gruyter, Berlin, New York, **1980**.

[111] G. H. Stout, L. H. Jensen, *X-ray Structure Determination - A Practical Guide*, The Macmillan Company, London, **1968**.

[112] W. Massa, R. O. Gould, *Crystal Structure Determination*, 2nd edition, Springer-Verlag, Berlin, **2004**.

[113] E. Clementi, D. L. Raimondi, *J. Chem. Phys.* **1963**, *38*, 2686–2689.

[114] E. Clementi, C. Roetti, *Atomic and Nuclear Data Tables* **1974**, *14*, 177–478.

[115] Z. Su, P. Coppens, *Acta Cryst. A* **1998**, *54*, 646–652.

[116] P. Macchi, P. Coppens, *Acta Cryst. A* **2001**, *57*, 656–662.

[117] K. Kurki-Suonio, *Isr. J. Chem.* **1977**, *16*, 115–123.

[118] I. N. Levine, *Quantum Chemistry*, 5th edition, Prentice Hall, Upper Saddle River, New Jersey, USA, **2000**.

[119] R. G. Parr, *Annu. Rev. Phys. Chem.* **1983**, *34*, 631–656.

[120] R. G. Parr, W. Yang, *Annu. Rev. Phys. Chem.* **1995**, *46*, 701–728.

[121] K. Capelle, *arXiv:cond-mat.mtrl-sci* **2006**, *0211443v5*, 1–69.

[122] C. Lee, W. Yang, R. G. Parr, *PHRB* **1988**, *37*, 785–789.

[123] A. D. Becke, *J. Chem. Phys.* **1993**, *98*, 1372–1377.

[124] J. B. Foresman, A. Frisch, *Exploring Chemistry with Electronic Structure Methods*, 2nd edition, Gaussian, Pittsburgh, USA, **1996**.

[125] D. C. Young, *Computational chemistry: a practical guide for applying techniques to real world problems*, Wiley, New York, USA, **2001**.

[126] S. F. Boys, F. Bernardi, *Mol. Phys.* **1970**, *19*, 553–566.

[127] M. P. Andersson, P. Uvdal, *J. Phys. Chem. A* **2005**, *109*, 2937–2941.

[128] S. M. Bachrach, J. M. Hayes, T. Dao, J. L. Mynar, *Theor. Chem. Acc.* **2002**, *107*, 266–271.

[129] A. E. Reed, L. A. Curtiss, F. Weinhold, *Chem. Rev.* **1988**, *88*, 899–926.

[130] F. Weinhold, *J. Mol. Struct. (Theochem)* **1997**, *398-399*, 181–197.

[131] F. Weinhold, C. R. Landis, *Chem. Educ. Res. Pract. Eur.* **2001**, *2*, 91–104.

[132] M. Mladenovic, M. Arnone, R. F. Fink, B. Engels, *J. Phys. Chem. B* **2009**, *113*, 5072–5082.

[133] B. Civalleri, P. D′Arco, R. Orlando, V. R. Saunders, R. Dovesi, *Chem. Phys. Lett.* **2001**, *348*, 131–138.

[134] M. D. Towler, A. Zupan, M. Causa, *Comp. Phys. Comm.* **1996**, *98*, 181–205.

[135] A. Lichanot, M. Rerat, M. Catti, *Acta Cryst. A* **1995**, *51*, 323–328.

[136] P. Popelier, *Coord. Chem. Rev.* **2000**, *197*, 169–189.

[137] R. F. W. Bader, T. S. Slee, D. Cremer, E. Kraka, *J. Am. Chem. Soc.* **1983**, *105*, 5061–5068.

[138] L. J. Farrugia, P. Macchi, *J. Phys. Chem. A* **2009**, *113*, 10058–10067.

[139] C. Gatti, D. Lasi, *Faraday Discuss.* **2007**, *135*, 55–78.

[140] L. J. Farrugia, C. Evans, M. Tegel, *J. Phys. Chem. A* **2006**, *110*, 7952–7961.

[141] L. J. Farrugia, C. Evans, D. Lentz, M. Roemer, *J. Am. Chem. Soc.* **2009**, *131*, 1251–1268.

[142] G. Náray-Szabo, G. G. Ferenczy, *Chem. Rev.* **1995**, *95*, 829–847.

[143] M. A. Spackmann, J. J. McKinnon, D. Jayatilaka, *CrystEngComm* **2008**, *10*, 377–388.

[144] C. Lecomte, N. Ghermani, V. Pichon-Pesme, M. Souhassou, *J. Mol. Struct. (Theochem)* **1992**, *255*, 241–260.

[145] A. Volkov, H. F. King, P. Coppens, L. J. Farrugia, *Acta Cryst. A* **2006**, *62*, 400–408.

[146] G. te Velde, F. M. Bickelhaupt, E. J. Baerends, C. F. Guerra, S. J. A. van Gisbergen, J. G. Snijders, T. Ziegler, *J. Comput. Chem.* **2001**, *22*, 931–967.

[147] A. J. Stone, *The Theory of Intermolecular Forces*, No. 32 in The International Series of Monographs on Chemistry, Oxford University Press, Oxford, U.K., **1997**.

[148] D. E. Williams, S. R. Cox, *Acta Cryst. B* **1984**, *40*, 404–417.

[149] M. A. Spackman, *J. Chem. Phys.* **1986**, *85*, 6579–6586.

[150] A. Volkov, T. Koritsánzky, P. Coppens, *Chem. Phys. Lett.* **2004**, *391*, 170–175.

[151] R. F. W. Bader, M. E. Stephens, *J. Am. Chem. Soc.* **1975**, *97*, 7391–7399.

[152] J. M. Molina, J. A. Dobado, *Theor. Chem. Acc.* **2001**, *105*, 328–337.

[153] P. Macchi, A. Sironi, *Coord. Chem. Rev.* **2003**, *238–239*, 383–412.

[154] J. S. Murray, P. Lane, P. Politzer, *J. Am. Chem. Soc.* **1995**, *85*, 1–8.

[155] P. Politzer, J. S. Murray, Z. Preralta-Inga, *Int. J. Quant. Chem.* **2001**, *85*, 676–684.

[156] C. B. Hübschle, S. Scheins, M. Weber, P. Luger, A. Wagner, T. Koritsánszky, S. I. Troyanov, O. V. Boltalina, I. V. Goldt, *Chem. Eur. J.* **2007**, *13*, 1910–1920.

[157] W.-T. Chan, I. P. Hamilton, *J. Chem. Phys.* **1998**, *108*, 2473–2485.

[158] M. A. Spackman, P. G. Byrom, *Chem. Phys. Lett.* **1997**, *267*, 215–220.

[159] F. L. Hirshfeld, *Theor. Chim. Acta* **1977**, *44*, 129–138.

[160] A. Savin, O. Jepsen, J. Flad, O. K. Andersen, H. Preuss, H. G. von Schnering, *Angew. Chem. Int. Ed.* **1992**, *31*, 187–188.

[161] C. B. Hübschle, B. Dittrich, S. Grabowsky, M. Messerschmidt, P. Luger, *Acta Cryst. B* **2008**, *64*, 363–374.

[162] F. R. Wagner, V. Bezugly, M. Kohout, Y. Grin, *Chem. Eur. J.* **2007**, *13*, 5724–5741.

[163] F. R. Wagner, M. Kohout, Y. Grin, *J. Phys. Chem. A* **2008**, *112*, 9814–9828.

[164] S. Raub, G. Jansen, *Theor. Chem. Acc.* **2001**, *106*, 223–232.

[165] M. Kohout, A. Savin, *Int. J. Quant. Chem.* **1996**, *60*, 875–882.

[166] M. Kohout, F. R. Wagner, Y. Grin, *Int. J. Quant. Chem.* **2006**, *106*, 1499–1507.

[167] A. Savin, B. Silvi, F. Colonna, *Can. J. Chem.* **1996**, *74*, 1088–1096.

[168] M. Calatayud, J. Andres, A. Beltran, B. Silvi, *Theor. Chem. Acc.* **2001**, *105*, 299–308.

[169] S. Berski, K. Mierzwicki, A. Bil, Z. Latajka, *Chem. Phys. Lett.* **2008**, *460*, 559–562.

[170] X. Krokidis, S. Noury, B. Silvi, *J. Phys. Chem. A* **1997**, *101*, 7277–7282.

[171] F. H. Allen, *Acta Cryst. B* **2002**, *58*, 380–388.

[172] A. Spielberger, P. Gspaltl, H. Siegl, E. Hengge, K. Gruber, *J. Organomet. Chem.* **1995**, *499*, 241–246.

[173] C. Eaborn, P. B. Hitchcock, P. D. Lickiss, *J. Organomet. Chem.* **1984**, *264*, 119–126.

[174] A. I. Gusev, M. G. Los', Y. M. Varezhkin, M. M. Morgunova, D. Y. Zhinkin, *J. Struct. Chem.* **1976**, *17*, 329–331.

[175] V. E. Shklover, H.-B. Bürgi, A. Raselli, T. Armbruster, W. Hummel, *Acta Cryst. B* **1991**, *47*, 544–548.

[176] Y. Kabe, K. Ohkubo, H. Ishikawa, W. Ando, *J. Am. Chem. Soc.* **2000**, *122*, 3775–3776.

[177] S. Shambayati, S. L. Schreiber, J. F. Blake, S. G. Wierschke, W. L. Jorgensen, *J. Am. Chem. Soc.* **1990**, *112*, 697–703.

[178] R. J. Hill, G. V. Gibbs, *Acta Cryst. B* **1979**, *35*, 25–30.

[179] C. A. Coulson, *Valence*, 2nd edition, Oxford University Press, London, **1963**.

[180] K. B. Wiberg, *Acc. Chem. Res.* **1996**, *29*, 229–234.

[181] T. Förster, *Z. Phys. Chem. B* **1939**, *43*, 58.

[182] C. A. Coulson, W. E. Moffitt, *Phil. Mag.* **1949**, *40*, 1.

[183] C. A. Coulson, T. H. Goodwin, *J. Chem. Soc.* **1962**, 2851–2854.

[184] A. D. Walsh, *Nature* **1947**, *159*, 712–713.

[185] A. D. Walsh, *Trans. Faraday. Soc.* **1949**, *45*, 179–190.

[186] P. Chakrabarti, P. Seiler, J. D. Dunitz, A.-D. Schlüter, G. Szeimies, *J. Am. Chem. Soc.* **1981**, *103*, 7378–7380.

[187] R. Boese, T. Miebach, A. de Meijere, *J. Am. Chem. Soc.* **1991**, *113*, 1743–1748.

[188] T. Koritsánszky, J. Buschmann, P. Luger, *J. Phys. Chem.* **1996**, *100*, 10547–10553.

[189] P. Luger, M. Messerschmidt, S. Scheins, A. Wagner, *Acta Cryst. A* **2004**, *60*, 390–396.

[190] C. L. Klein, E. D. Stevens, *Acta Cryst. B* **1988**, *44*, 50–55.

[191] A. Vila, R. A. Mosquera, *Tetrahedron* **2001**, *57*, 9415–9422.

[192] A. Vila, R. A. Mosquera, *J. Mol. Struct. (Theochem)* **2002**, *586*, 47–56.

[193] Y. L. Frolov, S. M. Shostakovskii, G. I. Kagan, *Teor. i Eksp. Khim.* **1969**, *5*, 153–159.

[194] L. A. Strait, R. Ketcham, D. Jambotkar, V. P. Shah, *J. Am. Chem. Soc.* **1964**, *86*, 4628–4630.

[195] J. Beckmann, M. Hesse, *Z. Anorg. Allg. Chem.* **2007**, *633*, 1233–1238.

[196] W. Fink, *Helv. Chim. Acta* **1974**, *57*, 1010–1015.

[197] H. Gilman, H. N. Benedict, H. Hartzfeld, *J. Org. Chem.* **1954**, *19*, 419–427.

[198] R. H. Blessing, C. Lecomte, *Experimental Requirements for Charge Density Analysis*, Plenum Press, New York, chap. 155–185, The Application of Charge Density Research to Chemistry and Drug Design, **1991**, 155–185.

[199] W. Kabsch, *J. Appl. Crystallogr.* **1988**, *21*, 916–924.

[200] W. Kabsch, *J. Appl. Crystallogr.* **1988**, *21*, 67–71.

[201] W. Kabsch, *J. Appl. Crystallogr.* **1993**, *26*, 795–800.

[202] R. H. Blessing, D. A. Langs, *J. Appl. Crystallogr.* **1987**, *20*, 427–428.

[203] R. H. Blessing, *J. Appl. Crystallogr.* **1989**, *22*, 396–397.

[204] R. H. Blessing, *J. Appl. Crystallogr.* **1997**, *30*, 421–426.

[205] G. M. Sheldrick, *Acta Cryst. A* **2008**, *64*, 112–122.

[206] M. N. Burnett, C. K. Johnson, ORTEP-III, Oak Ridge Thermal Ellipsoid Plot Program for Crystal Structure Illustrations, *Tech. rep.*, Oak Ridge National Laboratory Report ORNL-6895, Oak Ridge, Tennessee, U.S.A., **1996**.

[207] A. Volkov, P. Macchi, L. J. Farrugia, C. Gatti, P. R. Mallinson, T. Richter, T. S. Koritsánszky, *XD2006 - a Computer Program for Multipole Refinement, Topological Analysis and Evaluation of Intermolecular Energies from Experimental and Theoretical Structure Factors*, **2006**.

[208] A. Volkov, Y. Abramov, P. Coppens, *Acta Cryst. A* **2001**, *57*, 272–282.

[209] F. H. Allen, O. Kennard, D. G. Watson, L. Brammer, A. G. Orpen, R. Taylor, *International Tables for X-ray Crystallography*, Kluwer Academic Publishers, Amsterdam, vol. C, chap. 9.5, **1992**, 685–706.

[210] P. M. Dominiak, P. Coppens, *Acta Cryst. A* **2006**, *62*, 224–227.

[211] S. Mebs, A. Lüth, W. Löwe, C. Paulmann, P. Luger, *Z. Kristallogr.* **2008**, *223*, 502–514.

[212] N. Kocher, C. Selinka, D. Leusser, D. Kost, I. Kalikhman, D. Stalke, *Z. Anorg. Allg. Chem.* **2004**, *630*, 1777–1793.

[213] A. Volkov, P. Coppens, *Acta Cryst. A* **2001**, *57*, 395–405.

[214] T. Williams, C. Kelley, *et al.*, gnuplot 4.0 - An Interactive Plotting Program, *Tech. rep.*, **2004**.

[215] G. Bergerhoff, M. Berndt, K. Brandenburg, *J. Res. Natl. Inst. Stand. Technol.* **1996**, *101*, 221–225.

[216] C. B. Hübschle, P. Luger, *J. Appl. Crystallogr.* **2006**, *39*, 901–904.

[217] E. Keller, Schakal99 - A Fortran Program for the Graphical Representation of Molecular and Solid-State Structure Models, *Tech. rep.*, Albert-Ludwigs-Universität Freiburg, Freiburg, Germany, **1999**.

[218] D. Jayatilaka, D. J. Grimwood, *Computational Science - ICCS 2003, Part 4*, Springer Verlag, chap. Tonto: A Fortran Based Object-Oriented System for Quantum Chemistry and Crystallography, **2003**, 142–151.

[219] M. Kohout, DGrid version 4.4, *Tech. rep.*, Radebeul, **2008**.

[220] R. F. W. Bader, *Atoms in Molecules: A Quantum Theory*, 2nd edition, No. 22 in The International Series of Monographs on Chemistry, Clarendon Press, Oxford, **1994**.

[221] M. J. Frisch, *et al.*, Gaussian 03, Revision E.01, *Tech. rep.*, Gaussian, Inc., Wallington CT, **2004**.

[222] F. Biegler-König, J. Schönbohm, D. Bayles, *J. Comput. Chem.* **2001**, *22*, 545–559.

[223] R. Dovesi, V. R. Saunders, C. Roetti, R. Orlando, C. M. Zicovich-Wilson, F. Pascale, B. Civalleri, K. Doll, N. Harrison, I. Bush, P. DArco, M. Llunell, *CRYSTAL06, version 1.0.2*, **2008**.

[224] R. Nada, J. B. Nicholas, M. I. McCarthy, A. C. Hess, *Int. J. Quant. Chem.* **1996**, *60*, 809–820.

[225] C. Gatti, V. R. Saunders, C. Roetti, *J. Chem. Phys.* **1994**, *101*, 10686–10696.

[226] A. Okninski, *Catastrophe Theory*, No. 33 in Comprehensive Chemical Kinetics, (editor: R. G. Compton), Elsevier, Amsterdam, **1992**.

[227] S. Berski, J. Andres, B. Silvi, L. R. Domingo, *J. Phys. Chem. A* **2003**, *107*, 6014–6024.

[228] Microcal Software Inc., One Roundhouse Plaza, Northampton, MA 01060, USA, *Origin, version 5.0*, **1991–1997**.

[229] M. J. Barrow, E. A. V. Ebsworth, M. M. Harding, *Acta Cryst. B* **1979**, *35*, 2093–2099.

[230] J. Beckmann, S. Grabowsky, *J. Phys. Chem. A* **2007**, *111*, 2011–2019.

[231] R. West, R. H. Baney, *J. Am. Chem. Soc.* **1959**, *81*, 6145–6148.

[232] A. Reisinger, N. Trapp, I. Krossing, S. Altmannshofer, V. Herz, M. Presnitz, W. Scherer, *Angew. Chem. Int. Ed.* **2007**, *46*, 8295–8298.

[233] D. Himmel, N. Trapp, I. Krossing, S. Altmannshofer, V. Herz, G. Eickerling, W. Scherer, *Angew. Chem. Int. Ed.* **2008**, *47*, 7798–7801.

[234] T.-H. Tang, E. Deretey, S. J. K. Jensen, I. G. Csizmadia, *Eur. Phys. J. D* **2006**, *37*, 217–222.

[235] S. J. Grabowski, *Chem. Phys. Lett.* **2001**, *338*, 361–366.

[236] M. Ziolkowski, S. J. Grabowski, J. Leszczynski, *J. Phys. Chem. A* **2006**, *110*, 6514–6521.

[237] U. Koch, P. L. A. Popelier, *J. Phys. Chem.* **1995**, *99*, 9747–9754.

[238] G. A. Jeffrey, H. Maluszynska, J. Mitra, *Int. J. Biol. Macromol.* **1985**, *7*, 336–348.

[239] G. A. Jeffrey, *An Introduction to Hydrogen Bonding*, Oxford University Press, Oxford, U.K., **1997**.

[240] T. Steiner, *Angew. Chem.* **2002**, *114*, 50–80.

[241] J. P. Glusker, *Acta Cryst. D* **1995**, *51*, 418–427.

[242] J. Sola, A. Riera, X. Verdaguer, M. A. Maestro, *J. Am. Chem. Soc.* **2005**, *127*, 13629–13633.

[243] G. L. Sosa, N. Peruchena, R. H. Contreras, E. A. Castro, *J. Mol. Struct. (Theochem)* **1997**, *401*, 77–85.

[244] Bruker AXS Inc., Madison, WI, USA, *APEX2, SAINT, XPREP and SADABS*, **2004-2009**.

[245] A. J. Blake, E. A. V. Ebsworth, S. G. D. Henderson, *Acta Cryst. C* **1988**, *44*, 1–3.

[246] K. Vojinovic, U. Losehand, N. W. Mitzel, *Dalton Trans.* **2004**, 2578–2581.

[247] S. Grabowsky, R. Kalinowski, M. Weber, D. Förster, C. Paulmann, P. Luger, *Acta Cryst. B* **2009**, *65*, 488–501.

[248] P. Luger, J. Buschmann, *J. Am. Chem. Soc.* **1984**, *106*, 7118–7121.

[249] M. W. Miller, *J. Med. Chem.* **1963**, *6*, 233–237.

[250] W. J. Linn, O. W. Webster, R. E. Benson, *J. Am. Chem. Soc.* **1965**, *87*, 3651–3656.

[251] Bruker AXS Inc., Madison, WI, *SMART and SAINT Data Collection and Processing Software for the SMART System*, **1995–2005**.

[252] A. Volkov, Y. Abramov, P. Coppens, C. Gatti, *Acta Cryst. A* **2000**, *56*, 332–339.

[253] B. Dittrich, M. Weber, R. Kalinowski, S. Grabowsky, C. B. Hübschle, P. Luger, *Acta Cryst. B* **2009**, *65*, 749–756.

[254] R. Vicik, H. Helten, T. Schirmeister, B. Engels, *Chem. Med. Chem.* **2006**, *1*, 1021–1028.

[255] R. Vicik, M. Busemann, K. Baumann, T. Schirmeister, *Curr. Top. Med. Chem.* **2006**, *6*, 331–353.

[256] S. Grabowsky, T. Pfeuffer, W. Morgenroth, C. Paulmann, T. Schirmeister, P. Luger, *Photon Science 2008 - Highlights and HASYLAB Annual Report* **2008**, 30–31.

[257] E. Rödel, M. Messerschmidt, B. Dittrich, P. Luger, *Org. Biomol. Chem.* **2006**, *4*, 475–481.

[258] L. Chęcińska, S. Mebs, C. B. Hübschle, D. Förster, W. Morgenroth, P. Luger, *Org. Biomol. Chem.* **2006**, *4*, 3242–3251.

[259] D. Förster, A. Wagner, C. B. Hübschle, C. Paulmann, P. Luger, *Z. Naturforsch.* **2006**, *62b*, 696–704.

[260] R. Kalinowski, B. Dittrich, C. B. Hübschle, C. Paulmann, P. Luger, *Acta Cryst. B* **2007**, *63*, 753–767.

List of Publications

Publications in Scientific Journals

1. J. Beckmann, S. Grabowsky: Supramolecular Silanol Chemistry in the Gas Phase. Topological (AIM) and Population (NBO) Analyses of Hydrogen-Bonded Complexes between H_3SiOH and Selected O- and N- Acceptor Molecules. *J. Phys. Chem. A* **2007**, *111*, 2011-2019.

2. S. Grabowsky, T. Pfeuffer, L. Chęcińska, M. Weber, W. Morgenroth, P. Luger, T. Schirmeister: Electron Density Determination of Electrophilic Building Blocks as Model Compounds for Protease Inhibitors. *Eur. J. Org. Chem.* **2007**, *17*, 2759-2768, including cover title.

3. C. B. Hübschle, B. Dittrich, S. Grabowsky, M. Messerschmidt, P. Luger: Comparative experimental electron density and electron localization function study of thymidine based on 20 K X-ray diffraction data. *Acta Cryst. B* **2008**, *64*, 363-374.

4. S. Grabowsky, M. Weber, J. Buschmann, P. Luger: Experimental electron density study of ethylene oxide at 100K. *Acta Cryst. B* **2008**, *64*, 397-400.

5. S. Grabowsky, T. Pfeuffer, W. Morgenroth, C. Paulmann, T. Schirmeister, P. Luger: A Comparative Study on the Experimentally Derived Electron Densities of three Protease Inhibitor Model Compounds. *Org. Biomol. Chem.* **2008**, *6*, 2295-2307.

6. S. Grabowsky, M. F. Hesse, C. Paulmann, P. Luger, J. Beckmann: How to Make the Ionic Si-O Bond More Covalent and the Si-O-Si Linkage a Better Acceptor for Hydrogen Bonding. *Inorg. Chem.* **2009**, *48*, 4384-4393.

7. S. Grabowsky, R. Kalinowski, M. Weber, D. Förster, C. Paulmann, P. Luger: Transferability and reproducibility in electron-density studies - bond topo-

logical and atomic properties of tripeptides of the type L-alanyl-X-L-alanine. *Acta Cryst. B* **2009**, *65*, 488-501.

8. B. Dittrich, M. Weber, R. Kalinowski, S. Grabowsky, C. B. Hübschle, P. Luger: How to easily replace the independent atom model the example of bergenin, a potential anti-HIV agent of traditional Asian medicine. *Acta Cryst. B* **2009**, *65*, 749-756.

9. S. Grabowsky, M. Weber, Y.-S. Chen, D. Lentz, B. Schmidt, M. Hesse, P. Luger: Electron density of corannulene from synchrotron data at 12 K, comparison with fullerene results. *Z. Naturforsch.*, submitted.

10. S. Mebs, S. Grabowsky, D. Förster, R. Kickbusch, M. Hartl, L. L. Daemen, W. Morgenroth, P. Luger, B. Paulus, D. Lentz: On the Nature of the Dative Bond - An Experimental and Theoretical Electron Density Determination of Hydrazine Borane, Hydrazine Bisborane Dioxane Solvate and Ammonia Trifluoroborane. *J. Am. Chem. Soc.*, to be submitted.

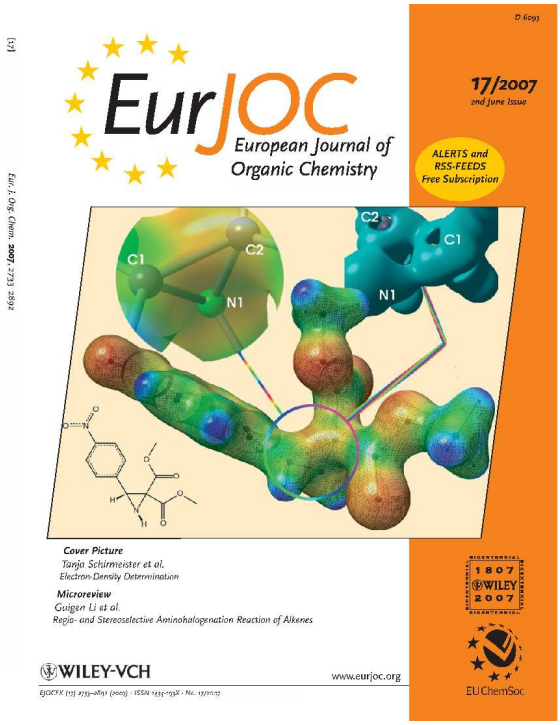

Cover title of of the European Journal of Organic Chemistry (17/2007, 2nd June issue)

Published Reports

1. S.Grabowsky, T.Pfeuffer, L.Chęcińska, M. Weber, W. Morgenroth, T.Schirmeister: Charge Density and Drug Development - Model Compound for Protease Inhibitors. *HASYLAB Annual Report* **2006**, pp. 1267-1268.

2. S. Grabowsky, T. Pfeuffer, W. Morgenroth, C. Paulmann, T. Schirmeister, P. Luger: A Comparative Study on the Experimentally Derived Electron Density of three Protease Inhibitor Model Compounds. *HASYLAB Annual Report* **2007**, pp. 1461-1462.

3. S. Grabowsky, J. Holstein, W. Morgenroth, C. Paulmann, P. Luger: Structures of the Tripeptides L-Alanyl-L-phenylalanyl-L-alanine (AFA) and Tri-L-aspartic acid (DDD) at Low Temperatures. *HASYLAB Annual Report* **2007**, pp.1533-1534.

4. S. Grabowsky, J. Beckmann, M. Hesse, C. Paulmann, P. Luger: Electron-Density Study on a Siloxanol Compound with an Unusual Hydrogen Bond. *HASYLAB Annual Report* **2007**, pp.549-550.

5. D. Förster, S. Grabowsky, W. Morgenroth, R. Kickbusch, D. Lentz, P. Luger: Charge density analysis of the closo-boranates B10H102- and B12H12 2-. *HASYLAB Annual Report* **2007**, pp.1249-1250.

6. S. Grabowsky, T. Pfeuffer, W. Morgenroth, C. Paulmann, T. Schirmeister, P. Luger: Insight into the reactivity. Study of biologically active molecules from ground-state electron densities. *Photon Science 2008 - Highlights and HASYLAB Annual Report* **2008**, pp. 30-31. (web-article: http://hasylab.desy.de/ news__events/ research_highlights/ insight_into_the_reactivity/ index_eng.html)

7. S. Grabowsky, S. D. Hoffmann, U. Ahmad, J. Beckmann, J. Richter, P. Luger: Electron-Density Determination of a Boroxine Compound from High-Resolution X-Ray Data Measured with a STOE IPDS 2T. *Stoe & Cie GmbH*, Labnote, **June 2009**. (web-article: http://www.stoe.com/pages/brochure/ Labnote_ED.pdf)

Talks at Conferences

1. T. Pfeuffer, L. Chęcińska, M. Weber, S. Grabowsky, P. Luger, T. Schirmeister: Synthesis, Crystallization and Electron Density Determination of Electrophilic Building Blocks as Model Compounds for Protease Inhibitors. *First Report Colloquium of the DFG Priority Program SPP 1178*, Hamburg, Germany, **July 2006**.

2. S. Grabowsky, T. Pfeuffer, W. Morgenroth, C. Paulmann, T. Schirmeister, P. Luger: An Experimental Electron Density and ELF Study of Protease Inhibitor Model Compounds. *Gordon Conference on Electron Distribution and Chemical Bonding*, South Hadley, USA, **July 2007**, (short oral presentation).

3. S. Grabowsky, J. Beckmann, M. Hesse, W. Morgenroth, C. Paulmann, P. Luger: Exploring the Electron-Density Distribution and the Electron Localization Function for Several Siloxane Linkages: How Does the Electronic Situation Change with Different Si-O-Si Angles? *16. Jahrestagung der Deutschen Gesellschaft für Kristallographie*, Erlangen, Germany, **March 2008**.

4. S. Grabowsky, J. Beckmann, M. Hesse, W. Morgenroth, C. Paulmann, P. Luger: How to Tune the Siloxane Linkage into a Good Acceptor for Hydrogen Bonding? *Tag der Chemie*, Berlin, Germany, **April 2008**.

5. S. Grabowsky, D. Jayatilaka, T. Schirmeister, P. Luger: Theoretical and Experimental ELI-D and Electron-Density Topologies of Four Epoxide Derivatives. *XVI. Sagamore Conference*, Santa Fe, USA, **August 2009**, (short oral presentation).

Poster Presentations at Conferences

1. S. Grabowsky, P. Luger, T. Pfeuffer, L. Chęcińska, M. Weber, W. Morgenroth, T. Schirmeister: Application of ELF to a Protease Inhibitor Model Compound: Preliminary Results. *AK 14 Workshop der Deutschen Gesellschaft für Kristallographie (DGK)*, Aachen, Germany, **February 2007**.

2. S. Grabowsky, T. Pfeuffer, L. Chęcińska, M. Weber, P. Luger, T. Schirmeister: Correlation of Molecular Properties from Experimentally Derived Electron Density with Biological Activity - A Protease Inhibitor Model Compound. *Frontiers in Medicinal Chemistry, Joint German-Swiss Meeting on Medicinal Chemistry*, Berlin, Germany, **March 2007**.

3. S. Grabowsky, T. Pfeuffer, W. Morgenroth, C. Paulmann, T. Schirmeister, P. Luger: An Experimental Electron Density and ELF Study of Protease Inhibitor Model Compounds. *Gordon Conference on Electron Distribution and Chemical Bonding*, South Hadley, USA, **July 2007**.

4. S. Grabowsky, J. Beckmann, M. Hesse, C. Paulmann, P. Luger: Electron-Density and ELF Study on a Siloxanol Compound with an Unusual Hydrogen Bond. *Workshop on Electron Localizability and Analysis of Chemical Bonding*, Dresden, Germany, **February 2008**.

5. S. Grabowsky, J. Beckmann, M. Hesse, W. Morgenroth, C. Paulmann, P. Luger: How to Tune the Siloxane Linkage into a Good Acceptor for Hydrogen Bonding? *Tag der Chemie*, Berlin, Germany, **April 2008**.

6. S. Grabowsky, J. Beckmann, M. Hesse, W. Morgenroth, C. Paulmann, P. Luger: How to Tune the Siloxane Linkage into a Good Acceptor for Hydrogen Bonding? - Exploring the ED and the ELF for Different Si-O-Si Angles. *5th European Charge Density Meeting in Conjunction with DFG 1178 Annual Meeting*, Gravedona, Italy, **June 2008**.

7. S. Grabowsky, T. Pfeuffer, M. Weber, S. Mebs, J. Buschmann, C. Paulmann, T. Schirmeister, P. Luger: Electronic situation in the oxirane ring – charge density and ELF study on several oxirane derivatives. *21st Congress and General Assembly of the International Union of Crystallography*, Osaka, Japan, **August 2008**. *Acta Cryst. A* **2008**, *64*, C567.

8. S. Grabowsky, D. Jayatilaka, T. Schirmeister, P. Luger: Theoretical and Experimental ELI-D and Electron-Density Topologies of Four Epoxide Derivatives. *XVI. Sagamore Conference*, Santa Fe, USA, **August 2009**.

Contributions to Talks at Conferences

The person who gave the talk is underlined.

1. T. Schirmeister, T. Pfeuffer, L. Chęcińska, M. Weber, S. Grabowsky, P. Luger: Synthesis, Crystallization and Electron Density Determination of Electrophilic Building Blocks as Model Compounds for Protease Inhibitors. *PhD Students Symposium of the German Pharmaceutical Society (DPhG-Doktorandentagung)*, Nürnberg, Germany, **September 2006**.

2. R. Kalinowski, S. Grabowsky, D. Förster, C. Paulmann, W. Morgenroth, M. Weber, P. Luger: Comparative Charge Density Study on Tripeptides of the Type ALA-XXX-ALA. *5th European Charge Density Meeting in Conjunction with DFG 1178 Annual Meeting*, Gravedona, Italy, **June 2008**.

3. T. Schirmeister, S. Grabowsky, M. Anone, T. Pfeuffer, W. Morgenroth, C. Paulmann, R. Fink, P. Luger, B. Engels: Electron Density Determination and Quantum Chemical Computations of Protease Inhibitor Model Compounds: Prediction of Reactivity. *5th European Charge Density Meeting in Conjunction with DFG 1178 Annual Meeting*, Gravedona, Italy, **June 2008**.

4. T. Schirmeister, T. Pfeuffer, S. Grabowsky, P. Luger, M. Mladenovic, M. Arnone, R. Fink, B. Engels: Correlation of electron density derived molecular properties with biological activity: a new tool in rational ligand design. *Proposal Colloquium of the DFG Priority Program SPP 1178*, Kloster Banz, Bad Staffelstein, Germany, **February 2009**.

Contributions to Poster Presentations at Conferences

The person who presented the poster is underlined.

1. T. Schirmeister, T. Pfeuffer, L. Chęcińska, M. Weber, S. Grabowsky, P. Luger: Synthesis, Crystallization and Electron Density Determination of Electrophilic Building Blocks as Model Compounds for Protease Inhibitors. *Annual Meeting of the German Pharmaceutical Society (DPhG-Jahrestagung), Joint Meeting with the Czech Pharmaceutical Sciences*, Marburg, Germany, **October 2006**.

2. P. Luger, S. Grabowsky, T. Pfeuffer, L. Chęcińska, M. Weber, W. Morgenroth, T. Schirmeister: Elektronendichte und Drug-Design: Protease-Inhibitor-Modellverbindungen. *Gemeinsame Jahrestagung der Deutschen Gesellschaft*

für Kristallographie und der Deutschen Gesellschaft für Kristallwachstum und Kristallzüchtung, Bremen, Germany, **March 2007**.

3. J. Beckmann, S. Grabowsky, M. Thöne: How to make the siloxane bond a better acceptor for hydrogen bonding. *4th European Silicon Days*, Bath, England, **September 2007**.

4. T. Pfeuffer, T. Schirmeister, L. Chęcińska, M. Weber, S. Grabowsky, P. Luger: Synthesis, Crystallization and Electron Density Determination of Electrophilic Building Blocks as Model Compounds for Protease Inhibitors. *5th General Meeting of the International Proteolysis Society (IPS2007)*, Patras, Greece, **October 2007**.

5. C. B. Hübschle, B. Dittrich, S. Grabowsky, C. Paulmann, P. Luger: A comparative experimental charge density and ELF study of adenosine based on 100 K X-ray diffraction data. *Workshop on Electron Localizability and Analysis of Chemical Bonding*, Dresden, Germany, **February 2008**.

6. J. Holstein, D. Jayatilaka, S. Grabowsky, P. Luger, B. Dittrich: Achieving a Reasonable Parameterisation in Multipole Refinements: A Study Based on Rfree, Deformation Density Maps and Residual Density Analysis. *5th European Charge Density Meeting in Conjunction with DFG 1178 Annual Meeting*, Gravedona, Italy, **June 2008**.

7. M. Hesse, S. Grabowsky, P. Luger, J. Beckmann: How to make the siloxane bond a better acceptor for hydrogen bonding. *23rd International Conference on Organometallic Chemistry*, Rennes, France, **July 2008**.

8. P. Luger, M. Weber, R. Kalinowski, S. Grabowsky, B. Dittrich, C. B. Hübschle: Teaching how to simply replace the independent atom model - the example of Bergenin. *21st Congress and General Assembly of the International Union of Crystallography*, Osaka, Japan, **August 2008**. *Acta Cryst. A* **2008**, *64*, A4.

9. T. Schirmeister, T. Pfeuffer, S. Grabowsky, P. Luger, M. Mladenovic, M. Arnone, R. Fink, B. Engels: Correlation of electron density derived molecular properties with biological activity: a new tool in rational ligand design. *Proposal Colloquium of the DFG Priority Program SPP 1178*, Kloster Banz, Bad Staffelstein, Germany, **February 2009**.

Acknowledgement

Mein besonderer Dank gilt Prof. Dr. Peter Luger für die Betreuung dieser Doktorarbeit. Er hat mir sowohl in der Auswahl der Themen und Kooperationspartner als auch in der konkreten methodischen Ausgestaltung der Arbeit außerordentlich viel Vertrauen geschenkt und Freiheiten gegeben, mir aber auch immer wieder den Blick für die Machbarkeit der Projekte geschärft. Die Einführung ins wissenschaftliche Arbeiten und Publizieren sowie in die wissenschaftliche Gemeinschaft, die ich durch ihn erhalten habe, wird die beste Grundlage für meinen weiteren wissenschaftlichen Weg sein. Prof. Luger hat es allen Doktoranden weit über das übliche Maß hinaus ermöglicht, internationale Tagungen zu besuchen und Messungen an verschiedenen Großforschungseinrichtungen in aller Welt durchzuführen. So werden mir unsere gemeinsamen Reisen nach England, Italien, Japan und in die USA in bester Erinnerung bleiben.
Die Idee, den Einfluss der Änderung eines Bindungswinkels auf die elektronischen Eigenschaften der funktionellen Gruppe mit Methoden der Elektronendichte zu untersuchen, verdanke ich Prof. Dr. Jens Beckmann. Über mehrere Jahre hinweg hat er dieses Thema mit mir soweit entwickelt, dass ich letztlich in der Lage war, dieses in der vorliegenden Arbeit umfassend zu bewältigen. Er hat nicht nur viel Mühe und Interesse aufgewandt, die Konzepte mit mir zu diskutieren und neue Ideen oder chemischen Sachverstand einfließen zu lassen, sondern er hat mir enorme praktische Hilfe für anstehende Messzeiten zukommen lassen. Die Hälfte der gemessenen Verbindungen wurden von ihm oder seiner Arbeitsgruppe synthetisiert. In diesem Zusammenhang gilt mein spezieller Dank Dipl.-Chem. Maxie F. Hesse.
Die substituierten Epoxid-Verbindungen stammen aus der Arbeitsgruppe von Prof. Dr. Tanja Schirmeister und wurden dort von Dipl.-Chem. Thomas Pfeuffer hergestellt. Ihnen danke ich für diese und unzählige weitere Verbindungen, die mich über viele Messzeiten beschäftigt haben und noch weitere Studien möglich machen werden. Unser regelmäßiger Kontakt und unsere gute Zusammenarbeit bei etlichen

Konferenzbeiträgen und Publikationen sorgten für ein sehr effizientes gegenseitiges Vorantreiben des Projekts der Proteaseinhibitoren.

Die gesamte Arbeitsgruppe um Prof. Luger hat ein ausgesprochen angenehmes Forschen in sehr freundschaftlicher Atmosphäre ermöglicht. Kollegiale Zusammenarbeit sowohl am Institut als auch auf Messreisen, aber auch gemeinsames Mittagessen oder gemeinsame Feiern haben mir die drei Jahre der Doktorarbeit leicht gemacht. Ich möchte mich bei allen dafür bedanken und Folgendes im Speziellen herausheben:

Dr. Christian B. Hübschle hat mich im ersten Jahr meiner Doktorarbeit als Mentor betreut und mir alles Wesentliche beigebracht, ohne das meine Doktorarbeit nicht hätte erfolgreich abgeschlossen werden können. Ohne ihn wäre ich niemals versiert in der Benutzung von Linux und etlichen Programmen zur Elektronendichteauswertung und -veranschaulichung geworden. Er war jederzeit ansprechbar und hilfsbereit. Ich bin ihm dafür ausgeprochen dankbar. Vielen Dank auch für die Entwicklung großartiger Programme wie MOLISO und MOLECOOL, die ich als ständige Hilfsmittel verwende. Zusammen mit Dipl.-Chem. Julian Holstein, mit dem ich auch eine sehr gute Zusammenarbeit im selben Büro während seiner Diplomarbeit verbinde, haben wir sehr schöne Aufenthalte auf Konferenzen im In- und Ausland verlebt.

Meinem Bürokollegen während der letzten zwei Jahre, Dr. Stefan Mebs, bin ich ebenfalls sehr dankbar für die stets gute Zusammenarbeit. Ich habe ihm unzählige hervorragende Ideen und Anregungen zu verdanken, die direkt in die Ausgestaltung der vorliegenden Doktorarbeit eingeflossen sind. Darüber hinaus hat er mir bei etlichen Messungen sowohl am arbeitsgruppeninternen Diffraktometer als auch am Gerät der Anorganischen Chemie oder an Synchrotronmessplätzen sehr geholfen. Besonders unsere Reise nach New York und zur Gordon-Konferenz sowie die Messung an DIAMOND in England werden mir im Gedächtnis bleiben.

Manuela Weber hat einen entscheidenden Beitrag zum Gelingen meiner Arbeit geleistet, weil sie mir nicht nur durch kontinuierliche und äußerst effiziente Hilfestellungen bei kleinen und großen Problemen vieles erleichtert hat, sondern ein absolut verlässlicher Ansprechpartner für alle Belange rund um den Arbeitsgruppenalltag ist. Das gemeinsame Mittagessen ist mir eine sehr wichtige Konstante während der Anfertigung der Doktorarbeit gewesen.

Dipl.-Chem. Roman Kalinowski war über die gesamte Zeit meiner Doktorarbeit ein hilfsbereiter Kollege, der mir mit seinem großen Fachwissen oft weiterhelfen

konnte. Die gemeinsame Messzeit am HASYLAB war für mich in allen Belangen ein voller Erfolg. Mit Dr. Diana Förster habe ich meine erste Messzeit an einem Synchrotronmessplatz verbracht, bei der sie mir vieles beibringen konnte. Ihr gilt mein Dank genau so wie Dr. Stephan Scheins für die freundschaftliche Aufnahme in die Arbeitsgruppe zu Beginn meiner Doktorarbeitszeit sowie für immerwährende große Hilfsbereitschaft.
Dr. Dieter Zobel danke ich für seine uneigennützige Hilfe bei allen technischen Fragen rund um Diffraktometer und Labor sowie für viele interessante und lustige Gespräche. Auch die Hilfe von Irene Jödicke bei etlichen organisatorischen Fragen war von großer Bedeutung für das Gelingen meiner Doktorarbeit.

Für den Erfolg der Messfahrt ans APS nach Chicago möchte ich Dr. Malte Hesse danken. Ohne seine praktische Hilfe vor Ort und seine Testmessungen im Vorfeld wäre das Experimentieren dort nicht möglich gewesen. Den Messplatzbetreuern Dr. Wolfgang Morgenroth und Dr. Carsten Paulmann (HASYLAB) sowie Dr. Yu-Sheng Chen (APS) gilt ebenso ein Dank für den reibungslosen Ablauf der Synchrotronmessungen.
I would especially like to thank Dr. Yu-Sheng Chen for his great support during the time at his beamline 15-ID-B at APS. His patience with us and his help also at night times were outstanding. Moreover, Katie Tietz and Dr. Yu-Sheng Chen are acknowledged for the efforts they made concerning our package that was lost at US customs.
I am thankful to Prof. Dr. Dylan Jayatilaka for the implementation of the ELI code into TONTO. During his visit to Berlin, he dedicated time to answer my specific questions and over the last one and a half years, he helped to successfully perform the study on the ELI-D of the epoxide compounds.
Ich bedanke mich bei Dr. Miroslav Kohout für seine Hilfe bei der Interpretation der vollständigen ELI-Topologie der Epoxid-Derivate. Ebenso danke ich Prof. Dr. Yuri Grin und Prof. Dr. Andreas Savin für einige sehr hilfreiche Anregungen im Zusammenhang mit ELF und ELI.
Prof. Dr. Carlo Gatti is acknowledged for his very kind help with the periodic-boundary calculation of the epoxide compounds as well as for his interpretation of the epoxide bond paths.
Ich danke Hendrik Lingemann und Dr. Stefan Mebs für das intensive und kritische Lesen des Manuskripts der Doktorarbeit.

Appendix A

Refinement Strategies and Coordinates of Compounds 1 to 4

Table A.1: Multipole refinement strategies and κ/κ' values of siloxanol (**1**, left) and trisilo (**2**, right)

Theo = periodic-boundary calculation at experimental geometry

atom	sym	cons	κ_{exp}	κ_{theo}	κ'	atom	sym	cons	κ_{exp}	κ_{theo}	κ'
Si1	m		1.1283	0.9535	0.8500	Si1	m		1.1224	0.9517	0.8500
Si2	m	Si1	1.1283	0.9535	0.8500	Si2	m	Si1	1.1224	0.9517	0.8500
Si3	1		1.1294	0.9547	0.8500						
O1	m		0.9649	0.9902	1.0000	O1	m		0.9641	0.9925	1.0000
O2	m		0.9456	0.9860	1.0000						
C1	m		0.9794	1.0044	1.0000	C1	m		0.9928	1.0017	1.0000
C2	m	C1	0.9794	1.0044	1.0000	C2	m	C1	0.9928	1.0017	1.0000
C3	m		1.0100	0.9946	1.0000	C3	m		1.0116	1.0140	1.0000
C4	m	C3	1.0100	0.9946	1.0000	C4	3		0.9662	1.0175	1.0000
C5	m	C3	1.0100	0.9946	1.0000	C5	3	C4	0.9662	1.0175	1.0000
C6	m	C1	0.9794	1.0044	1.0000	C6	3	C4	0.9662	1.0175	1.0000
C7	3		0.9252	1.0030	1.0000	C7	3	C4	0.9662	1.0175	1.0000
C8	3	C7	0.9252	1.0030	1.0000						
C9	3	C7	0.9252	1.0030	1.0000						
C10	3	C7	0.9252	1.0030	1.0000						
C11	3	C7	0.9252	1.0030	1.0000						
C12	3	C7	0.9252	1.0030	1.0000						
H3	6		1.1300	1.1300	1.2900	H3	6		1.1300	1.1300	1.2900
H4	6	H3	1.1300	1.1300	1.2900	H4A	6		1.1300	1.1300	1.2900
H5	6	H3	1.1300	1.1300	1.2900	H4B	6	H4A	1.1300	1.1300	1.2900
H7A	6		1.1300	1.1300	1.2900	H4C	6	H4A	1.1300	1.1300	1.2900
H7B	6	H7A	1.1300	1.1300	1.2900	H5A	6	H4A	1.1300	1.1300	1.2900
H7C	6	H7A	1.1300	1.1300	1.2900	H5B	6	H4A	1.1300	1.1300	1.2900
H8A	6	H7A	1.1300	1.1300	1.2900	H5C	6	H4A	1.1300	1.1300	1.2900
H8B	6	H7A	1.1300	1.1300	1.2900	H6A	6	H4A	1.1300	1.1300	1.2900
H8C	6	H7A	1.1300	1.1300	1.2900	H6B	6	H4A	1.1300	1.1300	1.2900
H9A	6	H7A	1.1300	1.1300	1.2900	H6C	6	H4A	1.1300	1.1300	1.2900
H9B	6	H7A	1.1300	1.1300	1.2900	H7A	6	H4A	1.1300	1.1300	1.2900
H9C	6	H7A	1.1300	1.1300	1.2900	H7B	6	H4A	1.1300	1.1300	1.2900
H10A	6	H7A	1.1300	1.1300	1.2900	H7C	6	H4A	1.1300	1.1300	1.2900
H10B	6	H7A	1.1300	1.1300	1.2900						
H10C	6	H7A	1.1300	1.1300	1.2900						
H11A	6	H7A	1.1300	1.1300	1.2900						
H11B	6	H7A	1.1300	1.1300	1.2900						
H11C	6	H7A	1.1300	1.1300	1.2900						
H12A	6	H7A	1.1300	1.1300	1.2900						
H12B	6	H7A	1.1300	1.1300	1.2900						
H12C	6	H7A	1.1300	1.1300	1.2900						
H2O	6		1.1300	1.1300	1.2900						

Table A.2: Multipole refinement strategies and κ/κ' values of pentaphe (**3**, left) and hexaphe (**4**, right)

Theo = periodic-boundary calculation at experimental geometry

atom	sym	cons	κ_{exp}	κ_{theo}	κ'	atom	sym	cons	κ_{exp}	κ_{theo}	κ'
Si1	1		1.0049	0.9358	0.8500	Si1	1		1.0338	0.9218	0.8500
Si2	1		0.9816	0.9299	0.8500						
O1	m		0.9867	0.9954	1.0000	O1	$\overline{3}$		0.9921	0.9938	1.0000
C1	mm2		1.0032	1.0100	1.0000	C1	mm2		0.9945	1.0108	1.0000
C2	mm2		0.9849	1.0058	1.0000	C2	mm2		0.9959	1.0086	1.0000
C3	mm2	C2	0.9849	1.0058	1.0000	C3	mm2	C2	0.9959	1.0086	1.0000
C4	mm2	C2	0.9849	1.0058	1.0000	C4	mm2	C2	0.9959	1.0086	1.0000
C5	mm2	C2	0.9849	1.0058	1.0000	C5	mm2	C2	0.9959	1.0086	1.0000
C6	mm2	C2	0.9849	1.0058	1.0000	C6	mm2	C2	0.9959	1.0086	1.0000
C7	mm2	C1	1.0032	1.0100	1.0000	C7	mm2	C1	0.9945	1.0108	1.0000
C8	mm2	C2	0.9849	1.0058	1.0000	C8	mm2	C2	0.9959	1.0086	1.0000
C9	mm2	C2	0.9849	1.0058	1.0000	C9	mm2	C2	0.9959	1.0086	1.0000
C10	mm2	C2	0.9849	1.0058	1.0000	C10	mm2	C2	0.9959	1.0086	1.0000
C11	mm2	C2	0.9849	1.0058	1.0000	C11	mm2	C2	0.9959	1.0086	1.0000
C12	mm2	C2	0.9849	1.0058	1.0000	C12	mm2	C2	0.9959	1.0086	1.0000
C13	mm2		1.0119	1.0118	1.0000	C13	mm2	C1	0.9945	1.0108	1.0000
C14	mm2		1.0046	1.0069	1.0000	C14	mm2	C2	0.9959	1.0086	1.0000
C15	mm2	C14	1.0046	1.0069	1.0000	C15	mm2	C2	0.9959	1.0086	1.0000
C16	mm2	C14	1.0046	1.0069	1.0000	C16	mm2	C2	0.9959	1.0086	1.0000
C17	mm2	C14	1.0046	1.0069	1.0000	C17	mm2	C2	0.9959	1.0086	1.0000
C18	mm2	C14	1.0046	1.0069	1.0000	C18	mm2	C2	0.9959	1.0086	1.0000
C19	mm2	C13	1.0119	1.0118	1.0000						
C20	mm2	C14	1.0046	1.0069	1.0000						
C21	mm2	C14	1.0046	1.0069	1.0000						
C22	mm2	C14	1.0046	1.0069	1.0000						
C23	mm2	C14	1.0046	1.0069	1.0000						
C24	mm2	C14	1.0046	1.0069	1.0000						
C25	mm2	C13	1.0119	1.0118	1.0000						
C26	mm2	C14	1.0046	1.0069	1.0000						
C27	mm2	C14	1.0046	1.0069	1.0000						
C28	mm2	C14	1.0046	1.0069	1.0000						
C29	mm2	C14	1.0046	1.0069	1.0000						
C30	mm2	C14	1.0046	1.0069	1.0000						
H2	6		1.1300	1.1300	1.2900	H2	6		1.1300	1.1300	1.2900
H3	6	H2	1.1300	1.1300	1.2900	H3	6	H2	1.1300	1.1300	1.2900
H4	6	H2	1.1300	1.1300	1.2900	H4	6	H2	1.1300	1.1300	1.2900
H5	6	H2	1.1300	1.1300	1.2900	H5	6	H2	1.1300	1.1300	1.2900
H6	6	H2	1.1300	1.1300	1.2900	H6	6	H2	1.1300	1.1300	1.2900
H8	6	H2	1.1300	1.1300	1.2900	H8	6	H2	1.1300	1.1300	1.2900
H9	6	H2	1.1300	1.1300	1.2900	H9	6	H2	1.1300	1.1300	1.2900
H10	6	H2	1.1300	1.1300	1.2900	H10	6	H2	1.1300	1.1300	1.2900
H11	6	H2	1.1300	1.1300	1.2900	H11	6	H2	1.1300	1.1300	1.2900
H12	6	H2	1.1300	1.1300	1.2900	H12	6	H2	1.1300	1.1300	1.2900
H14	6	H2	1.1300	1.1300	1.2900	H14	6	H2	1.1300	1.1300	1.2900
H15	6	H2	1.1300	1.1300	1.2900	H15	6	H2	1.1300	1.1300	1.2900
H16	6	H2	1.1300	1.1300	1.2900	H16	6	H2	1.1300	1.1300	1.2900
H17	6	H2	1.1300	1.1300	1.2900	H17	6	H2	1.1300	1.1300	1.2900
H18	6	H2	1.1300	1.1300	1.2900	H18	6	H2	1.1300	1.1300	1.2900
H20	6	H2	1.1300	1.1300	1.2900						
H21	6	H2	1.1300	1.1300	1.2900						
H22	6	H2	1.1300	1.1300	1.2900						
H23	6	H2	1.1300	1.1300	1.2900						
H24	6	H2	1.1300	1.1300	1.2900						
H26	6	H2	1.1300	1.1300	1.2900						
H27	6	H2	1.1300	1.1300	1.2900						
H28	6	H2	1.1300	1.1300	1.2900						
H29	6	H2	1.1300	1.1300	1.2900						
H30	6	H2	1.1300	1.1300	1.2900						
H1Si	6		1.0500	1.0500	1.0500						

Table A.3: Experimental fractional and cartesian coordinates of siloxanol (**1**)

atom	xf	yf	zf	x	y	z
Si1	0.9611	0.2215	0.5141	7.2282838	3.6996011	5.5720474
Si2	0.6415	0.2324	0.5051	4.4008026	3.8818983	5.4747350
Si3	1.2028	0.0760	0.7233	8.8367632	1.2693670	7.8402009
O1	0.7857	0.2542	0.4402	5.8570648	4.2449396	4.7714913
O2	1.2871	0.1631	0.7149	9.6106495	2.7241207	7.7490451
C1	0.9030	0.1510	0.6284	6.4105992	2.5220173	6.8110400
C2	0.7446	0.1603	0.6246	5.0073875	2.6767762	6.7698194
C3	0.6742	0.1142	0.7004	4.1802516	1.9074740	7.5915331
C4	0.7595	0.0570	0.7778	4.7390746	0.9512320	8.4305350
C5	0.9157	0.0469	0.7806	6.1254210	0.7825787	8.4603964
C6	0.9908	0.0935	0.7081	6.9849480	1.5615168	7.6753618
C7	0.5727	0.3238	0.5691	3.6188932	5.4080445	6.1685596
C8	0.4812	0.1844	0.3939	3.2617666	3.0793965	4.2695274
C9	1.0475	0.1748	0.3966	8.3071226	2.9183918	4.2989119
C10	1.0740	0.3108	0.5785	8.0665804	5.1908276	6.2701642
C11	1.2880	0.0278	0.8741	9.2018346	0.4636421	9.4739925
C12	1.2427	0.0131	0.5975	9.5224322	0.2189203	6.4766684
H3	0.5532	0.1232	0.6977	3.1079190	2.0569056	7.5622462
H4	0.7087	0.0198	0.8374	4.1297026	0.3310608	9.0763863
H5	0.9813	0.0008	0.8383	6.5590270	0.0126085	9.0865858
H7A	0.6602	0.3458	0.6430	4.2059232	5.7750604	6.9697010
H7B	0.4732	0.3107	0.6019	2.6453975	5.1885564	6.5235253
H7C	0.5459	0.3685	0.5000	3.5613206	6.1539500	5.4190335
H8A	0.4277	0.2266	0.3265	2.9609612	3.7843703	3.5386877
H8B	0.3994	0.1627	0.4411	2.4079471	2.7174574	4.7811163
H8C	0.5239	0.1358	0.3507	3.7559353	2.2683944	3.8009693
H9A	0.9752	0.1280	0.3523	7.7778351	2.1369487	3.8184851
H9B	1.1566	0.1505	0.4394	9.1685920	2.5131663	4.7627334
H9C	1.0606	0.2179	0.3303	8.5978446	3.6393642	3.5798541
H10A	1.1027	0.3441	0.5062	8.5125735	5.7466704	5.4867880
H10B	1.1767	0.2925	0.6412	8.8185750	4.8847834	6.9501149
H10C	1.0085	0.3469	0.6253	7.3596306	5.7937978	6.7778944
H11A	1.4071	0.0172	0.8831	10.2409669	0.2873068	9.5723237
H11B	1.2314	-0.0273	0.8802	8.6812608	-0.4564444	9.5399369
H11C	1.2725	0.0653	0.9468	8.8735253	1.0910945	10.2620837
H12A	1.1690	0.0304	0.5125	9.0876030	0.5080808	5.5553553
H12B	1.2225	-0.0478	0.6149	9.2967230	-0.7984270	6.6644754
H12C	1.3590	0.0206	0.5927	10.5727382	0.3442037	6.4239151
H2O	1.2847	0.1981	0.7836	9.4092339	3.3084203	8.4931084

Table A.4: Experimental fractional and cartesian coordinates of trisilo (**2**)

atom	xf	yf	zf	x	y	z
Si1	0.3268	0.5676	1.0474	-1.8068211	5.0746165	10.7564929
Si2	0.1819	0.3423	0.8613	-2.3967146	3.0606027	8.8454902
O1	0.3291	0.4391	0.9438	-1.2647875	3.9256891	9.6921410
C1	0.1408	0.5377	1.0273	-3.6572018	4.8073164	10.5501190
C2	0.0681	0.4253	0.9342	-3.9541733	3.8024732	9.5934007
C3	-0.0717	0.3893	0.9081	-5.2910891	3.4805614	9.3259751
C4	0.4612	0.5258	1.2156	-1.2374087	4.7010705	12.4835809
C5	0.3522	0.7565	0.9936	-1.2717405	6.7637324	10.2038141
C6	0.1130	0.3783	0.6838	-2.2326871	3.3825323	7.0221779
C7	0.2177	0.1395	0.8937	-2.1829924	1.2472159	9.1777671
H3	-0.1266	0.3025	0.8379	-5.5156595	2.7047419	8.6044673
H4A	0.4464	0.4154	1.2409	-1.5199098	3.7140735	12.7433968
H4B	0.4499	0.6024	1.2811	-1.6838715	5.3860226	13.1566377
H4C	0.5641	0.5362	1.2206	-0.1837211	4.7938870	12.5346506
H5A	0.4562	0.7653	1.0010	-0.2184556	6.8427887	10.2800439
H5B	0.3376	0.8384	1.0536	-1.7249153	7.4958483	10.8203583
H5C	0.2774	0.7736	0.8957	-1.5667204	6.9170616	9.1983469
H6A	0.1016	0.4950	0.6664	-2.2653665	4.4258755	6.8437367
H6B	0.0132	0.3256	0.6337	-3.0290407	2.9110555	6.5073932
H6C	0.1849	0.3349	0.6502	-1.3099616	2.9942157	6.6768486
H7A	0.2920	0.1045	0.8596	-1.2336864	0.9343166	8.8279090
H7B	0.1221	0.0789	0.8447	-2.9410897	0.7051051	8.6748948
H7C	0.2594	0.1196	0.9951	-2.2523933	1.0689323	10.2193414
Si1a	-0.3268	0.4324	0.9526	-8.1888913	3.8663835	9.7823166
Si2a	-0.1819	0.6577	1.1387	-7.5989978	5.8803973	11.6933194
O1a	-0.3291	0.5609	1.0562	-8.7309249	5.0153109	10.8466686
C1a	-0.1408	0.4623	0.9727	-6.3385105	4.1336836	9.9886906
C2a	-0.0681	0.5747	1.0658	-6.0415391	5.1385268	10.9454089
C3a	0.0717	0.6107	1.0919	-4.7046233	5.4604386	11.2128345
C4a	-0.4612	0.4742	0.7844	-8.7583037	4.2399295	8.0552287
C5a	-0.3522	0.2435	1.0064	-8.7239718	2.1772676	10.3349955
C6a	-0.1130	0.6217	1.3162	-7.7630253	5.5584677	13.5166317
C7a	-0.2177	0.8605	1.1063	-7.8127200	7.6937841	11.3610425
H3a	0.1266	0.6975	1.1621	-4.4800529	6.2362581	11.9343423
H4Aa	-0.4464	0.5846	0.7591	-8.4758026	5.2269265	7.7954127
H4Ba	-0.4499	0.3976	0.7189	-8.3118409	3.5549774	7.3821719
H4Ca	-0.5641	0.4638	0.7794	-9.8119913	4.1471130	8.0041589
H5Aa	-0.4562	0.2347	0.9990	-9.7772567	2.0982113	10.2587657
H5Ba	-0.3376	0.1616	0.9464	-8.2707971	1.4451517	9.7184512
H5Ca	-0.2774	0.2264	1.1043	-8.4289920	2.0239384	11.3404626
H6Aa	-0.1016	0.5050	1.3336	-7.7303458	4.5151245	13.6950728
H6Ba	-0.0132	0.6744	1.3663	-6.9666717	6.0299445	14.0314164
H6Ca	-0.1849	0.6651	1.3498	-8.6857507	5.9467843	13.8619609
H7Aa	-0.2920	0.8955	1.1404	-8.7620259	8.0066834	11.7109006
H7Ba	-0.1221	0.9211	1.1553	-7.0546227	8.2358949	11.8639147
H7Ca	-0.2594	0.8804	1.0049	-7.7433191	7.8720677	10.3194681

Table A.5: Experimental fractional and cartesian coordinates of pentaphe (**3**)

atom	xf	yf	zf	x	y	z
Si1	0.0470	-0.0324	0.2019	-0.3525918	-0.5883211	2.6150043
Si2	0.1416	0.2680	0.2479	0.1643928	2.5181883	3.2107735
O1	0.0665	0.1220	0.2164	-0.3158950	1.0194719	2.8029865
C1	0.1801	-0.0988	0.3144	0.4516363	-1.4256385	4.0720413
C2	0.2214	-0.0359	0.4145	0.3981119	-0.8865219	5.3689036
C3	0.3200	-0.0890	0.4975	0.9968940	-1.5466976	6.4435262
C4	0.3801	-0.2050	0.4817	1.6702467	-2.7486985	6.2390046
C5	0.3406	-0.2686	0.3829	1.7353749	-3.2968918	4.9591739
C6	0.2410	-0.2159	0.3004	1.1255004	-2.6413431	3.8902760
C7	-0.1575	-0.0853	0.1857	-2.1223289	-1.1255349	2.4049134
C8	-0.2074	-0.1131	0.2706	-2.8976812	-1.5221623	3.5053619
C9	-0.3609	-0.1525	0.2581	-4.2252476	-1.9219440	3.3426874
C10	-0.4669	-0.1642	0.1599	-4.7958585	-1.9244165	2.0703559
C11	-0.4196	-0.1379	0.0742	-4.0407212	-1.5423597	0.9608800
C12	-0.2658	-0.0989	0.0873	-2.7131500	-1.1479955	1.1308463
C13	0.0106	0.3728	0.1645	-0.7564550	3.7236211	2.1307500
C14	-0.0773	0.3305	0.0631	-1.1335351	3.4022754	0.8174131
C15	-0.1795	0.4088	0.0037	-1.8719140	4.2992405	0.0475849
C16	-0.1952	0.5311	0.0442	-2.2421029	5.5373774	0.5720674
C17	-0.1075	0.5752	0.1442	-1.8619761	5.8793256	1.8672978
C18	-0.0056	0.4964	0.2035	-1.1260015	4.9775237	2.6361675
C19	0.3357	0.2831	0.2284	2.0013022	2.7008263	2.9577474
C20	0.3931	0.4017	0.2086	2.5381923	3.9736111	2.7012503
C21	0.5385	0.4180	0.1951	3.9070190	4.1620543	2.5262846
C22	0.6300	0.3151	0.2014	4.7715144	3.0709423	2.6081528
C23	0.5754	0.1963	0.2208	4.2620840	1.7961999	2.8598578
C24	0.4294	0.1806	0.2341	2.8877067	1.6150386	3.0325310
C25	0.1544	0.3173	0.3848	-0.2873845	2.8687983	4.9843262
C26	0.2786	0.3975	0.4482	0.5495039	3.6361553	5.8053011
C27	0.2827	0.4424	0.5482	0.1674280	3.9865595	7.0999615
C28	0.1631	0.4060	0.5870	-1.0560941	3.5549700	7.6030348
C29	0.0385	0.3253	0.5256	-1.9041095	2.7808921	6.8075750
C30	0.0341	0.2822	0.4252	-1.5242265	2.4501129	5.5076949
H2	0.1762	0.0545	0.4282	-0.1171164	0.0494328	5.5465114
H3	0.3518	-0.0390	0.5741	0.9563605	-1.1139542	7.4355423
H4	0.4574	-0.2452	0.5463	2.1405824	-3.2511571	7.0752754
H5	0.3885	-0.3579	0.3696	2.2734289	-4.2209346	4.7866431
H6	0.2110	-0.2678	0.2245	1.1802030	-3.0949207	2.9082457
H8	-0.1267	-0.1070	0.3474	-2.4694116	-1.5521861	4.4997093
H9	-0.4027	-0.1747	0.3222	-4.8468544	-2.2345090	4.1727933
H10	-0.5857	-0.1980	0.1478	-5.8116590	-2.2659158	1.9136392
H11	-0.4994	-0.1490	-0.0030	-4.4565392	-1.5656555	-0.0389072
H12	-0.2286	-0.0792	0.0209	-2.1217203	-0.8595274	0.2705498
H14	-0.0619	0.2359	0.0325	-0.8206540	2.4442153	0.4206869
H15	-0.2462	0.3729	-0.0741	-2.1525167	4.0169724	-0.9597403
H16	-0.2747	0.5940	0.0007	-2.8284082	6.2532594	0.0091310
H17	-0.1165	0.6704	0.1767	-2.1251321	6.8415042	2.2891504
H18	0.0604	0.5319	0.2816	-0.8524536	5.2556465	3.6465752
H20	0.3224	0.4819	0.2033	1.8714255	4.8244747	2.6332793
H21	0.5764	0.5110	0.1786	4.2672541	5.1609672	2.3129946
H22	0.7408	0.3281	0.1875	5.8285622	3.2242767	2.4284598
H23	0.6431	0.1145	0.2230	4.9148862	0.9324079	2.8887662
H24	0.3854	0.0882	0.2476	2.4844302	0.6249169	3.2063310
H26	0.3721	0.4286	0.4193	1.4987283	3.9990608	5.4308779
H27	0.3792	0.5057	0.5950	0.8269787	4.5952910	7.7060662
H28	0.1686	0.4415	0.6650	-1.3329766	3.8334764	8.6123933
H29	-0.0566	0.2978	0.5542	-2.8685522	2.4564005	7.1782810
H30	-0.0665	0.2235	0.3782	-2.2227194	1.8894208	4.8987408
H1Si	0.0843	-0.0754	0.1061	0.3891673	-0.9237902	1.3742492

Table A.6: Experimental fractional and cartesian coordinates of hexaphe (**4**)

atom	xf	yf	zf	x	y	z
Si1	0.0384	0.0677	0.1564	-0.5594227	0.1188873	1.5169053
O1	0.0000	0.0000	0.0000	0.0000000	0.0000000	0.0000000
C1	0.2908	0.1229	0.2763	0.8936087	0.2395354	2.6794729
C2	0.4116	0.2672	0.3843	0.9437745	1.1717261	3.7272968
C3	0.5979	0.3030	0.4749	2.0262863	1.2111981	4.6062157
C4	0.6659	0.1936	0.4599	3.0717779	0.3030579	4.4610645
C5	0.5484	0.0491	0.3537	3.0421593	-0.6369522	3.4310002
C6	0.3630	0.0149	0.2625	1.9648390	-0.6601309	2.5460191
C7	0.0004	0.2479	0.1727	-1.6200744	1.6408434	1.6748597
C8	-0.1348	0.2547	0.2141	-2.9613751	1.5749792	2.0770153
C9	-0.1591	0.3921	0.2275	-3.7335539	2.7318605	2.2067154
C10	-0.0468	0.5257	0.2004	-3.1677545	3.9772649	1.9438817
C11	0.0894	0.5215	0.1600	-1.8313035	4.0624149	1.5514351
C12	0.1114	0.3837	0.1452	-1.0718959	2.9061106	1.4086699
C13	-0.1304	-0.0940	0.1968	-1.5541025	-1.4117278	1.9090803
C14	-0.3188	-0.2008	0.0966	-2.3505794	-2.0403780	0.9366593
C15	-0.4440	-0.3204	0.1283	-3.0967802	-3.1785051	1.2448086
C16	-0.3828	-0.3355	0.2613	-3.0589390	-3.7096246	2.5343314
C17	-0.1966	-0.2306	0.3623	-2.2778971	-3.0997167	3.5144730
C18	-0.0722	-0.1109	0.3300	-1.5360253	-1.9596044	3.2008242
H2	0.3542	0.3488	0.3957	0.1059414	1.8484245	3.8384905
H3	0.6931	0.4174	0.5545	2.0859242	1.9680379	5.3784997
H4	0.8087	0.2188	0.5324	3.8971063	0.3044535	5.1635809
H5	0.5963	-0.0386	0.3377	3.8403669	-1.3521591	3.2752184
H6	0.2736	-0.0962	0.1787	1.9586075	-1.3760375	1.7332209
H8	-0.2294	0.1490	0.2289	-3.4304470	0.6094699	2.2201976
H9	-0.2670	0.3947	0.2566	-4.7773308	2.6669913	2.4883854
H10	-0.0649	0.6327	0.2074	-3.7482583	4.8888894	2.0112439
H11	0.1798	0.6262	0.1416	-1.3801663	5.0306860	1.3733739
H12	0.2211	0.3855	0.1164	-0.0302910	3.0087276	1.1288525
H14	-0.3707	-0.1923	-0.0075	-2.4009711	-1.6528799	-0.0732206
H15	-0.5873	-0.4006	0.0472	-3.6857713	-3.6327020	0.4574130
H16	-0.4784	-0.4256	0.2890	-3.6476113	-4.5781434	2.8033049
H17	-0.1510	-0.2410	0.4660	-2.2709018	-3.5024752	4.5197846
H18	0.0720	-0.0283	0.4086	-0.9372021	-1.4761526	3.9632148
Si1a	-0.0384	-0.0677	-0.1564	0.5594227	-0.1188873	-1.5169053
C1a	-0.2908	-0.1229	-0.2763	-0.8936087	-0.2395354	-2.6794729
C2a	-0.4116	-0.2672	-0.3843	-0.9437745	-1.1717261	-3.7272968
C3a	-0.5979	-0.3030	-0.4749	-2.0262863	-1.2111981	-4.6062157
C4a	-0.6659	-0.1936	-0.4599	-3.0717779	-0.3030579	-4.4610645
C5a	-0.5484	-0.0491	-0.3537	-3.0421593	0.6369522	-3.4310002
C6a	-0.3630	-0.0149	-0.2625	-1.9648390	0.6601309	-2.5460191
C7a	-0.0004	-0.2479	-0.1727	1.6200744	-1.6408434	-1.6748597
C8a	0.1348	-0.2547	-0.2141	2.9613751	-1.5749792	-2.0770153
C9a	0.1591	-0.3921	-0.2275	3.7335539	-2.7318605	-2.2067154
C10a	0.0468	-0.5257	-0.2004	3.1677545	-3.9772649	-1.9438817
C11a	-0.0894	-0.5215	-0.1600	1.8313035	-4.0624149	-1.5514351
C12a	-0.1114	-0.3837	-0.1452	1.0718959	-2.9061106	-1.4086699
C13a	0.1304	0.0940	-0.1968	1.5541025	1.4117278	-1.9090803
C14a	0.3188	0.2008	-0.0966	2.3505794	2.0403780	-0.9366593
C15a	0.4440	0.3204	-0.1283	3.0967802	3.1785051	-1.2448086
C16a	0.3828	0.3355	-0.2613	3.0589390	3.7096246	-2.5343314
C17a	0.1966	0.2306	-0.3623	2.2778971	3.0997167	-3.5144730
C18a	0.0722	0.1109	-0.3300	1.5360253	1.9596044	-3.2008242
H2a	-0.3542	-0.3488	-0.3957	-0.1059414	-1.8484245	-3.8384905
H3a	-0.6931	-0.4174	-0.5545	-2.0859242	-1.9680379	-5.3784997
H4a	-0.8087	-0.2188	-0.5324	-3.8971063	-0.3044535	-5.1635809
H5a	-0.5963	0.0386	-0.3377	-3.8403669	1.3521591	-3.2752184
H6a	-0.2736	0.0962	-0.1787	-1.9586075	1.3760375	-1.7332209
H8a	0.2294	-0.1490	-0.2289	3.4304470	-0.6094699	-2.2201976
H9a	0.2670	-0.3947	-0.2566	4.7773308	-2.6669913	-2.4883854
H10a	0.0649	-0.6327	-0.2074	3.7482583	-4.8888894	-2.0112439
H11a	-0.1798	-0.6262	-0.1416	1.3801663	-5.0306860	-1.3733739
H12a	-0.2211	-0.3855	-0.1164	0.0302910	-3.0087276	-1.1288525
H14a	0.3707	0.1923	0.0075	2.4009711	1.6528799	0.0732206
H15a	0.5873	0.4006	-0.0472	3.6857713	3.6327020	-0.4574130
H16a	0.4784	0.4256	-0.2890	3.6476113	4.5781434	-2.8033049
H17a	0.1510	0.2410	-0.4660	2.2709018	3.5024752	-4.5197846
H18a	-0.0720	0.0283	-0.4086	0.9372021	1.4761526	-3.9632148

Results of the PES Scans on Model Compounds of the Type $H_3SiOSiH_3$

All values are dependent on the Si–O–Si angle a(Si–O–Si) in °.

If not otherwise specified, average values are given for Si–O bonds and Si atoms in symmetric model compounds.

Table A.7: Si-O bond distances (d) and bond-path lengths (bp) in Å, ED (ϱ) at the Si–O bcps in eÅ^{-3}, Laplacian ($\nabla^2\varrho$) at the Si–O bcps in eÅ^{-5}, and Si–O delocalization indices (δ) for free disiloxane $H_3SiOSiH_3$, [1] alternatively critical point between bcp_{Si-Si} and O atom

a(Si–O–Si)	d(Si–O)	d(bp)	ϱ(Si–O) or [1] $\varrho(bcp_{Si-Si}$–O)	$\nabla^2\varrho$(Si–O) or [1] $\nabla^2\varrho(bcp_{Si-Si}$–O)	δ(Si–O)
50	2.6479		[1]0.2057	[1] 1.127	0.3272
55	2.3400		[1]0.3782	[1] 0.987	0.4960
60	2.1385		[1]0.4997	[1] 0.054	0.5513
65	2.0081	2.0776	0.5518	0.772	0.5383
70	1.9190	1.9375	0.6059	4.834	0.5056
75	1.8547	1.8627	0.6606	7.742	0.4864
80	1.8077	1.8178	0.7087	10.075	0.4723
85	1.7721	1.7743	0.7500	12.012	0.4618
90	1.7448	1.7461	0.7844	13.623	0.4538
95	1.7237	1.7245	0.8121	14.951	0.4474
100	1.7074	1.7080	0.8340	16.039	0.4425
105	1.6945	1.6950	0.8513	16.944	0.4385
110	1.6846	1.6849	0.8640	17.676	0.4350
115	1.6766	1.6770	0.8734	18.286	0.4320
120	1.6701	1.6705	0.8803	18.811	0.4292
125	1.6645	1.6650	0.8854	19.278	0.4265
130	1.6597	1.6601	0.8891	19.702	0.4240
135	1.6554	1.6559	0.8919	20.095	0.4216
140	1.6515	1.6520	0.8939	20.460	0.4194
145	1.6481	1.6485	0.8956	20.799	0.4174
150	1.6450	1.6454	0.8968	21.109	0.4139
155	1.6423	1.6427	0.8978	21.383	0.4140
160	1.6401	1.6403	0.8986	21.618	0.4127
165	1.6384	1.6385	0.8993	21.808	0.4116
170	1.6371	1.6371	0.8997	21.948	0.4109
175	1.6363	1.6363	0.8999	22.033	0.4105
180	1.6361	1.6361	0.9000	22.060	0.4102

Table A.8: Si-Si bond distances (d) in Å, ED (ϱ) at the Si–Si bcps in eÅ^{-3}, Laplacian ($\nabla^2\varrho$) at the Si–O bcps in eÅ^{-5}, and Si–Si delocalization indices (δ) for free disiloxane $H_3SiOSiH_3$

a(Si–O–Si)	d(Si–Si)	d(bp)	ϱ(Si–Si)	$\nabla^2\varrho$(Si–Si)	δ(Si–Si)
50	2.2381	2.2568	0.5989	-3.709	0.4539
55	2.1609	2.1893	0.5876	-3.468	0.3276
60	2.1385	2.1804	0.5581	-2.836	0.2211
65	2.1579				0.1246
70	2.2014				0.0742
75	2.2582				0.0522
80	2.3240				0.0374
85	2.3945				0.0273
90	2.4675				0.0204
95	2.5417				0.0156
100	2.6159				0.0123
105	2.6887				0.0100
110	2.7598				0.0084
115	2.8281				0.0073
120	2.8927				0.0067
125	2.9529				0.0063
130	3.0084				0.0060
135	3.0588				0.0060
140	3.1039				0.0060
145	3.1436				0.0061
150	3.1779				0.0062
155	3.2068				0.0063
160	3.2304				0.0064
165	3.2487				0.0065
170	3.2617				0.0066
175	3.2695				0.0067
180	3.2721				0.0067

Table A.9: Si-O bond distances (d) in Å, ED (ϱ) at the Si–O bcps in eÅ^{-3}, Laplacian ($\nabla^2\varrho$) at the Si–O bcps in eÅ^{-5}, and Si–O delocalization indices (δ) for the siloxane group in disiloxane$\cdots$silanol

a(Si–O–Si)	d(Si–O)	ϱ(Si–O)	$\nabla^2\varrho$(Si–O)	δ(Si–O)
85	1.7717	0.7439	12.154	0.4337
90	1.7472	0.7743	13.587	0.4287
95	1.7278	0.7993	14.827	0.4244
100	1.7163	0.8179	15.591	0.4225
105	1.7026	0.8320	16.333	0.4196
110	1.6963	0.8389	16.866	0.4194
115	1.6886	0.8478	17.431	0.4168
120	1.6823	0.8543	17.913	0.4145
125	1.6769	0.8589	18.339	0.4123
130	1.6724	0.8620	18.717	0.4101
135	1.6682	0.8646	19.086	0.4082
140	1.6643	0.8667	19.431	0.4065
145	1.6606	0.8687	19.774	0.4051
150	1.6573	0.8702	20.093	0.4039
155	1.6543	0.8719	20.385	0.4031
160	1.6507	0.8756	20.723	0.4031
165	1.6474	0.8796	21.044	0.4030

Table A.10: Si-O bond distances (d) in Å, ED (ϱ) at the Si–O bcps in eÅ^{-3}, Laplacian ($\nabla^2\varrho$) at the Si–O bcps in eÅ^{-5}, and Si–O delocalization indices (δ) for the shorter Si–O bonds in disiloxane$\cdots$water

a(Si–O–Si)	d(Si–O)	ϱ(Si–O)	$\nabla^2\varrho$(Si–O)	δ(Si–O)
90	1.7410	0.7859	13.442	0.4403
95	1.7236	0.8077	14.628	0.4339
100	1.7080	0.8296	15.566	0.4329
105	1.6965	0.8446	16.438	0.4296
110	1.6882	0.8546	17.022	0.4273
115	1.6805	0.8639	17.652	0.4253
120	1.6749	0.8689	18.275	0.4219
125	1.6695	0.8738	18.779	0.4201
130	1.6649	0.8773	19.216	0.4182
135	1.6609	0.8797	19.600	0.4163
140	1.6574	0.8811	19.939	0.4145
145	1.6542	0.8824	20.273	0.4130
150	1.6509	0.8842	20.602	0.4120
155	1.6474	0.8873	20.957	0.4115
160	1.6436	0.8919	21.287	0.4124
165	1.6378	0.9018	21.861	0.4151

Table A.11: Si-O bond distances (d) in Å, ED (ϱ) at the Si–O bcps in eÅ^{-3}, Laplacian ($\nabla^2\varrho$) at the Si–O bcps in eÅ^{-5}, and Si–O delocalization indices (δ) for the longer Si–O bonds in disiloxane$\cdots$water

a(Si–O–Si)	d(Si–O)	ϱ(Si–O)	$\nabla^2\varrho$(Si–O)	δ(Si–O)
90	1.7481	0.7753	13.499	0.4305
95	1.7276	0.8018	14.740	0.4272
100	1.7142	0.8191	15.635	0.4228
105	1.7038	0.8318	16.335	0.4195
110	1.6954	0.8414	16.928	0.4165
115	1.6872	0.8512	17.526	0.4146
120	1.6815	0.8566	17.958	0.4112
125	1.6764	0.8606	18.366	0.4098
130	1.6719	0.8635	18.745	0.4076
135	1.6678	0.8656	19.099	0.4057
140	1.6640	0.8673	19.440	0.4040
145	1.6603	0.8690	19.783	0.4026
150	1.6570	0.8706	20.099	0.4014
155	1.6541	0.8719	20.381	0.4004
160	1.6516	0.8733	20.674	0.3995
165	1.6485	0.8761	20.922	0.3993

Table A.12: H$\cdots$O and O$\cdots$O distances (d) in Å, ED (ϱ) at the H$\cdots$O bcps in eÅ^{-3}, Laplacian ($\nabla^2\varrho$) at the H$\cdots$O bcps in eÅ^{-5}, and H$\cdots$O delocalization indices (δ) in disiloxane$\cdots$silanol

a(Si–O–Si)	d(H$\cdots$O)	d(O$\cdots$O)	ϱ(H$\cdots$O)	$\nabla^2\varrho$(H$\cdots$O)	δ(H$\cdots$O)
85	1.8917	2.8575	0.1812	2.044	0.0744
90	1.8956	2.8597	0.1803	2.036	0.0742
95	1.9038	2.8710	0.1741	2.007	0.0718
100	1.9051	2.8719	0.1750	2.003	0.0727
105	1.9073	2.8743	0.1765	1.993	0.0733
110	1.9149	2.8818	0.1732	1.967	0.0728
115	1.9210	2.8878	0.1718	1.947	0.0728
120	1.9290	2.8956	0.1697	1.921	0.0726
125	1.9396	2.9059	0.1666	1.888	0.0720
130	1.9491	2.9141	0.1645	1.861	0.0718
135	1.9646	2.9285	0.1599	1.816	0.0709
140	1.9867	2.9496	0.1529	1.752	0.0690
145	2.0109	2.9719	0.1458	1.684	0.0671
150	2.0358	2.9947	0.1395	1.614	0.0658
155	2.0762	3.0335	0.1284	1.503	0.0623
160	2.1518	3.0853	0.1082	1.324	0.0590
165	2.2499	3.1484	0.0876	1.105	0.0426

Table A.13: H$\cdots$O and O$\cdots$O distances (d) in Å, ED (ϱ) at the H$\cdots$O bcps in eÅ^{-3}, Laplacian ($\nabla^2\varrho$) at the H$\cdots$O bcps in eÅ^{-5}, and H$\cdots$O delocalization indices (δ) in disiloxane$\cdots$water

a(Si–O–Si)	d(H$\cdots$O)	d(O$\cdots$O)	ϱ(H$\cdots$O)	$\nabla^2\varrho$(H$\cdots$O)	δ(H$\cdots$O)
90	2.0572	2.9050	0.1298	1.763	0.0538
95	2.0104	2.9189	0.1403	1.824	0.0598
100	2.0628	2.9117	0.1281	1.737	0.0536
105	2.0448	2.9096	0.1331	1.781	0.0559
110	2.0369	2.9008	0.1368	1.813	0.0575
115	2.0686	2.9189	0.1279	1.713	0.0543
120	2.0610	2.9203	0.1298	1.724	0.0553
125	2.0735	2.9317	0.1270	1.680	0.0547
130	2.0826	2.9467	0.1253	1.640	0.0547
135	2.0925	2.9641	0.1233	1.596	0.0547
140	2.1037	2.9846	0.1212	1.549	0.0549
145	2.1219	3.0102	0.1174	1.484	0.0544
150	2.1590	3.0431	0.1093	1.378	0.0516
155	2.2176	3.0809	0.0974	1.232	0.0460
160	2.3069	3.1254	0.0822	1.035	0.0373
165	2.5327	3.1897	0.0574	0.680	0.0201

Table A.14: O–H$\cdots$O angle (a) in °, O–H distances (d) in Å, ED (ϱ) at the O–H bcps in eÅ^{-3}, Laplacian ($\nabla^2\varrho$) at the O–H bcps in eÅ^{-5}, and O–H delocalization indices (δ) in the silanol group of disiloxane$\cdots$silanol

a(Si–O–Si)	a(O–H$\cdots$O)	d(O–H)	ϱ(O–H)	$\nabla^2\varrho$(O–H)	δ(O–H)
85	175.23	0.9680	2.3961	-62.583	0.5450
90	173.78	0.9678	2.3972	-62.620	0.5455
95	179.71	0.9673	2.4024	-62.853	0.5459
100	177.69	0.9673	2.4020	-62.828	0.5460
105	178.19	0.9673	2.4020	-62.812	0.5460
110	178.85	0.9671	2.4037	-62.833	0.5470
115	178.70	0.9670	2.4047	-62.835	0.5478
120	178.43	0.9668	2.4063	-62.846	0.5496
125	178.00	0.9666	2.4084	-62.865	0.5521
130	176.14	0.9664	2.4106	-62.874	0.5544
135	175.45	0.9660	2.4141	-62.918	0.5578
140	174.93	0.9655	2.4189	-62.986	0.5622
145	173.77	0.9649	2.4243	-63.067	0.5668
150	172.66	0.9643	2.4297	-63.132	0.5724
155	172.10	0.9635	2.4369	-63.237	0.5787
160	163.10	0.9624	2.4471	-63.392	0.5902
165	155.17	0.9613	2.4571	-63.528	0.6025

Table A.15: O–H$\cdots$O angle (a) in °, O–H distances (d) in Å, ED (ϱ) at the O–H bcps in eÅ^{-3}, Laplacian ($\nabla^2\varrho$) at the O–H bcps in eÅ^{-5}, and O–H delocalization indices (δ) in the water group of disiloxane$\cdots$water

a(Si–O–Si)	a(O–H$\cdots$O)	d(O–H)	ϱ(O–H)	$\nabla^2\varrho$(O–H)	δ(O–H)
90	145.48	0.9658	2.4702	-63.622	0.6149
95	155.95	0.9656	2.4709	-63.682	0.6070
100	145.72	0.9654	2.4728	-63.692	0.6163
105	148.10	0.9655	2.4720	-63.685	0.6131
110	147.91	0.9657	2.4712	-63.645	0.6123
115	145.95	0.9653	2.4743	-63.700	0.6171
120	147.30	0.9654	2.4737	-63.684	0.6150
125	147.18	0.9652	2.4752	-63.700	0.6168
130	148.15	0.9651	2.4765	-63.729	0.6179
135	149.42	0.9649	2.4782	-63.774	0.6191
140	151.05	0.9647	2.4802	-63.823	0.6211
145	152.46	0.9644	2.4831	-63.868	0.6242
150	151.87	0.9639	2.4873	-63.913	0.6298
155	148.58	0.9634	2.4918	-63.940	0.6374
160	142.39	0.9629	2.4969	-63.595	0.6483
165	125.55	0.9621	2.5036	-63.616	0.6609

Table A.16: Si–O distances (d) in Å, ED (ϱ) at the Si–O bcps in eÅ^{-3}, Laplacian ($\nabla^2\varrho$) at the Si–O bcps in eÅ^{-5}, and Si–O delocalization indices (δ) in the silanol group of disiloxane$\cdots$silanol

a(Si–O–Si)	d(Si–O)	ϱ(Si–O)	$\nabla^2\varrho$(Si–O)	δ(Si–O)
85	1.6514	0.9269	19.806	0.4504
90	1.6515	0.9265	19.790	0.4501
95	1.6511	0.9278	19.932	0.4501
100	1.6513	0.9273	19.921	0.4498
105	1.6514	0.9268	19.923	0.4494
110	1.6517	0.9261	19.895	0.4490
115	1.6520	0.9255	19.883	0.4487
120	1.6522	0.9247	19.864	0.4482
125	1.6525	0.9238	19.836	0.4477
130	1.6530	0.9225	19.779	0.4470
135	1.6536	0.9211	19.734	0.4463
140	1.6542	0.9197	19.688	0.4455
145	1.6549	0.9179	19.628	0.4445
150	1.6558	0.9156	19.552	0.4434
155	1.6566	0.9136	19.491	0.4423
160	1.6576	0.9112	19.397	0.4413
165	1.6587	0.9086	19.340	0.4401

Table A.17: Bending-potential energies (E_{rel}) in kJ mol^{-1}

a(Si–O–Si)	E_{rel}(free disiloxane)	E_{rel}(disiloxane$\cdots$silanol)	E_{rel}(disiloxane$\cdots$water)
50	813.901	–	–
55	722.932	–	–
60	604.312	–	–
65	484.913	–	–
70	381.008	–	–
75	292.308	–	–
80	220.086	–	–
85	162.971	141.441	–
90	118.921	101.588	103.314
95	85.598	71.590	73.866
100	60.799	49.446	51.471
105	42.582	33.297	35.353
110	29.298	23.052	23.728
115	19.716	13.973	15.175
120	12.817	7.674	9.213
125	7.993	3.560	5.017
130	4.685	1.171	2.342
135	2.585	0.202	0.772
140	1.258	0.000	0.120
145	0.584	0.546	0.000
150	0.236	1.455	0.036
155	0.000	2.891	0.947
160	0.010	4.130	1.490
165	0.029	5.445	2.007
170	0.257	–	–
175	0.432	–	–
180	0.498	–	–

Table A.18: Hydrogen-bond (E_{HB}) and NBO delocalization (ΔE_{deloc}) energies in $kJ\,mol^{-1}$ as well as IR red shifts (ΔIR) of the O–H stretching vibrations in donor molecules in cm^{-1} for 1: disiloxane$\cdots$silanol and 2: disiloxane$\cdots$water
Symm/asymm = symmetric/asymmetric stretching vibrations of the O–H bonds in water

a(Si–O–Si)	$E_{HB}(1)$	$E_{HB}(2)$	$\Delta E_{deloc}(1)$	$\Delta E_{deloc}(2)$	$\Delta IR(1)$	$\Delta IR_{symm}(2)$	$\Delta IR_{asymm}(2)$
85	-26.486	–	28.805	–	188.10		
90	-22.233	-14.298	29.433	11.221	185.79	53.23	30.01
95	-18.903	-11.321	25.958	14.068	179.05	51.81	25.65
100	-16.153	-8.064	26.921	11.346	177.78	48.57	28.20
105	-14.353	-5.785	27.800	12.728	175.14	50.43	25.02
110	-12.497	-4.151	27.507	13.900	172.12	53.47	28.89
115	-11.091	-3.250	27.675	12.309	170.91	47.15	26.57
120	-9.835	-2.309	27.591	12.770	168.42	48.82	28.51
125	-9.144	-1.662	27.214	12.519	164.43	46.57	28.18
130	-8.303	-1.068	26.963	12.644	160.67	44.66	27.72
135	-7.238	-0.572	25.916	12.602	153.71	42.51	27.12
140	-6.193	0.029	24.283	12.602	143.82	39.86	26.51
145	-5.069	0.475	22.441	12.184	132.50	36.16	25.69
150	-3.857	0.838	20.641	10.634	121.96	29.58	23.54
155	-2.213	2.073	17.710	8.290	106.25	22.26	20.51
160	-1.027	2.780	13.147	5.443	79.82	14.22	15.81
165	-0.255	3.699	8.374	1.507	55.17	5.39	8.25

Table A.19: Atomic charges (Q_{001}) in e and volumes (V_{001}) in $Å^3$ of Si and O atoms in free disiloxane

a(Si–O–Si)	Q_{001}(Si)	V_{001}(Si)	Q_{001}(O)	V_{001}(O)
50	2.1573	9.676	-0.4118	22.136
55	2.2501	8.507	-0.6390	21.992
60	2.3824	7.528	-0.9124	21.982
65	2.5600	6.663	-1.2896	22.313
70	2.6678	6.229	-1.4436	21.986
75	2.7243	6.027	-1.5024	21.495
80	2.7650	5.909	-1.5381	21.097
85	2.7949	5.844	-1.5627	20.753
90	2.8165	5.809	-1.5805	20.464
95	2.8327	5.793	-1.5940	20.243
100	2.8466	5.788	-1.6041	20.051
105	2.8546	5.788	-1.6124	19.925
110	2.8618	5.793	-1.6190	19.834
115	2.8679	5.799	-1.6245	19.782
120	2.8730	5.804	-1.6297	19.785
125	2.8773	5.804	-1.6345	19.815
130	2.8814	5.799	-1.6393	19.923
135	2.8849	5.788	-1.6438	19.989
140	2.8883	5.774	-1.6480	20.088
145	2.8912	5.758	-1.6517	20.153
150	2.8937	5.744	-1.6550	20.204
155	2.8958	5.733	-1.6578	20.236
160	2.8977	5.721	-1.6603	20.255
165	2.8993	5.712	-1.6622	20.267
170	2.9003	5.706	-1.6638	20.279
175	2.9009	5.702	-1.6648	20.294
180	2.9013	5.700	-1.6655	20.306

Table A.20: Atomic charges (Q_{001}) in e and volumes (V_{001}) in Å^3 of Si and O atoms in the siloxane group of disiloxane$\cdots$silanol

a(Si–O–Si)	Q_{001}(Si)	V_{001}(Si)	Q_{001}(O)	V_{001}(O)
85	2.8167	5.715	-1.5686	19.669
90	2.8321	5.712	-1.5852	19.404
95	2.8432	5.719	-1.5944	19.257
100	2.8553	5.735	-1.6209	19.149
105	2.8619	5.753	-1.6269	18.990
110	2.8610	5.824	-1.6209	18.858
115	2.8665	5.831	-1.6270	18.772
120	2.8711	5.836	-1.6322	18.726
125	2.8752	5.836	-1.6370	18.720
130	2.8790	5.831	-1.6410	18.762
135	2.8824	5.819	-1.6461	18.838
140	2.8851	5.804	-1.6503	18.909
145	2.8873	5.790	-1.6546	18.983
150	2.8882	5.783	-1.6584	19.036
155	2.8900	5.770	-1.6619	19.122
160	2.8930	5.751	-1.6652	19.272
165	2.8953	5.720	-1.6681	19.430

Table A.21: Atomic charges (Q_{001}) in e and volumes (V_{001}) in Å^3 of Si and O atoms in the siloxane group of disiloxane$\cdots$water
1 = long bond; 2 = short bond

a(Si–O–Si)	Q_{001}(Si1)	V_{001}(Si1)	Q_{001}(Si2)	V_{001}(Si2)	Q_{001}(O)	V_{001}(O)
90	2.8340	5.640	2.8352	5.671	-1.6069	19.461
95	2.8427	5.738	2.8465	5.697	-1.6119	19.275
100	2.8540	5.665	2.8561	5.693	-1.6274	19.083
105	2.8597	5.693	2.8631	5.718	-1.6317	18.939
110	2.8656	5.696	2.8687	5.733	-1.6383	18.827
115	2.8714	5.720	2.8735	5.741	-1.6425	18.822
120	2.8760	5.756	2.8781	5.752	-1.6417	18.816
125	2.8800	5.750	2.8815	5.769	-1.6444	18.847
130	2.8836	5.743	2.8846	5.785	-1.6480	18.900
135	2.8865	5.735	2.8876	5.793	-1.6517	18.972
140	2.8889	5.728	2.8897	5.791	-1.6553	18.051
145	2.8912	5.718	2.8909	5.781	-1.6587	19.126
150	2.8935	5.702	2.8932	5.771	-1.6622	19.217
155	2.8959	5.680	2.8958	5.755	-1.6659	19.322
160	2.8974	5.665	2.8991	5.725	-1.6699	19.453
165	2.9007	5.639	2.9021	5.704	-1.6747	19.706

Table A.22: Atomic charges (Q_{001}) in e and volumes (V_{001}) in Å^3 of Si, O and H atoms in the silanol group of disiloxane$\cdots$silanol

a(Si–O–Si)	Q_{001}(Si)	V_{001}(Si)	Q_{001}(O)	V_{001}(O)	Q_{001}(H)	V_{001}(H)
85	2.8889	5.770	-1.4419	21.378	0.6267	2.115
90	2.8888	5.770	-1.4436	21.396	0.6267	2.120
95	2.8885	5.775	-1.4344	21.320	0.6274	2.136
100	2.8887	5.775	-1.4342	21.337	0.6268	2.137
105	2.8887	5.775	-1.4345	21.356	0.6263	2.141
110	2.8886	5.776	-1.4340	21.397	0.6276	2.157
115	2.8881	5.778	-1.4335	21.432	0.6246	2.166
120	2.8882	5.778	-1.4341	21.488	0.6234	2.175
125	2.8876	5.780	-1.4335	21.541	0.6217	2.184
130	2.8875	5.780	-1.4340	21.577	0.6199	2.194
135	2.8877	5.781	-1.4329	21.593	0.6177	2.211
140	2.8873	5.784	-1.4330	21.622	0.6156	2.236
145	2.8870	5.787	-1.4307	21.628	0.6130	2.269
150	2.8867	5.790	-1.4292	21.646	0.6099	2.326
155	2.8865	5.793	-1.4245	21.648	0.6067	2.388
160	2.8866	5.794	-1.4241	21.621	0.6035	2.488
165	2.8860	5.798	-1.4207	21.604	0.6005	2.636

Table A.23: Atomic charges (Q_{001}) in e and volumes (V_{001}) in Å^3 of O and H atoms in the water group of disiloxane$\cdots$water

a(Si–O–Si)	Q_{001}(O)	V_{001}(O)	Q_{001}(H)	V_{001}(H)
90	-1.1121	21.473	0.5952	2.613
95	-1.1080	21.640	0.5959	2.491
100	-1.1116	21.491	0.5944	2.622
105	-1.1113	21.494	0.5948	2.577
110	-1.1116	21.458	0.5943	2.569
115	-1.1108	21.455	0.5933	2.632
120	-1.1080	21.491	0.5936	2.611
125	-1.1067	21.484	0.5927	2.633
130	-1.1060	21.497	0.5916	2.648
135	-1.1042	21.517	0.5902	2.668
140	-1.1032	21.528	0.5879	2.695
145	-1.1015	21.543	0.5853	2.735
150	-1.0995	21.533	0.5825	2.812
155	-1.0972	21.473	0.5799	2.927
160	-1.0946	21.384	0.5765	3.083
165	-1.0900	21.250	0.5747	3.369

Table A.24: Number of ELI attractors belonging to oxygen lone-pair basins ($V_1(O)$) and distance from each other in Å, sum of the populations of both oxygen lone-pair basins ($\Sigma N_{001}(V_1(O))$) in e, and sum of the volumes of both oxygen lone-pair basins ($\Sigma V_{001}(V_1(O))$) in Å^3 for the ELI of free disiloxane

a(Si–O–Si)	no(attr)	dist(attr)	$\Sigma N_{001}(V_1(O))$	$\Sigma V_{001}(V_1(O))$
50	4		6.2360	21.586
55	2	1.125	6.3587	21.383
60	2	1.120	6.6366	21.782
65	2	1.113	7.0888	22.403
70	2	1.103	7.3383	22.121
75	2	1.088	7.8240	22.687
80	2	1.068	7.7850	21.960
85	2	1.042	6.2427	19.195
90	2	1.012	5.5275	17.756
95	2	0.976	5.1805	16.874
100	2	0.935	4.9865	16.327
105	2	0.888	4.8410	15.900
110	2	0.835	4.7135	15.549
115	2	0.774	4.6248	15.253
120	2	0.703	4.5586	15.028
125	2	0.621	4.5005	14.826
130	2	0.528	4.4674	14.683
135	2	0.430	4.4337	14.563
140	2	0.343	4.4257	14.490
145	2	0.306	4.4136	14.440
150	2	0.347	4.4277	14.447
155	2	0.447	4.4636	14.489
160	2	0.566	4.5310	14.536
165	2	0.687	4.5680	14.415
170	3	0.799	5.4760	17.546
175	3	0.901	5.7916	18.118
180	3	0.993	5.8631	18.286

Table A.25: Sum of the populations in e and volumes in Å^3 of both Si–O bond basins ($\Sigma N_{001}(V_2(Si,O))$ and $\Sigma V_{001}(V_2(Si,O))$), populations and volumes of the Si–Si bond basins ($N_{001}(V_2(Si,Si))$ and $V_{001}(V_2(Si,Si))$), distances of the Si–O bond attractors to the oxygen atom (d(att-O)) in Å, and distances of the Si–O bond attractors to the Si–O bond axis (d(att-axis)) in Å for the ELI of free disiloxane

a(Si–O–Si)	$\Sigma N_{001}(V_2(Si,O))$	$\Sigma V_{001}(V_2(Si,O))$	$N_{001}(V_2(Si,Si))$	$V_{001}(V_2(Si,Si))$
50			1.7079	8.410
55			1.6205	6.586
60			1.3412	4.417
65			0.8451	2.417
70			0.5392	1.510
75				
80			d(att-O)	d(att-axis)
85	1.5128	2.170	0.6340	0.238
90	2.2078	3.118	0.6338	0.171
95	2.5444	3.610	0.6333	0.129
100	2.7352	3.859	0.6330	0.096
105	2.8770	4.045	0.6327	0.068
110	2.9989	4.213	0.6312	0.041
115	3.0910	4.374	0.6304	0.014
120	3.1600	4.523	0.6293	0.012
125	3.2174	4.690	0.6279	0.037
130	3.2616	4.872	0.6275	0.061
135	3.2898	5.069	0.6271	0.085
140	3.3004	5.266	0.6265	0.107
145	3.3132	5.436	0.6262	0.128
150	3.3004	5.536	0.6256	0.147
155	3.2706	5.568	0.6251	0.164
160	3.2060	5.570	0.6248	0.177
165	3.1680	5.722	0.6247	0.184
170	2.2589	2.602	0.6237	0.189
175	1.9548	2.047	0.6229	0.192
180	1.8732	1.891	0.6197	

Table A.26: ELI values at the Si–O bond and oxygen lone-pair attractors in free disiloxane

a(Si–O–Si)	ELI(V_2(Si,O))	ELI(V_1(O))
50		1.7970
55		1.7335
60		1.6868
65		1.6545
70		1.6327
75		1.6179
80		1.6080
85	1.4662	1.6012
90	1.4723	1.5964
95	1.4791	1.5928
100	1.4850	1.5899
105	1.4898	1.5872
110	1.4933	1.5847
115	1.4957	1.5821
120	1.4972	1.5792
125	1.4978	1.5759
130	1.4977	1.5721
135	1.4969	1.5675
140	1.4954	1.5620
145	1.4932	1.5554
150	1.4906	1.5478
155	1.4874	1.5393
160	1.4837	1.5303
165	1.4798	1.5212
170	1.4757	1.5125
175	1.4718	1.5047
180	1.4694	1.4981

Table A.27: Number of ELI attractors belonging to oxygen lone-pair basins ($V_1(O)$), individual populations in e and volumes in Å^3 of the lone pair involved in the hydrogen bond ($N_{001}(V_1(O)_{hbond})$ and $V_{001}(V_1(O)_{hbond})$) and not involved in the hydrogen bond ($N_{001}(V_1(O))$ and $V_{001}(V_1(O))$, sum of the populations and volumes of both oxygen lone-pair basins or of the only oxygen lone-pair basin for a(Si–O–Si) $\geq 130\,°$, respectively, ($\Sigma N_{001}(V_1(O))$ and $\Sigma V_{001}(V_1(O))$) for the ELI of the siloxane group of disiloxane$\cdots$silanol

a(Si–O–Si)	no(attr)	N_{001} ($V_1(O)_{hbond}$)	V_{001} ($V_1(O)_{hbond}$)	N_{001} ($V_1(O)$)	V_{001} ($V_1(O)$)	ΣN_{001} ($V_1(O)$)	ΣV_{001} ($V_1(O)$)
85	2	2.7527	7.570	2.9551	9.630	5.7078	17.200
90	2	2.6000	7.172	2.7046	9.023	5.3046	16.195
95	2	2.5421	7.446	2.5359	8.285	5.0780	15.731
100	2	2.4791	7.220	2.4340	7.998	4.9131	15.218
105	2	2.4205	7.045	2.3581	7.755	4.7786	14.800
110	2	2.3970	6.955	2.3002	7.553	4.6972	14.508
115	2	2.3536	6.835	2.2659	7.364	4.6195	14.199
120	2	2.3383	6.759	2.2178	7.159	4.5561	13.918
125	2	2.3856	6.813	2.1358	6.918	4.5214	13.731
130	1					4.4736	13.529
135	1					4.4675	13.456
140	1					4.4624	13.447
145	1					4.4712	13.514
150	1					4.5607	13.922
155	1					4.6962	14.432
160	1					4.7756	14.754
165	1					5.0680	15.757

Table A.28: Sum of the populations in e and volumes in Å^3 of both Si–O bond basins ($\Sigma N_{001}(V_2(Si,O))$ and $\Sigma V_{001}(V_2(Si,O))$) for the ELI of the siloxane group of disiloxane$\cdots$silanol

a(Si–O–Si)	$\Sigma N_{001}(V_2(Si,O))$	$\Sigma V_{001}(V_2(Si,O))$
85	2.0127	2.894
90	2.4176	3.486
95	2.6389	3.756
100	2.8031	3.970
105	2.9332	4.134
110	3.0156	4.257
115	3.0922	4.379
120	3.1561	4.516
125	3.1979	4.656
130	3.2436	4.842
135	3.2628	5.006
140	3.2664	5.129
145	3.2565	5.159
150	3.1662	4.794
155	3.0368	4.389
160	2.9528	4.306
165	2.6613	3.500

Table A.29: Number of ELI attractors belonging to oxygen lone-pair basins ($V_1(O)$), individual populations in e and volumes in Å^3 of the lone pair involved in the hydrogen bond ($N_{001}(V_1(O)_{hbond})$ and $V_{001}(V_1(O)_{hbond})$) and not involved in the hydrogen bond ($N_{001}(V_1(O))$ and $V_{001}(V_1(O))$, sum of the populations and volumes of both oxygen lone-pair basins or of the only oxygen lone-pair basin for a(Si–O–Si) $\geq 120\,°$, respectively, ($\Sigma N_{001}(V_1(O))$ and $\Sigma V_{001}(V_1(O))$) for the ELI of the siloxane group of disiloxane$\cdots$water

a(Si–O–Si)	no(attr)	N_{001} ($V_1(O)_{hbond}$)	V_{001} ($V_1(O)_{hbond}$)	N_{001} ($V_1(O)$)	V_{001} ($V_1(O)$)	ΣN_{001} ($V_1(O)$)	ΣV_{001} ($V_1(O)$)
90	2	2.6183	7.187	2.7048	8.978	5.3231	16.165
95	2	2.5110	7.021	2.5797	8.553	5.0907	15.574
100	2	2.4225	6.706	2.4703	8.344	4.8928	15.050
105	2	2.4178	6.738	2.3606	7.948	4.7784	14.686
110	2	2.3605	6.516	2.3084	7.824	4.6689	14.340
115	2	2.3749	6.649	2.2156	7.501	4.5905	14.150
120	1					4.5397	13.963
125	1					4.4901	13.831
130	1					4.4631	13.735
135	1					4.4458	13.674
140	1					4.4474	13.690
145	1					4.4854	13.856
150	1					4.5434	14.091
155	1					4.6426	14.443
160	1					4.7784	14.851
165	1					5.0476	15.723

Table A.30: Individual populations in e and volumes in Å^3 of the bond basins belonging to the long ($N_{001}(V_2(Si,O)_{long})$ and $V_{001}(V_2(Si,O)_{long})$) and the short ($N_{001}(V_2(Si,O)_{short})$ and $V_{001}(V_2(Si,O)_{short})$) Si–O bonds as well as sums of the populations and volumes of both Si–O bond basins ($\Sigma N_{001}(V_2(Si,O))$ and $\Sigma V_{001}(V_2(Si,O))$) for the ELI of the siloxane group of disiloxane$\cdots$water

a(Si–O–Si)	N_{001} ($V_2(Si,O)_{long}$)	V_{001} ($V_2(Si,O)_{long}$)	N_{001} ($V_2(Si,O)_{short}$)	V_{001} ($V_2(Si,O)_{short}$)	ΣN_{001} ($V_2(Si,O)$)	ΣV_{001} ($V_2(Si,O)$)
90	1.2007	1.809	1.2001	1.716	2.4008	3.525
95	1.3161	1.928	1.3122	1.866	2.6283	3.794
100	1.4145	2.092	1.4095	1.985	2.8240	4.077
105	1.4718	2.153	1.4683	2.067	2.9401	4.220
110	1.5328	2.237	1.5175	2.143	3.0503	4.380
115	1.5724	2.309	1.5566	2.192	3.1290	4.501
120	1.6110	2.425	1.5746	2.215	3.1856	4.640
125	1.6428	2.500	1.5895	2.270	3.2323	4.770
130	1.6610	2.555	1.6000	2.232	3.2610	4.787
135	1.6726	2.581	1.6076	2.396	3.2802	4.977
140	1.6700	2.560	1.6031	2.382	3.2731	4.942
145	1.6458	2.467	1.5941	2.299	3.2399	4.766
150	1.6150	2.365	1.5723	2.201	3.1873	4.566
155	1.5665	2.219	1.5262	2.094	3.0927	4.313
160	1.4946	2.030	1.4629	1.905	2.9575	3.935
165	1.3569	1.690	1.3385	1.569	2.6954	3.259

Table A.31: Population in e and volume in Å^3 of the Si–O bond basin ($N_{001}(V_2(Si,O))$ and $V_{001}(V_2(Si,O))$), sum of populations and volumes of both oxygen lone-pair basins ($\Sigma N_{001}(V_1(O))$ and $\Sigma V_{001}(V_1(O))$), populations and volumes of the O–H bond basin ($N_{001}(V_1(O,H))$ and $V_{001}(V_1(O,H))$) for the ELI of the silanol group of disiloxane$\cdots$silanol

a(Si–O–Si)	N_{001} (V_2(Si,O))	V_{001} (V_2(Si,O))	ΣN_{001} (V_1(O))	ΣV_{001} (V_1(O))	N_{001} (V_1(O,H))	V_{001} (V_1(O,H))
85	1.5863	2.407	4.5373	15.751	1.6605	5.098
90	1.5917	2.408	4.5389	15.748	1.6570	5.113
95	1.5882	2.436	4.5356	15.669	1.6615	5.140
100	1.5842	2.429	4.5443	15.699	1.6615	5.139
105	1.5906	2.445	4.5308	15.696	1.6637	5.151
110	1.6019	2.451	4.5300	15.701	1.6612	5.208
115	1.5879	2.430	4.5371	15.746	1.6638	5.231
120	1.5914	2.432	4.5430	15.776	1.6618	5.252
125	1.5922	2.443	4.5384	15.795	1.6613	5.274
130	1.5944	2.431	4.5297	15.841	1.6644	5.283
135	1.6039	2.448	4.5190	15.836	1.6630	5.299
140	1.5934	2.427	4.5310	15.864	1.6675	5.329
145	1.6045	2.433	4.5262	15.848	1.6665	5.364
150	1.6020	2.426	4.5344	15.859	1.6670	5.442
155	1.5993	2.422	4.5320	15.838	1.6615	5.527
160	1.5922	2.385	4.5376	15.819	1.6589	5.619
165	1.5832	2.365	4.5434	15.769	1.6598	5.801

Table A.32: Sum of populations in e and volumes in Å^3 of both oxygen lone-pair basins ($\Sigma N_{001}(V_1(O))$ and $\Sigma V_{001}(V_1(O))$), populations and volumes of the O–H bond basin ($N_{001}(V_1(O,H))$ and $V_{001}(V_1(O,H))$) for the ELI of the water group of disiloxane$\cdots$water

a(Si–O–Si)	$\Sigma N_{001}(V_1(O))$	$\Sigma V_{001}(V_1(O))$	$N_{001}(V_1(O,H))$	$V_{001}(V_1(O,H))$
90	4.5179	14.976	1.6648	5.437
95	4.5174	15.139	1.6640	5.452
100	4.5093	15.139	1.6649	5.384
105	4.5109	15.108	1.6644	5.368
110	4.5156	15.090	1.6636	5.460
115	4.5156	15.090	1.6636	5.460
120	4.5239	15.147	1.6624	5.424
125	4.5142	15.129	1.6668	5.453
130	4.5176	15.148	1.6644	5.466
135	4.5138	15.177	1.6630	5.482
140	4.5194	15.205	1.6654	5.508
145	4.5215	15.145	1.6621	5.545
150	4.5201	15.175	1.6626	5.637
155	4.5211	15.074	1.6594	5.783
160	4.5184	14.937	1.6582	5.958
165	4.5162	14.636	1.6600	6.366

Geometries of Compounds 1 to 4

Table A.33: Bonds distances (Å) in siloxanol (**1**)

Exp = experimental geom., theo = optimised geometry from isolated-molecule calculation

bond	exp	theo	bond	exp	theo	bond	exp	theo
Si1–O1	1.6788(12)	1.6771	C2–C3	1.3969(9)	1.3961	C9–H9A	1.0591	1.0922
Si1–C1	1.8948(6)	1.9192	C3–C4	1.3895(11)	1.3859	C9–H9B	1.0590	1.0908
Si1–C9	1.8426(9)	1.8764	C4–C5	1.3969(11)	1.3895	C9–H9C	1.0589	1.0894
Si1–C10	1.8477(9)	1.8849	C5–C6	1.4006(10)	1.4017	C10–H10A	1.0590	1.0921
Si2–O1	1.6574(11)	1.6633	C3–H3	1.0831	1.0845	C10–H10B	1.0590	1.0912
Si2–C2	1.8702(6)	1.8898	C4–H4	1.0831	1.0827	C10–H10C	1.0588	1.0889
Si2–C7	1.8498(10)	1.8794	C5–H5	1.0830	1.0834	C11–H11A	1.0586	1.0911
Si2–C8	1.8423(11)	1.8785	C7–H7A	1.0588	1.0918	C11–H11B	1.0592	1.0916
Si3–O2	1.6503(14)	1.6748	C7–H7B	1.0592	1.0921	C11–H11C	1.0595	1.0918
Si3–C6	1.8820(6)	1.8936	C7–H7C	1.0590	1.0906	C12–H12A	1.0590	1.0902
Si3–C11	1.8579(10)	1.8847	C8–H8A	1.0591	1.0918	C12–H12B	1.0589	1.0914
Si3–C12	1.8528(9)	1.8757	C8–H8B	1.0591	1.0921	C12–H12C	1.0591	1.0914
C1–C2	1.4123(7)	1.4172	C8–H8C	1.0590	1.0906	O2–H2O	0.9673	0.9592
C1–C6	1.4140(8)	1.4155						

Table A.34: Bond angles (°) in siloxanol (**1**)

Exp = experimental geom., theo = optimised geometry from isolated-molecule calculation

angle	exp	theo	angle	exp	theo	angle	exp	theo
O1–Si1–C1	99.28(4)	98.77	C2–C3–C4	119.74(6)	120.46	Si1–C9–H9A	109.49	109.36
O1–Si1–C9	106.65(4)	108.56	C3–C4–C5	119.68(5)	119.45	Si1–C9–H9B	109.63	111.38
O1–Si1–C10	106.77(4)	106.62	C4–C5–C6	122.00(6)	122.12	Si1–C9–H9C	109.95	111.37
C1–Si1–C9	116.17(4)	115.51	Si3–C6–C1	123.96(5)	124.99	H9A–C9–H9B	108.84	107.75
C1–Si1–C10	116.76(3)	115.22	Si3–C6–C5	117.93(6)	116.62	H9A–C9–H9C	109.36	108.04
C9–Si1–C10	109.73(5)	110.86	C1–C6–C5	118.11(5)	118.28	H9B–C9–H9C	109.55	108.82
O1–Si2–C2	98.63(5)	98.32	Si3–O2–H2O	113.10	116.96	Si1–C10–H10A	109.58	108.52
O1–Si2–C7	110.48(4)	110.95	C2–C3–H3	119.63	120.30	Si1–C10–H10B	109.36	111.79
O1–Si2–C8	111.17(4)	110.95	C4–C3–H3	120.63	119.25	Si1–C10–H10C	109.75	112.26
C2–Si2–C7	114.14(4)	113.50	C3–C4–H4	121.86	120.49	H10A–C10–H10B	109.12	107.50
C2–Si2–C8	111.89(4)	112.80	C5–C4–H4	118.46	120.06	H10A–C10–H10C	109.69	107.77
C7–Si2–C8	110.08(6)	109.88	C4–C5–H5	119.70	118.08	H10B–C10–H10C	109.32	108.81
O2–Si3–C6	108.65(3)	110.44	C6–C5–H5	118.28	119.80	Si3–C11–H11A	110.29	112.29
O2–Si3–C11	109.80(5)	109.54	Si2–C7–H7A	109.60	110.68	Si3–C11–H11B	109.57	111.86
O2–Si3–C12	106.59(7)	104.90	Si2–C7–H7B	110.07	111.26	Si3–C11–H11C	109.66	109.54
C6–Si3–C11	109.74(4)	110.39	Si2–C7–H7C	109.79	111.14	H11A–C11–H11B	109.39	107.57
C6–Si3–C12	112.81(3)	110.89	H7A–C7–H7B	109.14	107.64	H11A–C11–H11C	109.50	107.39
C11–Si3–C12	109.18(4)	110.55	H7A–C7–H7C	108.75	108.05	H11B–C11–H11C	108.41	108.01
Si1–O1–Si2	116.37(7)	118.07	H7B–C7–H7C	109.46	107.92	Si3–C12–H12A	109.48	111.22
Si1–C1–C2	109.97(5)	110.43	Si2–C8–H8A	109.70	110.80	Si3–C12–H12B	109.59	110.72
Si1–C1–C6	130.28(5)	130.11	Si2–C8–H8B	109.35	111.22	Si3–C12–H12C	109.67	110.83
C2–C1–C6	119.72(4)	119.46	Si2–C8–H8C	109.54	111.02	H12A–C12–H12B	109.22	107.72
Si2–C2–C1	114.40(5)	114.20	H8A–C8–H8B	109.38	107.66	H12A–C12–H12C	109.36	108.09
Si2–C2–C3	124.76(6)	125.55	H8A–C8–H8C	109.69	108.07	H12B–C12–H12C	109.50	108.13
C1–C2–C3	120.72(5)	120.23	H8B–C8–H8C	109.16	107.93			

Table A.35: Torsion angles (°) in siloxanol (**1**)

Exp = experimental geom., theo = optimised geometry from isolated-molecule calculation

angle	exp	theo	angle	exp	theo	angle	exp	theo
C1–Si1–O1–Si2	12.18(5)	4.21	C3–C4–C5–C6	0.67(7)	0.48	C8–Si2–C7–H7C	-69.73	-59.22
O1–Si1–C1–C2	-9.03(5)	-4.30	C4–C5–C6–Si3	178.37(10)	-175.95	C7–Si2–C8–H8A	53.48	59.22
O1–Si1–C1–C6	169.23(7)	176.12	C4–C5–C6–C1	-1.42(7)	0.47	C7–Si2–C8–H8B	-66.47	-60.49
C9–Si1–O1–Si2	133.19(7)	124.98	O1–Si1–C9–H9A	-57.87	-63.00	C7–Si2–C8–H8C	173.94	179.31
C10–Si1–O1–Si2	-109.54(7)	-115.53	O1–Si1–C9–H9B	-177.20	175.33	C6–Si3–O2–H2O	65.84	70.83
C9–Si1–C1–C2	-122.84(6)	-119.81	O1–Si1–C9–H9C	62.31	55.99	O2–Si3–C11–H11A	-61.15	-53.49
C9–Si1–C1–C6	55.42(6)	60.62	O1–Si1–C10–H10A	-72.19	-40.73	O2–Si3–C11–H11B	178.38	-172.71
C10–Si1–C1–C2	105.17(6)	108.82	O1–Si1–C10–H10B	168.24	-159.34	O2–Si3–C11–H11C	59.51	66.24
C10–Si1–C1–C6	-76.57(6)	-70.76	O1–Si1–C10–H10C	48.33	78.06	C11–Si3–O2–H2O	-54.18	-50.95
C2–Si2–O1–Si1	-10.47(5)	-2.78	C1–Si1–C9–H9A	51.67	46.79	O2–Si3–C12–H12A	-77.77	-59.50
O1–Si2–C2–C1	3.68(5)	-0.52	C1–Si1–C9–H9B	-67.66	-74.89	O2–Si3–C12–H12B	162.47	-179.23
O1–Si2–C2–C3	-172.35(7)	-178.78	C1–Si1–C9–H9C	171.85	165.77	O2–Si3–C12–H12C	42.23	60.77
C7–Si2–O1–Si1	109.41(7)	116.39	C1–Si1–C10–H10A	177.90	-148.79	C12–Si3–O2–H2O	-172.32	-169.63
C8–Si2–O1–Si1	-128.06(7)	-121.16	C1–Si1–C10–H10B	58.33	92.21	C6–Si3–C11–H11A	179.50	-175.30
C7–Si2–C2–C1	-113.43(6)	-117.75	C1–Si1–C10–H10C	-61.58	-30.39	C6–Si3–C11–H11B	59.03	65.48
C7–Si2–C2–C3	70.54(7)	63.99	C10–Si1–C9–H9A	-173.16	-179.80	C6–Si3–C11–H11C	-59.84	-55.57
C8–Si2–C2–C1	120.72(6)	116.45	C10–Si1–C9–H9B	67.51	58.52	C6–Si3–C12–H12A	41.40	59.73
C8–Si2–C2–C3	-55.31(7)	-61.81	C10–Si1–C9–H9C	-52.98	-60.82	C6–Si3–C12–H12B	-78.37	-60.00
O2–Si3–C6–C1	37.83(7)	29.12	C9–Si1–C10–H10A	43.03	77.66	C6–Si3–C12–H12C	161.39	180.00
O2–Si3–C6–C5	-141.95(7)	-154.73	C9–Si1–C10–H10B	-76.55	-41.35	C12–Si3–C11–H11A	55.38	61.63
C11–Si3–C6–C1	157.89(6)	150.40	C9–Si1–C10–H10C	163.54	-163.95	C12–Si3–C11–H11B	-65.09	-57.59
C11–Si3–C6–C5	-21.89(6)	-33.45	O1–Si2–C7–H7A	-65.97	-56.23	C12–Si3–C11–H11C	176.04	-178.64
C12–Si3–C6–C1	-80.13(6)	-86.73	O1–Si2–C7–H7B	173.99	-176.52	C11–Si3–C12–H12A	163.69	-177.49
C12–Si3–C6–C5	100.09(6)	89.42	O1–Si2–C7–H7C	53.42	63.84	C11–Si3–C12–H12B	43.92	62.78
Si1–C1–C2–Si2	3.41(3)	3.05	O1–Si2–C8–H8A	-69.27	-63.85	C11–Si3–C12–H12C	-76.32	-57.22
Si1–C1–C2–C3	179.62(8)	-178.59	O1–Si2–C8–H8B	170.78	176.45	Si2–C2–C3–H3	-5.63	-1.80
Si1–C1–C6–Si3	2.61(3)	-5.58	O1–Si2–C8–H8C	51.19	56.25	C1–C2–C3–H3	178.58	-179.96
Si1–C1–C6–C5	-177.61(9)	178.33	C2–Si2–C7–H7A	44.08	53.38	C2–C3–C4–H4	-179.55	179.68
C6–C1–C2–Si2	-175.06(7)	-177.33	C2–Si2–C7–H7B	-75.96	-66.92	H3–C3–C4–C5	-179.48	179.21
C2–C1–C6–Si3	-179.27(8)	174.88	C2–Si2–C7–H7C	163.47	173.44	H3–C3–C4–H4	-0.06	-0.44
C6–C1–C2–C3	1.15(6)	1.04	C2–Si2–C8–H8A	-178.47	-173.06	C3–C4–C5–H5	-177.74	-179.47
C2–C1–C6–C5	0.51(6)	-1.21	C2–Si2–C8–H8B	61.57	67.24	H4–C4–C5–C6	-178.78	-179.88
Si2–C2–C3–C4	173.87(10)	178.08	C2–Si2–C8–H8C	-58.01	-52.97	H4–C4–C5–H5	2.82	0.18
C1–C2–C3–C4	-1.93(7)	-0.08	C8–Si2–C7–H7A	170.87	-179.29	H5–C5–C6–Si3	-3.20	4.00
C2–C3–C4–C5	1.02(7)	-0.67	C8–Si2–C7–H7B	50.83	60.41	H5–C5–C6–C1	177.01	-179.58

Table A.36: Bonds distances (Å) in trisilo (**2**)

Exp = experimental geom., theo = optimised geometry from isolated-molecule calculation

bond	exp	theo	bond	exp	theo	bond	exp	theo
Si1–O1	1.6573(4)	1.6723	C1–C2	1.4189(2)	1.4144	C5–H5B	1.0590	1.0921
Si1–C1	1.8810(5)	1.8939	C1–C3a	1.4010(2)	1.3963	C5–H5C	1.0590	1.0906
Si1–C4	1.8565(5)	1.8779	C2–C3	1.4009(2)	1.3963	C6–H6A	1.0590	1.0905
Si1–C5	1.8560(5)	1.8783	C3–H3	1.0830	1.0865	C6–H6B	1.0590	1.0921
Si2–O1	1.6573(4)	1.6723	C4–H4A	1.0590	1.0905	C6–H6C	1.0590	1.0918
Si2–C2	1.8803(5)	1.8936	C4–H4B	1.0590	1.0921	C7–H7A	1.0590	1.0917
Si2–C6	1.8588(5)	1.8783	C4–H4C	1.0590	1.0917	C7–H7B	1.0590	1.0921
Si2–C7	1.8559(5)	1.8784	C5–H5A	1.0590	1.0917	C7–H7C	1.0590	1.0905

Table A.37: Bond angles (°) in trisilo (**2**)

Exp = experimental geom., theo = optimised geometry from isolated-molecule calculation

angle	exp	theo	angle	exp	theo	angle	exp	theo
O1–Si1–C1	98.79(3)	98.71	Si2–C2–C1	111.98(3)	112.46	H5A–C5–H5B	109.40	107.70
O1–Si1–C4	110.96(3)	110.46	Si2–C2–C3	128.60(3)	128.22	H5A–C5–H5C	109.55	108.10
O1–Si1–C5	110.21(3)	110.53	C1–C2–C3	119.42(3)	119.33	H5B–C5–H5C	109.48	107.90
C1–Si1–C4	112.04(3)	113.23	C1–C3a–C2a	121.07(2)	121.35	Si2–C6–H6A	109.46	111.19
C1–Si1–C5	112.35(3)	113.33	C1–C3a–H3a	119.61	119.32	Si2–C6–H6B	109.47	111.13
C4–Si1–C5	111.82(3)	110.10	C2–C3–H3	119.32	119.33	Si2–C6–H6C	109.47	110.72
O1–Si2–C2	99.01(3)	98.72	Si1–C4–H4A	109.51	111.07	H6A–C6–H6B	109.48	107.90
O1–Si2–C6	110.52(3)	110.49	Si1–C4–H4B	109.38	111.14	H6A–C6–H6C	109.46	108.09
O1–Si2–C7	109.87(3)	110.51	Si1–C4–H4C	109.42	110.83	H6B–C6–H6C	109.48	107.67
C2–Si2–C6	113.26(3)	113.33	H4A–C4–H4B	109.54	107.89	Si2–C7–H7A	109.44	110.71
C2–Si2–C7	114.18(3)	113.39	H4A–C4–H4C	109.59	108.08	Si2–C7–H7B	109.43	111.10
C6–Si2–C7	109.55(3)	109.93	H4B–C4–H4C	109.40	107.89	Si2–C7–H7C	109.45	111.23
Si1–O1–Si2	117.81(3)	117.64	Si1–C5–H5A	109.47	110.80	H7A–C7–H7B	109.49	107.67
Si1–C1–C2	112.37(3)	112.46	Si1–C5–H5B	109.42	111.10	H7A–C7–H7C	109.51	108.08
Si1–C1–C3a	128.12(1)	128.21	Si1–C5–H5C	109.52	111.10	H7B–C7–H7C	109.51	107.91
C2–C1–C3a	119.51(1)	119.33						

Table A.38: Torsion angles (°) in trisilo (**2**)

exp = experimental geom., theo = optimised geometry from isolated-molecule calculation

angle	exp	theo	angle	exp	theo	angle	exp	theo
C1–Si1–O1–Si2	2.23(1)	-0.19	C3a–C1–C2–C3	0.06(1)	0.00	O1–Si2–C6–H6A	-53.61	-56.48
O1–Si1–C1–C2	-1.35(1)	0.19	C1–C3a–C2a–Si2a	179.53(2)	179.91	O1–Si2–C6–H6B	-173.62	-176.09
C4–Si1–O1–Si2	120.00(1)	118.69	C1–C3a–C2a–C1a	-0.06(1)	0.00	O1–Si2–C6–H6C	66.37	63.70
C5–Si1–O1–Si2	-115.60(1)	-119.21	O1–Si1–C4–H4A	-53.73	-56.61	O1–Si2–C7–H7A	-63.02	-63.70
C4–Si1–C1–C2	-118.29(1)	-116.58	O1–Si1–C4–H4B	-173.78	-176.73	O1–Si2–C7–H7B	177.01	176.72
C5–Si1–C1–C2	114.85(1)	117.09	O1–Si1–C4–H4C	66.40	63.56	O1–Si2–C7–H7C	57.00	56.49
C2–Si2–O1–Si1	-2.16(1)	0.13	O1–Si1–C5–H5A	-67.23	-63.82	C2–Si2–C6–H6A	56.44	53.24
O1–Si2–C2–C1	1.10(1)	0.02	O1–Si1–C5–H5B	172.90	176.50	C2–Si2–C6–H6B	-63.57	-66.97
O1–Si2–C2–C3	-178.52(2)	179.94	O1–Si1–C5–H5C	52.89	56.36	C2–Si2–C6–H6C	176.42	173.42
C6–Si2–O1–Si1	116.94(1)	119.14	C1–Si1–C4–H4A	55.63	53.03	C2–Si2–C7–H7A	-173.19	-173.46
C7–Si2–O1–Si1	-122.05(1)	-118.96	C1–Si1–C4–H4B	-64.42	-67.10	C2–Si2–C7–H7B	66.84	66.95
C6–Si2–C2–C1	-115.93(1)	-116.85	C1–Si1–C4–H4C	175.76	173.19	C2–Si2–C7–H7C	-53.18	-53.28
C6–Si2–C2–C3	64.45(2)	63.07	C1–Si1–C5–H5A	-176.34	-173.55	C7–Si2–C6–H6A	-174.81	-178.72
C7–Si2–C2–C1	117.75(1)	116.93	C1–Si1–C5–H5B	63.79	66.77	C7–Si2–C6–H6B	65.18	61.07
C7–Si2–C2–C3	-61.88(2)	-63.16	C1–Si1–C5–H5C	-56.22	-53.37	C7–Si2–C6–H6C	-54.83	-58.54
Si1–C1–C2–Si2	0.16(3)	-0.13	C5–Si1–C4–H4A	-177.22	-178.95	C6–Si2–C7–H7A	58.57	58.53
Si1–C1–C2–C3	179.82(2)	179.94	C5–Si1–C4–H4B	62.74	60.93	C6–Si2–C7–H7B	-61.40	-61.06
C3a–C1–Si1–O1	178.38(2)	179.94	C5–Si1–C4–H4C	-57.08	-58.79	C6–Si2–C7–H7C	178.58	178.71
C3a–C1–Si1–C4	61.45(1)	63.36	C4–Si1–C5–H5A	56.68	58.48	Si2–C2–C3–H3	0.35	0.10
C3a–C1–Si1–C5	-65.42(1)	-62.97	C4–Si1–C5–H5B	-63.20	-61.20	C1–C2–C3–H3	-179.24	-179.98
C3a–C1–C2–Si2	-179.60(2)	179.92	C4–Si1–C5–H5C	176.80	178.67			

Table A.39: Bond distances (Å) in pentaphe (**3**)

Exp = experimental geom., theo = optimised geometry from isolated-molecule calculation

bond	exp	theo	bond	exp	theo	bond	exp	theo
Si1–O1	1.6192(3)	1.6478	C14–C15	1.3937(3)	1.3892	C6–H6	1.0830	1.0840
Si1–C1	1.8630(3)	1.8783	C15–C16	1.3947(4)	1.3913	C8–H8	1.0830	1.0831
Si1–C7	1.8614(3)	1.8805	C16–C17	1.3925(3)	1.3892	C9–H9	1.0830	1.0832
Si2–O1	1.6258(3)	1.6523	C17–C18	1.3950(3)	1.3912	C10–H10	1.0830	1.0822
Si2–C13	1.8621(5)	1.8876	C19–C20	1.4050(3)	1.4008	C11–H11	1.0830	1.0822
Si2–C19	1.8632(5)	1.8847	C19–C24	1.4037(3)	1.4004	C12–H12	1.0830	1.0834
Si2–C25	1.8635(5)	1.8840	C20–C21	1.3928(3)	1.3901	C14–H14	1.0830	1.0834
C1–C2	1.4055(4)	1.3995	C21–C22	1.3945(4)	1.3900	C15–H15	1.0830	1.0823
C1–C6	1.4018(3)	1.4003	C22–C23	1.3957(4)	1.3903	C16–H16	1.0830	1.0822
C2–C3	1.3961(4)	1.3910	C23–C24	1.3970(3)	1.3901	C17–H17	1.0830	1.0823
C3–C4	1.3929(4)	1.3897	C25–C26	1.4011(3)	1.4001	C18–H18	1.0830	1.0823
C4–C5	1.3938(4)	1.3909	C25–C30	1.4068(3)	1.4013	C20–H20	1.0830	1.0833
C5–C6	1.3944(4)	1.3894	C26–C27	1.3946(3)	1.3905	C21–H21	1.0830	1.0823
C7–C8	1.4034(4)	1.4005	C27–C28	1.3915(4)	1.3898	C22–H22	1.0830	1.0822
C7–C12	1.4046(3)	1.4008	C28–C29	1.3968(4)	1.3903	C23–H23	1.0830	1.0823
C8–C9	1.3960(4)	1.3901	C29–C30	1.3941(4)	1.3901	C24–H24	1.0830	1.0825
C9–C10	1.3944(4)	1.3904	Si1–H1Si	1.4840	1.4876	C26–H26	1.0830	1.0829
C10–C11	1.3954(4)	1.3903	C2–H2	1.0830	1.0825	C27–H27	1.0830	1.0823
C11–C12	1.3953(4)	1.3898	C3–H3	1.0830	1.0823	C28–H28	1.0830	1.0822
C13–C14	1.4037(3)	1.4026	C4–H4	1.0830	1.0821	C29–H29	1.0830	1.0823
C13–C18	1.4015(3)	1.3996	C5–H5	1.0830	1.0822	C30–H30	1.0830	1.0827

Table A.40: Bond angles (°) in pentaphe (**3**)
Exp = experimental geom., theo = optimised geometry from isolated-molecule calculation

angle	exp	theo	angle	exp	theo	angle	exp	theo
O1–Si1–C1	110.23(3)	107.24	Si2–C19–C24	122.65(2)	120.81	C10–C11–H11	121.35	120.09
C1–Si1–C7	111.66(3)	111.63	C20–C19–C24	117.98(2)	117.79	C12–C11–H11	118.94	119.96
O1–Si1–C7	108.74(3)	110.68	C19–C20–C21	121.40(2)	121.25	C7–C12–H12	119.11	119.81
O1–Si2–C13	107.77(3)	110.27	C20–C21–C22	119.74(2)	119.99	C11–C12–H12	119.87	119.02
O1–Si2–C19	110.34(3)	108.17	C21–C22–C23	119.93(2)	119.72	C13–C14–H14	117.88	119.85
O1–Si2–C25	109.91(3)	106.75	C22–C23–C24	119.99(2)	120.06	C15–C14–H14	121.33	118.86
C13–Si2–C19	110.20(3)	109.61	C19–C24–C23	120.96(2)	121.20	C14–C15–H15	118.90	119.96
C13–Si2–C25	108.08(3)	110.74	Si2–C25–C26	121.06(2)	121.72	C16–C15–H15	120.82	120.08
C19–Si2–C25	110.48(3)	111.23	Si2–C25–C30	120.75(2)	120.49	C15–C16–H16	122.34	120.10
Si1–O1–Si2	162.03(2)	153.90	C26–C25–C30	118.04(2)	117.79	C17–C16–H16	117.96	120.16
Si1–C1–C2	122.20(2)	121.58	C25–C26–C27	121.19(2)	121.24	C16–C17–H17	120.94	120.07
Si1–C1–C6	119.73(2)	120.44	C26–C27–C28	119.91(2)	120.04	C18–C17–H17	119.20	119.88
C2–C1–C6	118.07(2)	117.98	C27–C28–C29	119.99(2)	119.70	C13–C18–H18	119.97	119.69
C1–C2–C3	120.83(2)	121.07	C28–C29–C30	119.81(2)	120.04	C17–C18–H18	118.78	119.09
C2–C3–C4	120.16(2)	120.04	C25–C30–C29	121.06(2)	121.20	C19–C20–H20	119.20	119.85
C3–C4–C5	119.79(2)	119.77	O1–Si1–H1Si	108.07	109.74	C21–C20–H20	119.40	118.90
C4–C5–C6	119.90(2)	119.96	C1–Si1–H1Si	109.67	109.87	C20–C21–H21	118.45	119.93
C1–C6–C5	121.24(2)	121.18	C7–Si1–H1Si	108.40	107.50	C22–C21–H21	121.80	120.08
Si1–C7–C8	121.22(2)	121.90	C1–C2–H2	120.06	119.63	C21–C22–H22	118.98	120.13
Si1–C7–C12	120.46(2)	120.16	C3–C2–H2	119.11	119.30	C23–C22–H22	121.03	120.15
C8–C7–C12	118.32(2)	117.93	C2–C3–H3	120.00	119.90	C22–C23–H23	120.88	120.06
C7–C8–C9	121.00(2)	121.12	C4–C3–H3	119.83	120.06	C24–C23–H23	119.09	119.88
C8–C9–C10	119.74(2)	119.99	C3–C4–H4	119.80	120.15	C19–C24–H24	118.72	119.68
C9–C10–C11	120.23(2)	119.82	C5–C4–H4	120.41	120.08	C23–C24–H24	120.31	119.12
C10–C11–C12	119.70(2)	119.95	C4–C5–H5	120.33	120.07	C25–C26–H26	120.29	119.89
C7–C12–C11	121.01(2)	121.18	C6–C5–H5	119.75	119.97	C27–C26–H26	118.48	118.87
Si2–C13–C14	121.82(2)	120.13	C1–C6–H6	120.33	119.91	C26–C27–H27	119.60	119.90
Si2–C13–C18	120.03(2)	122.12	C5–C6–H6	118.43	118.92	C28–C27–H27	120.50	120.06
C14–C13–C18	118.12(2)	117.74	C7–C8–H8	120.62	119.78	C27–C28–H28	118.81	120.10
C13–C14–C15	120.78(2)	121.29	C9–C8–H8	118.37	119.09	C29–C28–H28	121.20	120.15
C14–C15–C16	120.28(2)	119.96	C8–C9–H9	122.62	119.96	C28–C29–H29	120.78	120.08
C15–C16–C17	119.69(2)	119.74	C10–C9–H9	117.64	120.05	C30–C29–H29	119.39	119.87
C16–C17–C18	119.86(2)	120.05	C9–C10–H10	121.09	120.09	C25–C30–H30	120.79	119.80
C13–C18–C17	121.25(2)	121.22	C11–C10–H10	118.61	120.09	C29–C30–H30	118.12	119.00
Si2–C19–C20	119.36(2)	121.37						

Table A.41: Torsion angles (°) in pentaphe (**3**)

Exp = experimental geom., theo = optimised geometry from isolated-molecule calculation

angle	exp	theo	angle	exp	theo	angle	exp	theo
C1–Si1–O1–Si2	34.65(6)	158.40	C14–C15–C16–C17	0.48(2)	-0.01	H10–C10–C11–H11	1.09	
O1–Si1–C1–C2	32.28(2)	18.67	C15–C16–C17–C18	-0.65(2)	-0.14	C10–C11–C12–H12	179.44	
O1–Si1–C1–C6	-148.38(2)	-162.02	C16–C17–C18–C13	0.01(2)	0.05	H11–C11–C12–C7	-178.82	
C7–Si1–O1–Si2	157.35(7)	-79.50	Si2–C19–C20–C21	178.99(3)	177.78	H11–C11–C12–H12	0.79	
O1–Si1–C7–C8	-92.52(2)	-90.57	Si2–C19–C24–C23	-178.87(3)	-178.05	Si2–C13–C14–H14	-3.59	
O1–Si1–C7–C12	87.74(2)	88.24	C24–C19–C20–C21	-0.05(2)	-0.43	Si2–C13–C18–H18	1.65	
C7–Si1–C1–C2	-88.69(2)	-102.84	C20–C19–C24–C23	0.14(2)	0.18	C18–C13–C14–H14	178.22	
C7–Si1–C1–C6	90.65(2)	76.47	C19–C20–C21–C22	-0.13(2)	0.33	C14–C13–C18–H18	179.87	
C1–Si1–C7–C8	29.31(2)	29.03	C20–C21–C22–C23	0.23(2)	0.04	C13–C14–C15–H15	-179.57	
C1–Si1–C7–C12	-150.42(2)	-152.16	C21–C22–C23–C24	-0.15(2)	-0.29	H14–C14–C15–C16	-178.81	
C13–Si2–O1–Si1	158.79(7)	16.16	C22–C23–C24–C19	-0.04(2)	0.18	H14–C14–C15–H15	1.29	
O1–Si2–C13–C14	-32.02(2)	-68.74	Si2–C25–C26–C27	175.03(3)	178.92	C14–C15–C16–H16	-179.04	
O1–Si2–C13–C18	146.13(2)	110.03	Si2–C25–C30–C29	-175.96(3)	-178.99	H15–C15–C16–C17	-179.62	
C19–Si2–O1–Si1	38.43(6)	-103.69	C30–C25–C26–C27	-0.52(2)	-0.22	H15–C15–C16–H16	0.86	
O1–Si2–C19–C20	153.57(2)	157.39	C26–C25–C30–C29	-0.40(2)	0.16	C15–C16–C17–H17	179.03	
O1–Si2–C19–C24	-27.44(2)	-24.45	C25–C26–C27–C28	0.98(2)	0.12	H16–C16–C17–C18	178.89	
C25–Si2–O1–Si1	-83.65(6)	136.52	C26–C27–C28–C29	-0.51(2)	0.04	H16–C16–C17–H17	-1.42	
O1– Si2–C25–C26	144.12(2)	146.20	C27–C28–C29–C30	-0.39(2)	-0.10	C16–C17–C18–H18	-179.09	
O1– Si2–C25–C30	-40.45(2)	-34.69	C28–C29–C30–C25	0.85(2)	0.00	H17–C17–C18–C13	-179.68	
C19–Si2–C13–C14	88.43(2)	50.24	H1Si–Si1–O1–Si2	-85.18	38.99	H17–C17–C18–H18	1.22	
C19–Si2–C13–C18	-93.42(2)	-130.99	H1Si–Si1–C1–C2	151.14	138.00	Si2–C19–C20–H20	-1.34	
C13–Si2–C19–C20	34.68(2)	37.12	H1Si–Si1–C1–C6	-29.52	-42.69	Si2–C19–C24–H24	2.43	
C13–Si2–C19–C24	-146.33(2)	-144.71	H1Si–Si1–C7–C8	150.22	149.59	C24–C19–C20–H20	179.62	
C25–Si2–C13–C14	-150.76(2)	173.33	H1Si–Si1–C7–C12	-29.52	-31.60	C20–C19–C24–H24	-178.57	
C25–Si2–C13–C18	27.40(2)	-7.90	Si1–C1–C2–H2	-0.44		C19–C20–C21–H21	178.91	
C13–Si2–C25–C26	-98.52(2)	-93.75	Si1–C1–C6–H6	-0.01		H20–C20–C21–C22	-179.80	
C13–Si2–C25–C30	76.91(2)	85.36	C6–C1–C2–H2	-179.79		H20–C20–C21–H21	-0.77	
C25–Si2–C19–C20	-84.69(2)	-85.68	C2–C1–C6–H6	179.36		C20–C21–C22–H22	177.43	
C25–Si2–C19–C24	94.30(2)	92.48	C1–C2–C3–H3	179.36		H21–C21–C22–C23	-178.77	
C19–Si2–C25–C26	22.13(2)	28.40	H2–C2–C3–C4	-179.72		H21–C21–C22–H22	-1.58	
C19–Si2–C25–C30	-162.45(2)	-152.49	H2–C2–C3–H3	-1.00		C21–C22–C23–H23	177.63	
Si1–C1–C2–C3	179.20(4)	179.21	C2–C3–C4–H4	179.43		H22–C22–C23–C24	-177.29	
Si1–C1–C6–C5	-179.82(3)	-179.32	H3–C3–C4–C5	-179.25		H22–C22–C23–H23	0.49	
C6–C1–C2–C3	-0.15(2)	-0.12	H3–C3–C4–H4	0.71		C22–C23–C24–H24	178.64	
C2–C1–C6–C5	-0.46(2)	0.02	C3–C4–C5–H5	178.78		H23–C23–C24–C19	-177.85	
C1–C2–C3–C4	0.65(3)	0.12	H4–C4–C5–C6	179.97		H23–C23–C24–H24	0.83	
C2–C3–C4–C5	-0.53(3)	-0.02	H4–C4–C5–H5	-1.17		Si2–C25–C26–H26	-2.90	
C3–C4–C5–C6	-0.08(3)	-0.08	C4–C5–C6–H6	-179.24		Si2–C25–C30–H30	1.95	
C4–C5–C6–C1	0.58(2)	0.08	H5–C5–C6–C1	-178.29		C30–C25–C26–H26	-178.45	
Si1–C7–C8–C9	179.89(3)	178.51	H5–C5–C6–H6	1.90		C26–C25–C30–H30	177.51	
Si1–C7–C12– C11	-179.68(4)	-178.53	Si1–C7–C8–H8	-1.88		C25–C26–C27–H27	-178.92	
C12–C7–C8–C9	-0.37(2)	-0.32	Si1–C7–C12–H12	0.71		H26–C26–C27–C28	178.94	
C8–C7–C12–C11	0.58(3)	0.32	C12–C7–C8–H8	177.86		H26–C26–C27–H27	-0.96	
C7–C8–C9–C10	-0.24(3)	0.14	C8–C7–C12–H12	-179.04		C26–C27–C28–H28	179.71	
C8–C9–C10–C11	0.66(3)	0.04	C7–C8–C9–H9	179.90		H27–C27–C28–C29	179.39	
C9–C10–C11–C12	-0.46(3)	-0.04	H8–C8–C9–C10	-178.50		H27–C27–C28–H28	-0.39	
C10–C11–C12–C7	-0.17(3)	-0.15	H8–C8–C9–H9	1.63		C27–C28–C29–H29	-178.65	
Si2–C13–C14–C15	177.24(3)	178.47	C8–C9–C10–H10	177.66		H28–C28–C29–C30	179.38	
Si2–C13–C18–C17	-177.44(3)	-178.60	H9–C9–C10–C11	-179.47		H28–C28–C29–H29	1.13	
C18–C13–C14–C15	-0.95(2)	-0.36	H9–C9–C10–H10	-2.47		C28–C29–C30–H30	-177.11	
C14–C13–C18–C17	0.78(2)	0.20	C9–C10–C11–H11	178.16		H29–C29–C30–C25	179.13	
C13–C14–C15–C16	0.33(2)	0.27	H10–C10–C11–C12	-177.53		H29–C29–C30–H30	1.17	

Table A.42: Bond distances (Å) in hexaphe (**4**)

Exp = experimental geom., theo = optimised geometry from isolated-molecule calculation

bond	exp	theo	bond	exp	theo	bond	exp	theo
Si1–O1	1.6211(4)	1.6440	C9–C10	1.3929(3)	1.3893	C5–H5	1.0830	1.0823
Si1–C1	1.8648(5)	1.8857	C10–C11	1.3955(3)	1.3911	C6–H6	1.0830	1.0831
Si1–C7	1.8618(5)	1.8864	C11–C12	1.3907(3)	1.3894	C8–H8	1.0830	1.0827
Si1–C13	1.8673(5)	1.8861	C13–C14	1.4054(3)	1.4021	C9–H9	1.0830	1.0823
C1–C2	1.4034(3)	1.3998	C13–C18	1.4032(3)	1.3997	C10–H10	1.0830	1.0822
C1–C6	1.4053(3)	1.4019	C14–C15	1.3954(3)	1.3895	C11–H11	1.0830	1.0823
C2–C3	1.3949(3)	1.3912	C15–C16	1.3951(3)	1.3910	C12–H12	1.0830	1.0832
C3–C4	1.3924(3)	1.3894	C16–C17	1.3938(3)	1.3893	C14–H14	1.0830	1.0831
C4–C5	1.3948(3)	1.3910	C17–C18	1.3959(3)	1.3912	C15–H15	1.0830	1.0823
C5–C6	1.3944(3)	1.3895	C2–H2	1.0830	1.0828	C16–H16	1.0830	1.0822
C7–C8	1.4018(3)	1.3996	C3–H3	1.0830	1.0823	C17–H17	1.0830	1.0823
C7–C12	1.4044(3)	1.4022	C4–H4	1.0830	1.0822	C18–H18	1.0830	1.0827
C8–C9	1.3969(3)	1.3913						

Table A.43: Bond angles (°) in hexaphe (**4**)

Exp = experimental geom., theo = optimised geometry from isolated-molecule calculation

angle	exp	theo	angle	exp	theo	angle	exp	theo
O1–Si1–C1	108.61(3)	108.58	C8–C9–C10	119.89(2)	120.03	C5–C6–H6	119.45	118.90
O1–Si1–C7	109.63(3)	108.57	C9–C10–C11	119.78(2)	119.73	C7–C8–H8	119.62	119.75
O1–Si1–C13	108.68(3)	108.64	C10–C11–C12	120.07(2)	120.01	C9–C8–H8	119.12	119.04
O1–Si1–C1a	108.62(3)	108.58	C7–C12–C11	121.10(2)	121.22	C8–C9–H9	120.48	119.90
O1–Si1–C7a	109.63(3)	108.57	Si1–C13–C14	121.55(2)	120.48	C10–C9–H9	119.61	120.07
O1–Si1–C13a	108.68(3)	108.64	Si1–C13–C18	120.44(2)	121.74	C9–C10–H10	121.55	120.15
C1–Si1–C7	109.76(3)	110.40	C14–C13–C18	118.01(2)	117.78	C11–C10–H10	118.65	120.12
C1–Si1–C13	109.71(3)	110.30	C13–C14–C15	121.00(2)	121.21	C10–C11–H11	119.98	120.09
C7–Si1–C13	110.42(3)	110.30	C14–C15–C16	120.01(2)	120.04	C12–C11–H11	119.94	119.90
Si1–O1–Si1a	180.00	180.00	C15–C16–C17	119.91(2)	119.71	C7–C12–H12	120.64	119.90
Si1–C1–C2	122.43(3)	121.84	C16–C17–C18	119.82(2)	120.02	C11–C12–H12	118.21	118.89
Si1–C1–C6	119.56(3)	120.35	C13–C18–C17	121.26(2)	121.25	C13–C14–H14	120.77	119.90
C2–C1–C6	117.96(2)	117.80	C1–C2–H2	117.66	119.70	C15–C14–H14	118.23	118.89
C1–C2–C3	121.13(2)	121.23	C3–C2–H2	121.21	119.01	C14–C15–H15	118.18	119.89
C2–C3–C4	119.90(2)	120.02	C2–C3–H3	120.79	119.89	C16–C15–H15	121.81	120.08
C3–C4–C5	120.04(2)	119.72	C4–C3–H3	119.26	120.09	C15–C16–H16	121.34	120.21
C4–C5–C6	119.76(2)	120.03	C3–C4–H4	120.22	120.15	C17–C16–H16	118.74	120.17
C1–C6–C5	121.20(2)	121.20	C5–C4–H4	119.72	120.13	C16–C17–H17	119.58	120.08
Si1–C7–C8	122.07(2)	121.89	C4–C5–H5	122.39	120.07	C18–C17–H17	120.59	119.90
Si1–C7–C12	119.87(2)	120.31	C6–C5–H5	117.85	119.89	C13–C18–H18	118.73	119.74
C8–C7–C12	118.05(2)	117.80	C1–C6–H6	119.34	119.89	C17–C18–H18	120.01	119.02
C7–C8–C9	121.11(2)	121.21						

Table A.44: Torsion angles (°) in hexaphe (**4**)

Exp = experimental geom., theo = optimised geometry from isolated-molecule calculation

angle	exp	theo	angle	exp	theo	angle	exp	theo
O1–Si1–C1–C2	134.82(2)	139.81	Si1–C7–C8–C9	179.10(3)	179.14	Si1–C7–C8–H8	-5.43	
O1–Si1–C1–C6	-47.55(2)	-41.33	Si1–C7–C12–C11	-178.35(3)	-179.31	Si1–C7–C12–H12	-1.12	
O1–Si1–C7–C8	121.48(2)	137.80	C12–C7–C8–C9	0.16(2)	-0.12	C12–C7–C8–H8	175.63	
O1–Si1–C7–C12	-59.60(2)	-42.96	C8–C7–C12–C11	0.61(2)	-0.04	C8–C7–C12–H12	177.84	
O1–Si1–C13–C14	-36.10(2)	-41.99	C7–C8–C9–C10	-0.48(2)	0.18	C7–C8–C9–H9	178.10	
O1–Si1–C13–C18	144.63(2)	139.16	C8–C9–C10–C11	0.03(2)	-0.06	H8–C8–C9–C10	-175.97	
O1–Si1–C1–C2	134.82(2)	139.81	C9–C10–C11–C12	0.73(2)	-0.10	H8–C8–C9–H9	2.60	
O1–Si1–C1–C6	-47.55(2)	-41.33	C10–C11–C12–C7	-1.06(2)	0.15	C8–C9–C10–H10	178.41	
O1–Si1–C7–C8	121.48(2)	137.80	Si1–C13–C14–C15	-179.54(3)	-178.92	H9–C9–C10–C11	-178.56	
O1–Si1–C7–C12	-59.60(2)	-42.96	Si1–C13–C18–C17	179.70(3)	178.73	H9–C9–C10–H10	-0.18	
O1–Si1–C13–C14	-36.10(2)	-41.99	C18–C13–C14–C15	-0.26(2)	-0.02	C9–C10–C11–H11	-178.27	
O1–Si1–C13–C18	144.63(2)	139.16	C14–C13–C18–C17	0.41(2)	-0.15	H10–C10–C11–C12	-177.69	
C7–Si1–C1–C2	14.98(2)	20.90	C13–C14–C15–C16	-0.03(2)	0.17	H10–C10–C11–H11	3.30	
C7–Si1–C1–C6	-167.40(2)	-160.25	C14–C15–C16–C17	0.17(2)	-0.15	C10–C11–C12–H12	-178.36	
C1–Si1–C7–C8	-119.29(2)	-103.29	C15–C16–C17–C18	-0.03(2)	-0.02	H11–C11–C12–C7	177.94	
C1–Si1–C7–C12	59.62(2)	75.96	C16–C17–C18–C13	-0.27(2)	0.18	H11–C11–C12–H12	0.64	
C13–Si1–C1–C2	-106.52(2)	-101.25	Si1–C1–C2–H2	-1.05		Si1–C13–C14–H14	0.45	
C13–Si1–C1–C6	71.11(2)	77.61	Si1–C1–C6–H6	3.48		Si1–C13–C18–H18	0.16	
C1–Si1–C13–C14	-154.72(2)	-160.90	C6–C1–C2–H2	-178.71		C18–C13–C14–H14	179.74	
C1–Si1–C13–C18	26.01(2)	20.25	C2–C1–C6–H6	-178.79		C14–C13–C18–H18	-179.14	
C13–Si1–C7–C8	1.77(2)	18.87	C1–C2–C3–H3	176.55		C13–C14–C15–H15	-179.30	
C13–Si1–C7–C12	-179.31(2)	-161.89	H2–C2–C3–C4	178.17		H14–C14–C15–C16	179.98	
C7–Si1–C13–C14	84.18(2)	76.89	H2–C2–C3–H3	-4.41		H14–C14–C15–H15	0.70	
C7–Si1–C13–C18	-95.09(2)	-101.96	C2–C3–C4–H4	-177.67		C14–C15–C16–H16	178.53	
Si1–C1–C2–C3	178.02(3)	178.74	H3–C3–C4–C5	-176.89		H15–C15–C16–C17	179.43	
Si1–C1–C6–C5	-177.29(3)	-178.98	H3–C3–C4–H4	4.87		H15–C15–C16–H16	-2.22	
C6–C1–C2–C3	0.36(2)	-0.14	C3–C4–C5–H5	179.19		C15–C16–C17–H17	178.54	
C2–C1–C6–C5	0.44(2)	-0.08	H4–C4–C5–C6	178.47		H16–C16–C17–C18	-178.43	
C1–C2–C3–C4	-0.86(2)	0.24	H4–C4–C5–H5	-2.56		H16–C16–C17–H17	0.14	
C2–C3–C4–C5	0.57(2)	-0.11	C4–C5–C6–H6	178.49		C16–C17–C18–H18	179.27	
C3–C4–C5–C6	0.22(2)	-0.11	H5–C5–C6–C1	-179.75		H17–C17–C18–C13	-178.83	
C4–C5–C6–C1	-0.73(2)	-0.08	H5–C5–C6–H6	-0.52		H17–C17–C18–H18	0.71	

Results of the Topological Analyses of the ED of Compounds 1 to 4

Table A.45: Electron density (ϱ) at bcps in eÅ^{-3}, Laplacian ($\nabla^2\varrho$) at bcps in eÅ^{-5}, distances of the bcps to first (d1) and second (d2) atom of the bond X1–X2 in Å, and ellipticity at bcps (ε) for siloxanol (**1**)

First row: experiment, second row: periodic-boundary calculation at experimental geometry, third/fourth row: isolated-molecule calculations at experimental/optimised geometries, values not given for C–H bonds

bond	ϱ	$\nabla^2\varrho$	d1	d2	ε	bond	ϱ	$\nabla^2\varrho$	d1	d2	ε
Si1–O1	0.86(1)	16.7(1)	0.7073	0.9726	0.04	C5–H5	1.94(9)	-19.2(2)	0.5062	0.5769	0.15
	0.76	20.0	0.6880	0.9909	0.03		1.93	-20.5	0.6924	0.3906	0.02
	0.86	18.4	0.6833	0.9958	0.03						
	0.87	18.5	0.6828	0.9946	0.03						
Si1–C1	0.78(1)	2.3(1)	0.7947	1.1015	0.03	C7–H7A	1.57(7)	-9.2(3)	0.7499	0.3110	0.18
	0.74	6.7	0.7314	1.1644	0.11		1.95	-21.5	0.6664	0.3924	0.02
	0.81	4.2	0.7285	1.1678	0.07						
	0.78	3.4	0.7351	1.1855	0.07						
Si1–C9	0.82(1)	8.0(1)	0.7298	1.1131	0.05	C7–H7B	1.58(7)	-9.2(3)	0.7501	0.3111	0.18
	0.80	8.8	0.7168	1.1259	0.07		1.95	-21.5	0.6663	0.3930	0.02
	0.87	5.3	0.7161	1.1267	0.02						
	0.83	4.0	0.7255	1.1511	0.03						
Si1–C10	0.81(1)	7.8(1)	0.7310	1.1171	0.05	C7–H7C	1.58(7)	-9.2(3)	0.7495	0.3116	0.18
	0.80	8.7	0.7177	1.1300	0.07		1.96	-21.6	0.6659	0.3931	0.03
	0.86	5.0	0.7181	1.1298	0.03						
	0.82	3.8	0.7282	1.1570	0.03						
Si2–O1	0.90(1)	18.3(1)	0.7003	0.9577	0.04	C8–H8A	1.58(7)	-9.3(3)	0.7498	0.3113	0.18
	0.79	21.5	0.6833	0.9742	0.03		1.96	-21.7	0.6662	0.3929	0.03
	0.91	20.1	0.6768	0.9807	0.03						
	0.89	19.6	0.6786	0.9849	0.03						
Si2–C2	0.82(1)	2.9(1)	0.7816	1.0887	0.03	C8–H8B	1.57(7)	-9.2(3)	0.7498	0.3115	0.18
	0.77	7.6	0.7255	1.1450	0.09		1.95	-21.5	0.6661	0.3930	0.02
	0.83	5.2	0.7209	1.1500	0.07						
	0.81	4.4	0.7264	1.1642	0.07						
Si2–C7	0.81(1)	7.7(1)	0.7319	1.1183	0.06	C8–H8C	1.57(7)	-9.2(3)	0.7501	0.3110	0.18
	0.79	8.6	0.7182	1.1318	0.08		1.95	-21.5	0.6666	0.3925	0.02
	0.86	4.9	0.7194	1.1305	0.03						
	0.82	3.8	0.7278	1.1517	0.03						
Si2–C8	0.82(1)	7.9(1)	0.7304	1.1121	0.06	C9–H9A	1.57(7)	-9.2(3)	0.7500	0.3112	0.18
	0.80	8.8	0.7169	1.1257	0.09		1.95	-21.5	0.6666	0.3924	0.02
	0.87	5.2	0.7169	1.1257	0.03						
	0.83	4.0	0.7266	1.1252	0.03						
Si3–O2	0.97(1)	19.6(1)	0.6896	0.9645	0.13	C9–H9B	1.58(7)	-9.3(3)	0.7500	0.3110	0.18
	0.87	21.0	0.6812	0.9699	0.01		1.96	-21.6	0.6663	0.3926	0.03
	0.93	20.9	0.6737	0.9772	0.07						
	0.87	18.8	0.6811	0.9945	0.07						
Si3–C6	0.74(1)	4.4(1)	0.7698	1.1122	0.06	C9–H9C	1.58(7)	-9.3(3)	0.7497	0.3112	0.18
	0.72	8.1	0.7262	1.1559	0.10		1.95	-21.5	0.6659	0.3932	0.02
	0.82	4.7	0.7240	1.1579	0.08						
	0.81	4.1	0.7278	1.1658	0.08						

Table A.46: Continuation of Table A.45

bond	ϱ	$\nabla^2\varrho$	d1	d2	ε	bond	ϱ	$\nabla^2\varrho$	d1	d2	ε
Si3–C11	0.77(1)	6.8(1)	0.7471	1.1109	0.09	C10–H10A	1.58(7)	-9.2(3)	0.7497	0.3114	0.18
	0.75	8.8	0.7204	1.1378	0.08		1.95	-21.5	0.6658	0.3932	0.02
	0.85	4.6	0.7217	1.1363	0.02						
	0.82	3.6	0.7297	1.1553	0.02						
Si3–C12	0.86(1)	6.3(1)	0.7379	1.1159	0.05	C10–H10B	1.58(7)	-9.3(3)	0.7497	0.3113	0.18
	0.80	8.0	0.7218	1.1313	0.01		1.96	-21.5	0.6662	0.3928	0.03
	0.86	4.8	0.7191	1.1337	0.04						
	0.83	4.1	0.7252	1.1505	0.04						
C1–C2	2.11(4)	-20.3(1)	0.6748	0.7376	0.16	C10–H10C	1.57(7)	-9.3(3)	0.7501	0.3108	0.18
	1.97	-15.0	0.7051	0.7072	0.13		1.95	-21.5	0.6664	0.3924	0.02
	2.06	-22.3	0.7047	0.7077	0.12						
	2.04	-21.9	0.7073	0.7099	0.12						
C1–C6	2.11(3)	-20.4(1)	0.7390	0.6751	0.15	C11–H11A	1.57(7)	-9.2(3)	0.7484	0.3120	0.19
	1.96	-15.0	0.7086	0.7055	0.13		1.96	-21.6	0.6661	0.3925	0.02
	2.05	-22.5	0.7069	0.7071	0.12						
	2.05	-22.3	0.7067	0.7089	0.12						
C2–C3	2.18(4)	-21.7(1)	0.6445	0.7524	0.15	C11–H11B	1.57(7)	-9.2(3)	0.7492	0.3124	0.19
	2.06	-16.9	0.6869	0.7100	0.14		1.95	-21.5	0.6667	0.3924	0.02
	2.14	-24.8	0.6835	0.7133	0.15						
	2.15	-24.9	0.6843	0.7118	0.15						
C3–C4	2.17(5)	-18.8(1)	0.6595	0.7300	0.24	C11–H11C	1.56(7)	-9.2(3)	0.7491	0.3125	0.18
	2.12	-18.1	0.6942	0.6953	0.20		1.94	-21.5	0.6664	0.3931	0.02
	2.19	-25.9	0.6907	0.6988	0.20						
	2.20	-26.4	0.6906	0.6953	0.19						
C4–C5	2.15(3)	-18.2(1)	0.6626	0.7344	0.24	C12–H12A	1.57(7)	-9.2(3)	0.7494	0.3117	0.18
	2.10	-17.5	0.6980	0.6989	0.20		1.95	-21.5	0.6662	0.3929	0.02
	2.16	-25.3	0.6987	0.6982	0.19						
	2.19	-26.1	0.6958	0.6937	0.19						
C5–C6	2.13(4)	-18.8(1)	0.6833	0.7174	0.23	C12–H12B	1.58(7)	-9.2(3)	0.7494	0.3117	0.18
	2.05	-16.6	0.7103	0.6902	0.18		1.95	-21.5	0.6658	0.3930	0.02
	2.13	-24.2	0.7151	0.6856	0.16						
	2.12	-24.1	0.7162	0.6856	0.16						
C3–H3	1.94(9)	-19.2(2)	0.5062	0.5770	0.16	C12–H12C	1.56(7)	-9.1(3)	0.7490	0.3121	0.18
	1.93	-20.6	0.6920	0.3911	0.02		1.94	-21.5	0.6658	0.3933	0.02
C4–H4	1.94(9)	-19.1(2)	0.5049	0.5782	0.16	O2–H2O	1.82(13)	-31.7(6)	0.8097	0.1578	0.05
	1.93	-20.6	0.6917	0.3914	0.02		2.42	-48.7	0.7472	0.2202	0.00
							2.44	-60.8	0.7707	0.1966	0.00
							2.49	-63.4	0.7684	0.1909	0.00
silox	0.19	2.7				phenyl	0.17	3.3			
ring	0.17	3.3				ring	0.22	3.0			
	0.20	3.1					0.17	3.5			
	0.19	3.0					0.17	3.6			

Table A.47: Electron density (ϱ) at bcps in eÅ^{-3}, Laplacian ($\nabla^2\varrho$) at bcps in eÅ^{-5}, distances of bcps to first (d1) and second (d2) atom of the bond X1–X2 in Å, and ellipticity at bcps (ε) for trisilo (**2**)

First row: experiment, second row: periodic-boundary calculation at experimental geometry, third/fourth row: isolated-molecule calculations at experimental/optimised geometries, values not given for C–H bonds

bond	ϱ	$\nabla^2\varrho$	d1	d2	ε	bond	ϱ	$\nabla^2\varrho$	d1	d2	ε
Si1–O1	0.94(1)	16.0(1)	0.7040	0.9533	0.00	C4–H4A	1.75(2)	-14.7(2)	0.7192	0.3402	0.03
	0.82	20.6	0.6842	0.9740	0.03		1.94	-21.0	0.6611	0.3979	0.02
	0.90	20.1	0.6771	0.9804	0.03						
	0.88	18.9	0.6813	0.9911	0.03						
Si1–C1	0.77(1)	2.8(1)	0.7783	1.1029	0.04	C4–H4B	1.77(2)	-14.7(1)	0.7190	0.3404	0.03
	0.75	7.6	0.7281	1.1529	0.04		1.95	-21.0	0.6608	0.3983	0.03
	0.82	4.9	0.7236	1.1582	0.07						
	0.81	4.3	0.7275	1.1674	0.07						
Si1–C4	0.81(1)	4.5(1)	0.7556	1.1009	0.03	C4–H4C	1.76(2)	-14.7(1)	0.7190	0.3404	0.03
	0.78	8.2	0.7199	1.1366	0.07		1.95	-21.0	0.6608	0.3982	0.03
	0.85	4.8	0.7202	1.1358	0.03						
	0.83	4.1	0.7260	1.1519	0.03						
Si1–C5	0.81(1)	4.5(1)	0.7555	1.1005	0.03	C5–H5A	1.76(2)	-14.7(1)	0.7190	0.3404	0.03
	0.78	8.2	0.7198	1.1362	0.06		1.95	-21.0	0.6607	0.3982	0.03
	0.85	4.7	0.7203	1.1362	0.03						
	0.83	4.1	0.7260	1.1523	0.03						
Si2–O1	0.95(1)	16.4(1)	0.7016	0.9557	0.03	C5–H5B	1.77(2)	-14.8(1)	0.7189	0.3404	0.03
	0.82	20.7	0.6839	0.9745	0.03		1.95	-21.0	0.6608	0.3983	0.03
	0.90	20.1	0.6771	0.9903	0.03						
	0.87	18.9	0.6813	0.9911	0.03						
Si2–C2	0.77(1)	2.8(1)	0.7781	1.1025	0.04	C5–H5C	1.75(2)	-14.7(1)	0.7192	0.3402	0.03
	0.75	7.6	0.7279	1.1523	0.04		1.94	-21.0	0.6611	0.3979	0.02
	0.82	4.8	0.7238	1.1574	0.07						
	0.81	4.3	0.7275	1.1671	0.07						
Si2–C6	0.81(1)	4.4(1)	0.7563	1.1024	0.03	C6–H6A	1.75(2)	-14.7(1)	0.7192	0.3400	0.03
	0.78	8.2	0.7203	1.1384	0.07		1.94	-21.0	0.6612	0.3978	0.02
	0.85	4.8	0.7202	1.1385	0.03						
	0.83	4.0	0.7262	1.1521	0.03						
Si2–C7	0.81(1)	4.5(1)	0.7555	1.1004	0.03	C6–H6B	1.77(2)	-14.8(1)	0.7189	0.3403	0.03
	0.78	8.2	0.7198	1.1362	0.06		1.95	-21.0	0.6608	0.3983	0.03
	0.85	4.7	0.7210	1.1378	0.03						
	0.83	4.0	0.7263	1.1521	0.03						
C1–C2	2.05(1)	-17.7(1)	0.7099	0.7090	0.18	C6–H6C	1.76(2)	-14.8(1)	0.7189	0.3404	0.03
	1.98	-14.9	0.7094	0.7096	0.16		1.95	-21.0	0.6608	0.3983	0.03
	2.04	-21.8	0.7092	0.7098	0.11						
	2.06	-22.3	0.7072	0.7073	0.11						
C1–C3a	2.19(3)	-19.4(1)	0.6951	0.7059	0.05	C7–H7A	1.75(2)	-14.6(1)	0.7188	0.3407	0.03
	2.05	-15.9	0.6935	0.7075	0.19		1.94	-21.0	0.6607	0.3984	0.03
	2.12	-24.2	0.6913	0.7097	0.16						
	2.14	-24.8	0.6900	0.7063	0.16						
C2–C3	2.15(2)	-17.8(1)	0.7027	0.6982	0.12	C7–H7B	1.77(2)	-14.7(1)	0.7190	0.3405	0.03
	2.04	-15.8	0.6931	0.7079	0.19		1.95	-21.0	0.6608	0.3982	0.03
	2.12	-24.3	0.6922	0.7087	0.16						
	2.14	-24.8	0.6900	0.7063	0.16						
C3–H3	1.83(5)	-18.2(2)	0.7153	0.3679	0.05	C7–H7C	1.75(2)	-14.6(1)	0.7193	0.3403	0.03
	1.90	-20.1	0.6839	0.3991	0.04		1.94	-21.0	0.6612	0.3978	0.02
silox	0.12	3.4				phenyl	0.22	3.1			
ring	0.21	3.4				ring	0.21	3.0			
	0.20	3.1					0.17	3.5			
	0.19	3.0					0.17	3.6			

Table A.48: Electron density (ϱ) at bcps in eÅ^{-3}, Laplacian ($\nabla^2\varrho$) at bcps in eÅ^{-5}, distances of bcps to first (d1) and second (d2) atom of the bond X1–X2 in Å, and ellipticity at bcps (ε) for pentaphe (**3**)

First row: experiment, second row: periodic-boundary calculation at experimental geometry, third/fourth row: isolated-molecule calculations at experimental/optimised geometries, values not given for C–H bonds

bond	ϱ	$\nabla^2\varrho$	d1	d2	ε	bond	ϱ	$\nabla^2\varrho$	d1	d2	ε
Si1–O1	0.92(1)	20.9(1)	0.6838	0.9368	0.02	C25–C30	2.09(1)	-17.4(1)	0.6911	0.7156	0.15
	0.84	24.3	0.6751	0.9442	0.03		2.01	-15.5	0.6927	0.7141	0.19
	0.94	23.4	0.6687	0.9505	0.00		2.09	-23.5	0.6925	0.7142	0.15
	0.89	20.5	0.6776	0.9703	0.01		2.12	-24.2	0.6915	0.7099	0.15
Si1–C1	0.74(1)	5.6(1)	0.7503	1.1128	0.03	C26–C27	2.18(1)	-19.7(1)	0.6972	0.6974	0.16
	0.76	8.1	0.7262	1.1369	0.05		2.08	-17.1	0.6975	0.6971	0.21
	0.85	5.2	0.7190	1.1440	0.09		2.17	-25.5	0.6952	0.6994	0.19
	0.83	4.4	0.7240	1.1543	0.10		2.18	-25.9	0.6938	0.6967	0.19
Si1–C7	0.72(1)	7.6(1)	0.7322	1.1315	0.02	C27–C28	2.19(1)	-19.9(1)	0.6957	0.6958	0.16
	0.75	8.4	0.7244	1.1378	0.04		2.09	-17.4	0.6958	0.6958	0.21
	0.85	5.1	0.7191	1.1423	0.02		2.18	-25.8	0.6941	0.6974	0.19
	0.83	4.6	0.7239	1.1567	0.02		2.19	-26.0	0.6928	0.6971	0.19
Si2–O1	0.87(1)	23.3(1)	0.6778	0.9486	0.01	C28–C29	2.17(1)	-19.5(1)	0.6984	0.6984	0.16
	0.81	24.7	0.6749	0.9509	0.01		2.07	-17.0	0.6984	0.6984	0.21
	0.93	22.4	0.6717	0.9541	0.00		2.15	-25.2	0.7005	0.6963	0.19
	0.88	20.4	0.6782	0.9742	0.01		2.18	-25.9	0.6972	0.6931	0.19
Si2–C13	0.74(1)	7.2(1)	0.7337	1.1293	0.06	C29–C30	2.18(1)	-19.7(1)	0.6972	0.6969	0.16
	0.74	8.9	0.7215	1.1407	0.05		2.08	-17.2	0.6968	0.6972	0.21
	0.85	5.3	0.7184	1.1438	0.08		2.17	-25.4	0.6996	0.6945	0.20
	0.82	4.3	0.7263	1.1613	0.04		2.18	-25.9	0.6971	0.6931	0.20
Si2–C19	0.73(1)	8.2(1)	0.7255	1.1379	0.04	Si1–H1Si	0.73(2)	5.7(1)	0.7444	0.7421	0.05
	0.74	9.4	0.7192	1.1442	0.08		0.72	9.5	0.7191	0.7649	0.03
	0.85	5.1	0.7195	1.1438	0.08		0.82	4.5	0.7210	0.7630	0.03
	0.82	4.4	0.7248	1.1591	0.08		0.82	4.4	0.7222	0.7654	0.03
Si2–C25	0.76(1)	6.5(1)	0.7373	1.1268	0.10	C2–H2	1.86(2)	-19.5(1)	0.6947	0.3884	0.04
	0.73	9.3	0.7200	1.1437	0.06		1.92	-21.0	0.6906	0.3924	0.02
	0.84	5.2	0.7194	1.1441	0.07						
	0.82	4.3	0.7252	1.1596	0.08						
C1–C2	2.09(1)	-18.5(1)	0.6891	0.7164	0.18	C3–H3	1.865(2)	-19.4(1)	0.694	0.3882	0.04
	2.01	-15.6	0.6930	0.7124	0.18		1.915	-21.0	0.690	0.3927	0.02
	2.10	-23.8	0.6953	0.7102	0.15						
	2.13	-24.4	0.6921	0.7074	0.16						
C1–C6	2.10(1)	-18.8(1)	0.6872	0.7146	0.18	C4–H4	1.86(2)	-19.4(1)	0.6948	0.3883	0.04
	2.03	-15.9	0.6913	0.7105	0.18		1.92	-21.0	0.6904	0.3928	0.02
	2.12	-24.1	0.6901	0.7117	0.16						
	2.13	-24.3	0.6914	0.7090	0.15						
C2–C3	2.19(1)	-20.8(1)	0.6978	0.6984	0.19	C5–H5	1.86(2)	-19.4(1)	0.6948	0.3883	0.04
	2.07	-17.2	0.6981	0.6980	0.20		1.92	-21.0	0.6904	0.3928	0.02
	2.16	-25.2	0.6959	0.7002	0.20						
	2.18	-25.8	0.6938	0.6972	0.19						
C3–C4	2.20(1)	-21.1(1)	0.6964	0.6964	0.19	C6–H6	1.86(2)	-19.4(1)	0.6948	0.3883	0.04
	2.08	-17.5	0.6964	0.6964	0.20		1.91	-21.0	0.6908	0.3924	0.02
	2.17	-25.7	0.6942	0.6986	0.19						
	2.19	-26.0	0.6928	0.6969	0.19						
C4–C5	2.20(1)	-21.0(1)	0.6969	0.6970	0.19	C8–H8	1.86(2)	-19.4(1)	0.6947	0.3884	0.04
	2.08	-17.4	0.6969	0.6970	0.20		1.91	-21.0	0.6907	0.3924	0.02
	2.17	-25.7	0.6985	0.6953	0.18						
	2.18	-25.9	0.6969	0.6940	0.19						
C5–C6	2.20(1)	-21.0(1)	0.6973	0.6970	0.19	C9–H9	1.86(2)	-19.4(1)	0.6948	0.3883	0.04
	2.08	-17.4	0.6970	0.6973	0.20		1.91	-20.9	0.6903	0.3928	0.02
	2.17	-25.4	0.6982	0.6962	0.20						
	2.19	-25.9	0.6955	0.6939	0.20						
C7–C8	2.11(1)	-18.7(1)	0.6899	0.7135	0.18	C10–H10	1.86(2)	-19.4(1)	0.6948	0.3883	0.04
	2.02	-16.0	0.6924	0.7110	0.19		1.91	-20.9	0.6903	0.3928	0.02
	2.11	-24.1	0.6906	0.7128	0.14						
	2.12	-24.4	0.6912	0.7093	0.14						
C7–C12	2.10(1)	-18.6(1)	0.6904	0.7141	0.18	C11–H11	1.86(2)	-19.4(1)	0.6948	0.3883	0.04
	2.01	-15.7	0.6929	0.7117	0.19		1.91	-20.9	0.6903	0.3928	0.02
	2.10	-23.8	0.6928	0.7117	0.16						
	2.12	-24.2	0.6906	0.7102	0.16						
C8–C9	2.19(1)	-20.8(1)	0.6980	0.6980	0.19	C12–H12	1.86(2)	-19.4(1)	0.6949	0.3883	0.04
	2.07	-17.2	0.6983	0.6977	0.20		1.91	-21.0	0.6906	0.3925	0.02
	2.16	-25.1	0.6936	0.7024	0.20						
	2.18	-26.1	0.6937	0.6964	0.18						
C9–C10	2.20(1)	-21.0(1)	0.6975	0.6969	0.19	C14–H14	1.87(2)	-19.7(1)	0.6998	0.3834	0.04
	2.08	-17.4	0.6975	0.6970	0.20		1.91	-20.9	0.6905	0.3927	0.02
	2.17	-25.5	0.6919	0.7026	0.19						
	2.18	-25.9	0.6930	0.6975	0.19						
C10–C11	2.19(1)	-20.9(1)	0.6978	0.6976	0.19	C15–H15	1.87(2)	-19.7(1)	0.6996	0.3836	0.04
	2.08	-17.3	0.6978	0.6976	0.20		1.91	-20.9	0.6902	0.3928	0.02
	2.16	-25.6	0.6970	0.6984	0.18						
	2.18	-26.1	0.6975	0.6928	0.18						

Table A.49: Continuation of Table A.48

bond	ϱ	$\nabla^2\varrho$	d1	d2	ε	bond	ϱ	$\nabla^2\varrho$	d1	d2	ε
C11–C12	2.19(1)	-20.9(1)	0.6979	0.6974	0.19	C16–H16	1.87(2)	-19.7(1)	0.6995	0.3836	0.04
	2.08	-17.3	0.6978	0.6975	0.20		1.91	-20.8	0.6902	0.3929	0.02
	2.16	-25.2	0.6966	0.6987	0.20						
	2.18	-26.1	0.6961	0.6937	0.18						
C13–C14	2.11(1)	-17.7(1)	0.6898	0.7139	0.15	C17–H17	1.87(2)	-19.7(1)	0.6995	0.3836	0.04
	2.02	-15.7	0.6910	0.7127	0.19		1.91	-20.9	0.6902	0.3929	0.02
	2.11	-24.1	0.6936	0.7101	0.15						
	2.12	-24.0	0.6904	0.7121	0.15						
C13–C18	2.11(1)	-17.8(1)	0.6889	0.7127	0.15	C18–H18	1.87(2)	-19.7(1)	0.6997	0.3834	0.04
	2.03	-15.9	0.6902	0.7113	0.19		1.91	-20.9	0.6906	0.3925	0.02
	2.12	-24.1	0.6900	0.7116	0.15						
	2.13	-24.4	0.6910	0.7086	0.16						
C14–C15	2.19(1)	-19.8(1)	0.6967	0.6970	0.16	C20–H20	1.87(2)	-19.8(1)	0.7001	0.3830	0.04
	2.08	-17.2	0.6968	0.6969	0.21		1.91	-20.9	0.6907	0.3924	0.02
	2.17	-25.3	0.6960	0.6977	0.20						
	2.19	-25.9	0.6932	0.6960	0.20						
C15–C16	2.18(1)	-19.7(1)	0.6974	0.6973	0.16	C21–H21	1.87(2)	-19.7(1)	0.6995	0.3836	0.04
	2.08	-17.1	0.6974	0.6973	0.21		1.91	-20.8	0.6902	0.3930	0.02
	2.16	-25.4	0.6951	0.6996	0.19						
	2.18	-25.9	0.6936	0.6976	0.19						
C16–C17	2.19(1)	-19.8(1)	0.6964	0.6961	0.16	C22–H22	1.87(2)	-19.7(1)	0.6995	0.3837	0.04
	2.08	-17.3	0.6964	0.6961	0.21		1.91	-20.8	0.6902	0.3930	0.02
	2.18	-25.9	0.6966	0.6959	0.19						
	2.19	-26.0	0.6974	0.6918	0.19						
C17–C18	2.18(1)	-19.6(1)	0.6977	0.6974	0.16	C23–H23	1.87(2)	-19.7(1)	0.6995	0.3837	0.04
	2.08	-17.1	0.6974	0.6977	0.21		1.91	-20.8	0.6902	0.3930	0.02
	2.16	-25.3	0.6986	0.6964	0.19						
	2.18	-25.8	0.6975	0.6937	0.19						
C19–C20	2.11(1)	-17.6(1)	0.6909	0.7141	0.15	C24–H24	1.87(2)	-19.7(1)	0.6994	0.3838	0.04
	2.02	-15.6	0.6921	0.7129	0.19		1.91	-20.9	0.6903	0.3928	0.02
	2.11	-23.8	0.6924	0.7126	0.15						
	2.12	-24.2	0.6906	0.7102	0.16						
C19–C24	2.09(1)	-17.6(1)	0.6894	0.7142	0.15	C26–H26	1.87(2)	-19.7(1)	0.6997	0.3833	0.05
	2.01	-15.7	0.6909	0.7128	0.19		1.91	-20.9	0.6906	0.3924	0.02
	2.11	-23.9	0.6935	0.7102	0.15						
	2.12	-24.2	0.6915	0.7089	0.15						
C20–C21	2.19(1)	-19.8(1)	0.6964	0.6964	0.16	C27–H27	1.87(2)	-19.7(1)	0.6995	0.3835	0.04
	2.08	-17.3	0.6965	0.6963	0.21		1.91	-20.9	0.6902	0.3928	0.02
	2.17	-25.6	0.6962	0.6966	0.19						
	2.18	-25.9	0.6942	0.6962	0.20						
C21–C22	2.18(1)	-19.7(1)	0.6972	0.6973	0.16	C28–H28	1.87(2)	-19.7(1)	0.6995	0.3836	0.04
	2.08	-17.1	0.6972	0.6973	0.21		1.91	-20.9	0.6902	0.3929	0.02
	2.16	-25.4	0.6970	0.6975	0.19						
	2.19	-25.9	0.6932	0.6968	0.19						
C22–C23	2.18(1)	-19.6(1)	0.6979	0.6978	0.16	C29–H29	1.87(2)	-19.7(1)	0.6994	0.3836	0.04
	2.07	-17.1	0.6978	0.6979	0.21		1.91	-20.9	0.6901	0.3929	0.02
	2.16	-25.2	0.7002	0.6954	0.19						
	2.18	-26.0	0.6976	0.6926	0.19						
C23–C24	2.17(1)	-19.5(1)	0.6988	0.6982	0.16	C30–H30	1.87(2)	-19.7(1)	0.6994	0.3837	0.04
	2.07	-17.0	0.6985	0.6984	0.21		1.91	-20.8	0.6904	0.3927	0.02
	2.15	-25.1	0.6991	0.6979	0.19						
	2.18	-26.0	0.6971	0.6930	0.20						
C25–C26	2.11(1)	-17.9(1)	0.6882	0.7129	0.16						
	2.02	-15.9	0.6899	0.7113	0.19						
	2.12	-24.1	0.6901	0.7111	0.16						
	2.13	-24.3	0.6911	0.7090	0.16						
phenyl C1	0.20	3.1				phenylC19	0.20	3.1			
	0.20	3.0					0.20	3.0			
	0.16	3.6					0.16	3.6			
	0.17	3.7					0.17	3.6			
phenyl C7	0.20	3.1				phenylC25	0.20	3.1			
	0.20	3.0					0.20	3.0			
	0.16	3.6					0.16	3.6			
	0.17	3.6					0.17	3.7			
phenylC13	0.20	3.1									
	0.20	3.0									
	0.16	3.6									
	0.17	3.6									

Table A.50: Electron density (ϱ) at bcps in eÅ^{-3}, Laplacian ($\nabla^2\varrho$) at bcps in eÅ^{-5}, distances of bcps to first (d1) and second (d2) atom of the bond X1–X2 in Å, and ellipticity at bcps (ε) for hexaphe (**4**)

First row: experiment, second row: periodic-boundary calculation at experimental geometry, third/fourth row: isolated-molecule calculations at experimental/optimised geometries, values not given for C–H bonds

bond	ϱ	$\nabla^2\varrho$	d1	d2	ε	bond	ϱ	$\nabla^2\varrho$	d1	d2	ε
Si1–O1	0.92(1)	22.4(1)	0.6788	0.9434	0.03	C15–C16	2.15(1)	-19.3(1)	0.6975	0.6976	0.16
	0.85	25.2	0.6723	0.9489	0.01		2.06	-16.7	0.6975	0.6976	0.21
	0.93	23.6	0.6689	0.9522	0.01		2.16	-25.3	0.6959	0.6993	0.19
	0.89	21.4	0.6757	0.9683	0.01		2.18	-25.9	0.6933	0.6977	0.19
Si1–C1	0.75(1)	5.8(1)	0.7438	1.1225	0.05	C16–C17	2.16(1)	-19.4(1)	0.6969	0.6969	0.16
	0.73	10.2	0.7158	1.1492	0.03		2.07	-16.8	0.6969	0.6969	0.21
	0.84	4.7	0.7218	1.1431	0.07		2.17	-25.6	0.6989	0.6949	0.19
	0.82	3.9	0.7278	1.1580	0.07		2.19	-26.1	0.6968	0.6925	0.19
Si1–C7	0.82(1)	5.5(1)	0.7359	1.1276	0.03	C17–C18	2.15(1)	-19.2(1)	0.6976	0.6983	0.16
	0.74	10.1	0.7154	1.1464	0.02		2.06	-16.6	0.6978	0.6982	0.21
	0.85	5.1	0.7192	1.1426	0.05		2.16	-25.2	0.6994	0.6965	0.19
	0.82	4.2	0.7261	1.1603	0.07		2.18	-25.8	0.6972	0.6940	0.19
Si1–C13	0.80(1)	4.6(1)	0.7500	1.1173	0.12	C2–H2	1.87(2)	-20.2(1)	0.7038	0.3790	0.03
	0.75	9.9	0.7157	1.1514	0.05		1.90	-20.8	0.6885	0.3942	0.03
	0.84	5.1	0.7198	1.1473	0.08						
	0.82	4.4	0.7253	1.1608	0.08						
C1–C2	2.12(1)	-18.4(1)	0.6956	0.7078	0.15	C3–H3	1.88(2)	-20.1(1)	0.7031	0.3799	0.03
	2.02	-15.5	0.6945	0.7089	0.18		1.91	-20.8	0.6881	0.3948	0.03
	2.11	-23.9	0.6926	0.7108	0.16						
	2.13	-24.3	0.6906	0.7092	0.16						
C1–C6	2.12(1)	-18.3(1)	0.6966	0.7087	0.15	C4–H4	1.88(2)	-20.1(1)	0.7037	0.3801	0.03
	2.02	-15.4	0.6956	0.7096	0.18		1.90	-20.7	0.6888	0.3951	0.03
	2.10	-23.8	0.6923	0.7129	0.15						
	2.12	-24.1	0.6914	0.7106	0.15						
C2–C3	2.15(1)	-19.3(1)	0.6977	0.6973	0.16	C5–H5	1.88(2)	-20.1(1)	0.7032	0.3799	0.03
	2.06	-16.7	0.6975	0.6974	0.21		1.90	-20.8	0.6882	0.3949	0.03
	2.16	-25.3	0.6963	0.6987	0.19						
	2.18	-25.8	0.6940	0.6972	0.19						
C3–C4	2.16(1)	-19.5(1)	0.6963	0.6961	0.16	C6–H6	1.88(2)	-20.1(1)	0.7035	0.3797	0.03
	2.07	-16.9	0.6963	0.6961	0.21		1.91	-20.8	0.6887	0.3945	0.03
	2.17	-25.7	0.6930	0.6995	0.20						
	2.19	-26.0	0.6926	0.6968	0.19						
C4–C5	2.15(1)	-19.3(1)	0.6975	0.6973	0.16	C8–H8	1.87(2)	-20.1(1)	0.7039	0.3791	0.03
	2.06	-16.7	0.6976	0.6973	0.21		1.90	-20.8	0.6887	0.3943	0.03
	2.16	-25.4	0.6981	0.6967	0.19						
	2.18	-25.9	0.6977	0.6933	0.19						
C5–C6	2.16(1)	-19.3(1)	0.6971	0.6973	0.16	C9–H9	1.88(2)	-20.1(1)	0.7032	0.3799	0.03
	2.07	-16.7	0.6972	0.6972	0.21		1.91	-20.8	0.6883	0.3948	0.03
	2.17	-25.4	0.6974	0.6970	0.19						
	2.19	-25.9	0.6965	0.6929	0.19						
C7–C8	2.14(1)	-18.5(1)	0.6959	0.7060	0.15	C10–H10	1.88(2)	-20.1(1)	0.7031	0.3798	0.03
	2.03	-15.6	0.6942	0.7077	0.18		1.91	-20.8	0.6881	0.3948	0.03
	2.12	-24.1	0.6916	0.7102	0.16						
	2.13	-24.4	0.6913	0.7084	0.16						

Table A.51: Continuation of Table A.50

bond	ϱ	$\nabla^2\varrho$	d1	d2	ε	bond	ϱ	$\nabla^2\varrho$	d1	d2	ε
C7–C12	2.12(1)	-18.3(1)	0.6963	0.7081	0.14	C11–H11	1.88(2)	-20.1(1)	0.7032	0.3798	0.03
	2.01	-15.4	0.6952	0.7093	0.18		1.91	-20.8	0.6882	0.3947	0.03
	2.11	-23.9	0.6907	0.7137	0.16						
	2.12	-24.2	0.6916	0.7106	0.16						
C8–C9	2.15(1)	-19.1(1)	0.6989	0.6981	0.16	C12–H12	1.88(2)	-20.1(1)	0.7035	0.3800	0.03
	2.06	-16.6	0.6987	0.6982	0.21		1.91	-20.8	0.6887	0.3948	0.03
	2.15	-25.1	0.6956	0.7013	0.19						
	2.18	-25.7	0.6941	0.6973	0.19						
C9–C10	2.16(1)	-19.5(1)	0.6965	0.6964	0.16	C14–H14	1.87(2)	-20.2(1)	0.7033	0.3795	0.03
	2.07	-16.9	0.6966	0.6964	0.21		1.90	-20.8	0.6885	0.3944	0.03
	2.17	-25.7	0.6928	0.7002	0.20						
	2.19	-26.2	0.6925	0.6968	0.20						
C10–C11	2.15(1)	-19.3(1)	0.6978	0.6977	0.16	C15–H15	1.88(2)	-20.1(1)	0.7033	0.3799	0.03
	2.06	-16.6	0.6978	0.6977	0.21		1.90	-20.8	0.6883	0.3949	0.03
	2.16	-25.4	0.6990	0.6965	0.19						
	2.18	-25.9	0.6976	0.6935	0.19						
C11–C12	2.17(1)	-19.7(1)	0.6950	0.6958	0.16	C16–H16	1.88(2)	-20.1(1)	0.7033	0.3799	0.03
	2.08	-17.0	0.6952	0.6956	0.21		1.90	-20.8	0.6883	0.3949	0.03
	2.18	-25.8	0.6977	0.6931	0.19						
	2.19	-25.9	0.6968	0.6926	0.19						
C13–C14	2.12(1)	-18.3(1)	0.6975	0.7080	0.15	C17–H17	1.88(2)	-20.1(1)	0.7032	0.3798	0.03
	2.02	-15.4	0.6969	0.7085	0.18		1.91	-20.8	0.6882	0.3948	0.03
	2.10	-23.7	0.6921	0.7133	0.15						
	2.12	-24.1	0.6915	0.7106	0.15						
C13–C18	2.13(1)	-18.5(1)	0.6968	0.7065	0.15	C18–H18	1.87(2)	-20.1(1)	0.7041	0.3792	0.03
	2.03	-15.5	0.6959	0.7073	0.18		1.90	-20.8	0.6890	0.3943	0.03
	2.11	-23.9	0.6920	0.7113	0.16						
	2.13	-24.4	0.6906	0.7091	0.16						
C14–C15	2.15(1)	-19.3(1)	0.6979	0.6975	0.15						
	2.06	-16.7	0.6978	0.6976	0.21						
	2.16	-25.3	0.6957	0.6997	0.19						
	2.19	-25.8	0.6927	0.6968	0.20						
phenyl	0.21	3.2				phenyl	0.21	3.2			
C1	0.20	3.0				C13	0.20	3.0			
	0.16	3.6					0.16	3.6			
	0.17	3.6					0.17	3.6			
phenyl	0.21	3.2									
C7	0.20	3.2									
	0.16	3.6									
	0.17	3.6									

Table A.52: Atomic charges ($Q = Q_{001} = Q_{tot}$) in e, and atomic volumes (V_{001} and V_{tot}) in Å^3 of siloxanol (**1**)

First row: experiment, second row: periodic-boundary calculation at experimental geometry, third/fourth row: isolated-molecule calculations at experimental/optimised geometries, values only given for chemically different C atoms

atom	Q	V_{001}	V_{tot}	atom	Q	V_{001}	V_{tot}	atom	Q	V_{001}	V_{tot}
Si1	2.49	5.7	5.8	C10	-1.33	16.8	17.7	H9A	0.23	5.8	7.4
	2.82	4.5	4.7		-0.63	11.9	13.5		0.01	7.0	8.9
	2.97	4.3									
	2.95	4.6									
Si2	2.50	5.8	5.8	C11	-1.19	16.9	17.9	H9B	0.20	5.2	5.9
	2.82	4.6	4.6		-0.59	12.3	13.2		-0.01	6.2	7.2
	2.99	4.2									
	2.97	4.5									
Si3	2.46	5.9	6.0	C12	-1.35	16.9	18.2	H9C	0.19	6.2	7.0
	2.78	4.8	5.1		-0.62	12.1	13.5		0.00	7.1	8.5
	2.99	4.2									
	2.97	4.5									
O1	-1.23	14.1	15.6	H3	-0.28	7.1	7.9	H11A	0.21	6.1	8.0
	-1.57	13.7	16.8		0.02	6.5	7.6		0.00	7.5	9.1
	-1.64	19.0									
	-1.63	19.3									
O2	-1.61	19.7	21.5	H4	-0.28	7.8	11.2	H11B	0.20	6.2	7.6
	-1.48	17.4	19.9		-0.01	8.4	10.3		0.00	7.2	8.9
	-1.39	19.5									
	-1.39	19.7									
C1	-0.49	12.3	12.6	H5	-0.27	7.2	8.2	H11C	0.22	6.1	6.9
	-0.62	12.0	13.0		0.03	7.1	8.0		0.04	6.3	7.9
	-0.70	14.1									
	-0.68	14.0									
C2	-0.41	12.4	12.8	H2O	0.70	1.7	1.7	H12A	0.21	5.5	6.1
	-0.62	12.2	13.3		0.59	1.8	1.9		0.02	6.1	7.3
	-0.69	13.7			0.59	3.4					
	-0.68	14.0			0.59	3.3					
C3	0.26	10.7	12.6	H7A	0.22	6.2	7.7	H12B	0.19	6.1	7.3
	-0.14	12.2	14.4		0.00	7.6	9.4		0.01	6.4	8.5
	0.01	12.2									
	0.01	12.1									
C4	0.35	10.7	12.6	H7B	0.21	6.5	8.0	H12C	0.21	6.4	8.8
	-0.14	12.8	15.6		0.00	7.6	9.5		0.01	7.0	10.3
	0.01	12.3									
C5	0.27	10.4	10.9	H7C	0.19	6.7	7.4	H10A	0.20	6.4	8.3
	-0.18	12.5	13.1		-0.02	7.2	8.3		0.00	7.7	10.2
	0.00	12.0									
C6	-0.35	11.4	12.1	H8A	0.19	6.7	7.4	H10B	0.20	5.7	7.1
	-0.58	12.1	13.4		-0.02	7.0	8.8		0.00	6.2	8.6
	-0.69	14.0									
	-0.70	14.2									
C7	-1.33	17.4	19.0	H8B	0.20	6.3	7.4	H10C	0.23	5.6	7.3
	-0.65	12.4	13.6		0.00	6.9	9.1		0.02	6.8	9.3
C8	-1.33	17.8	20.3	H8C	0.23	5.8	7.8	sum	0.00	355.6	401.7
	-0.63	12.1	13.9		0.01	6.8	9.4		0.01	339.8	401.6
C9	-1.33	17.3	18.2								
	-0.64	11.7	12.9								
	-0.67	13.6									
	-0.73	14.4									

Table A.53: Atomic charges (Q = Q_{001} = Q_{tot}) in e, and atomic volumes (V_{001} and V_{tot}) in Å^3 of trisilo (**2**)

First row: experiment, second row: periodic-boundary calculation at experimental geometry, third/fourth row: isolated-molecule calculations at experimental/optimised geometries, values only given for chemically different C atoms

atom	Q	V_{001}	V_{tot}	atom	Q	V_{001}	V_{tot}	atom	Q	V_{001}	V_{tot}
Si1	2.43	5.5	5.7	C6	-0.83	13.1	14.2	H5C	0.09	6.9	9.4
	2.75	4.7	4.8		-0.61	11.9	13.2		0.02	7.1	9.1
	2.98	4.3									
	2.96	4.6									
Si2	2.43	5.8	6.2	C7	-0.83	12.9	13.9	H6A	0.09	6.9	9.7
	2.74	5.2	5.5		-0.60	11.8	12.8		0.01	7.1	9.9
	2.98	4.3									
	2.96	4.5									
O1	-1.56	14.9	17.5	H3	0.16	6.0	9.1	H6B	0.05	7.0	9.1
	-1.73	15.5	18.0		0.02	7.2	10.2		-0.01	7.0	9.1
	-1.64	19.2									
	-1.64	19.5									
C1	-0.39	11.1	13.2	H4A	0.10	6.3	8.6	H6C	0.07	7.0	8.9
	-0.69	12.7	14.3		0.03	6.5	8.9		-0.01	7.4	9.1
	-0.69	13.9									
	-0.68	14.1									
C2	-0.39	11.3	12.8	H4B	0.05	7.5	10.0	H7A	0.07	7.4	8.6
	-0.69	12.8	14.1		-0.01	7.3	10.4		0.00	7.2	8.8
	-0.70	14.1									
	-0.68	14.1									
C3	-0.23	11.4	12.8	H4C	0.09	6.4	8.2	H7B	-0.08	6.6	8.1
	-0.03	11.1	12.4		0.01	6.2	8.0		0.00	6.7	8.1
	0.00	12.3									
	0.01	12.2									
C4	-0.82	13.2	14.9	H5A	0.08	6.5	8.1	H7C	0.08	6.8	7.8
	-0.60	12.0	13.3		0.01	6.4	8.3		0.01	7.0	8.1
	-0.70	14.6									
C5	-0.83	13.4	15.0	H5B	0.04	6.9	9.0	sum	-0.14	200.8	240.9
	-0.60	12.1	13.6		-0.02	7.1	9.7		-0.01	200.1	239.9
	-0.67	14.0									
	-0.71	14.6									

Table A.54: Atomic charges ($Q = Q_{001} = Q_{tot}$) in e, and atomic volumes (V_{001} and V_{tot}) in $Å^3$ of pentaphe (**3**)

First row: experiment, second row: periodic-boundary calculation at experimental geometry, third/fourth row: isolated-molecule calculations at experimental/optimised geometries, values given for chemically different C atoms

atom	Q	V_{001}	V_{tot}	atom	Q	V_{001}	V_{tot}	atom	Q	V_{001}	V_{tot}
Si1	2.52	6.3	6.3	C18	-0.07	11.1	11.2	H10	0.05	7.0	8.1
	2.82	4.9	5.1		-0.04	10.8	11.0		0.03	7.1	8.1
	2.98	4.5									
	2.96	4.8									
Si2	2.79	5.0	5.2	C19	-0.47	11.8	13.3	H11	0.04	7.6	8.3
	2.88	4.6	4.7		-0.63	13.0	14.0		0.02	7.6	8.6
	3.02	4.1									
	2.98	4.4									
O1	-1.59	15.8	18.3	C20	-0.10	11.4	11.6	H12	0.08	7.1	10.3
	-1.72	15.7	18.0		-0.05	11.1	11.2		0.05	7.4	9.7
	-1.71	18.4									
	-1.69	18.7									
C1	-0.39	11.9	12.1	C21	-0.08	11.8	12.4	H14	0.08	7.2	9.7
	-0.61	12.4	12.8		-0.04	11.9	12.7		0.02	7.5	9.5
	-0.74	13.7									
	-0.76	14.1									
C2	-0.15	13.4	14.1	C22	-0.08	13.0	13.7	H15	0.06	7.3	7.5
	-0.05	12.5	13.4		-0.04	12.8	13.6		0.01	7.2	7.5
	-0.04	12.3									
	-0.01	12.3									
C3	-0.14	12.7	13.0	C23	-0.08	12.4	12.8	H16	0.06	7.1	8.5
	-0.02	12.4	12.7		-0.03	12.2	12.6		0.02	7.4	8.7
	0.01	12.3									
C4	-0.15	13.1	13.6	C24	-0.06	12.0	12.8	H17	0.06	6.6	6.9
	-0.03	12.7	13.2		-0.03	11.8	12.4		0.02	6.6	7.1
	0.02	12.3									
C5	-0.15	12.4	12.4	C25	-0.46	12.4	12.9	H18	0.08	6.3	6.4
	-0.03	11.9	11.9		-0.60	12.5	13.1		0.04	6.7	6.8
	0.02	12.3									
C6	-0.14	12.1	12.3	C26	-0.06	11.9	12.2	H20	0.09	6.6	6.9
	-0.03	11.6	11.9		-0.05	12.0	12.3		0.04	6.8	7.1
	0.01	12.2									
C7	-0.47	11.1	11.7	C27	-0.08	12.8	13.1	H21	0.06	7.8	8.9
	-0.63	11.9	12.4		-0.03	12.7	13.1		0.02	8.0	9.3
C8	-0.13	11.7	12.2	C28	-0.07	12.1	12.2	H22	0.06	6.1	7.0
	-0.03	11.1	11.6		-0.03	12.1	12.3		0.02	6.3	6.9
C9	-0.15	12.8	12.9	C29	-0.08	12.2	12.4	H23	0.06	6.7	7.5
	-0.03	12.4	12.6		-0.03	12.2	12.4		0.02	6.7	7.4
C10	-0.16	13.5	14.6	C30	-0.06	11.8	12.5	H24	0.07	7.5	8.1
	-0.04	13.0	14.1		-0.05	11.7	12.5		0.04	7.4	8.3
C11	-0.15	13.1	14.0	H2	0.06	7.1	8.2	H26	0.10	6.3	6.4
	-0.03	12.6	13.6		0.04	7.0	8.4		0.05	6.4	6.4
C12	-0.12	12.5	13.8	H3	0.04	7.5	7.7	H27	0.06	6.9	7.0
	-0.02	11.9	13.3		0.02	7.7	7.9		0.01	7.0	7.1
C13	-0.41	10.8	11.5	H4	0.05	7.2	7.3	H28	0.06	6.7	6.7
	-0.60	11.6	12.1		0.02	7.2	7.5		0.02	6.7	6.8
C14	-0.08	11.5	12.6	H5	0.04	7.2	7.4	H29	0.06	7.1	7.1
	-0.04	11.5	12.4		0.02	7.3	7.5		0.02	7.1	7.3
C15	-0.07	12.0	12.4	H6	0.05	6.9	7.0	H30	0.08	7.7	9.1
	-0.03	11.9	12.5		0.04	6.7	6.9		0.02	8.1	9.5
C16	-0.07	11.9	12.8	H8	0.06	7.2	8.3	H1Si	-0.56	12.9	15.9
	-0.03	12.0	12.9		0.04	7.4	8.6		-0.76	14.2	17.2
									-0.68	14.0	
									-0.67	14.2	
C17	-0.08	12.1	12.3	H9	0.04	7.4	7.9	sum	-0.03	581.4	621.1
	-0.04	12.02	12.2		0.01	7.6	8.3		-0.04	580.3	620.8

Table A.55: Atomic charges (Q = Q_{001} = Q_{tot}) in e, and atomic volumes (V_{001} and V_{tot}) in Å^3 of hexaphe (**4**)

First row: experiment, second row: periodic-boundary calculation at experimental geometry, third/fourth row: isolated-molecule calculations at experimental/optimised geometries, values only given for chemically different C atoms

atom	Q	V_{001}	V_{tot}	atom	Q	V_{001}	V_{tot}	atom	Q	V_{001}	V_{tot}
Si1	2.71	4.7	4.9	C11	-0.12	11.0	11.0	H6	0.10	7.0	8.9
	2.98	4.0	4.1		0.00	10.7	10.7		0.03	7.5	8.9
	3.02	4.1									
	2.98	4.4									
O1	-1.47	14.8	18.0	C12	-0.09	11.0	11.8	H8	0.14	5.5	6.7
	-1.92	16.8	18.3		-0.01	10.9	11.3		0.05	6.2	7.4
	-1.72	18.1									
	-1.71	18.1									
C1	-0.46	11.7	12.6	C13	-0.49	10.9	12.3	H9	0.07	7.4	8.0
	-0.71	13.2	13.5		-0.74	12.1	13.0		0.01	7.9	8.5
	-0.74	13.5									
	-0.73	13.7									
C2	-0.12	12.5	12.8	C14	-0.08	11.9	13.6	H10	0.07	6.4	6.8
	-0.03	12.3	12.4		0.00	11.8	13.3		0.02	6.5	6.9
	-0.05	12.3									
	-0.05	12.2									
C3	-0.13	13.0	13.7	C15	-0.13	12.7	13.2	H11	0.07	7.1	7.6
	-0.02	12.5	13.4		-0.01	12.4	12.9		0.01	7.5	7.7
C4	-0.13	12.0	12.4	C16	-0.13	12.4	12.5	H12	0.07	7.5	8.3
	-0.01	11.8	12.2		-0.01	12.0	12.2		0.02	7.5	7.9
C5	-0.13	12.3	12.5	C17	-0.12	11.7	12.0	H14	0.11	7.3	9.3
	-0.02	12.0	12.2		-0.01	11.3	11.6		0.04	7.8	9.6
C6	-0.10	12.0	13.7	C18	-0.10	10.9	11.7	H15	0.07	6.9	7.0
	-0.02	11.9	13.3		-0.01	10.7	11.1		0.02	7.2	7.3
C7	-0.59	11.9	13.4	H2	0.14	6.2	6.6	H16	0.07	7.1	7.2
	-0.73	13.1	13.9		0.04	6.8	6.9		0.02	7.3	7.4
C8	-0.13	12.6	14.9	H3	0.07	6.8	7.5	H17	0.07	7.5	9.0
	-0.03	12.3	14.6		0.01	7.0	7.7		0.02	7.7	9.2
C9	-0.13	12.6	14.1	H4	0.08	6.8	7.4	H18	0.13	5.7	6.0
	-0.01	12.3	13.9		0.02	7.0	7.6		0.05	6.4	6.5
C10	-0.13	12.2	12.3	H5	0.07	7.3	7.4	sum	-0.01	330.0	357.9
	-0.02	11.8	11.9		0.02	7.4	7.6		0.02	343.5	366.9

Table A.56: Absolute (relative) source-function contributions in eÅ^{-3} (%) to the bcps of the bonds Si1–O1, Si2–O1 and the hydrogen bond O2–H2O$\cdots$O1 in siloxanol (**1**)
Exp = experiment, theo = periodic-boundary calculation at experimental geometry, [1]: acceptor molecule, [2]: donor molecule

atom	Si1–O1 exp	Si1–O1 theo	Si2–O1 exp	Si2–O1 theo	Hbond exp [1]	Hbond exp [2]
Si1	0.2879(33.5)	0.2090(27.5)	0.0081(0.9)	0.0049(0.6)	0.0031(1.9)	-0.0007(-0.4)
Si2	0.0056(0.7)	0.0056(0.7)	0.2957(32.9)	0.2178(27.6)	0.0003(0.2)	-0.0006(-0.4)
Si3	-0.0008(-0.1)	-0.0058(-0.8)	-0.0006(-0.1)	-0.0046(-0.6)	-0.0004(-0.3)	0.0025(1.6)
O1	0.4092(47.6)	0.3748(49.3)	0.4320(48.0)	0.3902(49.4)	0.0194(12.1)	0.0027(1.7)
O2	-0.0022(-0.3)	-0.0023(-0.3)	-0.0004(0.0)	-0.0001(0.0)	-0.0012(-0.8)	0.1128(70.5)
C1	0.0085(1.0)	0.0161(2.1)	0.0056(0.6)	0.0047(0.6)	-0.0015(-0.9)	-0.0051(-3.2)
C2	0.0033(0.4)	0.0034(0.4)	0.0108(1.2)	0.0175(2.2)	-0.0012(-0.8)	0.0036(2.3)
C3	0.0081(0.9)	0.0094(1.2)	0.0106(1.2)	0.0110(1.4)	0.0035(2.2)	0.0023(1.4)
C4	0.0034(0.4)	0.0056(0.7)	0.0044(0.5)	0.0067(0.8)	0.0019(1.2)	0.0018(1.1)
C5	0.0020(0.2)	0.0058(0.8)	0.0014(0.2)	0.0048(0.6)	0.0005(0.3)	-0.0010(-0.6)
C6	0.0122(1.4)	0.0108(1.4)	0.0110(1.2)	0.0101(1.3)	0.0048(3.0)	-0.0081(-5.1)
C7	0.0001(0.0)	-0.0021(-0.3)	0.0180(2.0)	0.0183(2.3)	-0.0007(-0.4)	0.0004(0.3)
C8	-0.0025(-0.3)	-0.0001(0.0)	0.0136(1.5)	0.0199(2.5)	-0.0068(-4.3)	-0.0014(-0.9)
C9	0.0167(1.9)	0.0205(2.7)	-0.0006(-0.1)	0.0002(0.0)	-0.0051(-3.2)	-0.0008(-0.5)
C10	0.0174(2.0)	0.0184(2.4)	0.0000(0.0)	-0.0020(-0.3)	-0.0035(-2.2)	0.0030(1.9)
C11	0.0011(0.1)	-0.0009(-0.1)	0.0008(0.1)	-0.0008(-0.1)	0.0008(0.5)	-0.0005(-0.3)
C12	0.0002(0.0)	0.0002(0.0)	0.0002(0.0)	0.0003(0.0)	0.0004(0.3)	0.0013(0.8)
H3	0.0054(0.6)	0.0043(0.6)	0.0046(0.5)	0.0039(0.5)	0.0020(1.3)	0.0038(2.4)
H4	0.0053(0.6)	0.0043(0.6)	0.0055(0.6)	0.0045(0.6)	0.0031(1.9)	0.0037(2.3)
H5	0.0054(0.6)	0.0040(0.5)	0.0053(0.6)	0.0039(0.5)	0.0031(1.9)	0.0023(1.4)
H7A	0.0012(0.1)	0.0011(0.1)	0.0099(1.1)	0.0120(1.5)	0.0039(2.4)	-0.0022(-1.4)
H7B	0.0054(0.6)	0.0069(0.9)	0.0107(1.2)	0.0142(1.8)	0.0053(3.3)	0.0016(1.0)
H7C	0.0032(0.4)	0.0043(0.6)	0.0094(1.0)	0.0124(1.6)	-0.0018(-1.1)	0.0015(0.9)
H8A	0.0037(0.4)	0.0048(0.6)	0.0099(1.1)	0.0133(1.7)	0.0003(0.2)	0.0011(0.7)
H8B	0.0047(0.5)	0.0058(0.8)	0.0106(1.2)	0.0135(1.7)	0.0059(3.7)	0.0006(0.4)
H8C	0.0004(0.0)	0.0016(0.2)	0.0084(0.9)	0.0122(1.5)	0.0015(0.9)	0.0001(0.1)
H9A	0.0090(1.0)	0.0121(1.6)	0.0007(0.1)	0.0014(0.2)	0.0041(2.6)	0.0026(1.6)
H9B	0.0110(1.3)	0.0140(1.8)	0.0052(0.6)	0.0061(0.8)	0.0072(4.5)	-0.0030(-1.9)
H9C	0.0099(1.2)	0.0136(1.8)	0.0032(0.4)	0.0046(0.6)	-0.0022(-1.4)	0.0028(1.8)
H10A	0.0106(1.2)	0.0135(1.8)	0.0046(0.5)	0.0054(0.7)	0.0001(0.1)	0.0055(3.4)
H10B	0.0113(1.3)	0.0130(1.7)	0.0056(0.6)	0.0059(0.7)	0.0067(4.2)	-0.0130(-8.1)
H10C	0.0079(0.9)	0.0105(1.4)	-0.0013(-0.1)	-0.0013(-0.2)	0.0022(1.4)	0.0039(2.4)
H11A	0.0018(0.2)	0.0024(0.3)	0.0016(0.2)	0.0021(0.3)	0.0010(0.6)	0.0053(3.3)
H11B	0.0010(0.1)	0.0012(0.2)	0.0004(0.0)	0.0005(0.1)	0.0006(0.4)	0.0069(4.3)
H11C	0.0004(0.0)	0.0007(0.1)	0.0000(0.0)	0.0003(0.0)	0.0002(0.1)	-0.0052(-3.3)
H12A	-0.0036(-0.4)	-0.0033(-0.4)	-0.0024(-0.3)	-0.0021(-0.3)	-0.0026(-1.6)	0.0029(1.8)
H12B	0.0033(0.4)	0.0035(0.5)	0.0019(0.2)	0.0019(0.2)	0.0020(1.3)	0.0037(2.3)
H12C	0.0025(0.3)	0.0031(0.4)	0.0020(0.2)	0.0024(0.3)	0.0014(0.9)	0.0012(0.8)
H2O	0.0015(0.2)	0.0023(0.3)	0.0007(0.1)	0.0012(0.2)	0.0008(0.5)	-0.0612(-38.3)
sum	0.8719(101.4)	0.7922(104.2)	0.9071(100.8)	0.8171(103.4)	0.0590(36.9)	0.0772(48.3)
reference	0.86	0.76	0.90	0.79	0.16	0.16

Table A.57: Absolute (relative) source-function contributions in eÅ^{-3} (%) to the bcps of the Si1–O1 bonds in trisilo (**2**) and hexaphe (**4**)

*Exp = experiment, theo = periodic-boundary calculation at experimental geometry, [1]: trisilo (**2**), [2]: hexaphe (**4**)*

atom	Si1–O1 exp [1]	Si1–O1 theo [1]	atom	Si1–O1 exp [2]	Si1–O1 theo [2]
Si1	0.2761(29.4)	0.1825(22.3)	Si1	0.3084(33.5)	0.2192(25.8)
Si2	-0.0046(-0.5)	-0.0110(-1.3)	O1	0.4413(48.0)	0.4171(49.1)
O1	0.4111(43.7)	0.3741(45.6)	C1	0.0094(1.0)	0.0144(1.7)
C1	0.0053(0.6)	0.0183(2.2)	C2	0.0093(1.0)	0.0067(0.8)
C2	0.0021(0.2)	0.0065(0.8)	C3	0.0035(0.4)	0.0035(0.4)
C3	0.0067(0.7)	0.0067(0.8)	C4	0.0038(0.4)	0.0037(0.4)
C4	0.0125(1.3)	0.0185(2.3)	C5	0.0055(0.6)	0.0049(0.6)
C5	0.0116(1.2)	0.0173(2.1)	C6	0.0039(0.4)	0.0062(0.7)
C6	-0.0005(-0.1)	0.0014(0.2)	C7	0.0082(0.9)	0.0158(1.9)
C7	-0.0010(-0.1)	0.0012(0.1)	C8	0.0085(0.9)	0.0076(0.9)
H3	0.0043(0.5)	0.0043(0.5)	C9	0.0053(0.6)	0.0050(0.6)
H4A	0.0100(1.1)	0.0115(1.4)	C10	0.0028(0.3)	0.0026(0.3)
H4B	0.0124(1.3)	0.0143(1.7)	C11	0.0078(0.8)	0.0075(0.9)
H4C	0.0101(1.1)	0.0120(1.5)	C12	0.0012(0.1)	0.0033(0.4)
H5A	0.0107(1.1)	0.0124(1.5)	C13	0.0100(1.1)	0.0164(1.9)
H5B	0.0128(1.4)	0.0138(1.7)	C14	0.0024(0.3)	0.0044(0.5)
H5C	0.0102(1.1)	0.0110(1.3)	C15	0.0060(0.7)	0.0055(0.6)
H6A	0.0010(0.1)	0.0003(0.0)	C16	0.0042(0.5)	0.0040(0.5)
H6B	0.0058(0.6)	0.0063(0.8)	C17	0.0057(0.6)	0.0054(0.6)
H6C	0.0039(0.4)	0.0046(0.6)	C18	0.0059(0.6)	0.0077(0.9)
H7A	0.0029(0.3)	0.0043(0.5)	H2	0.0019(0.2)	0.0030(0.4)
H7B	0.0063(0.7)	0.0064(0.8)	H3	0.0038(0.4)	0.0038(0.4)
H7C	0.0012(0.1)	0.0006(0.1)	H4	0.0038(0.4)	0.0038(0.4)
			H5	0.0038(0.4)	0.0037(0.4)
			H6	-0.0002(0.0)	0.0006(0.1)
			H8	0.0023(0.3)	0.0026(0.3)
			H9	0.0039(0.4)	0.0039(0.5)
			H10	0.0039(0.4)	0.0038(0.4)
			H11	0.0039(0.4)	0.0040(0.5)
			H12	0.0010(0.1)	0.0013(0.2)
			H14	0.0013(0.1)	-0.0002(0.0)
			H15	0.0039(0.4)	0.0038(0.4)
			H16	0.0039(0.4)	0.0039(0.5)
			H17	0.0039(0.4)	0.0040(0.5)
			H18	0.0029(0.3)	0.0030(0.4)
Si1a	0.0007(0.1)	0.0017(0.2)	Si1a	0.0114(1.2)	0.0058(0.7)
Si2a	-0.0057(-0.6)	-0.0079(-1.0)	O1a	–	–
O1a	0.0021(0.2)	0.0027(0.3)	C1a	-0.0048(-0.5)	-0.0048(-0.6)
C1a	0.0051(0.5)	0.0041(0.5)	C2a	0.0036(0.4)	0.0020(0.2)
C2a	0.0075(0.8)	0.0062(0.8)	C3a	0.0013(0.1)	0.0014(0.2)
C3a	0.0078(0.8)	0.0079(1.0)	C4a	0.0024(0.3)	0.0024(0.3)
C4a	-0.0007(-0.1)	-0.0004(0.0)	C5a	0.0024(0.3)	0.0020(0.2)
C5a	-0.0012(-0.1)	-0.0008(-0.1)	C6a	-0.0024(-0.3)	-0.0004(0.0)
C6a	0.0002(0.0)	0.0006(0.1)	C7a	-0.0074(-0.8)	-0.0049(-0.6)
C7a	-0.0001(0.0)	0.0004(0.0)	C8a	0.0033(0.4)	0.0026(0.3)
H3a	0.0041(0.4)	0.0040(0.5)	C9a	0.0026(0.3)	0.0024(0.3)
H4Aa	-0.0002(0.0)	-0.0001(0.0)	C10a	0.0015(0.2)	0.0014(0.2)
H4Ba	-0.0002(0.0)	0.0000(0.0)	C11a	0.0043(0.5)	0.0041(0.5)
H4Ca	0.0017(0.2)	0.0019(0.2)	C12a	-0.0038(-0.4)	-0.0026(-0.3)
H5Aa	0.0018(0.2)	0.0020(0.2)	C13a	-0.0046(-0.5)	-0.0041(-0.5)
H5Ba	-0.0001(0.0)	-0.0002(0.0)	C14a	-0.0024(-0.3)	-0.0012(-0.1)
H5Ca	-0.0002(0.0)	-0.0002(0.0)	C15a	0.0029(0.3)	0.0027(0.3)
H6Aa	0.0004(0.0)	0.0001(0.0)	C16a	0.0027(0.3)	0.0025(0.3)
H6Ba	-0.0010(-0.1)	-0.0009(-0.1)	C17a	0.0030(0.3)	0.0029(0.3)
H6Ca	0.0019(0.2)	0.0022(0.3)	C18a	0.0021(0.2)	0.0032(0.4)
H7Aa	0.0017(0.2)	0.0023(0.3)	H2a	0.0011(0.1)	0.0018(0.2)
H7Ba	-0.0003(0.0)	-0.0006(-0.1)	H3a	0.0024(0.3)	0.0024(0.3)
H7Ca	0.0002(0.0)	-0.0001(0.0)	H4a	0.0026(0.3)	0.0026(0.3)
			H5a	0.0020(0.2)	0.0019(0.2)
			H6a	-0.0050(-0.5)	-0.0045(-0.5)
			H8a	0.0011(0.1)	0.0012(0.1)
			H9a	0.0025(0.3)	0.0025(0.3)
			H10a	0.0027(0.3)	0.0026(0.3)
			H11a	0.0023(0.3)	0.0023(0.3)
			H12a	-0.0026(-0.3)	-0.0023(-0.3)
			H14a	-0.0048(-0.5)	-0.0057(-0.7)
			H15a	0.0020(0.2)	0.0019(0.2)
			H16a	0.0027(0.3)	0.0027(0.3)
			H17a	0.0025(0.3)	0.0026(0.3)
			H18a	0.0018(0.2)	0.0018(0.2)
sum	0.8363(89.0)	0.7421(90.5)		0.9285(100.9)	0.8372(98.5)
reference	0.94	0.82		0.92	0.85

Table A.58: Absolute (relative) source-function contributions in e$\mathring{A}^{-3}$ (%) to the bcps of the bonds Si1–O1, Si2–O1 and Si1–H1Si in pentaphe (**3**)

Exp = experiment, theo = periodic-boundary calculation at experimental geometry

atom	Si1–O1 exp	Si1–O1 theo	Si2–O1 exp	Si2–O1 theo	Si1–H1Si exp	Si1–H1Si theo
Si1	0.2779(30.2)	0.2341(27.9)	0.0061(0.7)	0.0028(0.4)	0.2175(29.8)	0.1771(24.6)
Si2	-0.0034(-0.4)	-0.0063(-0.8)	0.2296(26.4)	0.1464(19.3)	-0.0040(-0.5)	-0.0057(-0.8)
O1	0.4712(51.2)	0.4342(51.7)	0.4536(52.1)	0.4561(60.0)	0.0511(7.0)	0.0497(6.9)
C1	0.0089(1.0)	0.0166(2.0)	-0.0039(-0.4)	-0.0032(-0.4)	0.0094(1.3)	0.0159(2.2)
C2	0.0013(0.1)	0.0027(0.3)	-0.0043(-0.5)	-0.0031(-0.4)	0.0053(0.7)	0.0061(0.8)
C3	0.0073(0.8)	0.0067(0.8)	0.0042(0.5)	0.0038(0.5)	0.0063(0.9)	0.0058(0.8)
C4	0.0036(0.4)	0.0033(0.4)	0.0024(0.3)	0.0022(0.3)	0.0036(0.5)	0.0034(0.5)
C5	0.0052(0.6)	0.0047(0.6)	0.0027(0.3)	0.0024(0.3)	0.0063(0.9)	0.0056(0.8)
C6	0.0059(0.6)	0.0062(0.7)	0.0022(0.3)	0.0024(0.3)	0.0020(0.3)	0.0024(0.3)
C7	0.0079(0.9)	0.0162(1.9)	-0.0046(-0.5)	-0.0037(-0.5)	0.0094(1.3)	0.0182(2.5)
C8	0.0062(0.7)	0.0076(0.9)	0.0006(0.1)	0.0017(0.2)	0.0078(1.1)	0.0090(1.3)
C9	0.0051(0.6)	0.0047(0.6)	0.0021(0.2)	0.0018(0.2)	0.0048(0.7)	0.0044(0.6)
C10	0.0021(0.2)	0.0018(0.2)	0.0006(0.1)	0.0005(0.1)	0.0022(0.3)	0.0019(0.3)
C11	0.0061(0.7)	0.0056(0.7)	0.0028(0.3)	0.0025(0.3)	0.0066(0.9)	0.0063(0.9)
C12	0.0049(0.5)	0.0044(0.5)	-0.0002(0.0)	-0.0005(-0.1)	0.0030(0.4)	0.0022(0.3)
C13	-0.0044(-0.5)	-0.0018(-0.2)	0.0073(0.8)	0.0172(2.3)	-0.0027(-0.4)	-0.0010(-0.1)
C14	-0.0023(-0.3)	-0.0031(-0.4)	0.0029(0.3)	0.0016(0.2)	-0.0019(-0.3)	-0.0026(-0.4)
C15	0.0031(0.3)	0.0031(0.4)	0.0064(0.7)	0.0063(0.8)	0.0021(0.3)	0.0022(0.3)
C16	0.0020(0.2)	0.0018(0.2)	0.0035(0.4)	0.0032(0.4)	0.0016(0.2)	0.0014(0.2)
C17	0.0021(0.2)	0.0022(0.3)	0.0046(0.5)	0.0047(0.6)	0.0016(0.2)	0.0016(0.2)
C18	0.0029(0.3)	0.0035(0.4)	0.0074(0.9)	0.0087(1.1)	0.0021(0.3)	0.0027(0.4)
C19	-0.0054(-0.6)	-0.0028(-0.3)	0.0074(0.9)	0.0160(2.1)	-0.0040(-0.5)	-0.0023(-0.3)
C20	0.0040(0.4)	0.0040(0.5)	0.0082(0.9)	0.0083(1.1)	0.0030(0.4)	0.0031(0.4)
C21	0.0028(0.3)	0.0022(0.3)	0.0053(0.6)	0.0044(0.6)	0.0022(0.3)	0.0017(0.2)
C22	0.0015(0.2)	0.0015(0.2)	0.0024(0.3)	0.0024(0.3)	0.0012(0.2)	0.0012(0.2)
C23	0.0035(0.4)	0.0036(0.4)	0.0061(0.7)	0.0061(0.8)	0.0022(0.3)	0.0025(0.3)
C24	-0.0037(-0.4)	-0.0026(-0.3)	0.0007(0.1)	0.0024(0.3)	-0.0040(-0.5)	-0.0032(-0.4)
C25	-0.0078(-0.8)	-0.0083(-1.0)	0.0068(0.8)	0.0094(1.2)	-0.0052(-0.7)	-0.0057(-0.8)
C26	0.0019(0.2)	0.0022(0.3)	0.0060(0.7)	0.0066(0.9)	0.0007(0.1)	0.0020(0.3)
C27	0.0017(0.2)	0.0017(0.2)	0.0039(0.4)	0.0039(0.5)	0.0010(0.1)	0.0011(0.2)
C28	0.0025(0.3)	0.0025(0.3)	0.0040(0.5)	0.0039(0.5)	0.0018(0.2)	0.0018(0.3)
C29	0.0028(0.3)	0.0027(0.3)	0.0060(0.7)	0.0057(0.8)	0.0016(0.2)	0.0015(0.2)
C30	-0.0031(-0.3)	-0.0027(-0.3)	0.0018(0.2)	0.0026(0.3)	-0.0021(-0.3)	-0.0019(0.0)
H2	0.0007(0.1)	0.0002(0.0)	-0.0060(-0.7)	-0.0061(-0.8)	0.0034(0.5)	0.0030(0.4)
H3	0.0040(0.4)	0.0040(0.5)	0.0023(0.3)	0.0023(0.3)	0.0040(0.5)	0.0039(0.5)
H4	0.0040(0.4)	0.0038(0.5)	0.0029(0.3)	0.0027(0.4)	0.0040(0.5)	0.0038(0.5)
H5	0.0040(0.4)	0.0039(0.5)	0.0028(0.3)	0.0027(0.4)	0.0041(0.6)	0.0040(0.6)
H6	0.0032(0.3)	0.0029(0.3)	0.0020(0.2)	0.0019(0.3)	0.0000(0.0)	-0.0005(-0.1)
H8	0.0029(0.3)	0.0028(0.3)	0.0005(0.1)	0.0004(0.1)	0.0035(0.5)	0.0034(0.5)
H9	0.0040(0.4)	0.0041(0.5)	0.0024(0.3)	0.0024(0.3)	0.0039(0.5)	0.0040(0.6)
H10	0.0039(0.4)	0.0039(0.5)	0.0026(0.3)	0.0026(0.3)	0.0038(0.5)	0.0038(0.5)
H11	0.0039(0.4)	0.0039(0.5)	0.0023(0.3)	0.0023(0.3)	0.0038(0.5)	0.0038(0.5)
H12	0.0023(0.3)	0.0025(0.3)	0.0003(0.0)	0.0004(0.1)	0.0000(0.0)	0.0002(0.0)
H14	-0.0054(-0.6)	-0.0057(-0.7)	0.0002(0.0)	-0.0001(0.0)	-0.0063(-0.9)	-0.0065(-0.9)
H15	0.0019(0.2)	0.0018(0.2)	0.0038(0.4)	0.0038(0.5)	0.0010(0.1)	0.0010(0.1)
H16	0.0025(0.3)	0.0025(0.3)	0.0038(0.4)	0.0038(0.5)	0.0021(0.3)	0.0020(0.3)
H17	0.0024(0.3)	0.0022(0.3)	0.0037(0.4)	0.0036(0.5)	0.0019(0.3)	0.0018(0.3)
H18	0.0019(0.2)	0.0018(0.2)	0.0034(0.4)	0.0035(0.5)	0.0015(0.2)	0.0015(0.2)
H20	0.0022(0.2)	0.0020(0.2)	0.0031(0.4)	0.0029(0.4)	0.0021(0.3)	0.0019(0.3)
H21	0.0027(0.3)	0.0027(0.3)	0.0039(0.4)	0.0039(0.5)	0.0024(0.3)	0.0024(0.3)
H22	0.0026(0.3)	0.0025(0.3)	0.0036(0.4)	0.0035(0.5)	0.0022(0.3)	0.0022(0.3)
H23	0.0019(0.2)	0.0019(0.2)	0.0037(0.4)	0.0037(0.5)	0.0011(0.2)	0.0012(0.2)
H24	-0.0078(-0.8)	-0.0078(-0.9)	0.0003(0.0)	0.0002(0.0)	-0.0086(-1.2)	-0.0084(-1.2)
H26	0.0013(0.1)	0.0015(0.2)	0.0024(0.3)	0.0028(0.4)	0.0005(0.1)	0.0007(0.1)
H27	0.0025(0.3)	0.0024(0.3)	0.0039(0.4)	0.0037(0.5)	0.0018(0.2)	0.0017(0.2)
H28	0.0024(0.3)	0.0025(0.3)	0.0036(0.4)	0.0036(0.5)	0.0018(0.2)	0.0018(0.3)
H29	0.0022(0.2)	0.0022(0.3)	0.0040(0.5)	0.0039(0.5)	0.0015(0.2)	0.0014(0.2)
H30	-0.0039(-0.4)	-0.0037(-0.4)	0.0006(0.1)	0.0011(0.1)	-0.0026(-0.4)	-0.0025(-0.3)
H1Si	0.0456(5.0)	0.0497(5.9)	0.0068(0.8)	0.0068(0.9)	0.3501(48.0)	0.3531(49.0)
sum	0.9021(98.1)	0.8424(100.3)	0.8472(97.4)	0.7875(103.6)	0.7160(98.1)	0.6923(96.2)
reference	0.92	0.84	0.87	0.76	0.73	0.72

Table A.59: Absolute (relative) source-function contributions in e$\mathring{A}^{-3}$ (%) to the bcps of the bonds Si1–C1 and C1–C2 in pentaphe (**3**)

Exp = experiment, theo = periodic-boundary calculation at experimental geometry

atom	Si1–C1 exp	Si1–C1 theo	C1–C2 exp	C1–C2 theo
Si1	0.1795(24.2)	0.1264(16.6)	0.0045(0.2)	0.0035(0.2)
Si2	-0.0048(-0.6)	-0.0064(-0.8)	-0.0056(-0.3)	-0.0064(-0.3)
O1	0.0486(6.6)	0.0466(6.1)	0.0039(0.2)	0.0026(0.1)
C1	0.2193(29.6)	0.2439(32.1)	0.9191(44.0)	0.8874(42.3)
C2	0.0234(3.2)	0.0235(3.1)	0.8889(42.5)	0.8518(40.6)
C3	0.0120(1.6)	0.0109(1.4)	0.0570(2.7)	0.0537(2.6)
C4	0.0058(0.8)	0.0053(0.7)	0.0146(0.7)	0.0136(0.6)
C5	0.0107(1.4)	0.0096(1.3)	0.0157(0.8)	0.0142(0.7)
C6	0.0248(3.4)	0.0242(3.2)	0.0544(2.6)	0.0533(2.5)
C7	0.0104(1.4)	0.0153(2.0)	-0.0012(-0.1)	-0.0013(-0.1)
C8	0.0046(0.6)	0.0056(0.7)	0.0003(0.0)	0.0010(0.0)
C9	0.0056(0.8)	0.0051(0.7)	0.0031(0.1)	0.0028(0.1)
C10	0.0021(0.3)	0.0019(0.3)	0.0013(0.1)	0.0011(0.1)
C11	0.0055(0.7)	0.0050(0.7)	0.0032(0.2)	0.0029(0.1)
C12	0.0065(0.9)	0.0058(0.8)	0.0033(0.2)	0.0029(0.1)
C13	-0.0029(-0.4)	-0.0012(-0.2)	-0.0023(-0.1)	-0.0010(0.0)
C14	-0.0015(-0.2)	-0.0021(-0.3)	-0.0007(0.0)	-0.0012(-0.1)
C15	0.0019(0.3)	0.0019(0.3)	0.0015(0.1)	0.0015(0.1)
C16	0.0013(0.2)	0.0012(0.2)	0.0010(0.0)	0.0009(0.0)
C17	0.0014(0.2)	0.0015(0.2)	0.0010(0.0)	0.0011(0.1)
C18	0.0015(0.2)	0.0021(0.3)	0.0008(0.0)	0.0013(0.1)
C19	-0.0031(-0.4)	-0.0014(-0.2)	-0.0024(-0.1)	-0.0009(0.0)
C20	0.0032(0.4)	0.0033(0.4)	0.0028(0.1)	0.0029(0.1)
C21	0.0023(0.3)	0.0018(0.0)	0.0021(0.1)	0.0016(0.0)
C22	0.0012(0.2)	0.0013(0.2)	0.0010(0.0)	0.0011(0.1)
C23	0.0025(0.3)	0.0027(0.4)	0.0018(0.1)	0.0020(0.1)
C24	-0.0028(-0.4)	-0.0017(-0.2)	-0.0030(-0.1)	-0.0017(-0.1)
C25	-0.0072(-1.0)	-0.0079(-1.0)	-0.0084(-0.4)	-0.0094(-0.4)
C26	0.0009(0.1)	0.0011(0.1)	-0.0002(0.0)	0.0000(0.0)
C27	0.0011(0.1)	0.0011(0.1)	0.0005(0.0)	0.0006(0.0)
C28	0.0020(0.3)	0.0020(0.3)	0.0016(0.1)	0.0016(0.1)
C29	0.0016(0.2)	0.0015(0.2)	0.0005(0.0)	0.0004(0.0)
C30	-0.0036(-0.5)	-0.0034(-0.4)	-0.0054(-0.3)	-0.0053(-0.3)
H2	0.0101(1.4)	0.0092(1.2)	0.0557(2.7)	0.0558(2.7)
H3	0.0064(0.9)	0.0063(0.8)	0.0169(0.8)	0.0168(0.8)
H4	0.0058(0.8)	0.0055(0.7)	0.0112(0.5)	0.0109(0.5)
H5	0.0065(0.9)	0.0063(0.8)	0.0112(0.5)	0.0110(0.5)
H6	0.0102(1.4)	0.0093(1.2)	0.0170(0.8)	0.0167(0.8)
H8	0.0007(0.1)	0.0004(0.1)	-0.0070(-0.3)	-0.0071(-0.3)
H9	0.0040(0.5)	0.0040(0.5)	0.0024(0.1)	0.0024(0.1)
H10	0.0038(0.5)	0.0038(0.5)	0.0028(0.1)	0.0028(0.1)
H11	0.0038(0.5)	0.0037(0.5)	0.0026(0.1)	0.0026(0.1)
H12	0.0032(0.4)	0.0032(0.4)	0.0022(0.1)	0.0022(0.1)
H14	-0.0034(-0.5)	-0.0036(-0.5)	-0.0015(-0.1)	-0.0016(-0.1)
H15	0.0012(0.2)	0.0011(0.1)	0.0010(0.0)	0.0010(0.0)
H16	0.0019(0.3)	0.0018(0.2)	0.0015(0.1)	0.0015(0.1)
H17	0.0017(0.2)	0.0016(0.2)	0.0013(0.1)	0.0012(0.1)
H18	0.0010(0.1)	0.0010(0.1)	0.0002(0.0)	0.0002(0.0)
H20	0.0020(0.3)	0.0019(0.3)	0.0019(0.1)	0.0018(0.1)
H21	0.0024(0.3)	0.0023(0.3)	0.0022(0.1)	0.0022(0.1)
H22	0.0022(0.3)	0.0021(0.3)	0.0020(0.1)	0.0020(0.1)
H23	0.0010(0.1)	0.0010(0.1)	0.0005(0.0)	0.0006(0.0)
H24	-0.0102(-1.4)	-0.0102(-1.3)	-0.0097(-0.5)	-0.0096(-0.5)
H26	0.0011(0.2)	0.0013(0.2)	0.0016(0.1)	0.0017(0.1)
H27	0.0022(0.3)	0.0021(0.3)	0.0025(0.1)	0.0024(0.1)
H28	0.0021(0.3)	0.0022(0.3)	0.0024(0.1)	0.0024(0.1)
H29	0.0018(0.2)	0.0018(0.2)	0.0022(0.1)	0.0021(0.1)
H30	-0.0027(-0.4)	-0.0026(-0.3)	-0.0005(0.0)	-0.0004(0.0)
H1Si	0.0444(6.0)	0.0459(6.0)	0.0096(0.5)	0.0089(0.4)
sum	0.6566(88.7)	0.6281(82.6)	2.0867(99.8)	2.009(95.7)
reference	0.74	0.76	2.09	2.10

Refinement Strategies and Coordinates of Cpds. 5 and 6

Table A.60: Multipole refinement strategies and κ/κ' values of butoxysilanol (**5**)
Periodic-boundary calculation at experimental geometry

atom	sym	cons	κ	κ'	atom	sym	cons	κ	κ'
Si1	1		0.9277	0.8500	Si1A	1		0.9277	0.8500
O1	m		0.9941	1.0000	O1A	m		0.9941	1.0000
O2	m		0.9991	1.0000	O2A	m		0.9991	1.0000
O3	m		0.9941	1.0000	O3A	m		0.9941	1.0000
O4	m		0.9941	1.0000	O4A	m		0.9941	1.0000
C1	3		1.0097	1.0000	C1A	3	C5	1.0097	1.0000
C2	3		1.0177	1.0000	C2A	3	C2	1.0177	1.0000
C3	3	C2	1.0177	1.0000	C3A	3	C2	1.0177	1.0000
C4	3	C2	1.0177	1.0000	C4A	3	C2	1.0177	1.0000
C5	3		1.0097	1.0000	C5A	3	C5	1.0097	1.0000
C6	3	C2	1.0177	1.0000	C6A	3	C2	1.0177	1.0000
C7	3	C2	1.0177	1.0000	C7A	3	C2	1.0177	1.0000
C8	3	C2	1.0177	1.0000	C8A	3	C2	1.0177	1.0000
C9	3	C5	1.0097	1.0000	C9A	3	C5	1.0097	1.0000
C10	3	C2	1.0177	1.0000	C10A	3	C2	1.0177	1.0000
C11	3	C2	1.0177	1.0000	C11A	3	C2	1.0177	1.0000
C12	3	C2	1.0177	1.0000	C12A	3	C2	1.0177	1.0000
H2O	6		1.1300	1.2900	H2OA	6		1.1300	1.2900
H2A	6		1.1300	1.2900	H2D	6	H2A	1.1300	1.2900
H2B	6	H2A	1.1300	1.2900	H2E	6	H2A	1.1300	1.2900
H2C	6	H2A	1.1300	1.2900	H2F	6	H2A	1.1300	1.2900
H3A	6	H2A	1.1300	1.2900	H3D	6	H2A	1.1300	1.2900
H3B	6	H2A	1.1300	1.2900	H3E	6	H2A	1.1300	1.2900
H3C	6	H2A	1.1300	1.2900	H3F	6	H2A	1.1300	1.2900
H4A	6	H2A	1.1300	1.2900	H4D	6	H2A	1.1300	1.2900
H4B	6	H2A	1.1300	1.2900	H4E	6	H2A	1.1300	1.2900
H4C	6	H2A	1.1300	1.2900	H4F	6	H2A	1.1300	1.2900
H6A	6	H2A	1.1300	1.2900	H6D	6	H2A	1.1300	1.2900
H6B	6	H2A	1.1300	1.2900	H6E	6	H2A	1.1300	1.2900
H6C	6	H2A	1.1300	1.2900	H6F	6	H2A	1.1300	1.2900
H7A	6	H2A	1.1300	1.2900	H7D	6	H2A	1.1300	1.2900
H7B	6	H2A	1.1300	1.2900	H7E	6	H2A	1.1300	1.2900
H7C	6	H2A	1.1300	1.2900	H7F	6	H2A	1.1300	1.2900
H8A	6	H2A	1.1300	1.2900	H8D	6	H2A	1.1300	1.2900
H8B	6	H2A	1.1300	1.2900	H8E	6	H2A	1.1300	1.2900
H8C	6	H2A	1.1300	1.2900	H8F	6	H2A	1.1300	1.2900
H10A	6	H2A	1.1300	1.2900	H10D	6	H2A	1.1300	1.2900
H10B	6	H2A	1.1300	1.2900	H10E	6	H2A	1.1300	1.2900
H10C	6	H2A	1.1300	1.2900	H10F	6	H2A	1.1300	1.2900
H11A	6	H2A	1.1300	1.2900	H11D	6	H2A	1.1300	1.2900
H11B	6	H2A	1.1300	1.2900	H11E	6	H2A	1.1300	1.2900
H11C	6	H2A	1.1300	1.2900	H11F	6	H2A	1.1300	1.2900
H12A	6	H2A	1.1300	1.2900	H12D	6	H2A	1.1300	1.2900
H12B	6	H2A	1.1300	1.2900	H12E	6	H2A	1.1300	1.2900
H12C	6	H2A	1.1300	1.2900	H12F	6	H2A	1.1300	1.2900

Table A.61: Multipole refinement strategies and κ/κ' values of sucrose (**6**)
Periodic-boundary calculation at experimental geometry

atom	symm	cons	κ	κ'	atom	sym	cons	κ	κ'
O1	m		0.9861	1.0000	H2O	6		1.1300	1.2900
O2	1		0.9889	1.0000	H3O	6		1.1300	1.2900
O3	1		0.9889	1.0000	H4O	6		1.1300	1.2900
O4	m		0.9889	1.0000	H6O	6		1.1300	1.2900
O5	1		0.9861	1.0000	H8O	6		1.1300	1.2900
O6	1		0.9889	1.0000	H9O	6		1.1300	1.2900
O7	m		0.9861	1.0000	H10O	6		1.1300	1.2900
O8	1		0.9889	1.0000	H11O	6		1.1300	1.2900
O9	1		0.9889	1.0000	H1	6		1.1300	1.2900
O10	1		0.9889	1.0000	H2	6		1.1300	1.2900
O11	1		0.9889	1.0000	H3	6		1.1300	1.2900
C1	1		1.0153	1.0000	H4	6		1.1300	1.2900
C2	m		1.0122	1.0000	H5	6		1.1300	1.2900
C3	m		1.0122	1.0000	H6A	6		1.1300	1.2900
C4	m		1.0122	1.0000	H6B	6	H6A	1.1300	1.2900
C5	1		1.0122	1.0000	H8	6		1.1300	1.2900
C6	m		1.0163	1.0000	H9	6		1.1300	1.2900
C7	1		1.0151	1.0000	H10	6		1.1300	1.2900
C8	m		1.0122	1.0000	H11A	6		1.1300	1.2900
C9	m		1.0122	1.0000	H11B	6	H11A	1.1300	1.2900
C10	1		1.0122	1.0000	H12A	6		1.1300	1.2900
C11	m		1.0163	1.0000	H12B	6	H12A	1.1300	1.2900
C12	m		1.0163	1.0000					

Table A.62: Experimental fractional and cartesian coordinates of butoxysilanol (**5**)

atom	xf	yf	zf	atom	xf	yf	zf	atom	x	y	z	atom	x	y	z
Si1	0.4627	0.1289	0.1591	Si1A	0.2421	0.3739	0.3332	Si1	5.4958268	1.6298182	3.2534147	Si1A	5.2223847	4.2884250	6.8135624
O1	0.3151	0.3135	0.1590	O1A	0.3174	0.3818	0.3952	O1	4.9756454	3.1836175	3.2513698	O1A	6.1903231	4.5671663	8.0813922
O2	0.5092	0.0595	0.2340	O2A	0.3387	0.4204	0.2669	O2	5.8856699	1.3019311	4.7850348	O2A	6.0909162	4.4529564	5.4578026
O3	0.6236	0.1207	0.1128	O3A	0.2688	0.1928	0.3316	O3	6.7841282	1.4022937	2.3066322	O3A	4.6267192	2.7582729	6.7808442
O4	0.3928	0.0342	0.1294	O4A	0.0464	0.4887	0.3388	O4	4.2963017	0.7308762	2.6460834	O4A	3.9523825	5.2740919	6.9280761
C1	0.1971	0.4178	0.1113	C1A	0.4856	0.3228	0.4082	C1	4.1826040	3.8984347	2.2759589	C1A	7.5316384	4.1149473	8.3472274
C2	0.2796	0.4028	0.0423	C2A	0.5928	0.1574	0.3887	C2	4.6251285	3.5359571	0.8649871	C2A	7.6917411	2.6556997	7.9484745
C3	0.0591	0.3710	0.1218	C3A	0.5453	0.4435	0.3713	C3	2.7199913	3.5403694	2.4906720	C3A	8.5092369	5.0048049	7.5926642
C4	0.1321	0.5881	0.1250	C4A	0.4816	0.3120	0.4818	C4	4.4165836	5.3790813	2.5561084	C4A	7.7177008	4.2759616	9.8522640
C5	0.7463	0.1651	0.1202	C5A	0.1726	0.1125	0.3653	C5	8.1596370	1.8014268	2.4579538	C5A	3.4843925	2.1975877	7.4699710
C6	0.6660	0.3313	0.1403	C6A	0.1169	0.1491	0.4347	C6	8.2559396	3.2694634	2.8689760	C6A	3.3928854	2.7432843	8.8891224
C7	0.8615	0.0381	0.1709	C7A	0.0276	0.1668	0.3254	C7	8.8326655	0.9057683	3.4947113	C7A	2.2374534	2.5181566	6.6540613
C8	0.8388	0.1669	0.0531	C8A	0.2879	-0.0672	0.3671	C8	8.7800992	1.5868918	1.0858348	C8A	3.7328143	0.6908607	7.5067790
C9	0.4560	-0.1344	0.1269	C9A	0.0457	0.6544	0.3484	C9	4.0950208	-0.6971196	2.5949612	C9A	3.8975071	6.7019766	7.1243852
C10	0.6424	-0.2149	0.1138	C10A	0.0429	0.7508	0.3119	C10	5.4093571	-1.4196890	2.3270810	C10A	5.0331996	7.3886225	6.3780016
C11	0.3745	-0.1388	0.0714	C11A	0.0667	0.6597	0.4212	C11	3.1096910	-0.9241444	1.4600491	C11A	3.9968357	6.9957979	8.6130627
C12	0.4063	-0.2140	0.1921	C12A	0.2104	0.7174	0.3213	C12	3.5058803	-1.1440842	3.9282273	C12A	2.5549397	7.1396060	6.5702209
H2O	0.5486	0.1235	0.2478	H2OA	0.2965	0.4141	0.2294	H2O	6.6000438	1.8879836	5.0672292	H2OA	5.5295654	4.2715511	4.6909700
H2A	0.3849	0.4207	0.0381	H2D	0.5534	0.0744	0.4174	H2A	5.6728739	3.6722797	0.7791018	H2D	7.0472308	2.0551679	8.5353570
H2B	0.1962	0.4908	0.0082	H2E	0.7168	0.1185	0.3963	H2B	4.1293047	4.1600991	0.1676807	H2E	8.6944904	2.3542173	8.1038859
H2C	0.3153	0.2865	0.0327	H2F	0.5829	0.1641	0.3386	H2C	4.3835257	2.5239694	0.6686779	H2F	7.4445358	2.5406101	6.9239863
H3A	0.1097	0.2456	0.1224	H3D	0.5490	0.4483	0.3204	H3A	2.6128779	2.4866846	2.5029413	H3D	8.3768994	4.8709808	6.5518169
H3B	-0.0199	0.4349	0.0834	H3E	0.6645	0.4074	0.3844	H3B	2.1376078	3.9468949	1.7054355	H3E	9.5006770	4.7457225	7.8605444
H3C	-0.0085	0.3998	0.1671	H3F	0.4638	0.5589	0.3836	H3C	2.3920810	3.9379015	3.4170056	H3F	8.3302420	6.0184578	7.8441853
H4A	0.0744	0.5959	0.1730	H4D	0.4034	0.4271	0.4948	H4A	4.0936694	5.6090575	3.5376540	H4D	7.5706437	5.2894851	10.1180993
H4B	0.0458	0.6710	0.0909	H4E	0.6019	0.2713	0.4949	H4B	3.8701485	5.9602865	1.8588020	H4E	8.6980893	3.9781521	10.1201442
H4C	0.2311	0.6157	0.1205	H4F	0.4368	0.2300	0.5067	H4C	5.4494563	5.5960409	2.4640885	H4F	7.0134279	3.6708411	10.3614408
H6A	0.5798	0.4159	0.1065	H6D	0.2208	0.1159	0.4597	H6A	7.7194191	3.8660078	2.1778043	H6D	4.2994759	2.5493517	9.4003441
H6B	0.7574	0.3665	0.1407	H6E	0.0539	0.0830	0.4596	H6B	9.2714232	3.5671804	2.8771556	H6E	2.5927501	2.2720253	9.3982992
H6C	0.6051	0.3268	0.1876	H6F	0.0373	0.2739	0.4330	H6C	7.8436915	3.3934901	3.8362074	H6F	3.2231090	3.7881523	8.8543593
H7A	0.7929	0.0300	0.2161	H7D	-0.0454	0.2931	0.3215	H7A	8.3242575	0.9922982	4.4190001	H7D	2.1279059	3.5681222	6.5743107
H7B	0.9511	0.0711	0.1768	H7E	-0.0444	0.1088	0.3490	H7B	9.8416280	1.2037905	3.6153597	H7E	1.3861851	2.1106412	7.1366545
H7C	0.9205	-0.0749	0.1548	H7F	0.0717	0.1361	0.2781	H7C	8.7991553	-0.1006868	3.1654846	H7F	2.3303262	2.0977822	5.6868299
H8A	0.8926	0.0510	0.0399	H8D	0.3201	-0.0927	0.3187	H8A	8.6955146	0.5659486	0.8159098	H8D	3.7348694	0.3104995	6.5170539
H8B	0.9322	0.1988	0.0545	H8E	0.2279	-0.1342	0.3943	H8B	9.8026427	1.8602492	1.1144632	H8E	2.9649874	0.2198977	8.0629882
H8C	0.7562	0.2520	0.0182	H8F	0.3954	-0.0991	0.3893	H8C	8.2753293	2.1838803	0.3721694	H8F	4.6685459	0.4982881	7.9607438
H10A	0.6749	-0.1585	0.0683	H10D	0.1576	0.7049	0.3313	H10A	5.8041003	-1.1006097	1.3966576	H10D	5.9607674	7.0685997	6.7747096
H10B	0.6860	-0.3384	0.1123	H10E	-0.0296	0.8733	0.3173	H10B	5.2380619	-2.4645662	2.2964077	H10E	4.9452511	8.4384308	6.4884254
H10C	0.6959	-0.2038	0.1515	H10F	0.0624	0.7413	0.2617	H10C	6.0988881	-1.1971881	3.0980033	H10F	4.9843833	7.1368033	5.3514684
H11A	0.2454	-0.0838	0.0820	H11D	-0.1196	0.5847	0.4466	H11A	2.2015660	-0.4248164	1.6768071	H11D	3.2514019	6.4513217	9.1324639
H11B	0.4171	-0.2600	0.0662	H11E	-0.1446	0.7796	0.4293	H11B	2.9259922	-1.9623234	1.3537150	H11E	3.8565965	8.0329592	8.7786985
H11C	0.4043	-0.0757	0.0273	H11F	0.0495	0.6186	0.4385	H11C	3.5155076	-0.5438656	0.5582541	H11F	4.9527922	6.7089977	8.9668281
H12A	0.4622	-0.2067	0.2300	H12D	-0.1913	0.6978	0.2724	H12A	4.2009104	-0.9528907	4.7032394	H12D	2.4604720	6.8072052	5.5702713
H12B	0.4452	-0.3364	0.1902	H12E	-0.2802	0.8423	0.3227	H12B	3.2944287	-2.1810698	3.8893745	H12E	2.4883883	8.1959275	6.5988493
H12C	0.2768	-0.1541	0.2012	H12F	-0.2747	0.6560	0.3500	H12C	2.6111434	-0.6086379	4.1143120	H12F	1.7785674	6.7209239	7.1571034

Table A.63: Experimental fractional and cartesian coordinates of sucrose (**6**)
Coordinates taken from Ref. [84]

atom	xf	yf	zf	x	y	z
O1	0.1079	0.2817	0.3289	0.0340779	2.4513534	3.4762407
O2	-0.2515	0.1938	0.2698	-2.6023742	1.6864476	2.8515955
O3	-0.2056	-0.1213	0.1913	-2.0562004	-1.0555526	2.0219059
O4	0.1448	-0.1870	0.1505	0.7538128	-1.6272740	1.5906787
O5	0.1310	0.2308	0.1214	0.7178938	2.0084216	1.2831123
O6	0.2133	0.0839	-0.0842	1.8550556	0.7300978	-0.8899345
O7	0.1804	0.5360	0.2880	0.6945002	4.6642720	3.0439566
O8	-0.1232	0.3891	0.4720	-2.1020579	3.3859482	4.9887067
O9	0.2981	0.3115	0.5760	0.9039532	2.7106730	6.0879132
O10	0.5911	0.5356	0.5212	3.3040000	4.6607912	5.5087159
O11	0.4582	0.3908	0.1722	3.1254513	3.4007416	1.8200324
C1	0.0137	0.2714	0.1997	-0.3801436	2.3617228	2.1106880
C2	-0.1389	0.1540	0.1863	-1.5280378	1.3401080	1.9690594
C3	-0.0658	-0.0092	0.2142	-1.0304527	-0.0800584	2.2639427
C4	0.0567	-0.0433	0.1244	0.1358061	-0.3767966	1.3148201
C5	0.2048	0.0774	0.1399	1.2437763	0.6735348	1.4786442
C6	0.3162	0.0577	0.0409	2.3465609	0.5021054	0.4322841
C7	0.1292	0.4365	0.3765	0.0829827	3.7984230	3.9793391
C8	0.2854	0.4395	0.4943	1.0045871	3.8245290	5.2244019
C9	0.4457	0.4651	0.4355	2.3878039	4.0473002	4.6029274
C10	0.3691	0.5704	0.3226	2.0700571	4.9636208	3.4096542
C11	-0.0474	0.4965	0.3988	-1.3374794	4.3205430	4.2150344
C12	0.4507	0.5488	0.2085	2.9790667	4.7756576	2.2036977
H2O	-0.3473	0.2599	0.2266	-3.2383219	2.2616498	2.3950020
H3O	-0.2430	-0.1377	0.2687	-2.5339405	-1.1982654	2.8399692
H4O	0.0653	-0.2635	0.1530	0.1327151	-2.2929770	1.6171019
H6O	0.2103	0.1896	-0.1082	1.8902705	1.6498992	-1.1435976
H8O	-0.1609	0.3035	0.4145	-2.2537337	2.6410570	4.3809723
H9O	0.3199	0.2202	0.5309	1.1823843	1.9161804	5.6112381
H10O	0.6994	0.4812	0.5156	4.1554408	4.1874024	5.4495279
H11O	0.3368	0.3539	0.1506	2.2388814	3.0796378	1.5917356
H1	-0.0433	0.3836	0.1647	-0.7358956	3.3380872	1.7407627
H2	-0.2210	0.1591	0.0890	-1.9263074	1.3844882	0.9406671
H3	0.0066	-0.0155	0.3134	-0.7118474	-0.1348810	3.3124167
H4	-0.0252	-0.0376	0.0272	-0.2611598	-0.3271952	0.2874848
H5	0.2897	0.0634	0.2356	1.6676016	0.5517068	2.4901256
H6A	0.3659	-0.0590	0.0527	2.7023156	-0.5134180	0.5570018
H6B	0.4315	0.1334	0.0596	3.1930006	1.1608468	0.6299299
H8	0.2734	0.5447	0.5483	0.7803037	4.7399794	5.7951438
H9	0.4868	0.3559	0.4004	2.7911969	3.0970418	4.2319452
H10	0.3919	0.6913	0.3523	2.1741397	6.0156926	3.7235622
H11A	-0.1355	0.5168	0.3061	-1.7933628	4.4971936	3.2352608
H11B	-0.0270	0.6068	0.4477	-1.2987016	5.2803736	4.7318728
H12A	0.5890	0.5845	0.2318	3.9922366	5.0863190	2.4499623
H12B	0.3713	0.6142	0.1298	2.5564066	5.3447684	1.3718943

Results of the PES Scans on Model Compounds of the Type H_3SiOCH_3 and H_3COCH_3

All values are dependent on the X–O–X angle a(X–O–X) in °.

If not otherwise specified, average values are given for C–O bonds and C atoms in symmetric model compounds.

Table A.64: Bending-potential energies (E_{rel}) in kJ mol^{-1}

1: free methoxysilane, 2: methoxysilane···silanol, 3: methoxysilane···water, 4: free dimethylether, 5: dimethylether···silanol, 6: dimethylether···water

a(X–O–X)	$E_{rel}(1)$	$E_{rel}(2)$	$E_{rel}(3)$	$E_{rel}(4)$	$E_{rel}(5)$	$E_{rel}(6)$
65	323.463	300.805		411.274	405.489	405.004
70	254.247	246.540		322.380	319.149	318.263
75	193.126	188.998		240.532	240.285	238.827
80	142.418	140.622	140.568	171.505	171.995	170.782
85	101.645	100.837	100.736	115.790	117.331	116.198
90	69.861	69.783	69.910	72.789	74.533	74.193
95	45.799	45.788	46.052	41.370	43.413	42.471
100	28.467	27.931	28.659	19.979	21.878	21.379
105	16.348	15.670	16.369	6.907	8.345	8.199
110	8.272	7.478	8.076	0.663	1.709	1.563
115	3.265	2.624	2.905	0.000	0.000	0.000
120	0.649	0.304	0.401	3.790	3.086	3.268
125	0.000	0.000	0.000	11.098	10.013	10.083
130	0.941	1.471	1.102	20.878	19.903	20.024
135	2.839	4.419	3.713	33.402	32.205	31.957
140	5.570	8.394	7.215	47.584	46.219	45.916
145	8.951	13.042	11.317	62.471	61.588	60.902
150	12.166	17.999	15.682	77.542	77.389	76.032
155	15.972	22.802	19.965	92.844	93.416	92.178
160	19.479	27.923	24.517	106.829	109.229	107.254
165	22.444	32.408	28.715	118.701	123.444	120.794
170	24.643	36.412	31.234	127.796	135.320	132.061
175	26.030	38.831	33.447	133.405	143.988	140.115
180	26.512	–	–	135.290	–	–

Table A.65: Hydrogen-bond energies (E_{HB}) in kJ mol^{-1}

1: methoxysilane$\cdots$silanol, 2: methoxysilane$\cdots$water, 3: dimethylether$\cdots$silanol, 4: dimethylether$\cdots$water

a(X–O–X)	$E_{HB}(1)$	$E_{HB}(2)$	$E_{HB}(3)$	$E_{HB}(4)$
65	-35.670	–	-23.827	-14.556
70	-21.622	–	-21.741	-12.569
75	-18.727	–	-18.921	-10.555
80	-17.012	-9.492	-18.611	-9.835
85	-16.062	-8.053	-17.704	-11.211
90	-15.319	-7.345	-17.699	-8.286
95	-15.292	-6.883	-17.591	-10.352
100	-15.371	-7.139	-17.623	-10.396
105	-15.421	-7.067	-17.958	-10.468
110	-15.463	-7.237	-18.195	-10.639
115	-15.236	-7.350	-19.038	-11.209
120	-14.888	-7.166	-19.558	-11.211
125	-14.517	-6.918	-19.574	-11.061
130	-13.992	-6.702	-19.183	-10.544
135	-12.968	-5.929	-19.241	-10.469
140	-11.777	-5.155	-19.127	-10.171
145	-10.587	-4.387	-18.458	-9.749
150	-8.986	-3.217	-17.620	-9.364
155	-8.261	-2.640	-16.835	-8.177
160	-6.878	-1.748	-15.102	-6.964
165	-5.538	-0.645	-12.968	-5.394
170	-3.806	-0.021	-10.572	-3.272
175	-2.927	0.833	-8.128	-1.040

Table A.66: Si–O and C–O bond distances (d) in Å, ED (ϱ) at the Si–O and C–O bcps in eÅ^{-3}, and Laplacian ($\nabla^2\varrho$) at the Si–O and C–O bcps in eÅ^{-5} for methoxysilane

a(Si–O–C)	d(Si–O)	ϱ(Si–O)	$\nabla^2\varrho$(Si–O)	d(C–O)	ϱ(C–O)	$\nabla^2\varrho$(C–O)
65	1.9477	0.5533	5.600	1.5276	1.4765	-7.531
70	1.8401	0.6573	9.276	1.5494	1.4063	-7.019
75	1.7872	0.7270	11.643	1.5352	1.4402	-8.528
80	1.7533	0.7789	13.405	1.5166	1.4862	-10.179
85	1.7296	0.8181	14.769	1.4978	1.5338	-11.669
90	1.7118	0.8486	15.893	1.4798	1.5806	-12.854
95	1.6980	0.8720	16.828	1.4651	1.6183	-13.537
100	1.6868	0.8898	17.629	1.4529	1.6489	-13.807
105	1.6777	0.9025	18.302	1.4428	1.6726	-13.758
110	1.6704	0.9108	18.873	1.4346	1.6903	-13.480
115	1.6640	0.9158	19.377	1.4279	1.7029	-13.040
120	1.6582	0.9184	19.849	1.4222	1.7114	-12.480
125	1.6526	0.9193	20.311	1.4171	1.7171	-11.820
130	1.6472	0.9189	20.778	1.4126	1.7206	-11.075
135	1.6416	0.9180	21.266	1.4087	1.7213	-10.275
140	1.6360	0.9169	21.785	1.4054	1.7200	-9.440
145	1.6307	0.9150	22.287	1.4024	1.7177	-8.584
150	1.6260	0.9124	22.758	1.3996	1.7154	-7.740
155	1.6217	0.9099	23.212	1.3972	1.7123	-6.953
160	1.6178	0.9077	23.628	1.3952	1.7095	-6.246
165	1.6146	0.9059	23.982	1.3936	1.7072	-5.654
170	1.6123	0.9044	24.253	1.3923	1.7057	-5.206
175	1.6109	0.9034	24.420	1.3916	1.7047	-4.931
180	1.6100	0.9040	24.517	1.3921	1.7016	-4.869

Table A.67: C–O bond distances (d) in Å, ED (ϱ) at the C–O bcps in eÅ^{-3}, Laplacian ($\nabla^2\varrho$) at the C–O bcps in eÅ^{-5}, atomic charges (Q_{001}) in e and volumes (V_{001}) in Å^3 of O and C atoms for dimethylether

a(C–O–C)	d(C–O)	ϱ(C–O)	$\nabla^2\varrho$(C–O)	Q_{001}(C)	V_{001}(C)	Q_{001}(O)	V_{001}(O)
65	1.6701	1.0602	-2.362	0.2874	8.573	-0.6292	17.609
70	1.6112	1.2126	-5.296	0.3388	8.495	-0.6835	17.176
75	1.5640	1.3455	-8.162	0.3836	8.468	-0.7345	16.781
80	1.5250	1.4621	-10.790	0.4211	8.460	-0.7868	16.419
85	1.4932	1.5610	-12.921	0.4570	8.463	-0.8400	16.096
90	1.4678	1.6415	-14.337	0.4893	8.479	-0.8914	15.833
95	1.4481	1.7039	-15.026	0.5165	8.507	-0.9379	15.605
100	1.4328	1.7504	-15.171	0.5382	8.547	-0.9782	15.415
105	1.4215	1.7820	-14.963	0.5544	8.600	-1.0113	15.262
110	1.4131	1.8014	-14.532	0.5687	8.653	-1.0387	15.144
115	1.4070	1.8104	-13.943	0.5800	8.709	-1.0623	15.060
120	1.4024	1.8113	-13.226	0.5911	8.754	-1.0838	15.013
125	1.3990	1.8057	-12.392	0.6000	8.794	-1.0965	14.981
130	1.3963	1.7952	-11.444	0.6090	8.810	-1.1146	15.007
135	1.3940	1.7811	-10.377	0.6182	8.806	-1.1399	15.088
140	1.3918	1.7646	-9.188	0.6276	8.779	-1.1583	15.158
145	1.3900	1.7464	-7.893	0.6364	8.744	-1.1761	15.215
150	1.3876	1.7278	-6.508	0.6478	8.697	-1.1937	15.265
155	1.3844	1.7128	-5.022	0.6578	8.653	-1.2120	15.307
160	1.3819	1.6974	-3.615	0.6664	8.615	-1.2272	15.319
165	1.3795	1.6849	-2.342	0.6740	8.580	-1.2402	15.335
170	1.3774	1.6757	-1.317	0.6803	8.552	-1.2495	15.334
175	1.3760	1.6702	-0.663	0.6851	8.532	-1.2556	15.330
180	1.3753	1.6692	-0.420	0.6865	8.525	-1.2580	15.329

Table A.68: Atomic charges (Q_{001}) in e and volumes (V_{001}) in Å^3 of C, Si and O atoms for methoxysilane

a(Si–O–C)	Q_{001}(C)	V_{001}(C)	Q_{001}(Si)	V_{001}(Si)	Q_{001}(O)	V_{001}(O)
65	-0.0231	9.128	2.8451	5.592	-0.9438	19.208
70	0.0537	9.187	2.8608	5.444	-1.0092	18.900
75	0.1573	9.072	2.8636	5.457	-1.0732	18.637
80	0.2468	8.970	2.8638	5.497	-1.1271	18.419
85	0.3207	8.890	2.8642	5.554	-1.1715	18.218
90	0.3809	8.836	2.8649	5.611	-1.2099	18.022
95	0.4289	8.813	2.8663	5.660	-1.2427	17.855
100	0.4714	8.793	2.8670	5.713	-1.2659	17.702
105	0.4998	8.809	2.8693	5.745	-1.2878	17.575
110	0.5230	8.834	2.8715	5.772	-1.3065	17.489
115	0.5412	8.862	2.8744	5.793	-1.3236	17.441
120	0.5571	8.884	2.8774	5.808	-1.3388	17.426
125	0.5713	8.895	2.8809	5.813	-1.3544	17.451
130	0.5825	8.899	2.8844	5.806	-1.3698	17.515
135	0.5922	8.891	2.8893	5.787	-1.3846	17.599
140	0.5999	8.877	2.8933	5.762	-1.3989	17.679
145	0.6084	8.851	2.8977	5.736	-1.4122	17.745
150	0.6152	8.830	2.9018	5.711	-1.4242	17.788
155	0.6191	8.817	2.9051	5.688	-1.4345	17.824
160	0.6238	8.801	2.9082	5.667	-1.4432	17.844
165	0.6269	8.791	2.9109	5.649	-1.4503	17.855
170	0.6304	8.777	2.9131	5.635	-1.4559	17.870
175	0.6316	8.774	2.9146	5.625	-1.4594	17.870
180	0.6379	8.757	2.9123	5.634	-1.4968	17.875

Table A.69: ED (ϱ) at the H$\cdots$O bcps in eÅ^{-3}

a(X–O–X)	methoxysilane$\cdots$ silanol	methoxysilane$\cdots$ water	dimethylether$\cdots$ silanol	dimethylether$\cdots$ water
65	0.2206	–	0.2631	0.1968
70	0.2174	–	0.2553	0.1879
75	0.2149	–	0.2436	0.1806
80	0.2129	0.1532	0.2404	0.1764
85	0.2095	0.1475	0.2350	0.1870
90	0.2083	0.1520	0.2347	0.1750
95	0.2051	0.1565	0.2321	0.1829
100	0.2065	0.1550	0.2324	0.1890
105	0.2053	0.1547	0.2321	0.1887
110	0.2069	0.1579	0.2339	0.1908
115	0.2081	0.1595	0.2388	0.1956
120	0.2086	0.1605	0.2363	0.1981
125	0.2081	0.1615	0.2508	0.2061
130	0.2065	0.1606	0.2608	0.2123
135	0.2028	0.1602	0.2623	0.2176
140	0.1969	0.1561	0.2732	0.2288
145	0.1891	0.1506	0.2770	0.2283
150	0.1780	0.1448	0.2768	0.2288
155	0.1627	0.1324	0.2728	0.2225
160	0.1445	0.1225	0.2626	0.2161
165	0.1228	0.1055	0.2457	0.2033
170	0.0962	0.0503	0.2218	0.1817
175	0.0643	0.0471	0.1946	0.1543

Table A.70: Number of ELI attractors belonging to oxygen lone-pair basins ($V_1(O)$), sum of the populations in e and volumes in Å^3 of both oxygen lone-pair basins ($\Sigma N_{001}(V_1(O))$ and $\Sigma V_{001}(V_1(O))$), sum of the populations in e and volumes in Å^3 of both C–O bond basins ($\Sigma N_{001}(V_2(C,O))$ and $\Sigma V_{001}(V_2(C,O))$) for the ELI of free dimethylether

a(Si–O–Si)	no(attr)	$\Sigma N_{001}(V_1(O))$	$\Sigma V_{001}(V_1(O))$	$\Sigma N_{001}(V_2(C,O))$	$\Sigma V_{001}(V_2(C,O))$
65	2	6.3211	17.4075	1.0034	1.2696
70	2	6.3029	16.8644	1.0264	1.1963
75	2	5.5871	15.8645	1.7638	1.6712
80	2	5.3672	15.2423	2.0106	1.7910
85	2	5.2187	14.2850	2.1926	1.8725
90	2	5.1015	14.2986	2.3288	1.9220
95	2	5.0302	13.9465	2.4186	1.9525
100	2	4.9625	13.6401	2.4916	1.9826
105	2	4.9205	13.3799	2.5488	2.0153
110	2	4.8900	13.1560	2.5865	2.0498
115	2	4.8739	12.9653	2.6208	2.1016
120	2	4.8635	12.8165	2.6344	2.1416
125	2	4.8640	12.6976	2.6351	2.1908
130	2	4.8710	12.6175	2.6383	2.2509
135	2	4.8821	12.5693	2.6233	2.3068
140	2	4.9241	12.6249	2.5889	2.3712
145	2	4.9751	12.7467	2.5408	2.3720
150	2	5.0857	13.0436	2.4352	2.2081
155	2	5.2869	13.5313	2.2337	1.7825
160	2	5.5456	13.9405	1.9703	1.4504
165	2	5.6966	14.1193	1.8145	1.3040
170	2	5.7942	14.2305	1.7136	1.2181
175	2	5.8484	14.2734	1.6599	1.1736
180	3	5.8632	14.2819	1.6481	1.1612

Table A.71: Number of ELI attractors belonging to oxygen lone-pair basins ($V_1(O)$), sum of the populations in e and volumes in Å^3 of both oxygen lone-pair basins ($\Sigma N_{001}(V_1(O))$ and $\Sigma V_{001}(V_1(O))$) for the ELI of free methoxysilane

a(Si–O–Si)	no(attr)	$\Sigma N_{001}(V_1(O))$	$\Sigma V_{001}(V_1(O))$
65	2	6.5839	19.4046
70	2	6.6282	18.9146
75	2	6.0086	17.8041
80	2	5.5371	16.8465
85	2	5.3052	16.1948
90	2	5.1223	15.6658
95	2	5.0123	15.2916
100	2	4.9177	14.9635
105	2	4.8444	14.6806
110	2	4.8082	14.4754
115	2	4.7756	14.2820
120	2	4.7487	14.1132
125	2	4.7505	14.0006
130	2	4.7522	13.8933
135	2	4.7534	13.7853
140	2	4.7962	13.7377
145	2	4.8409	13.6814
150	2	4.8845	13.6182
155	2	4.9454	13.5587
160	2	4.9789	13.4498
165	2	4.9285	13.1884
170	2	4.8148	12.7391
175	2	4.5914	12.0787
180	3	6.5165	17.0277

Table A.72: Populations in e and volumes in Å^3 of C–O and Si–O bond basins ($N_{001}(V_2(Si,O))$, $N_{001}(V_2(C,O))$, $V_{001}(V_2(Si,O))$ and $V_{001}(V_2(C,O))$ as well as sum of populations and volumes of both bond basins ($\Sigma N_{001}(V_2(Si/C,O))$ and $\Sigma V_{001}(V_2(Si/C,O))$) for the ELI of free methoxysilane

a(Si–O–Si)	$N_{001}(V_2(Si,O))$	$N_{001}(V_2(C,O))$	$\Sigma N_{001}(V_2(Si/C,O))$	$V_{001}(V_2(Si,O))$	$V_{001}(V_2(C,O))$	$\Sigma V_{001}(V_2(Si/C,O))$
65	–	0.8034	0.8034	–	0.7399	0.7399
70	–	0.7897	0.7897	–	0.7430	0.7430
75	0.6083	0.8618	1.4701	0.6904	0.7917	1.4821
80	1.0444	0.9287	1.9731	1.3025	0.8224	2.1249
85	1.2458	0.9913	2.2371	1.6293	0.8559	2.4852
90	1.3828	1.0528	2.4356	1.8533	0.8764	2.7297
95	1.4571	1.0970	2.5541	1.9431	0.8971	2.8402
100	1.5173	1.1309	2.6482	2.0187	0.9044	2.9231
105	1.5670	1.1648	2.7318	2.0872	0.9207	3.0079
110	1.5885	1.1848	2.7733	2.1290	0.9294	3.0584
115	1.6058	1.2051	2.8109	2.1869	0.9420	3.1289
120	1.6258	1.2213	2.8471	2.2620	0.9468	3.2088
125	1.6216	1.2276	2.8492	2.3330	0.9518	3.2848
130	1.6150	1.2322	2.8472	2.4406	0.9548	3.3954
135	1.6174	1.2333	2.8507	2.6110	0.9506	3.5616
140	1.5879	1.2239	2.8118	2.7666	0.9389	3.7055
145	1.5601	1.2128	2.7729	2.9573	0.9270	3.8843
150	1.5373	1.1960	2.7333	3.1307	0.9035	4.0342
155	1.4995	1.1766	2.6761	3.2818	0.8811	4.1629
160	1.4932	1.1542	2.6474	3.4622	0.8562	4.3184
165	1.5548	1.1406	2.6954	3.7796	0.8390	4.6186
170	1.6860	1.1223	2.8083	4.2508	0.8235	5.0743
175	1.9257	1.1121	3.0378	4.9399	0.8115	5.7514
180	–	1.1103	1.1103	–	0.8058	0.8058

Geometry of Compound 5

Table A.73: Experimental bond distances (Å) in butoxysilanol (**5**)

bond	dist	bond	dist	bond	dist
Si1–O1	1.6384(2)	C5–C8	1.5216(4)	O3A–C5A	1.4480(3)
Si1–O2	1.6138(2)	C9–C10	1.5235(4)	O4A–C9A	1.4429(3)
Si1–O3	1.6147(2)	C9–C11	1.5206(4)	C1A–C2A	1.5217(4)
Si1–O4	1.6178(2)	C9–C12	1.5240(4)	C1A–C3A	1.5222(4)
O1–C1	1.4463(3)	O2–H2O	0.9670	C1A–C4A	1.5238(4)
O3–C5	1.4392(3)	C–H	1.0590	C5A–C6A	1.5228(4)
O4–C9	1.4425(3)	Si1A–O1A	1.6202(2)	C5A–C7A	1.5242(4)
C1–C2	1.5228(4)	Si1A–O2A	1.6179(2)	C5A–C8A	1.5270(4)
C1–C3	1.5208(4)	Si1A–O3A	1.6425(2)	C9A–C10A	1.5230(4)
C1–C4	1.5247(4)	Si1A–O4A	1.6114(2)	C9A–C11A	1.5209(4)
C5–C6	1.5279(4)	O1A–C1A	1.4403(3)	C9A–C12A	1.5167(4)
C5–C7	1.5258(4)				

Table A.74: Experimental bond angles (°) in butoxysilanol (**5**)

angle		angle		angle	
Si1–O1–C1	130.03(5)	C7–C5–C8	110.44(11)	O1A–Si1A–O2A	108.51(6)
Si1–O3–C5	131.41(5)	O3–C5–C6	110.78(9)	O1A–C1A–C3A	108.83(9)
Si1–O4–C9	131.82(5)	O4–C9–C11	105.34(9)	O1A–C1A–C4A	105.20(9)
Si1–O2–H2O	109.47	O4–C9–C12	108.27(9)	O1A–C1A–C2A	110.55(9)
O1–Si1–O2	105.69(6)	C10–C9–C11	110.89(10)	C2A–C1A–C4A	110.35(10)
O1–Si1–O3	112.74(6)	C10–C9–C12	110.41(9)	C3A–C1A–C4A	110.42(11)
O1–Si1–O4	106.94(6)	C11–C9–C12	110.98(10)	C2A–C1A–C3A	111.31(10)
O2–Si1–O3	109.57(6)	O4–C9–C10	110.83(9)	O3A–C5A–C6A	110.64(9)
O2–Si1–O4	114.95(7)	C–C–H	109.47	O3A–C5A–C7A	107.99(9)
O3–Si1–O4	107.06(6)	H–C–H	109.47	C6A–C5A–C7A	111.97(12)
O1–C1–C3	108.39(9)	Si1A–O1A–C1A	130.30(5)	C6A–C5A–C8A	109.98(13)
O1–C1–C2	110.36(9)	Si1A–O3A–C5A	129.59(4)	O3A–C5A–C8A	105.35(9)
C3–C1–C4	110.52(11)	Si1A–O4A–C9A	130.16(5)	C7A–C5A–C8A	110.68(9)
O1–C1–C4	105.80(9)	Si1A–O2A–H2OA	109.47	O4A–C9A–C11A	108.79(10)
C2–C1–C3	110.78(10)	O1A–Si1A–O4A	108.06(5)	O4A–C9A–C12A	105.63(9)
C2–C1–C4	110.84(9)	O2A–Si1A–O3A	105.81(6)	O4A–C9A–C10A	110.56(9)
O3–C5–C7	109.30(9)	O2A–Si1A–O4A	114.86(6)	C10A–C9A–C12A	110.57(10)
O3–C5–C8	104.84(9)	O3A–Si1A–O4A	106.59(7)	C11A–C9A–C12A	111.08(11)
C6–C5–C7	110.71(11)	O1A–Si1A–O3A	113.14(5)	C10A–C9A–C11A	110.12(10)
C6–C5–C8	110.61(12)				

Table A.75: Experimental torsion angles (°) in butoxysilanol (**5**)

angle		angle	
Si1–O1–C1–C2	-41.0(1)	Si1A–O1A–C1A–C2A	-41.4(1)
Si1–O1–C1–C4	-161.0(1)	Si1A–O1A–C1A–C4A	-160.6(1)
Si1–O1–C1–C3	80.4(1)	Si1A–O1A–C1A–C3A	81.0(1)
Si1–O3–C5–C8	-166.4(1)	Si1A–O3A–C5A–C8A	-158.4(1)
Si1–O3–C5–C6	-47.1(1)	Si1A–O3A–C5A–C7A	83.3(1)
Si1–O3–C5–C7	75.1(1)	Si1A–O3A–C5A–C6A	-39.5(1)
Si1–O4–C9–C12	82.9(1)	Si1A–O4A–C9A–C10A	36.7(1)
Si1–O4–C9–C11	-158.2(1)	Si1A–O4A–C9A–C12A	156.3(1)
Si1–O4–C9–C10	-38.2(1)	Si1A–O4A–C9A–C11A	-84.3(1)
O2–Si1–O1–C1	-161.5(1)	O3A–Si1A–O1A–C1A	72.9(1)
O3–Si1–O1–C1	78.8(1)	O4A–Si1A–O1A–C1A	-169.3(1)
O4–Si1–O1–C1	-38.5(1)	O1A–Si1A–O4A–C9A	51.3(1)
O1–Si1–O3–C5	71.9(1)	O2A–Si1A–O4A–C9A	-69.9(1)
O2–Si1–O3–C5	-45.4(1)	O3A–Si1A–O4A–C9A	173.2(1)
O4–Si1–O3–C5	-170.7(1)	O2A–Si1A–O1A–C1A	-44.1(1)
O1–Si1–O4–C9	-168.9(1)	O1A–Si1A–O3A–C5A	83.0(1)
O2–Si1–O4–C9	-52.0(1)	O2A–Si1A–O3A–C5A	-158.2(1)
O3–Si1–O4–C9	69.9(1)	O4A–Si1A–O3A–C5A	-35.5(1)

Results of the Topological Analyses of the ED of Compounds 5 and 6

Table A.76: Electron density (ϱ) at bcps in eÅ^{-3}, Laplacian ($\nabla^2\varrho$) at bcps in eÅ^{-5}, distances of bcps to first (d1) and second (d2) atom of the bond X1–X2 in Å, and ellipticity at bcps (ε) for butoxysilanol (**5**)

Periodic-boundary calculation at experimental geometry

bond	ϱ	$\nabla^2\varrho$	d1	d2	ε	bond	ϱ	$\nabla^2\varrho$	d1	d2	ε
Si1–O1	0.85	22.5	0.6781	0.9608	0.03	Si1A–O1A	0.87	24.5	0.6719	0.9480	0.02
Si1–O2	0.90	25.6	0.6691	0.9461	0.08	Si1A–O2A	0.92	24.8	0.6703	0.9489	0.03
Si1–O3	0.91	23.7	0.6739	0.9418	0.02	Si1A–O3A	0.85	21.7	0.6803	0.9629	0.02
Si1–O4	0.88	24.4	0.6720	0.9458	0.04	Si1A–O4A	0.91	24.7	0.6713	0.9407	0.02
O1–C1	1.65	-10.3	0.8297	0.6165	0.01	O1A–C1A	1.66	-10.9	0.8367	0.6036	0.01
O3–C5	1.66	-10.8	0.8364	0.6039	0.01	O3A–C5A	1.64	-10.2	0.8346	0.6126	0.00
O4–C9	1.65	-10.6	0.8374	0.6057	0.00	O4A–C9A	1.65	-10.4	0.8353	0.6071	0.01
C1–C2	1.71	-12.2	0.7743	0.7485	0.06	C1A–C2A	1.71	-12.3	0.7736	0.7479	0.05
C1–C3	1.71	-12.4	0.7736	0.7475	0.06	C1A–C3A	1.71	-12.3	0.7740	0.7482	0.05
C1–C4	1.71	-12.2	0.7754	0.7495	0.06	C1A–C4A	1.71	-12.2	0.7754	0.7496	0.06
C5–C6	1.70	-12.0	0.7767	0.7511	0.05	C5A–C6A	1.71	-12.2	0.7746	0.7489	0.05
C5–C7	1.70	-12.1	0.7762	0.7504	0.05	C5A–C7A	1.71	-12.2	0.7750	0.7493	0.05
C5–C8	1.72	-12.4	0.7735	0.7477	0.06	C5A–C8A	1.70	-12.1	0.7767	0.7509	0.06
C9–C10	1.71	-12.2	0.7748	0.7491	0.05	C9A–C10A	1.71	-12.2	0.7745	0.7484	0.05
C9–C11	1.72	-12.5	0.7729	0.7472	0.06	C9A–C11A	1.72	-12.4	0.7735	0.7473	0.05
C9–C12	1.71	-12.2	0.7753	0.7494	0.05	C9A–C12A	1.73	-12.6	0.7715	0.7455	0.06
O2–H2O	2.91	-96.4	0.7649	0.2012	0.01	O2A–H2OA	2.84	-112.8	0.7923	0.1752	0.00
C2–H2A	2.32	-32.6	0.6498	0.4103	0.00	C2A–H2D	2.32	-32.8	0.6487	0.4098	0.00
C2–H2B	2.32	-32.7	0.6487	0.4104	0.00	C2A–H2E	2.32	-32.8	0.6484	0.4102	0.00
C2–H2C	2.32	-32.8	0.6488	0.4100	0.00	C2A–H2F	2.32	-32.6	0.6497	0.4104	0.00
C3–H3A	2.32	-32.7	0.6494	0.4098	0.00	C3A–H3D	2.32	-32.9	0.6483	0.4094	0.00
C3–H3B	2.32	-32.8	0.6485	0.4103	0.00	C3A–H3E	2.32	-32.7	0.6488	0.4103	0.00
C3–H3C	2.32	-32.6	0.6496	0.4105	0.00	C3A–H3F	2.32	-32.7	0.6493	0.4104	0.00
C4–H4A	2.32	-32.8	0.6485	0.4101	0.00	C4A–H4D	2.33	-32.9	0.6482	0.4099	0.00
C4–H4B	2.32	-32.7	0.6492	0.4104	0.00	C4A–H4E	2.32	-32.7	0.6489	0.4102	0.00
C4–H4C	2.32	-32.7	0.6492	0.4102	0.00	C4A–H4F	2.32	-32.8	0.6489	0.4101	0.00
C6–H6A	2.32	-32.8	0.6490	0.4100	0.00	C6A–H6D	2.32	-32.8	0.6488	0.4099	0.00
C6–H6B	2.32	-32.8	0.6481	0.4102	0.00	C6A–H6E	2.32	-32.7	0.6487	0.4104	0.00
C6–H6C	2.32	-32.8	0.6487	0.4100	0.00	C6A–H6F	2.32	-32.7	0.6492	0.4100	0.00
C7–H7A	2.32	-32.8	0.6488	0.4097	0.00	C7A–H7D	2.32	-32.8	0.6489	0.4097	0.00
C7–H7B	2.32	-32.8	0.6486	0.4103	0.00	C7A–H7E	2.32	-32.6	0.6494	0.4106	0.00
C7–H7C	2.32	-32.7	0.6491	0.4104	0.00	C7A–H7F	2.32	-32.8	0.6486	0.4101	0.00
C8–H8A	2.32	-32.7	0.6492	0.4103	0.00	C8A–H8D	2.32	-32.6	0.6497	0.4106	0.00
C8–H8B	2.32	-32.8	0.6488	0.4100	0.00	C8A–H8E	2.32	-32.8	0.6486	0.4101	0.00
C8–H8C	2.32	-32.8	0.6486	0.4100	0.00	C8A–H8F	2.33	-32.9	0.6479	0.4098	0.00
C10–H10A	2.32	-32.7	0.6496	0.4102	0.00	C10A–H10D	2.33	-32.8	0.6484	0.4100	0.00
C10–H10B	2.32	-32.7	0.6488	0.4105	0.00	C10A–H10E	2.32	-32.7	0.6489	0.4104	0.00
C10–H10C	2.33	-32.9	0.6481	0.4099	0.00	C10A–H10F	2.33	-32.9	0.6485	0.4096	0.00
C11–H11A	2.32	-32.8	0.6487	0.4101	0.00	C11A–H11D	2.32	-32.7	0.6490	0.4102	0.00
C11–H11B	2.32	-32.7	0.6493	0.4103	0.00	C11A–H11E	2.32	-32.7	0.6492	0.4105	0.00
C11–H11C	2.32	-32.7	0.6493	0.4102	0.00	C11A–H11F	2.32	-32.8	0.6491	0.4098	0.00
C12–H12A	2.32	-32.8	0.6486	0.4098	0.00	C12A–H12D	2.33	-32.9	0.6482	0.4098	0.00
C12–H12B	2.32	-32.7	0.6488	0.4103	0.00	C12A–H12E	2.32	-32.8	0.6488	0.4100	0.00
C12–H12C	2.32	-32.7	0.6490	0.4102	0.00	C12A–H12F	2.32	-32.7	0.6493	0.4102	0.00

Table A.77: Electron density (ϱ) at bcps in eÅ^{-3}, Laplacian ($\nabla^2\varrho$) at bcps in eÅ^{-5}, distances of bcps to first (d1) and second (d2) atom of the bond X1–X2 in Å, and ellipticity at bcps (ε) for sucrose (**6**)

bond	ϱ	$\nabla^2\varrho$	d1	d2	ε	bond	ϱ	$\nabla^2\varrho$	d1	d2	ε
O1–C1	1.78	-12.1	0.8172	0.6133	0.03	C10–C12	1.74	-13.1	0.7726	0.7496	0.05
O1–C7	1.75	-11.3	0.8196	0.6199	0.04	O2–H2O	2.48	-51.8	0.7417	0.2298	0.03
O2–C2	1.72	-11.1	0.8241	0.6087	0.06	O3–H3O	2.52	-54.7	0.7384	0.2197	0.02
O3–C3	1.73	-10.2	0.8161	0.6204	0.04	O4–H4O	2.98	-73.5	0.7039	0.2070	0.03
O4–C4	1.78	-11.5	0.8106	0.6114	0.03	O6–H6O	2.54	-59.9	0.7404	0.2145	0.02
O5–C1	1.84	-13.4	0.8123	0.6092	0.03	O8–H8O	2.48	-49.9	0.7397	0.2336	0.02
O5–C5	1.68	-10.4	0.8317	0.6171	0.04	O9–H9O	2.52	-53.7	0.7402	0.2272	0.02
O6–C6	1.71	-10.0	0.8184	0.6106	0.02	O10–H10O	2.46	-54.1	0.7505	0.2255	0.02
O7–C7	1.89	-13.6	0.8031	0.6108	0.03	O11–H11O	2.49	-49.7	0.7389	0.2313	0.03
O7–C10	1.65	-9.0	0.8295	0.6257	0.05	C1–H1	2.01	-25.7	0.7195	0.3836	0.04
O8–C11	1.74	-9.7	0.8114	0.6228	0.03	C2–H2	1.91	-22.4	0.7091	0.3947	0.05
O9–C8	1.82	-11.2	0.8051	0.6079	0.03	C3–H3	1.95	-23.1	0.7070	0.3902	0.04
O10–C9	1.76	-10.9	0.8135	0.6135	0.05	C4–H4	1.91	-21.7	0.7039	0.3987	0.03
O11–C12	1.69	-9.6	0.8232	0.6119	0.04	C5–H5	1.92	-22.8	0.7160	0.3875	0.05
C1–C2	1.74	-13.0	0.7833	0.7604	0.09	C6–H6A	1.96	-22.8	0.6822	0.4012	0.07
C2–C3	1.73	-12.9	0.7660	0.7676	0.06	C6–H6B	1.94	-22.2	0.6866	0.4043	0.07
C3–C4	1.72	-13.0	0.7722	0.7606	0.06	C8–H8	1.98	-24.8	0.7111	0.3907	0.05
C4–C5	1.73	-13.6	0.7610	0.7747	0.10	C9–H9	1.92	-21.6	0.6985	0.3985	0.03
C5–C6	1.72	-12.5	0.7856	0.7444	0.05	C10–H10	1.90	-22.9	0.7122	0.3907	0.04
C7–C8	1.71	-12.7	0.7895	0.7607	0.08	C11–H11A	1.95	-23.5	0.7000	0.3952	0.06
C7–C11	1.78	-13.9	0.7884	0.7435	0.08	C11–H11B	1.96	-23.9	0.6968	0.3941	0.06
C8–C9	1.71	-12.8	0.7621	0.7713	0.04	C12–H12A	1.97	-23.7	0.6921	0.3960	0.06
C9–C10	1.74	-13.1	0.7642	0.7736	0.12	C12–H12B	1.95	-23.2	0.6949	0.3981	0.06
hexose	0.15	2.5				pentose	0.29	5.3			

Table A.78: Atomic charges (Q = Q_{001} = Q_{tot}) in e, and atomic volumes (V_{001} and V_{tot}) in Å^3 of butoxysilanol (**5**)

atom	Q	V_{001}	V_{tot}	atom	Q	V_{001}	V_{tot}	atom	Q	V_{001}	V_{tot}
Si1	3.07	3.5	3.5	H7B	0.05	7.1	8.4	C12A	-0.09	9.8	11.0
O1	-1.36	13.6	14.9	H7C	0.05	6.5	7.6	H2OA	0.81	0.7	0.7
O2	-1.62	17.7	18.5	H8A	0.05	6.4	8.4	H2D	0.06	6.6	8.5
O3	-1.38	14.6	15.5	H8B	0.05	6.6	8.8	H2E	0.05	6.5	8.6
O4	-1.42	14.9	15.8	H8C	0.05	6.8	7.3	H2F	0.06	6.0	6.9
C1	0.38	5.6	5.6	H10A	0.06	6.3	8.7	H3D	0.07	5.7	9.4
C2	-0.06	9.0	9.6	H10B	0.05	6.6	7.8	H3E	0.05	6.7	8.9
C3	-0.07	9.5	9.8	H10C	0.05	6.7	7.9	H3F	0.05	6.6	8.1
C4	-0.08	9.2	9.9	H11A	0.05	6.6	8.5	H4D	0.05	6.8	9.3
C5	0.39	5.6	5.6	H11B	0.05	7.1	7.6	H4E	0.05	6.5	9.9
C6	-0.07	9.4	10.4	H11C	0.05	6.7	7.5	H4F	0.05	7.0	8.3
C7	-0.06	9.1	9.8	H12A	0.07	6.0	8.0	H6D	0.06	6.4	8.4
C8	-0.08	9.3	9.6	H12B	0.05	6.7	7.9	H6E	0.05	6.4	9.8
C9	0.39	5.6	5.6	H12C	0.05	6.9	8.1	H6F	0.07	5.9	7.7
C10	-0.07	9.2	10.1	Si1A	3.11	3.2	3.2	H7D	0.07	5.8	8.3
C11	-0.08	9.3	9.8	O1A	-1.40	15.1	16.1	H7E	0.05	6.5	7.8
C12	-0.07	9.2	10.4	O2A	-1.67	18.2	19.5	H7F	0.04	7.1	9.5
H2O	0.73	2.5	2.6	O3A	-1.34	13.5	14.5	H8D	0.06	6.0	7.0
H2A	0.06	6.8	7.6	O4A	-1.39	14.4	15.6	H8E	0.05	6.8	9.7
H2B	0.05	6.7	8.0	C1A	0.41	5.3	5.3	H8F	0.05	6.7	7.9
H2C	0.06	6.4	7.3	C2A	-0.07	9.2	9.6	H10D	0.06	6.6	7.3
H3A	0.08	6.0	6.6	C3A	-0.06	8.9	10.2	H10E	0.05	6.6	7.9
H3B	0.05	6.7	8.1	C4A	-0.09	9.4	10.1	H10F	0.07	6.2	7.0
H3C	0.05	6.5	10.9	C5A	0.38	5.7	6.1	H11D	0.05	6.9	8.1
H4A	0.06	6.2	7.6	C6A	-0.07	9.0	10.2	H11E	0.05	6.8	8.1
H4B	0.05	6.8	9.3	C7A	-0.07	9.1	11.3	H11F	0.07	6.2	8.2
H4C	0.05	6.7	7.7	C8A	-0.07	9.1	9.5	H12D	0.05	6.8	9.5
H6A	0.06	6.8	7.5	C9A	0.39	5.6	5.6	H12E	0.05	6.5	7.1
H6B	0.05	6.1	7.5	C10A	-0.06	9.1	9.6	H12F	0.05	6.5	8.4
H6C	0.06	5.7	6.9	C11A	-0.07	9.2	10.1	sum	0.16	682.3	794.8
H7A	0.08	5.7	6.5								

Table A.79: Atomic charges (Q = Q_{001} = Q_{tot}) in e, and atomic volumes (V_{001} and V_{tot}) in Å^3 of sucrose (**6**)

atom	Q	V_{001}	V_{tot}	atom	Q	V_{001}	V_{tot}	atom	Q	V_{001}	V_{tot}
O1	-0.87	12.0	12.0	C6	0.44	7.4	7.8	H1	0.11	4.5	4.5
O2	-1.02	15.0	15.7	C7	0.71	4.8	4.8	H2	0.04	7.2	7.5
O3	-1.01	15.9	18.2	C8	0.39	6.3	6.3	H3	0.07	6.0	6.3
O4	-1.03	14.9	15.7	C9	0.33	6.6	6.6	H4	0.02	6.6	6.7
O5	-0.89	11.9	12.0	C10	0.33	6.6	6.7	H5	0.06	6.6	7.8
O6	-0.99	14.3	14.3	C11	0.36	7.5	7.6	H6A	0.02	7.4	8.8
O7	-0.88	12.1	12.6	C12	0.40	7.8	8.2	H6B	0.03	6.8	7.3
O8	-0.99	15.1	16.0	H2O	0.60	1.8	1.8	H8	0.07	5.9	6.2
O9	-1.01	15.0	15.9	H3O	0.62	1.7	1.7	H9	0.04	6.7	7.0
O10	-0.99	15.8	16.2	H4O	0.55	2.7	2.8	H10	0.09	6.5	7.5
O11	-0.99	15.3	16.1	H6O	0.62	1.7	1.8	H11A	0.07	5.4	5.5
C1	0.71	5.6	5.6	H8O	0.58	1.8	1.8	H11B	0.07	6.4	6.6
C2	0.39	6.3	6.3	H9O	0.60	1.7	1.7	H12A	0.05	5.8	5.9
C3	0.33	6.5	6.7	H10O	0.62	1.5	1.5	H12B	0.05	6.8	7.2
C4	0.41	6.1	6.1	H11O	0.58	1.9	1.9	sum	0.04	339.1	353.8
C5	0.33	6.7	6.7								

Table A.80: Absolute (relative) source-function contributions in e$\mathring{A}^{-3}$ (%) to the bcps of the bonds Si1–O1, C1–O1, Si1–O3, C5–O3 and the hydrogen bond O2A–H2OA$\cdots$O1 in butoxysilanol (**5**)

Donor = contributions of donor molecule, acc = contributions of acceptor molecule

atom	Si1–O1	C1–O1	Si1–O3	C5–O3	Hbond donor	Hbond acc
Si1	0.1397(16.43)	0.0003(0.02)	0.1896(20.84)	-0.0010(-0.06)	0.0086(5.75)	-0.0023(-1.50)
O1	0.3507(41.26)	0.7699(46.66)	0.0414(4.55)	0.0025(0.15)	0.0041(2.70)	0.0137(9.10)
O2	0.0595(7.00)	0.0096(0.58)	0.0600(6.59)	0.0094(0.57)	0.1389(92.58)	0.0030(1.99)
O3	0.0433(5.09)	0.0019(0.12)	0.4327(47.55)	0.7617(45.88)	-0.0081(-5.40)	0.0036(2.39)
O4	0.0450(5.29)	-0.0014(-0.09)	0.0453(4.97)	0.0058(0.35)	-0.0030(-2.02)	0.0020(1.33)
C1	0.0105(1.24)	0.5663(34.32)	0.0038(0.41)	0.0021(0.13)	0.0052(3.45)	0.0070(4.63)
C2	0.0040(0.47)	0.0376(2.28)	0.0019(0.21)	0.0032(0.19)	0.0027(1.79)	0.0072(4.77)
C3	0.0050(0.59)	0.0367(2.22)	0.0040(0.44)	0.0030(0.18)	0.0032(2.15)	0.0056(3.72)
C4	0.0056(0.66)	0.0358(2.17)	0.0037(0.41)	0.0025(0.15)	0.0000(0.00)	-0.0048(-3.18)
C5	0.0027(0.32)	0.0017(0.10)	0.0091(1.00)	0.5679(34.21)	0.0015(0.99)	0.0016(1.06)
C6	-0.0053(-0.62)	-0.0026(-0.16)	-0.0042(-0.46)	0.0275(1.66)	0.0027(1.79)	-0.0025(-1.65)
C7	0.0024(0.28)	0.0019(0.11)	0.0028(0.31)	0.0333(2.01)	0.0013(0.87)	0.0017(1.11
C8	0.0032(0.38)	0.0025(0.15)	0.0043(0.48)	0.0344(2.07)	0.0051(3.39)	0.0026(1.75)
C9	0.0035(0.42)	0.0019(0.12)	0.0029(0.32)	0.0016(0.10)	0.0005(0.35)	0.0018(1.21)
C10	-0.0021(-0.25)	-0.0007(-0.04)	-0.0056(-0.62)	-0.0025(-0.15)	0.0017(1.11)	-0.0006(-0.38)
C11	0.0014(0.17)	0.0005(0.03)	0.0018(0.20)	0.0011(0.06)	0.0014(0.91)	0.0008(0.56)
C12	0.0011(0.13)	0.0011(0.07)	0.0025(0.27)	0.0022(0.13)	-0.0007(-0.45)	0.0009(0.62)
H2O	0.0081(0.96)	0.0020(0.12)	0.0080(0.88)	0.0007(0.04)	-0.0923(-61.54)	-0.0001(-0.05)
H2A	0.0040(0.47)	0.0186(1.13)	-0.0009(-0.10)	-0.0071(-0.43)	0.0027(1.78)	0.0018(1.18)
H2B	0.0111(1.31)	0.0203(1.23)	0.0091(1.00)	0.0065(0.39)	0.0041(2.74)	0.0069(4.62)
H2C	0.0019(0.22)	0.0189(1.15)	-0.0023(-0.26)	-0.0002(-0.01)	-0.0072(-4.81)	0.0056(3.77)
H3A	-0.0007(-0.08)	0.0185(1.12)	-0.0021(-0.23)	-0.0004(-0.03)	-0.0059(-3.95)	0.0061(4.06)
H3B	0.0098(1.16)	0.0207(1.25)	0.0059(0.65)	0.0032(0.19)	0.0042(2.82)	0.0089(5.92)
H3C	0.0070(0.82)	0.0199(1.21)	0.0046(0.51)	0.0028(0.17)	0.0025(1.64)	0.0002(0.13)
H4A	0.0046(0.55)	0.0201(1.22)	0.0035(0.38)	0.0030(0.18)	0.0014(0.91)	-0.0020(-1.34)
H4B	0.0082(0.96)	0.0211(1.28)	0.0053(0.59)	0.0039(0.24)	0.0023(1.55)	0.0149(9.94)
H4C	0.0032(0.37)	0.0197(1.19)	0.0004(0.04)	-0.0022(-0.13)	0.0012(0.81)	0.0059(3.94)
H6A	0.0008(0.09)	-0.0056(-0.34)	0.0048(0.53)	0.0189(1.14)	0.0017(1.15)	-0.0012(-0.82)
H6B	0.0090(1.06)	0.0067(0.41)	0.0108(1.19)	0.0202(1.22)	0.0037(2.49)	0.0075(5.02)
H6C	-0.0038(-0.45)	-0.0018(-0.11)	0.0011(0.12)	0.0186(1.12)	-0.0002(-0.12)	-0.0110(-7.33)
H7A	-0.0018(-0.21)	-0.0005(-0.03)	0.0009(0.10)	0.0192(1.16)	-0.0013(-0.87)	-0.0025(-1.68)
H7B	0.0064(0.75)	0.0035(0.21)	0.0102(1.12)	0.0207(1.25)	0.0058(3.90)	0.0034(2.26)
H7C	0.0043(0.50)	0.0027(0.17)	0.0061(0.67)	0.0194(1.17)	-0.0027(-1.78)	0.0038(2.56)
H8A	0.0033(0.39)	0.0029(0.18)	0.0044(0.48)	0.0203(1.23)	-0.0013(-0.88)	0.0030(1.99)
H8B	0.0054(0.63)	0.0038(0.23)	0.0083(0.92)	0.0214(1.29)	0.0042(2.81)	0.0028(1.89)
H8C	0.0008(0.09)	-0.0016(-0.10)	0.0036(0.39)	0.0203(1.22)	0.0018(1.19)	0.0001(0.05)
H10A	0.0016(0.18)	0.0000(0.00)	0.0010(0.11)	-0.0032(-0.19)	0.0011(0.76)	0.0007(0.44)
H10B	0.0067(0.79)	0.0041(0.25)	0.0095(1.04)	0.0067(0.40)	0.0061(4.06)	0.0032(2.17)
H10C	-0.0015(-0.17)	0.0003(0.02)	-0.0041(-0.45)	-0.0051(-0.31)	-0.0077(-5.14)	-0.0013(-0.89)
H11A	0.0018(0.21)	-0.0003(-0.02)	0.0037(0.40)	0.0028(0.17)	0.0020(1.36)	-0.0000(-0.02)
H11B	0.0054(0.64)	0.0045(0.27)	0.0055(0.60)	0.0032(0.19)	0.0032(2.11)	0.0030(1.97)
H11C	0.0010(0.11)	-0.0003(-0.02)	0.0004(0.04)	-0.0010(-0.06)	0.0004(0.28)	0.0005(0.31)
H12A	-0.0010(-0.12)	0.0005(0.03)	-0.0014(-0.16)	-0.0014(-0.08)	-0.0039(-2.61)	-0.0014(-0.94)
H12B	0.0064(0.76)	0.0043(0.26)	0.0063(0.69)	0.0034(0.20)	0.0039(2.60)	0.0037(2.45)
H12C	0.0020(0.24)	-0.0005(-0.03)	0.0041(0.45)	0.0029(0.17)	0.0033(2.18)	-0.0002(-0.15)
sum	0.7742(91.08)	1.6654(100.93)	0.9023(99.15)	1.6523(99.54)	0.0981(65.40)	0.1035(69.00)
ref	0.85	1.65	0.91	1.66	0.15	0.15

Table A.81: Absolute (relative) source-function contributions in eÅ^{-3} (%) to the bcps of the bonds C1–O1, C7–O1, C1–O5 and C5–O5 in sucrose (**6**)

atom	C1–O1	C7–O1	C1–O5	C5–O5
O1	0.8090(45.45)	0.8120(46.40)	0.0736(4.00)	0.0059(0.35)
O2	0.0127(0.71)	-0.0004(-0.02)	0.0166(0.90)	0.0097(0.58)
O3	0.0110(0.62)	0.0065(0.37)	0.0110(0.60)	0.0107(0.64)
O4	0.0076(0.42)	0.0037(0.21)	0.0109(0.59)	0.0179(1.06)
O5	0.0778(4.37)	0.0126(0.72)	0.8367(45.47)	0.7426(44.20)
O6	0.0037(0.21)	0.0032(0.18)	0.0043(0.23)	0.0164(0.98)
O7	0.0066(0.37)	0.0793(4.53)	-0.0050(-0.27)	-0.0024(-0.15)
O8	0.0103(0.58)	0.0168(0.96)	0.0068(0.37)	0.0035(0.21)
O9	0.0058(0.32)	0.0168(0.96)	0.0045(0.25)	0.0036(0.22)
O10	0.0058(0.33)	0.0095(0.55)	0.0048(0.26)	0.0043(0.25)
O11	0.0061(0.34)	0.0047(0.27)	0.0095(0.51)	0.0060(0.36)
C1	0.6226(34.98)	0.0118(0.67)	0.6479(35.21)	0.0170(1.01)
C2	0.0334(1.88)	0.0074(0.42)	0.0327(1.78)	0.0042(0.25)
C3	0.0001(0.00)	-0.0002(-0.01)	0.0012(0.06)	0.0013(0.08)
C4	0.0012(0.07)	0.0017(0.098)	0.0006(0.03)	0.0282(1.68)
C5	-0.0052(-0.29)	-0.0044(-0.25)	0.0051(0.28)	0.5855(34.85)
C6	0.0053(0.30)	0.0034(0.19)	0.0075(0.41)	0.0364(2.16)
C7	0.0097(0.55)	0.6063(34.65)	0.0017(0.09)	0.0012(0.07)
C8	0.0071(0.40)	0.0323(1.84)	0.0045(0.25)	0.0030(0.18)
C9	-0.0014(-0.08)	-0.0001(-0.01)	-0.0012(-0.06)	-0.0011(-0.07)
C10	0.0020(0.11)	0.0051(0.29)	0.0011(0.06)	0.0008(0.05)
C11	0.0008(0.04)	0.0321(1.84)	0.0006(0.03)	0.0008(0.05)
C12	0.0026(0.15)	0.0042(0.24)	0.0022(0.12)	0.0030(0.18)
H2O	0.0057(0.32)	0.0035(0.20)	0.0039(0.21)	0.0026(0.15)
H3O	0.0023(0.13)	0.0011(0.06)	0.0030(0.16)	0.0033(0.20)
H4O	0.0030(0.17)	0.0020(0.12)	0.0038(0.20)	0.0066(0.39)
H6O	0.0002(0.01)	-0.0001(-0.01)	0.0004(0.02)	0.0039(0.23)
H8O	-0.0041(-0.23)	0.0016(0.09)	-0.0029(-0.16)	-0.0020(-0.12)
H9O	-0.0016(-0.09)	0.0021(0.12)	-0.0017(-0.09)	-0.0025(-0.15)
H10O	0.0012(0.07)	0.0022(0.13)	0.0008(0.04)	0.0003(0.02)
H11O	-0.0079(-0.44)	-0.0042(-0.24)	-0.0121(-0.66)	-0.0115(-0.69)
H1	0.0631(3.54)	0.0123(0.71)	0.0630(3.43)	0.0142(0.85)
H2	0.0163(0.91)	0.0075(0.43)	0.0157(0.85)	0.0073(0.43)
H3	0.0028(0.16)	-0.0020(-0.11)	0.0068(0.37)	0.0069(0.41)
H4	0.0057(0.32)	0.0034(0.19)	0.0069(0.37)	0.0159(0.95)
H5	0.0045(0.25)	-0.0012(-0.07)	0.0144(0.78)	0.0646(3.85)
H6A	0.0049(0.27)	0.0032(0.18)	0.0076(0.41)	0.0178(1.06)
H6B	0.0030(0.17)	0.0010(0.054)	0.0055(0.30)	0.0175(1.04)
H8	0.0070(0.39)	0.0161(0.92)	0.0049(0.26)	0.0039(0.23)
H9	-0.0005(-0.03)	0.0053(0.30)	-0.0018(-0.10)	-0.0043(-0.26)
H10	0.0059(0.33)	0.0087(0.50)	0.0053(0.29)	0.0043(0.26)
H11A	0.0030(0.17)	0.0157(0.89)	-0.0006(-0.03)	0.0001(0.01)
H11B	0.0095(0.53)	0.0167(0.96)	0.0060(0.33)	0.0036(0.21)
H12A	0.0052(0.29)	0.0057(0.33)	0.0054(0.29)	0.0045(0.27)
H12B	0.0023(0.13)	0.0038(0.22)	0.0017(0.09)	0.0021(0.13)
sum	1.7658(99.20)	1.7688(101.07)	1.8134(98.55)	1.6577(98.67)
ref	1.78	1.75	1.84	1.68

Table A.82: Absolute (relative) source-function contributions in eÅ^{-3} (%) to the bcps of the bonds C7–O7, C10–O7 and the hydrogen bond O11–H11O$\cdots$O5 in sucrose (**6**)

atom	C7–O7	C10–O7	Hbond
O1	0.0719(3.80)	0.0129(0.78)	0.0014(0.72)
O2	-0.0001(-0.01)	0.0008(0.046)	0.0050(2.52)
O3	0.0045(0.24)	0.0033(0.20)	0.0053(2.67)
O4	0.0028(0.15)	0.0020(0.12)	0.0050(2.51)
O5	0.0045(0.24)	-0.0026(-0.16)	0.0139(6.97)
O6	0.0030(0.16)	0.0033(0.20)	0.0098(4.92)
O7	0.8639(45.71)	0.7288(44.17)	-0.0119(-5.93)
O8	0.0183(0.97)	0.0077(0.47)	0.0043(2.15)
O9	0.0200(1.06)	0.0147(0.89)	0.0055(2.76)
O10	0.0115(0.61)	0.0167(1.01)	0.0065(3.24)
O11	0.0079(0.42)	0.0195(1.18)	0.1048(52.39)
C1	-0.0015(-0.08)	-0.0014(-0.08)	0.0058(2.92)
C2	0.0057(0.30)	0.0040(0.24)	0.0057(2.86)
C3	0.0004(0.02)	0.0004(0.023)	0.0006(0.29)
C4	0.0016(0.09)	0.0017(0.10)	0.0043(2.15)
C5	-0.0038(-0.20)	-0.0038(-0.23)	-0.0068(-3.38)
C6	0.0028(0.15)	0.0024(0.14)	0.0007(0.33)
C7	0.6537(34.59)	0.0141(0.86)	0.0011(0.56)
C8	0.0317(1.68)	0.0070(0.43)	0.0039(1.97)
C9	0.0022(0.12)	0.0286(1.73)	-0.0016(-0.78)
C10	0.0160(0.84)	0.5895(35.73)	-0.0001(-0.05)
C11	0.0322(1.71)	0.0039(0.24)	0.0016(0.80)
C12	0.0066(0.35)	0.0341(2.07)	0.0049(2.44)
H2O	0.0018(0.10)	0.0010(0.06)	0.0016(0.78)
H3O	0.0009(0.05)	0.0008(0.05)	0.0018(0.91)
H4O	0.0017(0.09)	0.0016(0.10)	0.0033(1.67)
H6O	-0.0005(-0.03)	-0.0009(-0.06)	-0.0017(-0.85)
H8O	0.0025(0.13)	0.0012(0.07)	-0.0009(-0.43)
H9O	0.0028(0.15)	0.0018(0.11)	-0.0015(-0.75)
H10O	0.0029(0.16)	0.0041(0.25)	0.0007(0.37)
H11O	-0.0032(-0.17)	0.0010(0.06)	-0.0565(-28.25)
H1	0.0013(0.07)	-0.0008(-0.05)	0.0088(4.42)
H2	0.0047(0.25)	0.0028(0.17)	0.0037(1.87)
H3	-0.0008(-0.04)	-0.0004(-0.03)	0.0018(0.91)
H4	0.0023(0.12)	0.0017(0.10)	0.0038(1.89)
H5	-0.0005(-0.02)	-0.0005(-0.03)	0.0103(5.15)
H6A	0.0030(0.16)	0.0031(0.19)	0.0107(5.37)
H6B	0.0002(0.01)	-0.0012(-0.07)	0.0004(0.22)
H8	0.0162(0.86)	0.0095(0.58)	0.0048(2.38)
H9	0.0106(0.56)	0.0176(1.06)	-0.0042(-2.12)
H10	0.0150(0.79)	0.0616(3.73)	0.0079(3.95)
H11A	0.0150(0.79)	0.0044(0.26)	0.0003(0.13)
H11B	0.0161(0.85)	0.0035(0.21)	0.0036(1.80)
H12A	0.0078(0.41)	0.0168(1.02)	0.0104(5.21)
H12B	0.0050(0.27)	0.0158(0.96)	0.0062(3.11)
sum	1.8607(98.45)	1.6317(98.89)	0.1854(92.71)
ref	1.89	1.65	0.20

Refinement Strategies and Coordinates of Cpds. 7 to 10

Table A.83: Multipole refinement strategies and κ/κ' values of moc-epoxide (**8**, left) and niphe-epoxide (**9**, right)
Exp = experiment, theoSP/theoopt = periodic-boundary calculations at experimental/optimised geometry

atom	sym	κ_{exp}	κ_{theoSP}	$\kappa_{theoopt}$	κ'	atom	sym	κ_{exp}	κ_{theoSP}	$\kappa_{theoopt}$	κ'
O1	mm2	0.9850	0.9850	0.9826	1.0000	O1	mm2	0.9816	0.9905	0.9899	1.0000
C1	1	1.0152	1.0152	1.0185	1.0000	C1	1	0.9541	1.0163	1.0156	1.0000
C2	1	1.0152	1.0152	1.0185	1.0000	C2	1	0.9452	1.0196	1.0181	1.0000
O2	m	0.9783	0.9783	0.9796	1.0000	O2	m	0.9732	0.9920	0.9918	1.0000
O3	m	0.9884	0.9884	0.9876	1.0000	O3	m	0.9732	0.9920	0.9918	1.0000
O4	m	0.9783	0.9783	0.9796	1.0000	O4	m	0.9831	0.9904	0.9896	1.0000
O5	m	0.9884	0.9884	0.9876	1.0000	O5	m	1.0027	0.9936	0.9930	1.0000
C3	m	1.0104	1.0104	1.0026	1.0000	O6	m	0.9831	0.9904	0.9896	1.0000
C4	3	1.0186	1.0186	1.0119	1.0000	O7	m	1.0027	0.9936	0.9930	1.0000
C5	m	1.0104	1.0104	1.0026	1.0000	N1	mm2	0.9751	1.0011	0.9988	1.0000
C6	3	1.0186	1.0186	1.0119	1.0000	C3	m	0.9372	1.0148	1.0143	1.0000
H1	6	1.1300	1.1300	1.1300	1.2900	C4	m	0.9566	1.0172	1.0144	1.0000
H2	6	1.1300	1.1300	1.1300	1.2900	C5	m	0.9566	1.0172	1.0144	1.0000
H4A	6	1.1300	1.1300	1.1300	1.2900	C6	m	0.9566	1.0172	1.0144	1.0000
H4B	6	1.1300	1.1300	1.1300	1.2900	C7	m	0.9566	1.0172	1.0144	1.0000
H4C	6	1.1300	1.1300	1.1300	1.2900	C8	mm2	0.9417	1.0243	1.0234	1.0000
H6A	6	1.1300	1.1300	1.1300	1.2900	C9	m	0.9372	1.0211	1.0197	1.0000
H6B	6	1.1300	1.1300	1.1300	1.2900	C10	3	0.9027	1.0325	1.0264	1.0000
H6C	6	1.1300	1.1300	1.1300	1.2900	C11	m	0.9372	1.0211	1.0197	1.0000
O1A	mm2	0.9850	0.9850	0.9826	1.0000	C12	3	0.9027	1.0325	1.0264	1.0000
C1A	1	1.0152	1.0152	1.0185	1.0000	H1	6	1.1300	1.1300	1.1300	1.2900
C2A	1	1.0152	1.0152	1.0185	1.0000	H4	6	1.1300	1.1300	1.1300	1.2900
O2A	m	0.9783	0.9783	0.9796	1.0000	H5	6	1.1300	1.1300	1.1300	1.2900
O3A	m	0.9884	0.9884	0.9876	1.0000	H6	6	1.1300	1.1300	1.1300	1.2900
O4A	m	0.9783	0.9783	0.9796	1.0000	H7	6	1.1300	1.1300	1.1300	1.2900
O5A	m	0.9884	0.9884	0.9876	1.0000	H10A	6	1.1300	1.1300	1.1300	1.2900
C3A	m	1.0104	1.0104	1.0026	1.0000	H10B	6	1.1300	1.1300	1.1300	1.2900
C4A	3	1.0186	1.0186	1.0119	1.0000	H10C	6	1.1300	1.1300	1.1300	1.2900
C5A	m	1.0104	1.0104	1.0026	1.0000	H12A	6	1.1300	1.1300	1.1300	1.2900
C6A	3	1.0186	1.0186	1.0119	1.0000	H12B	6	1.1300	1.1300	1.1300	1.2900
H1A	6	1.1300	1.1300	1.1300	1.2900	H12C	6	1.1300	1.1300	1.1300	1.2900
H2A	6	1.1300	1.1300	1.1300	1.2900						
H4D	6	1.1300	1.1300	1.1300	1.2900						
H4E	6	1.1300	1.1300	1.1300	1.2900						
H4F	6	1.1300	1.1300	1.1300	1.2900						
H6D	6	1.1300	1.1300	1.1300	1.2900						
H6E	6	1.1300	1.1300	1.1300	1.2900						
H6F	6	1.1300	1.1300	1.1300	1.2900						

Table A.84: Multipole refinement strategies and κ/κ' values of etox (**7**, left) and cyano-epoxide (**10**, right)
Exp = experiment, theoSP/theoopt = periodic-boundary calculations at experimental/optimised geometry

atom	sym	κ_{exp}	κ_{theoSP}	$\kappa_{theoopt}$	κ'
O1	mm2	0.9849	0.9845	0.9823	1.0000
C1	m	1.0286	1.0116	1.0132	1.0000
C2	m	1.0013	1.0132	1.0078	1.0000
H1	6	1.1300	1.1300	1.1300	1.2900
H2	6	1.1300	1.1300	1.1300	1.2900
H3	6	1.1300	1.1300	1.1300	1.2900
H4	6	1.1300	1.1300	1.1300	1.2900

atom	sym	κ_{exp}	κ_{theoSP}	$\kappa_{theoopt}$	κ'
O1	mm2	0.9984	0.9944	0.9935	1.0000
C1	m	1.0118	1.0421	1.0393	1.0000
C2	m	1.0118	1.0421	1.0393	1.0000
C3	6	1.0214	1.0446	1.0429	1.0000
C4	6	1.0214	1.0446	1.0429	1.0000
C5	6	1.0214	1.0446	1.0429	1.0000
C6	6	1.0214	1.0446	1.0429	1.0000
N1	6	0.9857	0.9925	0.9897	1.0000
N2	6	0.9857	0.9925	0.9897	1.0000
N3	6	0.9857	0.9925	0.9897	1.0000
N4	6	0.9857	0.9925	0.9897	1.0000

Table A.85: Experimental fractional and cartesian coordinates of etox (**7**)

atom	xf	yf	zf	x	y	z
O1	0.1169	0.8310	0.1241	0.3944516	6.9800304	0.8031195
C1	0.1485	0.9386	0.2959	0.3374961	7.8843996	1.9143329
C2	-0.1344	0.8647	0.2181	-0.8809944	7.2636144	1.4110004
H1	0.2882	0.8919	0.4360	0.8192498	7.4920524	2.8208879
H2	0.1758	1.0634	0.2529	0.5150613	8.9323836	1.6364390
H3	-0.3043	0.9368	0.1221	-1.5543632	7.8690192	0.7897210
H4	-0.2066	0.7650	0.3049	-1.3179473	6.4260924	1.9726561

Table A.86: Experimental fractional and cartesian coordinates of moc-epoxide (**8**)

atom	xf	yf	zf	x	y	z
O1	0.3791	0.0908	0.5345	5.3031225	0.3674729	9.0374759
O2	0.3240	0.2574	0.3699	4.9849358	1.0415603	6.2538633
O3	0.2489	0.5475	0.4095	3.1788603	2.2152031	6.9229515
O4	0.4384	0.5021	0.6673	5.8788783	2.0312926	11.2814255
O5	0.5079	0.6761	0.6006	7.7042343	2.7355544	10.1548604
C1	0.3436	0.3874	0.5076	4.6867838	1.5673452	8.5813347
C2	0.4157	0.3801	0.5287	6.1140633	1.5379922	8.9392785
C3	0.3055	0.3879	0.4210	4.3249982	1.5692225	7.1180952
C4	0.2090	0.5779	0.3277	2.7529474	2.3382915	5.5404949
C5	0.4540	0.5263	0.6071	6.5225287	2.1294340	10.2637432
C6	0.5508	0.8163	0.6729	8.2441273	3.3025225	11.3775602
H1	0.3213	0.4940	0.5507	3.9879523	1.9985451	9.3116442
H2	0.4388	0.4067	0.4810	6.8523169	1.6456253	8.1328863
H4A	0.2335	0.7330	0.2965	3.4355823	2.9655314	5.0137659
H4B	0.1629	0.6865	0.3254	1.7823541	2.7773242	5.5016758
H4C	0.2013	0.3400	0.3007	2.7298780	1.3754199	5.0832209
H6A	0.5248	0.9996	0.6949	7.5755215	4.0444435	11.7484042
H6B	0.5921	0.9287	0.6609	9.1862866	3.7575244	11.1741827
H6C	0.5670	0.6264	0.7161	8.3664434	2.5343396	12.1066185
O1A	0.1345	1.1656	0.0253	2.7343433	4.7160265	0.4278722
O2A	0.1467	0.7607	0.1598	2.2965515	3.0776150	2.7018491
O3A	0.0450	0.5702	0.0985	0.4471008	2.3070288	1.6661944
O4A	0.1109	0.9921	-0.1384	3.0812092	4.0137594	-2.3406591
O5A	0.2068	0.7163	-0.0981	4.9141965	2.8981470	-1.6589412
C1A	0.0977	0.8671	0.0215	1.9704406	3.5080138	0.3629990
C2A	0.1593	0.8731	-0.0005	3.3955910	3.5323539	-0.0084367
C3A	0.1006	0.7267	0.1014	1.6165010	2.9403255	1.7142448
C4A	0.0412	0.4327	0.1731	-0.0206426	1.7505274	2.9272230
C5A	0.1549	0.8694	-0.0870	3.7503535	3.5176754	-1.4708478
C6A	0.2088	0.6978	-0.1793	5.3770275	2.8231521	-3.0310505
H1A	0.0521	0.8659	-0.0278	1.2549506	3.5031870	-0.4700390
H2A	0.2042	0.7675	0.0398	4.1440115	3.1051028	0.6732136
H4D	0.0810	0.2659	0.1956	0.7104313	1.0758210	3.3078901
H4E	-0.0044	0.3069	0.1640	-0.9440873	1.2416705	2.7722002
H4F	0.0444	0.6288	0.2144	-0.1660945	2.5441914	3.6243435
H6D	0.1684	0.5537	-0.2132	4.6928131	2.2404009	-3.6041393
H6E	0.2537	0.5879	-0.1812	6.3446944	2.3786493	-3.0627685
H6F	0.2052	0.9406	-0.2036	5.4273302	3.8057556	-3.4429116

Table A.87: Experimental fractional and cartesian coordinates (exp. geom.) of niphepoxide (**9**)

atom	xf	yf	zf	x	y	z
O1	0.2585	0.5831	0.1751	4.8774064	3.9460211	1.9870408
O2	0.2297	1.2458	0.5405	8.4616520	8.2784164	6.1325255
O3	0.2377	1.0688	0.6860	8.2945232	6.8973556	7.7830002
O4	0.6248	0.6166	0.0688	7.5026164	4.2804798	0.7799927
O5	0.7623	0.4158	0.2008	8.2015155	2.7443148	2.2779654
O6	0.4037	0.1801	0.1686	4.3862972	1.1131902	1.9125937
O7	0.7102	0.1531	0.0681	6.3279511	1.0160886	0.7728453
N1	0.2403	1.0995	0.5832	8.1032915	7.2086252	6.6160346
C1	0.2926	0.5350	0.2889	5.3200764	3.5024968	3.2781454
C2	0.4606	0.4438	0.1780	5.9009851	2.9620796	2.0195902
C3	0.2798	0.6838	0.3635	6.0518581	4.4823997	4.1242238
C4	0.2833	0.8460	0.3162	6.5673510	5.6683542	3.5868138
C5	0.2631	0.6596	0.4836	6.2158896	4.2010857	5.4864400
C6	0.2519	0.7951	0.5562	6.9006315	5.0888299	6.3100777
C7	0.2720	0.9824	0.3879	7.2522318	6.5631411	4.4007513
C8	0.2562	0.9541	0.5065	7.4019733	6.2547545	5.7463128
C9	0.6240	0.5033	0.1406	7.2813271	3.4161114	1.5946223
C10	0.9250	0.4640	0.1793	9.5822651	3.1033658	2.0344864
C11	0.5201	0.2436	0.1385	5.4415509	1.5887480	1.5707974
C12	0.7761	-0.0353	0.0207	5.9388374	-0.2677995	0.2347432
H1	0.2261	0.4487	0.3367	4.6183010	2.8507070	3.8199233
H4	0.2892	0.8725	0.2245	6.4204982	5.9399107	2.5466080
H5	0.2591	0.5349	0.5209	5.8127657	3.2884460	5.9101032
H6	0.2397	0.7762	0.6491	7.0328816	4.8702302	7.3641246
H7	0.2765	1.1056	0.3484	7.6466557	7.4678809	3.9526506
H10A	1.0045	0.4378	0.0876	9.7974559	3.0035558	0.9938948
H10B	1.0307	0.3793	0.2284	10.2250355	2.4616417	2.5913761
H10C	0.8599	0.6110	0.2056	9.7454771	4.1148762	2.3320479
H12A	0.7685	-0.1229	0.0914	5.7623192	-0.9502336	1.0372561
H12B	0.9309	-0.0966	-0.0338	6.7184546	-0.6496780	-0.3839324
H12C	0.6779	-0.0270	-0.0300	5.0466757	-0.1627285	-0.3399471

Table A.88: Experimental fractional and cartesian coordinates of cyano-epoxide (**10**)

atom	xf	yf	zf	x	y	z
O1	0.1469	0.6576	0.0870	1.0380012	3.9992982	0.9752751
N1	0.3097	0.8134	0.3819	1.3422291	4.9470137	4.2826526
N2	0.0606	0.1989	0.2219	-0.3636617	1.2096186	2.4880066
N3	0.5246	0.7798	0.1741	4.2880382	4.7428409	1.9516378
N4	0.2721	0.1718	0.0037	2.5925422	1.0447781	0.0418353
C1	0.2017	0.5515	0.2003	1.0809443	3.3544420	2.2459090
C2	0.2840	0.5420	0.1149	2.2333360	3.2966447	1.2888324
C3	0.2596	0.6951	0.3030	1.1990708	4.2278415	3.3970022
C4	0.1223	0.3567	0.2140	0.2617052	2.1695406	2.3992789
C5	0.4181	0.6745	0.1433	3.3978156	4.1021509	1.6065498
C6	0.2797	0.3382	0.0512	2.4637066	2.0568837	0.5735395

Geometries of Compounds 7 to 10

Table A.89: Bond distances (Å) in etox (**7**)

Exp = experimental, theo: first row = optimised geometry of periodic-boundary calculation, second row = optimised geometry of isolated-molecule calculation

bond	exp	theo	bond	exp	theo
O1–C1	1.4338(7)	1.4486	C1–H2	1.0986	1.0885
		1.4280			1.0846
O1–C2	1.4411(7)	1.4536	C2–H3	1.0982	1.0874
		1.4276			1.0847
C1–C2	1.4572(8)	1.4681	C2–H4	1.0991	1.0880
		1.4638			1.0846
C1–H1	1.0991	1.0883			
		1.0846			

Table A.90: Bond angles (°) in etox (**7**)

Exp = experimental, theo: first row = optimised geometry of periodic-boundary calculation, second row = optimised geometry of isolated-molecule calculation

angle	exp	theo	angle	exp	theo
C1–O1–C2	60.91(4)	60.78	H1–C1–H2	118.58	115.77
		61.68			115.51
O1–C1–C2	59.79(3)	59.78	O1–C2–H3	114.37	113.98
		59.15			115.29
O1–C2–C1	59.30(3)	59.44	O1–C2–H4	114.68	114.86
		59.18			115.29
O1–C1–H1	113.37	114.16	C1–C2–H3	118.25	118.91
		115.29			119.53
O1–C1–H2	113.53	115.66	C1–C2–H4	118.72	118.99
		115.31			119.56
C2–C1–H1	119.96	119.27	H3–C2–H4	117.74	117.13
		119.55			115.53
C2–C1–H2	117.01	119.72			
		119.57			

Table A.91: Torsion angles (°) in etox (**7**)

Exp = experimental, theo: first row = optimised geometry of periodic-boundary calculation, second row = optimised geometry of isolated-molecule calculation

angle	exp	theo	angle	exp	theo
C2–O1–C1–H1	112.2(1)	111.0	H1–C1–C2–O1	-101.2(1)	-102.5
		110.7			-103.5
C2–O1–C1–H2	-108.6(1)	-110.9	H1–C1–C2–H3	155.8(1)	155.2
		-110.7			153.0
C1–O1–C2–H3	109.6(1)	110.6	H1–C1–C2–H4	2.0(1)	0.9
		110.7			0.0
C1–O1–C2–H4	-110.0(1)	-110.3	H2–C1–C2–O1	102.8(1)	104.2
		-110.7			103.5
O1–C1–C2–H3	-103.0(1)	-102.3	H2–C1–C2–H3	-0.2(1)	1.9
		-103.5			0.0
O1–C1–C2–H4	103.2(1)	103.4	H2–C1–C2–H4	-154.0(1)	-152.5
		103.5			-153.0

Table A.92: Bond distances (Å) in moc-epoxide (**8**)
Exp = experimental, theo: first row = optimised geometry of periodic-boundary calculation, second row = optimised geometry of isolated-molecule calculation

bond	exp	theo	bond	exp	theo
O1–C1	1.4241(16)	1.4311	O1A–C1A	1.4305(18)	1.4330
		1.4158			
O1–C2	1.4273(18)	1.4337	O1A–C2A	1.4242(18)	1.4317
		1.4158			
C1–C2	1.4718(10)	1.4769	C1A–C2A	1.4730(10)	1.4766
		1.4793			
O2–C3	1.2088(12)	1.2200	O2A–C3A	1.2070(10)	1.2197
		1.2020			
O3–C3	1.3299(12)	1.3382	O3A–C3A	1.3306(12)	1.3389
		1.3432			
O3–C4	1.4519(11)	1.4530	O3A–C4A	1.4554(13)	1.4518
		1.4394			
O4–C5	1.2081(10)	1.2193	O4A–C5A	1.2045(14)	1.2199
		1.2020			
O5–C5	1.3327(12)	1.3395	O5A–C5A	1.3317(13)	1.3389
		1.3432			
O5–C6	1.4520(13)	1.4505	O5A–C6A	1.4501(11)	1.4518
		1.4394			
C1–C3	1.5073(10)	1.5050	C1A–C3A	1.5079(13)	1.5068
		1.5036			
C2–C5	1.5070(12)	1.5062	C2A–C5A	1.5050(10)	1.5047
		1.5036			
C1–H1	1.0990	1.0851	C1A–H1A	1.0982	1.0861
		1.0827			
C2–H2	1.0985	1.0859	C2A–H2A	1.0989	1.0846
		1.0827			
C4–H4A	1.0660	1.0900	C4A–H4D	1.0653	1.0908
		1.0882			
C4–H4B	1.0662	1.0880	C4A–H4E	1.0658	1.0901
		1.0884			
C4–H4C	1.0662	1.0906	C4A–H4F	1.0663	1.0911
		1.0851			
C6–H6A	1.0659	1.0911	C6A–H6D	1.0660	1.0907
		1.0851			
C6–H6B	1.0662	1.0902	C6A–H6E	1.0653	1.0885
		1.0882			
C6–H6C	1.0652	1.0905	C6A–H6F	1.0665	1.0891
		1.0884			

Table A.93: Bond angles (°) in moc-epoxide (**8**)

Exp = experimental, theo: first row = optimised geometry of periodic-boundary calculation, second row = optimised geometry of isolated-molecule calculation

angle	exp	theo	angle	exp	theo
C1–O1–C2	62.15(8)	62.06	C1A–O1A–C2A	62.13(8)	62.05
		62.99			
O1–C1–C2	59.03(8)	59.05	O1A–C1A–C2A	58.73(9)	58.93
		58.50			
O1–C2–C1	58.82(7)	58.88	O1A–C2A–C1A	59.15(9)	59.02
		58.51			
C3–O3–C4	115.71(7)	118.05	C3A–O3A–C4A	115.66(7)	117.57
		115.67			
C5–O5–C6	116.01(7)	117.15	C5A–O5A–C6A	115.88(8)	116.43
		115.67			
O1–C1–C3	114.58(9)	114.83	O1A–C1A–C3A	113.75(9)	115.10
		116.10			
C2–C1–C3	117.97(6)	118.05	C2A–C1A–C3A	117.34(8)	119.12
		118.18			
O1–C2–C5	114.54(8)	114.98	O1A–C2A–C5A	114.55(11)	114.63
		116.10			
C1–C2–C5	117.95(8)	118.95	C1A–C2A–C5A	118.23(7)	118.02
		118.18			
O2–C3–O3	125.28(8)	125.28	O2A–C3A–O3A	125.38(9)	125.21
		124.96			
O2–C3–C1	124.23(8)	124.45	O2A–C3A–C1A	123.92(9)	125.01
		125.08			
O3–C3–C1	110.49(7)	110.26	O3A–C3A–C1A	110.68(7)	109.76
		109.96			
O5–C5–C2	110.31(7)	110.12	O4A–C5A–O5A	125.13(8)	125.10
		109.96			
O4–C5–O5	125.32(9)	124.91	O4A–C5A–C2A	124.51(10)	124.42
		124.96			
O4–C5–C2	124.35(9)	124.94	O5A–C5A–C2A	110.36(8)	110.49
		125.08			
O1–C1–H1	113.14	115.46	O1A–C1A–H1A	112.72	116.06
		115.38			
C2–C1–H1	117.58	119.02	C2A–C1A–H1A	116.05	118.63
		118.60			
C3–C1–H1	119.47	117.14	C3A–C1A–H1A	121.68	116.29
		116.93			
C5–C2–H2	115.12	116.41	O1A–C2A–H2A	116.70	115.46
		116.93			
O1–C2–H2	120.85	115.90	C1A–C2A–H2A	119.75	119.18
		115.38			
C1–C2–H2	118.11	118.83	C5A–C2A–H2A	116.00	117.16
		118.59			
O3–C4–H4B	109.68	105.51	O3A–C4A–H4D	109.35	110.94
		105.59			
H4A–C4–H4C	109.46	109.61	O3A–C4A–H4E	109.57	105.04
		109.11			
O3–C4–H4C	109.76	109.90	O3A–C4A–H4F	109.02	110.48
		110.29			
H4A–C4–H4B	108.82	110.84	H4D–C4A–H4E	110.13	110.94
		110.74			
O3–C4–H4A	109.42	109.69	H4D–C4A–H4F	109.35	109.97
		110.36			
H4B–C4–H4C	109.67	111.23	H4E–C4A–H4F	109.41	110.85
		110.71			
O5–C6–H6C	109.69	110.92	O5A–C6A–H6D	109.39	109.61
		110.37			
H6A–C6–H6C	109.62	109.67	O5A–C6A–H6E	109.85	105.49
		109.12			
H6B–C6–H6C	109.66	110.63	O5A–C6A–H6F	109.44	110.11
		110.74			
H6A–C6–H6B	108.91	111.19	H6D–C6A–H6E	109.81	111.17
		110.51			
O5–C6–H6A	109.38	109.26	H6D–C6A–H6F	109.05	109.26
		110.28			
O5–C6–H6B	109.55	105.10	H6E–C6A–H6F	109.28	111.16
		105.59			

Table A.94: Torsion angles (°) in moc-epoxide (**8**)

Exp = experimental, theo: first row = optimised geometry of periodic-boundary calculation, second row = optimised geometry of isolated-molecule calculation

angle	exp	theo	angle	exp	theo
C2–O1–C1–C3	109.1(1)	109.1	C2A–O1A–C1A–C3A	108.7(1)	110.2
		108.5			
C1–O1–C2–C5	109.0(1)	110.0	C1A–O1A–C2A–C5A	109.4(1)	109.1
		108.5			
C4–O3–C3–O2	-3.5(2)	-1.4	C4A–O3A–C3A–O2A	0.2(2)	1.7
		-0.6			
C4–O3–C3–C1	177.3(1)	178.8	C4A–O3A–C3A–C1A	-178.2(1)	-179.9
		178.6			
C6–O5–C5–O4	0.7(2)	2.8	C6A–O5A–C5A–C2A	-179.6(1)	-179.4
		-0.6			
C6–O5–C5–C2	-177.5(1)	-178.8	C6A–O5A–C5A–O4A	-0.6(2)	-1.0
		178.6			
C2–C1–C3–O2	30.7(2)	39.6	O1A–C1A–C2A–C5A	-103.2(2)	-103.4
		35.9			
O1–C1–C3–O2	-35.9(2)	-27.1	C3A–C1A–C2A–O1A	-102.5(1)	-103.4
		-30.7			
C2–C1–C3–O3	-150.1(1)	-140.5	C3A–C1A–C2A–C5A	154.3(1)	153.3
		-143.3			
C3–C1–C2–C5	153.5(1)	153.1	O1A–C1A–C3A–O3A	148.5(1)	144.0
		150.2			
O1–C1–C2–C5	-103.2(1)	-103.3	C2A–C1A–C3A–O2A	35.9(2)	32.5
		-104.9			
O1–C1–C3–O3	143.4(1)	152.8	C2A–C1A–C3A–O3A	-145.7(1)	-149.1
		150.1			
C3–C1–C2–O1	-103.3(1)	-103.6	O1A–C1A–C3A–O2A	-29.8(2)	-34.5
		-104.9			
O1–C2–C5–O5	149.9(1)	142.2	O1A–C2A–C5A–O4A	-34.9(2)	-28.3
		150.2			
C1–C2–C5–O4	38.0(2)	30.6	C1A–C2A–C5A–O4A	31.8(2)	38.3
		35.9			
O1–C2–C5–O4	-28.3(2)	-36.2	C1A–C2A–C5A–O5A	-149.1(1)	-142.1
		-30.6			
C1–C2–C5–O5	-143.8(1)	-151.0	O1A–C2A–C5A–O5A	144.1(1)	151.4
		-143.3			

Table A.95: Bond distances (Å) in niphe-epoxide (**9**)
Exp = experimental, theo: first row = optimised geometry of periodic-boundary calculation, second row = optimised geometry of isolated-molecule calculation

bond	exp	theo	bond	exp	theo
O1–C1	1.4352(7)	1.4356	C3–C5	1.4006(7)	1.4050
		1.4255			1.3972
O1–C2	1.4202(7)	1.4277	C4–C7	1.3901(8)	1.3909
		1.4198			1.3865
C1–C2	1.4878(7)	1.4971	C5–C6	1.3912(8)	1.3915
		1.4856			1.3847
O2–N1	1.2275(9)	1.2403	C6–C8	1.3888(7)	1.3965
		1.2216			1.3877
O3–N1	1.2228(9)	1.2372	C7–C8	1.3885(7)	1.3944
		1.2222			1.3869
O4–C9	1.2083(7)	1.2163	C1–H1	1.1004	1.0889
		1.2000			1.0853
O5–C9	1.3285(7)	1.3369	C4–H4	1.0850	1.0830
		1.3399			1.0795
O5–C10	1.4473(9)	1.4572	C5–H5	1.0839	1.0861
		1.4406			1.0821
O6–C11	1.2069(8)	1.2207	C6–H6	1.0846	1.0827
		1.2022			1.0785
O7–C11	1.3230(7)	1.3275	C7–H7	1.0839	1.0810
		1.3361			1.0786
O7–C12	1.4454(7)	1.4555	C10–H10A	1.0673	1.0884
		1.4413			1.0882
N1–C8	1.4690(7)	1.4621	C10–H10B	1.0654	1.0867
		1.4764			1.0850
C1–C3	1.4871(7)	1.4906	C10–H10C	1.0669	1.0913
		1.4869			1.0879
C2–C9	1.5140(7)	1.5183	C12–H12A	1.0681	1.0886
		1.5130			1.0881
C2–C11	1.5160(6)	1.5209	C12–H12B	1.0660	1.0886
		1.5210			1.0848
C3–C4	1.4004(7)	1.4023	C12–H12C	1.0664	1.0905
		1.3955			1.0878

Table A.96: Bond angles (°) in niphe-epoxide (**9**)

Exp = experimental, theo: first row = optimised geometry of periodic-boundary calculation, second row = optimised geometry of isolated-molecule calculation

angle	exp	theo	angle	exp	theo
C1–O1–C2	62.80(3)	63.05	O5–C9–C2	109.60(4)	110.30
		62.95			109.53
O1–C1–C2	58.10(3)	58.22	O6–C11–O7	125.87(5)	125.46
		58.34			125.02
O1–C2–C1	59.09(3)	58.73	O6–C11–C2	122.55(5)	122.08
		58.71			123.97
C9–O5–C10	116.67(5)	117.02	O7–C11–C2	111.57(4)	112.46
		115.84			110.95
C11–O7–C12	115.39(5)	116.35	O1–C1–H1	115.42	113.84
		115.99			113.92
O2–N1–O3	123.51(7)	123.78	C2–C1–H1	116.76	115.13
		124.73			114.30
O2–N1–C8	118.17(6)	118.09	C3–C1–H1	115.09	115.58
		117.66			115.68
O3–N1–C8	118.32(6)	118.13	C3–C4–H4	122.01	119.87
		117.61			119.45
O1–C1–C3	117.39(4)	117.57	C7–C4–H4	117.84	119.79
		118.42			120.34
C2–C1–C3	121.90(5)	123.75	C3–C5–H5	120.38	120.18
		123.69			119.82
O1–C2–C9	116.29(4)	115.52	C6–C5–H5	119.27	119.35
		116.33			119.54
O1–C2–C11	113.73(4)	113.01	C5–C6–H6	120.45	120.92
		112.96			121.73
C1–C2–C9	118.98(4)	119.27	C8–C6–H6	121.31	120.63
		120.45			119.69
C1–C2–C11	117.46(4)	116.76	C4–C7–H7	118.32	120.26
		116.89			121.44
C9–C2–C11	117.70(4)	118.83	C8–C7–H7	123.14	121.03
		117.54			119.59
C1–C3–C4	121.39(4)	121.11	O5–C10–H10A	109.46	110.86
		121.77			110.16
C1–C3–C5	118.59(4)	119.03	O5–C10–H10B	109.77	105.49
		118.57			105.54
C4–C3–C5	120.02(5)	119.82	O5–C10–H10C	109.52	109.23
		119.65			110.31
C3–C4–C7	120.12(5)	120.33	H10A–C10–H10B	109.37	109.29
		120.21			110.75
C3–C5–C6	120.35(5)	120.46	H10A–C10–H10C	109.25	110.67
		120.64			109.32
C5–C6–C8	118.24(5)	118.44	H10B–C10–H10C	109.45	111.19
		118.58			110.73
C4–C7–C8	118.53(5)	118.71	O7–C12–H12A	109.41	109.95
		118.98			110.16
N1–C8–C6	118.50(4)	118.97	O7–C12–H12B	109.72	105.27
		118.95			105.48
N1–C8–C7	118.75(4)	118.78	O7–C12–H12C	109.77	109.95
		119.11			110.18
C6–C8–C7	122.74(5)	122.24	H12A–C12–H12B	109.15	110.58
		121.95			110.81
O4–C9–O5	125.57(6)	125.67	H12A–C12–H12C	109.24	110.26
		125.34			109.36
O4–C9–C2	124.80(5)	123.99	H12B–C12–H12C	109.54	110.72
		125.12			110.81

Table A.97: Torsion angles (°) in niphe-epoxide (**9**)

Exp = experimental, theo: first row = optimised geometry of periodic-boundary calculation, second row = optimised geometry of isolated-molecule calculation

angle	exp	theo	angle	exp	theo
C2–O1–C1–C3	112.3(1)	114.4	O1–C2–C9–O5	147.6(1)	154.6
		114.0			164.1
C1–O1–C2–C9	-109.5(1)	-110.1	C1–C2–C9–O4	-98.5(1)	-90.1
		-111.2			-82.3
C1–O1–C2–C11	108.9(1)	113.0	C1–C2–C9–O5	80.00(1)	87.6
		108.5			96.5
C10–O5–C9–O4	1.1(1)	125.7	C11–C2–C9–O4	109.2(1)	116.1
		-2.6			123.8
C10–O5–C9–C2	-177.3(1)	-175.8	C11–C2–C9–O5	-72.4(1)	-66.2
		178.6			-57.4
C12–O7–C11–O6	2.8(1)	0.4	O1–C2–C11–O6	-42.7(1)	-45.0
		-0.4			-63.6
C12–O7–C11–C2	-176.7(1)	-179.9	C1–C2–C11–O7	-157.00(1)	-160.2
		-177.8			179.2
O2–N1–C8–C6	-175.0(1)	-171.9	O1–C2–C11–O7	136.8(1)	134.5
		-179.7			113.8
O2–N1–C8–C7	4.2(1)	6.5	C1–C2–C11–O6	23.5(1)	20.3
		0.0			1.7
O3–N1–C8–C6	4.7(1)	7.6	C9–C2–C11–O6	176.3(1)	174.8
		0.4			156.5
O3–N1–C8–C7	-176.1(1)	-174.0	C9–C2–C11–O7	-4.2(1)	-5.7
		-179.9			-28.0
C2–C1–C3–C4	53.0(1)	56.5	C1–C3–C5–C6	179.7(1)	177.9
		61.8			-179.7
C2–C1–C3–C5	-127.3(1)	-125.8	C1–C3–C4–C7	-179.7(1)	-177.5
		-119.4			179.4
O1–C1–C2–C9	105.0(1)	103.7	C5–C3–C4–C7	0.5(1)	0.1
		104.2			0.6
O1–C1–C2–C11	-102.6(1)	-101.9	C4–C3–C5–C6	-0.6(1)	-0.2
		-101.8			-0.9
C3–C1–C2–O1	-104.5(1)	-103.9	C3–C4–C7–C8	-0.4(1)	0.0
		-105.1			0.1
C3–C1–C2–C9	0.5(1)	0.2	C3–C5–C6–C8	0.5(1)	0.7
		-1.0			0.5
C3–C1–C2–C11	152.9(1)	154.2	C5–C6–C8–N1	178.8(1)	177.5
		153.1			179.8
O1–C1–C3–C4	-14.8(1)	-12.0	C5–C6–C8–C7	-0.3(1)	-0.8
		-7.3			0.1
O1–C1–C3–C5	165.0(1)	165.7	C4–C7–C8–N1	-178.9(1)	-177.9
		171.5			179.9
O1–C2–C9–O4	-30.9(1)	-23.2	C4–C7–C8–C6	0.2(1)	0.5
		-14.7			-0.4

Table A.98: Bond distances in cyano-epoxide (**10**)

Exp = experimental, theo: first row = optimised geometry of periodic-boundary calculation, second row = optimised geometry of isolated-molecule calculation

bond	exp	theo	bond	exp	theo
O1–C1	1.4256(3)	1.4331	N4–C6	1.1505(3)	1.1589
		1.4233			1.1490
O1–C2	1.4216(3)	1.4287	C1–C3	1.4498(3)	1.4535
		1.4237			1.4476
C1–C2	1.4991(3)	1.5193	C1–C4	1.4486(3)	1.4530
		1.5174			1.4477
N1–C3	1.1498(3)	1.1579	C2–C5	1.4511(3)	1.4547
		1.1490			1.4477
N2–C4	1.1491(3)	1.1584	C2–C6	1.4497(3)	1.4535
		1.1490			1.4478
N3–C5	1.1498(3)	1.1580			
		1.1490			

Table A.99: Bond angles (°) in cyano-epoxide (**10**)

Exp = experimental, theo: first row = optimised geometry of periodic-boundary calculation, second row = optimised geometry of isolated-molecule calculation

angle	exp	theo	angle	exp	theo
C1–O1–C2	63.54(3)	64.13	O1–C2–C6	116.58(3)	115.91
		64.38			116.62
O1–C1–C2	58.10(3)	57.79	C1–C2–C5	117.11(3)	118.53
		57.81			119.34
O1–C2–C1	58.36(3)	58.08	C1–C2–C6	118.04(3)	119.33
		57.81			119.34
O1–C1–C3	115.95(3)	115.28	C5–C2–C6	117.08(3)	116.09
		116.69			115.00
O1–C1–C4	116.57(3)	116.00	N1–C3–C1	176.89(3)	177.39
		116.69			179.15
C2–C1–C3	117.87(3)	118.74	N2–C4–C1	177.72(3)	178.77
		119.34			179.15
C2–C1–C4	118.08(3)	119.19	N3–C5–C2	175.07(3)	178.47
		119.34			179.15
C3–C1–C4	117.05(3)	116.48	N4–C6–C2	176.48(4)	178.52
		115.00			179.15
O1–C2–C5	116.66(3)	116.06			
		116.62			

Table A.100: Torsion angles (°) in cyano-epoxide (**10**)

Exp = experimental, theo: first row = optimised geometry of periodic-boundary calculation, second row = optimised geometry of isolated-molecule calculation

angle	exp	theo	angle	exp	theo
C2–O1–C1–C3	108.0(3)	109.3	C3–C1–C2–O1	-104.7(3)	103.3
		109.4			-104.6
C2–O1–C1–C4	-108.0(3)	-109.5	C3–C1–C2–C5	1.4(3)	1.2
		-109.3			0.0
C1–O1–C2–C5	-106.8(3)	-108.8	C3–C1–C2–C6	149.8(3)	152.8
		-109.4			150.5
C1–O1–C2–C6	108.0(3)	109.8	C4–C1–C2–O1	105.4(3)	104.0
		109.3			104.7
O1–C1–C2–C5	106.1(3)	104.5	C4–C1–C2–C5	-148.6(3)	-151.5
		104.7			-150.5
O1–C1–C2–C6	-105.5(3)	-103.9	C4–C1–C2–C6	-0.1(4)	-0.1
		-104.7			0.0

Table A.101: Hydrogen-bonding pattern of etox (**7**): H$\cdots$O distance in Å, C$\cdots$O distance in Å, C-H$\cdots$O angle in °, electron density (ϱ) at H$\cdots$O bcp in eÅ^{-3}, Laplacian ($\nabla^2\varrho$) at H$\cdots$O bcp in eÅ^{-5}, interaction energy (E_{int}) of hydrogen-bonded symmetry-related (sym) molecules

First row: exp, second/third row: periodic-boundary calculations at experimental/ optimised geometries

labels	H$\cdots$O	C$\cdots$O	C-H$\cdots$O	ϱ	$\nabla^2\varrho$	E_{int}	sym
C1–H1$\cdots$O1	2.584	3.579	150.20	0.03(1)	0.5(1)	-3.56	1/2+x, 3/2-y, 1/2+z
SP periodic				0.05	0.6	-1.45	
opt periodic	–	–	–	–	–	–	–
C1–H2$\cdots$O1	2.520	3.481	145.42	0.05(1)	0.7(1)	-4.29	1/2-x, 1/2+y, 1/2-z
SP periodic				0.06	0.7	-5.56	
opt periodic	2.453	3.470	154.89	0.07	0.7	-5.58	
C2–H3$\cdots$O1	–	–	–	–	–	–	–
SP periodic	–	–	–	–	–	–	–
opt periodic	2.502	3.377	136.73	0.06	0.8	-4.90	-x, -y, -z
C2–H4$\cdots$O1	2.519	3.503	148.39	0.03(1)	0.5(1)	-4.78	-1/2+x, 3/2-y, 1/2+z
SP periodic				0.05	0.6	-4.52	
opt periodic	2.596	3.529	143.40	0.05	0.5	-4.43	-1/2+x, -1/2-y, 1/2+z

Table A.102: Hydrogen-bonding pattern of moc-epoxide (**8**): H···O distance in Å, C···O distance in Å, C-H···O angle in °, electron density (ϱ) at H···O bcp in eÅ^{-3}, Laplacian ($\nabla^2\varrho$) at H···O bcp in eÅ^{-5}, interaction energy (E_{int}) of hydrogen-bonded symmetry-related (sym) molecules

First row: exp, second/third row: periodic-boundary calculations at experimental/ optimised geometries

labels	H···O	C···O	C-H···O	ϱ	$\nabla^2\varrho$	E_{int}	sym
C1–H1···O3	2.571	3.102	108.60	0.05	0.9	-9.84	1/2-x, -1/2+y, 1-z
SP periodic				0.05	0.9	-10.15	
opt periodic	2.580	3.369	128.91	0.05	0.7	-6.85	
C2–H2···O5	2.352	3.391	157.28	0.07	1.0	-4.72	1-x, y, 1-z
SP periodic				0.07	1.0	-4.85	
opt periodic	2.351	3.410	164.32	0.08	0.9	-4.78	
C4–H4A···O2A	2.580	2.969	100.70	0.06	0.9	-8.08	intra asu
SP periodic				0.06	0.9	-8.36	
opt periodic	2.763	3.269	108.03	0.03	0.5	-5.05	
C4–H4B···O4	2.543	3.602	172.38	0.06	0.6	-9.89	1/2-x, 1/2+y, 1-z
SP periodic				0.06	0.6	-10.25	
opt periodic	2.380	3.465	175.01	0.08	0.9	-6.84	
C6–H6A···O4	2.689	3.647	149.55	0.05	0.5	-11.51	x, 1+y, z
SP periodic				0.05	0.5	-12.64	
opt periodic	2.644	3.580	143.55	0.05	0.6	-10.04	
C6–H6B···O2	2.414	3.472	171.48	0.08	0.8	-9.96	1-x, 1+y, 1-z
SP periodic				0.08	0.8	-10.14	
opt periodic	2.621	3.707	173.67	0.05	0.5	-8.59	
C6–H6C···O4A	2.526	3.462	146.02	0.06	0.6	-7.12	1/2+x, -1/2+y, 1+z
SP periodic				0.06	0.6	-7.26	
opt periodic	2.602	3.431	132.24	0.05	0.5	-10.38	
C1A–H1A···O3A	2.400	3.377	147.41	0.07	0.9	-6.03	-x, y, -z
SP periodic				0.07	0.9	-6.14	
opt periodic	2.352	3.403	162.55	0.08	1.0	-5.55	
C2A–H2A···O5A	2.609	3.193	112.32	0.05	0.8	-6.68	1/2-x, 1/2+y, -z
SP periodic				0.05	0.8	-6.88	
opt periodic	2.572	3.326	125.89	0.04	0.7	-5.91	
C4A–H4D···O2A	2.657	3.579	144.63	0.05	0.6	-13.21	1/2-x, -1/2+y, -z
SP periodic				0.05	0.6	-14.31	
opt periodic	2.671	3.611	144.06	0.04	0.5	-16.56	
C4A–H4E···O4A	2.525	3.590	177.58	0.06	0.6	-9.33	-x, -1+y, -z
SP periodic				0.06	0.6	-9.47	
opt periodic	2.581	3.661	170.87	0.05	0.5	-9.52	
C4A–H4F···O4	2.520	3.570	168.21	0.06	0.6	-7.52	1/2-x, 1/2+y, 1-z
SP periodic				0.06	0.6	-7.60	
opt periodic	2.488	3.467	148.63	0.06	0.7	-5.46	
C6A–H6E···O2A	2.434	3.479	166.60	0.07	0.9	-6.63	1/2-x, -1/2+y, -z
SP periodic				0.07	0.9	-6.82	
opt periodic	2.412	3.498	175.54	0.07	0.8	-5.90	

Table A.103: Hydrogen-bonding pattern of niphe-epoxide (**9**): H$\cdots$O distance in Å, C$\cdots$O distance in Å, C-H$\cdots$O angle in °, electron density (ϱ) at H$\cdots$O bcp in eÅ^{-3}, Laplacian ($\nabla^2\varrho$) at H$\cdots$O bcp in eÅ^{-5}, interaction energy (E_{int}) of hydrogen-bonded symmetry-related (sym) molecules

First row: exp, second/third row: periodic-boundary calculations at experimental/ optimised geometries

labels	H$\cdots$O	C$\cdots$O	C-H$\cdots$O	ϱ	$\nabla^2\varrho$	E_{int}	sym
C5–H5$\cdots$O2	2.446	3.486	160.35	0.07	0.6	-5.62	x, -1+y, z
SP periodic				0.06	0.7	-8.58	
opt periodic	2.554	3.607	162.98	0.05	0.5	-5.50	
C6–H6$\cdots$O5	2.282	3.248	147.30	0.09	0.8	-11.70	1-x, 1-y, 1-z
SP periodic				0.09	1.0	-10.40	
opt periodic	2.422	3.367	145.08	0.06	0.8	-8.14	
C7–H7$\cdots$O6	2.264	3.150	137.65	0.09	1.2	-7.22	x, 1+y, z
SP periodic				0.08	1.1	-11.44	
opt periodic	2.318	3.197	137.23	0.08	1.0	-8.80	
C10–H10A$\cdots$O4	–	–	–	–	–	–	–
SP periodic	–	–	–	–	–	–	–
opt periodic	2.571	3.534	147.06	0.05	0.6	-6.49	2-x, 1-x, -z
C10–H10B$\cdots$O6	2.433	3.237	131.39	0.07	0.9	-11.80	1+x, y, z
SP periodic				0.05	0.8	-9.24	
opt periodic	2.462	3.346	137.69	0.06	0.8	-9.00	
C10–H10C$\cdots$O3	2.628	3.663	163.46	0.04	0.7	-12.55	1-x, 2-y, 1-z
SP periodic				0.05	0.5	-14.42	
opt periodic	2.570	3.656	173.33	0.06	0.6	-14.06	
C12–H12A$\cdots$O3	2.682	3.440	127.62	0.04	0.5	-5.20	1-x, 1-y, 1-z
SP periodic				0.03	0.5	-3.47	
opt periodic	2.616	3.410	129.23	0.04	0.6	-5.43	
C12–H12B$\cdots$O7	2.503	3.461	148.99	0.06	0.5	-8.34	2-x, -y, -z
SP periodic				0.05	0.6	-6.24	
opt periodic	2.674	3.710	158.92	0.04	0.5	-3.86	
C12–H12C$\cdots$O6	2.495	3.461	150.23	0.05	0.8	-4.46	1-x, -y, -z
SP periodic				0.05	0.6	-6.09	
opt periodic	2.486	3.500	154.13	0.06	0.6	-6.80	

Table A.104: Intermolecular contact pattern of cyano-epoxide (**10**): N$\cdots$C distance in Å, electron density (ϱ) at N$\cdots$C bcp in eÅ^{-3}, Laplacian ($\nabla^2\varrho$) at N$\cdots$C bcp in eÅ^{-5}, interaction energy (E_{int}) of symmetry-related (sym) contact pair

First row: exp, second/third row: periodic-boundary calculations at experimental/ optimised geometries

labels	C$\cdots$N	ϱ	$\nabla^2\varrho$	E_{int}	sym
N1$\cdots$C5	2.932	0.08	0.9	-7.77	x, 3/2-y, 1/2+z
SP periodic		0.07	0.9	-9.88	
opt periodic	3.107	0.06	0.8	-11.00	
N2$\cdots$C4	2.993	0.07	0.8	-8.72	-x, -1/2+y, 1/2-z
SP periodic		0.06	0.8	-11.27	
opt periodic	3.272	0.05	0.8	-9.34	

Results of the Topological Analyses of the ED of Compounds 7 to 10

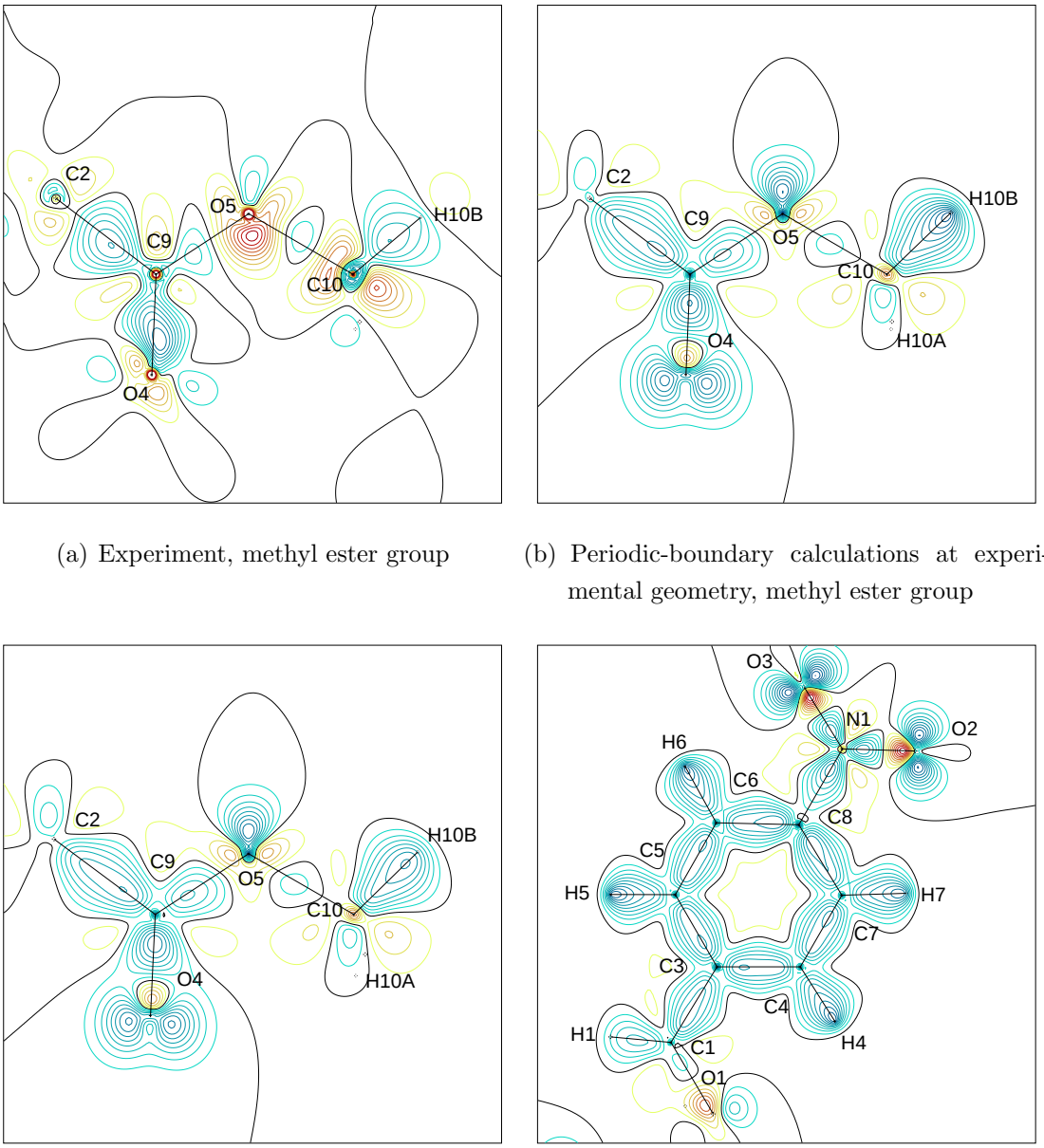

(a) Experiment, methyl ester group

(b) Periodic-boundary calculations at experimental geometry, methyl ester group

(c) periodic-boundary calculations at optimised geometry, methyl ester group

(d) periodic-boundary calculations at experimental geometry, nitro-phenyl group

Figure A.1: Static deformation-density maps in the methyl ester and nitro-phenyl group of niphe-epoxide (**9**)
Contour interval = 0.1 e Å^{-3}, blue = positive, red = negative, black = zero

Table A.105: Electron density (ϱ) at bcps in eÅ^{-3}, Laplacian ($\nabla^2\varrho$) at bcps in eÅ^{-5}, distances of the bcps to first (d1) and second (d2) atom of the bond X1–X2 in Å, and ellipticity at bcps (ε) for etox (**7**)

First row: experiment, second/third row: periodic-boundary calculation at experimental/optimised geometry, fourth/fifth row: isolated-molecule calculations at experimental/optimised geometries

bond	ϱ	$\nabla^2\varrho$	d1	d2	ε	bond	ϱ	$\nabla^2\varrho$	d1	d2	ε
O1–C1	1.66(3)	-1.8(1)	0.8282	0.6065	0.21	C1–H2	1.87(7)	-18.8(3)	0.7248	0.3745	0.03
	1.68	-3.5	0.8064	0.6283	0.49		1.91	-21.9	0.7046	0.3947	0.05
	1.64	-2.6	0.8089	0.6398	0.48		1.95	-23.3	0.6968	0.3918	0.05
	1.71	-10.0	0.8953	0.5386	0.69		1.94	-27.2	0.7079	0.3907	0.03
	1.73	-10.1	0.8968	0.5312	0.66		2.00	-28.8	0.6965	0.3881	0.03
O1–C2	1.77(4)	-10.3(1)	0.8440	0.5972	0.52	C2–H3	1.67(6)	-14.0(2)	0.7212	0.3777	0.04
	1.64	-2.6	0.8090	0.6322	0.52		1.90	-21.4	0.7023	0.3966	0.05
	1.61	-2.9	0.8162	0.6375	0.49		1.96	-23.7	0.6941	0.3933	0.05
	1.68	-9.8	0.8947	0.5464	0.73		1.95	-27.3	0.7081	0.3900	0.03
	1.73	-10.1	0.8968	0.5308	0.66		2.00	-28.8	0.6967	0.3880	0.03
C1–C2	1.68(3)	-6.6(1)	0.6887	0.7748	0.59	C2–H4	1.73(7)	-13.8(3)	0.7029	0.3969	0.04
	1.72	-8.4	0.7332	0.7303	0.40		1.92	-22.1	0.7018	0.3980	0.05
	1.68	-7.7	0.7442	0.7321	0.38		1.98	-24.4	0.6932	0.3949	0.05
	1.81	-16.7	0.7322	0.7316	0.28		1.94	-27.2	0.7087	0.3903	0.03
	1.77	-15.8	0.7352	0.7352	0.31		2.00	-28.8	0.6968	0.3879	0.03
C1–H1	1.67(6)	-12.1(3)	0.7423	0.3580	0.03	epoxide	1.39	9.4			
	1.90	-21.6	0.7051	0.3952	0.05	ring	1.38	8.6			
	1.97	-23.4	0.6924	0.3960	0.05		1.35	8.6			
	1.94	-27.2	0.7089	0.3901	0.03		1.45	6.8			
	2.00	-28.8	0.6968	0.3879	0.03		1.46	6.5			

Table A.106: Electron density (ϱ) at bcps in eÅ^{-3}, Laplacian ($\nabla^2\varrho$) at bcps in eÅ^{-5}, distances of the bcps to first (d1) and second (d2) atom of the bond X1–X2 in Å, and ellipticity at bcps (ε) for moc-epoxide (**8**)

First row: experiment, second/third row: periodic-boundary calculation at experimental/optimised geometry, fourth/fifth row: isolated-molecule calculations at experimental/optimised geometries

bond	ϱ	$\nabla^2\varrho$	d1	d2	ε	bond	ϱ	$\nabla^2\varrho$	d1	d2	ε
O1–C1	1.70	-5.4	0.8028	0.6215	0.46	O1A–C1A	1.62	-4.8	0.8113	0.6195	0.64
	1.71	-5.4	0.8026	0.6208	0.46		1.62	-4.8	0.8111	0.6187	0.64
	1.64	-3.0	0.8072	0.6239	0.45		1.59	-4.4	0.8144	0.6192	0.49
	1.75	-10.6	0.8919	0.5321	0.60						
	1.77	-11.2	0.8900	0.5261	0.49						
O1–C2	1.65	-3.0	0.8036	0.6238	0.58	O1A–C2A	1.67	-4.9	0.8029	0.6215	0.60
	1.65	-3.0	0.8034	0.6230	0.58		1.67	-5.0	0.8027	0.6205	0.60
	1.63	-2.6	0.8066	0.6273	0.51		1.62	-5.2	0.8124	0.6204	0.47
	1.74	-10.8	0.8882	0.5394	0.56						
	1.78	-10.8	0.8922	0.5238	0.57						
C1–C2	1.58	-6.5	0.7381	0.7391	0.62	C1A–C2A	1.64	-6.7	0.7339	0.7491	0.48
	1.59	-6.5	0.7375	0.7386	0.63		1.65	-6.8	0.7330	0.7484	0.48
	1.64	-7.6	0.7564	0.7284	0.49		1.61	-8.4	0.7456	0.7423	0.43
	1.73	-14.6	0.7400	0.7371	0.36						
	1.69	-13.6	0.7421	0.7424	0.41						
O2–C3	2.89	-33.3	0.7544	0.4544	0.08	O2A–C3A	2.86	-30.8	0.7608	0.4462	0.15
	2.88	-33.5	0.7542	0.4576	0.08		2.85	-31.1	0.7610	0.4490	0.15
	2.77	-34.2	0.7634	0.4572	0.09		2.83	-33.8	0.7602	0.4596	0.18
	2.88	-10.1	0.7931	0.4157	0.13						
	2.92	-8.9	0.7895	0.4127	0.14						
O3–C3	2.19	-24.7	0.8036	0.5266	0.14	O3A–C3A	2.15	-24.3	0.8059	0.5253	0.14
	2.18	-24.6	0.8036	0.5272	0.14		2.15	-24.2	0.8058	0.5265	0.14
	2.17	-25.2	0.8080	0.5305	0.10		2.16	-23.0	0.8017	0.5380	0.19
	2.16	-14.7	0.8699	0.4605	0.06						
	2.10	-15.6	0.8747	0.4688	0.05						
O3–C4	1.47	-8.5	0.8678	0.5840	0.04	O3A–C4A	1.55	-8.3	0.8482	0.6074	0.02
	1.46	-8.5	0.8679	0.5850	0.04		1.55	-8.3	0.8482	0.6071	0.02
	1.51	-9.1	0.8656	0.5874	0.00		1.56	-8.5	0.8507	0.6012	0.01
	1.59	-10.5	0.9414	0.5108	0.03						
	1.63	-10.3	0.9391	0.5007	0.01						
O4–C5	2.93	-33.3	0.7552	0.4530	0.08	O4A–C5A	2.90	-32.4	0.7596	0.4451	0.16
	2.92	-33.5	0.7550	0.4567	0.08		2.89	-32.8	0.7598	0.4479	0.16
	2.84	-34.7	0.7555	0.4639	0.18		2.82	-34.6	0.7650	0.4550	0.13
	2.88	-10.1	0.7929	0.4154	0.14						
	2.92	-8.8	0.7894	0.4127	0.13						
O5–C5	2.11	-24.2	0.8126	0.5204	0.21	O5A–C5A	2.22	-23.7	0.7925	0.5396	0.12
	2.11	-24.1	0.8126	0.5207	0.21		2.21	-23.5	0.7923	0.5413	0.12
	2.14	-24.7	0.8118	0.5285	0.17		2.23	-25.5	0.7947	0.5445	0.07
	2.14	-14.7	0.8713	0.4615	0.05						
	2.10	-15.4	0.8757	0.4678	0.06						
O5–C6	1.49	-7.1	0.8524	0.5996	0.02	O5A–C6A	1.57	-8.1	0.8455	0.6046	0.03
	1.49	-7.1	0.8524	0.5996	0.02		1.57	-8.1	0.8456	0.6049	0.03
	1.50	-7.7	0.8555	0.5950	0.00		1.58	-8.6	0.8477	0.6041	0.01
	1.59	-10.5	0.9405	0.5117	0.02						
	1.63	-10.9	0.9336	0.5061	0.01						

Table A.107: Continuation of Table A.106

bond	ϱ	$\nabla^2\varrho$	d1	d2	ε	bond	ϱ	$\nabla^2\varrho$	d1	d2	ε
C1–C3	1.75	-13.0	0.7412	0.7662	0.15	C1A–C3A	1.77	-13.4	0.7468	0.7610	0.09
	1.75	-13.0	0.7411	0.7660	0.15		1.77	-13.4	0.7468	0.7608	0.09
	1.74	-13.4	0.7280	0.7772	0.08		1.75	-13.3	0.7411	0.7657	0.10
	1.82	-18.2	0.7413	0.7660	0.10						
	1.83	-18.5	0.7383	0.7652	0.11						
C2–C5	1.73	-13.6	0.7393	0.7676	0.15	C2A–C5A	1.72	-11.6	0.7375	0.7675	0.19
	1.73	-13.6	0.7392	0.7674	0.15		1.72	-11.7	0.7372	0.7671	0.19
	1.75	-14.1	0.7426	0.7636	0.14		1.77	-13.0	0.7244	0.7803	0.13
	1.82	-18.2	0.7397	0.7673	0.11						
	1.83	-18.5	0.7385	0.7651	0.11						
C1–H1	1.87	-21.3	0.7084	0.3907	0.05	C1A–H1A	1.88	-20.7	0.7208	0.3775	0.05
	1.87	-21.3	0.7085	0.3907	0.05		1.88	-20.7	0.7213	0.3779	0.05
	1.93	-21.8	0.7027	0.3826	0.03		1.94	-21.4	0.7124	0.3738	0.05
	1.96	-27.6	0.7195	0.3795	0.03						
	2.03	-29.6	0.7070	0.3758	0.03						
C2–H2	1.90	-19.9	0.7140	0.3850	0.04	C2A–H2A	1.90	-22.1	0.7200	0.3790	0.06
	1.90	-19.8	0.7143	0.3851	0.04		1.90	-22.1	0.7202	0.3790	0.06
	1.98	-23.1	0.7094	0.3766	0.05		1.95	-22.9	0.7008	0.3838	0.08
	1.96	-27.6	0.7195	0.3791	0.03						
	2.03	-29.6	0.7070	0.3758	0.03						
C4–H4A	2.01	-25.3	0.6713	0.3950	0.05	C4A–H4D	1.99	-24.1	0.6823	0.3832	0.07
	2.02	-25.3	0.6711	0.3950	0.05		1.99	-24.0	0.6829	0.3835	0.07
	1.91	-23.2	0.6961	0.3941	0.05		1.87	-21.9	0.7138	0.3773	0.05
	2.09	-31.1	0.6815	0.3848	0.04						
	1.99	-28.5	0.7012	0.3873	0.04						
C4–H4B	1.96	-25.0	0.6852	0.3808	0.05	C4A–H4E	1.97	-23.3	0.6843	0.3817	0.07
	1.96	-25.0	0.6853	0.3808	0.05		1.97	-23.3	0.6845	0.3818	0.07
	1.92	-22.3	0.6880	0.4001	0.06		1.96	-24.5	0.7050	0.3850	0.05
	2.09	-31.2	0.6818	0.3843	0.05						
	1.99	-29.0	0.6975	0.3876	0.04						
C4–H4C	1.97	-24.4	0.6788	0.3875	0.05	C4A–H4F	2.00	-24.6	0.6830	0.3836	0.07
	1.97	-24.4	0.6787	0.3874	0.05		2.00	-24.6	0.6828	0.3835	0.07
	1.92	-23.9	0.6971	0.3937	0.05		1.96	-22.8	0.6938	0.3977	0.05
	2.09	-31.3	0.6849	0.3813	0.04						
	2.01	-28.6	0.7011	0.3871	0.04						
C6–H6A	1.98	-24.9	0.6784	0.3871	0.07	C6A–H6D	2.00	-24.9	0.6943	0.3717	0.04
	1.98	-24.8	0.6788	0.3873	0.07		2.00	-24.9	0.6944	0.3717	0.04
	1.87	-21.0	0.6923	0.3990	0.06		1.91	-22.1	0.7110	0.3799	0.05
	2.09	-31.3	0.6820	0.3834	0.04						
	1.99	-28.5	0.7012	0.3873	0.04						
C6–H6B	1.99	-24.6	0.6734	0.3926	0.07	C6A–H6E	2.03	-24.3	0.6827	0.3828	0.05
	1.99	-24.5	0.6735	0.3926	0.07		2.03	-24.3	0.6831	0.3830	0.05
	1.87	-22.5	0.7034	0.3868	0.06		1.96	-23.4	0.7069	0.3817	0.05
	2.09	-31.2	0.6820	0.3840	0.05						
	2.01	-29.0	0.6972	0.3879	0.04						
C6–H6C	2.05	-28.4	0.6758	0.3904	0.06	C6A–H6F	2.06	-25.8	0.6822	0.3845	0.05
	2.05	-28.4	0.6758	0.3904	0.06		2.06	-25.9	0.6818	0.3843	0.05
	1.91	-25.0	0.7030	0.3877	0.06		2.01	-23.4	0.6926	0.3968	0.05
	2.09	-31.3	0.6830	0.3832	0.04						
	1.99	-28.6	0.7018	0.3864	0.04						
epoxide	1.36	7.3				epoxide	1.36	7.3			
	1.36	7.3					1.36	7.3			
	1.35	8.4					1.28	8.2			
	1.46	6.2									
	1.47	5.8									

Table A.108: Electron density (ϱ) at bcps in eÅ^{-3}, Laplacian ($\nabla^2\varrho$) at bcps in eÅ^{-5}, distances of the bcps to first (d1) and second (d2) atom of the bond X1–X2 in Å, and ellipticity at bcps (ε) for niphe-epoxide (**9**)

First row: experiment, second/third row: periodic-boundary calculation at experimental/optimised geometry, fourth/fifth row: isolated-molecule calculations at experimental/optimised geometries

bond	ϱ	$\nabla^2\varrho$	d1	d2	ε	bond	ϱ	$\nabla^2\varrho$	d1	d2	ε
O1–C1	1.71(4)	-16.6(2)	0.8830	0.5605	0.35	C3–C5	2.20(5)	-29.1(2)	0.8009	0.5998	0.09
	1.70	-3.3	0.7984	0.6370	0.37		2.07	-16.8	0.7050	0.6955	0.22
	1.70	-3.5	0.7984	0.6375	0.33		2.06	-16.8	0.7069	0.6982	0.21
	1.71	-10.7	0.8968	0.5384	0.54		2.14	-24.8	0.7078	0.6928	0.19
	1.74	-10.7	0.8983	0.5274	0.51		2.16	-25.2	0.7060	0.6912	0.19
O1–C2	1.72(4)	-7.9(2)	0.8413	0.5793	0.62	C4–C7	2.12(4)	-18.1(1)	0.6692	0.7209	0.08
	1.76	-4.2	0.7902	0.6311	0.36		2.09	-16.8	0.6875	0.7031	0.21
	1.74	-3.9	0.7917	0.6362	0.37		2.09	-17.0	0.6904	0.7005	0.20
	1.78	-11.8	0.8862	0.5342	0.51		2.18	-25.8	0.6883	0.7018	0.19
	1.77	-11.6	0.8873	0.5327	0.54		2.19	-26.1	0.6860	0.7005	0.19
C1–C2	1.52(3)	-8.4(1)	0.7318	0.7661	0.52	C5–C6	2.14(4)	-19.5(1)	0.6901	0.7013	0.20
	1.60	-5.9	0.7403	0.7545	0.56		2.09	-16.6	0.6913	0.6987	0.20
	1.57	-5.5	0.7406	0.7629	0.57		2.09	-16.9	0.6917	0.6997	0.21
	1.68	-13.2	0.7333	0.7603	0.35		2.17	-25.6	0.6907	0.7004	0.19
	1.68	-13.3	0.7300	0.7615	0.36		2.20	-26.2	0.6870	0.6977	0.20
O2–N1	3.32(6)	-15.8(3)	0.6561	0.5717	0.11	C6–C8	2.23(4)	-23.9(1)	0.6757	0.7133	0.03
	3.16	-3.5	0.6140	0.6137	0.08		2.11	-17.0	0.6811	0.7072	0.22
	3.06	-1.7	0.6176	0.6227	0.08		2.08	-16.4	0.6869	0.7098	0.22
	3.40	-26.7	0.6434	0.5841	0.12		2.19	-26.1	0.6675	0.7214	0.20
	3.45	-28.1	0.6421	0.5795	0.12		2.20	-26.2	0.6666	0.7212	0.20
O3–N1	3.39(6)	-19.2(3)	0.6575	0.5653	0.02	C7–C8	2.31(4)	-28.5(1)	0.6738	0.7150	0.05
	3.23	-6.0	0.6129	0.6084	0.09		2.12	-17.6	0.6806	0.7078	0.23
	3.10	-3.5	0.6173	0.6199	0.08		2.09	-17.2	0.6852	0.7095	0.23
	3.44	-28.1	0.6425	0.5803	0.12		2.19	-26.1	0.6663	0.7225	0.21
	3.44	-28.2	0.6423	0.5799	0.12		2.20	-26.4	0.6640	0.7231	0.21
O4–C9	2.73(6)	-8.6(5)	0.8173	0.3917	0.38	C1–H1	1.79(9)	-17.3(3)	0.6687	0.4334	0.14
	2.95	-32.9	0.7317	0.4736	0.15		1.93	-22.7	0.7067	0.3924	0.06
	2.88	-30.9	0.7324	0.4841	0.15		1.97	-23.9	0.6990	0.3899	0.06
	2.88	-9.7	0.7927	0.4156	0.14		1.96	-27.6	0.7194	0.3810	0.03
	2.93	-8.1	0.7882	0.4119	0.13		2.03	-29.5	0.7087	0.3766	0.03
O5–C9	2.07(5)	-17.9(3)	0.7960	0.5329	0.16	C4–H4	1.90(8)	-25.6(2)	0.5539	0.5323	0.08
	2.24	-22.4	0.7845	0.5448	0.17		1.95	-22.7	0.6875	0.3955	0.03
	2.21	-21.1	0.7839	0.5534	0.16		1.95	-23.0	0.6915	0.3915	0.03
	2.16	-14.4	0.8698	0.4591	0.06		1.71	-28.6	0.7059	0.3792	0.01
	2.12	-15.5	0.8736	0.4666	0.06		2.02	-29.3	0.7016	0.3779	0.01
O5–C10	1.73(6)	-15.6(3)	1.0121	0.4352	0.05	C5–H5	2.05(9)	-27.1(3)	0.5786	0.5054	0.15
	1.60	-8.4	0.8416	0.6062	0.02		1.95	-22.4	0.6867	0.3963	0.02
	1.56	-8.0	0.8478	0.6094	0.02		1.94	-22.2	0.6854	0.4007	0.03
	1.59	-9.8	0.9438	0.5039	0.02		1.98	-28.2	0.6951	0.3889	0.02
	1.62	-9.9	0.9409	0.5001	0.01		1.99	-28.4	0.6932	0.3889	0.01
O6–C11	2.76(6)	-21.5(4)	0.7880	0.4199	0.03	C6–H6	2.12(9)	-35.6(3)	0.5295	0.5557	0.08
	2.98	-35.6	0.7315	0.4764	0.12		1.95	-23.1	0.6943	0.3887	0.02
	2.90	-33.7	0.7319	0.4889	0.13		1.95	-23.1	0.6953	0.3874	0.03
	2.89	-9.5	0.7919	0.4150	0.13		1.99	-28.6	0.7067	0.3779	0.01
	2.92	-8.5	0.7896	0.4127	0.13		2.02	-29.3	0.7013	0.3772	0.01

Table A.109: Continuation of Table A.108

bond	ϱ	$\nabla^2\varrho$	d1	d2	ε	bond	ϱ	$\nabla^2\varrho$	d1	d2	ε
O7–C11	2.09(5)	-19.9(3)	0.8817	0.4414	0.17	C7–H7	2.07(13)	-25.5(5)	0.6850	0.4002	0.08
	2.30	-23.9	0.7815	0.5404	0.15		1.96	-23.1	0.6920	0.3910	0.02
	2.28	-22.9	0.7810	0.5468	0.15		1.98	-23.6	0.6896	0.3914	0.03
	2.19	-14.4	0.8671	0.4562	0.07		1.99	-28.7	0.7062	0.3778	0.01
	2.14	-15.3	0.8726	0.4638	0.07		2.02	-29.4	0.7019	0.3779	0.01
O7–C12	1.71(6)	-13.7(3)	1.0123	0.4332	0.04	C10–H10A	1.73(11)	-15.9(6)	0.7612	0.3061	0.09
	1.59	-7.8	0.8412	0.6052	0.02		2.05	-25.5	0.6716	0.3947	0.07
	1.56	-7.8	0.8436	0.6119	0.02		1.95	-22.9	0.6903	0.3984	0.06
	1.60	-9.6	0.9436	0.5022	0.03		2.09	-31.1	0.6845	0.3828	0.04
	1.62	-9.8	0.9417	0.5000	0.01		1.99	-28.6	0.7015	0.3867	0.04
N1–C8	1.79(4)	-14.1(2)	0.8850	0.5841	0.12	C10–H10B	1.74(10)	-16.6(6)	0.7604	0.3050	0.09
	1.76	-12.6	0.8559	0.6137	0.12		2.05	-25.3	0.6718	0.3942	0.07
	1.79	-13.5	0.8532	0.6088	0.12		1.97	-23.2	0.6877	0.3990	0.06
	1.79	-17.6	0.8882	0.5808	0.14		2.09	-31.3	0.6814	0.3842	0.05
	1.77	-17.1	0.8869	0.5895	0.14		2.01	-29.1	0.6973	0.3877	0.04
C1–C3	1.87(3)	-16.5(1)	0.7832	0.7040	0.19	C10–H10C	1.83(10)	-19.7(5)	0.7485	0.3185	0.09
	1.81	-13.5	0.7511	0.7363	0.10		2.06	-25.6	0.6724	0.3938	0.07
	1.79	-13.0	0.7536	0.7371	0.10		1.95	-22.9	0.6929	0.3985	0.06
	1.85	-18.8	0.7531	0.7342	0.08		2.09	-31.1	0.6835	0.3835	0.04
	1.84	-18.8	0.7546	0.7324	0.08		2.00	-28.7	0.7018	0.3861	0.04
C2–C9	1.78(3)	-17.1(1)	0.7057	0.8096	0.14	C12–H12A	1.92(13)	-26.4(5)	0.7054	0.3630	0.14
	1.79	-13.9	0.7459	0.7682	0.10		2.05	-25.4	0.6720	0.3942	0.07
	1.77	-13.5	0.7515	0.7668	0.10		1.96	-23.2	0.6908	0.3979	0.06
	1.80	-17.6	0.7508	0.7632	0.08		2.08	-31.0	0.6851	0.3831	0.04
	1.80	-17.5	0.7511	0.7619	0.10		1.99	-28.6	0.7015	0.3866	0.04
C2–C11	1.88(3)	-18.4(1)	0.7590	0.7580	0.03	C12–H12B	1.47(9)	-8.5(5)	0.7463	0.3204	0.19
	1.75	-12.6	0.7513	0.7649	0.14		2.04	-25.4	0.6727	0.3935	0.06
	1.72	-12.1	0.7533	0.7677	0.14		1.95	-22.9	0.6926	0.3961	0.06
	1.78	-17.1	0.7510	0.7652	0.10		2.09	-31.3	0.6817	0.3844	0.05
	1.77	-16.9	0.7520	0.7691	0.06		2.01	-29.2	0.6976	0.3873	0.04
C3–C4	2.12(4)	-21.2(1)	0.6730	0.7276	0.01	C12–H12C	1.73(10)	-15.0(4)	0.7020	0.3648	0.19
	2.05	-15.9	0.7042	0.6967	0.20		2.07	-25.8	0.6729	0.3932	0.06
	2.05	-15.9	0.7066	0.6957	0.21		1.95	-23.1	0.6927	0.3980	0.06
	2.14	-24.7	0.7125	0.6879	0.18		2.09	-31.2	0.6850	0.3815	0.04
	2.16	-25.2	0.7120	0.6836	0.18		2.00	-28.6	0.7027	0.3852	0.04
epoxide	1.31	7.2				aryl	0.26	3.2			
	1.37	8.7					0.19	3.0			
	1.35	8.5					0.19	2.9			
	1.43	6.5					0.17	3.6			
	1.44	6.3					0.17	3.6			

Table A.110: Electron density (ϱ) at bcps in eÅ^{-3}, Laplacian ($\nabla^2\varrho$) at bcps in eÅ^{-5}, distances of the bcps to first (d1) and second (d2) atom of the bond X1–X2 in Å, and ellipticity at bcps (ε) for cyano-epoxide (**10**)
First row: experiment, second/third row: periodic-boundary calculation at experimental/optimised geometry, fourth/fifth row: isolated-molecule calculations at experimental/optimised geometries

bond	ϱ	$\nabla^2\varrho$	d1	d2	ε	bond	ϱ	$\nabla^2\varrho$	d1	d2	ε
O1–C1	1.78(2)	-4.1(7)	0.7878	0.6387	0.34	N4–C6	3.15(2)	-5.3(14)	0.7428	0.4078	0.00
	1.74	-2.5	0.7819	0.6436	0.36		3.02	-2.2	0.7288	0.4217	0.00
	1.72	-2.8	0.7847	0.6485	0.32		2.98	-4.1	0.7345	0.4244	0.00
	1.78	-12.5	0.8742	0.5518	0.44		3.32	-1.8	0.7486	0.4019	0.01
	1.79	-13.1	0.8719	0.5527	0.35		3.34	-1.7	0.7472	0.4017	0.02
O1–C2	1.76(2)	-3.7(7)	0.7903	0.6313	0.33	C1–C3	1.85(1)	-12.4(5)	0.6765	0.7733	0.07
	1.76	-2.9	0.7805	0.6415	0.33		1.80	-10.6	0.6827	0.7671	0.08
	1.73	-3.0	0.7840	0.6449	0.29		1.78	-10.2	0.6846	0.7689	0.08
	1.80	-12.8	0.8736	0.5484	0.43		1.93	-21.2	0.7073	0.7424	0.06
	1.79	-13.1	0.8718	0.5523	0.35		1.93	-21.4	0.7047	0.7430	0.06
C1–C2	1.58(2)	-6.8(5)	0.7499	0.7546	0.65	C1–C4	1.89(1)	-13.3(5)	0.6679	0.7808	0.07
	1.56	-5.2	0.7516	0.7523	0.72		1.80	-10.5	0.6828	0.7661	0.08
	1.48	-3.8	0.7622	0.7622	0.76		1.78	-10.1	0.6850	0.7682	0.08
	1.65	-12.4	0.7523	0.7519	0.43		1.93	-21.2	0.7062	0.7425	0.06
	1.58	-10.8	0.7602	0.7613	0.48		1.93	-21.3	0.7042	0.7434	0.06
N1–C3	3.21(2)	-11.5(14)	0.7404	0.4094	0.00	C2–C5	1.86(1)	-12.4(5)	0.6770	0.7741	0.04
	3.04	-4.0	0.7279	0.4219	0.00		1.79	-10.5	0.6835	0.7677	0.07
	2.98	-3.4	0.7334	0.4245	0.00		1.79	-10.5	0.6877	0.7671	0.07
	3.33	-3.3	0.7461	0.4037	0.01		1.92	-21.0	0.7061	0.7450	0.06
	3.34	-2.2	0.7471	0.4018	0.01		1.93	-21.4	0.7047	0.7431	0.06
N2–C4	3.20(2)	-10.5(14)	0.7383	0.4108	0.00	C2–C6	1.85(1)	-12.4(5)	0.6794	0.7703	0.04
	3.02	-2.0	0.7278	0.4213	0.00		1.80	-10.7	0.6823	0.7676	0.07
	2.97	-3.8	0.7331	0.4253	0.00		1.79	-10.5	0.6885	0.7652	0.07
	3.33	-3.1	0.7457	0.4034	0.01		1.93	-21.2	0.7055	0.7443	0.06
	3.34	-1.8	0.7472	0.4018	0.02		1.93	-21.3	0.7042	0.7435	0.06
N3–C5	3.20(2)	-9.0(14)	0.7410	0.4088	0.00	epoxide	1.38	7.7			
	3.04	-3.6	0.7286	0.4211	0.00		1.36	7.9			
	2.98	-4.1	0.7330	0.4250	0.00		1.31	7.8			
	3.33	-1.6	0.7482	0.4016	0.01		1.43	6.5			
	3.34	-2.2	0.7471	0.4018	0.01		1.40	6.4			

Table A.111: Atomic charges (Q = Q_{001} = Q_{tot}) in e, and atomic volumes (V_{001} and V_{tot}) in Å^3 of etox (**7**)
First row: experiment, second/third row: periodic-boundary calculation at experimental/optimised geometry, fourth/fifth row: isolated-molecule calculations at experimental/optimised geometries

atom	Q	V_{001}	V_{tot}	atom	Q	V_{001}	V_{tot}
O1	-0.81	14.6	14.8	H2	0.06	6.7	6.7
	-0.77	15.0	15.0		0.07	6.6	6.6
	-0.76	16.1	16.4		0.07	6.9	7.3
	-0.87	16.7			0.06	7.2	
	-0.89	16.6			0.05	7.2	
C1	0.33	9.3	9.4	H3	0.12	6.7	6.8
	0.25	10.1	10.2		0.06	6.8	6.9
	0.24	10.5	10.6		0.07	6.8	7.1
	0.41	9.8			0.06	7.2	
	0.44	9.7			0.05	7.2	
C2	0.15	10.4	10.4	H4	0.08	6.9	7.1
	0.26	10.5	10.5		0.07	7.0	7.1
	0.26	10.7	10.9		0.07	7.3	7.7
	0.40	9.9			0.06	7.2	
	0.44	9.7			0.05	7.2	
H1	0.08	6.8	7.0	sum	0.02	61.4	62.2
	0.06	6.8	6.8		0.00	62.8	63.1
	0.05	7.9	8.2		0.01	66.1	68.2
	0.06	7.2			0.18	65.2	
	0.05	7.2			0.19	64.8	

Table A.112: Atomic charges (Q = Q_{001} = Q_{tot}) in e, and atomic volumes (V_{001} and V_{tot}) in Å^3 of moc-epoxide (**8**)

First row: experiment, second/third row: periodic-boundary calculation at experimental/optimised geometry, fourth/fifth row: isolated-molecule calculations at experimental/optimised geometries

atom	Q	V_{001}	V_{tot}	atom	Q	V_{001}	V_{tot}	atom	Q	V_{001}	V_{tot}
O1	-0.72	14.1	14.3	H4A	0.02	6.7	6.8	C3A	1.38	5.6	5.6
	-0.72	14.1	14.3		0.02	6.7	6.8		1.37	5.7	5.6
	-0.83	15.1	15.9		0.06	7.4	7.5		1.33	6.0	6.1
	-0.84	15.8			0.04	6.9					
	-0.87	15.8			0.06	7.0					
C1	0.35	7.9	7.9	H4B	0.09	6.3	6.4	C4A	0.43	9.5	9.5
	0.35	7.9	7.9		0.09	6.3	6.4		0.43	9.5	9.5
	0.31	8.8	8.9		0.00	6.8	7.4		0.33	10.6	10.8
	0.35	8.4			0.05	6.9					
	0.39	8.3			0.06	7.0					
C2	0.33	8.5	8.7	H4C	0.04	7.3	7.3	C5A	1.31	6.6	6.6
	0.33	8.5	8.7		0.04	7.3	7.3		1.30	6.6	6.7
	0.33	8.2	8.5		0.11	6.9	7.4		1.25	7.0	7.1
	0.36	8.4			0.06	6.7					
	0.38	8.3			0.06	6.9					
O2	-1.15	18.2	18.8	H6A	0.06	6.4	6.7	C6A	0.44	8.7	8.6
	-1.14	18.2	18.7		0.06	6.4	6.7		0.44	8.7	8.6
	-1.06	18.6	19.6		0.02	7.2	7.7		0.22	10.1	10.4
	-1.17	19.4			0.05	6.8					
	-1.17	19.4			0.06	6.9					
O3	-0.88	13.9	13.9	H6B	0.04	6.7	7.1	H1A	0.10	6.2	6.4
	-0.88	13.9	13.9		0.04	6.7	7.1		0.10	6.2	6.4
	-0.92	14.7	15.2		0.10	7.1	7.9		0.07	6.2	6.5
	-1.09	15.0			0.05	6.9					
	-1.08	14.9			0.05	7.0					
O4	-1.21	18.0	18.2	H6C	0.12	6.3	6.5	H2A	0.14	6.2	6.2
	-1.20	17.9	18.2		0.12	6.3	6.5		0.14	6.2	6.2
	-1.08	18.0	19.4		0.15	6.8	7.4		0.13	6.5	6.8
	-1.17	19.4			0.05	6.8					
	-1.16	19.3			0.06	6.9					
O5	-0.84	13.9	14.4	O1A	-0.62	14.0	14.3	H4D	0.03	6.6	6.6
	-0.84	13.9	14.4		-0.62	14.0	14.2		0.03	6.6	6.6
	-0.89	13.9	14.7		-0.65	14.9	15.6		0.12	6.6	7.0
	-1.08	15.0									
	-1.08	14.9									
C3	1.31	6.6	6.7	C1A	0.30	8.3	8.5	H4E	0.04	7.2	7.6
	1.30	6.7	6.8		0.31	8.3	8.5		0.04	7.2	7.6
	1.36	6.8	6.9		0.34	8.2	8.5		0.12	6.8	7.5
	1.60	5.3									
	1.60	5.3									
C4	0.58	8.4	8.4	C2A	0.21	8.5	8.6	H4F	0.07	6.5	6.6
	0.58	8.4	8.4		0.21	8.5	8.6		0.07	6.5	6.6
	0.52	9.4	9.7		0.35	8.5	8.6		0.00	7.2	7.8
	0.52	8.8									
	0.51	8.9									
C5	1.37	5.7	5.7	O2A	-1.15	17.4	17.5	H6D	0.07	6.9	7.1
	1.35	5.8	5.8		-1.14	17.4	17.5		0.07	6.9	7.1
	1.36	5.9	5.9		-1.09	18.2	19.3		0.11	7.3 0	7.6
	1.60	5.3									
	1.59	5.3									
C6	0.49	9.2	9.4	O3A	-0.89	13.9	14.4	H6E	-0.02	7.0	7.0
	0.49	9.2	9.4		-0.89	13.9	14.3		-0.02	7.0	7.0
	0.47	10.1	10.5		-0.95	14.1	14.8		0.11	6.3	6.7
	0.52	8.7									
	0.50	9.0									
H1	0.12	6.0	6.0	O4A	-1.13	18.6	19.3	H6F	0.01	7.2	7.4
	0.12	6.0	6.0		-1.12	18.6	19.3		0.01	7.2	7.4
	0.10	6.7	7.0		-1.09	18.7	19.7		0.02	7.4	8.0
	0.10	6.6									
	0.10	6.5									
H2	0.07	6.2	6.5	O5A	-0.88	14.1	14.1	sum	0.02	356.8	363.2
	0.07	6.2	6.4		-0.88	14.1	14.1		0.01	356.8	363.2
	0.09	6.0	6.4		-0.92	14.6	15.1		0.01	371.5	389.6
	0.11	6.6							0.11	367.4	
	0.10	6.5							0.16	368.2	

Table A.113: Atomic charges (Q = Q_{001} = Q_{tot}) in e, and atomic volumes (V_{001} and V_{tot}) in Å^3 of niphe-epoxide (**9**)

First row: experiment, second/third row: periodic-boundary calculation at experimental/optimised geometry, fourth/fifth row: isolated-molecule calculations at experimental/optimised geometries

atom	Q	V_{001}	V_{tot}	atom	Q	V_{001}	V_{tot}	atom	Q	V_{001}	V_{tot}
O1	-0.56	14.6	15.1	C4	0.29	10.6	10.8	H5	-0.21	7.2	7.5
	-0.70	14.8	16.1		0.02	11.5	12.3		0.08	6.6	7.0
	-0.70	15.2	17.0		0.01	12.1	13.7		0.07	6.9	8.0
	-0.87	15.5									
	-0.89	15.5									
C1	0.38	8.7	8.7	C5	0.48	10.2	10.2	H6	-0.29	6.8	7.2
	0.28	8.7	8.8		0.02	11.3	11.4		0.11	5.7	6.3
	0.29	8.8	9.0		0.02	12.2	13.0		0.11	6.2	7.2
	0.42	8.0									
	0.43	7.9									
C2	0.22	7.7	7.7	C6	0.45	9.8	9.8	H7	-0.05	6.4	6.6
	0.28	7.2	7.2		0.02	11.6	11.8		0.10	5.7	5.9
	0.27	7.6	7.6		0.01	12.4	13.1		0.10	5.9	6.5
	0.40	6.9									
	0.40	6.9									
O2	-0.22	16.6	17.2	C7	-0.16	11.7	11.7	H10A	0.13	6.0	6.0
	-0.41	16.7	17.7		0.03	11.2	11.4		0.04	6.5	6.8
	-0.40	17.4	19.4		0.03	11.9	12.3		0.06	6.3	6.9
	-0.43	17.3									
	-0.43	17.3									
O3	-0.27	16.5	17.2	C8	0.13	9.1	9.1	H10B	0.18	6.3	6.6
	-0.40	16.6	17.7		0.22	9.0	9.0		0.03	6.9	7.4
	-0.39	17.1	19.6		0.23	9.8	10.0		0.05	6.7	8.2
	-0.43	17.3									
	-0.43	17.3									
O4	-1.07	17.3	17.4	C9	1.53	4.5	4.5	H10C	0.10	6.6	6.6
	-0.95	16.9	17.2		1.24	5.3	5.4		0.04	6.5	6.9
	-0.92	17.7	18.1		1.20	6.0	6.2		0.07	6.7	7.2
	-1.12	19.2			1.63	4.6					
	-1.13	19.1			1.63	4.9					
O5	-1.00	14.0	14.2	C10	-0.03	12.3	12.4	H12A	0.26	5.3	5.3
	-0.88	13.6	14.1		0.47	8.8	8.9		0.04	6.4	6.9
	-0.87	14.2	14.8		0.41	9.5	10.1		0.07	6.7	7.1
	-1.13	14.7									
	-1.12	14.8									
O6	-1.01	16.3	16.3	C11	1.73	5.0	5.0	H12B	0.24	5.8	6.5
	-0.94	16.2	16.3		1.25	6.0	6.0		0.05	6.3	7.7
	-0.91	16.9	17.2		1.20	6.6	6.8		0.06	6.7	8.5
	-1.11	19.0			1.65	5.2					
	-1.11	19.1			1.64	5.1					
O7	-1.14	14.3	14.5	C12	0.02	13.9	14.6	H12C	0.04	6.0	6.0
	-0.89	13.6	14.3		0.46	8.9	9.6		0.04	6.1	6.2
	-0.88	14.4	15.7		0.40	9.5	11.1		0.07	6.7	6.9
	-1.10	14.5									
	-1.08	14.5									
N1	0.31	8.1	8.1	H1	-0.01	6.8	7.1	sum	0.06	301.8	307.8
	0.19	8.1	8.1		0.09	6.7	7.2		-0.01	295.3	308.7
	0.17	8.6	8.6		0.08	6.9	8.0		0.00	310.2	335.8
	0.42	7.4			0.09	6.6					
C3	-0.14	10.1	10.1	H4	-0.26	7.4	7.8				
	0.01	9.5	9.6		0.08	6.4	7.3				
	0.01	10.1	10.3		0.09	6.7	7.8				
	0.01	10.0									
	0.00	10.1									

Table A.114: Atomic charges (Q = Q_{001} = Q_{tot}) in e, and atomic volumes (V_{001} and V_{tot}) in Å^3 of cyano-epoxide (**10**)

First row: experiment, second/third row: periodic-boundary calculation at experimental/optimised geometry, fourth/fifth row: isolated-molecule calculations at experimental/optimised geometries

atom	Q	V001	Vtot	atom	Q	V001	Vtot	atom	Q	V001	Vtot
O1	-0.53	16.1	17.9	C4	0.72	10.9	11.0	N2	-0.85	21.0	22.9
	-0.60	16.3	18.3		0.75	10.1	10.2		-0.89	21.1	23.3
	-0.60	14.8	21.8		0.71	11.3	12.8		-0.86	21.4	31.9
	-0.80	15.4			0.92	10.6			-1.03	22.9	
	-0.77	15.4			0.96	10.6			-0.96	22.7	
C1	0.51	6.6	6.6	C5	0.76	10.4	10.6	N3	-0.88	20.6	21.1
	0.58	6.5	6.5		0.75	10.0	10.2		-0.89	20.8	21.4
	0.59	6.5	6.5		0.73	10.7	11.9		-0.88	21.6	27.8
	0.52	6.8			0.97	10.5			-0.96	22.6	
	0.59	6.7			0.94	10.6			-1.00	22.8	
C2	0.51	6.1	6.1	C6	0.79	10.6	10.8	N4	-0.90	22.2	24.4
	0.59	6.0	6.0		0.71	10.6	10.8		-0.86	22.0	24.4
	0.61	6.0	6.0		0.72	11.1	12.7		-0.85	22.4	31.0
	0.61	6.6			0.97	10.5			-0.96	22.7	
	0.59	6.7			0.96	10.6			-0.96	22.7	
C3	0.81	10.5	10.6	N1	-0.94	21.0	21.5	sum	-0.01	156.1	163.6
	0.75	10.3	10.3		-0.89	21.0	21.6		-0.01	154.7	163.0
	0.73	10.9	12.2		-0.86	21.1	30.3		0.03	157.9	205.0
	0.92	10.6			-1.02	22.8			0.14	162.0	
	0.94	10.6			-1.00	22.8			0.29	162.2	

Table A.115: Absolute (relative) source-function contributions in eÅ^{-3} (%) to the bcps of the bonds C1–O1, C2–O1 and C1–C2 in etox (**7**)
Exp = experiment, theo = periodic-boundary calculations at experimental (first row) and optimised (second row) geometry

atom	C1–O1 exp	C1–O1 theo	C2–O1 exp	C2–O1 theo	C1–C2 exp	C1–C2 theo
O1	0.7096(42.7)	0.7293(43.4)	0.7585(42.9)	0.7097(43.3)	0.2218(13.2)	0.2082(12.1)
		0.7157(43.6)		0.7005(43.5)		0.2044(12.2)
C1	0.6096(36.7)	0.6111(36.4)	0.1271(7.2)	0.1350(8.2)	0.6196(36.9)	0.6349(36.9)
		0.5906(36.0)		0.1299(8.1)		0.6185(36.8)
C2	0.1545(9.3)	0.1354(8.1)	0.6836(38.6)	0.5950(36.3)	0.6345(37.8)	0.6552(38.1)
		0.1299(7.9)		0.5795(36.0)		0.6395(38.1)
H1	0.0597(3.6)	0.0620(3.7)	0.0272(1.5)	0.0280(1.7)	0.0538(3.2)	0.0528(3.1)
		0.0653(4.0)		0.0297(1.8)		0.0557(3.3)
H2	0.0632(3.8)	0.0614(3.7)	0.0286(1.6)	0.0283(1.7)	0.0578(3.4)	0.0532(3.1)
		0.0622(3.8)		0.0284(1.8)		0.0534(3.2)
H3	0.0266(1.6)	0.0286(1.7)	0.0589(3.3)	0.0622(3.8)	0.0457(2.7)	0.0534(3.1)
		0.0291(1.8)		0.0641(4.0)		0.0552(3.3)
H4	0.0301(1.8)	0.0285(1.7)	0.0669(3.8)	0.0628(3.8)	0.0518(3.1)	0.0541(3.1)
		0.0292(1.8)		0.0642(4.0)		0.0556(3.3)
sum	1.6534(99.6)	1.6561(98.6)	1.7508(98.9)	1.6211(98.8)	1.6851(100.3)	1.7117(99.5)
		1.6221(98.9)		1.5962(99.1)		1.6823(100.1)
reference	1.66	1.68	1.77	1.64	1.68	1.72
		1.64		1.61		1.68

Table A.116: Absolute (relative) source-function contributions in eÅ^{-3} (%) to the bcps of the bonds C1–O1, C2–O1 and C1–C2 in moc-epoxide (**8**)
Exp = experiment, theo = periodic-boundary calculations at experimental (first row) and optimised (second row) geometry

atom	C1–O1 exp	C1–O1 theo	C2–O1 exp	C2–O1 theo	C1–C2 exp	C1–C2 theo
O1	0.7396(43.5)	0.7407(43.3)	0.7070(42.8)	0.7081(42.9)	0.2155(13.6)	0.2160(13.6)
		0.7143(43.6)		0.7080(43.4)		0.2103(12.8)
C1	0.6057(35.6)	0.6068(35.5)	0.1147(7.0)	0.1152(7.0)	0.5412(34.3)	0.5424(34.1)
		0.5739(35.0)		0.1110(6.8)		0.5657(34.5)
C2	0.1107(6.5)	0.1111(6.5)	0.5840(35.4)	0.5852(35.5)	0.5446(34.5)	0.5458(34.3)
		0.1174(7.2)		0.5728(35.1)		0.5962(36.4)
O2	0.0340(2.0)	0.0339(2.0)	0.0149(0.9)	0.0150(0.9)	0.0298(1.9)	0.0297(1.9)
		0.0313(1.9)		0.0143(0.9)		0.0282(1.7)
O3	0.0181(1.1)	0.0182(1.1)	0.0117(0.7)	0.0117(0.7)	0.0164(1.0)	0.0164(1.0)
		0.0190(1.2)		0.0121(0.7)		0.0166(1.0)
O4	0.0147(0.9)	0.0148(0.9)	0.0336(2.0)	0.0336(2.0)	0.0303(1.9)	0.0303(1.9)
		0.0142(0.9)		0.0324(2.0)		0.0288(1.8)
O5	0.0097(0.6)	0.0097(0.6)	0.0158(1.0)	0.0157(1.0)	0.0138(0.9)	0.0137(0.9)
		0.0112(0.7)		0.0174(1.1)		0.0157(1.0)
C3	0.0228(1.3)	0.0196(1.1)	0.0069(0.4)	0.0037(0.2)	0.0170(1.1)	0.0136(0.9)
		0.0192(1.2)		0.0030(0.2)		0.0134(0.8)
C4	0.0028(0.2)	0.0029(0.2)	0.0022(0.1)	0.0022(0.1)	0.0027(0.2)	0.0027(0.2)
		0.0014(0.1)		0.0009(0.1)		0.0013(0.1)
C5	0.0058(0.3)	0.0049(0.3)	0.0213(1.3)	0.0203(1.2)	0.0153(1.0)	0.0143(0.9)
		0.0121(0.7)		0.0296(1.8)		0.0246(1.5)
C6	0.0022(0.1)	0.0022(0.1)	0.0029(0.2)	0.0029(0.2)	0.0027(0.2)	0.0027(0.2)
		0.0036(0.2)		0.0046(0.3)		0.0044(0.3)
H1	0.0612(3.6)	0.0612(3.6)	0.0276(1.7)	0.0277(1.7)	0.0511(3.2)	0.0511(3.2)
		0.0615(3.8)		0.0282(1.7)		0.0513(3.1)
H2	0.0282(1.7)	0.0282(1.6)	0.0605(3.7)	0.0605(3.7)	0.0539(3.4)	0.0538(3.4)
		0.0279(1.7)		0.0614(3.8)		0.0541(3.3)
H4A	0.0028(0.2)	0.0028(0.2)	0.0015(0.1)	0.0015(0.1)	0.0018(0.1)	0.0018(0.1)
		0.0026(0.2)		0.0014(0.1)		0.0018(0.1)
H4B	0.0041(0.2)	0.0041(0.2)	0.0033(0.2)	0.0033(0.2)	0.0040(0.3)	0.0040(0.3)
		0.0041(0.3)		0.0033(0.2)		0.0039(0.2)
H4C	0.0021(0.1)	0.0021(0.1)	0.0015(0.1)	0.0015(0.1)	0.0026(0.2)	0.0026(0.2)
		0.0022(0.1)		0.0018(0.1)		0.0028(0.2)
H6A	0.0014(0.1)	0.0014(0.1)	0.0026(0.2)	0.0026(0.2)	0.0018(0.1)	0.0018(0.1)
		0.0014(0.1)		0.0026(0.2)		0.0018(0.1)
H6B	0.0034(0.2)	0.0034(0.2)	0.0042(0.3)	0.0042(0.3)	0.0041(0.3)	0.0041(0.3)
		0.0030(0.2)		0.0038(0.2)		0.0037(0.2)
H6C	0.0015(0.1)	0.0015(0.1)	0.0020(0.1)	0.0020(0.1)	0.0026(0.2)	0.0026(0.2)
		0.0017(0.1)		0.0022(0.1)		0.0027(0.2)
sum	1.6709(98.3)	1.6694(97.6)	1.6183(98.1)	1.6170(98.0)	1.5510(98.2)	1.5496(97.5)
		1.6219(98.9)		1.6108(98.8)		1.6274(99.2)
reference	1.70	1.71	1.65	1.65	1.58	1.59
		1.64		1.63		1.64

Table A.117: Absolute (relative) source-function contributions in eÅ^{-3} (%) to the bcps of the bonds C1–O1, C2–O1 and C1–C2 in niphe-epoxide (**9**)
Exp = experiment, theo = periodic-boundary calculations at experimental (first row) and optimised (second row) geometry

atom	C1–O1 exp	C1–O1 theo	C2–O1 exp	C2–O1 theo	C1–C2 exp	C1–C2 theo
O1	0.7109(41.6)	0.7485(44.0)	0.7453(43.3)	0.7885(44.8)	0.2158(14.2)	0.2188(13.7)
		0.7421(43.7)		0.7708(44.3)		0.2166(13.8)
C1	0.6258(36.6)	0.6102(35.9)	0.1010(5.9)	0.1154(6.6)	0.5371(35.3)	0.5719(35.7)
		0.6301(37.1)		0.1155(6.6)		0.5515(35.1)
C2	0.0848(5.0)	0.1054(6.2)	0.6239(36.3)	0.6256(35.5)	0.4976(32.7)	0.5440(34.0)
		0.1044(6.1)		0.6113(35.1)		0.5236(33.4)
O2	0.0034(0.2)	0.0031(0.2)	0.0026(0.2)	0.0024(0.1)	0.0034(0.2)	0.0032(0.2)
		0.0030(0.2)		0.0024(0.1)		0.0032(0.2)
O3	0.0042(0.2)	0.0038(0.2)	0.0036(0.2)	0.0033(0.2)	0.0038(0.3)	0.0035(0.2)
		0.0038(0.2)		0.0033(0.2)		0.0035(0.2)
O4	0.0182(1.1)	0.0186(1.1)	0.0333(1.9)	0.0314(1.8)	0.0339(2.2)	0.0328(2.1)
		0.0177(1.0)		0.0309(1.8)		0.0318(2.0)
O5	0.0073(0.4)	0.0075(0.4)	0.0182(1.1)	0.0168(1.0)	0.0103(0.7)	0.0102(0.6)
		0.0071(0.4)		0.0157(0.9)		0.0098(0.6)
O6	0.0134(0.8)	0.0137(0.8)	0.0368(2.1)	0.0327(1.9)	0.0291(1.9)	0.0276(1.7)
		0.0126(0.7)		0.0314(1.8)		0.0259(1.6)
O7	0.0117(0.7)	0.0109(0.6)	0.0203(1.2)	0.0169(1.0)	0.0178(1.2)	0.0154(1.0)
		0.0116(0.7)		0.0178(1.0)		0.0162(1.0)
N1	-0.0001(0.0)	-0.0013(-0.1)	-0.0002(0.0)	-0.0013(-0.1)	-0.0002(0.0)	-0.0014(-0.1)
		0.0002(0.0)		0.0001(0.0)		0.0002(0.0)
C3	0.0446(2.6)	0.0329(1.9)	0.0135(0.8)	0.0101(0.6)	0.0315(2.1)	0.0265(1.7)
		0.0326(1.9)		0.0097(0.6)		0.0259(1.6)
C4	0.0103(0.6)	0.0045(0.3)	0.0036(0.2)	-0.0002(0.0)	0.0084(0.6)	0.0046(0.3)
		0.0057(0.3)		0.0010(0.1)		0.0055(0.4)
C5	0.0116(0.7)	0.0100(0.6)	0.0068(0.4)	0.0059(0.3)	0.0093(0.6)	0.0084(0.5)
		0.0099(0.6)		0.0057(0.3)		0.0081(0.5)
C6	0.0091(0.5)	0.0049(0.3)	0.0066(0.4)	0.0033(0.2)	0.0085(0.6)	0.0047(0.3)
		0.0051(0.3)		0.0035(0.2)		0.0050(0.3)
C7	0.0099(0.6)	0.0071(0.4)	0.0072(0.4)	0.0052(0.3)	0.0085(0.6)	0.0064(0.4)
		0.0073(0.4)		0.0052(0.3)		0.0063(0.4)
C8	0.0033(0.2)	0.0031(0.2)	0.0026(0.2)	0.0025(0.1)	0.0030(0.2)	0.0029(0.2)
		0.0025(0.1)		0.0020(0.1)		0.0023(0.1)
C9	0.0118(0.7)	0.0034(0.2)	0.0365(2.1)	0.0212(0.7)	0.0276(1.8)	0.0159(1.0)
		0.0055(0.3)		0.0242(1.4)		0.0170(1.1)
C10	0.0035(0.2)	0.0026(0.2)	0.0044(0.3)	0.0031(0.2)	0.0047(0.3)	0.0035(0.2)
		0.0016(0.1)		0.0021(0.1)		0.0023(0.1)
C11	0.0144(0.8)	-0.0014(-0.1)	0.0347(2.0)	0.0117(0.7)	0.0279(1.8)	0.0075(0.5)
		0.0012(0.1)		0.0157(0.9)		0.0108(0.7)
C12	0.0033(0.2)	0.0045(0.3)	0.0049(0.3)	0.0057(0.3)	0.0044(0.3)	0.0052(0.3)
		0.0023(0.1)		0.0031(0.2)		0.0028(0.2)
H1	0.0732(4.3)	0.0605(3.6)	0.0312(1.8)	0.0274(1.6)	0.0601(4.0)	0.0530(3.3)
		0.0636(3.7)		0.0283(1.6)		0.0554(3.5)
H4	0.0053(0.3)	0.0036(0.2)	-0.0003(0.0)	-0.0006(0.0)	0.0049(0.3)	0.0038(0.2)
		0.0030(0.2)		-0.0012(-0.1)		0.0033(0.2)
H5	0.0062(0.4)	0.0046(0.3)	0.0037(0.2)	0.0030(0.2)	0.0049(0.3)	0.0040(0.3)
		0.0046(0.3)		0.0029(0.2)		0.0039(0.2)
H6	0.0055(0.3)	0.0043(0.3)	0.0042(0.2)	0.0035(0.2)	0.0051(0.3)	0.0042(0.3)
		0.0043(0.3)		0.0034(0.2)		0.0042(0.3)
H7	0.0052(0.3)	0.0047(0.3)	0.0038(0.2)	0.0037(0.2)	0.0047(0.3)	0.0045(0.3)
		0.0045(0.3)		0.0035(0.2)		0.0043(0.3)
H10A	0.0027(0.2)	0.0028(0.2)	0.0027(0.2)	0.0027(0.2)	0.0035(0.2)	0.0038(0.2)
		0.0026(0.2)		0.0027(0.2)		0.0036(0.2)
H10B	0.0032(0.2)	0.0033(0.2)	0.0041(0.2)	0.0042(0.2)	0.0040(0.3)	0.0041(0.3)
		0.0033(0.2)		0.0040(0.2)		0.0039(0.2)
H10C	0.0012(0.1)	0.0010(0.1)	0.0024(0.1)	0.0021(0.1)	0.0025(0.2)	0.0022(0.1)
		0.0011(0.1)		0.0022(0.1)		0.0021(0.1)
H12A	0.0011(0.1)	0.0014(0.1)	0.0023(0.1)	0.0027(0.2)	0.0014(0.1)	0.0017(0.1)
		0.0016(0.1)		0.0029(0.2)		0.0019(0.1)
H12B	0.0027(0.2)	0.0036(0.2)	0.0036(0.2)	0.0045(0.3)	0.0033(0.2)	0.0042(0.3)
		0.0033(0.2)		0.0042(0.2)		0.0039(0.2)
H12C	0.0015(0.1)	0.0010(0.1)	0.0022(0.1)	0.0015(0.1)	0.0026(0.2)	0.0021(0.1)
		0.0015(0.1)		0.0022(0.1)		0.0026(0.2)
sum	1.7093(100.0)	1.6829(99.0)	1.7655(102.6)	1.7551(99.7	1.5793(103.9)	1.5990(99.9)
		1.7000(100.0)		1.7265(99.2)		1.5575(99.2)
reference	1.71	1.70	1.72	1.76	1.52	1.60
		1.70		1.74		1.57

Table A.118: Absolute (relative) source-function contributions in eÅ^{-3} (%) to the bcps of the bonds C1–O1, C2–O1 and C1–C2 in niphe-epoxide (**9**)
Exp = experiment, theo = periodic-boundary calculations at experimental (first row) and optimised (second row) geometry

atom	C1–O1 exp	C1–O1 theo	C2–O1 exp	C2–O1 theo	C1–C2 exp	C1–C2 theo
O1	0.7903(44.4)	0.7761(44.6)	0.7735(43.9)	0.7879(44.8)	0.2283(14.4)	0.2263(14.5)
		0.7667(44.6)		0.7748(44.8)		0.2189(14.8)
C1	0.6017(33.8)	0.5809(33.4)	0.0920(5.2)	0.0891(5.1)	0.4973(31.5)	0.4932(31.6)
		0.5994(34.8)		0.1022(5.9)		0.4809(32.5)
C2	0.0909(5.1)	0.0954(5.5)	0.5938(33.7)	0.5996(34.1)	0.5270(33.4)	0.5168(33.1)
		0.1011(5.9)		0.6041(34.9)		0.4773(32.3)
N1	0.0498(2.8)	0.0499(2.9)	0.0312(1.8)	0.0317(1.8)	0.0461(2.9)	0.0465(3.0)
		0.0496(2.9)		0.0312(1.8)		0.0456(3.1)
N2	0.0507(2.8)	0.0500(2.9)	0.0320(1.8)	0.0318(1.8)	0.0469(3.0)	0.0466(3.0)
		0.0493(2.9)		0.0311(1.8)		0.0454(3.1)
N3	0.0315(1.8)	0.0318(1.8)	0.0504(2.9)	0.0498(2.8)	0.0468(3.0)	0.0465(3.0)
		0.0313(1.8)		0.0493(2.8)		0.0455(3.1)
N4	0.0317(1.8)	0.0321(1.8)	0.0509(2.9)	0.0503(2.9)	0.0470(3.0)	0.0468(3.0)
		0.0315(1.8)		0.0498(2.9)		0.0456(3.1)
C3	0.0433(2.4)	0.0390(2.2)	0.0116(0.7)	0.0088(0.5)	0.0353(2.2)	0.0313(2.0)
		0.0396(2.3)		0.0089(0.5)		0.0310(2.1)
C4	0.0424(2.4)	0.0384(2.2)	0.0100(0.6)	0.0085(0.5)	0.0341(2.1)	0.0309(2.0)
		0.0392(2.3)		0.0085(0.5)		0.0307(2.1)
C5	0.0098(0.6)	0.0088(0.5)	0.0417(2.4)	0.0383(2.2)	0.0339(2.1)	0.0311(2.0)
		0.0084(0.5)		0.0388(2.2)		0.0302(2.0)
C6	0.0105(0.6)	0.0090(0.5)	0.0423(2.4)	0.0388(2.2)	0.0342(2.2)	0.0314(2.0)
		0.0086(0.5)		0.0391(2.3)		0.0305(2.1)
sum	1.7525(98.5)	1.7114(98.4)	1.7295(98.3)	1.7346(98.6)	1.5770(99.8)	1.5474(99.2)
		1.7248(100.3)		1.7378(100.5)		1.4816(100.1)
reference	1.78	1.74	1.76	1.76	1.58	1.56
		1.72		1.73		1.48